Universität Hamburg
DER FORSCHUNG | DER LEHRE | DER BILDUNG

Dissertation

Advances in Vitrimer Design and their Application as Matrix Materials in Composites

submitted by

Philipp Haida

Hamburg 2023

Faculty of Mathematics, Informatics, and Natural Science

Department of Chemistry

in conformity with requirements for the degree of

Doctor rerum naturalium (Dr. rer. nat.)

submitted to the Universität Hamburg

"The greatest obstacle to discovery is not ignorance – it is the illusion of knowledge"

Daniel J. Boorstin

The submitted dissertation was written under the supervision of Prof. Dr. Volker Abetz at the Institute of Physical Chemistry of the University of Hamburg. The practical work of the dissertation was carried out from May 2019 to May 2023. The dissertation was submitted in October 2023 and represents a cumulative dissertation with the approval of the audit committee. The dissertation contains three first-author publications, which were published with the help of cooperation partners and co-workers mentioned in the publications. Contributions for presented unpublished results are acknowledged in this dissertation in the particular subchapter as well.

Publications

This cumulative thesis contains three first-author publications that have been published prior to this work. The publications are shown as a reprint in chapter 5.

Publication 1:
Acid-Mediated Autocatalysis in Vinylogous Urethane Vitrimers

Philipp Haida and Volker Abetz

Publication 2:
Blended Vinylogous Urethane/Urea Vitrimers Derived from Aromatic Alcohols

Philipp Haida, Gloria Signorato and Volker Abetz

Publication 3:
Starch-Reinforced Vinylogous Urethane Vitrimer Composites: An Approach to Biobased, Reprocessable, and Biodegradable Materials

Philipp Haida, Suwabun Chirachanchai and Volker Abetz

Table of Contents

Index of Symbols

Δ	Heat
E	E-modulus
α	Alpha
σ_m	Tensile Strength or ultimate Strength
σ_b	Stress at break
ε_b	Elongation at break or ultimate strain
ε_m	Elongation at ultimate strength
ω	Circular frequency
γ	Torsional deformation
T	Temperature
R	Acetoacetate/epoxide to amine ratio
s	Seconds
h	Hours
Min	Minutes
kJ	kilo Joule
MPa	Megapascal
G'	Storage modulus
G''	Loss modulus
Tan δ	Loss factor
η	Viscosity
e	Euler's number
R_g	Gas constant
τ	Stress-relaxation time
$G(t)$	Stress-relaxation modulus
Mol%	Mole fraction
Wt%	Weight fraction
pKa	Acid dissociation constant
$\Delta G^{\#}$	Free Gibbs energy (transition state)
ΔG°	Free Gibbs energy (activation energy)
f	Functionality

q	Cross-linking density
M_c	Molecular mass in between cross-links
NRU	Number of repeating units
M_{RU}	Molecular mass of the repeating unit

Index of Abbreviations

3D	Three-dimensional
4D	Four-dimensional
AA	Acetic acid
AcAc	Acetoacetate
AcAm	Acetoacetamide
Al_2O_3	Alumina oxide
APTMS	Aminopropyltrimethoxysilane
ATR-FT-IR	Attenuated total reflection-fourier transform-infrared
BADGE	Bisphenol-A diglycidylether
BAP	N,N Bis(3-aminopropylpiperazin)
BPA	Bisphenol-A
BSA	Benzenesulfonic acid
BZ	1,3-Benzoldimethanol
CAN	Covalent adaptable network
CH	1,4-Cyclohexandimethanol (cis and trans)
CHDA	1,3-Bis-(aminomethyl)-cyclohexan
Chi	Chitin
Chs	Chitosan
CL	Cellulose
CLB	Cellulose nanoparticles (bacteria)
CLL	Cellulose cotton linters
CLMW	Cellulose milkweed fibers
CS	Corn starch
DAB	1,4 Diaminobutane/Putrescine
DAD	1,10-Diaminodecan
DADD	1,12-Diaminododecane
DAE	1,2-Diaminoethan

DAH	1,6-Diaminohexan
DAO	1,8-Diaminooktan
DAP	1,5-Diaminopentan/Cadaverine
DBAT	Butyleneadipate-co-terephthalate
DBN	1,5-Diazabicyclo[4.3.0]non-5-ene
DBTL	Dibutyltindilaurate
DC	4,4′-Methylen-bis-cyclohexylamin
DCH	4,4′-(Propane-2,2-diyl)dicyclohexanol (isomeric mixture)
DCM	Bis-(4-amino-3-methylcyclohexyl)-methan, stereoisomeres
DMA	Dynamic mechanical analysis
DMAP	(Dimethylamino)pyridine
DMF	Dimethylformamide
DMSO	Dimethylsulfoxide
DMTA	Temperature-dependent dynamic mechanical analysis
DOD	1,12-Dodecanediol
DP	(1R,2R)-(+)-1,2-Diphenyl-ethylendiamin
DSC	Differential scanning calorimetry
EDDET	(2,2′-(ethylenedioxy)diethanethiol
EG	Ethylene glycol
EI	Electron ionization
ESB	Energy selective backscattering
ESI	Electrospray ionization
FRU	*D*-Fructose
GL	Glycerol
GLU	*D*-Glucose
HM	1,6 Hexanediol
HT	1,2,6-Hexantriol
HTFSI	Bis(trifluoromethanesulfonyl)azanide
HUPA	11-hydroxyundecylphosphonic acid
In-lens	Immersion lens

IV

IP	Isophorone diamine
J2000	Jeffamine® D2000
J230	Jeffamine® D230
J400	Jeffamine® D400
J3000	Jeffamine® T3000
J403/JA	Jeffamine® T403
LAC	D-Lactose
m-X	*Meta*-xylylendiamine
MD	1,8-Diamino-*p*-menthan
MNR	Molecular network rearrangement
MS	Mass spectrometry
N-Me	3,3′-Diamino-N-methyldipropylamin
NDO	2,7-Napthtalenediol
NGP	Neighboring group participation
NMR	Nuclear magnetic resonance
Nu	Nucleophile
OA	Oleic acid
ODD	1,4-Bis-(3-aminopropyloxy)-butan
OE	2,2′-(Ethylendioxy)diethylamin
Oli	Oligomer
OM	Optical microscopy
p-TsOH	*para*-Toluolsulfonic acid
PA	Priamine®
PBS	Polybutylene succinate
PCAN	Permanent covalent adaptable network
PDMS	Poly(dimethylsiloxane)
PEG	Poly(ethylene glycol)
PETMP	Pentaerythritol-tetrakis-(3-mercaptopropionate)
PH	Phenol
PI	Piperazin

PLA	Poly(lactic acid)
PPG	Poly(propylene glycol)
PPh3	Triphenylphosphine
PTFE	Poly(tetrafluoroethylene)
PTHF	Poly(tetrahydrofuran)
PU	Poly(urethane)
RCAN	Reversible covalent adaptable network
RE	Resorcin
SAC	*D*-Sucrose
S_N2	Biomolecular reaction mechanism (Hughes-Ingold symbol)
SEM	Scanning electron microscopy
SFB	Collaborative research center (german research foundation)
SO	*D*-Sorbitol
TBA	*Tert*-butylacetoacetate
TEMPO	2,2,6,6-Tetramethylpiperidinyloxyl
T_g	Glass transition temperature
TGA	Thermogravimetric analysis
THPE	1,1,1-Tris-(4-hydroxyphenyl)-ethan
TMDO	2,2,6-trimethyl-1,3-dioxin-4-one
TREN	Tris(2-aminoethyl)amine
TS	Transition state
TUHH	Technical University of Hamburg
T_v	Topology freezing temperature
TCA	Trichloracetic acid
UV	Ultraviolet
VUC	Vinylogous urethane composite
VUCH	Vinylogous urethane hierarchical composite
V-UREA	Vinylogous urea
Vipoxy	Vitrimer-epoxy
VU	Vinylogous urethane

VI

WLF   Williams Landel Ferry

XRD   X-Ray Diffraction

Abbreviations of the acetoacetate monomers and vitrimers:

Acetoacetate monomers are abbreviated according to the corresponding abbreviation of the alcohol with the addition of AcAc (*e.g.,* acetoacetylated ethylene glycol = EG_{AcAc}).

Vitrimers are usually abbreviated according to the used acetoacetylated alcohol or epoxide, the used amine and the *R*-value (acetoacetate/epoxide$_{Amine, \; R\text{-value}}$, *e.g.* $EG_{J403, \; 0.75}$).

1   Abstract

For almost 100 years, plastics have gained an increasingly important role in industrial applications and in private households. Within the last decade, more and more conventional materials have been replaced by different types of plastics. The durability and versatility of established plastics is both their advantage and disadvantage. On the one hand, they can be used for long-term applications and behave very durable, but on the other hand, they get into the environment and cause heavy, long-lasting pollution due to their fragmentation to microplastics and/or release of toxic compounds. Thermosets represent a group of high-performance plastics, which represent cross-linked and non-recyclable polymers that have been disposed of thermally so far. A solution to this problem is the implementation of dynamic, covalent bonds, which enable reprocessing through a thermally-induced exchange reaction of the cross-linking points. These dynamically cross-linked polymers are called permanent covalent adaptable networks or vitrimers and enable applications such as malleability, weldability, or grinding and compression molding.   In the last decades, research and development have been increasingly working on solutions to these problems. Solutions include the improvement of recyclability, using renewable raw materials or biodegradable materials as feedstocks. The main part of this work represents the synthesis and characterization of vinylogous urethane vitrimers polymerized by the condensation reaction of acetoacetates and primary amines. Within three publications and unpublished results, numerous different vitrimers were investigated to understand the influence of various synthetic parameters on the cross-linking chemistry, the mechanical properties, and in particular the reprocessability of the vitrimers. The studies were carried out to further understand and improve the vitrimers properties and customize them for certain processing methods and composite materials within the scope of the collaborative research center SFB986 - area A. Area A is inspired by nacre-like, natural materials and aims to synthesize thermoreversible, hierarchical composite materials based on inorganic-organic composites with high loads of inorganic particles and outstanding mechanical properties. This work was integrated into subproject A2 and was in charge of the development of the organic phase, which includes the synthesis of suitable thermoreversible polymers and ligands. Factors such as the stereoisomerism of the vinylogous urethane bond in different solvents, the use of

different acetoacetate to amine ratios, catalysts, different monomers with respect to the backbone and the nucleophilicity of the amine, cross-linking densities and additional heteroatoms in the network were explored. Through in-depth characterization of these networks, crucial trends and correlations were identified, which influence the thermomechanical properties. In particular, heteroatoms in the monomer backbone, a high excess of amines, highly nucleophilic amines, a high concentration of functional groups, low crosslinking densities, the use of long-chained monomers and the use of catalysts were identified as accelerating factors for the transamination reaction. The choice of solvents and raw materials was led by a strong focus on utilizing bio-based and non-toxic substances to improve the established reactions and reduce the carbon footprint. The knowledge gained was used in the preparation of composite materials, some of them were synthesized in the scope of this work and some were developed in cooperation projects.

Within the framework of the SFB 986 - area A, thermoreversible composite materials were developed, which improve the mechanical properties of the pure polymers and enable the incorporation of functional components such as magnetic nanoparticles, supramolecular natural granules or anisotropic inorganic platelets. As a part of this, biodegradable polymer-polymer composites of starch, nacreous inorganic-organic composites of aluminina oxide, and magnetic inorganic-organic nanocomposites of iron-oxide particles were prepared and analyzed. Moreover, a phosphonic acid ligand bearing an acetoacetate group was developed and used to bind the interface of iron-oxide nanoparticles to the vitrimers. It was found that the mechanical properties of the composites, *e.g.* the elastic moduli and tensile strengths greatly increased while maintaining the characteristic reprocessability of the vitrimers. Furthermore, it was shown that the particles could be aligned within the material by heat compression, enabling a solid-state postmodification within the anisotropic material. Magnetic, elastomeric or thermosetting composites, on the other hand, offer potential opportunities in the fields of high-performance materials, sensoric or robotic technologies. Furthermore, a first hierarchical vitrimer composite was successfully synthesized by using iron-oxide nanoparticle clusters. This work offers an in-depth understanding of the crucial factors in the recyclability of vinylogous urethane vitrimers and the incorporation of particles to prepare composite materials. Moreover, the results offer future potential for the

development of smart and high performance, yet reprocessable materials for other applications.

2   Zusammenfassung

Seit fast 100 Jahren spielen Kunststoffe eine immer wichtigere Rolle in industriellen Anwendungen und in privaten Haushalten. In den letzten zehn Jahren wurden immer mehr herkömmliche Materialien durch verschiedene Arten von Kunststoffen ersetzt. Die Langlebigkeit und Vielseitigkeit etablierter Kunststoffe ist sowohl ihr Vorteil als auch ihr Nachteil. Einerseits können sie für langfristige Anwendungen eingesetzt werden und verhalten sich sehr langlebig, andererseits gelangen sie in die Umwelt und verursachen durch ihre Fragmentierung in Mikroplastik und/oder die Freisetzung giftiger Substanzen eine starke, lang-anhaltende Verschmutzung. Duroplasten stellen eine Gruppe von Hochleistungskunststoffen dar, bei denen es sich um vernetzte und nicht recycelbare Polymere handelt, die bisher thermisch entsorgt wurden. Eine Lösung für dieses Problem ist die Implementierung dynamischer, kovalenter Bindungen, die durch eine thermisch induzierte Austauschreaktion der Vernetzungspunkte eine Reprozessierung ermöglichen. Diese dynamisch vernetzten Polymere werden als permanente kovalente anpassungsfähige Netzwerke oder Vitrimere bezeichnet und ermöglichen Anwendungen wie Verformbarkeit, Schweißbarkeit oder Schleif- und Formpressen.   In den letzten Jahrzehnten haben Forschung und Entwicklung verstärkt an Lösungen für diese Probleme gearbeitet. Zu den Lösungen gehören die Verbesserung der Recyclingfähigkeit, die Verwendung erneuerbarer Rohstoffe oder biologisch abbaubarer Materialien als Ausgangsmaterial. Der Hauptteil dieser Arbeit befasst sich mit der Synthese und Charakterisierung von vinylogen Urethan-Vitrimeren, die durch die Kondensationsreaktion von Acetoacetaten und primären Aminen polymerisiert werden. Im Rahmen von drei Veröffentlichungen und unveröffentlichten Ergebnissen wurden zahlreiche verschiedene Vitrimere untersucht, um verschiedene Auswirkungen auf die mechanischen Eigenschaften und insbesondere die Wiederverarbeitbarkeit der Vitrimere zu beleuchten. Die Untersuchungen wurden im Rahmen des Sonderforschungsbereichs SFB986 - Bereich A durchgeführt, um die Eigenschaften der Vitrimere weiter zu verstehen und zu verbessern und sie für bestimmte Verarbeitungsverfahren und Verbundwerkstoffe anzupassen. Bereich A wurde inspiriert von perlmuttartigen, natürlichen Materialien und zielt auf die Synthese von thermoreversiblen, hierarchischen Verbundwerkstoffen auf der Basis anorganisch-organischer Komposite mit hohem Anteil

anorganischer Partikel und hervorragenden mechanischen Eigenschaften ab. Diese Arbeit wurde in das Teilprojekt A2 integriert und war für die Entwicklung der organischen Phase verantwortlich, welche die Synthese geeigneter thermoreversibler Polymere und Liganden umfasst. Dabei wurden Faktoren wie die Stereoisomerie der vinylogen Urethanbindung in verschiedenen Lösungsmitteln, die Verwendung verschiedener Acetoacetat-Amin-Verhältnisse, Katalysatoren, verschiedene Monomere in Bezug auf das Rückgrat und die Nukleophilie des Amins, Vernetzungsdichten und zusätzliche Heteroatome im Netzwerk untersucht. Durch eine eingehende Charakterisierung dieser Netzwerke wurden entscheidende Trends und Korrelationen identifiziert, die die thermomechanischen Eigenschaften beeinflussen. Insbesondere Heteroatome im Monomer-Rückgrat, ein hoher Überschuss an Aminen, stark nukleophile Amine, eine hohe Konzentration an funktionellen Gruppen, niedrige Vernetzungsdichten, die Verwendung langkettiger Monomere und der Einsatz von Katalysatoren wurden als entscheidende Faktoren für die Austauschreaktion, bei welcher es sich im die Transaminationsreaktion handelt, identifiziert. Bei der Wahl der Lösungsmittel und Rohstoffe wurde ein starker Fokus auf die Verwendung biobasierter und ungiftiger Lösungsmittel gelegt, um die etablierten Reaktionen zu verbessern und den Kohlenstoff-Fußabdruck zu reduzieren. Die gewonnenen Erkenntnisse wurden für die Herstellung von Verbundwerkstoffen genutzt, die zum Teil im Rahmen dieser Arbeit synthetisiert und zum Teil in Kooperationsprojekten entwickelt wurden. Im Rahmen des SFB 986 - Bereich A wurden thermoreversible Kompositmaterialien entwickelt, die die mechanischen Eigenschaften der reinen Polymere verbessern und den Einbau von funktionellen Komponenten wie magnetischen Nanopartikeln, supramolekularen natürlichen Granulaten oder anisotropen anorganischen Plättchen ermöglichen. In diesem Zusammenhang wurden biologisch abbaubare Polymer-Polymer-Komposite aus Stärke, perlmuttartige anorganisch-organische Komposite aus Aluminiumoxid und magnetische anorganisch-organische Nanokomposite aus Eisenoxidpartikeln hergestellt und analysiert. Darüber hinaus wurde ein Phosphonsäure-Ligand mit einer Acetoacetat-Gruppe entwickelt und verwendet, um die Oberfäche von Eisenoxid-Nanopartikeln an die Vitrimere zu binden. Es wurde festgestellt, dass die mechanischen Eigenschaften der Verbundwerkstoffe, z. B. die Elastizitätsmodule und die Zugfestigkeit, stark zunahmen, während die charakteristische Reprozessierbarkeit der Vitrimere erhalten blieb. Darüber hinaus konnte gezeigt werden, dass die Partikel durch Heizpressen im Material

ausgerichtet werden können, was eine Postmodifikation im festen Zustand des anisotropen Materials ermöglicht. Magnetische, elastomere oder duroplastische Verbundwerkstoffe bieten dagegen potenzielle Möglichkeiten im Bereich der Hochleistungsmaterialien-, Sensorik- oder Robotertechnologien. Darüber hinaus wurde mit Hilfe von Eisenoxid-Nanopartikeln ein erster hierarchischer Vitrimer-Verbundwerkstoff erfolgreich synthetisiert. Diese Arbeit bietet ein tiefgreifendes Verständnis der entscheidenden Faktoren für die Recyclingfähigkeit von vinylogen Urethan-Vitrimeren und die Einbindung von Partikeln zur Herstellung von Verbundwerkstoffen. Darüber hinaus bieten die Ergebnisse zukünftiges Potenzial für die Entwicklung intelligenter und hochleistungsfähiger, aber dennoch wiederverwertbarer Materialien, die auch für andere Anwendungen weiter erforscht werden können.

3   Introduction

Synthetic polymers are an indispensable part of modern life and are used as materials for numerous applications in industry or for end consumer products. To name just a few major areas, polymers are used in construction, transport, communication, household items, packaging, and many, many more. The dominant use of synthetic polymeric materials started with the first fully synthetic produced polymer bakelite, which was invented by Leo Baekeland in 1907 and coined "plastic" for synthetic polymers.[1] The plastics industry started to grow rapidly in the 1950s with the availability of cheap and readily available petroleum as a raw material for polymer synthesis.[2, 3] The cheap availability and widely adaptable properties for different applications quickly displaced established materials and products made from ceramics, metals, or natural products like wood.[4] Nowadays, around 380 million tons of plastics per year are consumed worldwide with a rising perspective. Since 1950, the average annual growth rate between 1950–2017 has been 8.4%.[5] Moreover, it is estimated that 8300 million metric tons of virgin plastic have been produced to date, which of approximately 6500 metric tons have been end up as plastic waste (2015). Roughly 9% of the plastic waste had been recycled, 12% was incinerated, and 79% was accumulated in landfills or the natural environment. For 2050 it is estimated, that around 12.000 million metric tons of plastic will have been end up in landfills or in the natural environment.[5]

Because of the exploitation of fossil resources, the dramatic pollution of the environment, and health risks for humans, the massive production of plastics poses a growing problem for humanity. For this reason, a great focus of research and development in academia and industry is nowadays on developing novel recycling and production methods, easily reprocessable polymers, and adapting raw material sources to renewable resources. Especially, bio-based polymers have been greatly focused in scientific research in the last decade, with thousands of new publications each year.[6]

3.1   Polymer Classification and Thermoreversible Polymers

Polymers are classified according to their processing and material properties and are typically divided into thermoplastics and thermosets.[7] Thermoplastics such as polyethylene, polypropylene, poly(ethylene terephthalate), polystyrene, and many more are materials that consist of long, linear or slightly branched polymer chains. Thermoplastics are held together by non-covalent, intermolecular forces between the polymer chains, which are overcome at higher temperatures. Therefore, thermoplastics show a glass transition or melting point above which the polymers behave like a viscoelastic fluid. This behavior makes them eminently processable and usable in several mass-produced products.[8] However, strong mechanical properties, thermal and chemical resistance are decisive factors for many applications and limit the field of application for thermoplastics.

Thermosets, such as epoxy resins, cross-linked polyesters and polyurethanes, consist of covalently bonded, interlinked chains that build a three-dimensional polymer network. As a result, thermosets show excellent mechanical and chemical properties in terms of stiffness, dimensional stability, creep- and chemical resistance as well as good mechanical properties. However, after the network formation, they can no longer be remolded or reprocessed, which makes, once the polymerization is complete, recycling very difficult.[9, 10]

In the past, the established polymer materials were designed to be chemically inert and exhibit a solid molecular composition. The chemical reactivity of these polymers was often considered disturbing, and therefore, attempts were made to control it by the molecular compositions or by adding stabilizers. Due to the growing interest in dynamic polymer systems, this attitude has changed in recent decades. Properties such as self-healing, shape memory, reprocessability, stimulability, and adaptability offer a variety of new applications.[11] (Thermo)reversible polymers contain different non-covalent or covalent cross-linking points, which enable a dynamic behavior of the polymers when a specific stimulus is applied. Supramolecular polymers are defined as "polymeric assemblies of monomeric units held together by highly directional and reversible non-covalent interactions, resulting in polymer-like properties in bulk as well as in solution".[12] In general, supramolecular polymers consist of covalently linked units of arbitrary length, which in turn are linked together by weaker, non-covalent bonds. Examples of these non-

covalent interactions are hydrogen bonds, coordination to metal atoms, or π-π interactions of aromatics exemplified shown in **Figure 1**.[12-18] In contrast, covalent adaptable networks (CANs) represent other types of thermoreversible polymers. The cross-links are of covalent nature but remain reactive when heat or another stimulus is applied. Reversible covalent adaptable networks (RCANs) undergo depolymerization by a dissociative mechanism at elevated temperatures (*e.g.* Diels-Alder reaction). Permanent covalent adaptable networks (PCANs) undergo associative exchange reactions, which enable a reorganization of the cross-linking points at elevated temperatures (*e.g.* transamination of vinylogous urethanes). The number of cross-linking points always remains constant during the exchange reaction, leading to a constant stiffness and dimensional stability of the material at high temperatures. PCANs are also titled as vitrimers, according to their inventor Ludwik Leibler.[19] This work includes new investigations about vitrimers. The introductions to CANs, especially PCANs, are described in detail in the following chapters.
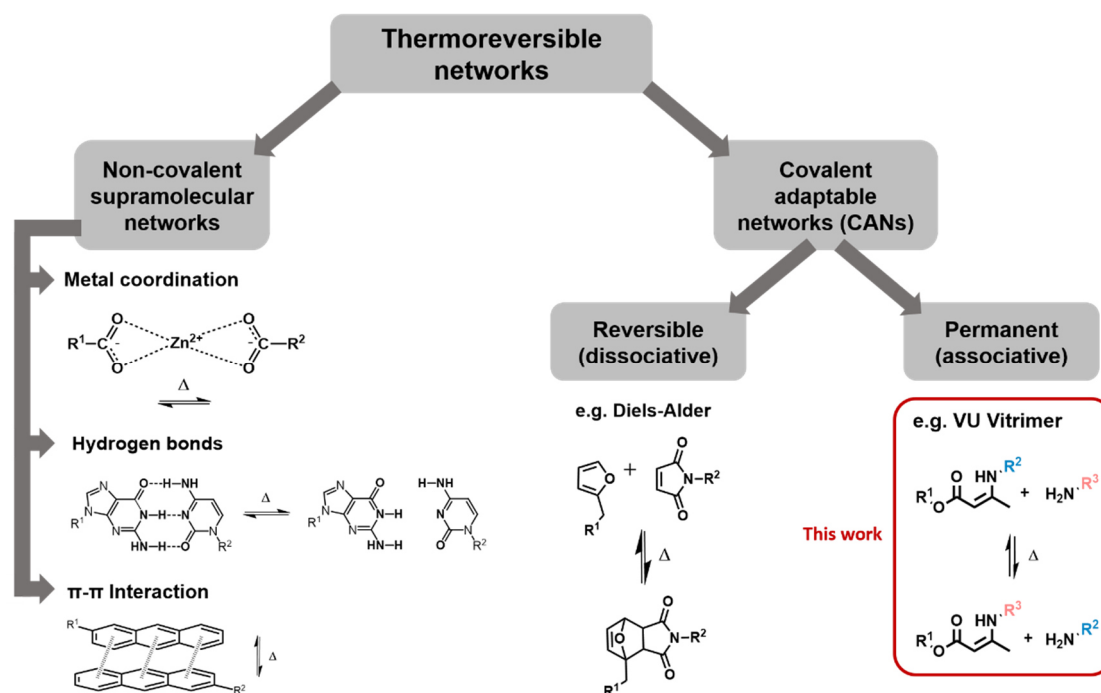
Figure 1: Illustration of thermoreversible polymer networks based on non-covalent interactions, *e.g.,* hydrogen bonds, π-π interactions, or metal-ionic interactions. Reversible (RCANs) and permanent covalent adaptable networks (PCANs) based on dissociative or associative exchange mechanisms, *e.g.,* Diels-Alder reaction or the transamination of vinylogous urethane vitrimers. This work includes results about PCANs (Vitrimers).

3.1.1 Macroscopic Properties of Vitrimers

The benefit of vitrimers is the combination of the desired properties of classic thermosets and thermoplastics in terms of their mechanical strength, chemical resistance, creep resistance and thermomechanical stability while remaining reprocessable and weldable (**Figure 2**).
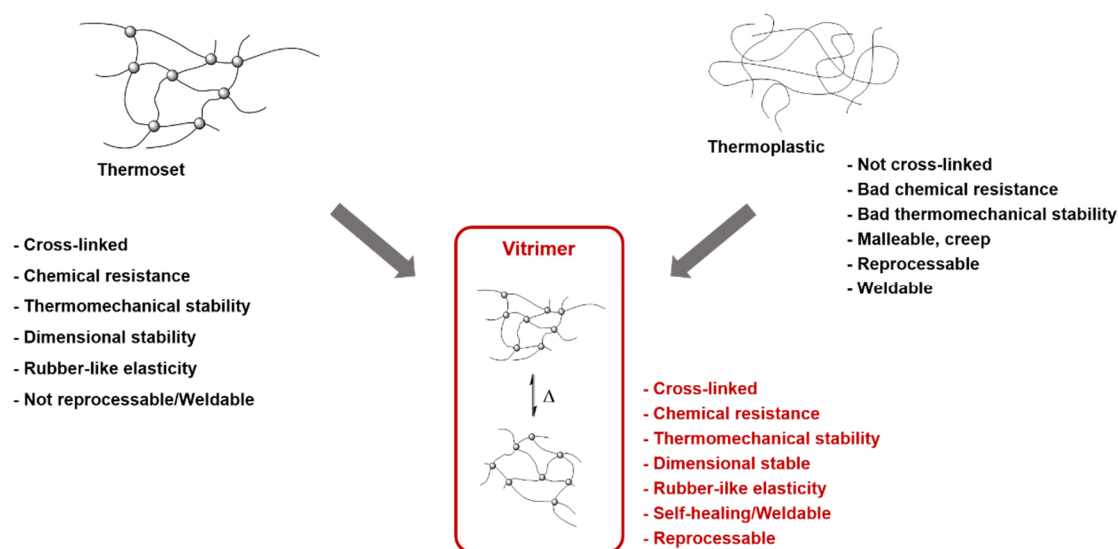

Figure 2: Illustration of the network structure and the characteristic properties of classic thermosets and thermoplastics compared to vitrimer networks.

The unique properties of vitrimers lead to remarkable behavior on the macroscopic scale. Since the exchange reactions usually proceed only at elevated temperatures, the reaction is unmeasurably slow at the service temperature of many applications (< 50 °C). At this temperature, the vitrimers behave like a normal elastomer or thermoset, show creep resistance, chemical resistance, and can be used for high-performance materials, *e.g.,* composites.[20-22] Vitrimers show stimuli-responsiveness to the temperature and show viscoelastic properties, which enables various remarkable properties for distinct applications. For example, vitrimers show therm-adapt shape memory and reshaping at the same time depending on the temperature, pressure and duration of heating. When the vitrimer is heated for a short time above the glass transition temperature (T_g), set in a new shape, and cooled down again, the material shows shape-memory when heated above the T_g again. The temperature and duration of time were too short for the exchange reactions to proceed. However, when the material is heated for a more extended period of time at a temperature where the exchange reaction proceeds efficiently, new permanent shapes are

generated. In addition, self-healing of cracks and cuts is possible by the same mechanism, enabling the confluence of material.[23, 24] Furthermore, mechanical recycling can be carried out by consecutive grinding and remolding of the materials. The material is cut or ground into small fragments (*e.g.* cutting, ball milling) and heat-pressed to a dense film again, showing similar properties to the previous material.[23, 25, 26] The already used and ground vitrimers can even be mixed with other compounds, *e.g.* polymers, fillers, particles, fibers and enable not only recycling but also upcycling.[25, 27] Also chemical recycling can be carried out in several ways. For example, the vitrimer can be dissolved by adding a, for the exchange reaction suitable, monofunctional reactant to the material. Due to the proceeding exchange reactions, the cross-linking density is reduced until the fragments are soluble. By removing this monofunctional reactant, the cross-linked material can be regenerated. Another way for chemical recycling is to depolymerize the vitrimer by promoting the backward reaction using catalysts, *e.g.* Brønsted acids/bases or Lewis acids/bases. This method likewise offers the opportunity to isolate the monomers for separate re-usage in other applications.[25, 28-30] A graphical illustration of the macroscopic properties is shown in **Figure 3**.
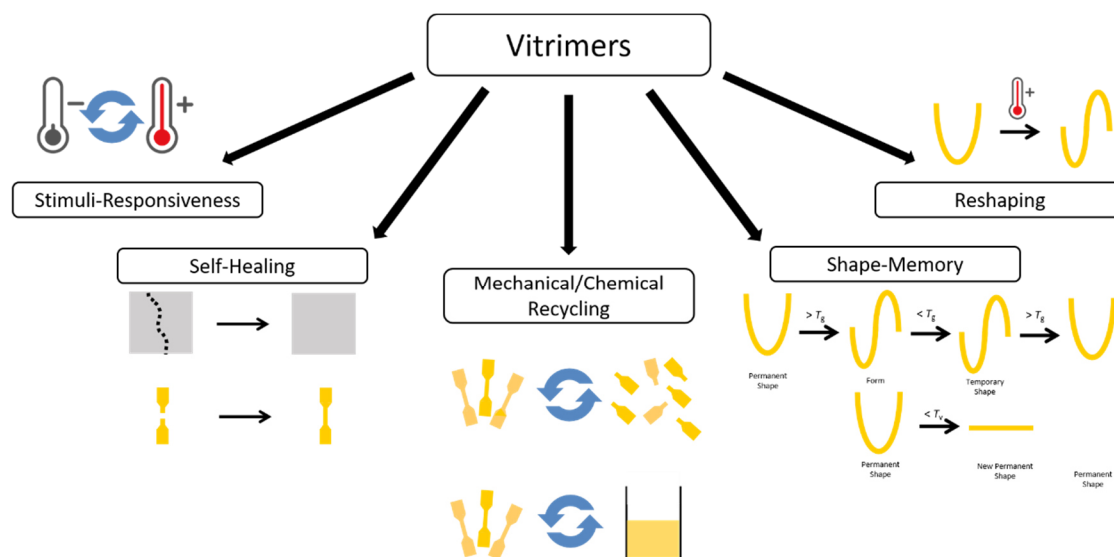
Figure 3: Macroscopic properties of vitrimers. The materials show stimuli-responsiveness, self-healing, therm-adapt shape-memory, reshaping, mechanical recycling by consecutive grinding and remolding as well as different chemical recycling routes and recovery of the monomers.

3.2   Covalent Adaptable Networks

3.2.1   Covalent Adaptable Networks – Exchange Mechanisms

CANs are classified according to their undergoing exchange mechanism. Polymers reacting by a dissociative pathway are assigned to reversible CANs (RCANs) and show depolymerization during energy supply, *e.g.* heat or light. In these networks, the cross-linking density decreases constantly when energy is applied until the polymer behaves like a viscoelastic fluid, with a mold as intermediate. In the intermediate state, the cross-links are predominantly depolymerized and the equilibrium is shifted to the monomers (*e.g.* Diels-Alder reaction). Polymers reacting by a concerted or associative mechanism are called permanent CANs or vitrimers and show no depolymerization during energy supply (*e.g.* transesterification reaction).
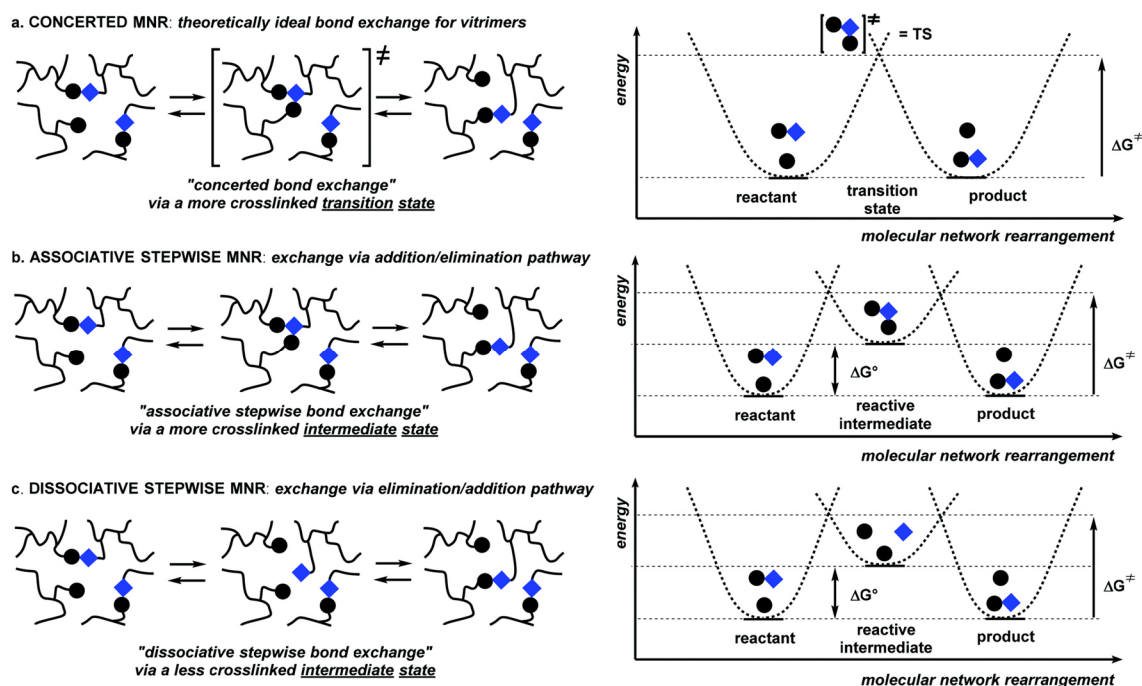
Figure 4: Scheme of the stepwise exchange pathway of CANs based on dissociative, concerted or associative mechanisms triggered by energy supply (left). Scheme of the energy course during the exchange mechanism (right). The black circles and blue squares represent different reactants of a bimolecular reaction, while a free black circle indicates a free functional group, which can initiate the exchange reaction ($\Delta G°$ = activation energy, $\Delta G^{\#}$ = free enthalpy to transition state, TS = transition state). Reproduced from Ref. Polym. Chem., 2019, 10, 6091-6108 (DOI: 10.1039/C9PY01260E) with permission from the Royal Society of Chemistry.[11]

The number of cross-linking points always remains constant, which leads to a molecular network rearrangement (MNR) in the materials without the intermediate state of a mold. The number of cross-linking points always remains constant, making these networks permanent as well as dynamic. **Figure 4** shows the exchange mechanism and energy schemes of the different mechanisms.

3.2.2 Reversible Covalent Adaptable Networks

Reversible CANs are already known for a long time. In principle, all bimolecular addition reactions are reversible and are determined by the temperature dependence of the equilibrium constant. However, in reality, most of the reactions are essentially irreversible because of a limiting temperature range, side reactions or the degradation temperature. Moreover, the time scale of the forward and reverse reaction has to be in a suitable range so that the network can adapt to a stimulus and rearrange. For this reason, both the thermodynamics and kinetics of a thermoreversible reaction must be considered, including the application and time scale.[31, 32] In **Figure 5**, several thermoreversible cross-linking reactions are shown, which work at practical rates and temperatures without any catalyst. Well-known examples are the addition reactions of isocyanate and imidazole[33], the carbene dimerization[34], the reversible radical coupling between TEMPO and a styryl radical[35] and the Diels-Alder cycloaddition between furan and maleimide.[36] In addition, also light can serve as an energy supplier for cyclization reactions. Coumarines[37], cinnamates[38], anthracenes[39] and thymines[40] have been investigated for RCANs by photodimerization. Photodimerizations typically proceed by a [2+2] cycloaddition (except [4+4] for anthracenes), while near ultraviolet light effects the forward and shorter wavelengths the backward reaction. Consequently, the RCANs cross-linking density is controlled by light (Figure 5e).[31] Recently, also RCANs received a great deal of renewed attention, because of the emerging research field of permanent covalent adaptable network (vitrimers), which are described in the next chapter.[11]
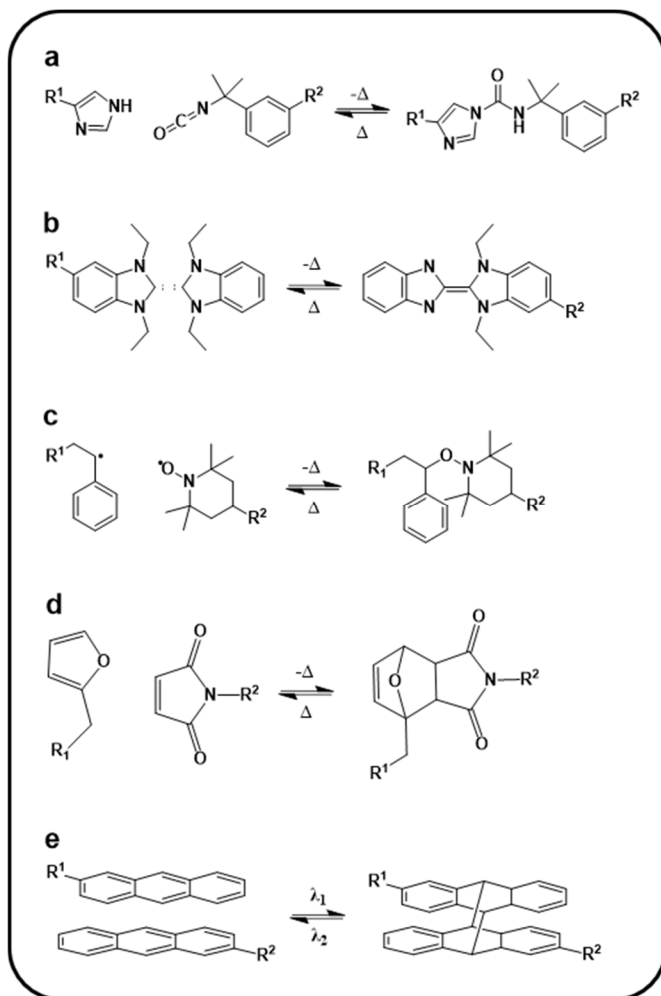
Figure 5: Scheme of thermoreversible cross-linking addition reactions. (a) Nucleophilic addition between isocyanate and imidazole, (b) carbene dimerization, (c) reversible radical coupling between TEMPO and a styryl radical, and (d) the Diels-Alder cycloaddition between furan and maleimide. (e) Exemplary scheme of the [4+4] cycloaddition of anthracenes.[31]

3.2.2.1 Small Molecule Mediated Dissociative Stepwise MNR

Another pathway for dissociative stepwise MNR proceeds by mediating a reactive small molecule, acting as a rearrangement catalyst. In this pathway, polymer chains are reversibly linked through a condensation reaction, releasing a small molecule under certain conditions and linking these polymer chains. In most cases, water acts as this small molecule, undergoing hydrolysis reactions as backward reactions. Nevertheless, also other groups *e.g.,* halogenides can act as a mediator. A scheme of the exchange reaction and the energetic course *via* the intermediate state is shown in **Figure 6**.
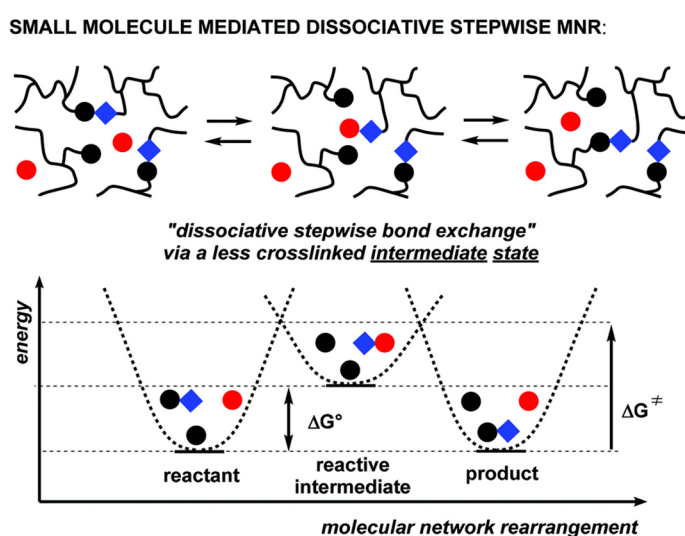
Figure 6: Energy scheme and graphical illustration of the exchange pathway via small molecule mediated dissociative stepwise MNR ($\Delta G°$ = activation energy, $\Delta G^{\#}$ = free enthalpy to transition state). Reproduced from Ref. Polym. Chem., 2019, 10, 6091-6108 (DOI: 10.1039/C9PY01260E) with permission from the Royal Society of Chemistry.[11]

Examples of this exchange mechanism are the water-mediated polyimine and poly(acyl) hydrazone-based network exchange (**Figure 7a**) [41], the implementation of transalkylation reactions of quarternary amines *via* temporary de-cross-linking by bromide ions as good nucleophiles (Figure 7b) [42, 43] and the water-mediated boronic ester exchange (Figure 7c).[11, 44]
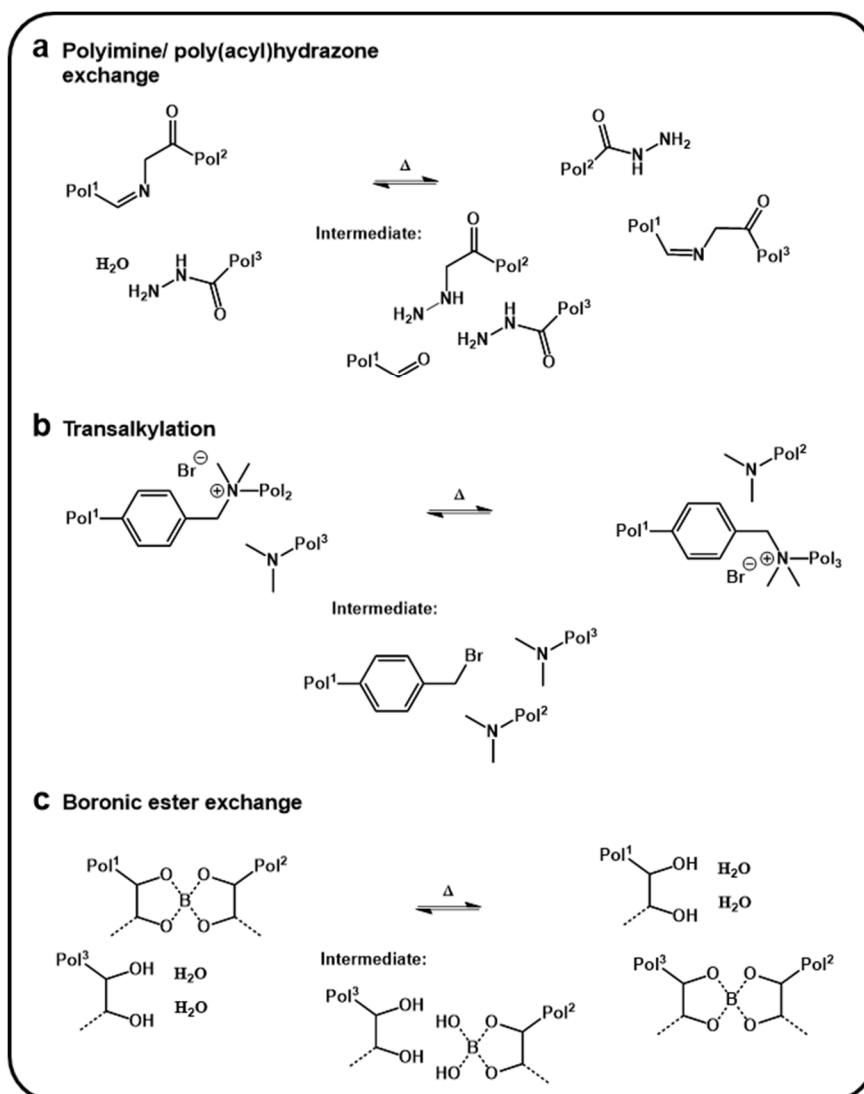
Figure 7: Examples of different polymers which exchange reactions proceeds by a small molecule mediated dissociative stepwise MNR (Pol = Polymer). (a) The water mediated boronic ester exchange, (b) polyimine and poly(acyl)hydrazone-based network exchanges and (c) the implementation of transalkylation reactions of quarternary amines, *via* temporary de-cross-linking by adventitious bromide ions as good nucleophiles.

3.2.3 Permanent Covalent Adaptable Networks – Vitrimers

Vitrimers belong to CANs and are classified into the subclass of permanent CANs. In contrast to reversible CANs, the exchange mechanism proceeds *via* an associative or concerted exchange mechanism, resulting in a permanent cross-linked network with the cross-linking density always remaining constant. When heated, vitrimers behave like viscoelastic fluids, while maintaining a chemically inert network even when swelling in

good solvents. No depolymerization takes place in these networks, making them permanent as well as dynamic. Because of the unique properties this class of polymers is often said to be the third category of polymers, since it combines the classifying properties of thermosets and thermoplastics.

Vitrimers were first introduced by Ludwik Leibler and co-workers in 2011.[19] In their work zinc acetate was used as a suitable transesterification catalyst and added to a polyester network based on diglycidyl ether of bisphenol-A and a mixture of fatty dicarboxylic and tricarboxylic acids (**Figure 8a**). The thermally activated transesterification reactions based on an associative exchange mechanism resulted in permanent polyester/polyol networks that showed an astonishing viscosity decrease upon heating, while maintaining a cross-linked polymer network (Figure 8b). The exchange pathway is graphically shown in Figure 8c. To date, this behavior was only observed for vitreous silica, but never for organic polymers. Hence, the name vitrimer was introduced for this novel class of polymers.[19, 45]
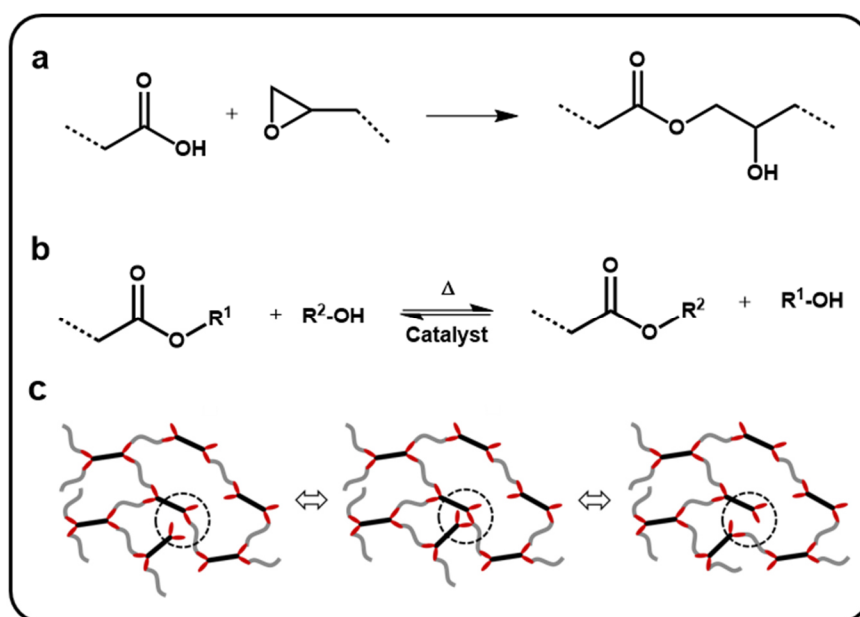
Figure 8: (a) Reaction scheme of the reaction of a carboxylic acid and an epoxide, leading to the formation of a polyol/polyester network. **(b)** Thermally-activated, catalytic transesterification reaction as associative exchange pathway for vitrimers (Pol = Polymer). **(c)** Graphic of the cross-linked network, which undergoes associative exchange mechanism.

3.2.3.1 Transition Temperatures and Viscoelastic Behavior

Vitrimers show two characteristic transition temperatures. The glass transition temperature (T_g) and the freezing transition temperature (T_v). T_v is conventionally chosen as the temperature were the material reaches a viscosity of 10^{12} Pa s^{-1} and determines the transition from the liquid to the glassy state.[46, 47] The viscosity change in the glass transition area gives information about the broadness of the glass transition.[47] Silica and other inorganic compounds show a broad, Arrhenius-like behavior in the transition zone and are titled as strong glass formers. However, organic liquids or polymers show a more rapid increase of viscosity when cooled down, not following an Arrhenius-like behavior. These organic compounds are titled as fragile glass formers. In contrast, vitrimers show a broad, Arrhenius-like behavior and can be assigned to the strong glass formers (*e.g.* silica), which was never observed for polymers before. Since the activation energies for the monomer friction and exchange reactions are different, the topology freezing transition temperature can also occur above the glass transition temperature. The stress-relaxation times and viscosity follow an Arrhenius law, while the vitrimers represent covalently bonded, cross-linked polymer networks with silica like behavior.
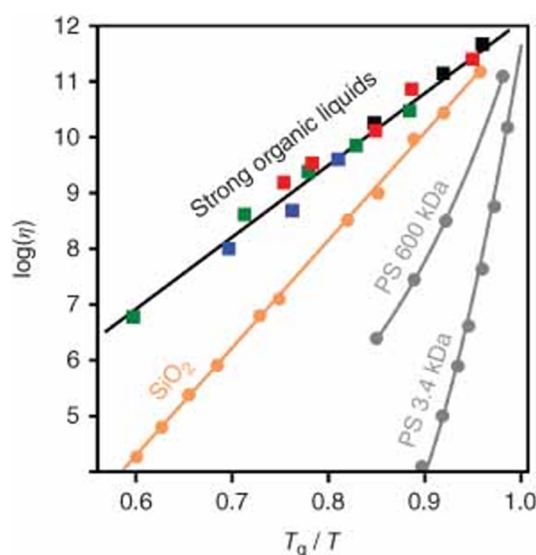
Figure 9: Angell fragility plot, showing viscosity as a function of inverse temperature normalized to 1 at the glass transition temperature (T_g) for different epoxy vitrimers as example for strong organic liquids. Moreover, a comparison for silica and polystyrene is shown. Reproduced from Vitrimer Chemistry and Applications, Macromolecular Engineering: From Precise Synthesis to Macroscopic Materials and Applications, 2022, 1-38 (DOI: 10.1002/9783527815562.mme0029) with permission from Wiley.[48]

Figure 9 shows an Angell fragility plot of the viscosity *versus* the inverse temperature normalized to 1 at the glass transition temperature.

Strong organic liquids, e.g. an epoxy/anhydride or epoxy/acid vitrimer systems with different amounts of $Zn(acac)_2$ as catalyst are shown.[19] For a comparison the viscoelastic behavior of classic polymers like silica[49] and polystyrene[50] are shown in the graphic.[19, 51] The T_v can also be observed experimentally by dilatometry, since a reorganising network has a higher expansion coefficient than a static network.[45] According to the polymer backbone and the used covalent dynamic bond the T_g is below or above the T_v. In case of an elastomer, the T_g is usually lower than T_v, which lead to the fact that the transition from a viscoelastic solid to a viscoelastic fluid appears slowly, while heating obove the T_v. As characteristic of vitrimers, the viscosity drop correlates with the Arrhenius law and depends on the chemical reactions in the material (**Figure 10**, elastomer). If the T_g is higher than T_v no segmental motions can occur in the frozen, glassy state of the network. Heating above the T_g, a dramatic decrease in viscosity, according to the Williams–Landel–Ferry model (WLF), is observed. At higher temperatures an Arrhenius-like behavior, determined through the chemical exchange reaction, again takes over and show the typical exponential decrease (Figure 10, thermoset).[45]
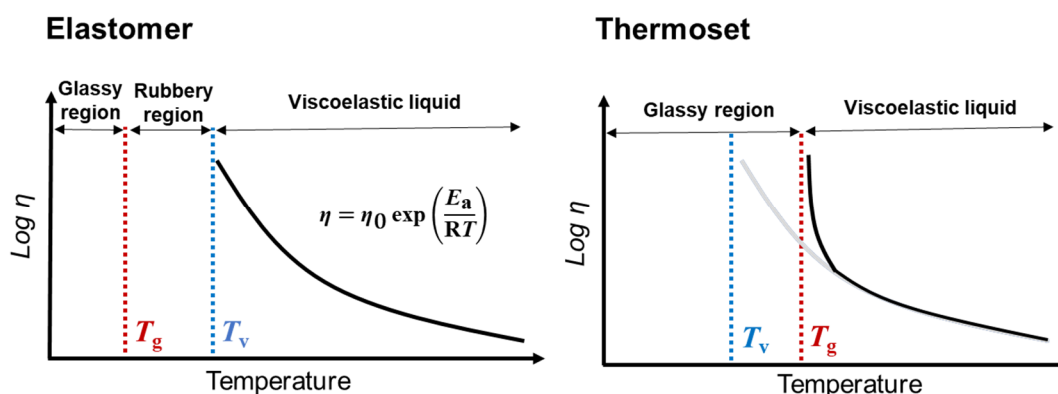
Figure 10: Illustration of the viscosity behavior of vitrimers in case the glass transition temperature (T_g) is below or above the topology freezing temperature (T_v).

Nevertheless, the theoretical concept of T_v is discussed controversially from its introduction in the early state of vitrimer research. T_v is obtained by extrapolating viscosity trends into regions where viscosity almost becomes unmeasurable within reasonable time frames. The extrapolation takes place over a large temperature range and

depends on many factors, even at low temperatures. For these reasons, a comparison between different values of T_v in different polymers is often very inaccurate and does not reflect the actual topology freezing temperature. **Figure 11a** shows a plot of $\log \eta$ against the reciprocal temperature for determining the T_v. The graphic indicates that the actual topology freezing temperature often differs significantly from the calculated extrapolation. Moreover, the T_v is only of interest for elastomers with very low T_gs and should be determined by stringent creep experiments at low temperatures and not by extrapolation at high temperatures.[20] For these reasons, the T_v is only being considered in special polymer compositions and generally less discussed in the vitrimer community nowadays.[45, 52] Figure 11b shows an exemplary creep experiment on an elastomeric vinylogous urethane vitrimer at 25 °C and 80 °C, showing constant stress and strain values at 25 °C. In contrast, at 80 °C the material started to creep and show viscoelastic properties, pointing out the running exchange reactions above the T_v.[20] Even if the T_g of this elastomer is at a low temperature of -41 °C, the exchange reaction proceeds unmeasurably slow at 25 °C, while it already occurs at 80 °C. This example impressively shows the influences of the type of the exchange reaction and the temperature on the interaction of the T_g and T_v, which can vary a lot by using different types of exchange mechanisms and/or monomer backbone (*e.g.* transamination, transesterification).
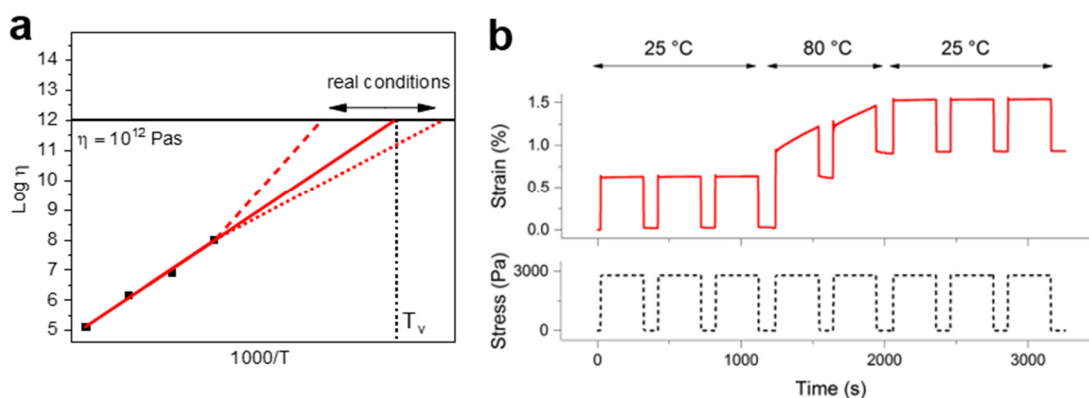
Figure 11: Angel fragility plot to calculate the topology freezing temperature, which in by convention defined as the temperature where the viscosity reaches 10^{12} Pa s^{-1}. Depending on different factors of the vitrimer composition, *e.g.* polarity, or hydrogen bonds, the real T_v is often determined at a different temperature. Adapted from Chem. Sci., 2020, 11, 4855 (DOI: 10.1039/D0SC01069C) with permission from the Royal Society of Chemistry.[52] (**b**) An exemplary creep experiment of an elastomeric vinylogous urethane vitrimer at 25 °C and 80 °C.

3.2.3.2 Viscoelastic Properties – Oscillatory Shear Experiments

Since rheology measurements belong to the standard analysis methods for polymers, the measuring principle is not described in this thesis. The following presents only a short chapter about the standard measurements to unambiguously identify vitrimer networks. The characteristic properties of vitrimers can be analysed by dynamic mechanical analysis (DMA). Since vitrimers behave like normal, permanent cross-linked thermosets, temperature-dependent oscillatory shear experiments (DMTA) show a glassy state, glass transition state and a rubbery plateau at elevated temperatures. This behavior proves the formation of a cross-linked network, which is stable over a large temperature range until the degradation temperature is reached (**Figure 12**).
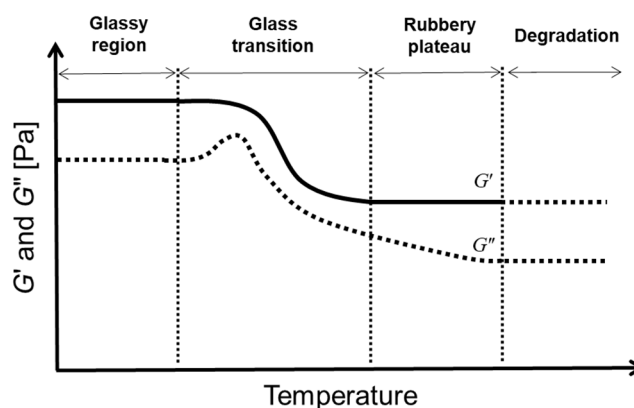
Figure 12: Temperature-dependent DMA measurement of a thermoset, showing a glassy state, glass transition state and a rubbery plateau, indicating a cross-linked network.

To explore the dynamic behavior of the cross-linked networks, stress-relaxation measurements were carried out. This static shear experiment analyses the viscoelastic properties of melts, gels or solids when a torsional deformation is applied at a specific temperature. The stress-relaxation modulus $G_{(t)}/G_{(0)}$ is recorded as a function of time. Depending on the type of material, different stress-relaxation curves are observed (**Figure 13**). Ideal elastic solids show no stress-relaxation since the tension cannot be removed due to the fixed, cross-linked network. After the deformation is applied, the stress-relaxation modulus remains constant at a higher value than before. Ideal viscous

fluids, on the other hand, immediately reduce the total tension. The curves show a sharp maximum with a quick drop to no tension. However, a partial or complete stress relaxation is observed when a torsional deformation is applied to viscoelastic materials. The decay follows an exponential function according to the Maxwell model for viscoelastic fluids. The relaxation time for the Maxwell model is the time needed for the stress to relax and reduce to 37% (1/e) of the initial value.[53] Viscoelastic liquids (*e.g.* thermoplastics) show a complete stress-relaxation when the time is sufficiently long. Viscoelastic solids (*e.g.* thermosets, elastomers, gels) show only stress-relaxation until a certain level and no full stress-relaxation due to chemical or physical bonds which cannot move freely.[54]
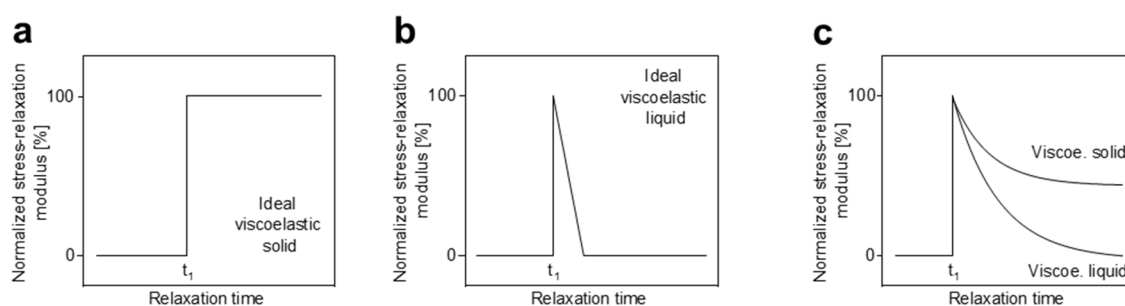
Figure 13: Stress-relaxation curves of ideal viscoelastic solids and viscoelastic liquids as well as real viscoelastic solids and liquids.

When a torsional deformation is applied to a vitrimer at a temperature where the type of exchange reactions already sufficiently proceeds, the vitrimer shows full stress-relaxation as usually observed for viscoelastic liquids. This is because the thermal exchange reactions in the network reorganize the cross-linking points and, therefore, can remove the full tension in the material. Since the stress-relaxation time directly depends on the chemical exchange reactions in the material, an Arrhenius-like behavior can be observed when measuring at different temperatures. By measuring the stress-relaxation at different temperatures and plotting the stress relaxation times τ (37%, determined by 1/e, e = Euler's number) against the reciprocal temperature, the activation energies can be calculated from the slope of the linear fit (**Figure 14**).[55, 56]
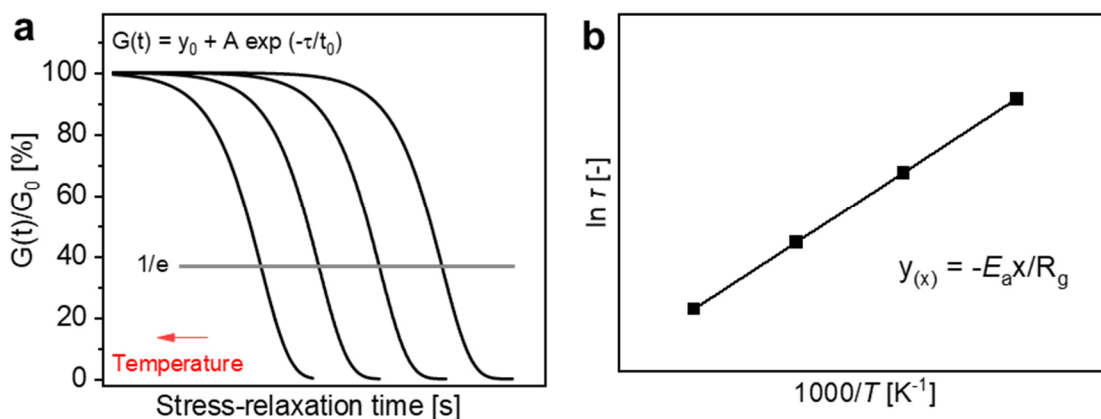
Figure 14: (**a**) Normalized stress-relaxation measurements at different temperatures. (**b**) Plot of the stress-relaxation time against the reciprocal temperature. The activation energies (E_a) can be calculated from the slope of the linear fit using the universal gas constant (R_g).

3.2.3.3 Types of Dynamic Covalent Bonds for Vitrimers

From a historical point of view, associative exchange mechanisms in polymers are not new and were already discussed in the early days of polymer science. Classic polysulfide rubbers contain S-S linkages and even if the exact mechanism of vulcanization processes in rubbers is not entirely understood nowadays, it was clear early on, that it proceeds *via* an associative pathway and does not involve disulfide bond cleavage (**Figure 15a**). However, polysulfide rubbers also contain other linkages, *e.g.* thioetherbonds, which are of permanent nature and can hinder a total relaxation and reorganization of the networks.[57] In 1954 Osthoff *et al.* reported about polydimethylsiloxane (PDMS) elastomers,[58] which were contemporaneously studied by Tobolsky *et al.* in 1966.[59-61] In retroperspective, the well-established alkoxide-mediated addition-elimination that can happen at PDMS chain ends shows stress relaxation and represents an overlooked and forgotten class of dynamic materials (Figure 15b). Nowadays, the transesterification in siloxanes is an established exchange pathway for vitrimers. Nevertheless, unfavorable reactions like backbiting or depolymerization by ring opening polymerization interfered with the available associative mechanism and made them appear less clear and attractive at that time. This leads to the conclusion that associative networks were already known in principle for a long time, but the molecular design was not yet matured, and side

reactions were hindering. Moreover, at that time, the focus in science was more on chemically inactive polymers because further reactions were considered disturbing.[11]
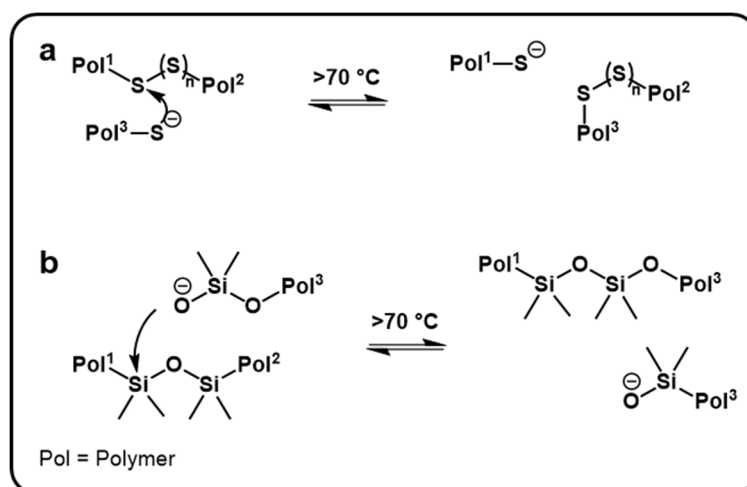

Figure 15: Reaction schemes of the early associative exchange mechanism observed in (**a**) vulcanized rubbers or (**b**) PDMS polymers.

However, since the research field of vitrimers is growing rapidly, various dynamic covalent exchange mechanisms, *e.g.* transesterification, transcarbonation, transalkylation, transcarbamoylation, boronic ester exchange, thiol–disulfide exchange, thiol-thioester exchange, trans-N-alkylation, transamination, transimination and more reactions have been investigated and applied with innumerable molecules, oligomers or modified polymers. The exchange mechanism and transition states of exemplary associative vitrimer exchange reactions are shown in **Figure 16**.[11, 45, 48, 52]
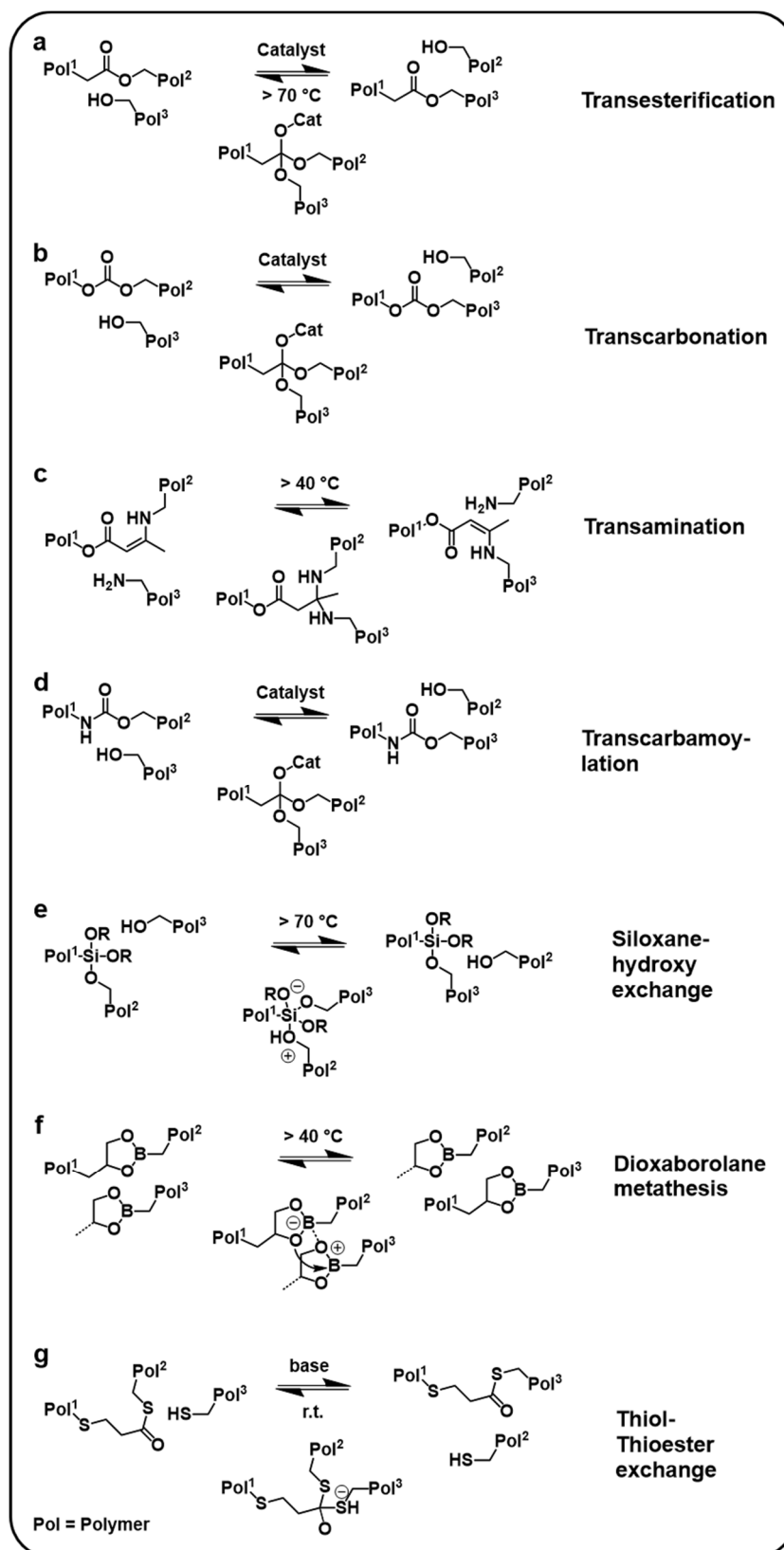
Figure 16: Reaction schemes of associative exchange mechanism for vitrimers. (**a**) Transesterification, (**b**) transcarbonation, (**c**) transamination, (**d**) transcarbamoylation, (**e**) siloxane-hydroxy exchange, (**f**) dioxaborolane metathesis, (**g**) thiol-thioester exchange.

3.2.3.4 External and Internal Catalysis, Neighboring Group Participation
and Matrix Effects

For most vitrimer systems, a catalyst is required and is usually represented by an external catalyst, *e.g.* Brønstedt acid/base or a Lewis acid/base. The catalyst lowers the energy barrier for the exchange reaction, and accelerates the exchange reaction rates. Nevertheless, the amount of catalyst has to be carefully chosen because at high temperatures, a sufficient exchange rate is desired, while at low temperatures the exchange rate should be unmeasurably slow to obtain a resilient and creep resistant material. For the most utilized, ester-based vitrimers with a transesterification mechanism, catalysts like 1,5,7-Triazabicyclo[4.4.0]dec-5-en (TBD), zincacetate $(Zn(OAc)_2)$ or triphenylphosphine (PPh_3) have been chosen and compared (**Figure 17a₂**). Experiments showed, that with an increasing amount of a catalyst, the stress relaxation times shorten in a linear dependency, while the activation energies stay constant. Using different catalysts, the activation energies differ significantly, because of different energetic intermediate states. For example, the use of PPh_3 lead to much lower activation energies than $Zn(OAc)_2$ or TBD, which can be determined by the slope of the Arrhenius fit.[52, 62] In case of using protons as a catalyst, Brønsted acids with different pK_a values have been compared. Trifluoromethanesulfonic acid (Triflic, pK_a = -12), Bis(trifluoromethanesulfonyl)azanide (HTFSI, pK_a = -9.7), benzenesulfonic acid (BSA, pK_a = -7), methanesulfonic acid (MSA, pK_a = -1.9) and trichloracetic acid (TCA, pK_a = 0.8) were compared and show activation energies of 50–67 kJ mol^{-1}, with the strong acids exhibiting slightly higher activation energies than the weaker acids (Figure 17a₃). Nevertheless, the differences in the activation energies, depending on the strength of the acid, are not very pronounced, while a clear correlation of the pK_a value and the stress relaxation times was observed. A lower pK_a value leads to shorter stress-relaxation times (Figure 17a₄).[52, 63]
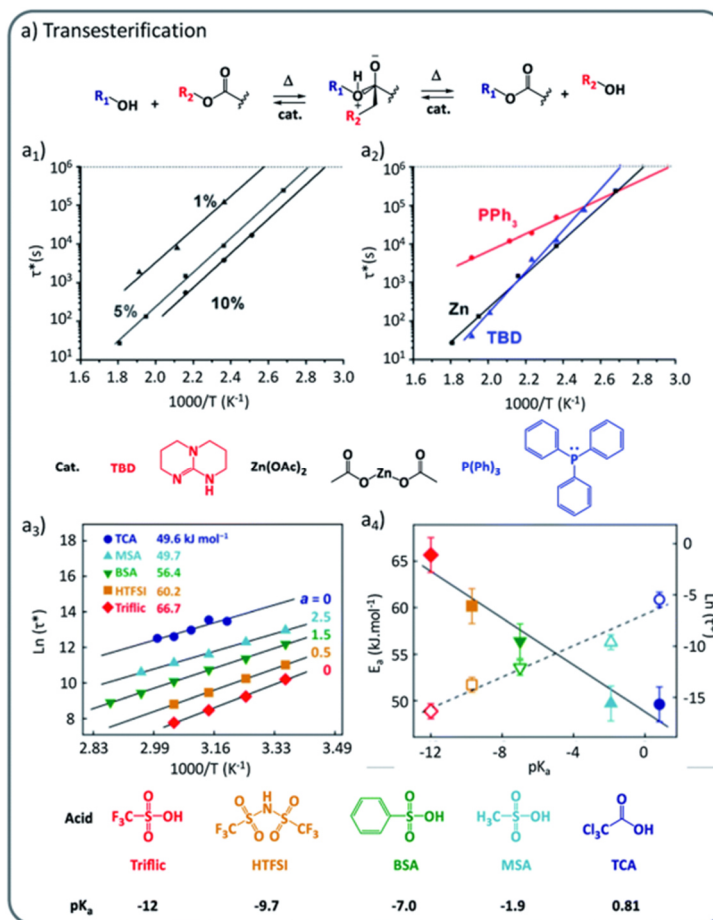
Figure 17: Effect of catalysts on the stress-relaxation times and activation energies of the transesterification reaction comparing different amounts of a catalyst and different Lewis acid/base or Brønstedt acid/base as catalysts. (a_1) Different wt% of the catalyst $Zn(OAc)_2$. (a_2) Comparison of TBD, ($Zn(OAc)_2$) or $P(Ph)_3$ as catalyst. (a_3) Comparison of the different Brønsted acids Triflic, HTFSI, BSA, MSA and TCA as catalyst. (a_4) Comparison of the activation energies of the different Brønsted acids *versus* the respective pK_a values of the acids. Reproduced from Chem. Sci., 2020, 11, 4855 (DOI: 10.1039/D0SC01069C) with permission from the Royal Society of Chemistry.[52]

However, it is quite common to use external catalysts in materials, but due to their low compatibility, stability or catalyst leaching, they might show some disadvantages. For this reason, it can be helpful if a catalytic functional group is directly introduced within the used monomers/polymers. For this reason, a possible concept is to include a Brønsted acid, *e.g.* a carboxy group bond to the monomer backbone, which can act as a internal catalyst. Another concept is to include a functional group for neighbouring group participation (NGP). The term NGP is reserved for substituent effects, in which an

accelerated exchange rate is caused by a substituent binding covalently to the reaction center, initiating an internal group transfer or cyclisation reaction. All other rate-enhancing effects should be termed internal catalysis (*e.g.* electrostatic). Examples of NGPs are citric acid-based esters with unreacted carboxyl groups close to the ester bonds[64], boronic ester exchanges with near tertiary amino moiety[65], silylether exchanges with secondary amino influence[66] or phthalate monoester with free carboxyl or sulfonic acid groups close to the ester bond (**Figure 18**).[67] Since the functional groups are located near to the exchange reaction center, they actively interact with the ground and intermediate state and can accelerate the exchange rate and/or lower the activation energy.
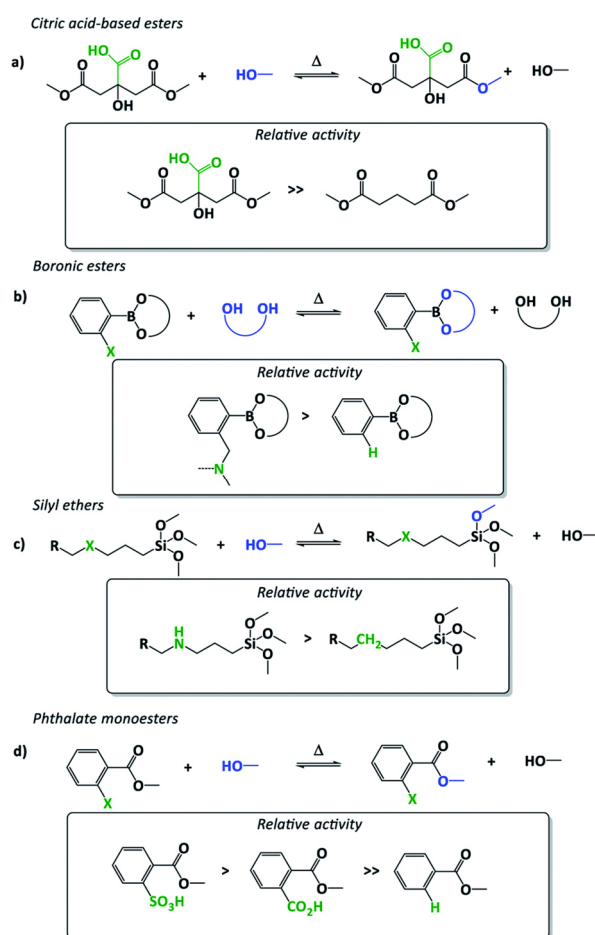
Figure 18: Examples of internal catalysis by neighboring group participation (nucleophile in blue, catalyst in green). (**a**) Citric acid-based esters with unreacted carboxyl groups close to the ester bonds, (**b**) boronic ester exchanges and amino, (**c**) silyl ether exchanges with amino influence, and (**d**) phthalate monoester with free carboxyl or sulfonic acid groups close to the ester bond. Reproduced from *Chem. Sci.*, 2020, 11, 4855 (DOI: 10.1039/D0SC01069C) with permission from the Royal Society of Chemistry.[52]

As a solvent significantly influences chemical reactions, likewise, the vitrimer matrix influences the exchange rate and activation energies. Hydrophobicity and polarity of the monomer/polymer backbone are apparent factors for the ionic exchange mechanism and can also influence the mobility of catalysts in the material. Moreover, hydrogen bonding or metal coordination influences the reorganization processes at elevated temperatures. For example, the combination of hydrogen bonds and disulfide exchanges leads to materials with a strong viscosity-temperature dependence with almost no stress-relaxation at 25 °C.[68] Dynamic covalent boronic esters and non-covalent sacrificial Zn^{2+}-O bonds lead to a dual cross-linking.[69] These additional non-covalent cross-links provide additional stability at service temperature and further improve the mechanical properties. Du Prez *et al.* presented a comparison between vinylogous urethane vitrimers synthesized by fourteen different diol-derived materials with backbones ranging from silicone (polydimethylsiloxane, PDMS), to polyethers (polytetrahydrofuran, PTHF), poly(ethylene glycol9 (PEG) and poly(propylene glycol) (PPG) as well as more hydrophobic backbone spacers (1,10-decanediol, pripol® 2033). To investigate the influence of the cross-linking density on the stress-relaxation, the focus was on two different polyethers, used with different molecular weights: PTHF (M_n: 250, 650, 1000, 2000, and 2900 g mol^{-1}) and PPG (M_n: 400, 725 and 2000 g mol^{-1}). As an amine cross-linker the trifunctional TREN was used. The materials show activation energies in the range of 68–117 kJ mol^{-1}, stress-relaxation times of 2–345 s at 140 °C and T_g of -120–31 °C. As a result, the publication stated that it is hard to spot any trends since many parameters such as polarity, solvation, cross-linking density, degree of flexibility, mass ratio and many more influence the exchange rate and activation energies.[70]

Wang *et al.* synthesized polyimine vitrimers based on modified vanillin, cured with different diamines. Activation energies of 49–81 kJ mol^{-1} were calculated for different backbones but didn't show any exact trends.[71] These results show that the matrix composition has a crucial influence on the exchange rate and activation energies, since it is affecting the flexibility, mobility, cross-linking density, stabilization of the intermediate state and activation of the ground state. Nevertheless, it has to be noted that many studies were sporadically and not systematically carried out to give exact trends. This is, because often the influence of changing a parameter cannot be considered entirely alone. For example, if the acetoacetate to amine ratio R is changed, likewise the cross-linking density, mass ratio and possibly the ratio of hydrophobic/hydrophilic backbones

is changed at the same time. For these reasons, crucial factors and dependencies need to be carefully studied in the future to fully understand and predict stress-relaxation rates and activation energies.[52]

3.2.3.5 Concerted Exchange Mechanisms

In principle, also concerted mechanisms are suitable for vitrimers and theoretically provide the best possible mechanism for fast exchange reactions. So far, only two mechanisms are known, which undergo a typical Sn2 reaction at elevated temperatures. A transalkylation chemistry in polythioether was reported, proceeding *via* a cationic ring opening polymerization of cyclic thioethers supported by sulfonium sulfonate ion pairs (**Figure 19a**).[72] And a polyionic network including N-alkylated triazolium iodide was reported using a transalkylation reaction of triazoles (Figure 19b).[73] Nevertheless, the exchange reactions in these dynamic polymer networks are still subject to investigations to gain an in-depth understanding of the undergoing processes but might be subject to finely tuned vitrimers for specific applications and efficient exchange reactions.
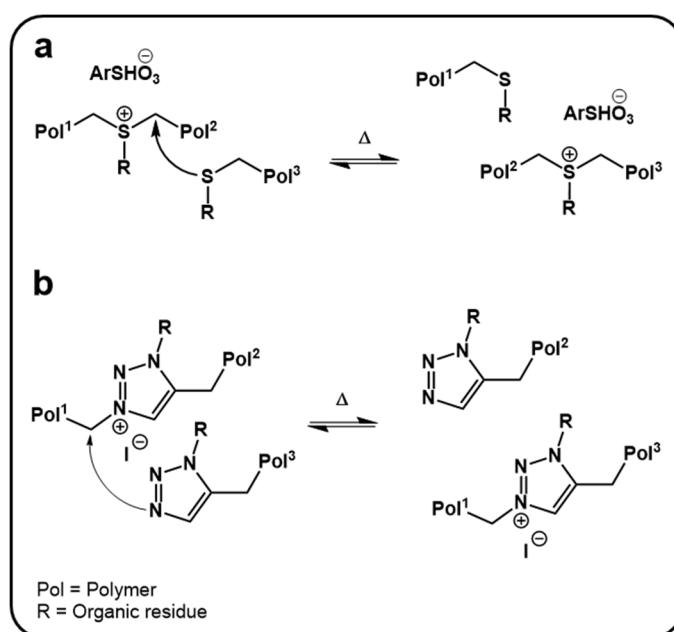
Figure 19: Examples of concerted mechanisms for vitrimers. **(a)** A cationic ring opening polymerization of cyclic thioethers supported by sulfonium sulfonate ion pairs. **(b)** A polyionic network including *N*-alkylated triazolium iodide, proceeding by a transalkylation reaction of triazoles.

3.2.3.6 Dissociative Vitrimers

An essential characteristic of vitrimers is the temperature-dependent Arrhenius behavior, caused by chemical reactions proceeding by associative or concerted exchange mechanisms. Moreover, vitrimers are insoluble in good solvents and show no sol-gel transition.[52] Interestingly, also dissociative pathways can show this behavior under certain circumstances, giving a schematic example of the energy scheme during such a reaction in **Figure 20**. Comparing two dissociative mechanisms with the same activation energy, the energy barrier for the backward reaction can be quite different. If the barrier is low, the backward reaction occurs very fast, while in the other case, it is much slower, even if the debond rate is theoretically the same at all temperatures. Nevertheless, their viscosity profiles and mechanical properties will differ significantly with the extreme case that the cross-linking density stays constant at a high level and over a large temperature range. In these networks, the temperature to shift the debonding significantly to the endothermic side is higher than the degradation temperature. Concluding that in a specific temperature range the cross-linking density in dissociative CANs can likewise be considered as constant and negligible low depolymerization grades and therefore show a vitrimer-like, Arrhenius dependence, caused by the chemical exchange reaction. Such examples are already reported by transalkylation exchanges of C–N bonds, but to date rarely investigated.[73] However, another difference to real vitrimers is the solubility in good, non-reactive solvents. In dissociative CANs the equilibrium shifts toward the debonded state by dilution effect, whilein vitrimers the networks stay the same at all temperatures.[52, 73]

dissociative network
with high reaction enthalpy

dissociative network
with low reaction enthalpy
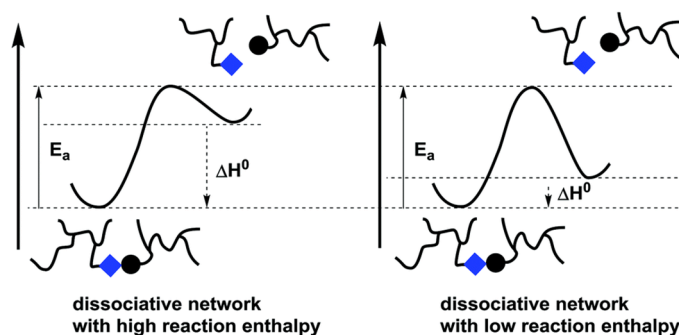
Figure 20: Energy scheme of dissociative networks with the same activation energy, but different reaction enthalpies, effecting the speed of the backward reaction and therefore the viscoelastic behavior. By fast backward reactions, dissociative CANs can be considered with a constant cross-linking ratio in a specific temperature range. Reproduced from Ref. *Polym. Chem.*, 2019, 10, 6091-6108 (DOI: 10.1039/C9PY01260E) with permission from the Royal Society of Chemistry.[11]

3.3 Vinylogous Urethane/Urea Vitrimers

3.3.1 Monomer Synthesis

Vinylogous urethane/urea vitrimers are synthesized by the condensation reaction of acetoaceteates/acetoacetamides and primary amines. The acetoacetates are typically generated from the corresponding alcohols/amines and converted by an acetoacetylation/acetoacetamidation reaction. *Tert*-butylacetoacetate (TBA) is readily known as a reactant for various alcohols and other nucleophiles.[21, 55, 74] At elevated temperatures above 110 °C TBA splits into a reactive acetylketene and *tert*-butanol as a byproduct. The highly electrophilic acetylketene undergoes fast addition reactions with almost any available nucleophile, *e.g.* to form acetoacetates, acetoacetamides or thioacetoacetates (**Figure 21**). In this work mainly, acetoacetates were used. Moreover, TBA is used for several steps in the organic synthesis of complex molecules.[74-76]
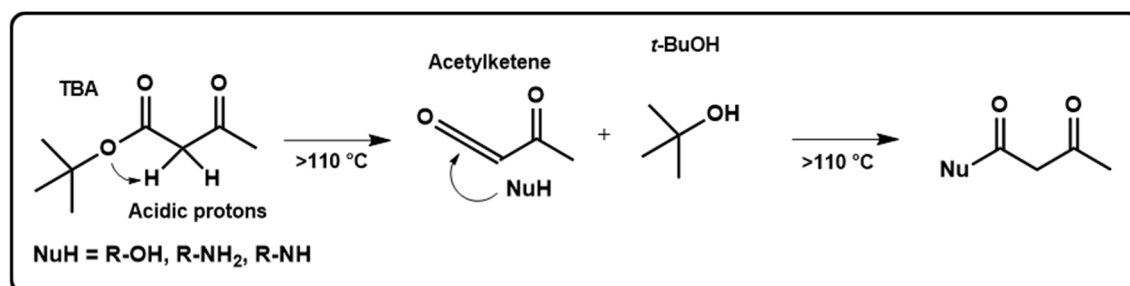
Figure 21: Acetoacetylation agent TBA dissociates to a reactive acetylketene at elevated temperatures above 110 °C. A nucleophile attacks the electrophilic acetylketene and produces the desired acetoacetate or acetoacetamide.

Furthermore, it has been known from literature for many decades that acetoacetates undergo keto-enol tautomerism, with the formation of a 6-membered cyclic structure stabilized by intramolecular hydrogen bonds. Usually, the keto form is thermodynamically preferred, while the equilibrium is determined by the surround protic/aprotic polarity (solvent, monomer), temperature, substituents and time. For this reason, in every acetoacetate monomer, a little amount of the enol form can be found (**Figure 22**).[77-80]
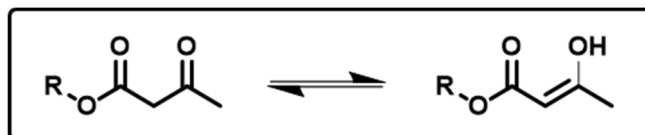
Figure 22: Keto-enol tautomerism in acetoacetates. The keto form is usually thermodynamically preferred.

3.3.2 Vinylogous Urethane Vitrimers

Vinylogous urethane vitrimers were introduced by Ludwik Leibler and Filip Du Prez as suitable covalent dynamic chemistry for vitrimers in 2015.[55] The condensation reaction of ketones or acetoacetates and primary amines follows the mechanism for the imine formation in typical polyimine networks, releasing water as a byproduct. However, the intramolecular stabilization by conjugation and intramolecular hydrogen bonds leads to a dominant formation of the enamine tautomer, instead of the usually thermodynamically preferred imine tautomer (**Figure 23**). The stabilization of the enamine-one tautomer is so much preferred that the imine form cannot be measured in significant amounts. Comparing the reactivity of the imines and enamines, the enamines electrophilicity is lower than the imines, making them less reactive. For this reason, the condensation reaction can be carried out in water, since the backward reaction is highly suppressed and the equilibrium is widely shifted to the products.[45, 55]
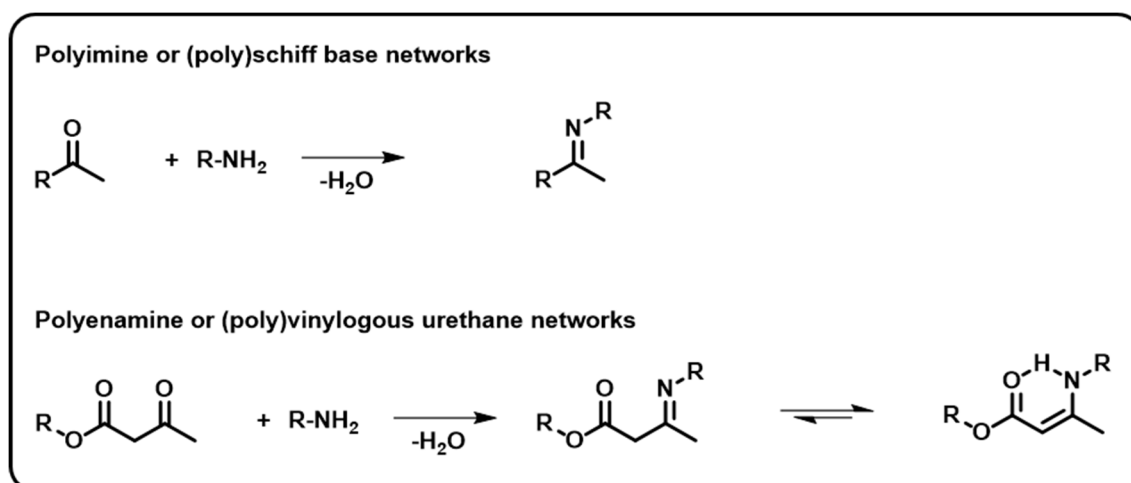
Figure 23: Condensation reaction of ketones and acetoacetates with primary amines to form the imine or enamine as thermodynamically preferred tautomer.

Moreover, it is known that imine-enamine tautomerism and enamine *cis-trans* stereoisomerism depend on the structure of the molecular, temperature, surrounding polarity and competing external hydrogen bond stabilization to the intramolecular hydrogen bonds, which has already been extensively investigated on soluble organic compounds[81-84] (**Figure 24**).
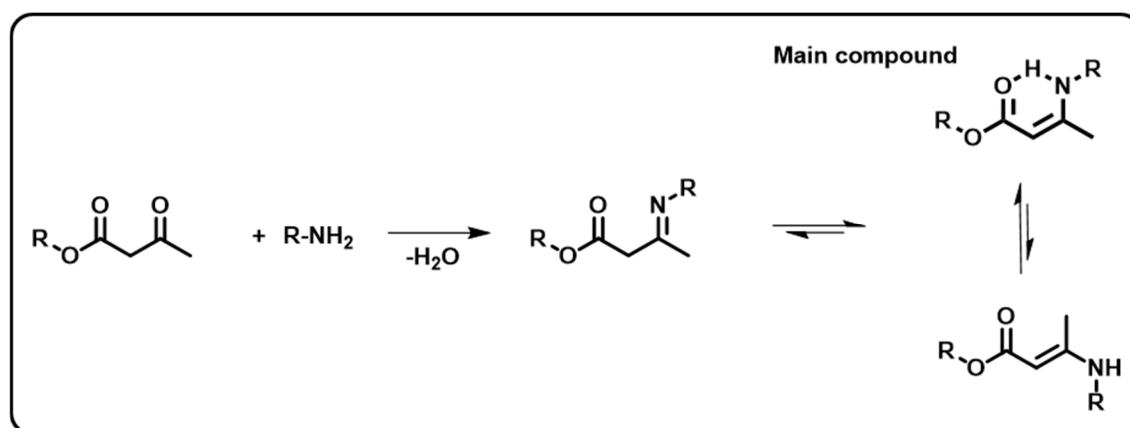
Figure 24: Reaction of acetoacetates and primary amines to the imine as intermediate, followed by fast equilibration the thermodynamically preferred enamine-one tautomer. The enamine-one tautomer can exist in different configurations, *e.g. cis* or *trans* configuration, while the *cis* form is usually thermodynamically preferred.

3.3.3 Exchange Mechanism – Transamination

For vinylogous urethane vitrimers, different exchange pathways for the transamination reaction were proposed. A protic-catalyzed iminium pathway was determined as the dominant exchange mechanism with activation energies around 75 kJ mol^{-1}. Another mechanism is the Lewis acid-catalyzed aprotic Michael-type acceptor pathway, where the Lewis acid accumulates to the C=O bond and activates the C=C double bond by shifting electrons and stabilizing the zwitterionic intermediate state. Moreover, an aprotic Michael-type pathway with higher activation energies around 150 kJ mol^{-1} was observed. Another exchange reaction is based on the dissociative backward reaction with water (**Figure 25**).[20] To the state of the art, many different vinylogous urethane vitrimers based on countless different backbones have been prepared. Comparing the catalyst-free transamination pathways, activation energies of 68–149 kJ mol^{-1} have been reported for the protic iminium pathway and 142–521 kJ mol^{-1} for the aprotic Michael-type pathway.

These results show that the activation energies can vary a lot and depend on various factors like cross-linking density, polarity, flexibility and other factors.[70] Besides these associative pathways, the dissociative backward reaction (hydrolysis) with water is also possible and is accelerated with a rising amount of a catalyst and/or water in the material.[85]
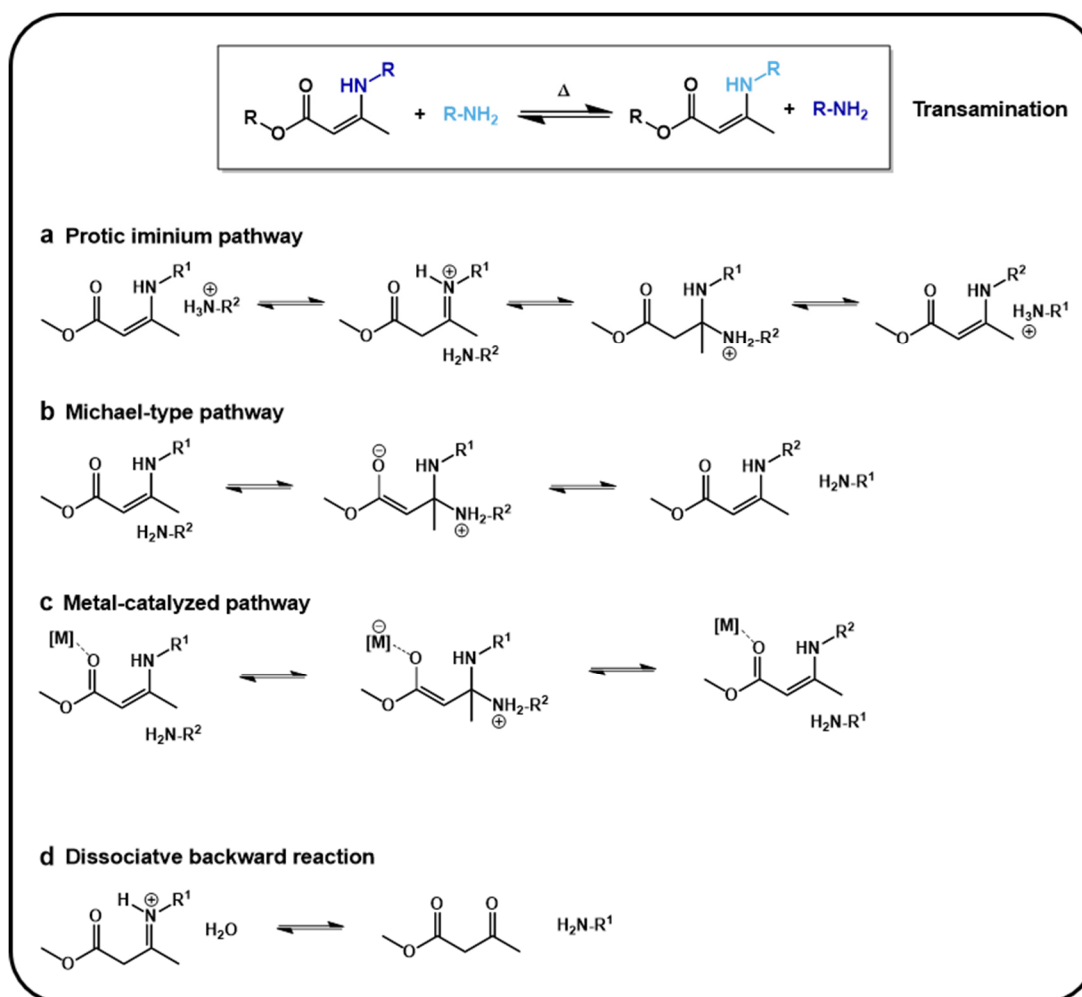
Figure 25: Exchange mechanism of vinylogous urethanes. (**a**) The dominant mechanism is proposed as the protic iminium pathway, in which the enamine is converted into a highly reactive iminium-ion and substituted by another free amine. (**b**) Lewis acid catalyzed aprotic Michael-type acceptor pathway, where the lewis acid activates the C=C double bond by shifting electrons and stabilizing the zwitterionic intermediate state. (**c**) Direct attack of the amine to the electrophilic C=C bond and stabilization in the zwitterionic intermediate state. (**d**) Dissociative mechanism of the hydrolysis with water, initiating the backward reaction and depolymerization.

Adding a catalyst, *e.g.* a Brønsted acid to a vinylogous urethane, the enamine-one is partly present as iminium-ion. The iminium-ion is highly electrophilic and can easily undergo substitution reactions with free primary amines. Interestingly, the protic iminium pathway was even identified as the predominant mechanism in materials without adding an additional catalyst, leading to the conclusion that the materials contain enough protons for the exchange reaction to proceed (**Figure 26a**). Only if a base is added, the exchange mechanism is suppressed and the Michael-type acceptor pathway is pronounced.[86]

In addition, vitrimers can show both the protic iminium pathway and the aprotic Michael-type pathway in the same material at different temperatures. When the temperature is high enough, the Michael-type pathway is pronounced, enabling a dual temperature response, which is proven by different slopes in the linear Arrhenius fit (Figure 26b).[20] Moreover, it was observed that with a rising amount of free amines and/or catalyst in the network, the stress-relaxation times were accelerated and only the protic iminium pathway is pronounced, even at high temperatures (Figure 26b-d).[70]
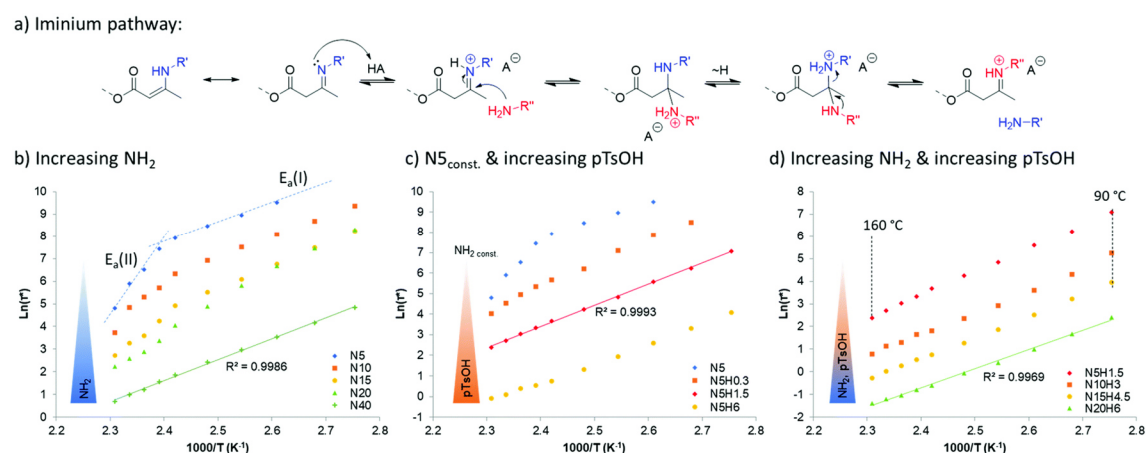
Figure 26: Plots of the stress-relaxation times versus the reciprocal temperature with a linear fit of the measurement points. The results show that with rising amounts of free amines and/or catalyst (*p*-TsOH) in the network, only the protic iminium pathway is pronounced. Without catalyst and low excess of amines, the iminium pathway, and the aprotic Michael pathway can both be measured. Reproduced from Mater. Horiz., 2020, 7, 104-110 (DOI: 10.1039/C9MH01062A) with permission from the Royal Society of Chemistry.[56]

Comparing different Brønsted acid catalysts, *e.g.* sulfuric acid or *para*-toluolsulfonic acid, faster exchange rates were observed, but no significant changes in the activation energies compared to uncatalyzed conditions. Adding the Lewis acid dibutyltin dilaurate (DBTL), a much lower activation energy of 45 kJ mol^{-1} was determined. The Lewis acid binds to the ester bond and increases the electrophilicity at the C=C bond, making a nucleophilic attack more attractive and stabilizing the zwitterionic intermediate state. Adding the base 1,5,7-triazabicyclo[4.4.0]dec-5-en (TBD) or 1,5-diazabicyclo[4.3.0]non-5-ene (DBN), the aprotic Michael-type acceptor pathway is pronounced with higher activation energies of 150 kJ mol^{-1} or more.[52, 86]

3.3.4 Vinylogous Urea Vitrimers

Vinylogous urea vitrimers are synthesized by the condensation reaction of acetoacetamides and primary amines and follow the same reactions and exchange conditions as the vinylogous urethane vitrimers (**Figure 27**). Similar exchange mechanisms were reported for vinylogous urea vitrimers, with slightly lower activation energies of 49–54 kJ mol^{-1}.[21] While vinylogous urea vitrimers did not gain much attention, with only one reported publication, many works for vinylogous urethanes have been published.
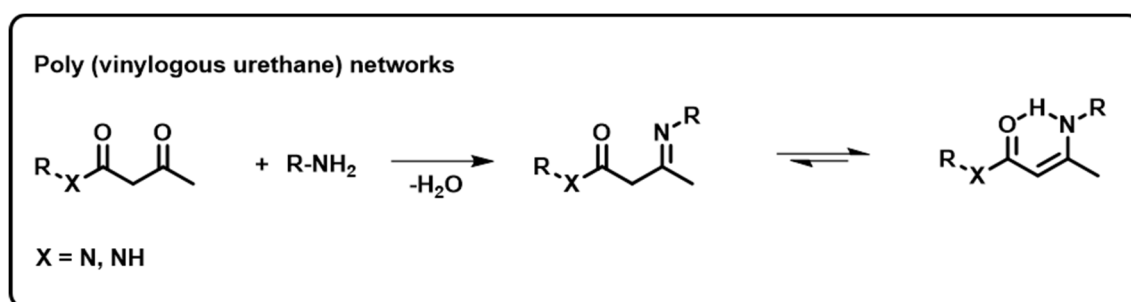
Figure 27: Condensation reaction of acetoacetamides and primary amines to form vinylogous urea bonds.

Denissen *et. al* synthesized different vinylogous urea vitrimers in order to use them in a fiber-reinforced composite material. It was found that the acetoacetamide monomer using secondary amines exhibits the shortest intrinsic stress-relaxation times with remarkably good properties (T_g = 110 °C, E-modulus = 2.2 GPa, tensile strength = 70 MPa). The matrix enables enduring prepregs, which still allow an efficient thermal fusion of multiple

layers as well as thermoforming and fiber recycling by solvolysis.[21] Vinylogous urea vitrimers are further discussed in chapter unpublished results 6.3.6.

3.3.5 Vitrimers in Different Research Fields

Nowadays, vinylogous urethanes have been used for several applications and applied with innumerable molecules, oligomers or modified polymers. Besides the functional groups for the exchange reaction, the backbone of the monomers/polymers is a decisive factor for the vitrimers properties. Since the concentration of the functional groups is of major importance, the backbone likewise influences the condensation reaction rate and the exchange speed. Most important, the backbone defines the cross-linking density and glass transition temperature of the materials.[70]

Michael O. Wolf and co-workers combined vinylogous urethane chemistry, activated by heat, with photoactive aromatic diamines using UV-irridiation ([4+4] cycloaddition) of anthracene for a dual respond exchange mechanism. The networks rearranged under thermal treatment due to transamination reactions and additionally lowered their viscosity under UV-irradiation by dissociative depolymerization of the anthracene bonds.[87]

Yangju Lin *et al.* synthesized three different bio-based vitrimers derived from acetoacetylated cardanol and two different diamines (*m*-xylylendiamine and 4,4-diaminocyclohexylmethane). The modified cardanol was reacted with each of the amine and a mixture of the amines. Afterward, the pure vitrimers were investigated by their mechanical properties, ground and fused to a homogeneously mixed material by heat compression. Experiments showed that after three cycles of compression molding, the vitrimers showed precisely the same properties as the directly prepared mixture of the diamines, pointing out the excellent compatibility and ability for easy postmodification of these type of vitrimers.[27]

Giving a few examples for block copolymer vitrimers, polystyrene was copolymerized with (2-acetoacetoxy)ethyl methacrylate by radical polymerization. The copolymer showed molecular weights considerably higher than the entanglement threshold. Moreover, the copolymers were cross-linked by *m*-xylylendiamine and the reaction was catalyzed by *p*-toluenesulfonic acid, generating a material with a high T_g (120 °C) and remarkably short stress-relaxation times. [88]

The same group introduced catalyst-free copolymers derived by controlled radical polymerization from methyl methracrylate and (2-acetoacetoxy)ethyl methacrylate, likewise enabling soft, acetoacetylated copolymers as suitable monomer for vinylogous urethane vitrimers. The cross-linking was conducted with TREN and showed a good processability in terms of chemical and mechanical recycling.[89]

3.4 Bio-based Vitrimers

Due to the increasing environmental impact of plastics derived from fossil resources, the life cycle assessment of plastics is becoming more and more important for all types of materials and products. In this context, in particular bio-based raw materials offer a very sustainable alternative to conventional raw materials, since they are obtained from renewable sources and leave a significantly better carbon footprint even in the case of subsequent thermal recycling. The global production of bio-based polymers is growing from 1.7 mt in 2014 to 2.1 mt in 2020[90, 91], which, however, is only a fraction of the global plastic production of 380 metric tons.[92] The primary industrially produced bio-based polymers are thermoplastics such as starch-based compounds, cellulose acetate, poly(lactic acid) (PLA), poly(butyleneadipate-co-terephthalate) (PBAT), poly(butylene succinate) (PBS), and green polyolefins.[90, 93, 94]

Moreover, also thermosetting bio-based polymers like polyether, polyester, polyols and polyurethanes (PU) are produced for mainly foams or coatings, while also first productions of vegetable oil and fatty acid -based epoxy resins started.[95, 96]

As society has become increasingly aware of the problems caused by plastic waste, the research field of bio-based polymers has grown rapidly in recent years. Nature delivers many aliphatic, cycloaliphatic or aromatic substances, which enable the synthesis of bio-based polymers with a broad range of thermomechanical properties.[97] Vegetable oils represent a class of aliphatic hydrocarbons, which are cheap, widely available and contain functional groups such as hydroxy groups or carbon double bonds for chemical reactions. For example, triglycerides can be directly used as a trifunctional monomer for polymer networks[98-101] or split into well-defined fatty acids and glycerol.[102] Fatty acids can be modified and dimerized to di- and trifunctional acids, which are sold under the trade name Pripol®.[103, 104]

By further modification, fatty acids can likewise be dimerized to di- and trifunctional amines with the trade name Priamine®.[91, 105] Another potentially very interesting feedstock is represented by polysaccharides (carbohydrates), which represent the most available bio-polymers on earth. Cellulose, starch, hemicellulose, chitin, chitosan or alginate are composed of monosaccharides, which are bonded by glycosidic bonds and contain different functional groups, *e.g.*, hydroxy groups, carboxy groups or amine groups. The polymers can be either used as polymers or degraded into low molecular monosaccharides as monomers for new materials. Low molecular saccharides can be converted into precursors of a broad range of platform chemicals, such as isosorbide, isomannide and isoidide, aromatic furan-based monomers, or short aliphatic molecules such as itaconic acid, levulinic acid or succinic acid.[97, 106-108]

The second most abundant class of biomass is represented by lignin, derived from wood. Lignin offers the extraction of several aromatic and phenolic compounds as precursors like vanillin, syringaldehyde, or hydroxybenzoic acid for bio-based materials.[109-111]

3.5   (Nano-)composite Materials

Composites are produced from two or more different materials, which show different physical and/or chemical properties. The resulting composites exhibit different properties compared to the individual base materials. A composite material as studied in this work always contains a matrix and a filler compound. The filler compounds are homogeneously distributed in the matrix. A first classification of composites is based on the matrix and exhibits polymer matrix composites, metal matrix composites, carbon matrix composites or ceramic matrix composites. The second classification is according to the filler, which can appear in many different shapes, *e.g.* particles, platelets, fibers, or lamella structures. In general, composites can consist of any type of organic and inorganic material or even the same class, turning many materials into a composite. For example, wood is an organic polymer-polymer composite made from cellulose fibers and lignin as a matrix. The benefits of composites are their high specific strength and high specific modulus. The specific strength is defined as the ratio of strength to density, while the specific modulus is the ratio of modulus to density. Especially polymer composites show exceptional strength-to-weight ratio, high stiffness, durability, and resistance to corrosion, chemicals,

and environmental exposures, which is highly favorable for many modern applications, *e.g.* airplanes or wind turbines.[112]

3.5.1 Bio-inspired Organic-inorganic Composites

Nature has produced remarkable materials over million years with a small set of building blocks and ambient conditions.[113] Under these circumstances, it is even more impressive how diverse fundamental molecular interactions were used for the fabrication of multilayer and often hierarchical materials with astonishing properties. The implementation of sometimes contradictory properties like combining high strength and toughness offer great examples for the engineering of new, man-made materials, which have already been used for some applications (*e.g.* metal mimics).[114] However, the fabrication of bioinspired structures faces great challenges, such as structural coupling between hard and soft building blocks, the retention of mechanical integrity while maintaining other desired functional properties and the molecular-scale precision within each level of hierarchy. Nevertheless, the possibility for a fast and large-scale production must be considered.[115]

One prominent example for a natural organic-inorganic composite is the natural material nacre. Nacre is the inner shell layer of some molluska and contains of 95 wt% aragonite ($CaCO_3$) and 5 wt% of proteins and polysascharides. Nacre exhibits a high fracture toughness, which is much greater than pure aragonite due to its ingenious structure. The complex hierarchical microarchitecture of nacre ranges from the nano- to the micrometer scale. The structure contains columnar architectures and sheet tiles, mineral bridges, polygonal nanograins, nanoasperities, plastic microbuckling, crack deflection and interlocking bricks (**Figure 28**). Due to these properties the materials exhibit a remarkable combination of stiffness, low weight, and strength. For this reason, the structure of nacre attracted scientists' interest in mimicking the unique properties and developing new materials such as laminated composite materials, biomineralization or molecular scale self-assembly.[116]
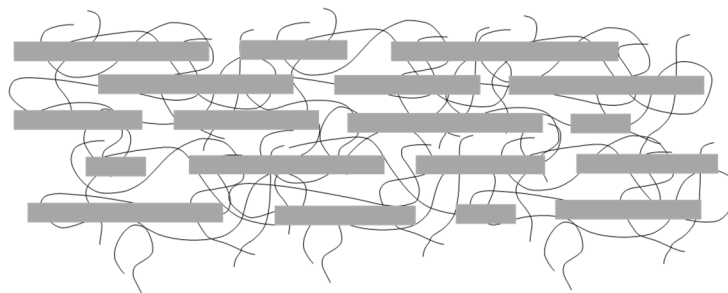
Figure 28: Structure of natural nacre, showing the brick and mortar-like structure of the anisotropic platelets (aragonite) in the polymer matrix (polysaccharides).

3.5.2 Vitrimer (Nano-)composites

Nowadays, the use of thermosetting polymers for high-demand applications in composite materials is a growing research field, due to their excellent properties and easy production.[117]

However, these materials still face the central problem of non-recyclability in terms of their cross-linked polymer network with the incooperation of other materials, *e.g.* glass fibers, carbon fibers, wood or metal, which makes them even more difficult to separate or to recycle. One of the main challenges is to separate the fillers from the matrix. Current processes use thermolysis, solvolysis or other methods enabling reinforcement recovery but often with altered mechanical properties. Because of this reason, the fillers cannot be reused for the same applications in most cases.[118-120]

Vitrimers enable covalent dynamic networks in the composite materials, which allow the cross-linked matrix to rearrange at elevated temperatures and pressure. For this reason, the concept of covalent adaptable networks was rapidly used in composite research to implement their unique properties. Carbon fibers[121], carbon nanotubes[122, 123], graphene[124], carbon black nanodots[125], glass fibers[121, 126], cellulose-based reinforcement[127, 128], silica- and aluminaoxide fillers[129-131], polyhedral oligomeric silsesquioxane nanostructures[132] and iron oxide particles[133] have been used as fillers for different composites.[22] However, adding fillers lowers the flexibility and mobility in the network while the T_g and the cross-linking density usually increase. For these reasons, it is even more challenging to reprocess a composite material, especially with high filler loadings.[22]

As an example for an iron oxide based composite, a magneto-responsive elastomer doped with iron oxide microparticles wasreported.[133] The elastomeric vitrimer was made of a

thioplast, epoxy-terminated monomer EPS25 and mixed in a stoichiometric ratio of two sulfhydryls (2,2′-(ethylenedioxy)diethanethiol (EDDET) and pentaerythritol tetrakis (3-mercaptopropionate) (PETMP)). (Dimethylamino)pyridine (DMAP) was chosen as a catalyst and iron-oxide particles in the micrometer range were added. The vitrimer show viscoelastic properties under thermal treatment/UV-light by disulfide metathesis. As known for vitrimers, the materials showed shape-memory, remolding, repcrocessing and self-healing. Moreover, the material could be moved by magnetic fields and pass through small tunnels due to the flexibility of the elastomeric network.[133]

4 Objectives of the Work

This Ph.D. thesis is a part into the collaborated research center SFB986 in project area A. Area A aimed to synthesize hierarchical composite materials based on inorganic-organic composites with high loads of inorganic particles. The project was inspired by natural materials like nacre, which show remarkable properties, *e.g.* high strength, toughness or high fracture toughness (chapter 3.5.1). The unique properties were achieved through a multiscale hierarchical structure from the nano- to the micro-scale. The goal was to mimic these structures by clustering nanoparticles into nanoparticle clusters and embedding them into a thermoreversible polymer matrix. To obtain a well-designed, and from the mechanical perspective promising hierarchical material, the composite should be heat compressed to a brick and mortar structure. To achieve that, the used polymer must be malleable, which can be achieved by using covalent adaptable networks (chapter 3.2). Subproject A2 was responsible for the development of thermoreversible polymers and ligands to connect the interfaces of the nanoparticles (provided by subproject A1) and polymers. Moreover, milestones were to be reached on the way to the final goal, which initially involved the implementation and investigation of individual nanoparticles and ligands in thermoreversible polymers separately. Various thermoreversible polymers have been synthesized and tested in terms of their properties to provide a suitable material for different processing methods and properties. This was essentially important for different processing techniques like 3D-printing, spouted bed granulation or infiltration technique, which require different physical or chemical properties of the monomers and polymers (*e.g.* for 3D-printing the solvent and polarity must be suitable for the printing process). These projects were carried out in cooperation with subprojects A1, A3 and A6. The focus of this work was on the synthesis and in-depth investigation of vinylogous urethane vitrimers, which represent a suitable, robust and catalyst-free type of vitrimers (chapter 3.3). **Figure 29** displays the overall goal of the SFB986 - Area A to synthesize a hierarchical material by using clustered nanoparticles embedded into a thermoreversible polymer matrix.
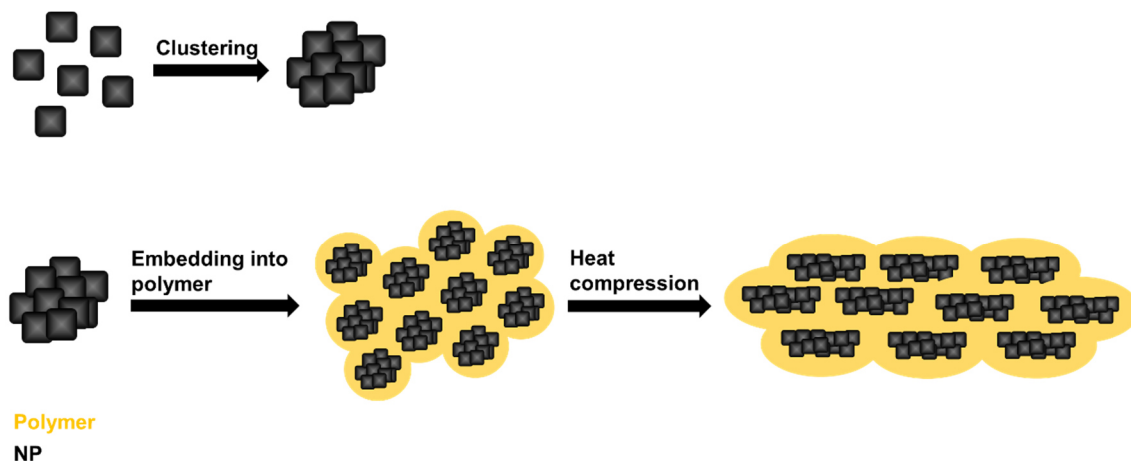
Figure 29: Scheme of the overall goal of the SFB986 - Area A to synthesize a hierarchical material by clustered nano-particles embedded into a thermoreversible polymer matrix.

To achieve the overall goals, the prepared vinylogous urethane vitrimers were investigated in terms of their basic reaction behavior and structure by solvent-based model reactions and cross-linked materials. Effects such as the solvent, catalyst, monomer backbone, nucleophilicity, cross-linking density, backbone structure or spatial arrangement were investigated in terms of their influence on the structure, the polymerization and the thermomechanic behavior. The base research is mainly shown in publication 1 and the chapters of unpublished works 6.1 (monomer synthesis), 6.2 (Polymerization), 6.3.1-6.3.3 (Influence of different amines and acetoacetates to the dynamic properties of the vitrimers) and 6.3.6 (Vinylogous urea vitrimers).

Moreover, a focus was on optimizing the synthetic routes in terms of sustainability, non-toxicity and applicability. To reduce the carbon footprint, bio-based and non-toxic raw materials were used as raw materials and organic solvents were reduced to a minimum. This was essentially important for different processing techniques, *e.g.* for 3D-printing the solvent and polarity must be suitable for the printing process. Moreover, several vitrimers have been developed with the objective of certain applications, *e.g.* reprocessable epoxy resins or porous vitrimer membranes. The results are shown in publication 2 and the unpublished chapters 6.3.4 (Vipoxy – Epoxy-vitrimers derived from aromatic alcohols) and 6.3.5 (Porous and dense vitrimer films based on sugars).

The last overarching topic is about vitrimer composite and shows different polymer-polymer and inorganic-polymer composites, which were achieved by cooperation with different partners. The results are shown in publication 3

(starch-reinforced vinylogous urethane composites) and the chapters of unpublished works 6.4.1 (iron-oxide nanocomposites) and 6.4.2 (nacre-inspired organic-ceramic vitrimer composites). Starch-reinforced vitrimer composites were synthesized from bio-based raw materials and represent an organic-hierarchical polymer-polymer composite based on complex supramolecular starch granules embedded into thermoreversible vitrimer matrix. This project was carried out in the scope of a cooperation project with Professor Suwabun Chirachanchai (research visit, Chulalongkorn University, Bangkok). Iron oxide-nanoparticles/clusters have been embedded into a vitrimer matrix with low and high particle loads and carried out together with subproject A1. Nacre-like structures were prepared and investigated in the scope of a cooperation project with subproject A6. An *in-situ* 3D printing process was developed, which enables the alignment of anisotropic alumina platelets during the 3d- printing process as well as in a post modification process by heat compression molding. The topics are summarized shown in **Figure 30**.
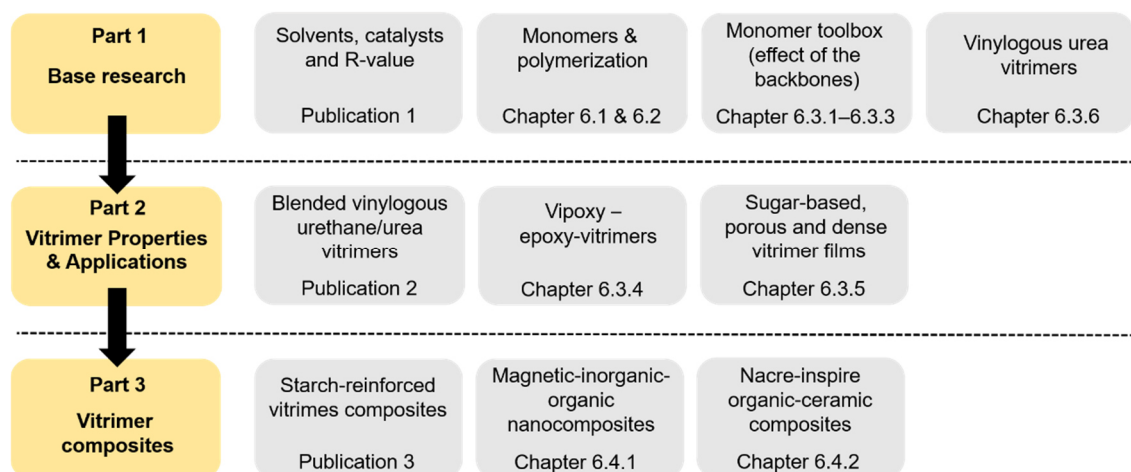
Figure 30: Overview of the investigated and discussed topics in this dissertation. In the first part, the fundamental reaction behavior of the vitrimers were enlighten by model reactions and material investigations. In the second part, different application-related vitrimer composition were investigated and discussed in terms of their properties. As last part, vitrimers were reacted with particles to form different composite materials with specific properties.

5 Results and Discussion – Published Works

This chapter contains the reprints of three published first-author articles that represent the central part of this dissertation. The support of collaborators, students, and colleagues is acknowledged. A short synopsis is given for each publication.

5.1 Publication 1: Acid-Mediated Autocat. in Vinylogous Urethane Vitrimers

Acid-Mediated Autocatalysis in Vinylogous Urethane Vitrimers

In the first publication, the reaction behavior of the condensation reaction of acetoacetates and primary amines as well as the resulting enamine-one (vinylogous urethane) species were investigated in solvent-based model studies and cross-linked vitrimer networks. The motivation was to explore the influence of solvents, temperature, catalysts and the decisive role of water on the structure of the resulting vinylogous urethane moieties and the characteristic exchange reaction (transamination reaction). In this context, it was of major interest if, besides the well-known transimination reaction, a reported imine-metathesis reaction for typical poly(imine) networks[30, 134, 135] can also proceed as an additional exchange mechanism in vinylogous urethane networks, especially in networks without free amines.

First, the acid-induced imine-enamine tautomerism and *cis-trans* equilibration were examined as fundamental mechanisms in vinylogous urethanes. In addition, an acid-mediated autocatalysis was investigated as exchange pathway for this type of vitrimer. Vinylogous urethanes are highly stabilized as *cis*-enamine-one, because of an intrinsic conjugated Michael system and intramolecular hydrogen bonds. It was explored, that the thermodynamic preference for the *cis*- and *trans*-stereoisomer depends on the polarity and proton donation ability of the solvent, while the preference for the *cis*-isomer was least in DMSO and highly pronounced in benzene. Furthermore, the kinetics of acid-mediated autocatalyzed transimination reactions were examined using low molecular model compounds, while the roles of a Brønsted catalyst and remaining water were investigated. Enamine-one species with different residues on both sides of the

enamine bond showed a fast exchange of the residues at elevated temperatures, indicating the same reaction products as expected for imine metathesis. In addition, poly(vinylogous urethane) networks with and without free amine groups and *para*-toluenesulfonic acid as a catalyst were prepared and characterized in terms of their thermal and mechanical properties. Surprisingly, the networks without free amines also showed a relatively fast exchange reaction by stress relaxation measurements.

As a result, this work pointed out the decisive role of a Brønsted acid catalyst and traces of water for the exchange reaction in vinylogous urethanes, especially in materials without free amines. Using a catalyst, these materials still showed remarkably fast stress-relaxation, indicating an additional exchange mechanism, *e.g.* protic imine metathesis. However, since traces of water or free amines cannot be verifiable excluded and the materials were analyzed under an ambient atmosphere, the exchange reaction is most likely proceeding by an acid-mediated autocatalysis, partly liberating free amines for typical transimination reactions. These findings participate in a discussion in literature where a similar autocatalysis reaction was explored for poly(imine) networks and contribute insights into yet not fully understood exchange pathways in this type of vitrimer.[136, 137] Further investigations of the fundamental reaction behavior and the dynamics of the transamination reaction in vinylogous urethane vitrimers networks are shown in chapters 6.1, 6.2 and 6.3.1–6.3.2.

The publication is reprinted with permission from P. Haida and V. Abetz, *Macromol. Rapid Commun.*, **2020**, *41*(14), 2000273 – published by Wiley. The related supporting information is available in Section 9.2.

Acid-Mediated Autocatalysis in Vinylogous Urethane Vitrimers

Philipp Haida and Volker Abetz*

Vitrimers are a class of polymeric materials with outstanding properties. Intramolecular substitution reactions lead to a dynamic exchange within the polymer network which enables thermoreversible stress relaxation in yet permanently crosslinked materials. In this paper, the acid-mediated autocatalysis is explored as a rearrangement pathway for vinylogous urethane vitrimers. The autocatalysis enables transimination reactions, resulting in a dynamic exchange among the enamine-one species, without an excess of free amines. Therefore, the enamine-ones are protonated by a Brønsted acid and turn into electrophilic iminium-ones, thus enabling fast backward and substitution reactions with water and free amines. This work provides an in-depth investigation of the mechanism by kinetic studies of selected compounds. In addition, novel elastomeric and thermosetting poly(vinylogous urethane) networks with and without free amine groups and additional *para*-toluene sulfonic acid as a Brønsted catalyst are prepared by bulk polymerization of hexane-1,6-diylbis(3-oxobutanoate) and tris(2-aminoethyl)amine. The underlying exchange mechanisms are determined by stress-relaxation experiments with stress relaxation times of 0.3–54 000 s at 110 °C.

Thermosets are used for many applications due to their unique properties in terms of structural and mechanical stability as well as their chemical resistance. However, as a result of their permanent 3D network, thermosets cannot be processed, reshaped, or recycled.[1]

The use of reversible bonds within polymer networks enables a dynamic rearrangement of the crosslinking points, which leads to a macroscopic flow behavior of the material without permanently changing the network integrity or its mechanical properties.

P. Haida, Prof. V. Abetz
Institute of Physical Chemistry
Universität Hamburg
Grindelallee 117, Hamburg 20146, Germany
E-mail: volker.abetz@hzg.de
Prof. V. Abetz
Institute of Polymer Research
Helmholtz-Zentrum Geesthacht
Max-Planck-Straße 1, Geesthacht 21502, Germany

The ORCID identification number(s) for the author(s) of this article can be found under https://doi.org/10.1002/marc.202000273.

Polymers and networks based on thermoreversible noncovalent bonds are known since many decades and the works of Meijer, Stadler, and Binder have contributed substantially to their development based on supramolecular concepts using tailored hydrogen bonding motifs, leading also to self-healing materials with adjustable properties.[2] Polymers with covalently exchangeable bonds are known, in principle, since the vulcanization of natural rubber with sulfur.[3] Covalent adaptable networks (CANs) with well-controllable chemical bonds are divided into dissociative and associative exchange mechanisms.[4] A typical dissociative exchange mechanism is the well-known retro-Diels-Alder reaction, e.g., between furan and maleimide. By applying heat, the equilibrium is shifted to the endothermic side and thus the polymer network is split covalently, which leads to a sudden reduction in viscosity, as in the case of thermoplastics above glass transition or melting temperature.[5]

CANs based on associative exchange mechanisms do not undergo depolymerization because the number of crosslinking points always remains constant. Covalent bonds are only broken when new ones are formed, making these networks permanent and dynamic at the same time.[6]

In 2011, Leibler and co-workers introduced a new class of CANs based on an associative exchange mechanism by adding a compatible transesterification catalyst to epoxy/acid or epoxy/anhydride polyester-based networks. This thermally triggered catalytic transesterification reaction resulted in durable polyester/polyol networks that show a slow viscosity decrease upon heating, which had never been observed in organic polymer materials before. Hence, the authors introduced the name vitrimers for those novel polymeric materials.[7]

Since this initial work, various dynamic covalent bonds for rearrangement reactions in vitrimers have been investigated.[8]

Further examples for associative exchange mechanisms are the transalkylation,[9] transcarbonation,[10] transcarbamoylation,[11] thiol-disulfide exchange,[12] transamination[13] or transimination reactions.[14] The use of numerous monomers and catalysts lead to a variety of exchange rates and activation energies.[13a,15,33] In all of these vitrimer-types, however, nonstoichiometric polymer networks are synthesized, with the excess component always initiating the exchange reaction. Another

**ADVANCED
SCIENCE NEWS**
www.advancedsciencenews.com

**Macromolecular
Rapid Communications**
www.mrc-journal.de

type of rearrangement mechanism for vitrimer-like materials, which does not require an excess compound, is based on metathesis reactions. Examples are the disulfide metathesis,[16] olefin metathesis,[17] or imine metathesis.[14,18]

In 2014, Winne and co-workers investigated the vinylogous amide-type enamine-one species, which are synthesized with primary amines and acetoacetates, giving a covalently dynamic bond for vitrimeric materials.[13b] This bond can be regarded as a vinylogous urethane with a vinylic bond and is stabilized by the conjugation through the ester unit and an intramolecular hydrogen bond, that turns vinylogous urethanes into thermodynamically stable bonds. While normal urethanes cannot undergo spontaneous addition reactions due to the weak electrophilicity, the vinylogous urethanes are significantly more reactive, which enables dynamic exchange reactions.[19] It is known from literature that the condensation reaction of aldehydes and ketones with primary amines produces imines and one equivalent of water.[20] However, in case a conjugated system is formed, the enamine structure can also be the preferred tautomer. As an example, the reaction of benzaldehyde and a primary amine produces predominantly the conjugated imine,[21] while the recently described reaction of acetoacetates and primary amines leads to the formation of the conjugated enamine.[13b,22] In both cases, the product is strongly thermodynamically favored by the conjugation, and yet, different. In addition, the enamine tautomer can exist as a *cis*- or a *trans*-stereoisomer. Depending on the chemical environment (e.g., polarity), one stereoisomer is usually thermodynamically preferred.[23] The basic knowledge of imine metathesis has already been known for approximately a century, using acid or metal catalysts.[24] However, it has recently been shown that imine metathesis reactions can also proceed at moderate temperatures and without adding an additional catalyst.[18a,25] Stefano and co-workers showed that aromatic imines undergo autocatalyzed transimination reactions at moderate temperatures, while the exchange rate can be easily accelerated by adding additional free primary amines.[25b,26]

Here, we investigated the Brønsted acid and autocatalyzed exchange pathway for vinylogous urethane vitrimers for the first time. Traces of water enable autocatalyzed transimination reactions, resulting in dynamic exchanges between the residues of the enamine-one species (**Figure 1**). Vinylogous urethanes are thermodynamically stabilized as a *cis*-enamine-one stereoisomer. Adding a Brønsted acid, the equilibrium of the imine-enamine tautomerism shifts to the side of the protonated, electrophilic iminium-one, which in turn enables nucleophilic substitution reactions. In addition, a solvent-dependent *cis–trans* stereoisomerism of the enamine-one species is investigated. The exchange mechanism is proven by stress relaxation experiments in poly(vinylogous urethane) networks, exploring vitrimers with and without additional free amines and *p*-toluene sulfonic acid as catalyst. Furthermore, novel elastomeric and thermosetting vinylogous urethane vitrimers are synthesized by carrying out nonstoichiometric crosslinking and using easily accessible, low molecular weight monomers, exhibiting short stress relaxation times and excellent mechanical properties.

Vinylogous urethanes can be easily synthesized by mixing primary amines and acetoacetates under elimination of one equivalent of water. The condensation reaction of ethylacetoacetate (**1**) and hexylamine (**2**) at room temperature was considered as a model compound reaction.

Characterization by ^{1}H NMR spectroscopy showed a fast condensation reaction, in which the formation of a stereoisomeric mixture of *cis*- and *trans*-enamine-ones was observed (**Figure 2**) (^{1}H NMR spectra, Figures S1 and S2, Supporting Information). The results pointed out that the *cis*-enamine-one (*cis*-en) (**3**) is predominantly present, while the *trans*-enamine-one (*trans*-en) (**4**) only represented a small amount. Furthermore, 2D NMR-experiments (13C DEPTQ-135 (distortionless enhancement by polarization transfer), correlated spectroscopy (COSY), heteronuclear single quantum coherence (HSQC), heteronuclear multiple bond correlation (HMBC), nuclear overhauser enhancement spectroscopy (NOESY)—Figures S3–S7, Supporting Information) clearly demonstrated the formation of the *cis*- and *trans*-enamine-ones as stereoisomers. As mentioned earlier, a conjugation thermodynamically stabilizes the respective tautomer.[22] In this case, the formation of a conjugated Michael system highly favors the enamine-one tautomers. Furthermore, the formation of an intramolecular hydrogen bond in the *cis*-en provides additional stabilization to the stereoisomer, which leads to the almost exclusive formation of the *cis*-en. Attenuated total reflection-fourier-transform-infrared (ATR-FT-IR) measurements supported the formation of the enamine-one by measuring the respective C=C band (1603 cm^{-1}) and the C=O ester band (1650 cm^{-1}) (Figure S8, Supporting Information).

It has been shown that solvent effects likewise influence the imine-enamine tautomerism and *cis–trans* stereoisomerism regarding aromatic and aliphatic imines in low molecular weight studies.[22,23,27] It is hence assumed that the solvent plays a major role for imine-enamine tautomerism and *cis–trans* stereoisomerism in vinylogous urethanes as well. To investigate this feature in our study, the isomeric mixture was stirred in deuterated benzene, chloroform, methanol, dimethylsulfoxide (DMSO), and without solvent for 8 d at room temperature and characterized by ^{1}H NMR-spectroscopy in different time
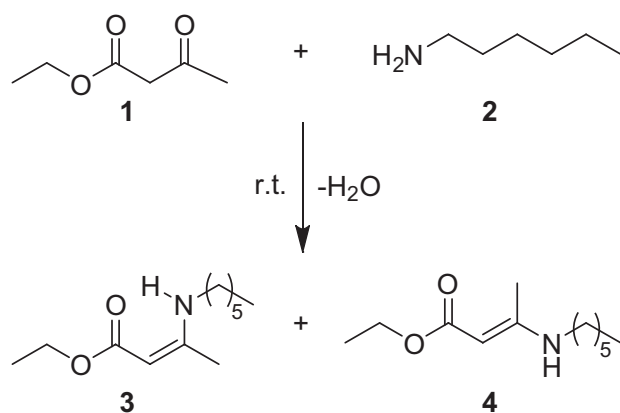

Figure 1. Schematic representation of the acid-mediated autocatalyzed exchange pathway for vinylogous urethane vitrimers. The enamine-ones are protonated by a Brønsted acid, giving an electrophilic iminium-one, which undergoes the backward reaction with water. Thus, the liberated amines initiate fast transimination reactions as exchange mechanism even in networks without an excess of free amines.

**ADVANCED
SCIENCE NEWS**
www.advancedsciencenews.com

**Macromolecular
Rapid Communications**
www.mrc-journal.de

Figure 2. Schematic representation of the condensation reaction with ethylacetoacetate (**1**) and hexylamine (**2**). The cis-enamine-one (**3**) and trans-enamine-one (**4**) stereoisomers were synthesized under elimination of one equivalent of water, with the cis-enamine-one (**3**) representing the predominant species.

intervals (Figure S9, Supporting Information). The spectra showed that the thermodynamic preference for the *cis*-en disappears slowly with increasing polarity of the aprotic solvents, while the *cis*-en was still predominant (**Table 1**).

This can be explained by the fact that a polar, aprotic solvent forms hydrogen bonds with the NH bond and thus competes with the intramolecular hydrogen bonds of the *cis*-en. The sterically preferred *trans*-en is therefore more strongly present in the polar, aprotic DMSO. In nonpolar aprotic solvents, on the contrary, stabilization can only take place via the intramolecular hydrogen bond of the *cis*-en. In comparison of the aprotic, polar DMSO and the protic, polar MeOD, the preference for the *cis*-en is more pronounced in DMSO. This can be explained by the fact that DMSO is a better hydrogen bond acceptor than MeOD. Considering the reaction times until the *cis*–*trans* equilibria were set, DMSO and MeOD show significantly different rates. The protic MeOD highly accelerates the reaction times in comparison to the other solvents. However, the mechanism for the isomerization requires further investigations since the mechanism might proceed via the protic catalyzed dissociation and renewed condensation reaction with water or the protonated iminium-one as direct intermediate.

Furthermore, it is reported that the imine-enamine tautomerism in general can be influenced by temperature.[23f,28] For this reason, temperature dependent ^{1}H NMR spectra

were measured in deuterated benzene, DMSO, and without solvent. In temperature-dependent NMR measurements, the temperature range is limited by the boiling points of the available deuterated solvents. With this in mind, the homogeneous stereoisomeric mixture was measured in deuterated benzene in a range of 20–60 °C, in deuterated DMSO in a range of 20–110 °C, and without solvent in a range of 20–90 °C (Figure S10, Supporting Information). The measurements in deuterated benzene showed no significant shift of the *cis*–*trans* stereoisomerism (98:2–97:3 mol%) in a temperature range of 20–60 °C. In the more polar deuterated DMSO, heating from 20–70 °C showed a slight shift (87:13–85:15 mol%). In the range from 70 to 110 °C, however, a significant increase (85:15–60:40 mol%) was found.

Thus, at 110 °C, the same *cis*–*trans* equilibrium state was reached as observed at room temperature after 144 h. Apparently, the temperature is not a decisive factor here, since the *cis*–*trans* equilibrium does not show a significant shift at higher temperatures, just a faster equilibration (Table S1, Supporting Information).

The metal- and acid-catalyzed imine metathesis for imine species is known for a long time.[24a,d,25a] For the protic imine metathesis pathway a stepwise mechanism is suggested in which a protonated iminium serves as electrophile and the nonprotonated imine serves as nucleophile (Figure S11, Supporting Information).[24a] In this work, we examined the exchange mechanism of the protic imine metathesis for vinylogous urethanes, considering enamine-ones as reactants. In order to investigate the exchange reaction, two enamine-one species with different residues on both sides of the enamine bond were synthesized and it was examined whether the four expected products arose during stirring at elevated temperatures (**Figure 3**). Xylene was used as solvent because of the high boiling point and the nonpolar, aprotic character. As mentioned earlier, the preference for the *cis*-enamine-one is thermodynamically highly pronounced in nonpolar solvents. This should ensure a clear evaluation of the expected four *cis*-enamine-one products.

Compounds **6** and **7** were mixed equally in xylene and stirred for 7 h at 140 °C. Characterization by ^{1}H NMR spectroscopy showed the formation of the four expected products (**6**, **7**, **8**, and **9**) and an equilibrium state where the share of each product amounted to 25%. As a reference, the four expected products **6**, **7**, **8**, and **9** were synthesized separately and mixed in the same ratio and concentration as in the model compound reaction. In comparison, the obtained ^{1}H NMR spectra show the same equilibrium signals and intensities, which is a clear evidence for the

Table 1. Molar ratio of cis-trans-stereoisomers in solvents with different polarity at room temperature. With increasing polarity of the aprotic solvents, the thermodynamic preference for the cis-isomer disappears slowly. The protic solvent MeOD acts as a protic catalyst since the equilibration proceeds significantly faster compared to aprotic solvents.

Solvent	6 h	17 h	24 h	41 h	72 h	144 h	204 h	
Benzene-d_6	97:3	97:3	98:2	–	98:2	–	98:2	
CDCl$_3$-d_1	96:4	97:3	–	97:3	97:3	–	97:3	
DMSO-d_6	87:13	79:21	–	71:29	66:34	61:39	61:39	*Cis:trans*
MeOD-d_4	74:26	74:26	–	74:26	–	74:26	74:26	
No Solvent	91:9	–	–	–	–	–	91:9	
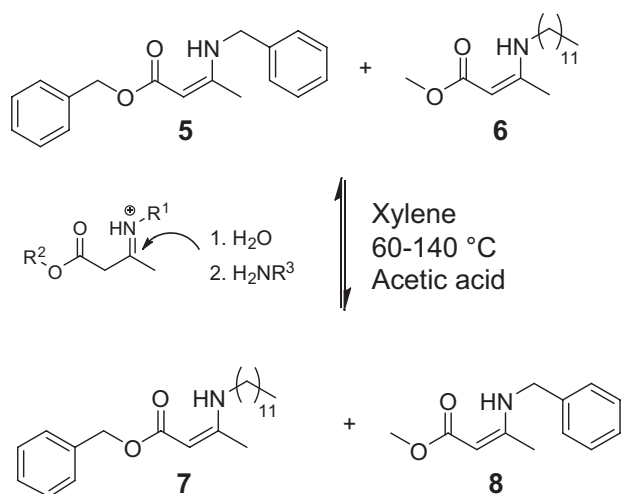
Figure 3. Schematic representation of the model compound exchange experiment for the acid-mediated autocatalysis reaction. The enamine-ones (**5** and **6**) were dissolved in xylene and different amounts of acetic acid were added as Brønsted catalyst. The exchange reaction (yielding **7** and **8**) was monitored over time at different temperatures.

exchange reaction in vinylogous urethanes (**Figure 4**). (Full ^{1}H NMR spectra, Figure S12, Supporting Information).

The transimination reaction in vinylogous urethanes is initiated by free primary amines. Consequently, the existence of such primary amine would yield the same product as

the exchange reaction in this synthetic scheme. This makes a removal of all free primary amines before the experiment mandatory. To achieve that, an excess of acetoacetates (0.1 eq.) was added and the absence of amines was proven by ^{1}H NMR spectroscopy.

In order to investigate the role of an acid catalyst during the reaction, equal amounts of compounds **5** and **6** were dissolved in xylene and stirred for 4 h at 80 °C with different amounts of acetic acid (0–10 eq.) (**Figure 5**).

The results clearly show accelerated conversion by using an increased amount of the Brønsted acid. Consequently, the exchange reaction could be quenched by adding the weak base sodium acetate to the reaction mixture with no conversion after 4 h at 80 °C. Furthermore, the imine metathesis in imines can be quenched by adding an excess of a strong Brønsted acid, as all nucleophiles are protonated instantly with no nucleophiles remaining. To prove this, the reaction mixture was added to an excess of trifluoroacetic acid with the result that all enamine-ones were present as protonated iminium-ones (Figure S13, Supporting Information). These findings match with the reported investigations of the protic imine metathesis using aliphatic and aromatic imines.[24a,25a] The experiments show that the exchange reaction is catalyzed by Brønsted acids and even proceeds slowly without adding an additional catalyst.

Moreover, the role of water is of major interest for the mechanistic investigation of the exchange reaction since water initiates the backward reaction to acetoacetates and amines. These free amines can undergo fast condensation and transimination reactions, leading to an exchange of the different
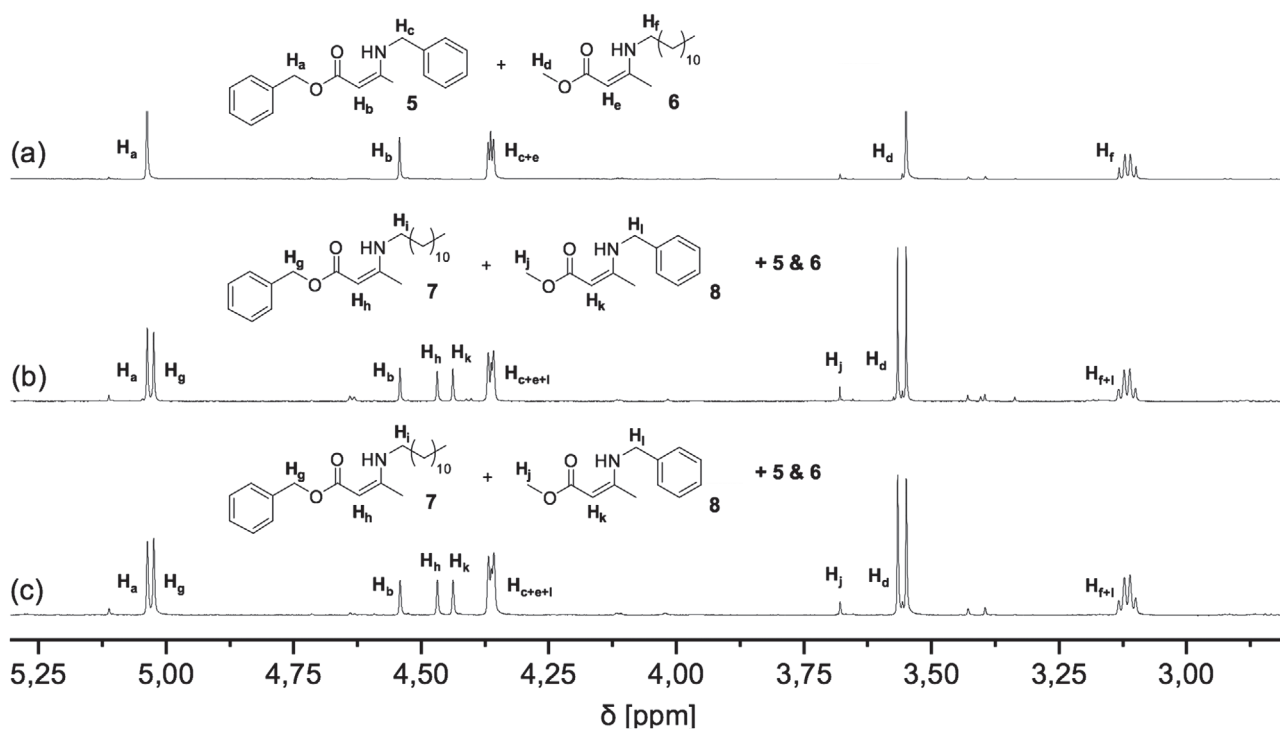
Figure 4. ^{1}H NMR-spectra of the model compound exchange reaction for the acid-mediated autocatalysis in vinylogous urethanes in comparison to a reference spectrum. a) ^{1}H NMR-spectrum of the reactants **5** and **6** before heating. b) ^{1}H NMR-spectrum of the products **5**, **6**, **7**, and **8** equilibrated after stirring for 7 h at 140 °C. c) ^{1}H NMR-spectrum of the reference with compounds **5**, **6**, **7**, and **8** in the same concentration.

**ADVANCED
SCIENCE NEWS**
www.advancedsciencenews.com

**Macromolecular
Rapid Communications**
www.mrc-journal.de
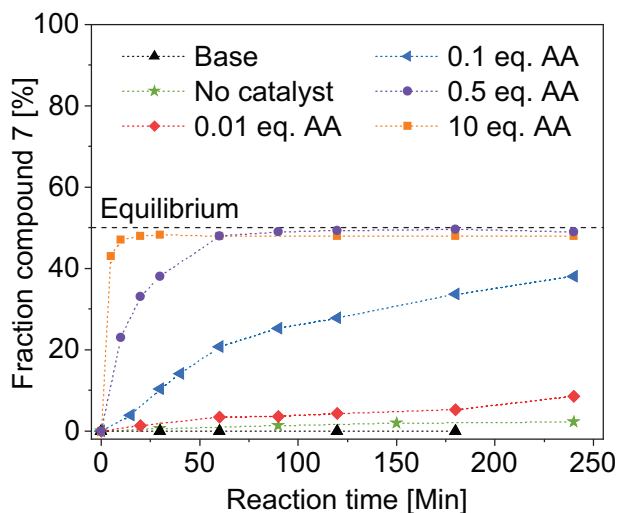
Figure 5. Conversions using different equivalents of acetic acid (AA) as catalyst. An increased amount of acid accelerated the exchange reaction, while the addition of a base quenched the reaction.

residues of the enamine-one species as well. The predominant enamine-one species is resistant to hydrolysis due to the weak electrophilicity of the conjugated C=C bond, which enables the condensation reaction of acetoacetates and amines even in aqueous medium. However, the protonated iminium-one shows a significant higher electrophilicity and undergoes hydrolysis reactions. Thereby, the concentration of the electrophilic, protonated iminium-one is a decisive factor and depends on the amount of acid catalyst in the experiment. In order to examine the influence of water, another exchange experiment was carried out. An enamine-one (**5**) was synthesized with dodecylamine and an excess of methylacetoacetate (1.2 eq.) and dried in vacuo, with the excess of acetoacetates saturating all free amines. Next, an excess of benzylacetoacetate (1 eq.) (**9**) was added to the mixture and stirred for 6 h at 80 °C in xylene. The backward reaction of the protonated iminium-one and water produces free dodecylamine, which then undergo a fast condensation reaction with the excess of benzylacetoacetate (**9**), that is, another enamine-one (**7**) (**Figure 6**). ^{1}H NMR spectra clearly show the formation of compound **7**, leading to an equilibrium state of the involved acetoacetates (Figure S14, Supporting Information). This proves that the backward reaction with water play a major role for the enamine-one exchange reaction, even if the mixture contains just traces of water. Furthermore, it was found that the addition of acetic acid accelerated the equilibration, which can be explained by the fact, that the concentration of the electrophilic iminium-one was increased and thus made a nucleophilic attack of water more likely (Figure S15, Supporting Information).

To prove a catalyst effect of water, the enamine-one exchange reaction was carried out with different amounts of water and stirred for 11 h at 120 °C (Figure 3). Therefore, one part of the mixture was dried in vacuo (oil pump) for 2 h and the exchange reaction was carried out under nitrogen atmosphere. The second part of the mixture was dried after the synthesis of the involved enamine-ones, but stirred under atmospheric

conditions during the exchange reaction, while 1 eq. of water was added to a third part. The results show a faster equilibration with increased amount of water. Interestingly, part one, which was dried in vacuo and contained just traces of water, shows a sigmoidal conversion. This behavior can be attributed to an autocatalysis. The amount of the electrophilic iminium-one and nucleophilic water is extremely low, giving a slow release of free amines and the resulting transimination reactions. If the amount of the electrophilic iminium-one was increased through an acid catalyst or a higher amount of water was present, the autocatalytic behavior could not be observed due to an instant release of free amines (**Figure 7**). Moreover, a model compound exchange experiment with the equilibration of acetoacetates (Figure 6) showed the same sigmoidal curve with a similar conversion rate under dry conditions (Figure S16, Supporting Information). Finally, this result proves that the acid-mediated autocatalyzed transimination reaction is initiated even by traces of water and seems to be the only exchange pathway for enamine-ones. As it is reported for imines, no direct, acid catalyzed imine metathesis pathway was observed.[24a] The amine catalyzed imine metathesis for aromatic imines was investigated by Stefano and co-workers. Interestingly, the group observed an autocatalytic behavior exploring the imine-equilibration in experiments without additional free amines, accompanied by low concentrations of free reactants after a few hours of reaction time. However, they proposed that a low concentration of water is capable for a dissociation reaction giving free amines, which in turn catalyze the imine metathesis exchange reactions.[25b,26] These findings support our investigations for the autocatalyzed transimination reactions in vinylogous urethane vitrimers.

In order to determine the activation energies of the exchange reaction, compounds **5** and **6** were mixed with an excess of
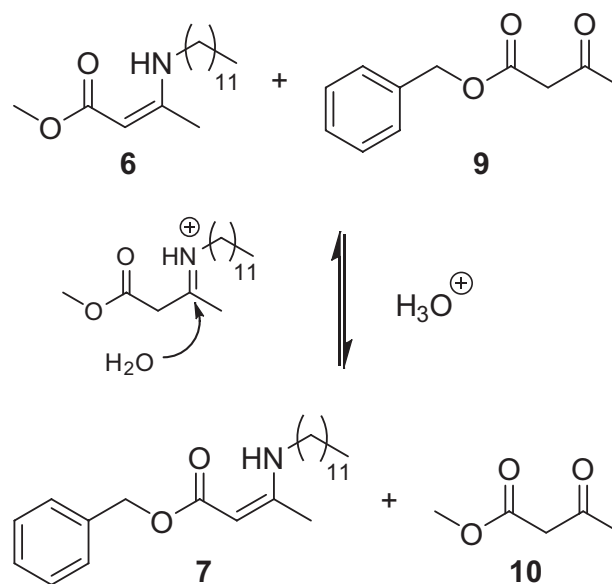
Figure 6. Model compound experiment to determine the role of water for the exchange reactions. The backward reaction of the protonated iminium-one with water leads to the formation of free methylacetoacetate and dodecylamine, which undergo a renewed condensation reaction with the excess of benzylacetoacetate, thus giving another enamine-one.

2000273 (5 of 12)

**ADVANCED
SCIENCE NEWS**
www.advancedsciencenews.com

**Macromolecular
Rapid Communications**
www.mrc-journal.de
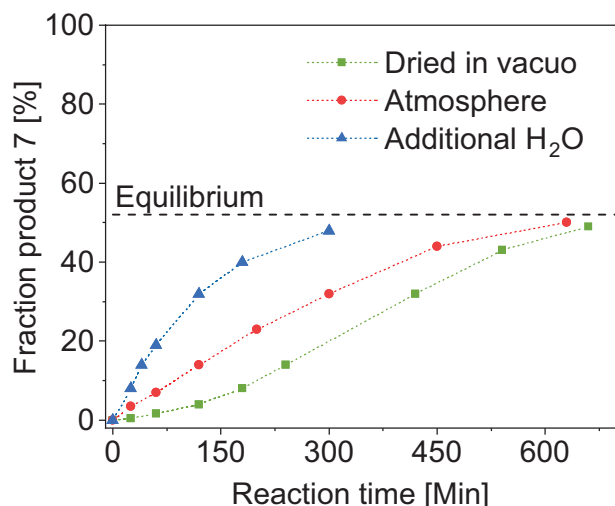
Figure 7. Conversions of the autocatalyzed enamine-one exchange reaction (Figure 3) using different amounts of water. A sigmoidal curve is observed in the experiments containing low amounts of water, showing the autocatalytic behavior of this exchange mechanism (dried in vacuo). With increased amount of water, the amines were liberated almost instantly.

compound **6** to ensure a pseudo first order kinetics at low conversions. Since the exchange reaction results in an equilibrium state, the backward reaction became significant at high conversions. The reactions were carried out in xylene at 60, 80, and 100 °C. The conversion of reactant **7** was plotted against the reaction time (**Figure 8**). Next, first order kinetics at low conversions were fitted and used to determine the initial rates of the conversion curves. (Figure S17, Supporting Information). The activation energy was obtained using an Arrhenius law. (Equation (S1) and Figure S18, Supporting Information).[13b,29]

With this, an activation energy of 54 kJ mol^{-1} was calculated for the exchange reaction of the enamine-ones. For
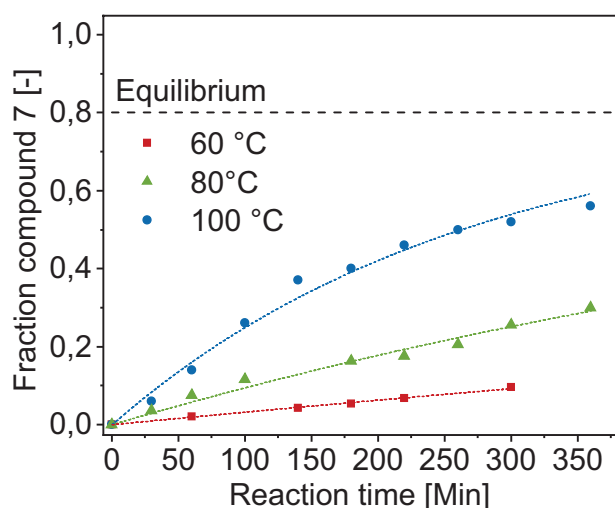
Figure 8. Schematic representation of the enamine-one model exchange reaction of compounds **5** and **6** (Figure 3). Conversion of **7** during the exchange reaction at 60, 80, and 100 °C in xylene.

comparison, the activation energy of the transimination reaction with an excess of free primary amines was calculated using an Arrhenius law as well. Doing so, the enamine-one methyl 3-(benzylamino)but-2-enoate (**11**) was mixed with an excess of dodecylamine (**12**) to ensure a pseudo first order kinetics. The solution was stirred for 3 h at 100, 120, and 140 °C, respectively, in xylene and characterized by ^{1}H NMR spectroscopy in different time intervals (Figure S19, Supporting Information). The conversions of compound **11** were plotted against the reaction time (Figure S20, Supporting Information). Next, a first order law was fitted at low conversions and the initial rates were determined. (Figure S21, Supporting Information).[29] With this, an activation energy of 60 kJ mol^{-1} was calculated by using an Arrhenius law (Equation (S1) and Figure S22, Supporting Information).[13b,29] Du Prez and co-workers determined the activation energy for vinylogous urethanes by a similar model experiment, with a calculated activation energy of 59 kJ mol^{-1}, which agrees well with our result.[13b] Regarding the calculated activation energies, the experiment showed that the exchange reaction proceeds via the protic iminium pathway, even if no additional catalyst was added.[30]

In comparison, the transimination reaction with additional free amines and the exchange reaction of the enamine-ones without additional free amines show similar calculated activation energies. This supports the hypothesis that the reactions proceed via the same transition state and proves that the transamination reactions proceed with an excess of free amines or by acid-mediated autocatalysis.

The calculated activation energies are comparable to values reported for imine metathesis and transimination reactions of aromatic imines (64 kJ mol^{-1}).[14] Furthermore, it is reported that an imine metathesis in aromatic and aliphatic imines can proceed without an additional catalyst and at moderate temperatures, with calculated activation energies of 48–89 kJ mol^{-1}.[14,18,20c,25a,25b,31] In comparison, our calculated activation energies of 54–60 kJ mol^{-1} are in good agreement, but nevertheless the mechanism is based on a fast acid-mediated autocatalysis reaction, which enables a transimination reaction. A direct exchange mechanism of the enamine-one species was not observed.

Vinylogous urethane networks were prepared using the condensation reaction between acetoacetates and primary amines following the work of Winne and co-workers.[13b] A wide range of polyacetoacetate monomers can be easily prepared from broadly available polyols.[32] A combination of these monomers with various commercially available polyamine monomers gives access to a wide selection of poly(vinylogous urethane) vitrimers. Hexane-1,6-diylbis(3-oxobutanoate) and tris(2-aminoethyl)amine (TREN) as trifunctional crosslinking agent were used as monomers. In addition, *para*-toluenesulfonic acid (*p*-TsOH) was used as catalyst in selected vitrimers. The condensation reaction between primary amines and acetoacetates already occurs at room temperature and generates one equivalent of water that needs to be removed. For this reason, the vitrimeric networks were cured in vacuo at 100 °C for 20 h and then postcured for 30 min at 150 °C to ensure full curing and removal of water. The stoichiometry of the functional groups is an important factor in the prepared poly(vinylogous urethane)

**ADVANCED
SCIENCE NEWS**
www.advancedsciencenews.com

**Macromolecular
Rapid Communications**
www.mrc-journal.de
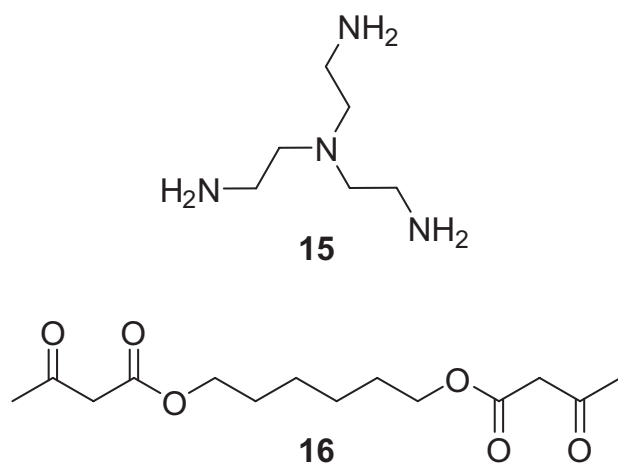
Figure 9. Schematic representation of the used monomers to synthesize the poly(vinylogous urethane) networks. Hexane-1,6-diylbis(3-oxobutanoate) (**16**) and tris(2-aminoethyl)amine (TREN) (**15**) were mixed in different ratios to obtain **VU-A**, **VU-A$_{H+}$**, **VU-E$_{H+}$**, **VU-NA**, and **VU-NA$_{H+}$** with an excess of amines or acetoacetates and p-TsOH as catalyst.

networks. The availability of free primary amines leads to transimination reactions, which are strongly accelerating the reorganization process in the vitrimeric network. Nevertheless, synthesizing a network with an excess of amines or acetoacetates implies working under nonstoichiometric conditions, which affects the network topology. For this reason, a compromise between rearrangement rate and a resilient network integrity (gel point) must be made.

For further investigations of the exchange reactions in poly(vinylogous urethanes), different vitrimers with bisacetoacetate (**16**) and TREN (**15**) as crosslinking agent were synthesized (**Figure 9**). For comparison, vitrimeric networks with an acetoacetate to amine ratio (R) of $R = 0.7$ (excess of amines) and $R = 1.35$ (excess of acetoacetates) were prepared. This ratio provides nonstoichiometric crosslinking while maintaining the integrity of the polymer networks. As described in literature, vitrimeric networks with free primary amines undergo rapid transimination reactions, which can be highly accelerated by using a Brønsted acid as catalyst.[13b,30,33]

Since networks with a high excess of acetoacetates contain low amounts of free amines, another mechanism is considered as exchange pathway in these networks. To investigate that, five different vinylogous urethane vitrimers were prepared. **VU-A** with an excess of amines ($R = 0.7$), **VU-A$_{H+}$** with an excess of amines ($R = 0.7$) and 0.05 wt% p-TsOH as catalyst, **VU-E$_{H+}$** with an equal ratio of amines and acetoacetates ($R = 1.0$) and 0.05 wt% p-TsOH, **VU-NA** with an excess of acetoacetates ($R = 1.35$) and **VU-NA$_{H+}$** with an excess of acetoacetates ($R = 1.35$) and 0.05 wt% p-TsOH.

ATR-FT-IR measurements proved the formation of the vitrimers by measuring the respective C=O ester (1650 cm^{-1}) and C=C band (1602 cm^{-1}) as well as the C=O ester (1735 cm^{-1}) and C=O ketone band (1724 cm^{-1}) of the acetoacetate monomer in networks with an excess of acetoacetates (Figure S23, Supporting Information).

In terms of a thermomechanical classification elastomeric and thermosetting vinylogous urethane vitrimers with glass

transition temperatures (T_g) of 13 °C (**VU-A**), 17 °C (**VU-A$_{H+}$**), −8 °C (**VU-NA**), 29 °C (**VU-NA$_{H+}$**), and 51 °C (**VU-E$_{H+}$**) were synthesized (T_g on-set obtained by differential scanning calorimetry, DSC) (Figure S24, Supporting Information). As expected, the vitrimers synthesized under highly nonstoichiometric ratios showed a low T_g, in comparison to **VU-E$_{H+}$**, which was synthesized with equimolar fractions of amines and acetoacetates (thermosetting vitrimer). The thermomechanical classification of vinylogous urethane vitrimers can be facilely adjusted by a variation of the monomers and stoichiometry. Regarding that, elastomeric vinylogous urethane vitrimers were synthesized by using bulky amine- and acetoacetate-functionalized molecules and polymers like pripol-, poly(propylene-glycol)-, or perfluoropolyether-derivates as described in literature.[15,30] Admittedly, these elastomeric vinylogous urethane vitrimers have lower glass transitions temperatures (−100–5 °C) than ours, but show comparable stress relaxation times (acid catalyzed and noncatalyzed).[15,30] This shows that elastomeric vitrimers can be synthesized by using easily accessible, low molecular weight molecules as monomers, instead of bulky ones. Furthermore, the thermal stability was investigated by thermal gravimetric analysis (TGA) measurements and showed degradation points up to 281 °C (**VU-A**), 226 °C (**VU-A$_{H+}$**), 222 °C (**VU-E$_{H+}$**), 251 °C (**VU-NA**), and 220 °C (**VU-NA$_{H+}$**) under oxygen atmosphere with no significant change by measuring under nitrogen atmosphere (Figure S25, Supporting Information). Interestingly, the vitrimer with an excess of amines and without catalyst (**VU-A**) is the most stable one, while the vitrimer with an excess of acetoacetates (**VU-NA**) showed a 30 °C lower degradation point. In addition, the vitrimers with additional p-TsOH (**VU-A$_{H+}$**, **VU-NA$_{H+}$**, **VU-E$_{H+}$**) showed significantly lower degradation points with a difference of ≈60 °C compared to the most stable one. Consequently, it can be assumed that p-TsOH is accelerating the degradation process. In addition, **VU-E$_{H+}$** ($R = 1$) showed the least mass loss until the degradation point, which can be explained by its tight network topology.

For further investigations of the mechanical properties, temperature dependent dynamical-mechanical analysis (DMA) measurements were carried out and showed similar storage moduli of 0.3–0.7 GPa and rubbery plateaus of 0.2–4 MPa for the synthesized vitrimers (Figures S26–S30, Supporting Information). Moreover, stress relaxation experiments were carried out at different temperatures to examine the exchange mechanisms in these networks and an Arrhenius law was used to calculate the activation energies. The stress relaxation experiments were measured with a torsional deformation of 1% and the relaxation modulus was recorded as a function of time in the range of 90–160 °C. According to the Maxwell model of viscoelastic fluids the relaxation times were determined at 37% (1/e) of the normalized stress relaxation modulus.[13b] According to literature, a dual temperature response was measured by stress relaxation experiments using a low amount of amine or Brønsted acid in the formulation of the vitrimers.[30] This response can be attributed to two different exchange mechanisms. A protic iminium pathway (transimination) with an activation energy of 60–102 kJ mol^{-1} and an aprotic Michael-type pathway (transamination) with an activation energy of 99–141 kJ mol^{-1}.[15,30,34] In addition, the protic iminium pathway

ADVANCED
SCIENCE NEWS
www.advancedsciencenews.com

Macromolecular
Rapid Communications
www.mrc-journal.de
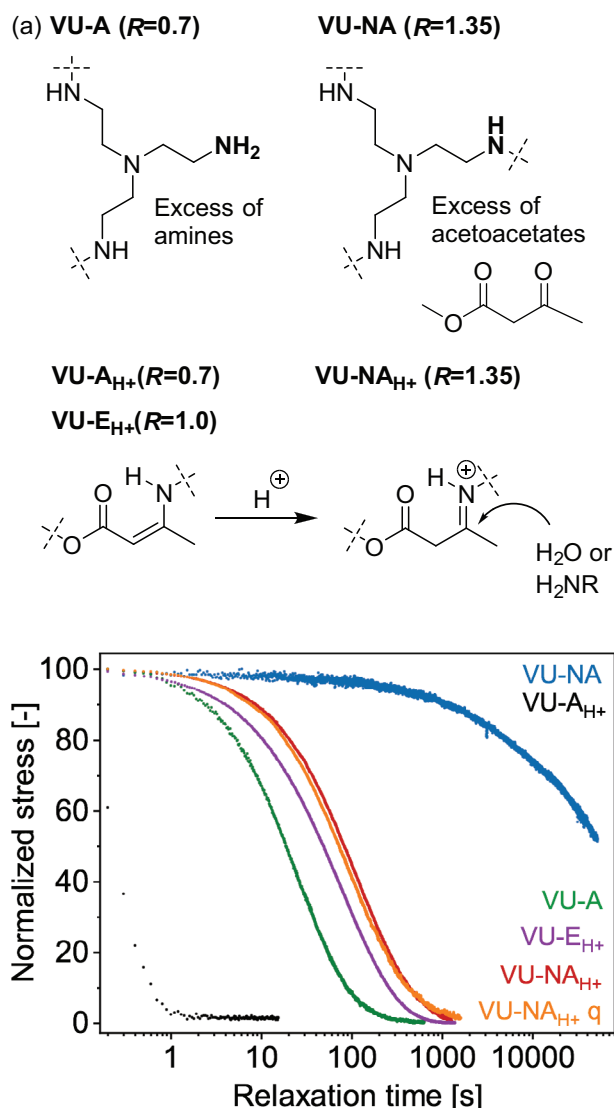
Figure 10. Normalized stress relaxation curves of the considered vinylogous urethane vitrimers at 110 °C to prove the underlying exchange mechanism. Without amines and acid catalyst (**VU-NA**) long relaxation of >13 h could be measured. In networks with free amines (**VU-A**) and additional catalyst (**VU-A$_{H+}$** and **VU-E$_{H+}$**) short relaxation times were observed, which can be attributed to fast transamination and transimination reactions (0.3–80 s). Most interesting, **VU-NA$_{H+}$** showed a relatively short relaxation time of 134 s in comparison to **VU-NA** (>13 h). In addition, another quenching step (by adding methylacetoacetate) did not change the relaxation times significantly (123 s). This behavior can be attributed to acid-mediated autocatalyzed transimination reactions in network **VU-NA$_{H+}$**.

is supposed to be the predominant exchange mechanism, at least if a high excess of free primary amines or a Brønsted acid as catalyst is used in the temperature range of 90–160 °C.[30]

For the investigation of the exchange mechanisms, the normalized stress relaxation curves of the vitrimers at 110 °C are shown in **Figure 10**. In networks without additional Brønsted acid the concentration of the protonated iminium-one (electrophile) is quite low. Therefore, networks with an excess of free amines undergo transimination, showing a stress relaxation

time of 29 s (**VU-A**). On the contrary, vitrimer **VU-NA** contains a high excess of acetoacetates, which means there are almost no free amines left in the network. In addition, the concentration of the electrophilic protonated iminium-one is likewise low. Hence, the network showed long relaxation times over 15 h.

Preparing networks with a Brønsted acid means that the concentration of the protonated iminium-one is highly increased and the protic exchange mechanisms are preferred.

VU-A$_{H+}$ was synthesized with an excess of free amines ($R = 0.7$) and p-TsOH and showed extremely short relaxation times of 0.3 s at 110 °C, which can be attributed to fast transimination reactions with a huge excess of free amines as strong nucleophiles.[30,33] Interestingly, the network **VU-NA$_{H+}$**, with an excess of acetoacetates ($R = 1.35$) and p-TsOH showed relatively short relaxation times of 134 s, compared to **VU-NA** without an acid catalyst (>15 h). This can be explained by the fact that the concentration of the electrophilic iminium-one was highly increased and nucleophilic attacks occurred much more likely. To prove that all amines were saturated, **VU-NA$_{H+}$** was swelled in tetrahydrofuran (THF) and a high concentration of methylacetoacetate was added to quench free amines. After swelling for 3 h and drying in vacuo for 8 h at 100 °C, the stress relaxation was measured at 110 °C once again. Apparently, no significant change was measured regarding **VU-NA$_{H+}$** (134 s) and **VU-NA$_{H+quenched}$** (123 s). This behavior was incidentally reported in studies on quenching free amine groups in polydimethylsiloxane polymers with methylacetoacetates, without exploring this finding in further detail.[35]

For further comparisons, the activation energies of the vitrimers were determined from stress relaxation measurements at different temperatures (Figures S31–S35, Supporting Information). Activation energies of 75.9 kJ mol^{-1} (**VU-A**), 60.3 kJ mol^{-1} (**VU-A$_{H+}$**), 84.9 kJ mol^{-1} (**VU-E$_{H+}$**), and 75.8 kJ mol^{-1} (**VU-NA$_{H+}$**) were calculated (**Figure 11**). An estimation for **VU-NA** was impossible due to long relaxation times and the related problems during processing (cracks in the material).
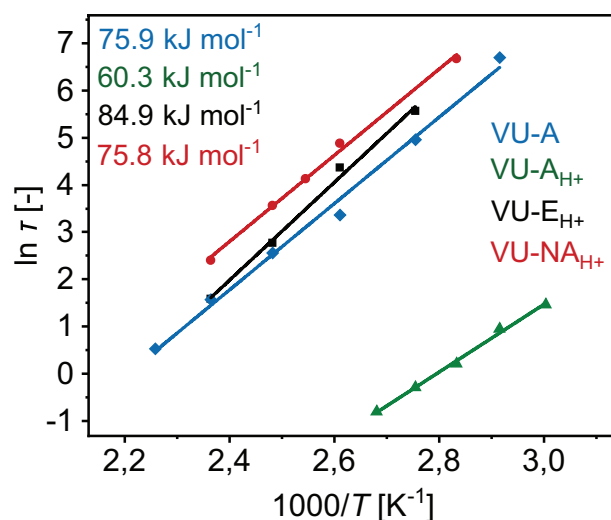
Figure 11. Arrhenius fit by using the normalized stress relaxation times (37%) at different temperatures to determine the activation energies of the respective vitrimers. Activation energies of 60.3–85.9 kJ mol^{-1} were calculated.

**ADVANCED
SCIENCE NEWS**

www.advancedsciencenews.com

**Macromolecular
Rapid Communications**

www.mrc-journal.de

According to literature, activation energies of 60–102 kJ mol^{-1} are typical for vinylogous urethane vitrimers.[13b,15,30] Our observations are hence in good agreement with the reported values. As investigated in the model compound studies, even small amounts of water combined with an acid catalyst enable fast backward reactions, thus releasing free amines for fast transimination reactions. Even if the poly(vinylogous urethane) networks synthesized by a condensation reaction were postcured in vacuo for a long time, traces of water will always remain in the network. In summary, these findings lead to the conclusion that in vitrimers with an excess of acetoacetate and additional acid as catalyst, fast depolymerization, polymerization (condensation reaction), and transimination reactions occur and ensure a fast exchange compared to networks without acid catalyst.

The acid induced imine-enamine tautomerism and *cis–trans* equilibration were examined as fundamental mechanisms in vinylogous urethanes. In addition, an acid-mediated autocatalysis was investigated as exchange pathway for this type of vitrimer. Vinylogous urethanes are highly stabilized as *cis*-enamine-one, because of an intrinsic conjugated Michael system and intramolecular hydrogen bonds. We explored, that the thermodynamic preference for the *cis*- and *trans*-stereoisomer depends on the polarity and proton donation ability of the solvent, while the preference for the *cis*-isomer was least in DMSO and highly pronounced in benzene. Furthermore, the kinetics of acid-mediated autocatalyzed transimination reactions were examined using low molecular model compounds, while the decisive roles of Brønsted catalyst and remaining water were of major interest for the exchange mechanism. Enamine-one species with different residues on both sides of the enamine bond showed a fast exchange of the residues during stirring at elevated temperatures. In addition, poly(vinylogous urethane) networks with and without additional free amine groups and *p*-toluenesulfonic acid as catalyst were prepared and proved short relaxation times even in networks without additional free amines. This evidences the decisive role of water, acid catalysts, or other protic donors for the exchange mechanisms in vinylogous urethane vitrimers.

Moreover, novel elastomeric and thermosetting poly(vinylogous urethane) networks with glass transition temperatures of −8–19 °C, thermal stabilities up to 220–281 °C, storage moduli of 0.2–0.7 GPa, rubbery plateaus of 0.2–4 MPa, and stress-relaxation times of 0.3–54 000 s at 110 °C are presented by using adjustable nonstoichiometric crosslinking. The investigations of the acid-mediated autocatalyzed transimination reactions in vinylogous urethane vitrimers underline the outstanding properties of this type of vitrimers, which form highly resilient, but nevertheless crosslinked materials.

Experimental Section

Chemicals: Hexylamine (99%), *para*-toluene sulfonic acid monohydrate (99%), trifluoroacetic acid (99%), and *tert*-butyl-acetoacetate (≥98%) were purchased from Sigma-Aldrich. Benzylamine (≥99%) and benzylacetoacetate (≥95%) were obtained from TCI Deutschland GmbH. Methylacetoacetate (≥99%) and tris(2-aminoethyl)amine (97%) were purchased from Alfa Aesar. Ethylacetoacetate (98%) and 1,6-hexanediol (≥97%) were purchased from MERCK KG aA. Acetic acid (95%) was obtained by VWR and dodecylamine (≥98%) was purchased from Fluka.

Sodiumacetate (99%) was purchased from pro analysis. Xylene (99%, isomeric mixture) and MgSO$_4$ (99%) were purchased from Grüssing. Benzene-d_6, DMSO-d_6, methanol-d_4, and CDCl$_3$ were purchased from Deutero GmbH.

Instrumentation: Proton nuclear magnetic resonance (^{1}H NMR, ^{13}C NMR and COSY, HSQC, HMBC, NOESY) spectra were recorded on a Bruker AVANCEII (Bruker BioSpin GmbH, Karlsruhe, Germany) at 400–600 MHz. Tetramethylsilane was used as internal standard and chloroform-d_1 (CDCl$_3$), benzene-d_6, dioxane-d_8, or DMSO-d_6 were used as solvents. Sample concentration was between 10 and 20 mg mL^{-1}. Measurements were usually recorded at 300 K (excluded temperature-dependent measurements). Data processing was carried out with MestReNova (Version 9.0.1, Mestrelab Research S.L., Santiago de Compostela, Spain).

FT-IR spectra were recorded on a Bruker FT-IR Vertex 70 (Bruker, Ettlingen, Germany) with a diamond ATR-probe. The measuring software was Opus 7.5. All samples were measured in the range of 3600–600 cm^{-1} with a resolution of 2 cm^{-1} and 32 scans.

For thermogravimetric analysis a TGA 209 F1 Iris (NETZSCH-Gerätebau GmbH, Selb, Germany) was used to determine the mass loss during heat treatment. A temperature range of 25–600 °C with a heating rate of 10 K min^{-1} was chosen. About 5–10 mg of polymer were weighed into a ceramic crucible. Dynamic air and nitrogen atmosphere were used with a flow rate of 20 mL min^{-1}. Data processing was performed with Proteus analysis (NETZSCH-Gerätebau GmbH, Selb, Germany).

To determine the glass transition temperature (T_g) of the vinylogous urethane vitrimers, a differential scanning calorimeter DSC 204 F1 Phoenix (NETZSCH-Gerätebau GmbH, Selb, Germany) was used. Therefore, 5–10 mg polymer was weighed into an aluminum crucible. The measurements were performed at one bar under nitrogen atmosphere (flow rate of 20 mL min^{-1}) in the temperature range between −50 and 150 °C. The heating and cooling rates were 10 K min^{-1}. The thermal properties were analyzed using the DSC data of the second and third heating curve. Data processing was performed by Proteus analysis (NETZSCH-Gerätebau GmbH, Selb, Germany).

For oscillatory shear experiments, a rotational rheometer (MCR 502, Anton Paar GmbH, Graz, Austria) with a 8 mm plate-plate geometry and a heat chamber with nitrogen atmosphere was used. The temperature was controlled by a Peltier plate and by a constant nitrogen flow into the chamber. The gap between the lower and the upper plate was set to 1.0 mm. Amplitude sweeps between 0.01% and 1% shear strain (*g*) at a constant angular frequency (*w*) of 10 rad s^{-1} were carried out at 110 °C before each measurement, This should ensure that the chosen strain amplitude g_0 was inside the linear viscoelastic regime, so that the storage modulus *G′* and the loss modulus *G″* were independent of strain. The temperature-dependent measurements were carried out at 10 rad s^{-1} and a deformation of 0.1 %. The temperature was first raised from 90 to 160 °C. at a rate of 2 K min^{-1} and, after a waiting period of five minutes, decreased from 160 to 20 °C. One measuring point per 1 K was recorded. The gap was kept constant during measurement.

The stress relaxation experiments were carried out with a deformation of 1% and the relaxation module was recorded as a function of time. The comparative measurements were carried out in temperature ranges of 50–170 °C. Data processing was performed by RheoCompass software (version 1.19.266, Anton Paar GmbH, Graz, Austria).

The test specimens for the dynamic-mechanical analysis and the relaxation tests were pushed out with an 8 mm punch. The vitrimer plates were previously placed in a drying chamber at 100 °C for a few seconds in order to heat them above the glass transition temperature to prevent splintering during processing.

Synthetic Procedures—Ethyl(cis)-3-(hexylamino)but-2-enoate and Ethyl(trans)-3-(hexylamino)but-2-enoate: Ethylacetoacetate (1.08 g, 0.0078 м) and hexylamine (1.02 mL, 0.0078 mol) were stirred for 4 h at room temperature. When the formation of the vinylogous urethane was complete (^{1}H NMR, FT-IR), water and excess reactants were removed in vacuo yielding the desired product.

Yield of Ethyl(cis)-3-(hexylamino)but-2-enoate and Ethyl(trans)-3-(hexylamino)but-2-enoate Stereoisomers: 97%, 1.61 g: Ethyl(cis)-3-(hexylamino)but-2-enoate: ^{1}H NMR (500 MHz, CDCl$_3$, δ): 8.50

(t, 1H; NH), 4.36 (s, 1H; CH), 4.14 (q, $J = 6.62$ Hz, 2H; CH$_2$), 3.12 (q, $J = 6.41$ Hz,2H; CH$_2$), 1.84 (s, 3H; CH$_3$), 1.53–1.43 (m, 2H; CH$_2$), 1.33–1.13 (m, 6H; CH$_2$), 1.18 (t, $J = 7.08$ Hz, 3H; CH$_3$), 0.82 (t, $J = 7.50$ Hz, 3H; CH$_3$).

Ethyl(cis)-3-(hexylamino)but-2-enoate: ^{1}H NMR (600 MHz, benzene-d_6, δ): 8.99 (s, 1H; NH), 4.78 (s, 1H; CH), 4.20 (q, $J = 6.97$ Hz, 2H; CH$_2$), 2.60 (q, $J = 5.77$ Hz, 2H; CH$_2$), 1.42 (s, 3H; CH$_3$), 1.17–1.09 (m, 2H; CH$_2$), 1.09–0.99 (m, 6H; CH$_2$), 1.13 (t, $J = 8.15$ Hz, 3H; CH$_3$), 0.83 (t, $J = 7.19$ Hz, 3H; CH$_3$).

Ethyl(cis)-3-(hexylamino)but-2-enoate: ^{1}H NMR (600 MHz, methanol-d_4, δ): 8.50 (1H; NH), 4.41 (s, 1H; CH), 4.03 (q, $J = 7.45$ Hz, 2H; CH$_2$), 3.26 (t, $J = 6.92$ Hz, 2H; CH$_2$), 1.94 (s, 3H; CH$_3$), 1.65–1.51 (m, 2H: CH$_2$), 1.49–1.30 (m, 6H; CH$_2$), 1.23 (t, $J = 7.16$ Hz, 3H; CH$_3$), 0.94 (t, $J = 7.29$ Hz, 3H; CH$_3$).

Ethyl(cis)-3-(hexylamino)but-2-enoate: ^{1}H NMR (600 MHz, DMSO-d_6, δ): 8.50 (t, $J = 5.37$ Hz, 1H; CH), 4.32 (s, 1H), 3.95 (q, $J = 7.10$ Hz, 2H; CH$_2$), 3.18 (q, $J = 6.92$ Hz, 2H; CH$_2$), 1.88 (s, 3H; CH$_3$), 1.52–1.43 (m, 2H, CH$_2$), 1.33–1.22 (m, 6H; CH$_2$), 1.13 (t, $J = 7.54$ Hz, 3H; CH$_3$), 0.87 (t, $J = 7.10$ Hz, 3H; CH$_3$).

Ethyl(cis)-3-(hexylamino)but-2-enoate: ^{13}C NMR (600 MHz, DMSO-d_6, δ): 169.9 (C=O), 162.6 (C4), 81.5 (C3), 57.9 (C2), 42.7 (C2), 31.5 (C2), 30.5 (HNC2), 26.9 (C2), 22.6 (C2), 19.4 (C1), 15.1 (C1), 14.4 (C1).

Ethyl(cis)-3-(hexylamino)but-2-enoate: ^{1}H NMR (600 MHz, no solvent, δ): 8.58 (t, $J = 5.87$ Hz, 1H; NH), 4.32 (s, 1H; CH), 3.94 (q, $J = 7.35$ Hz, 2H; CH$_2$), 3.10 (q, $J = 6.82$ Hz, 2H; CH$_2$), 1.81 (s, 3H; CH$_3$), 1.52–1.40 (m, 2H; CH$_2$), 1.33–1.20 (m, 6H; CH$_2$), 1.11 (t, $J = 7.60$ Hz, 3H; CH$_3$), 0.85 (t, $J = 7.20$ Hz, 3H; CH$_3$).

Ethyl(trans)-3-(hexylamino)but-2-enoate: ^{1}H NMR (500 MHz, CDCl$_3$, δ): 5.35 (t, 1H; NH), 4.52 (s, 1H; CH), 4.01 (q, $J = 7.24$ Hz, 2H; CH$_2$), 2.93 (q, $J = 5.00$ Hz, 2H; CH$_2$), 2.20 (s, 3H; CH$_3$), 1.53–1.42 (m, 2H; CH$_2$), 1.33–1.13 (m, 6H; CH$_2$), 1.18 (t, $J = 7.08$ Hz, 3H; CH$_3$), 0.82 (t, $J = 7.50$ Hz, 3H; CH$_3$).

Ethyl(trans)-3-(hexylamino)but-2-enoate: ^{1}H NMR (600 MHz, benzene-d_6, δ): 8.07 (s, 1H; NH), 4.91 (s, 1H; CH), 3.90 (q, $J = 7.00$ Hz, 2H), 2.50 (q, $J = 5.41$ Hz, 2H; CH$_2$), 2.24 (s, 3H; CH$_3$), 1.09–1.17 (m, 2H; CH$_2$), 1.09–0.99 (m, 6H; CH$_2$), 1.12 (t, $J = 8.15$ Hz, 3H; CH$_3$), 0.83 (t, $J = 7.19$ Hz, 3H; CH$_3$).

Ethyl(trans)-3-(hexylamino)but-2-enoate: ^{1}H NMR (600 MHz, methanol-d_4, δ): 6.28 (1H; NH), 4.52 (s, 1H; CH), 4.03 (q, $J = 7.45$ Hz, 2H; CH$_2$), 2.99 (t, $J = 8.16$ Hz, 2H; CH$_2$), 2.25 (s, 3H; CH$_3$), 1.65–1.51 (m, 2H; CH$_2$), 1.49–1.30 (m, 6H; CH$_2$), 1.24 (t, $J = 7.15$ Hz, 3H; CH$_3$), 0.94 (t, $J = 7.29$ Hz, 3H; CH$_3$).

Ethyl(trans)-3-(hexylamino)but-2-enoate: ^{1}H NMR (600 MHz, DMSO-d_6, δ): 6.64 (t, $J = 5.37$ Hz, 1H; NH), 4.34 (s, 1H; CH), 3.90 (q, $J = 7.02$ Hz, 2H; CH$_2$), 2.87 (q, $J = 6.71$ Hz, 2H; CH$_2$), 2.16 (s, 3H; CH$_3$), 1.52–1.42 (m, 2H ; CH$_2$), 1.33–1.22 (m, 6H; CH$_2$), 1.12 (t, $J = 7.54$ Hz, 3H; CH$_3$), 0.87 (t, $J = 7.10$ Hz, 3H; CH$_3$).

Ethyl(trans)-3-(hexylamino)but-2-enoate: ^{13}C NMR (600 MHz, DMSO-d_6, δ): 168.4 (C=O), 162.6 (C4), 80.5 (C3), 57.5 (C2), 43. 1 (C2), 31.5 (C2), 28.2 (NC2), 26.9 (C2), 22.6 (C2), 19.4 (C1), 15.1 (C1), 14.4 (C1).

Ethyl(trans)-3-(hexylamino)but-2-enoate: NMR (600 MHz, no solvent, δ): 5.36 (t, $J = 4.33$ Hz 1H), 4.45 (s, 1H), 4.06 (q, $J = 6.75$ Hz, 2H), 2.88 (q, $J = 6.31$ Hz, 2H), 2.20 (s, 3H), 1.52–1.40 (m, 2H), 1.33–1.20 (m, 6H), 1.11 (t, $J = 7.60$ Hz, 3H), 0.85 (t, $J = 7.20$ Hz, 3H).

Synthetic Procedures—Methyl-3-(dodecylamino)but-2-enoate, Benzyl-3-(benzylamino)but-2-enoate, Benzyl-3-(dodecylamino)but-2-enoate, and Methyl-3-(benzylamino)but-2-enoate: Methyl-,benzylacetoacetate (0.01 mol) and dodecyl-, benzylamine (0.01 mol) were stirred for 4 h at room temperature. When the formation of the vinylogous urethane was complete (^{1}H NMR, FT-IR), water and excess reactants were removed in vacuo yielding the desired product.

Yield of Methyl(cis)-3-(dodecylamino)but-2-enoate, Methyl(cis)-3-(benzylamino)but-2-enoate, Benzyl(cis)-3-(dodecylamino)butanoate, and Benzyl(cis)-3-(benzylamino)butanoate: 97%: *Methyl(cis)-3-(dodecylamino)but-2-enoate*: ^{1}H NMR (500 MHz, CDCl$_3$, δ): 8.47 (t, 1H; NH), 4.36 (s, 1H; CH), 3.55 (s, 3H; CH$_3$), 3.12 (q, $J = 6.02$ Hz, 2H; CH$_2$), 1.84 (s, 3H; CH$_3$), 1.53–1.44 (m, 2H; CH$_2$), 1.32–1.14 (m, 6H; CH$_2$), 0.81 (t, $J = 7.42$ Hz, 3H; CH$_3$).

Methyl(cis)-3-(benzylamino)but-2-enoate: ^{1}H-NMR (500 MHz, CDCl$_3$, δ): 8.86 (t, 1H; NH), 7.30–7.15 (m, 5H; Ar H), 4.46 (s, 1H; CH), 4.35 (d, $J = 6.07$ Hz, 2H; CH$_2$), 3.56 (s, 3H; CH$_3$), 1.83 (s, 3H; CH$_3$).

Benzyl(cis)-3-(benzylamino)but-2-enoate: ^{1}H NMR (400 MHz, CDCl$_3$, δ): 8.87 (t, 1H; NH), 7.34–7.14 (m, 10H; Ar H) 5.02 (s, 2H; CH$_2$), 4.54 (s, 1H; CH), 4.36 (d, $J = 5.94$ Hz, 2H; CH$_2$), 1.85 (s, 3H; CH$_3$).

Benzyl(cis)-3-(dodecylamino)but-2-enoate: ^{1}H NMR (500 MHz, CDCl$_3$, δ): 8.48 (t, 1H; NH), 7.33–7.13 (m, 10H; Ar H) 5.02 (s, 2H; CH$_2$), 4.44 (s, 1H; CH), 3.11 (q, $J = 6.78$ Hz, 2H), 1.85 (s, 3H; CH$_3$), 1.52–1.45 (m, 2H; CH$_2$), 1.30–1.13 (m, 6H; CH$_2$) 0.81 (t, $J = 7.29$ Hz, 3H; CH$_3$).

Hexane-1,6-diyl-bis(3-oxobutanoate): Hexanediol (54.1 g, 0.458 mol) and *tert*-butylacetoacetate (160 mL, 0.961 mol) were dissolved in 90 mL of xylene in a 500 mL flask. The mixture was heated for 200 min at 135 °C. The *tert*-butanol product was removed by distillation during the reaction. When the temperature in the still head dropped to 50 °C, xylene and the *tert*-butylacetoacetate were removed in vacuo. The resulting product crystallized after 24 h at room temperature. Repeated crystallization and decanting of the excess liquid phase yielded the desired product (transparent crystals). Yield: 60%, 78.59 g. ^{1}H NMR (400 MHz, CDCl$_3$, δ): 4.07 (t, $J = 6.64$ Hz, 2H; CH$_2$), 3.39 (s, 2H; CH$_2$), 2.20 (s, 3H; CH$_3$), 1.63–1.55 (m, 4H, CH$_2$), 1.36–1.28 (m, 4H; CH$_2$).

Model Compound Reactions (Autocatalysis): Benzyl-3-(benzylamino)but-2-enoate (2.4 mmol, 0.68 g) and methyl-3-(dodecylamino)but-2-enoate (9.6 mmol, 2.72 g) were dissolved in 2.43 mL xylene (or without solvent). Four equivalents of methyl-3-(dodecylamino)but-2-enoate were used to obtain a pseudo first order kinetic at low conversions. Different amounts of acetic acid (0–1000 mol%), natriumacetate (100 mol%), or trifluoracetic acid (high excess) were added to the solution mixture as catalyst/quenching agent. The solution was heated to 60–140 °C in a pressure-resistant, thick-walled 10 mL glass vials with rubber-sealed crimp caps and NMR samples (0.01 mL) were taken at different time intervals (measured in chloroform-d_1). The reaction was followed by integration of the two vinylic signals at 4.47 ppm (chloroform-d_1) and 4.54 ppm (chloroform-d_1) for dodecyl-3-(benzylamino)but-2-enoate and benzyl-3-(benzylamino)but-2-enoate, respectively.

Model Compound Reactions (Backward Reaction with Water): Methyl-3-(dodecylamino)but-2-enoate (2.4 mmol, 0.68 g) with an excess of methylacetoacetate (0.48 mmol, 0.06 g) was dissolved in 4.8 mL xylene (or without solvent) and benzylacetoacetate (2.4 mmol, 0.46 g) was added in an equal ratio to the mixture. The solution was heated to 80 and 120 °C in a pressure-resistant, thick-walled 10 mL glass vials with rubber-sealed crimp caps and NMR samples (0.01 mL) were taken at different time intervals (measured in chloroform-d_1). The reaction was followed by integration of the two vinylic signals at 4.47 ppm (chloroform-d_1) for benzyl-3-(dodecylamino)but-2-enoate, respectively.

Model Compound Reaction (Transimination, Excess of Free Amines): Benzylamine (6.84 mmol, 1.72 g) was added to a solution of methyl-3-(benzylamino)but-2-enoate (1.71 mmol, 0.352 g) in 8.55 mL xylene. Four equivalents of dodecylamine were used to obtain a pseudo first order kinetic at low conversions. The mixture was heated up to 100, 120, and 140 °C in a pressure-resistant, thick-walled 10 mL glass vials with rubber-sealed crimp caps and NMR samples (0.01 mL) were taken at different time intervals (measured in chloroform-d_1). The reaction was followed by integration of the two vinylic signals at 4.47 ppm (chloroform-d_1) and 4.37 ppm (chloroform-d_1) for methyl-3-(benzylamino)but-2-enoate and methyl-3-(dodecylamino)but-2-enoate model compounds, respectively.

Synthesis of the Vinylogous Urethane Vitrimers: According to literature the synthesis was slightly variated.[13b] **VU-A**: Hexane-1,6-diyl-bis(3-oxobutanoate) (4.00 g, 14.0 mmol) was provided in a rolled rim glass and heated up in an oil bath at 60 °C. Tris(2-aminoethyl)amine (1.985 mL, 13.27 mmol) was added under constant stirring. As soon as a homogeneous liquid mixture was obtained, the mixture was taken out of the oil under continues stirring. After a few seconds an opaque mass could be observed, which was filled onto a Teflon sheet and pressed for 10 min at 90 °C to a 2 mm plate. Afterward the plate was postcured for 20 h at 100 °C and 30 min at 150 °C, followed by pressing a 1 mm plate for 10 min at 150 °C.

VU-NA, **VU-A$_{H+}$**, and **VU-NA$_{H+}$** were synthesized under the same conditions. In the following, just the used amounts of monomers and

catalyst are shown. **VU-NA**: *Hexane-1,6-diyl-bis(3-oxobutanoate)* (4.00 g, 14.0 mmol) was provided in a rolled rim glass and tris(2-aminoethyl)amine (1.031 mL, 6.90 mmol) was added under constant stirring.

VU-A$_{H+}$: *Hexane-1,6-diyl-bis(3-oxobutanoate)* (3.27 g, 11.4 mmol) and *p*-toluene sulfonic acid (0.243 g, 0.05 wt%) monohydrate were provided in a rolled rim glass and tris(2-aminoethyl)amine (1.630 mL, 10.9 mmol) was added under constant stirring.

VU-NA$_{H+}$: *Hexane-1,6-diyl-bis(3-oxobutanoate)* (4.00 g, 14.0 mmol) and *p*-toluene sulfonic acid (0.250 g, 0.05 wt%) monohydrate were provided in a rolled rim glass and tris(2-aminoethyl)amine (1.031 mL, 6.90 mmol) was added under constant stirring.

Quenching VU-NA$_{H+}$: **VU-NA$_{H+}$** was placed in a high concentrated solution of methylacetoacetate in THF (1$_M$) at room temperature. After 3 h of swelling the vitrimer was taken and dried in vacuo at 100 °C for 8 h.

Conflict of Interest

The authors declare no conflict of interest.

[1] a) J.-P. Pascault, H. Sautereau, J. Verdu, R. J. Williams, *Thermosetting Polymers*, CRC Press, Florida, United States **2002**; b) A. D. McNaught, A. Wilkinson, *Compendium of Chemical Terminology*, Blackwell Science, Oxford **1997**.

[2] a) R. F. M. Lange, M. Van Gurp, E. W. Meijer, *J. Polym. Sci., Part A: Polym. Chem.* **1999**, *37*, 3657; b) W. P. Appel, M. M. Nieuwenhuizen, E. Meijer, *Supramol. Polym. Chem.* **2012**, *1*, 3; c) C. Hilger, R. Stadler, *Makromol. Chem.: Macromol. Chem. Phys.* **1990**, *191*, 1347; d) U. Seidel, J. Hellman, D. Schollmeyer, C. Hilger, R. Stadler, *Supramol. Sci.* **1995**, *2*, 45; e) M. J. Kunz, G. Hayn, R. Saf, W. H. Binder, *J. Polym. Sci., Part A: Polym. Chem.* **2004**, *42*, 661; f) W. H. Binder, R. Zirbs, in *Hydrogen Bonded Polymers* (Ed: W. Binder), Springer, Berlin, Germany **2007**, p. 1.

[3] M. Hernández, A. Grande, W. Dierkes, J. Bijleveld, S. Zwaag, S. García, *ACS Sustainable Chem. Eng.* **2016**, 4, 5776.

[4] a) C. J. Kloxin, C. N. Bowman, *Chem. Soc. Rev.* **2013**, *42*, 7161; b) C. J. Kloxin, T. F. Scott, B. J. Adzima, C. N. Bowman, *Macromolecules* **2010**, *43*, 2643; c) H. Yang, K. Yu, X. Mu, X. Shi, Y. Wei, Y. Guo, H. J. Qi, *Soft Matter* **2015**, *11*, 6305.

[5] a) A. Gandini, *Prog. Polym. Sci.* **2013**, *38*, 1; b) B. Strachota, A. Morand, J. Dybal, L. Matějka, *Polymers* **2019**, *11*, 930.

[6] a) W. Denissen, J. M. Winne, F. E. Du Prez, *Chem. Sci.* **2016**, *7*, 30; b) J. M. Winne, L. Leibler, F. E. Du Prez, *Polym. Chem.* **2019**, *10*, 6091.

[7] a) D. Montarnal, M. Capelot, F. Tournilhac, L. Leibler, *Science* **2011**, *334*, 965; b) M. Capelot, M. M. Unterlass, F. Tournilhac, L. Leibler, *ACS Macro Lett.* **2012**, *1*, 789; c) M. Capelot, D. Montarnal, F. Tournilhac, L. Leibler, *J. Am. Chem. Soc.* **2012**, *134*, 7664.

[8] B. Krishnakumar, R. V. S. P. Sanka, W. H. Binder, V. Parthasarthy, S. Rana, N. Karak, *Chem. Eng. J.* **2020**, *385*, 123820.

[9] M. M. Obadia, B. P. Mudraboyina, A. Serghei, D. Montarnal, E. Drockenmuller, *J. Am. Chem. Soc.* **2015**, *137*, 6078.

[10] R. L. Snyder, D. J. Fortman, G. X. De Hoe, M. A. Hillmyer, W. R. Dichtel, *Macromolecules* **2018**, *51*, 389.

[11] D. J. Fortman, J. P. Brutman, M. A. Hillmyer, W. R. Dichtel, *J. Appl. Polym. Sci.* **2017**, *134*, 44984.

[12] M. Pepels, I. Filot, B. Klumperman, H. Goossens, *Polym. Chem.* **2013**, *4*, 4955.

[13] a) Y. Spiesschaert, M. Guerre, L. Imbernon, J. M. Winne, F. Du Prez, *Polymer* **2019**, *172*, 239; b) W. Denissen, G. Rivero, R. Nicolaÿ, L. Leibler, J. M. Winne, F. E. Du Prez, *Adv. Funct. Mater.* **2015**, *25*, 2451; c) W. Denissen, I. De Baere, W. Van Paepegem, L. Leibler, J. Winne, F. E. Du Prez, *Macromolecules* **2018**, *51*, 2054.

[14] S. Dhers, G. Vantomme, L. Avérous, *Green Chem.* **2019**, *21*, 1596.

[15] M. Guerre, C. Taplan, R. Nicolaÿ, J. M. Winne, F. E. Du Prez, *J. Am. Chem. Soc.* **2018**, *140*, 13272.

[16] a) J. Canadell, H. Goossens, B. Klumperman, *Macromolecules* **2011**, *44*, 2536; b) U. Lafont, H. van Zeijl, S. van der Zwaag, *ACS Appl. Mater. Interfaces* **2012**, *4*, 6280; c) Y. Amamoto, H. Otsuka, A. Takahara, K. Matyjaszewski, *Adv. Mater.* **2012**, *24*, 3975.

[17] a) R. Martin, A. Rekondo, A. R. de Luzuriaga, G. Cabañero, H. J. Grande, I. Odriozola, *J. Mater. Chem. A* **2014**, *2*, 5710; b) Y.-X. Lu, F. Tournilhac, L. Leibler, Z. Guan, *J. Am. Chem. Soc.* **2012**, *134*, 8424.

[18] a) Z. Q. Lei, P. Xie, M. Z. Rong, M. Q. Zhang, *J. Mater. Chem. A* **2015**, *3*, 19662; b) P. Taynton, K. Yu, R. K. Shoemaker, Y. Jin, H. J. Qi, W. Zhang, *Adv. Mater.* **2014**, *26*, 3938; c) H. Zhang, D. Wang, W. Liu, P. Li, J. Liu, C. Liu, J. Zhang, N. Zhao, J. Xu, *J. Polym. Sci., Part A: Polym. Chem.* **2017**, *55*, 2011; d) H. Zheng, Q. Liu, X. Lei, Y. Chen, B. Zhang, Q. Zhang, *J. Polym. Sci., Part A: Polym. Chem.* **2018**, *56*, 2531; e) S. Wang, S. Ma, Q. Li, W. Yuan, B. Wang, J. Zhu, *Macromolecules* **2018**, *51*, 8001.

[19] a) R. J. Friary, V. Seidl, J. H. Schwerdt, T.-M. Chan, M. P. Cohen, E. R. Conklin, T. Duelfer, D. Hou, M. Nafissi, R. L. Runkle, *Tetrahedron* **1993**, *49*, 7179; b) K. Ostrowska, M. Ciechanowicz-Rutkowska, T. Pilati, G. Zżuchowski, *Chem. Mon.* **1999**, *130*, 555.

[20] a) *Brockhaus ABC Chemie*, VEB F. A. Brockhaus Verlag Leipzig, **1965**, S. 668; b) R. W. Layer, *Chem. Rev.* **1963**, *63*, 489; c) Y. Liu, Z. Tang, J. Chen, J. Xiong, D. Wang, S. Wang, S. Wu, B. Guo, *Polym. Chem.* **2020**, *11*, 1348.

[21] a) M. A. Sprung, *Chem. Rev.* **1940**, *26*, 297; b) A. Chao, I. Negulescu, D. Zhang, *Macromolecules* **2016**, *49*, 6277.

[22] R. F. Martínez, M. Ávalos, R. Babiano, P. Cintas, J. L. Jiménez, M. E. Light, J. C. Palacios, *Org. Biomol. Chem.* **2011**, *9*, 8268.

[23] a) H. Ahlbrecht, *Tetrahedron Lett.* **1968**, *9*, 4421; b) H. Ahlbrecht, J. Blecher, F. Kröhnke, *Tetrahedron Lett.* **1969**, *10*, 439; c) H. Ahlbrecht, H. Hanisch, W. Funk, R. Kalas, *Tetrahedron* **1972**, *28*, 5481; d) G. O. Dudek, R. H. Holm, *J. Am. Chem. Soc.* **1961**, *83*, 2099; e) C.-g. Shin, M. Masaki, M. Ohta, *Bull. Chem. Soc. Jpn.* **1971**, *44*, 1657; f) R. A. Clark, D. C. Parker, *J. Am. Chem. Soc.* **1971**, *93*, 7257.

[24] a) G. Tóth, I. Pintér, A. Messmer, *Tetrahedron Lett.* **1974**, *15*, 735; b) C. K. Ingold, H. A. Piggott, *J. Chem. Soc., Trans.* **1922**, *121*,

**ADVANCED
SCIENCE NEWS**

www.advancedsciencenews.com

**Macromolecular
Rapid Communications**

www.mrc-journal.de

2793; c) C. K. Ingold, H. A. Piggott, *J. Chem. Soc., Trans.* **1923**, *123*, 2745; d) G. K. Cantrell, T. Y. Meyer, *Organometallics* **1997**, *16*, 5381; e) J. McInnes, *Chem. Commun.* **1998**, 1669.

[25] a) M. Ciaccia, S. Di Stefano, *Org. Biomol. Chem.* **2015**, *13*, 646; b) M. Ciaccia, R. Cacciapaglia, P. Mencarelli, L. Mandolini, S. Di Stefano, *Chem. Sci.* **2013**, *4*, 2253; c) M. E. Belowich, J. F. Stoddart, *Chem. Soc. Rev.* **2012**, *41*, 2003.

[26] M. Ciaccia, S. Pilati, R. Cacciapaglia, L. Mandolini, S. Di Stefano, *Org. Biomol. Chem.* **2014**, *12*, 3282.

[27] a) M. Yıldız, Z. Kılıç, T. Hökelek, *J. Mol. Struct.* **1998**, *441*, 1; b) H. Ünver, *Spectrosc. Lett.* **2001**, *34*, 783.

[28] T. Seki, Y. Iwanami, Y. Kuwatani, M. Iyoda, *J. Heterocycl. Chem.* **1997**, *34*, 773.

[29] S. Logan, *J. Chem. Educ.* **1990**, *67*, 371.

[30] C. Taplan, M. Guerre, J. M. Winne, F. E. Du Prez, *Mater. Horiz.* **2020**, *7*, 104.

[31] S. Kulchat, Thesis, English, *Université de Strasbourg* **2015**.

[32] a) R. J. Clemens, J. A. Hyatt, *J. Org. Chem.* **1985**, *50*, 2431; b) J. S. Witzeman, W. D. Nottingham, *J. Org. Chem.* **1991**, *56*, 1713.

[33] W. Denissen, M. Droesbeke, R. Nicolaÿ, L. Leibler, J. M. Winne, F. E. Du Prez, *Nat. Commun.* **2017**, *8*, 14857.

[34] a) Y. Spiesschaert, M. Guerre, I. De Baere, W. Van Paepegem, J. M. Winne, F. E. Du Prez, *Macromolecules* **2020**, *53*, 2485; b) M. Guerre, C. Taplan, J. M. Winne, F. Du Prez, *Chem. Sci.* **2020**, *11*, 4855.

[35] T. Stukenbroeker, W. Wang, J. M. Winne, F. E. Du Prez, R. Nicolaÿ, L. Leibler, *Polym. Chem.* **2017**, *8*, 6590.

2000273 (12 of 12)

5.2   Publication 2: Blended Vinylogous Urethane/Urea Vitrimers

Blended vinylogous urethane/urea vitrimers derived from aromatic alcohols

This work was partially created with the assistance of Gloria Signorato (Universität Hamburg) within the scope of an internship within her master's degree. Glorias help is grateful acknowledged.

The second publication focuses on using aromatic alcohols as raw materials for vitrimers. Aromatic alcohols like bisphenol-A or resorcin are used for countless applications, *e.g.* epoxy resins, phenolic resins and polyester-networks, which are mostly cross-linked polymers and, therefore, not reprocessable.[138-140] Nevertheless, the aromatic backbone structure of these polymers lead to polymers with outstanding mechanical and chemical properties, making them attractive for many applications where light, flexible and yet very resistant material are needed (*e.g.* airplanes, wind turbine blades).[141-143]

For these reasons, bisphenol-A, resorcin, 2,7-naphthalenediol and 1,1,1-tris(4-hydroxyphenyl)ethane were chosen as raw materials and converted into acetoacetates as suitable monomers for vinylogous urethane vitrimers. The aromatic acetoacetates provide the basis for the prepared vitrimers, representing a reprocessable alternative to the established materials. Acetoacetates undergo a fast condensation reaction (polymerization) with primary amines to form a vinylogous urethane network. For a comparison, the commercial used Jeffamine® T-403 known as a typical curing agent for epoxy resins was used as reactant for the vitrimers.[144, 145] At the time of publishing, only aliphatic alcohols were used as raw materials, because the established synthesis route for the acetoacetylation of aliphatic alcohol with TBA works well for aliphatic alcohols but not efficiently for the less nucleophilic aromatic alcohols. Using TMDO, a feasible synthesis route for the acetoacetylation of aromatic alcohols was found. Model studies were carried out to enlighten the condensation, substitution and transamination reactions of the synthesized acetoacetates with the primary amines, investigating solvent and catalyst effects and activation energies compared to the use of established aliphatic acetoacetates. Utilizing the findings from the model studies for the preparation of vitrimers, 16 elastomeric and thermosetting blended poly(vinylogous urethane/urea)

networks are prepared by bulk/solvent polymerization and compared in terms of their dynamic and mechanical properties. These networks can also be considered as a co-network. Moreover, the materials show remarkable reprocessing, reshaping, shape-memory and self-healing properties.

Related to publication 2, epoxy-vitrimers (vipoxy) were prepared by using acetoacetylated bisphenol-A, bisphenol-A diglycidylether and JA to investigate their reprocessability (chapter 6.5.1.4). The vipoxy materials were especially compared to an established and fixed epoxy resin network without any covalent dynamic bond and showed remarkably fast stress-relaxation even when only 30 mol% of the bonds were dynamic.

Reproduced from *Polym. Chem*, **2022**, *13*, 946-958 (DOI: 10.1039/d1py01237a) with permission from The Royal Society of Chemistry. The related supporting information is available in Section 9.3.

PAPER

Check for updates

Blended vinylogous urethane/urea vitrimers derived from aromatic alcohols†

Philipp Haida,[a] Gloria Signorato[a] and Volker Abetz (ID) *[a,b]

Vitrimers belong to the class of covalent adaptable networks and are cross-linked polymers, which undergo dynamic, associative exchange reactions under thermal treatment, making these networks permanent as well as dynamic. In this work a feasible synthesis route for the acetoacetylation of aromatic alcohols, which expands the selection of acetoacetate monomers for the synthesis of vitrimers, is introduced. Bisphenol-A, resorcin, 2,7-naphthalenediol and 1,1,1-tris(4-hydroxyphenyl)ethane are chosen as examples for commercially relevant di- and trifunctional alcohols used for countless applications, *e.g.* epoxy resins, phenolic resins and polyester-networks, which are in general not reprocessable. In contrast, aromatic alcohols provide the basis for the prepared vitrimers, representing a reprocessable alternative to the established materials. Model studies are conducted to enlighten the undergoing condensation, substitution and transamination reactions in the emerging vinylogous urethane/urea mixtures, investigating solvent and catalyst effects and determining activation energies. Utilizing the findings from the model studies for the preparation of vitrimers, 16 elastomeric and thermosetting blended poly(vinylogous urethane/urea) networks are prepared by bulk/solvent polymerization, showing short stress-relaxation times of up to 0.7 s at 130 °C and activation energies of ca. 45–150 kJ mol^{-1} with a broad range of material properties. Moreover, the materials show remarkable reprocessing, reshaping, shape-memory and self-healing properties.

Introduction

The outstanding properties of thermosets with respect to their mechanical stability and chemical resistance make this class of polymers attractive for various applications. However, thermosets cannot be reprocessed or recycled due to their permanent cross-linked networks.[1–3] For this reason, a great deal of focus has been placed on the field of chemically and physically robust, but still reprocessable polymer networks over the last few decades. The use of reversible covalent bonds within polymer networks enables a dynamic reorganization of cross-linking points and leads to a macroscopic flow behavior of the material without a permanent change in the physical or chemical properties. Polymers with covalently exchangeable bonds are assigned to the class of covalent adaptable networks (CANs) and classified according to the underlying associative, dissociative, or concerted exchange mechanism.[4–10] Considering CANs based on an associative exchange mecha-

nism, the number of cross-linking points always remains constant during the rearrangement process, providing permanent and dynamic polymer networks at the same time.[11–13]

In 2011, Leibler and co-workers established a novel class of CANs by adding a suitable transesterification catalyst to polyester-based networks. The thermally activated, catalytic transesterification reaction based on an associative exchange mechanism resulted in permanent polyester/polyol networks that showed an astonishing viscosity decrease upon heating, while maintaining a cross-linked polymer network. Hence, Leibler invented the name "vitrimers" for this novel subcategory of thermosetting polymers.[14–16] Since this initial finding, various dynamic covalent exchange mechanisms, *e.g.* transcarbonation,[17] transalkylation,[18] transcarbamoylation,[19,20] thiol–disulfide exchange,[21] trans-*N*-alkylation,[22] transamination[23–25] and transimination reactions[26] have been investigated and applied with innumerable molecules, oligomers or modified polymers.[11,22,27–31] In 2014, Du Prez, Leibler and co-workers examined vinylogous amide-type enamine-one species as a suitable covalent dynamic bond for vitrimers, which are synthesized by the condensation reaction of primary amines and acetoacetates.[24] This bond can be regarded as a vinylogous urethane, stabilized by the vinylic bond and the conjugation through the ester unit. In contrast to conventional urethane bonds, the electrophilicity of vinylogous urethane bonds is

[a]Institute of Physical Chemistry, Universität Hamburg, Grindelallee 117, 20146 Hamburg, Germany
[b]Institute of Membrane Research, Helmholtz-Zentrum Hereon, Max-Planck-Straße 1, 21502 Geesthacht, Germany. E-mail: volker.abetz@hereon.de
†Electronic supplementary information (ESI) available. See DOI: 10.1039/d1py01237a

highly increased, thus enabling thermally induced, dynamic exchange reactions with primary amines.[32,33]

In this work, a synthetic route for the acetoacetylation of aromatic alcohols as suitable raw materials for vinylogous urethane vitrimers was investigated using 2,2,6-trimethyl-1,3-dioxin-4-one (TMDO) as a reactant. In particular, the acetoacetylation of aromatic alcohols and the use of the prepared aromatic acetoacetates have not been described in the literature for vitrimers which increases the number of possible reactants multiple times. For example, phenol, bisphenol-A, resorcin, 2,7-naphthalenediol and 1,1,1-tris(4-hydroxyphenyl)ethane were chosen as commercially accessible and broadly established mono-, di-, and trifunctional reactants. Nowadays, these aromatic alcohols are used for countless applications, *e.g.* epoxy resins,[34–36] phenolic resins (resorcinol),[37–40] polyesters,[41–46] dyes (fluorescein and eosin),[47,48] medical diagnostics[49] and other usages,[50] which make them promising candidates for the use of recyclable and reprocessable polymer networks. Moreover, we introduce 2,7-naphthalenediol and 1,1,1-tris(4-hydroxyphenyl)ethane as less toxic alternatives to the widely established toxic and carcinogenic bisphenol-A and resorcin-based polymers, which are increasingly being avoided and replaced by industry.[51–56]

The condensation and substitution reactions of the prepared aromatic acetoacetates with aliphatic primary amines lead to the formation of blended vinylogous urethane and vinylogous urea compounds, which both undergo thermally induced exchange reactions, thus representing the required dynamic covalent bonds for vitrimers. Model studies are conducted to enlighten the undergoing condensation, substitution and exchange reactions in the emerging vinylogous urethane/urea mixtures, investigate the solvent or catalyst effects and compare the activation energies. Utilizing the findings from the model studies for the preparation of vitrimers, 16 elastomeric and thermosetting blended poly(vinylogous urethane/urea) networks have been prepared and characterized in terms of their material properties and remarkable reshaping, reprocessing, shape-memory and self-healing properties.

Results and discussion

Synthesis of aromatic acetoacetates

According to the literature, the established synthetic route for the acetoacetylation of various aliphatic alcohols was carried out with *tert*-butylacetoacetate (*t*-buacac).[24,25,57] However, another synthesis route using TMDO is described for monofunctional aliphatic and aromatic alcohols (basic organic chemistry) in the literature and turned out to proceed in a much more efficient way for aromatic alcohols, thus enabling aromatic acetoacetates to be used as suitable monomers for this type of vitrimer.[58–61] In both synthetic routes the thermal dissociation of the reactant into a highly reactive, electrophilic acetylketene is the crucial step for acetoacetylation with the corresponding nucleophile (Fig. S1, ESI†). TMDO undergoes a *retro*-Diels Alder reaction at elevated temperatures (>110 °C),

thus releasing the reactive acetylketene and acetone, with acetone being removed by distillation. In comparison, the established acetoacetylation with *t*-buacac proceeds by dissociation into the same reactive acetylketene and *tert*-butanol. Due to the delocalized electrons, aromatic alcohols show significantly lower nucleophilicity in comparison to aliphatic alcohols. Experiments showed that the acetoacetylation of aromatic alcohols with *t*-buacac proceeds slowly with low conversions and emerging byproducts after a long time of stirring at high temperatures, while the synthesis could not be significantly improved by changing the solvent, temperature, reaction time, and reactant concentration, or even using a catalyst. Nevertheless, the desired di- and trifunctional acetoacetate products may be isolated by complicated and time-consuming purification steps. In contrast, the use of TMDO instead of *t*-buacac enables a fast and selective acetoacetylation at 135 °C in xylene after 45 min. Obviously, in the dissociation step, the backward reaction of the byproducts or the removal of acetone proceeds more efficiently. The synthetic route using TMDO works for aliphatic alcohols as well but does not offer any major advantages compared to the established synthesis route using *t*-buacac. Since the reaction times are significantly increased for aromatic alcohols, the acetoacetylation using
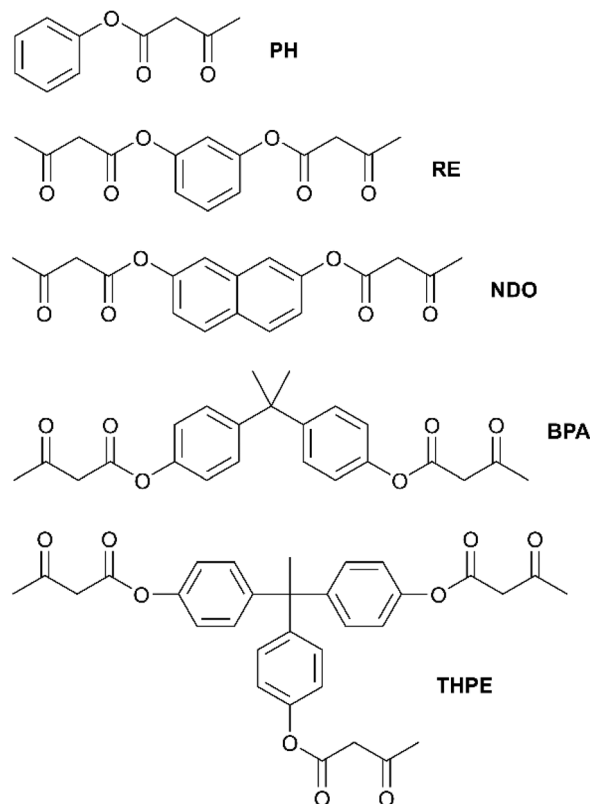
Fig. 1 Representation of the synthesized acetoacetate monomers phenyl-3-oxobutanoate (**PH**), 1,3-phenylene bis(3-oxobutanoate) (**RE**), naphthalene-2,7-diyl bis(3-oxobutanoate) (**NDO**), propane-2,2-diylbis (4,1-phenylene) bis(3-oxobutanoate) (**BPA**) and ethane-1,1,1-triyltris (benzene-4,1-diyl) tris(3-oxobutanoate) (**THPE**).

TMDO represents an effective synthesis route, which allows easy access to aromatic acetoacetates (Fig. S1, ESI†).

Herein, the aromatic alcohols phenol, bisphenol-A, resorcin, 2,7-naphthalenediol and 1,1,1-tris(4-hydroxyphenyl)ethane were used as raw materials for the mono-, di-, and trifunctional monomers phenyl-3-oxobutanoate (**PH**), 1,3-phenylene-bis(3-oxobutanoate) (**RE**), naphthalene-2,7-diyl-bis(3-oxobutanoate) (**NDO**), propane-2,2-diylbis(4,1-phenylene)-bis(3-oxobutanoate) (**BPA**) and ethane-1,1,1-triyltris(benzene-4,1-diyl)-tris(3-oxobutanoate) (**THPE**) (Fig. 1). The synthesized acetoacetate monomers were characterized by Attenuated-total-reflection-Fourier-transform infrared (ATR-FT-IR) spectroscopy (Fig. S2, ESI†), ^{1}H/^{13}C nuclear magnetic resonance (NMR) spectroscopy (Fig. S3, ESI†) and mass spectrometry (MS) (Fig. S4, ESI†).

Model studies – condensation, substitution and exchange reactions

In order to investigate the characteristic condensation, substitution and exchange reactions, model studies with monofunctional reactants have been carried out. In the following text and illustrations, the vinylogous urethane (VUT) and vinylogous urea (VUA) compounds are abbreviated with the respective substituent on each side of the dynamic covalent bonds (Phe = phenyl, Hex = hexyl, Bz = benzyl, and AcAc = acetoacetate, *e.g.*: **Phe-VUT-Hex**). Aliphatic acetoacetates undergo a selective condensation reaction with primary amines to give a vinylogous urethane.[24,62] However, aromatic acetoacetates show a different reaction behavior due to their variant electron configuration. For the model study, phenylacetoacetate (**PH**) was mixed with an excess of hexylamine (2 equivalents) in chloroform at room temperature to give the vinylogous urethane phenyl-3-(hexylamino)but-2-enoate (**Phe-VUT-Hex**) (Fig. 2). Characterization by ^{1}H/^{13}C NMR spectroscopy, ATR-FT-IR spectroscopy and MS showed the formation of the vinylogous urethane with the characteristic chemical shifts

(Fig. S5, ESI†), the typical conjugated C=O ester band (1663 cm^{-1}) and C=C band (1606 cm^{-1}) (Fig. S6, ESI†) and the molecular ion peak m/z = 262.181 (M$^+$ + 1) (Fig. S7, ESI†). In addition, the spectra showed the temporary formation of the acetoacetamide **Hex-VUA-AcAc**, since the ester group of the aromatic acetoacetates is sufficiently electrophilic to undergo a substitution reaction with the nucleophilic hexylamine. Subsequently, the acetoacetamide undergoes a fast condensation reaction with another hexylamine, giving the vinylogous urea compound **Hex-VUA-Hex** together with **Phe-VUT-Hex** (^{1}H NMR, MS, and ATR-FT-IR, Fig. S8–10, ESI†). This is proven by individual reference measurements of the pure vinylogous urea compound **Hex-VUA-Hex** (^{1}H/^{13}C NMR, MS, and ATR-FT-IR, Fig. S11–14, ESI†). In this way two dynamic covalent bonds were synthesized simultaneously with an approximate proportion of 37% vinylogous urethane and 63% vinylogous urea products, respectively.

Due to the significantly lower electrophilicity of the conjugated C=O ester bond of the vinylogous urethane, this bond is resistant to further substitution reactions with free hexylamine, while the C=C bond enables dynamic covalent exchange reactions. Thus, mixtures of vinylogous urethane/urea compounds and pendant free amines could be obtained. In general, the nucleophilicity of the amines highly depends on solvation, steric hindrance or coordinating effects and can be adjusted by solvents, catalysts or other additives.[63–65] For example, the aromatic amine aniline undergoes a more selective condensation reaction, producing mainly the vinylogous urethane compound **Phe-VUT-Phe** (67%)(Fig. S15, ESI†), proved by reference measurements (^{1}H/MS and ATR-FT-IR, Fig. S16–21, ESI†).

Moreover, experiments showed that the ratio of the emerging vinylogous urethane and vinylogous urea products can be adjusted by the solvent (dimethyl sulfoxide (DMSO), benzene, and chloroform) (^{1}H NMR, Fig. S22, ESI†) and/or acetic acid as a
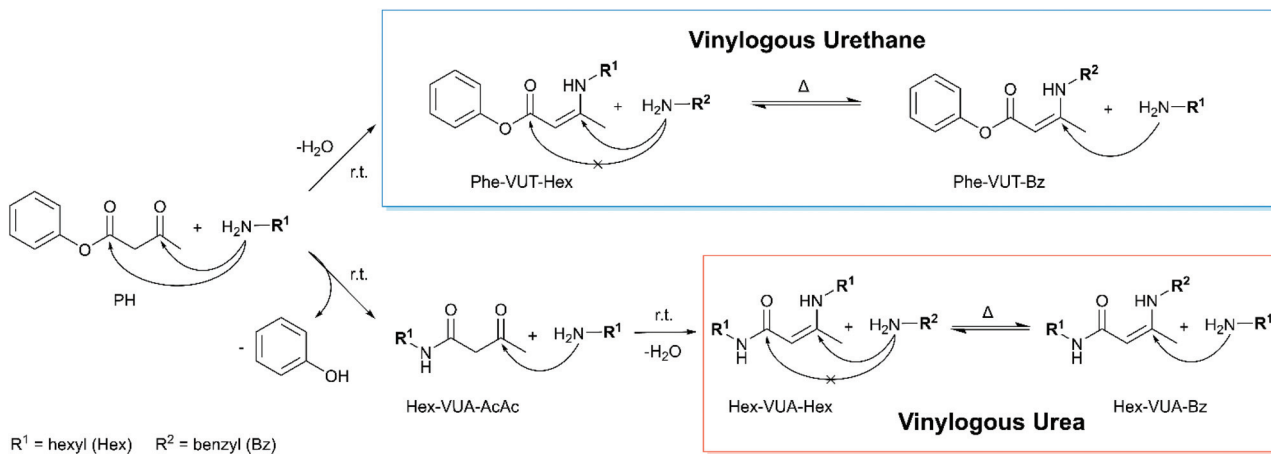
Fig. 2 Schematic representation of the condensation and substitution reactions of aromatic acetoacetates and aliphatic primary amines. The nucleophilic attack can either occur at the keto group, producing a vinylogous urethane, or at the ester unit, producing an acetoacetamide and vinylogous urea. Both types represent dynamic covalent bonds, which undergo fast exchange reactions with free primary amines at elevated temperatures in the absence of a catalyst. For the model studies phenylacetoacetate, hexylamine and benzylamine have been used.
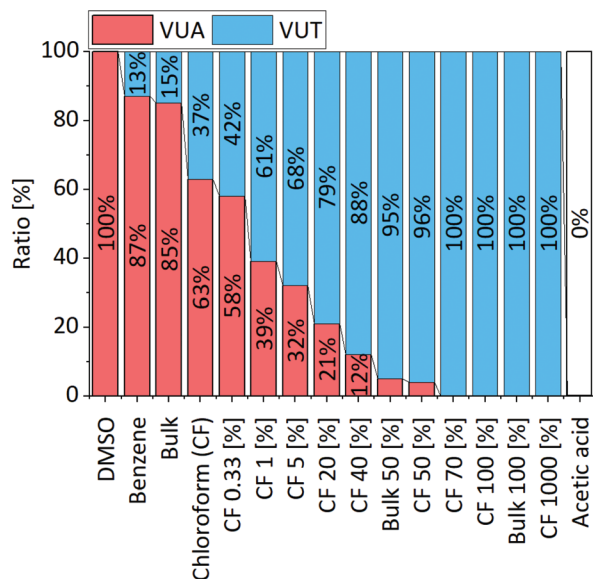
Fig. 3 Ratio of the vinylogous urethane and vinylogous urea compounds resulting from the condensation and substitution reactions of phenylacetoacetate and hexylamine in different solvents/bulk and with different amounts of acetic acid. The ratio can be shifted to a selective formation of either the vinylogous urethane or the vinylogous urea compound.

Fig. 4 Calculation of the activation energies from the slope of the linear fit by plotting $\ln k$ against the reciprocal temperature. The activation energies of aromatic and aliphatic vinylogous urethanes show comparable values of 64.5 ± 10.3 kJ mol^{-1} and 64.7 ± 8.1 kJ mol^{-1}. The vinylogous urea compounds show an activation energy of 52.2 ± 4.8 kJ mol^{-1}.

catalyst (Fig. 3) (^{1}H NMR, Fig. S23, ESI†). Available protons protonate the keto group of the acetoacetate and increase the electrophilicity, which shifts the ratio to the vinylogous urethane products and allows a selective conversion by using a sufficient amount of acetic acid. Furthermore, the conversion rates are highly increased by the addition of some acetic acid, while a higher amount of acetic acid slowed down the reaction and finally totally inhibited it due to the protonation of all nucleophilic amines (Fig. S24, ESI†). In comparison, the condensation reaction of the aliphatic methylacetoacetate and hexylamine selectively yields the vinylogous urethane compound in all considered solvents and acetic acid as a catalyst.[62] In addition, the characteristic exchange reactions of the vinylogous urethane and vinylogous urea compounds with pendant free amines were investigated and compared in terms of their activation energies (Fig. 4). For this, an excess of four equivalents of a different amine-type were added to the vinylogous urethane/vinylogous urea mixture to ensure a pseudo first order decay during the beginning of the exchange reaction (eqn (S1), ESI†). The vinylogous urethane exchange was monitored at 70, 90 and 110 °C, while the vinylogous urea exchange was monitored at 12, 22 and 32 °C (schematic overview of the used compounds, Fig. S25, ESI†). By plotting the rate constant ($\ln k$) against the reciprocal temperature ($1/K$), the activation energies can be calculated from the slope of the linear fit. ^{1}H NMR spectra show the exchange of benzyl- and hexylamine during the exchange reaction. Regarding the vinylogous urethanes the spectra show a shift of the characteristic vinylic proton at 4.68 ppm (**Phe-VUT-Bz**) to 4.58 ppm (**Phe-VUT-Hex**) (Fig. S26, ESI†). The vinylogous urea compounds show a shift of the characteristic NH protons at 8.93 ppm (**Hex-**

VUA-Hex) and 9.39 ppm (**Hex-VUA-Bz**) after the exchange reaction (Fig. S27, ESI†). ATR-FT-IR spectra did not show significant shifts of the characteristic C=O ester, C=O amide or C=C bands after the exchange reaction (Fig. S28, ESI†). An activation energy of 64.7 ± 8.1 kJ mol^{-1} was calculated for the aromatic vinylogous urethane exchange, while 52.2 ± 4.8 kJ mol^{-1} was calculated for the vinylogous urea exchange (Fig. 4). In addition, the activation energy for the exchange of aliphatic vinylogous urethanes synthesized by methylacetoacetate and hexylamine was determined and a similar activation energy of 64.5 ± 10.3 kJ mol^{-1} was obtained (Fig. S29, ESI†). The results were supported by comparing the expected exchange products with individual reference compounds (^{1}H/^{13}C NMR, MS, and ATR-FT-IR, Fig. S30–S32, ESI†). Furthermore, the calculated values are in good agreement with the values reported in the literature and point out that aromatic and aliphatic vinylogous urethanes show similar activation energies.[24,25]

Blended poly(vinylogous urethane/urea) networks

In this work four different di- and trifunctional acetoacetate monomers, used for the condensation/substitution reactions with trifunctional primary amines, are introduced. Jeffamine-T403 (**JA**) and tris(2-aminoethyl)amine (**TREN**) have been used as trifunctional cross-linking agents (Fig. 5). **TREN** has already been established as a suitable cross-linker for vinylogous urethane vitrimers and other vitrimer-types.[24,57,66,67] Furthermore, **JA** is a commercial, trifunctional amine based on poly(propylene oxide), which is used as a cross-linker in several industrial applications, especially epoxy resins. Moreover, **JA** has been of interest to scientific basic research in terms of epoxy chemistry, composite materials, and other applications, serving as an alternative as a less toxic cross-linker than the highly toxic **TREN**.[68–73] The monomers were
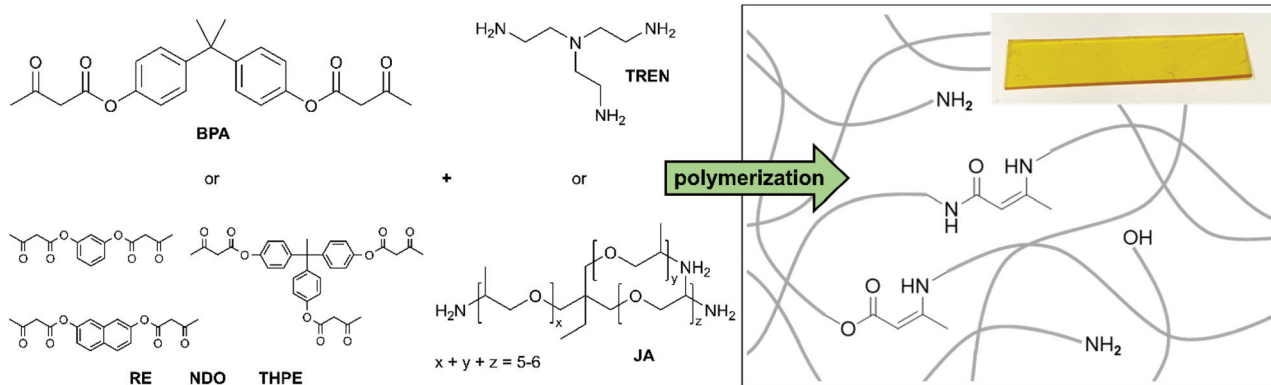
Fig. 5 Representation of the used di- and trifunctional acetoacetate and amine monomers and the resulting network structure, containing vinylogous urethane bonds, vinylogous urea bonds, and free aliphatic amine- and aromatic hydroxy groups.

mixed at 80 °C in a bulk reaction (with and without acetic acid) until an opaque, homogeneous mass was obtained. A solvent-based polymerization was carried out in chloroform. Herein, the solvent was slowly evaporated at room temperature until gelation of the vitrimers occurred. Next, the vitrimers were cured *in vacuo* for 20 h at 100 °C to complete the curing process and to remove excess water/acetic acid from the condensation reaction. Afterwards, the vitrimers were post-cured at 150 °C for 1 h and hot-pressed at 150 °C to obtain 1 mm thick films. The stoichiometry of the functional groups and the degree of cross-linking are important factors in the prepared poly(vinylogous urethane/urea) networks. The availability of free primary amine groups accelerates the reorganization process due to exchange reactions within the network. Nevertheless, the network topology is affected by synthesizing a material with an excess of amines, which implies working under non-stoichiometric conditions. Therefore, a compromise between the rearrangement rate and resilient network integrity must be made. In addition, the ratio of the emerging vinylogous urethane/urea compounds determines the required amount of amines (R) and can be estimated from the results of the model study. Furthermore, the choice of the monomer backbone is a decisive factor, since it determines the spatial arrangement of the polymer network and thus has a strong influence on the exchange rate and mechanical properties.[24,27] As discussed in the model study, blended poly(vinylogous urethane/urea) networks were synthesized simultaneously, containing two dynamic covalent bond types at the same time (Fig. 5). Because of that, acetoacetate to amine ratios (R) with an excess of amines (R = 0.5, 0.7, and 0.9) were set to ensure sufficient amine groups for the condensation, substitution, and exchange reactions depending on the polymerization conditions (with or without acetic acid). By performing that, 16 vitrimers were polymerized, providing new materials with a broad range of properties. The used monomers, compositions and the measurement results of differential scanning calorimetry (DSC), thermogravimetric analysis (TGA), dynamic mechanical analysis (DMA), and tensile tests as well as the calculated activation energies (E_a) are summarized in Table 1.

ATR-FT-IR spectra show the disappearance of the characteristic C=O ester and C=O ketone bands of the acetoacetate monomers after the polymerization (Fig. 6) (Fig. S33, ESI†). The vitrimers show the characteristic C=C band (1610 cm^{-1}) and C=O ester band (1664 cm^{-1}) of the vinylogous urethane bonds as well as the C=C band (1593 cm^{-1}) and C=O amide band (1616 cm^{-1}) of the vinylogous urea bonds, proving the formation of the blended poly(vinylogous urethane/urea) networks (all spectra, Fig. S34, ESI†). Nevertheless, the spectra show several overlapping bands, which lead back to the aromatic C=C stretching bands of the conjugated phenylic rings (1587–1605 cm^{-1}) and free primary amine groups (1591 cm^{-1}) in the same area. The reference spectra of the individual model compounds support these findings by measuring similar bands (Fig. S6–S12, ESI†). Furthermore, a qualitative shift regarding the vinylogous urethane/urea bond ratios could be observed, using acetic acid as an additional catalyst and/or carrying out a controlled polymerization in chloroform. As shown in the model study, this shifts the ratio towards the vinylogous urethane bonds. IR spectra support this finding by measuring the increased C=O ester band (1664 cm^{-1}) (Fig. 6). Nevertheless, it is not possible to determine exact ratios from the spectra.

Thermogravimetric analysis of the materials showed thermal degradation temperatures of 222–290 °C (5% mass loss) at ambient atmosphere (Fig. S35, ESI†). Relating the results to the values of vinylogous urethane vitrimers described in the literature (230–280 °C), the prepared blended vitrimers showed similar degradation temperatures.[27] The glass transition temperatures of the vitrimers have differed significantly by using various acetoacetate to amine ratios, cross-linking agents or acetoacetate backbones. With this, elastomeric and thermosetting vitrimers with T_g values between 11 and 73 °C could be prepared. In particular, the use of **JA** enabled low T_g, partially elastomeric vitrimers, while the use of **TREN** led exclusively to thermosetting vitrimers. By using additional acetic acid (ratio shifted to vinylogous urethane bonds) the materials show higher glass transition temperatures (Fig. S36, ESI†). Temperature-dependent DMA measure-

Table 1 Overview of the synthesized vitrimer compositions and characteristic properties measured by DSC, TGA, DMA and tensile test measurements

Vitrimer	T_g [°C]	$T_{95\%}$ [°C]	$\tau_{130\,°C}$ [s]	E_a [kJ mol^{-1}]	$G'_{20\,°C}$ [GPa]	$G'_{150\,°C}$ [MPa]	$E_{t\,\varnothing}$ r.t. [MPa]	$\sigma_{m\varnothing}$ r.t. [MPa]	$\varepsilon_{m\varnothing}$ r.t. [%]
Bulk									
VU-RE$_{JA,\,0.5}$	27	244	79	43.8 ± 2.6	0.70	2.00	290	14.6	7.4
VU-RE$_{JA,\,0.7}$	11	237	343	47.3 ± 2.5	0.10	0.43	5.0	5.60	340
VUH$^+$-RE$_{JA,\,0.9}$	32	222	686	55.5 ± 2.6	0.33	0.64	260	10.1	9.6
VU-NDO$_{JA,\,0.5}$	39	262	44	48.9 ± 2.4	0.42	1.70	1270	52.9	5.4
VU-NDO$_{JA,\,0.7}$	30	241	65	54.8 ± 5.9	0.77	0.80	350	31.1	6.5
VUH$^+$-NDO$_{JA,\,0.9}$	43	253	36	79.6 ± 3.8	0.78	0.70	1150	50.0	5.4
VU-THPE$_{JA,\,0.5}$	45	290	133	46.4 ± 1.4	0.81	1.40	870	62.8	6.7
VU-THPE$_{JA,\,0.7}$	42	267	136	44.6 ± 2.8	0.33	0.42	1240	30.9	2.5
VUH$^+$-THPE$_{JA,\,0.9}$	68	279	3193	149.7 ± 41.3	0.74	0.82	1540	20.3	1.8
VU-BPA$_{JA,\,0.5}$	33	260	58	52.2 ± 6.7	0.67	2.05	850	35.0	4.9
VU-BPA$_{JA,\,0.7}$	20	250	133	43.9 ± 10.6	0.47	0.25	320	12.5	5.9
VUH$^+$-BPA$_{JA,\,0.9}$	48	258	275	97.9 ± 2.6	0.78	0.12	1160	5.20	0.5
VU-BPA$_{TREN,\,0.5}$	68	244	0.7	50.2 ± 2.2	0.78	1.04	1100	33.6	2.7
VU-BPA$_{TREN,\,0.7}$	73	242	1.2	59.9 ± 2.4	0.67	1.57	1450	12.7	1.2
Solvent-based									
CFVUH$^+$-BPA$_{JA,\,0.7}$	45	266	355	90.2 ± 6.9	0.63	0.32	920	7.8	1.3
CFVUH$^+$-BPA$_{JA,\,0.9}$	57	269	814	149.5 ± 8.1	0.54	0.59	1170	53.0	4.6

The table shows the respective compositions of the vitrimers with the used acetoacetate monomers (RE, NDO, BPA or THPE), the used amine monomers (**JA** or **TREN**), the acetoacetate to amine ratio R and H$^+$ for the use of acetic acid (template: VUH$^+$-acetoacetate$_{amine,\,R}$). Poly(vinylogous urethane/urea) networks are abbreviated with VU. The glass transition temperatures ($T_{g\,on-set}$), thermal degradation temperatures at 5% mass loss under an ambient atmosphere ($T_{95\%}$), stress–relaxation times at 130 °C ($\tau_{130\,°C}$), activation energies (E_a), storage moduli at 20 °C (G', ω = 10 rad s^{-1}, y = 0.1%), rubbery plateaus at 150 °C ($G'_{150\,°C}$), average Young's moduli ($E_{t\,\varnothing}$), maximum tensile strengths ($\sigma_{m\varnothing}$) and strains ($\varepsilon_{m\varnothing}$) at room temperature are shown.
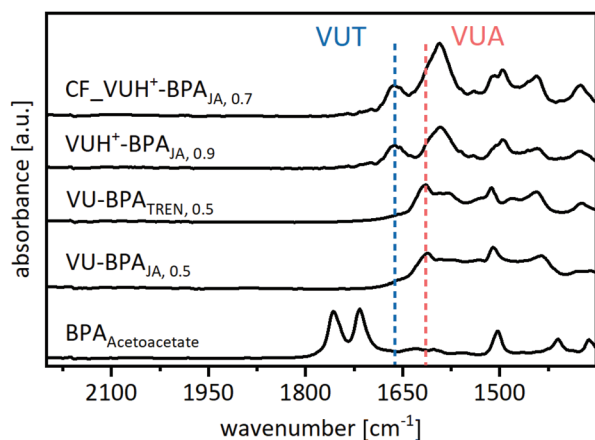
Fig. 6 Exemplary ATR-FT-IR spectra of the vitrimers cured with BPA and **JA/TREN** by different synthetic routes. The blue line marks the characteristic C=O ester band of the vinylogous urethane bond (1664 cm^{-1}), while the red line marks the characteristic C=O amide band of the vinylogous urea bond (1623 cm^{-1}). The vitrimers polymerized with additional acetic acid show a significantly higher intensity of the ester band (blue), while the vitrimers show a higher intensity of the amide band (red).

ments showed maximum storage moduli (G') of 0.10–0.81 GPA at 20 °C and rubbery plateaus of 0.12–2.05 MPA at 150 °C, measured within the linear viscoelastic regime, so that the storage modulus G' and the loss modulus G'' were independent of strain (ω = 10 rad s^{-1} and y = 0.1%) (Fig. S37, ESI†). In addition, the materials displayed stress-relaxation times of 0.7–3193 s at 130 °C, measured by a torsional deformation of 1% (Fig. S38, ESI†).

Moreover, the cross-linking agents **JA** and **TREN**, polymerized with BPA (R = 0.5), were compared in terms of the material properties. Interestingly, VU-BPA$_{TREN,\,0.5}$ shows significantly shorter stress-relaxation times of 0.7 s at 130 °C compared to VU-BPA$_{JA,\,0.5}$ with 58 s at 130 °C, even if VU-BPA$_{TREN,\,0.5}$ showed a significantly higher T_g (**JA**: 33 °C and **TREN**: 68 °C) (Fig. 7). Reasons for this might be the closer spatial arrangement of the functional groups regarding the network with the small molecule **TREN** in comparison to the bulkier molecule **JA** as well as a higher nucleophilicity of the terminal primary amine groups of **TREN** in comparison to the sterically hindered isopropyl-terminated primary amine groups of **JA**. The activation energies were calculated by using Maxwell's model for viscoelastic fluids and an Arrhenius law (eqn (S2), ESI†). Therefore, stress-relaxation curves at different temperatures (110–150 °C) were measured and normalized (Fig. S38, ESI†).

Next, the logarithm of the stress-relaxation time at 37% of the normalized stress-relaxation was plotted against 1000/T to calculate the activation energy from the slope. Even if the stress-relaxation times and T_g values differ significantly, the calculated activation energies of the vitrimers BPA$_{TREN,\,0.5}$ and VU-BPA$_{JA,\,0.5}$ showed comparable values, which were 50.2 kJ mol^{-1} and 52.2 kJ mol^{-1}, respectively (Fig. 8). The different acetoacetate monomers RE, NDO, BPA and THPE were equally cured with **JA** and compared in terms of the stress relaxation times and calculated activation energies (E_a). The activation energies were calculated in the range of 43.8–54.8 kJ mol^{-1}, while higher activation energies of 55.5–149.7 kJ mol^{-1} were determined when acetic acid was used during the synthesis. This is reasonable because the catalyst shifts the ratio of
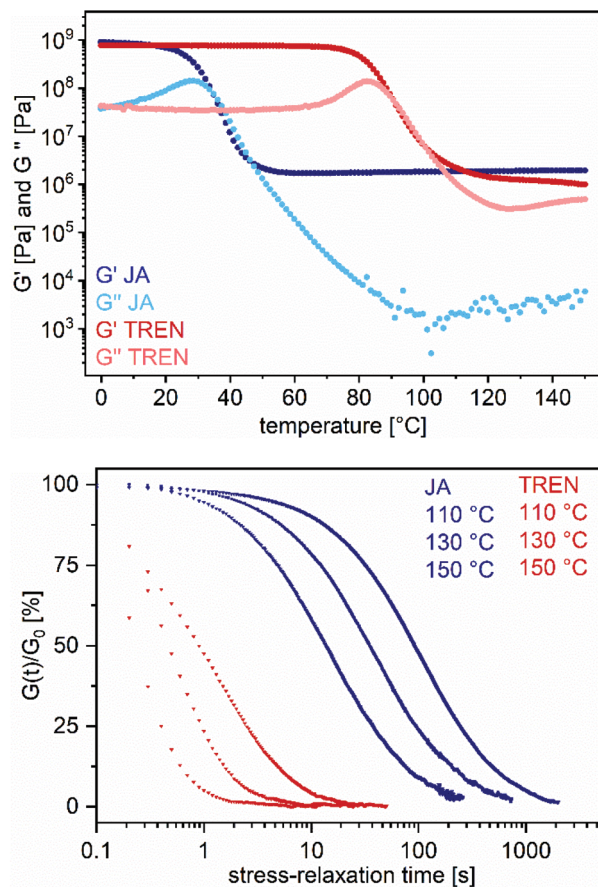
Fig. 7 Exemplary temperature-dependent DMA and stress-relaxation measurements in comparison with the vitrimers VU-BPA$_{TREN, 0.5}$ and VU-BPA$_{JA, 0.5}$. Temperature-dependent DMA measurements show cross-linked networks with the corresponding glass transition temperatures and the characteristic rubbery plateaus (top). Stress-relaxation measurements at 110, 130 and 150 °C show short stress-relaxation times (**TREN** notably shorter than **JA**) with an Arrhenius dependence (bottom).

Fig. 8 Plot of $\ln \tau$ against $1000/T$ to calculate the activation energies from the slope of the linear fit. The stress relaxation times τ (37%) were determined by different stress-relaxation experiments in the temperature range of 110–150 °C. The calculated activation energies of all 16 prepared vitrimers were calculated as summarized in Table 1.

vinylogous urethane and vinylogous urea bonds towards the side of the vinylogous urethanes, which show higher activation energies (Fig. 8). Comparing these results with activation energies reported for pure vinylogous urethane vitrimers (68–149 kJ mol⁻¹) and pure vinylogous urea vitrimers (49–53 kJ mol⁻¹), the calculated activation energies in this work reflect the results in good accordance.[25,27,57]

For further investigations of the mechanical properties of the materials, several stress-strain measurements have been carried out at room temperature for each vitrimer and showed significantly different resilience with averaged tensile strengths ($\sigma_{m\varnothing}$) of 5.2–62.8 MPa, elongation in tensile strengths ($\varepsilon_{m\varnothing}$) of 0.5–340% and Young's moduli of 5–1540 MPa (Table 1) (Fig. S39, ESI†). For comparison, one representative curve of each vitrimer is shown in Fig. 9. As expected, the elastomeric vitrimer VU-RE$_{0.7}$ shows the highest elongation of 340%, with a low tensile strength of 5.6 MPa and a Young's modulus of 5 MPa. The vitrimer with the highest tensile strength turned out to be VU-THPE$_{0.5}$ with a $\varepsilon_{m\varnothing}$ of 6.7%, a $\sigma_{m\varnothing}$ of 62.8 MPa and a

Young's modulus of 870 MPA. The highest Young's modulus was measured for VUH⁺-THPE$_{JA, 0.9}$ with a value of 1540 MPa.

Reprocessing and reshaping properties

Experiments were carried out to determine the reshaping, reprocessing and self-healing properties of the vitrimers. Two exemplary cycles of successive grinding and compression molding of the elastomeric vitrimer VU-RE$_{0.7}$ demonstrated a good reprocessability of the material, proven by repetitively measured ATR-FT-IR spectra and tensile tests. The reprocessing cycles produced always homogeneous, transparent, and bubble-free specimens (Fig. 10). Besides, the ATR-FT-IR spectra are rather similar (if not the same), while the stress–strain measurements show comparable results with slightly decreasing stress and strain at break after the first cycle (Fig. S40, ESI†).

Furthermore, the materials present reshaping and shape-memory properties using different temperature protocols (Fig. 11). Polymers with shape-memory properties are smart materials that are capable of memorizing their temporary shape and recovering the permanent shape due to entropic elasticity under an external stimulus,[74,75] while traditionally, the refinement of permanent shapes is limited by molding and processing methods.[76] However, the investigation of dynamic bonds with polymer networks provides an elegant solution to overcome this limitation. Vitrimers can be
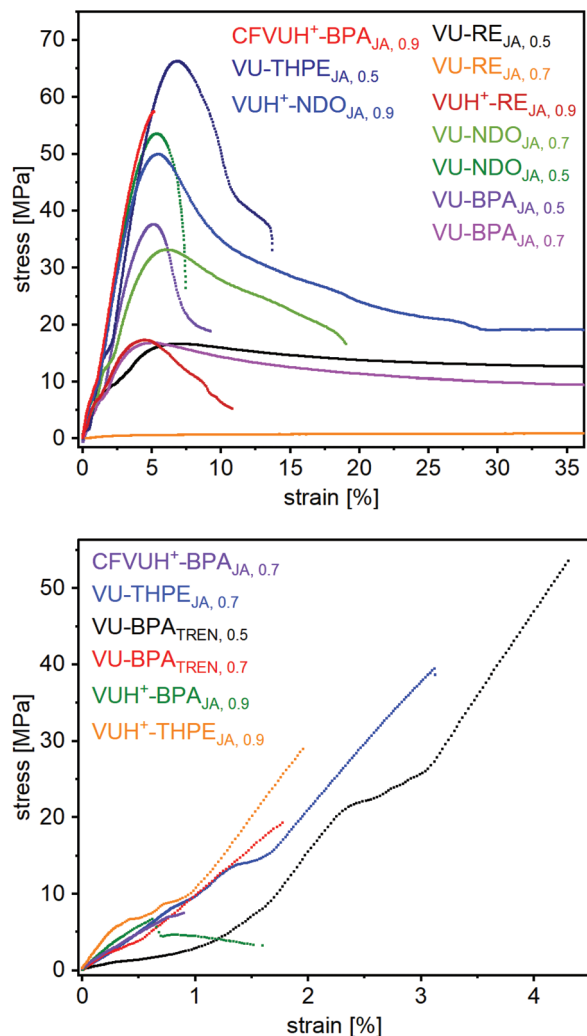
Fig. 9 Stress–strain curves of the prepared vitrimers. For comparison, one representative curve is shown for each vitrimer. The elastomeric vitrimer VU-RE$_{0.7}$ shows the stress–strain curve of an elastomer, with a high elongation at break of 340% strain. The most resilient vitrimer turned out to be VU-THPE$_{0.5}$ with a strain at break of 6.7%, a tensile strength of 62.8 MPa and a Young's modulus of 866 MPA. The highest Young's modulus was measured for VUH$^+$-THPE$_{JA, 0.9}$ with 1540 MPa.
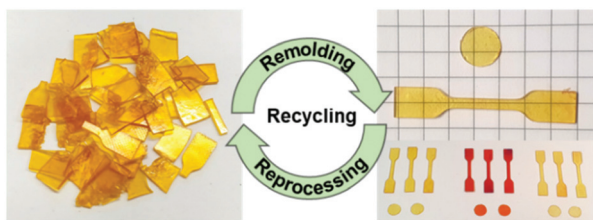
Fig. 10 Reprocessing cycles of the vitrimers by consecutive grinding and compression molding (150 °C, 300 s), generating homogeneous, transparent, and bubble-free films (specimen).

reshaped and reprocessed in the solid state due to the thermally induced associative exchange mechanism in the network. Thus, well defined shapes can be easily transformed into new defined
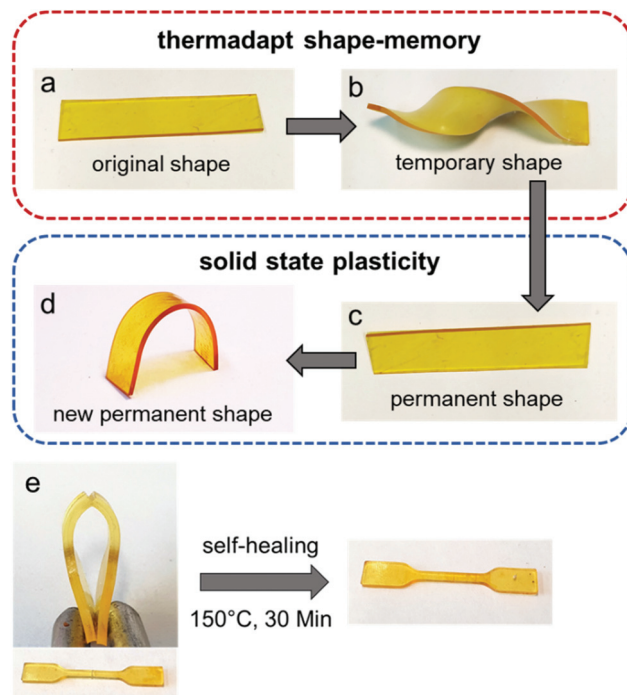
Fig. 11 Exemplary thermoadapt shape-memory properties (VU-RE$_{JA, 0.5}$) were investigated by twisting the original strip (a) at 80 °C for 5 s, freezing the topology below the T_g at room temperature (b) and letting it relax back to the original shape at 80 °C for 30 s (c). Solid state plasticity properties were explored by bending the permanent strip (c) at 150 °C for 300 s and reshaping the strip into a new shape (d). The specimens for tensile tests (1 mm) were cut in half in the middle (0.5 mm) and heated for 30 minutes at 150 °C. The cut and non-cut specimens were compared using tensile tests and they show self-healing by almost full recovery (e).

shapes without the intermediate step of a mold.[77] The presented materials show both thermo-adaptive shape-memory and solid state plasticity, depending on the applied temperature and duration. Heating up above the respective T_g for a short time (80 °C, 5 s) and twisting the material led to topology freezing with subsequent shape-memory when heating the material again above the T_g. Moreover, heating up at 150 °C for 5 min and bending the material, the thermal-induced exchange reactions enable a reorientation of the cross-linking points, leading to a new defined and permanent shape of the material. In addition, self-healing properties were observed by cutting the tensile test specimen (1 mm) in half in the middle (0.5 mm) and heating them for 30 minutes at 150 °C. Afterwards, the cut and non-cut specimens were compared using tensile tests and they show self-healing by almost full recovery and comparable results (Fig. S41, ESI†).

Experimental

Materials

Acetic acid and chloroform were purchased from VWR chemicals. Bisphenol-A (97%), 2,7-naphthalenediol (98%), and

hexylamine (99%) were purchased from Sigma-Aldrich. 2,2,6-Trimethyl-1,3-dioxin-4-one (95%), benzylamine (99%), aniline (98%), *tert*-butylacetoacetate (98%) and 1,1,1-tris(4-hydroxyphenyl)ethane (98%) were obtained from TCI. Tris(2-aminoethyl)amine (97%) was purchased from Alfa Aesar. Phenol (99.5%) was purchased from MERCK. Xylene (99%, isomeric mixture) and resorcin (98%) were purchased from Grüssing. CDCl$_3$, benzene-d6 and DMSO-d6 were purchased from Deutero GmbH. Jeffamine T-403 was purchased from Huntsman.

Instrumentation

Nuclear magnetic resonance (^{1}H NMR, ^{13}C NMR) spectroscopy: the spectra (broadband decoupled, ^{13}C NMR (DEPTQ135)) were recorded on a Bruker AVANCEII system (Bruker BioSpin GmbH, Karlsruhe, Germany) at 300 MHz/75 MHz with chloroform-d$_1$ (CDCl$_3$) as a solvent and tetramethylsilane (TMS) as an internal standard. Sample concentrations were between 20 and 40 mg mL^{-1} and measurements were recorded at 298 K. Data processing was carried out using MestReNova (Version 9.0.1, Mestrelab Research S.L., Santiago de Compostela, Spain). **Mass spectrometry (MS):** electrospray ionization (ESI) was measured using an Agilent 6224 ESI-TOF device coupled with an Agilent HPLC 1200 Series and direct injection (110–3200 *m/z*) system. Electron ionization (EI-DIP) was measured using a Thermo ISQ LT EI device coupled with a Thermo Trace 1300 and direct injection (40–800 *m/z*) system. Data processing was carried out using MestReNova (Version 9.0.1, Mestrelab Research S.L., Santiago de Compostela, Spain). **Attenuated total reflection-Fourier transform Infrared (ATR-FT-IR) spectroscopy:** ATR-FT-IR spectra were recorded on a Bruker FT-IR Vertex 70 spectrometer (Bruker, Ettlingen, Germany) with a diamond ATR-probe. The measurement software was Opus 8.1. All samples were measured in the range of 3600–600 cm^{-1} with a resolution of 4 cm^{-1} and 32 scans. **Thermogravimetric analysis (TGA):** for thermogravimetric analysis, a TGA 209 F1 Iris system (NETZSCH-Gerätebau GmbH, Selb, Germany) was used to determine the mass loss during heat treatment. A temperature range of 25–600 °C with a heating rate of 10 K min^{-1} was chosen. About 5–10 mg of the polymer was weighed into a ceramic crucible. A normal atmosphere (with oxygen) was used with a flow rate of 20 mL min^{-1}. Data processing was performed using Proteus analysis (NETZSCH-Gerätebau GmbH, Selb, Germany). **Differential scanning calorimetry (DSC):** to determine the glass transition temperature (T_g) of the vitrimers, a DSC 204 F1 Phoenix differential scanning calorimeter (NETZSCH-Gerätebau GmbH, Selb, Germany) was used. 5–10 mg of the polymer was weighed into an aluminum crucible. The measurements were performed at one bar under a nitrogen atmosphere (flow rate of 20 mL min^{-1}) in the temperature range between −50 and 150 °C. The heating and cooling rates were set to 10 K min^{-1} and the thermal properties were analyzed using the DSC data of the second and third heating curves. Data processing was performed by Proteus analysis (NETZSCH-Gerätebau GmbH, Selb, Germany). **Dynamic-mechanical analysis (DMA):** for oscil-

latory shear experiments, a rotational rheometer (MCR 502, Anton Paar GmbH, Graz, Austria) with an 8 mm plate-plate geometry and a heat chamber with a nitrogen atmosphere was used. The temperature was controlled using a Peltier plate and by a constant nitrogen flow into the chamber. The gap between the lower and the upper plates was usually set to 1 mm. Amplitude sweeps between 0.01% and 1% shear strain (*y*) at a constant angular frequency (*ω*) of 10 rad per s were carried out at 110 °C before each measurement. This should ensure that the chosen strain amplitude y_0 was within the linear viscoelastic regime, so that the storage modulus G' and the loss modulus G'' were independent of strain. The temperature-dependent measurements were carried out at 10 rad s^{-1} and a deformation of 0.1%. The temperature was first increased from 110 to 150 °C at a rate of 2 K min^{-1}, and then, after a waiting period of 5 min, it was decreased from 150 to 0 °C. Usually, one measuring point per 1 K was recorded. The stress relaxation experiments were carried out with a deformation of 1% and the relaxation modulus was recorded as a function of time. The comparative measurements were carried out in temperature ranges of 110–150 °C. Data processing was performed using the RheoCompass software (version 1.19.266, Anton Paar GmbH, Graz, Austria). The test specimens for the dynamic-mechanical analysis and the relaxation tests were pushed out with an 8 mm punch. The vitrimer films were previously placed in a drying chamber at 100 °C for a few seconds in order to heat them above the glass transition temperature to prevent splintering during processing. **Tensile tests:** tensile tests were carried out at room temperature on a universal testing machine type Z020 (Zwick Roell) using a 5 kN load cell. The measurements were carried out in accordance with the test standard DIN EN ISO 527-1. The initial force was 0.1 MPa and the clamping length was 13.24 mm. The modulus of elasticity was determined at a speed of 1 mm min^{-1} and the rest of the test was carried out at 10 mm min^{-1}. The test specimens for the tensile test were punched out with a cutting press type ZCP020 (Zwick Roell). The attachment was used for test specimens of type 5B (according to DIN EN ISO 527-2). The vitrimer films were placed in a drying cabinet at 100 °C for a few minutes in order to heat them above the glass transition temperature, to prevent splintering during processing

Synthetic procedures

Phenyl 3-oxobutanoate (PH). Phenol (4.21 g, 0.0448 mol) and 2,2,6-trimethyl-1,3-dioxin-4-one (6.68 g, 0.0470 mol) were dissolved in xylene (4 mL) in a 100 mL flask. The mixture was heated at 135 °C for 45 min, while the byproduct acetone was removed by distillation during the reaction. The temperature in the still head was usually between 75 and 90 °C, and when the temperature dropped to 35 °C, xylene, acetone, TMDO and dehydroacetic acid were removed *in vacuo* (oil pump). The residue represented the desired product in a high degree of purity, appearing as a brownish liquid. δH (300 MHz, CDCl$_3$, Me$_4$Si, 298 K): 7.43–7.35 (2H, m, Ph), 7.29–7.21 (1H, m, Ph), 7.15–7.09 (2H, m, Ph), 3.69 (2H, s, CH$_2$), 2.36 (3H, s, CH$_3$). δC (75 MHz, CDCl$_3$, Me$_4$Si): 200.06 (q, C=O), 165.83 (q, COO),

Polymer Chemistry

Paper

150.49 (q, Ph), 129.63 (t, Ph), 126.33 (t, Ph), 121.15 (t, Ph), 50.09 (s, CH$_2$), 30.37 (p, CH$_3$). δH (300 MHz, DMSO-d6, 298 K): 7.47–7.39 (2H, m, Ph), 7.31–7.24 (1H, m, Ph), 7.16–7.10 (2H, m, Ph), 3.89 (2H, s, CH$_2$), 2.27 (3H, s, CH$_3$). δC (75 MHz, DMSO-d6, 298 K): 201.46 (q, C=O), 166.17 (q, COO), 150.28 (q, Ph), 129.58 (t, Ph), 126.02 (t, Ph), 121.65 (t, Ph), 49.47 (s, CH$_2$), 30.19 (p, CH$_3$). δH (300 MHz, benzene-d6, 298 K): 7.11–6.97 (4H, m, Ph), 6.92–6.85 (1H, m, Ph), 3.00 (2H, s, CH$_2$), 1.62 (3H, s, CH$_3$). δC (75 MHz, benzene-d6, 298 K): 198.77 (q, C=O), 165.52 (q, COO), 151.23 (q, Ph), 129.62 (t, Ph), 126.08 (t, Ph), 121.89 (t, Ph), 49.55 (s, CH$_2$), 29.43 (p, CH$_3$). EI-DIP: m/z 179.152 (M$^+$ + 1, 2.73%) 178.113 (M$^+$, 24.72), 94.128 (90.19), 43.024 (100). Calculated for C$_{10}$H$_{10}$O$_3$ (M$^+$) 178.063, found 178.113.

1,3-Phenylene bis(3-oxobutanoate) (RE). The crude, brownish 2,2,6-trimethyl-1,3-dioxin-4-one was purified by vacuum distillation to obtain a pure colorless product. Resorcin (15.27 g, 0.139 mol) and the purified TMDO (41.45 g, 0.292 mol) were dissolved in xylene (25 mL) in a 250 mL flask. The mixture was heated at 135 °C for 45 min, while the byproduct acetone was removed by distillation during the reaction. The temperature in the still head was usually between 75 and 90 °C, and when the temperature dropped to 35 °C, xylene, acetone, TMDO and dehydroacetic acid were removed *in vacuo* (oil pump). The residue represented the desired product in a high degree of purity, appearing as a yellowish oil. The other aromatic acetoacetate monomers were synthesized using the same synthetic protocol. δH (300 MHz, CDCl$_3$): 7.44–7.35 (1H, m, Ph), 7.08–7.03 (2H, m, Ph), 7.00–6.98 (1H, m, Ph), 3.69 (4H, s, CH$_2$), 2.35 (6H, s, CH$_3$). δC (75 MHz, CDCl$_3$, Me$_4$Si): 199.97 (q, C=O), 165.38 (q, COO), 150.90 (q, Ph–O), 130.05 (t, Ph), 119.42 (t, Ph), 115.38 (t, Ph), 49.46 (s, CH$_2$), 30.41 (p, CH$_3$). EI-DIP: m/z 278.146 (M$^+$, 0.37%), 194.118 (17.92), 110.066 (100) 43.014 (31.53). Calculated for C$_{14}$H$_{14}$O$_6$ (M$^+$) 278.079, found 278.146.

Naphthalene-2,7-diyl bis(3-oxobutanoate) (NDO). δH (300 MHz, CDCl$_3$): 7.90–7.84 (2H, d, J = 11 Hz, Ph), 7.59–7.54 (2H, d, J = 2.2 Hz, Ph), 7.33–7.21 (2H, d, Ph), 3.75 (4H, s, CH$_2$), 2.39 (6H, s, CH$_3$). δC (75 MHz, CDCl$_3$, Me$_4$Si): 200.03 (q, C=O), 165.86 (q, COO), 148.89 (q, Ph–O), 134.25 (q, Ph), 129.86 (q, Ph), 129.63 (t, Ph), 121.08 (t, Ph), 118.53 (t, Ph), 50.13 (s, CH$_2$), 30.47 (p, CH$_3$). EI-DIP: m/z 328.064 (M$^+$, 0.03%), 160.087 (100.00), 131.086 (26.20), 43.002 (15.06). Calculated for C$_{18}$H$_{16}$O$_6$ (M$^+$) 328.094, found 328.064.

Propane-2,2-diylbis(4,1-phenylene)bis(3-oxobutanoate) (BPA). δH (300 MHz, CDCl$_3$): 7.25–7.20 (4H, m, Ph), 7.04–6.99 (4H, m, Ph), 3.68 (4H, s, CH$_2$), 2.35 (6H, s, CH$_3$), 1.67 (6H, s, CH$_3$). δC (75 MHz, CDCl$_3$, Me$_4$Si): 200.06 (q, C=O), 165.87 (q, COO), 148.37 (q, Ph), 148.28 (q, Ph–O), 127.96 (t, Ph), 120.86 (t, Ph), 50.06 (s, CH$_2$), 42.57 (q, C–CH$_3$), 30.95 (p, CH$_3$), 30.31 (p, O=C–CH$_3$). EI-DIP: m/z 396.210 (M$^+$, 0.05%), 228.162 (21.73), 213.154 (100.00), 119.081 (18.09), 43.020 (12.17). Calculated for C$_{23}$H$_{24}$O$_6$ (M$^+$) 396.157, found 396.210.

Ethane-1,1,1-triyltris(benzene-4,1-diyl)tris(3-oxobutanoate) (THPE). δH (300 MHz, CDCl$_3$): 7.2–7.06 (6H, m, Ph), 7.05–6.98 (6H, m, Ph) 3.67 (6H, s, CH$_2$), 2.35 (9H, s, CH$_3$), 2.15 (3H, s,

CH$_3$). δC (75 MHz, CDCl$_3$, Me$_4$Si): 200.01 (q, C=O), 165.81 (q, COO), 148.77 (q, Ph–O), 146.48 (q, Ph–C), 129.86 (t, Ph), 120.93 (t, Ph), 51.80 (q, C–CH$_3$) 50.15 (s, CH$_2$), 30.95 (p, C–CH$_3$), 30.40 (p, O=C–CH$_3$). EI-DIP: m/z 558.271 (0.01%) 306.146 (9.05), 291.136 (100.00), 197.105 (10.57) 43.038 (13.32). Calculated for C$_{32}$H$_{30}$O$_9$ (M$^+$) 558.189, found 558.271.

N-Hexyl-3-(hexylamino)but-2-enamide (Hex-VUA-Hex). The crude, brownish 2,2,6-trimethyl-1,3-dioxin-4-one was purified by vacuum distillation to obtain a pure colorless product. Hexylamine (1.43 g, 0.0141 mol) and the purified TMDO (1.00 g, 0.00707 mol) were mixed in a 10 mL flask. The mixture was heated at 120 °C for 30 min, while the byproduct acetone was removed by distillation during the reaction. The residue represents the desired product in a high degree of purity, appearing as an orange liquid. The other vinylogous urea reference compounds were synthesized using the same synthetic protocol. δH (300 MHz, CDCl$_3$): 9.00 (1H, s, NH), 4.78 (1H, s, NH), 4.22 (1H, s, CH), 3.18 (2H, d, CH$_2$), 3.13 (2H, d, CH$_2$), 1.85 (3H, s, CH$_3$), 1.60–1.42 (4H, m, CH$_2$), 1.40–1.20 (12H, m, CH$_2$), 0.87 (3H, t, CH$_3$), 0.86 (3H, t, CH$_3$). δC (75 MHz, CDCl$_3$, 25 °C): 171.10 (q, C=O), 158.61 (q, C–CH$_3$), 84.32 (t, CH), 43.04 (s, CH$_2$), 31.07 (s, CH$_2$), 30.73 (s, CH$_2$), 30.31 (s, CH$_2$), 26.83 (s, CH$_2$), 26.75 (s, CH$_2$), 22.72 (s, CH$_2$), 22.66 (s, CH$_2$), 19.53 (p, CH$_3$). 14.15 (p, CH$_3$). δH (300 MHz, DMSO-d6. 298 K): 8.92 (1H, t, NH), 6.89 (1H, t, NH), 4.28 (1H, s, CH), 3.08 (2H, dd, CH$_2$), 2.97 (2H, dd, CH$_2$), 1.77 (3H, s, CH$_3$), 1.51–1.05 (16H, m, CH$_2$), 0.86 (3H, t, CH$_3$), 0.85 (3H, t, CH$_3$). δC (75 MHz, DMSO, 298 K): 170.56 (q, C=O), 156.94 (q, C–CH$_3$), 85.90 (t, CH), 42.33 (s, CH$_2$), 38.24 (s, CH$_2$), 31.57 (s, CH$_2$), 31.48 (s, CH$_2$), 30.78 (s, CH$_2$), 30.17 (s, CH$_2$), 26.69 (s, CH$_2$), 26.49 (s, CH$_2$), 22.58 (s, CH$_2$), 22.54 (s, CH$_2$), 19.36 (p, CH$_3$), 14.38 (p, CH$_3$), 14.35 (p, CH$_3$). δH (300 MHz, benzene-d6, 298 K): 9.68 (1H, s, NH), 4.63 (1H, t, NH), 4.25 (1H, s, CH), 3.26 (2H, d, CH$_2$), 2.77 (2H, dd, CH$_2$), 1.61 (3H, s, CH$_3$), 1.42–1.02 (16H, m, CH$_2$, 0.84 (3H, t, CH$_3$), 0.83 (3H, t, CH$_3$). δC (75 MHz, benzene-d6, 298 K): 171.04 (q, C=O), 157.40 (q, C–CH$_3$), 85.78 (t, CH), 42.90 (s, CH$_2$), 32.02 (s, CH$_2$), 31.89 (s, CH$_2$), 31.08 (s, CH$_2$), 30.81 (s, CH$_2$), 27.09 (s, CH$_2$), 26.89 (s, CH$_2$), 23.03 (s, CH$_2$), 22.91 (s, CH$_2$), 19.24 (p, CH$_3$). 14.29 (p, CH$_3$), 14.26 (p, CH$_3$). ESI: m/z 270.262 (M$^+$ + 2, 16.07%), 269.259 (M$^+$ + 1, 100.00). Calculated for C$_{16}$H$_{32}$N$_2$O (M) 268.251.

N-Phenyl-3-(phenylamino)but-2-enamide (Phe-VUA-Bz). δH (300 MHz, CDCl$_3$): 11.06 (1H, s, NH), 7.43–7.34 (2H, d, Ph), 7.26–7.15 (4H, m, Ph), 7.08–6.91 (4H, m, Ph), 6.85 (1H, s, NH), 4.57 (1H, s, CH), 1.91 (3H, s, CH$_3$). δC (75 MHz, CDCl$_3$): 168.85 (q, C=O), 157.38 (q, C–CH$_3$), 139.71 (q, Ph), 138.91 (q, Ph), 129.08 (t, Ph), 129.00 (t, Ph), 124.56 (t, Ph), 124.18 (t, Ph), 123.37 (t, Ph), 120.11 (t, Ph), 88.66 (t, CH), 20.57 (p, CH$_3$). EI-DIP: m/z 252.174 (M$^+$, 13.25%), 160.134 (100.00), 132.109 (15.36), 118.105 (11.17). Calculated for C$_{16}$H$_{16}$N$_2$O$_6$ (M$^+$) 252.126, found 252.174. **Hexylamine** δH (300 MHz, CDCl$_3$, 25 °C): 2.62 (2H, t, N–CH$_2$), 1.43–1.32 (2H, m, CH$_2$), 1.32–1.17 (6H, m, CH$_2$), 1.11 (2H, s, NH$_2$), 0.83 (3H, t, CH$_3$). δC (75 MHz, CDCl$_3$): 42.35 (s, CH$_2$), 33.93 (s, CH$_2$), 31.78 (s, CH$_2$), 26.63 (s, CH$_2$), 22.70 (s, CH$_2$), 14.08 (s, CH$_3$). **Benzylamine** δH

(300 MHz, CDCl$_3$, 25 °C): 7.31–7.15 (5H, m, Ph), 3.80 (2H, s, CH$_2$), 1.37 (2H, s, NH$_2$). δC (75 MHz, CDCl$_3$): 143.42 (q, Ph), 128.56 (t, Ph), 127.08 (t, Ph), 126.79 (t, Ph), 46.56 (s, CH$_2$). **Anilin** δH (300 MHz, CDCl$_3$, 25 °C): 7.06 (2H, t, Ph), 6.66 (1H, t, Ph), 6.57 (2H, d, Ph), 3.52 (2H, s, NH$_2$). δC (75 MHz, CDCl$_3$): 146.47 (q, Ph), 129.35 (t, Ph), 118.59 (t, Ph), 115.17 (t, Ph).

Phenyl-3-(hexylamino)but-2-enoate (Phe-VUT-Hex). Phenyl 3-oxobutanoate (PH) (0.043 g, 0.24 mmol) and hexylamine (0.049 g, 0.48 mmol) were stirred for 24 h at room temperature in deuterated chloroform, benzene or DMSO (0.1 M), while the reaction was monitored by ^{1}H NMR spectroscopy. Different amounts of acetic acid (0.03–1000 mol%) were added to the PH solution in order to perform different kinetics. The pure vinylogous urethane reference compounds were synthesized by adding 100 mol% acetic acid and using the same synthetic protocol. δH (300 MHz, CDCl$_3$, 298 K): 8.62 (1H, s, NH), 7.40–7.30 (2 H, m, Ph), 7.23–7.12 (1H, m, Ph), 7.11–7.05 (2H, m, Ph), 4.65 (s, 1H; CH), 3.20 (2H, m, CH$_2$) 1.98 (3H, s, CH$_3$), 1.68–1.47 (2H, m, CH$_2$), 1.40–1.18 (6H, m, CH$_2$), 0.93–0.79 (3H, t, CH$_3$). δC (75 MHz, CDCl$_3$, Me$_4$Si): 169.16 (q, COO), 164.08 (q, C=C), 151.54 (q, Ph–O), 129.28 (t, Ph), 124.96 (t, Ph), 122.32 (t, Ph), 80.82 (t, CH), 43.38 (s, CH$_2$), 31.59 (s, CH$_2$), 31.32 (s, CH$_2$), 26.62 (s, CH$_2$), 22.49 (s, CH$_2$), 31.6 (p, C–CH$_3$) 14.11 (p, CH$_2$–CH$_3$). δH (300 MHz, DMSO-d6, 298 K): 8.52 (1H, s, NH), 7.19–7.06 (2 H, m, Ph), 6.79–6.66 (3H, m, Ph), 4.57 (s, 1H; CH), 3.23 (2H, m, CH$_2$) 1.77 (3H, s, CH$_3$), 1.57–1.40 (2H, m, CH$_2$), 1.35–1.14 (6H, m, CH$_2$), 0.90–0.78 (3H, t, CH$_3$). δH (300 MHz, benzene-d6, 298 K): 8.90 (1H, s, NH), 4.90 (1H, s, CH), 2.54 (2H, dd, CH$_2$) 1.41 (3H, s, CH$_3$), 1.33–1.03 (8H, m, CH$_2$), 0.89–0.78 (6H, t, CH$_3$). ESI: m/z 263.184 (M$^+$ + 2, 17.15%), 262.181 (M$^+$ + 1, 100.00). Calculated for C$_{16}$H$_{23}$NO$_2$ (M) 261.172.

Phenyl-3-(benzylamino)but-2-enoate (Phe-VUT-Bz). δH (300 MHz, CDCl$_3$, 298 K): 8.98 (1H, t, NH), 7.33–7.03 (10H, m, Ph), 4.72 (1H, s, CH), 4.36 (2H, d, CH$_2$), 1.94 (s, 3H, CH$_3$). δC (75 MHz, CDCl$_3$, Me$_4$Si): 168.69 (q, COO), 163.36 (q, C=C), 151.15 (q, Ph–O), 137.92 (q, Ph), 129.10 (t, Ph), 128.54 (t, Ph), 126.94 (t, Ph), 125.54 (t, Ph), 121.64 (t, Ph), 81.95 (t, CH), 46.86 (s, CH$_2$), 19.34 (p, CH$_3$). ESI-MS: m/z 269.138 (M$^+$ + 2, 17.16%), 268.36 (M$^+$ + 1, 100.00). Calculated for C$_{17}$H$_{17}$NO$_2$ (M) 267.126.

Phenyl-3-(phenylamino)but-2-enoate (Phe-VUT-Phe). δH (300 MHz, CDCl$_3$, 298 K): 10.33 (1H, t, NH), 7.50–6.97 (10H, m, Ph), 4.87 (1H, s, CH), 2.02 (3H, s, CH$_3$). δC (75 MHz, CDCl$_3$, Me$_4$Si): 169.04 (q, COO), 161.42 (q, C=C), 151.21 (q, Ph–O), 129.45 (t, Ph), 129.10 (t, Ph), 124.74 (t, Ph), 122.24 (t, Ph), 118.72 (t, Ph), 84.86 (t, CH), 20.74 (p, CH$_3$). ESI: m/z 255.119 (M$^+$ + 2, 4.41%), 254.116 (M$^+$ + 1, 24.44). Calculated for C$_{16}$H$_{15}$NO$_2$ (M) 253.111.

Model study – exchange reaction (*E*$_a$ calculation)

VUT$_{aromatic}$: 4 equivalents of hexylamine were added to a mixture of **Phe-VUT-Bz** (1 M) and stirred for 4 hours at 70, 90 and 110 °C in xylene, resulting in the formation of the transamination product **Phe-VUT-Hex**. VUT$_{aliphatic}$: the reaction was carried out under the same conditions for **Me-VUT-Bz** (aliphatic vinylogous urethane). VUA: 4 equivalents of benzyl-

amine were added to a mixture of **Hex-VUA-Hex** (0.0015 M) and stirred for 30 minutes at 12, 22 and 32 °C in benzene, resulting in the formation of the transamination product **Hex-VUA-Bz**.

Vitrimer synthesis

Bulk: All vitrimers were prepared by the following exemplary synthesis route: propane-2,2-diylbis(4,1-phenylene)bis(3-oxobutanoate) (BPA) (1.38 g, 3.48 mmol) was provided in a rolled rim glass and heated up in an oil bath at 80 °C. When the vitrimer was cured with additional acetic acid, the acid was added to the acetoacetate monomer before the amine. Jeffamine-T403 (2.05 g, 6.96 mmol) was added under constant stirring. As soon as a homogeneous, opaque and cross-linked mass was obtained, the vitrimer-gel was filled onto a Teflon sheet and cured for 20 h at 100 °C *in vacuo* (oil pump). Afterwards, the vitrimer was post-cured for 1 h at 150 °C *in vacuo*, in order to ensure full conversion and the removal of the remaining reaction water. Next, the samples were pressed for 5–10 min at 150 °C into a 1 mm thick film. Solvent-based: the acetoacetate monomer was dissolved in chloroform (0.3 M) and acetic acid was added to the solution (70 mol%). Afterwards, Jeffamine-T403 was added to the solution and stirred until gelation. The gel was filled onto a Teflon sheet and cured under the same conditions as those used for the bulk reaction.

Recycling/reprocessing

The vitrimers were reprocessed by consecutive grinding and remolding, cutting the films and specimens into small pieces and pressing them at 150 °C for 5–10 min into 1 mm films. In each cycle, ATR-FT-IR and tensile test measurements were carried out repeatedly.

Shape-memory, solid state plasticity and self-healing experiments

Exemplary thermoadapt shape-memory properties were investigated by twisting the original film at 80 °C for 5 s, freezing the topology by cooling down to room temperature (22 °C) (topology freezing) and letting it relax back to the original shape at 80 °C for 30 s. Solid state plasticity was explored by bending the film at 150 °C for 300 s, reshaping it into a new shape due to the rearrangement of the cross-linking points. The self-healing experiment is exemplarily described for VU-RE$_{JA, 0.5}$. The DIN 5B specimens for tensile tests (1 mm) were cut in half in the middle of the specimen (0.5 mm) and heated for 30 minutes at 150 °C. Thecut and non-cut specimens were compared using tensile tests.

Conclusions

A synthetic route for an easily feasible acetoacetylation of aromatic alcohols using 2,2,6-trimethyl-4*H*-1,3-dioxin-4-one instead of the established *tert*-butylacetoacetate is introduced and proceeds significantly more efficient by simple heating for 45 minutes at 135 °C. With this, the widely used and commercially relevant alcohols such as bisphenol-A, resorcin,

2,7-naphthalenediol, and 1,1,1-tris(4-hydroxyphenyl)ethane are introduced as raw materials for vinylogous urethane vitrimers by easy acetoacetylation and curing with the commercially available poly(propylene oxide)-based trifunctional amine Jeffamine T-403 (**JA**) and tris(2-aminoethyl)amine (**TREN**). Model studies with monofunctional compounds show that aromatic acetoacetates undergo fast condensation- and substitution reactions with primary amines, leading to mixtures of vinylogous urethane and vinylogous urea bonds, both representing dynamic covalent bonds for thermally induced transamination reactions. Furthermore, this ratio can be adjusted by the used solvent (DMSO, benzene, and chloroform) and/or acetic acid as a catalyst, where the ratio can be completely shifted either to vinylogous urethane or vinylogous urea bonds. By transferring the findings from the model study to the preparation of vitrimers, 16 different elastomeric and thermosetting blended poly(vinylogous urethane/urea) networks were synthesized, showing glass transition temperatures of 11–73 °C and thermal degradation temperatures of 222–290 °C at ambient atmosphere. Dynamic mechanical analysis shows short stress-relaxation times of up to 0.7 s at 130 °C, with calculated activation energies of 43.8–149.7 kJ mol^{-1}, storage moduli of 0.10–0.81 GPa at 20 °C and rubbery plateaus of 0.12–2.05 MPa at 150 °C. In addition, tensile tests showed maximum tensile strengths of 5.2–62.8 MPa with elongations of 0.5–340% (at break) and Young's moduli of 5–1540 MPa. Moreover, the prepared smart materials exhibit remarkable reprocessing, reshaping, shape-memory and self-healing properties, by undergoing two consecutive cycles of grinding and remolding, showing thermoadapt shape-memory and solid state plasticity. Notably, this work contributes detailed model- and material studies for the use of aromatic alcohols as an important class of raw materials for several applications and introduces reprocessable alternatives to the established materials, which offer potential for further investigation of highly resilient, but reprocessable cross-linked polymers.

Author contributions

P. H. and V. A.: conceptualization; P. H. and G. S.: methodology, investigation, data curation, formal analysis, and validation; V. A.: supervision and resources; P. H.: writing – the original draft; and P. H. and V. A.: writing – review and editing.

Conflicts of interest

There are no conflicts to declare.

Acknowledgements

Notes and references

1 J. P. Pascault, H. Sautereau, J. Verdu and R. J. Williams, *Thermosetting polymers*, CRC press, Boca Raton, 2002.
2 A. D. McNaught and A. Wilkinson, *Compendium of Chemical Terminology*, Blackwell Science Publications, Oxford, 1997.
3 H. Dodiuk and S. H. Goodman, *Handbook of Thermoset Plastics*, Elsevier, Amsterdam, 2013.
4 C. N. Bowman and C. J. Kloxin, *Angew. Chem., Int. Ed.*, 2012, **51**, 4272–4274.
5 C. J. Kloxin and C. N. Bowman, *Chem. Soc. Rev.*, 2013, **42**, 7161–7173.
6 C. J. Kloxin, T. F. Scott, B. J. Adzima and C. N. Bowman, *Macromolecules*, 2010, **43**, 2643–2653.
7 H. Yang, K. Yu, X. Mu, X. Shi, Y. Wei, Y. Guo and H. J. Qi, *Soft Matter*, 2015, **11**, 6305–6317.
8 C. Bowman, F. Du Prez and J. Kalow, *Polym. Chem.*, 2020, **11**, 5295–5296.
9 A. Khan, N. Ahmed and M. Rabnawaz, *Polymers*, 2020, **12**, 2027.
10 M. Thiessen and V. Abetz, *Polymers*, 2021, **13**, 1189.
11 W. Denissen, J. M. Winne and F. E. Du Prez, *Chem. Sci.*, 2016, **7**, 30–38.
12 J. M. Winne, L. Leibler and F. E. Du Prez, *Polym. Chem.*, 2019, **10**, 6091–6108.
13 N. J. Van Zee and R. Nicolaÿ, *Prog. Polym. Sci.*, 2020, **104**, 101233.
14 D. Montarnal, M. Capelot, F. Tournilhac and L. Leibler, *Science*, 2011, **334**, 965–968.
15 M. Capelot, D. Montarnal, F. Tournilhac and L. Leibler, *J. Am. Chem. Soc.*, 2012, **134**, 7664–7667.
16 M. Capelot, M. M. Unterlass, F. Tournilhac and L. Leibler, *ACS Macro Lett.*, 2012, **1**, 789–792.
17 R. L. Snyder, D. J. Fortman, G. X. De Hoe, M. A. Hillmyer and W. R. Dichtel, *Macromolecules*, 2018, **51**, 389–397.
18 M. M. Obadia, B. P. Mudraboyina, A. Serghei, D. Montarnal and E. Drockenmuller, *J. Am. Chem. Soc.*, 2015, **137**, 6078–6083.
19 D. J. Fortman, J. P. Brutman, C. J. Cramer, M. A. Hillmyer and W. R. Dichtel, *J. Am. Chem. Soc.*, 2015, **137**, 14019–14022.
20 D. J. Fortman, J. P. Brutman, M. A. Hillmyer and W. R. Dichtel, *J. Appl. Polym. Sci.*, 2017, **134**, 44984.
21 M. Pepels, I. Filot, B. Klumperman and H. Goossens, *Polym. Chem.*, 2013, **4**, 4955–4965.
22 M. Guerre, C. Taplan, J. M. Winne and F. E. Du Prez, *Chem. Sci.*, 2020, **11**, 4855–4870.
23 Y. Spiesschaert, M. Guerre, L. Imbernon, J. M. Winne and F. Du Prez, *Polymer*, 2019, **172**, 239–246.
24 W. Denissen, G. Rivero, R. Nicolaÿ, L. Leibler, J. M. Winne and F. E. Du Prez, *Adv. Funct. Mater.*, 2015, **25**, 2451–2457.
25 W. Denissen, I. De Baere, W. Van Paepegem, L. Leibler, J. Winne and F. E. Du Prez, *Macromolecules*, 2018, **51**, 2054–2064.
26 S. Dhers, G. Vantomme and L. Avérous, *Green Chem.*, 2019, **21**, 1596–1601.

27 Y. Spiesschaert, C. Taplan, L. Stricker, M. Guerre, J. M. Winne and F. E. Du Prez, *Polym. Chem.*, 2020, **11**, 5377–5385.

28 T. Wright, T. Tomkovic, S. G. Hatzikiriakos and M. O. Wolf, *Macromolecules*, 2018, **52**, 36–42.

29 J. J. Lessard, G. M. Scheutz, S. H. Sung, K. A. Lantz, T. H. Epps III and B. S. Sumerlin, *J. Am. Chem. Soc.*, 2019, **142**, 283–289.

30 B. Krishnakumar, R. P. Sanka, W. H. Binder, V. Parthasarthy, S. Rana and N. Karak, *Chem. Eng. J.*, 2020, **385**, 123820.

31 C. Ye, V. S. D. Voet, R. Folkersma and K. Loos, *Adv. Mater.*, 2021, **33**, 2008460.

32 R. J. Friary, V. Seidl, J. H. Schwerdt, T.-M. Chan, M. P. Cohen, E. R. Conklin, T. Duelfer, D. Hou, M. Nafissi and R. L. Runkle, *Tetrahedron*, 1993, **49**, 7179–7192.

33 K. Ostrowska, M. Ciechanowicz-Rutkowska, T. Pilati and G. Zżuchowski, *Monatsh. Chem.*, 1999, **130**, 555–562.

34 M. Irfan, *Chemistry and Technology of Thermosetting Polymers in Construction Applications*, Springer Science & Business Media, Luxembourg, 1998.

35 *Epoxy resins: Chemistry and Technology*, ed. M. Clayton, Routledge, London, 2018.

36 H. Q. Pham and M. J. Marks, Epoxy Resins, in *Ullmann's Encyclopedia of Industrial Chemistry*, Wiley, Weinheim, 7th edn, 2005.

37 K. W. Schmiedel and D. Decker, Resorcinol, in *Ullmann's Encyclopedia of Industrial Chemistry*, Wiley, Weinheim, 7th edn, 2011.

38 R. B. Durairaj, *Chemistry, Technology and Applications*, Springer Science & Business Media, Luxembourg, 2005.

39 A. Gardziella, L. A. Pilato and A. Knop, *Phenolic resins: Chemistry, Applications, Standardization, Safety and Ecology*, Springer Science & Business Media, Luxembourg, 2013.

40 M. Asim, N. Saba, M. Jawaid, M. Nasir, M. Pervaiz and O. Y. Alothman, *Curr. Anal. Chem.*, 2018, **14**, 185–197.

41 M. Miyasaka, T. Takazoe, H. Kudo and T. Nishikubo, *Polym. J.*, 2010, **42**, 852–859.

42 H. Domininghaus, P. Eyerer, P. Elsner and T. Hirth, *Die Kunststoffe und ihre Eigenschaften*, Springer-Verlag, Berlin, 2005.

43 M. Weber and P. Charoensirisomboon, *Macromol. Symp.*, 2003, **199**(1), 243–252.

44 I. Sluijs, J. Heijl, E. Sluyts and F. Bruynseels, *US Pat.*, US20170369642A1, 2016; Covestro Deutschland AG.

45 C. E. Scott, M. E. Stewart, D. S. Wilmoth, J. C. Morris and J. R. Bradley, *US Pat.*, US5942585A, 1997; Eastman Chemical Co.

46 W. Kaiser, *Kunststoffchemie für Ingenieure*, Hanser München, 2006.

47 H. Shindy, *Chem. Int*, 2016, **2**, 41–47.

48 H. P. Latscha and H. A. Klein, *Organische Chemie: Chemie—Basiswissen II*, Springer, Berlin, 1990, pp. 559–567.

49 R. L. Stamper, M. F. Lieberman and M. V. Drake, *Becker-Shaffer's Diagnosis and Therapy of the Glaucomas*, Elsevier Health Sciences, Amsterdam, 2009.

50 J. M. Dennis, R. J. Mondschein, J. D. Wolfgang, M. Hegde, R. Odle and T. E. Long, *ACS Appl. Polym. Mater.*, 2020, **2**, 958–965.

51 A. M. Nelson and T. E. Long, *Polym. Int.*, 2012, **61**, 1485–1491.

52 R. K. Shahni, M. Mabin, Z. Wang, A. Shaik, A. Ugrinov and Q. R. Chu, *Polym. Chem.*, 2020, **11**, 6081–6090.

53 T. Wang, J. P. Matinlinna, J. He, K. E. Ahmed and M. F. Burrow, *Mater. Sci. Eng., C*, 2020, **117**, 111309.

54 D. Schmidt, *US Pat.*, US9139690B2, 2012; UMass Lowell.

55 N. Jalal, A. R. Surendranath, J. L. Pathak, S. Yu and C. Y. Chung, *Toxicol. Rep.*, 2018, **5**, 76–84.

56 C. Erler and J. Novak, *J. Pediatr. Nurs.*, 2010, **25**, 400–407.

57 C. Taplan, M. Guerre, J. M. Winne and F. E. Du Prez, *Mater. Horiz.*, 2020, **7**, 104–110.

58 F. J. Zawacki and M. T. Crimmins, *Tetrahedron Lett.*, 1996, **37**, 6499–6502.

59 Y.-J. Li, H.-Y. Hung, Y.-W. Liu, P.-J. Lin and H.-J. Huang, *Tetrahedron*, 2011, **67**, 927–935.

60 V. Sridharan, M. Ruiz and J. C. Menéndez, *Synthesis*, 2010, 1053–1057.

61 R. J. Clemens and J. A. Hyatt, *J. Org. Chem.*, 1985, **50**, 2431–2435.

62 P. Haida and V. Abetz, *Macromol. Rapid Commun.*, 2020, **41**, 2000273.

63 D. Xin and K. Burgess, *Org. Lett.*, 2014, **16**, 2108–2110.

64 W. A. Henderson and C. J. Schultz, *J. Org. Chem.*, 1962, **27**, 4643–4646.

65 T. Kanzian, T. A. Nigst, A. Maier, S. Pichl and H. Mayr, *Eur. J. Org. Chem.*, 2009, 6379–6385.

66 P. Haida and V. Abetz, *Macromol. Rapid Commun.*, 2020, **41**, 2000273.

67 X. Kuang, G. Liu, X. Dong, X. Liu, J. Xu and D. Wang, *J. Polym. Sci., Part A: Polym. Chem.*, 2015, **53**, 2094–2103.

68 L. Liu and H. D. Wagner, *Compos. Sci. Technol.*, 2005, **65**, 1861–1868.

69 L.-Q. Liu and H. D. Wagner, *Compos. Interfaces*, 2007, **14**, 285–297.

70 H. Lu and G. Tan, *Mech. Time-Depend. Mater.*, 2001, **5**(2), 119–129.

71 W. Chen and B. Zhou, *Mech. Time-Depend. Mater.*, 1998, **2**, 103–111.

72 R. J. Morgan, F. M. Kong and C. M. Walkup, *Polymer*, 1984, **25**, 375–386.

73 R. J. Morgan and C. M. Walkup, *J. Appl. Polym. Sci.*, 1987, **34**, 37–46.

74 L. Bai and J. Zheng, *Compos. Sci. Technol.*, 2020, **190**, 108062.

75 Z. Tang, Y. Liu, B. Guo and L. Zhang, *Macromolecules*, 2017, **50**, 7584–7592.

76 N. Zheng, J. Hou, Y. Xu, Z. Fang, W. Zou, Q. Zhao and T. Xie, *ACS Macro Lett.*, 2017, **6**, 326–330.

77 Y. Chen, Z. Tang, Y. Liu, S. Wu and B. Guo, *Macromolecules*, 2019, **52**, 3805–3812.

5.3   Publication 3: Starch-Reinforced Vinylogous Urethane Vitrimer Composites

Starch-Reinforced Vinylogous Urethane Vitrimer Composites: An Approach to Biobased, Reprocessable, and Biodegradable Materials

This work was conducted within a cooperation between the Chulalongkorn University in Bangkok and the University of Hamburg. The project was started within a four months stay in the working group of Prof. Suwabun Chirachanchai. The helpful advice and supervision of professor Suwabun Chirachanchai and the group is gratefully acknowledged.

In publication 3, polymer-polymer composites were synthesized with the motivation to prepare bio-based, reprocessable and biodegradable composites with enhanced mechanical properties. Combining the benefits of vitrimers and the use of renewable raw material resources, the carbon footprint can be reduced, and new materials with distinct properties and the ability for mechanical, chemical, and biological recycling/reprocessing methods can be achieved. Starch-based polymers and starch-based blends like thermoplastic starch are among the most utilized polymers for commercially fabricated biodegradable materials.[146, 147] However, starch-based polymers and blends face some disadvantages, *e.g.*, high hydrophilicity leading to mechanical weakening, leaking out of plasticizers like glycerol or sorbitol and/or poor mechanical properties.[148] Nevertheless, starch shows unabated interest in polymer science and recently to the field of bio-based vitrimers.

It has been shown that starch granules can be surface acetoacetylated without destroying the inner semicrystalline, complex supramolecular structure and maintaining the densely packed granules. The modification enabled the implementation of the polyfunctional starch granules into the vitrimer network, which acted as an additional cross-linker and filler. The matrix vitrimers were prepared by vinylogous urethane vitrimers polymerized of fully acetoacetylated glycerol and different diamines. The cross-linked composites show enhanced mechanical properties with increased E-moduli, low swelling ratios and suppressing of the natural gelatinization of starch in contact with water even at high temperatures. Moreover, suitable thermomechanical, chemical and enzymatic recycling methods were developed for closed loop cycles, reusability and biodegradability. Seven

matrix vitrimers were synthesized and compared in terms of their properties with and without the modified starch. Reprocessable materials with up to 70 wt% of starch were achieved. This work shows the development of hierarchical polymer-polymer composites and the successful implementation of natural compounds as reinforcing filler and cross-linking agent, providing the basis for future biodegradable, high-performance et reprocessable materials.

The related supporting information is available in Section 9.4.

Research Article

Starch-Reinforced Vinylogous Urethane Vitrimer Composites: An Approach to Biobased, Reprocessable, and Biodegradable Materials

Philipp Haida, Suwabun Chirachanchai, and Volker Abetz*

Cite This: https://doi.org/10.1021/acssuschemeng.3c01340

Read Online

ACCESS | Metrics & More | Article Recommendations | Supporting Information
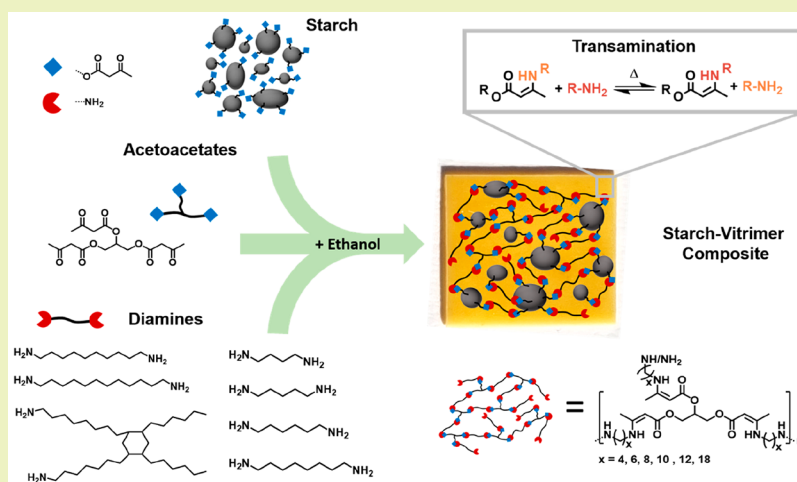
ABSTRACT: Vitrimers represent permanent and dynamic polymer networks at the same time. The combination of dynamic covalent bonds and widely available, biodegradable, and biobased raw materials enables new polymers with an excellent carbon footprint, mechanical properties, and outstanding features in terms of multiple recycling methods, e.g., thermomechanical, chemical, and biological reprocessing/reusability. Natural corn starch granules have been surface-modified by an acetoacetylation reaction without using any additional solvent and maintaining the inner semicrystalline structure, giving a polyfunctional cross-linker for starch-reinforced vitrimer composites. Vinylogous urethane vitrimer matrices were synthesized by the condensation reaction of fully acetoacetylated glycerol and different diamines, while glycerol and the diamines were deliberately selected as potentially biobased raw materials. Seven different matrix vitrimers were synthesized with a content of 0−70 wt % of modified starch and investigated in terms of their thermal and mechanical properties. In total, 20 elastomeric and thermosetting materials have been prepared, exhibiting high elastic moduli of 2 GPa with short stress relaxation times and a high content of modified starch up to 70 wt %. The composites show low swelling ratios, suppressing the natural gelatinization of starch in water. Moreover, suitable thermomechanical, chemical, and enzymatic recycling methods for closed-loop cycles, remolding, reusability, and biodegradability were developed.

KEYWORDS: covalent adaptable networks, biobased vitrimers, vinylogous urethane vitrimers, vitrimer-composites, biodegradable, starch

■ INTRODUCTION

Vitrimers have attracted increasing interest in scientific research and industry since their first introduction by Leibler's group,[1] and various polymers and applications were already demonstrated since then.[2,3] Due to their unique properties in terms of the mechanical and chemical stability in combination with available dynamic chemical bonds, the cross-linked materials merge the favorable properties of classic thermosets and thermoplastics. Vitrimers belong to the class of covalent adaptable networks (CANs) and contain covalent dynamic bonds, which proceed by a thermally induced, associative exchange mechanism, making these networks permanent as well as dynamic. Therefore, the innovative materials can be

reprocessed and remolded, show self-healing and shape-memory properties simultaneously.[2,4−7] The unique properties make them promising candidates to overcome the environmental and waste disposal problems of classic, nonrecyclable thermosets. In this context, also biobased polymers show highly increased research interest, with countless new

publications every year, especially in the past decade.[8,9] Combining the benefits of vitrimers and the use of renewable raw resources, the carbon footprint can be reduced, and new materials with distinct properties and the ability for mechanical, chemical, and biological recycling/reprocessing can be implemented. Motivated by that, vitrimers based on different exchange mechanisms, e.g., transesterification, transamination, transimination, boronic-ester exchange, transcarbamoylation, and thiol–disulfide exchanges, were fabricated on the basis of countless biobased raw materials derived from vegetable oils, terpenes, carbohydrates, lignin, and more. Especially, widely available and inexpensive polysaccharides like starch, cellulose, and chitin are of great interest.[8,10,11] Nowadays, starch-based polymers and starch blends like thermoplastic starch are among the most utilized polymers for commercially fabricated biodegradable materials.[12−14] However, starch-based polymers and blends face some disadvantages, e.g., high hydrophilicity leading to mechanical weakening, leaking out of plasticizers, and poor mechanical properties.[15] Nevertheless, starch shows unabated interest in polymer science and recently to the field of biobased vitrimers. The synthesis of a starch-based, elastomeric epoxy vitrimer through the incorporation of garlic-based diallyl disulfide was reported. Epoxidized amylopectin-rich starch and epoxidized bisphenol A, diallyl disulfide, and thiol cross-linkers were reacted via "click" reaction. After reprocessing, the fabricated elastomeric vitrimer displayed self-strengthening properties with increased glass transition temperature (25 °C), tensile strengths (18.5 MPa), E-modulus (268 MPa), and elongation at break (>900%).[16] In another approach, oxidized starch with 57% carboxyl content (30 phr) was fabricated and served as a cross-linking agent, reacting with epoxidized natural rubber latex to form a soft, elastomeric polymer network with glass transition temperatures below 0 °C. Consequently, the cross-linking density determined the performance of the biobased and biodegradable vitrimer and enabled it to achieve a high elongation at break (1108%) and elastic recovery (90%).[17] Moreover, catalyst-free, fully biobased hydroxyester vitrimers were synthesized by cross-linking and plasticizing epoxidized soybean oil and acetylated starch-succinate monoesters. The vitrimers possessed a lower glass transition temperature, better solvent resistance and reprocessing performance compared to traditional starch-based materials.[18,19] A summary of the state of art, epoxy-based, soft, and elastomeric vitrimer composites proceeded by catalyzed and noncatalyzed transesterification or thiol–disulfide exchanges is presented, using starch as a polyfunctional monomer, but not as the main compound with more than 50 wt % of the material. Adding modified starch as a cross-linker, an improvement of the mechanical properties could be achieved while maintaining the reprocessability and enabling partly biodegradability.[19,20]

In this work, acetoacetylated starch granules were used as a reinforcing cross-linking agent for elastomeric and thermosetting vinylogous urethane vitrimer matrices synthesized by the condensation reaction of acetoacetylated glycerol and diamines. In the process, particular attention was paid to maintain the semicrystalline structure of the starch granules during the preparation of the materials. Moreover, glycerol and seven diamines were deliberately selected as potentially biobased raw materials, which can be produced by biotechnological production methods, e.g., glycerol as a byproduct from biodiesel production and other methods.[21−23] With this, cross-linked, particulate-filled polymer–polymer

microcomposite vitrimers with a high content of up to 95 wt % renewable raw materials were fabricated. To tune the properties of the emerging composites, seven matrix vitrimers were synthesized and compared in terms of their properties and interaction with the acetoacetylated starch granules. A focus was set on maximizing the amount of starch and the improvement of the mechanical properties, while maintaining the reprocessability. Giving a rough techno-economic estimation, the cheap and widely available raw materials starch, glycerol and some of the diamines (1,6-diaminohexane and Priamine 1075) are already established for huge polymer productions in industry and the omission of solvents and relatively short heating periods opens up opportunities to use this process in bigger scales as well.

■ EXPERIMENTAL SECTION

Materials and methods sections are shown in the Supporting Information (SI, S1−S4).

Synthetic Procedures. Propane-1,2,3-triyl tris(3-oxobutanoate) (GlyAcAc): The synthesis route was adapted from Witzemann et al. and customized in terms of reaction conditions and acetoacetylation agent.[24] The crude, brownish 2,2,6-trimethyl-1-3-dioxin-4-one (TMDO) was purified by vacuum distillation at 60 °C and 0.1 mbar to obtain the pure colorless product. Glycerol (10.0 g, 0.108 mol) and the purified TMDO (48.6 g, 0.342 mol) were mixed in a 250 mL flask. The mixture was heated at 135 °C for 1 h, while the byproduct acetone was removed by distillation during the reaction. The remaining acetone, TMDO, and dehydroacetic acid were removed in vacuo at 135 °C and 0.1 mbar. The residue represented the desired product in a high degree of purity, appearing as a slightly yellowish liquid. Yield: 98%. The synthetic routes of EgAcAc, HexAcAc, and CsAcAc follow a similar protocol and are described in SI (SI, S5 and S6).

Vitrimer Synthesis. All vitrimers were prepared by the following exemplary synthesis route: In ethanol dispersed CsAcAc (1.03 g starch, 0.50 g mL^{-1}) was provided in a 10 mL beaker. GlyAcAc (1.42 g, 4.12 mmol) and a diamine, e.g., hexanediamine (0.98 g, 8.4 mmol) were added and mixed. After a few minutes, a homogeneous, opaque, and cross-linked gel was obtained. The obtained gel was cured for 18 h at 100 °C and postcured for 1 h at 150 °C in vacuo. Next, the samples were pressed for 5−10 min at 160 °C with a pressure of 500− 1000 N cm^{-2} into a 1 mm thick film. The acetoacetate to amine ratio was set to R = 0.75 for 0 wt % CsAcAc, R = 0.73 for 30 wt %, R = 0.7 for 50 wt %, and R = 0.65 for 70 wt %. Mechanical recycling/ reprocessing: The vitrimers were reprocessed by consecutive grinding and remolding, cutting the films and specimen into small pieces and pressing 5−10 min at 160 °C with a pressure of 500−1000 N cm^{-2} into a 1 mm thick film. Chemical recycling: The materials were dissolved in an aqueous acetic acid (10 wt %, 25 mg g^{-1}) solution. After 18 h at 20 °C, the degraded material was obtained, dried and pressed 5−10 min at 160 °C with a pressure of 500−1000 N cm^{-2} into a 1 mm thick film. Swelling ratio/gel content/soluble fraction: The dried materials were weighed, put into water for 3 h at 100 °C or tetrahydrofuran (THF) for 24 h at 20 °C, and weighed again in the swollen and dried state. To determine the soluble fraction, the remaining THF was removed and the residue weighed (equations, SI, S6-T1). Enzymatic hydrolysis (biodegradability): To investigate the enzymatic hydrolysis of corn starch and CsAcAc 20 mg powder were dispersed aqueous iodine solution (1 wt %, 3 mL), which turned purple due to the formation of triiodide-amylose complexes. Afterward, α-amylase was added (20 mg, pH = 7, 25 °C, *Aspergillus oryzae*) and a color change from purple to almost colorless was observed. To investigate the vitrimer composites, VU-PA$_{70}$ (40 mg) was put into an aqueous iodine solution (1 wt %, 6 mL), which caused the material to turn dark purple after 24 h at 20 °C The dark purple material was cut into half and put into an aqueous solution (3 mL) and in an aqueous α-amylase solution (0.05 g g^{-1}, 3 mL) for 30 min. The color change from purple to colorless was monitored. The

solution was filtered with 0.2 μm PTFE filters and characterized by ESI-MS. For an application-related experiment, the composites were left for 6 weeks under nonspecific, wet conditions, observing a mold growth of likewise raw starch conquering mold after a few days at room temperature.

RESULTS AND DISCUSSION

Acetoacetate Monomers. According to the literature, the acetoacetylation of various alcohols as monomers for vinylogous urethane vitrimers is carried out in organic, high-boiling solvents like xylene or dimethylformamide.[25−28] In times of increasing environmental pollution and the exploitation of fossil resources, it is desirable to use renewable raw materials and explore the expendability of (toxic) organic solvents. The acetoacetylation of several alcohols likewise takes place without using an additional organic solvent, only with the acetoacetylation agent, utilizing the same reaction conditions. In comparison, it was found that the acetoacetylation agent TMDO proceeds more efficiently than t-BuAcAc with faster conversions.[29] Glycerol, ethylene glycol, 1,6-hexanediol, or starch were mixed with an excess of TMDO and heated for 45−60 min at 135 °C to obtain the liquid products GlyAcAc, EgAcAc, and HexAcAc or the solid, modified starch granules (CsAcAc; Figure 1a). ATR-FT-IR spectroscopy proved a successful acetoacetylation by measuring the characteristic C= O ester (1738−1742 cm^{-1}) and C=O ketone stretching vibrations (1711 cm^{-1}), as well as decreasing O−H stretching vibrations (3000−3600 cm^{-1}; Figure 1b; all spectra, SI, S7-S1 and -S2). ^{1}H NMR spectra showed the characteristic chemical shifts, including the acetoacetate signals at 2.17 ppm (CH$_3$) and 3.62 ppm (CH$_2$) (Figure 1c). ^{13}C NMR spectra and mass spectrometry (MS, ESI/EI) likewise proved the formation (^{1}H NMR/^{13}C NMR, SI, S8-S1 and -S2, S9-S1 and -S2, S10-S1 and -S2) (MS, SI, S11-S1 and -S2, S12-S1 and -S2). Starch granules consist of α-D-glucose repeating units titled as anhydrous glucose units (AGU), which form the linear polymer amylose and the branched polymer amylopectin by 1,4- and 1,6-glycosidic bonds. These polymers build supramolecular, semicrystalline, and hydrogen-bonded granules in the micrometer range, while the amylose/amylopectin ratio, crystal structure, size, and morphology vary in the different types of starch (e.g., corn, tapioca, rice, wheat, and potato).[30−32] It was explored that TMDO-dispersed corn starch granules can be surface-acetoacetylated by this synthetic route without destroying the inner semicrystalline structure, shape, or size of the starch granules (Figure 1a). In contrast, Qi et al. reported an acetoacetylation of starch dissolved in dimethyl sulfoxide, leading to the degradation of the starch granules during the synthesis.[33,34] The surface modification works for wheat, tapioca, and rice starch as well, plausibly working for any type of starch. ATR-FT-IR spectra show the characteristic acetoacetate C=O ester (1746 cm^{-1}), C=O ketone (1713 cm^{-1}), and C−O stretching vibrations (1140 cm^{-1}; Figure 1b). Furthermore, the O−H (3000−3600 cm^{-1}) and C−O stretching vibrations of the AGU (995, 1078, and 1148 cm^{-1}) of native corn starch are represented.[35] ^{1}H NMR spectra show the characteristic chemical shifts of AGU and the acetoacetate group at 2.17 ppm (CH$_3$) and 3.62 ppm (CH$_2$) (Figure 1c).[36] Integrating the OH-signals and the CH$_3$ group (AcAc), about 2.0−2.5 mol % of the hydroxy groups were acetoacetylated. ^{13}C NMR spectra confirmed the acetoacetylation by measuring the characteristic CH$_3$ signal at 30.1 ppm,
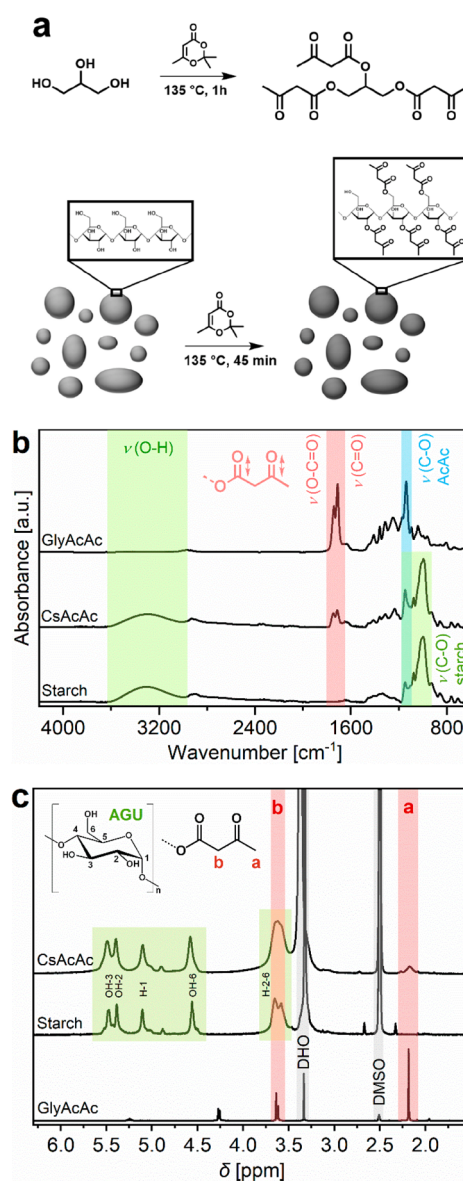
Figure 1. (a) Scheme of the acetoacetylation reaction of glycerol and corn starch granules using TMDO. (b) ATR-FT-IR spectra of GlyAcAc, CsAcAc, and corn starch showing the characteristic bands of the acetoacetate group with the C=O ester (1742−1746 cm^{-1}, red), C=O ketone (1711−1713 cm^{-1}, red), and C−O (1140−1148 cm^{-1}, blue) stretching vibration bands. The backbone AGU represents the C−O (995−1148 cm^{-1}) and O−H (3000−3600 cm^{-1}) stretching vibration bands (green). (c) ^{1}H NMR spectra of GlyAcAc and CsAcAc, showing the characteristic chemical shifts of the acetoacetate group at 2.17 ppm (CH$_3$, red a) and 3.62 ppm (CH$_2$, red b), as well as the backbone signals of the AGU (green).

besides the typical chemical shifts of AGU (full ^{1}H NMR/^{13}C NMR spectra, SI, S13-S1 and -S2).[37]

As another quantitative method, elemental analysis was carried out. The raw corn starch and CsAcAc were reacted with an excess of monofunctional isobutylamine to form vinylogous urethane bonds. After removing the excess of free amines through intensive washing with ethanol and evaporating the slightly volatile isobutylamine in vacuo, the results were compared regarding the nitrogen content. Doing that, an initial degree of acetoacetylation of 1.5−2 mol % of the hydroxy

c

groups was calculated, confirming the results determined by ^{1}H NMR spectroscopy (SI, S14-T1). Furthermore, this result showed that free amines do not undergo a significant amount of side reactions under these conditions, e.g., Maillard reaction, since the nitrogen content stays constant before and after the treatment with isobutylamine when using raw starch. Scanning electron microscope (SEM) and optical microscope (OM) images were recorded to evaluate the particle morphology before and after the modification. Corn starch consists of irregular polyhedron-shaped granules with an average diameter of 5−20 μm, while much smaller and bigger granules are present sporadically.[34,38,39] The images indicate no significant differences before and after the surface modification (Figure 2a) (different magnifications, SI, S14-S1, S15-S1). XRD
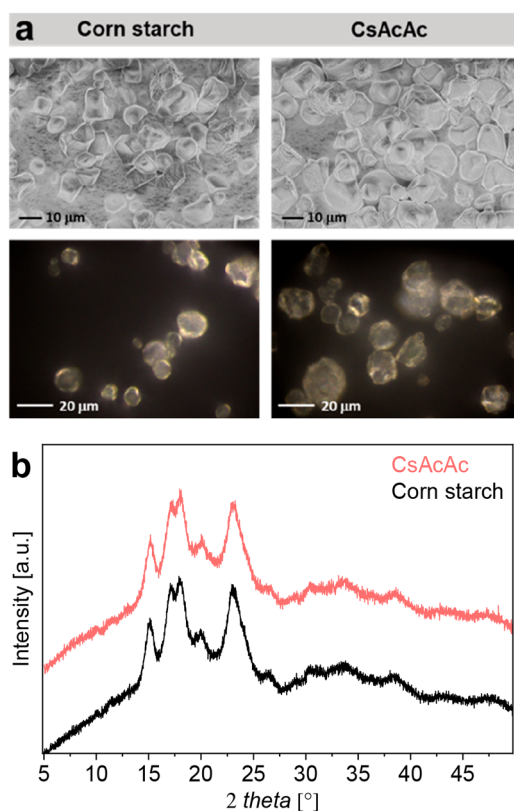
Figure 2. (a) SEM (top) and OM (bottom) images of the raw corn starch and CsAcAc, showing similar polyhedron-shaped granules with a diameter of 5−20 μm in all images. (b) XRD-powder diffractograms of raw corn starch and CsAcAc.

measurements proved that the inner semicrystalline structure of the starch granules is not affected by the modification reaction, exhibiting the characteristic Bragg peaks of corn starch before and after the modification (Figure 2b).[40,41] DSC measurements showed no significant difference in comparison to raw corn starch and CsAcAc, exhibiting melting points obove 200 °C (SI, S16-S1).[42,43]

Matrix Vitrimers and Starch-Reinforced Vitrimer Composites. For the preparation of the starch-vitrimer composites GlyAcAc, CsAcAc, and 1,4-diaminobutane (DAB), 1,5-diaminopentane (DAP) 1,6-diaminohexane (DAH), 1,8-diaminooctane (DAO), 1,10-diaminodecane (DAD), 1,12-diaminododecane (DADD), or Priamine 1075 (PA) were mixed at different ratios and compared in terms of the properties of the materials. DAB and DAP are biogenic

diamines, mainly produced by fermentation, whole-cell bioconversion, or enzymatic processes.[44,45] Especially for DAP, many different production pathways have been developed with first productions on an industrial scale.[22,46,47] Biotechnological methods can also generate DAH, DAO, DAD, and DADD from sugars with mostly the intermediate product of the corresponding diol.[22,48,49] PA is a commercially available, biobased diamine generated from terpenes.[50] The monomers were mixed with a small amount of ethanol (1/3 of the total monomer mass) until an opaque, homogeneous gel was obtained. To obtain homogeneous materials, ethanol was used as a green plasticizer, gelation retarder, and cosolvent (Figure 3). Due to the high viscosity and poor mixing performance, ethanol was especially essential for the synthesis of materials with high amounts of CsAcAc (50−70 wt %), while lower amounts (0−30 wt %), could also be prepared without ethanol by bulk reaction. The materials were labeled as VU-amine$_{wt\%CsAcAc}$ (e.g., VU-DAO$_{30}$), and the used monomer ratios are illustrated in SI (SI, S16-S2). It was found that vitrimers with relatively long alkyl chains of the diamine (DADD, PA) and a low cross-linking density allow the synthesis of vitrimer composites with a high share of CsAcAc up to 70 wt %. Regarding DAB, DAH, DAO, and DAD the highest amount was 30−50 wt %, since reprocessing did not work sufficiently well and led to brittle and cracked materials without efficient reprocessing during heat compression.

To evidence that modified starch acts as a multifunctional cross-linker, HexAcAc and DAH (R = 0.9) were mixed to prepare a soft, linear, and thermoplastic reference polymer without any cross-linker, which showed the characteristic vinylogous urethane bands (ATR-FT-IR, S17-S1). Polymerizing the linear polymer with 50 wt % raw corn starch as a filler, the prepared material still showed thermoplastic properties. Polymerizing with 50 wt % of CsAcAc, a cross-linked material was prepared, proven by temperature-dependent dynamic mechanical analysis (DMTA; SI, S17-S1 and S18-S1). Supporting this result, tensile tests showed a significant increase in the elastic modulus from 0.5 to 26 MPa, and increase in tensile strength from 0.7 to 3.1 MPa (SI, S18-S2). To prepare resilient composite materials, the modified starch granules were incorporated into a cross-linked vitrimer matrix synthesized by the trifunctional GlyAcAc and different diamines. ATR-FT-IR spectra showed the formation of the characteristic C=C (1592−1604 cm^{-1}) and C=O ester (1644−1654 cm^{-1}) bands of the vinylogous urethane bonds (all spectra, SI, S19-S1 and -S2). Moreover, spectra of the matrix vitrimer VU-PA$_0$ and composites with different amounts of CsAcAc were compared, showing the characteristic vinylogous urethane bands and an increase in O−H and C−O stretching vibrations of the AGU with a rising amount of CsAcAc in the materials (SI, S20-S1). XRD measurements show the characteristic Bragg peaks of CsAcAc in the composite material VU-PA$_{70}$, indicating that the inner semicrystalline structure remained intact throughout the process (SI, S20-S2).[10] Differential scanning calorimetry (DSC) measurements showed elastomeric and thermosetting vitrimers with T_g's of (−26)−71 °C (VU-DAB$_0$: 71 °C, VU-DAP$_0$: 63 °C, VU-DAH$_0$: 54 °C, VU-DAO$_0$: 47 °C, VU-DAD$_0$: 36 °C, VU-DADD$_0$: 29 °C, VU-PA$_0$: (−26) °C, o--set) (SI, S21-S1). The T_gs increased with a declined chain length of the diamine and showed a linear dependency with a calculated increase of 5 °C per additional CH$_2$ group (SI, S21-S2). PA is excluded from this trend due to its different molecular
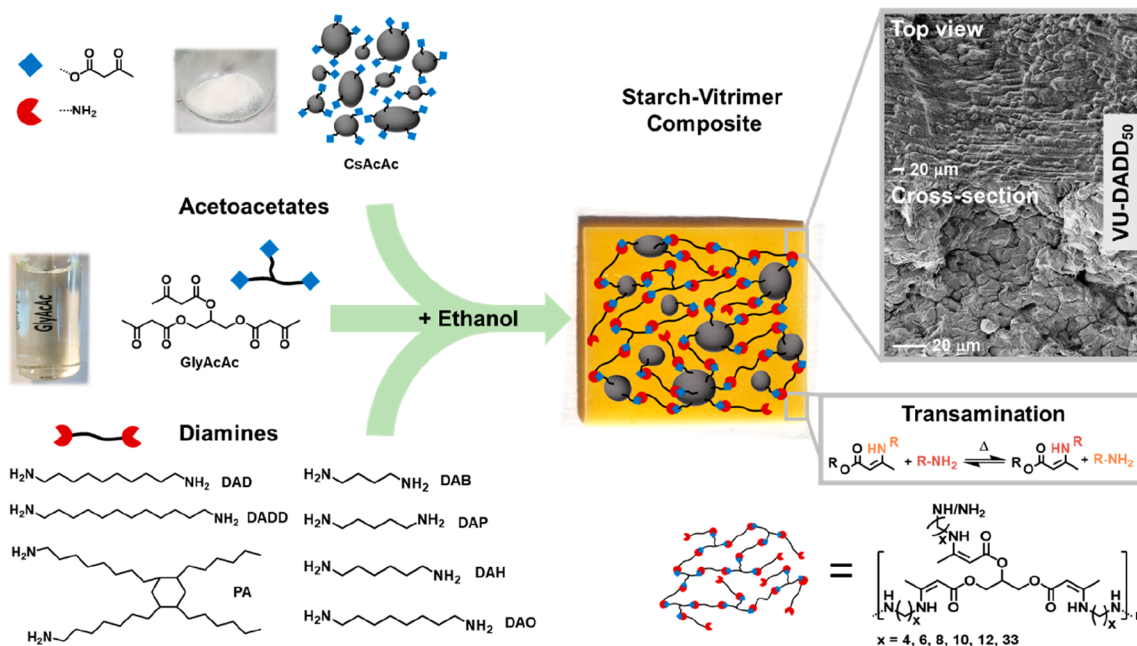
Figure 3. Illustration of the used monomers CsAcAc, GlyAcAc, and diamines, polymerized by a condensation reaction, and processed to starch-reinforced vinylogous urethane vitrimer composites. Vinylogous urethane vitrimers undergo thermal-induced transamination exchange reactions, enabling a reorganization of the cross-linking points in the material (reprocessing/remolding). SEM images show the top view and cross-section of the composite materials VU-DADD$_{50}$, picturing the starch granules homogeneously distributed in the material.
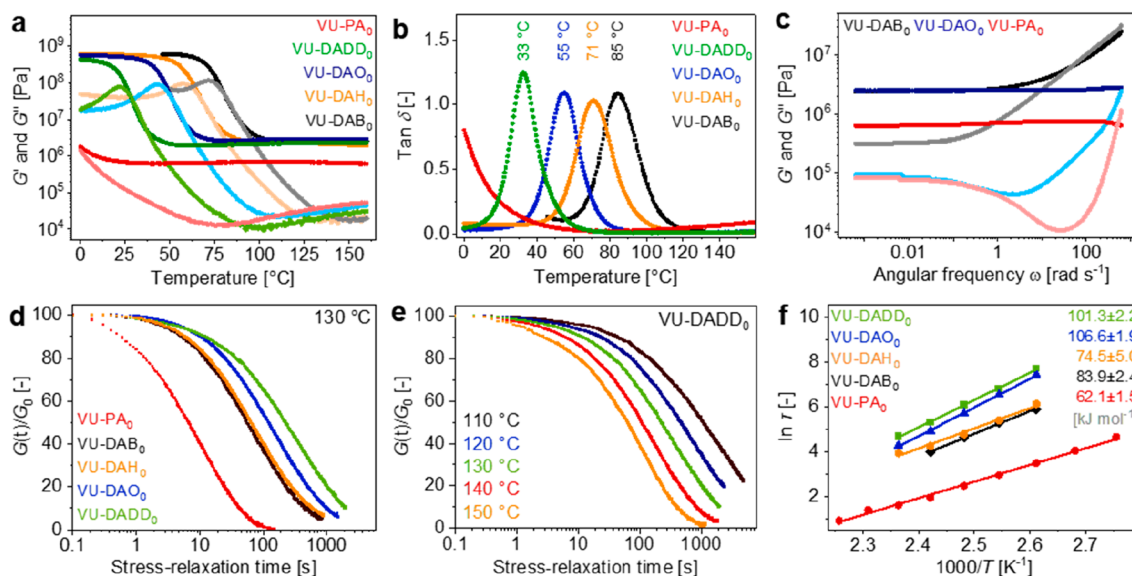
Figure 4. (a) DMTA measurements (G' = dark color, G'' = light color) of the matrix vitrimers (ω = 10 rad s^{-1}, γ = 0.1%). (b) Loss factors (DMTA) of the matrix vitrimers, showing the glass transition temperatures. (c) Frequency sweeps of the matrix vitrimers show cross-linked materials in a broad frequency range (100 °C, γ = 0.1%). (d) Stress relaxation measurements of the matrix vitrimers displaying stress-relaxation times of 12−425 s (γ = 1%). (e) Stress relaxation measurements in the temperature range of 110−150 °C, exemplified shown at VU-DADD$_0$ (γ = 1%). (f) Plot of ln τ vs the reciprocal temperature to calculate the activation energies from the slopes of the linear fits.

structure. Adding CsAcAc, the T_gs of the composite materials showed comparable values to the matrix vitrimers, exemplified shown by the materials VU-DADD$_0$ with 30, 50, and 70 wt % of CsAcAc, exhibiting values in the range of 21−29 °C (SI, S22-S1). Thermogravimetric analysis (TGA) from representative samples was carried out under an ambient atmosphere. The degradation temperatures of the matrix vitrimers correlate with the alkyl chain length of the diamine, exhibiting the most susceptible vitrimer VU-DAB$_0$ and the most resilient vitrimer

VU-PA$_0$ with degradation temperatures of 231−273 °C (SI, S22-S2). Corn starch and CsAcAc granules showed comparable degradation temperatures of 287 and 290 °C. Consequently, the vitrimer composites showed similar degradation temperatures of 250−255 °C to the respective matrix vitrimer, exemplarily shown by the materials VU-DADD$_0$ with 30 and 50 wt % of CsAcAc (SI, S23-S1).

Mechanical Properties. DMA measurements were carried out to investigate the material's mechanical properties by
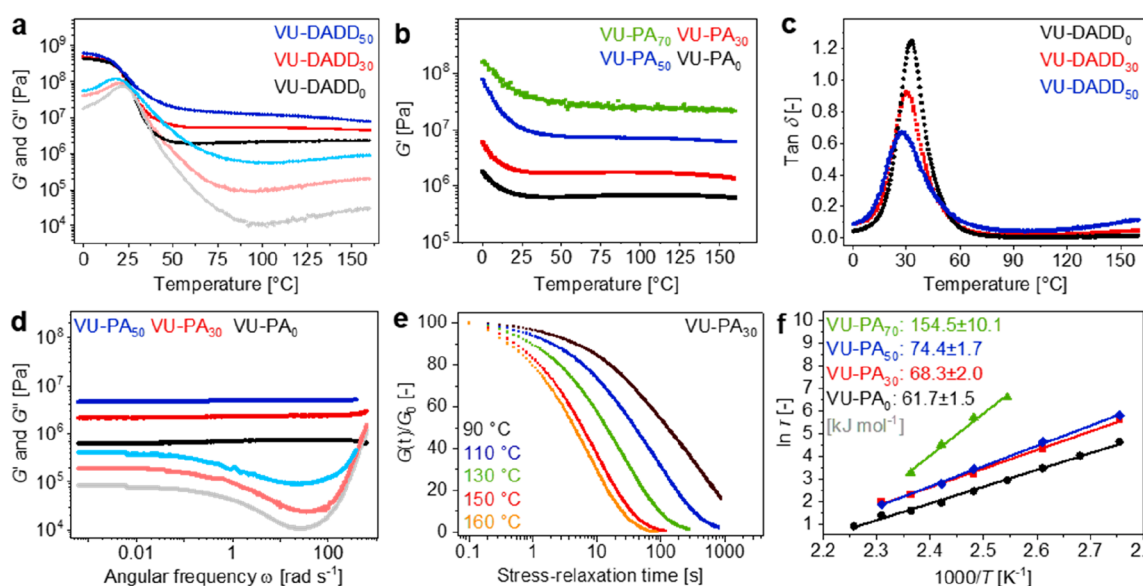
Figure 5. (a, b) DMTA measurements of VU-DADD$_0$, VU-DADD$_{30}$, VU-DADD$_{50}$ and VU-PA$_0$, VU-PA$_{30}$, VU-PA$_{50}$, and VU-PA$_{70}$ (G' = dark color, G'' = light color, ω = 10 rad s^{-1}, γ = 0.1) (c) Loss factor (DMTA) of VU-DADD$_0$, VU-DADD$_{30}$, and VU-DADD$_{50}$, pointing out similar glass transition temperatures of the composites. (d) Frequency sweeps of VU-PA$_0$, VU-PA$_{30}$, and VU-PA$_{50}$ prove cross-linked materials (100 °C, γ = 0.1%). (e) Stress-relaxation curves exemplified shown on the material VU-PA$_{30}$ in a temperature range of 90−160 °C. (f) Plot of ln τ vs the reciprocal temperature to calculate the E_as from the slopes of the linear fit.

oscillatory and step shear experiments. Five matrix vitrimers without CsAcAc were compared (VU-DAB$_0$, VU-DAH$_0$, VU-DAO$_0$, VU-DADD$_0$, VU-PA$_0$). The measurements were carried out within the linear viscoelastic regime so that the storage modulus G' and the loss modulus G'' were independent of strain. Amplitude sweeps show yield points of 1−20% at 100 °C (SI, S23-S2). DMTA measurements in the range of 0−160 °C display maximal storage moduli of 1−600 MPa and rubbery plateaus of 0.6−2.6 MPa, indicating cross-linked materials (Figure 4a). Rubbery plateaus demonstrate comparable values at elevated temperatures in case of VU-DAB$_0$, VU-DAP$_0$, VU-DAD$_0$, and VU-DADD$_0$, while VU-PA$_0$ displays a significantly lower value of 0.6 MPa. This can be explained by the lower cross-linking density and the free alkyl chains of PA, acting as a plasticizer. Figure 4b shows the loss factors, pointing out the T_g's of the materials. Cross-linked materials were likewise identified by measuring frequency sweeps (Figure 4c). In addition, the materials displayed stress-relaxation times of 12−425 s at 130 °C, with VU-PA$_0$ showing the shortest and VU-DADD$_0$ the longest (Figure 4d). The short stress-relaxation time of VU-PA$_0$ can be assigned to the low cross-linking density, high soluble fraction, and chain mobility in the material. VU-DAB$_0$, VU-DAP$_0$, VU-DAD$_0$, and VU-DADD$_0$ follow the trend of a shorter stress-relaxation time with shorter chain length of the diamine. This is probably due to the effect of a higher concentration of the relevant functional groups. The effect of a closer spatial arrangement outweighs the slowing effect of a higher cross-linking density. The soluble fractions of the materials were determined to comparable values of 3.2−5.5% in case of the matrix vitrimers, except for VU-PA$_0$, showing 15% (soluble fractions, SI, S24-T1). Activation energies (E_as) were determined by carrying out stress relaxation measurements at different temperatures, exemplified shown on VU-DADD$_0$ (Figure 4e; all stress-relaxation measurements, SI, S24-S1, S25-S1 and -S2, S26-S1). According to literature, the E_as were determined by an Arrhenius-like behavior of the material and calculated by

plotting ln τ (37%) versus the reciprocal temperature to calculate E_as of 62−107 kJ mol^{-1} from the slopes of the linear fits (Figure 4f).[26,51]

Next, the composite materials were investigated by DMA. Comparing amplitude sweeps of VU-PA$_0$, VU-PA$_{30}$, and VU-PA$_{70}$, a massive shift of the yield point from γ = 20 to 1 to 0.1% shear strain was measured at 100 °C, which can be explained by a rising cross-linking density of the composite materials (SI, S26-S2). DMTA measurements show increased storage and loss moduli in the glassy and especially in the rubbery state, displayed by the materials VU-DADD$_0$, VU-DADD$_{30}$, VU-DADD$_{50}$ and VU-PA$_0$, VU-PA$_{30}$, VU-PA$_{50}$, and VU-PA$_{70}$ with 0, 30, 50, and 70 wt % of CsAcAc (Figure 5a,b; G' and G'', SI, S27-S1). In addition, DMTA measurements (loss factor) show comparable T_gs of the composite materials with and without CsAcAc (Figure 5c). Frequency sweeps of VU-PA$_0$, VU-PA$_{30}$, and VU-PA$_{50}$ prove cross-linked materials (Figure 5d). Stress-relaxation curves were exemplified shown at the composite material VU-PA$_{30}$ in a temperature range of 90−160 °C (Figure 5e). Comparing VU-PA with different contents of CsAcAc, stress-relaxation times of 22−385 s at 130 °C and E_as of 62−155 kJ mol^{-1} were calculated for the composite materials (Figure 5f). In comparison, a trend toward higher activation energies with an increasing proportion of CsAcAc was observed. Furthermore, E_as of 81.4 ± 3.5 kJ mol^{-1} (VU-DADD$_{30}$), 84.4 ± 2.9 kJ mol^{-1} (VU-DADD$_{50}$), and 96.4 ± 6.8 kJ mol^{-1} (VU-DAB$_{30}$) were calculated (all stress-relaxation and E_as, SI, S27-S2, S28-S1 and -S2, S29-S1 and -S2, S30-S1). The determined values fit to reported values for vinylogous urethane vitrimers and concluded that the transamination reaction in the matrix and composite vitrimers mainly proceeds by a proposed protic iminium pathway.[51−53]

In order to investigate the mechanical properties of the vitrimers, tensile tests have been carried out at 20 °C. First, the matrix vitrimers without CsAcAc were compared, showing averaged elastic modulus (E) in the range of 4−1100 MPa, tensile strengths (σ_m) of 0.2−65.9 MPa, and elongations at an
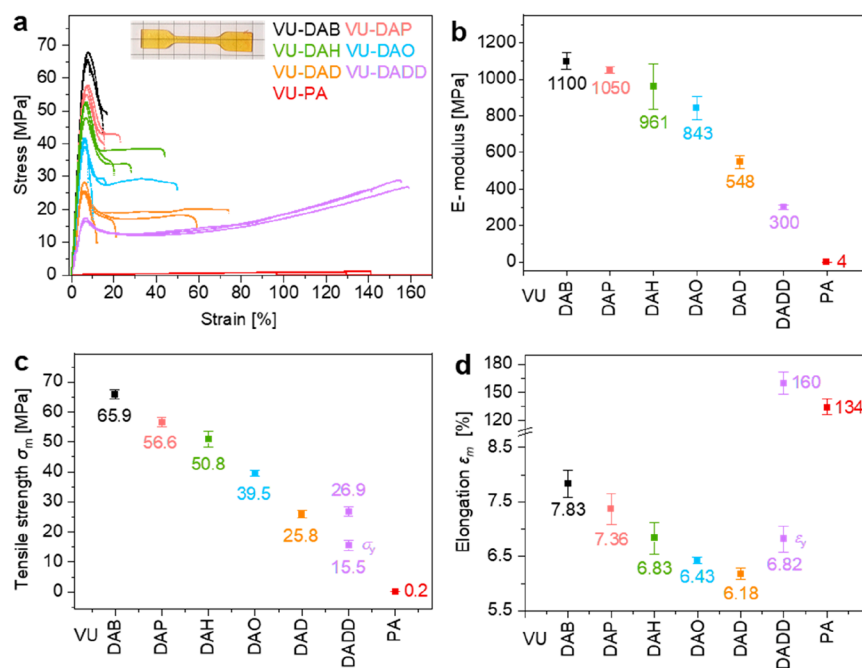
Figure 6. (a) Stress−strain curves derived from the matrix vitrimers. (b) E-moduli of the matrix vitrimers. (c) Tensile strengths of the matrix vitrimers. (d) Elongations at ultimate stress (ε_m, ε_y) of the matrix vitrimers.

ultimate stress (ε_m) of 6.18−160% (Figure 6a−d). The results indicate that, with a shorter aliphatic chain length, E, σ_m, and ε_m increase, with VU-DAB$_0$ exhibiting the highest values. The materials VU-DAB$_0$, VU-DAP$_0$, VU-DAH$_0$, VU-DAO$_0$, and VU-DAD$_0$ showed no significant difference in terms of the averaged toughness of 588−1129 N m^{-2}, while VU-DADD$_0$ showed a significantly higher value of 2549 N m^{-2} and VU-PA$_0$ a lower value of 69 N m^{-2} (SI, S30-S2).

The stress−strain curves of the composite materials VU-DADD$_0$ and VU-PA$_0$ with 0, 30, 50, and 70 wt % of CsAcAc are shown in Figure 7a,b (all stress−strain curves, SI, S31-S1 and -S2, S32-S1 and -S2). With a rising propotion of CsAcAc in the materials, increased E-moduli, and simultaniously decreased elongations at ultimate stress were measured for every composite. This can be explained by the higher cross-linking density and the filler effect of CsAcAc. The composites show averaged E-moduli of 6−2055 MPa, tensile strengths of 4.2−65.5 MPa, and elongations at ultimate stress of 2.8−85% (Figure 7c−e; zoom for small elongations at ultimate stress, SI, S33-S1). VU-DAB$_{30}$ shows the highest E-modulus of all composites with E = 2055 MPa. The composite VU-DAH$_{30}$ shows the highest tensile strength of σ_m = 65.5 MPa. The toughness is exemplified shown by the materials VU-DADD$_0$ with 30, 50, and 70 wt % of CsAcAc, pointing out a decreasing toughness of 2552−65 N m^{-2}, caused by the higher cross-linking density with a rising amount of CsAcAc (Figure 7f).

Swelling Ratio, Gel Content, and Soluble Fraction. A typical problem of starch-based materials is the hydrophilic nature, resulting in massive swelling ratios and gelatinization in water. At low temperatures, corn starch is reported to show a swelling ratio of 230% at 40 °C. Moreover, at temperatures above 60 °C, starch undergoes gelatinization, which leads to degradation of the hydrogen-bonded semicrystalline structure associated with massive swelling of the starch granules of 1280% when heating for 1 h at 90 °C.[54] To overcome this problem, a cross-linked matrix can suppress the swelling even

at high temperatures. To investigate that, matrix vitrimers/composites were kept at 100 °C in water for 3 h. For the vitrimer matrices, low swelling ratios of 0.3% were determined for the nonpolar VU-PA$_0$ and 4.2% for the most polar VU-DAB$_0$ (VU-DAB$_0$: 4.2%, VU-DAP$_0$: 4.4%, VU-DAH$_0$: 3.8%, VU-DAO$_0$: 1.8%, VU-DAD$_0$: 1.7%, VU-DADD$_0$: 1.5%, VU-PA$_0$: 0.3%; SI, S33-S2). Adding CsAcAc, more water can penetrate into the material, while the cross-linked matrix suppresses a massive swelling even at high temperatures. Following the trend, composites with a more polar matrix and 50 wt % of CsAcAc show higher swelling ratios than nonpolar matrices (VU-DAH$_{50}$: 16.7%, VU-DADD$_{50}$: 11.7%, VU-PA$_{50}$: 8.0%; SI, S34-S1). To determine the swelling ratios, gel content and soluble fractions of the materials, samples were put into THF at room temperature for 24 h. With rising chain lengths of the diamine, the swelling ratios increased from 49−325%, which can be explained by the lower cross-linking density. With a rising content of CsAcAc in the composites, the swelling ratios were lowered, mainly caused by the denser cross-linking densities and insolubility of starch in THF (e.g., VU-DADD$_0$: 148%, VU-DADD$_{30}$: 80%, VU-DADD$_{50}$: 55%). Gel contents of 92−98% and soluble fractions of 3−6% were calculated for all materials except for VU-PA$_0$ with a gel content of 84% and a soluble fraction of 15% (SI, S24, T-1).

Mechanical and Chemical Recycling. In order to investigate the reprocessability of the prepared vitrimer composites, five cycles of successive grinding and compression molding were carried out on the example of VU-DAB$_{30}$ (Figure 8a). Repetitively measured tensile tests and ATR-FT-IR spectra show rather similar results in Figure 8b (pristine: σ_m = 63.1 MPa, ε_m = 3.3%, E = 2055 MPa; 5× reprocessed: σ_m = 59.2 MPa, ε_m = 3.3%, E = 2000 MPa; ATR-FT-IR, SI, S34-S2). Chemical recycling was investigated by treating the materials with an aqueous acetic acid solution (10 wt %, pH ≈ 2). Vinylogous urethane bonds readily undergo acid-catalyzed hydrolysis, leading to a dissolution of the materials after 18 h at
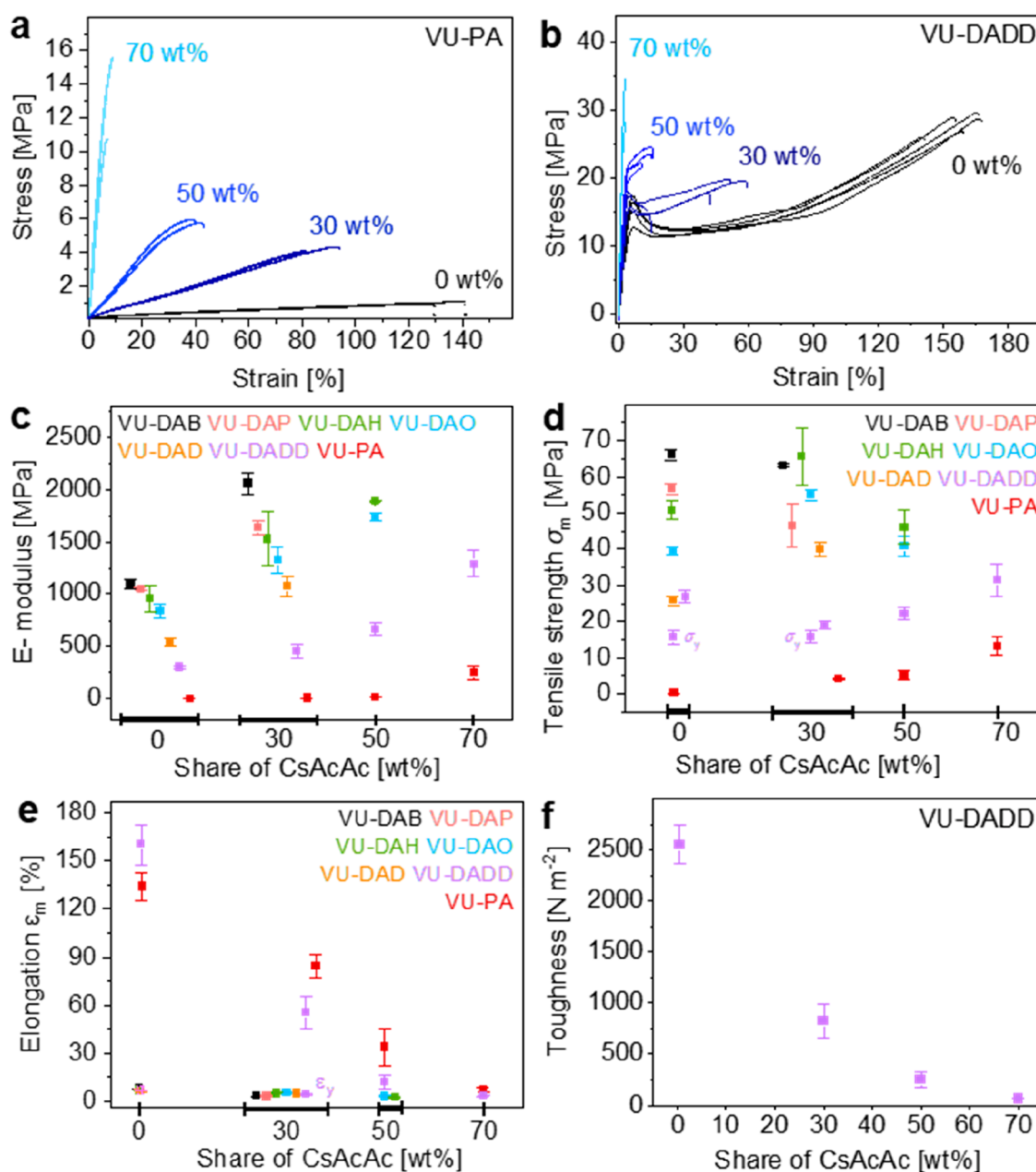
Figure 7. (a, b) Stress−strain curves derived from the vitrimer composite VU-DADD$_0$ and VU-PA$_0$ with 30, 50, 70 wt % CsAcAc. (c) Plot of the E-modulus vs the content of CsAcAc in the composite materials with values of 6−2055 MPa. (d) Plot of the tensile strengths vs the share of CsAcAc with values of 4−65.9 MPa. (e) Plot of the elongations at ultimate stress or break against the share of CsAcAc with values of 2.8−85%. (f) The toughness of the composites is exemplary shown by the materials VU-DADD$_0$ with 30, 50, and 70 wt % of CsAcAc.

20 °C and enabling closed-loop cycles by removing water/acetic acid or adding additional monomers for repolymerization as reported in literature (Figure 8c).[55] Moreover, the composites were treated in the same way and showed separation of the vinylogous urethane matrix and starch. After removing the aqueous acetic acid solution the received material was characterized. ATR-FT-IR measurements show a complete regeneration of the characteristic vinylogous urethane bands, while likewise a small increase in OH-bands has been noted, indicating acetic hydrolysis of the starch. Tensile tests showed increased brittleness by measuring a higher E-modulus and lower tensile strength after chemical recycling (SI, S35-S1). The acidic degradation of starch was

intensively investigated in literature and depends on factors like pH, temperature, and time, allowing either an extensive destruction of the starch to smaller building blocks (nanocrystals, oligosaccharides) or only a slight superficial change, regenerating the starch granules and easily separate them from the soluble vitrimer matrix.[56−59] Therefore, further investigations on chemical recycling routes of starch-based composites can be conducted, offering several ways for mechanical and chemical reprocessing.

Biodegradability. Enzymatic hydrolysis of starch is well-known and can also be performed on starch-based materials.[17,60−62] In order to make a statement about the biodegradability, enzymatic hydrolysis of the prepared
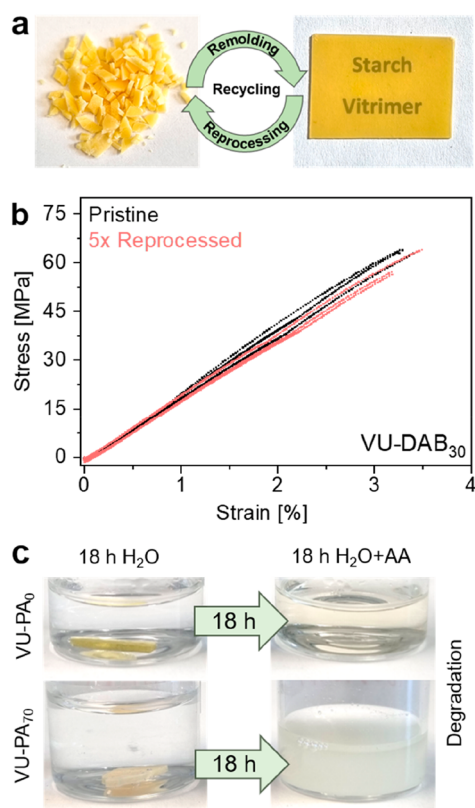
Figure 8. (a) Pictures of repetitive grinding and compression molding cycle, showing small vitrimer chunks and a reprocessed vitrimer film. (b) Stress−strain curves of the vitrimer VU-DAB$_{30}$ in comparison of the pristine specimens and 5x reprocessed specimens, showing rather similar curves. (c) Pictures showing acidic hydrolysis (chemical recycling) of the vinylogous urethane matrix/composites VU-PA$_0$ and VU-PA$_{70}$ in aqueous acetic acid solution after 18 h.

composite materials was investigated by using α-amylase, which is a class of enzymes utilized by bacteria, molds, and higher organisms in order to degrade the natural energy storage starch to smaller building blocks.[63] The enzyme depolymerizes 1,4-glycosidic bonds of α-1,4-glucan polysaccharides like starch to smaller blocks, e.g., oligosaccharides and disaccharides.[64] Corn starch and CsAcAc were mixed with an aqueous iodine-solution to form the characteristic purple triiodide-amylose complex.[65−67] Afterward α-amylase was added, and the decrease in purple color was monitored as an indicator for the enzymatic hydrolysis of the starch granules. After 5 min, a significant decrease in color was observed, while after 180 min, the mixtures were almost colorless, proving that both corn starch and CsAcAc undergo enzymatic hydrolysis. Next, the composite materials were investigated for this behavior. VU-PA$_{70}$ swelled in aqueous iodine solution and turned dark purple, indicating starch in the material. After that, the dark purple sample was placed partly in a pure aqueous solution and partly in an aqueous α-amylase solution. With amylase, the material turned yellow again, proving the enzymatic degradation, while the sample in water still showed intact starch−triiodide complexes (SI, S35-S2). The solution was filtered and analyzed in terms of the specific, water-soluble degradation products. ESI-MS showed the formation of glucose, maltose, and oligosaccharides (SI, S36-S1). Moreover, an application-related test was carried out. Raw corn starch was

wetted and conquered by nonspecific mold/bacteria from the air after a few days, known for degrading starch as an energy supplier. Interestingly, the modified starch CsAcAc and the composite materials were likewise conquered under humid conditions. Following the weight loss of the composites after 6 weeks at room temperature, a loss of 21−39 wt % was weighed, accompanied by optical deformation, crumbling and shrinking of the material (SI, S35-S1). ATR-FT-IR spectra of VU-DADD$_{50}$ before and after the treatment show a dramatic change of the material by measuring the monomer acetoacetate, while the vinylogous urethane bands almost disappeared (SI, S36-S2). Moreover, the characteristic bands of the AGU backbone are highly represented, indicating a predominant share of yet unmetabolized starch and a massive loss of the matrix vitrimer. Obviously, the biofilm is able to fragment or degrade both the vinylogous urethane matrix and the modified starch, while the exact mechanism is unclear. As mentioned, vinylogous urethane bonds can depolymerize by acidic hydrolysis, likewise found in mold crops. DAB and DAH are known to be metabolized in nature, which gives the outlook that one or more presented vinylogous urethane vitrimers/composites might be fully biodegradable as well.[68,69] However, for a detailed investigation, long time studies under normalized/certified conditions have to be carried out in order to give a detailed insight into the biodegradability and comparisons to established materials.

CONCLUSIONS

An easy pathway for preparing biobased, reprocessable and biodegradable elastomeric and thermosetting starch-based vitrimer composites with outstanding mechanical properties (e.g., E-modulus > 2 GPa) and a high content of up to 70 wt % of modified starch is presented. The acetoacetylation reaction was adjusted to the effect that typically used solvents can be avoided by performing an easy, one-step bulk reaction. The polymerization of the acetoacetates with diamines was carried out by a bulk reaction without or a minimum quantity of ethanol to lower the viscosity of the mixtures. Twenty matrix vitrimers and composite materials have been synthesized and compared in terms of their mechanical properties, showing elastic moduli of 4−2055 MPa, tensile strengths of 0.2−65.9 MPa, and elongations at maximum stress of 2.8−160% at 20 °C. Short stress relaxation times of 12−425 s at 130 °C and activation energies of 62−155 kJ mol^{-1} were calculated, exhibiting typical values for vinylogous urethane vitrimers and pointing out the remarkable catalyst-free reprocessability of the materials. Besides, the composites show excellent resistance against massive swelling and gelatinization of starch in water at 100 °C, caused by the suppressing effect of the cross-linked matrix vitrimers. In addition, the composites enable thermomechanical reprocessing by grinding and remolding, chemical reprocessing by acidic hydrolysis, and degradation/reusage by enzymatic hydrolysis using α-amylase. With this, several pathways for closed-loop cycles, repolymerization, and separate reusage of the monomers for various recycling methods were developed. Since mainly soft, elastomeric starch-based vitrimers were reported before, this work contributes to the development of biobased and biodegradable thermosetting vitrimer composites and offers new insights and future prospectives into recyclable polymer−polymer composites.

■ ASSOCIATED CONTENT

ⓈⒾ Supporting Information

The Supporting Information is available free of charge at https://pubs.acs.org/doi/10.1021/acssuschemeng.3c01340.

> Materials, methods, and experimental procedures used. In addition, ^{1}H/^{13}C NMR spectra, MS spectra, ATR-FT-IR spectra, DSC curves, TGA curves, DMA curves, elemental analysis, swelling ratios/gel contents/soluble fractions, optical microscope images, SEM images, and stress−strain curves of the used monomers, polymers, and composites are shown (PDF)

■ AUTHOR INFORMATION

Corresponding Author

Volker Abetz − *Institute of Membrane Research, Helmholtz-Zentrum Hereon, 21502 Geesthacht, Germany; Institute of Physical Chemistry, Universität Hamburg, 20146 Hamburg, Germany;* ⓘ orcid.org/0000-0002-4840-6611; Email: volker.abetz@hereon.de

Authors

Philipp Haida − *Institute of Physical Chemistry, Universität Hamburg, 20146 Hamburg, Germany*

Suwabun Chirachanchai − *Center of Excellence in Bioresources to Advanced Materials, The Petroleum and Petrochemical College, Chulalongkorn University, Wangmai, Pathumwan Bangkok 10330, Thailand;* ⓘ orcid.org/0000-0003-1355-8452

Complete contact information is available at:
https://pubs.acs.org/10.1021/acssuschemeng.3c01340

Author Contributions

The manuscript was written through contributions of all authors. All authors have given approval to the final version of the manuscript.

Notes

The authors declare no competing financial interest.

■ ACKNOWLEDGMENTS

■ REFERENCES

(1) Montarnal, D.; Capelot, M.; Tournilhac, F.; Leibler, L. Silica-like malleable materials from permanent organic networks. *Science* **2011**, *334* (6058), 965−968.

(2) Zheng, J.; Png, Z. M.; Ng, S. H.; Tham, G. X.; Ye, E.; Goh, S. S.; Loh, X. J.; Li, Z. Vitrimers: Current Research Trends and their Emerging Applications. *Mater. Today* **2021**, *51*, 586−625.

(3) Schenk, V.; Labastie, K.; Destarac, M.; Olivier, P.; Guerre, M. Vitrimer composites: current status and future challenges. *Materials Advances* **2022**, *3* (22), 8012−8029.

(4) Guerre, M.; Taplan, C.; Winne, J. M.; Du Prez, F. E. Vitrimers: directing chemical reactivity to control material properties. *Chemical Science* **2020**, *11* (19), 4855−4870.

(5) Chakma, P.; Konkolewicz, D. Dynamic Covalent Bonds in Polymeric Materials. *Angew. Chem., Int. Ed.* **2019**, *58* (29), 9682−9695.

(6) Krishnakumar, B.; Sanka, R. V. S. P.; Binder, W. H.; Parthasarthy, V.; Rana, S.; Karak, N. Vitrimers: Associative Dynamic Covalent Adaptive Networks in Thermoset Polymers. *Chemical Engineering Journal* **2020**, *385*, 123820.

(7) Van Zee, N. J.; Nicolaÿ, R. Vitrimers: Permanently Crosslinked Polymers with Dynamic Network Topology. *Prog. Polym. Sci.* **2020**, *104*, 101233.

(8) Krishnakumar, B.; Pucci, A.; Wadgaonkar, P. P.; Kumar, I.; Binder, W. H.; Rana, S. Vitrimers Based on Bio-Derived Chemicals: Overview and Future Prospects. *Chemical Engineering Journal* **2022**, *433*, 133261.

(9) Raquez, J. M.; Deléglise, M.; Lacrampe, M. F.; Krawczak, P. Thermosetting (Bio)materials Derived from Renewable Resources: A Critical Review. *Prog. Polym. Sci.* **2010**, *35* (4), 487−509.

(10) Vidil, T.; Llevot, A. Fully Biobased Vitrimers: Future Direction toward Sustainable Cross-Linked Polymers. *Macromol. Chem. Phys.* **2022**, *223* (13), 2100494.

(11) Lucherelli, M. A.; Duval, A.; Avérous, L. Biobased vitrimers: Towards sustainable and adaptable performing polymer materials. *Prog. Polym. Sci.* **2022**, *127*, 101515.

(12) Zhang, Y.; Rempel, C.; Liu, Q. Thermoplastic Starch Processing and Characteristics—A Review. *Critical Reviews in Food Science and Nutrition* **2014**, *54* (10), 1353−1370.

(13) Avérous, L.; Halley, P. J. Starch Polymers: From the Field to Industrial Products. In *Starch Polymers*; Halley, P. J., Avérous, L., Eds.; Elsevier, 2014; pp 3−10, Chapter 1.

(14) Laycock, B. G.; Halley, P. J. Starch Applications: State of Market and New Trends. In *Starch Polymers*; Halley, P. J., Avérous, L., Eds.; Elsevier, 2014; pp 381−419, Chapter 14.

(15) Ribba, L.; Garcia, N. L.; D'Accorso, N.; Goyanes, S. Disadvantages of Starch-Based Materials, Feasible Alternatives in Order to Overcome These Limitations. In *Starch-Based Materials in Food Packaging*; Villar, M. A., Barbosa, S. E., García, M. A., Castillo, L. A., López, O. V., Eds.; Academic Press, 2017; pp 37−76, Chapter 3.

(16) Tratnik, N.; Tanguy, N. R.; Yan, N. Recyclable, Self-Strengthening Starch-based Epoxy Vitrimer Facilitated by Exchangeable Disulfide Bonds. *Chemical Engineering Journal* **2023**, *451*, 138610.

(17) Tong, H.; Chen, Y.; Weng, Y.; Zhang, S. Biodegradable-Renewable Vitrimer Fabrication by Epoxidized Natural Rubber and Oxidized Starch with Robust Ductility and Elastic Recovery. *ACS Sustainable Chem. Eng.* **2022**, *10* (24), 7942−7953.

(18) Li, C.; Ju, B.; Zhang, S. Fully bio-based Hydroxy Ester Vitrimer Synthesized by Crosslinking Epoxidized Soybean Oil with Doubly Esterified Starch. *Carbohydr. Polym.* **2023**, *302*, 120442.

(19) Li, C.; Zhang, S.; Ju, B. Preparation of a Starch-Based Vitrimer Comprising a Crosslinkable Macromolecular Elasticizer by extrusion. *Industrial Crops and Products* **2023**, *191*, 115941.

(20) Vidil, T.; Llevot, A. Fully Biobased Vitrimers: Future Direction toward Sustainable Cross-Linked Polymers. *Macromol. Chem. Phys.* **2022**, *223* (13), 2100494.

(21) Nda-Umar, U. I.; Ramli, I.; Taufiq-Yap, Y. H.; Muhamad, E. N. An Overview of Recent Research in the Conversion of Glycerol into Biofuels, Fuel Additives and other Bio-Based Chemicals. *Catalysts* **2019**, *9* (1), 15.

(22) Wang, X.; Gao, S.; Wang, J.; Xu, S.; Li, H.; Chen, K.; Ouyang, P. The Production of Biobased Diamines from Renewable Carbon Sources: Current Advances and Perspectives. *Chinese Journal of Chemical Engineering* **2021**, *30*, 4−13.

(23) Monteiro, M. R.; Kugelmeier, C. L.; Pinheiro, R. S.; Batalha, M. O.; da Silva César, A. Glycerol from biodiesel production: Technological paths for sustainability. *Renewable and Sustainable Energy Reviews* **2018**, *88*, 109−122.

(24) Witzeman, J. S.; Nottingham, W. D. Transacetoacetylation with tert-butyl acetoacetate: synthetic applications. *Journal of Organic Chemistry* **1991**, *56* (5), 1713−1718.

(25) Weerathaworn, S.; Abetz, V. Tailor-Made Vinylogous Urethane Vitrimers Based on Binary and Ternary Block and Random Copolymers: An Approach toward Reprocessable Materials. *Macromol. Chem. Phys.* **2023**, *224* (1), 2200248.

(26) Denissen, W.; Rivero, G.; Nicolaÿ, R.; Leibler, L.; Winne, J. M.; Du Prez, F. E. Vinylogous Urethane Vitrimers. *Adv. Funct. Mater.* **2015**, *25* (16), 2451−2457.

(27) Haida, P.; Abetz, V. Acid-Mediated Autocatalysis in Vinylogous Urethane Vitrimers. *Macromol. Rapid Commun.* **2020**, *41* (16), 2000273.

(28) Witzeman, J. S.; Nottingham, W. D. Transacetoacetylation with tert-butyl acetoacetate: synthetic applications. *J. Org. Chem.* **1991**, *56*, 1713−1718.

(29) Haida, P.; Signorato, G.; Abetz, V. Blended vinylogous urethane/urea vitrimers derived from aromatic alcohols. *Polym. Chem.* **2022**, *13* (7), 946−958.

(30) Bertoft, E. Understanding Starch Structure: Recent Progress. *Agronomy* **2017**, *7* (3), 56.

(31) Geddes, R.; Greenwood, C. T.; Mackenzie, S. Studies on the Biosynthesis of Starch Granules: Part III. The Properties of the Components of Starches from the Growing Potato Tuber. *Carbohydr. Res.* **1965**, *1* (1), 71−82.

(32) Tester, R. F.; Karkalas, J.; Qi, X. Starch—Composition, Fine Structure and Architecture. *Journal of Cereal Science* **2004**, *39* (2), 151−165.

(33) Liu, H.; Guo, L.; Tao, S.; Huang, Z.; Qi, H. Freely Moldable Modified Starch as a Sustainable and Recyclable Plastic. *Biomacromolecules* **2021**, *22* (6), 2676−2683.

(34) Szymanowska-Powałowska, D.; Lewandowicz, G.; Błaszczak, W.; Szwengiel, A. Structural Changes of Corn Starch During Fuel Ethanol Production from Corn Flour. *BioTechnologia* **2012**, *3*, 333−341.

(35) Wang, Y.; Xie, W. Synthesis of Cationic Starch with a High Degree of Substitution in an Ionic Liquid. *Carbohydr. Polym.* **2010**, *80* (4), 1172−1177.

(36) Bunkerd, R.; Molloy, R.; Somsunan, R.; Punyodom, W.; Topham, P. D.; Tighe, B. J. Synthesis and Characterization of Chemically-Modified Cassava Starch Grafted with Poly(2-Ethylhexyl Acrylate) for Blending with Poly(Lactic Acid). *Starch - Stärke* **2018**, *70* (11−12), 1800093.

(37) Uliniuc, A.; Popa, M.; Drockenmuller, E.; Boisson, F.; Leonard, D.; Hamaide, T. Toward Tunable Amphiphilic Copolymers via CuAAC Click Chemistry of Oligocaprolactones onto Starch Backbone. *Carbohydr. Polym.* **2013**, *96* (1), 259−269.

(38) Tomoaia-Cotisel, M.; Cota, C.; Mocanu, A.; Horovitz, O. Micro and Nanostructure of Starch Granules from Potato and Maize. *Materiale Plastice* **2010**, *47*, 426−432.

(39) Chakraborty, I.; Pallen, S.; Shetty, Y.; Roy, N.; Mazumder, N. Advanced Microscopy Techniques for Revealing Molecular Structure of Starch Granules. *Biophysical Reviews* **2020**, *12* (1), 105−122.

(40) Huang, X.; Liu, H.; Ma, Y.; Mai, S.; Li, C. Effects of Extrusion on Starch Molecular Degradation, Order-Disorder Structural Transition and Digestibility-A Review. *Foods* **2022**, *11* (16), 2538.

(41) Santiago-Ramos, D.; Figueroa-Cárdenas, J. d. D.; Véles-Medina, J. J.; Reynoso-Camacho, R.; Ramos-Gómez, M.; Gaytán-Martínez, M.; Morales-Sánchez, E. Effects of Annealing and Concentration of Calcium Salts on Thermal and Rheological Properties of Maize Starch During an Ecological Nixtamalization Process. *Cereal Chem.* **2015**, *92* (5), 475−480.

(42) Wang, S.; Copeland, L. Molecular disassembly of starch granules during gelatinization and its effect on starch digestibility: a review. *Food & Function* **2013**, *4* (11), 1564−1580.

(43) Regazzi, A.; Dumont, P. J. J.; Harthong, B.; Imbault, D.; Peyroux, R.; Putaux, J.-L. Effectiveness of Thermo-Compression for Manufacturing Native Starch Bulk Materials. *J. Mater. Sci.* **2016**, *51* (11), 5146−5159.

(44) Kind, S.; Wittmann, C. Bio-based Production of the Platform Chemical 1,5-Diaminopentane. *Appl. Microbiol. Biotechnol.* **2011**, *91* (5), 1287−1296.

(45) Wendisch, V. F.; Mindt, M.; Pérez-García, F. Biotechnological production of mono- and diamines using bacteria: recent progress, applications, and perspectives. *Appl. Microbiol. Biotechnol.* **2018**, *102* (8), 3583−3594.

(46) Scott, E.; Peter, F.; Sanders, J. Biomass in the Manufacture of Industrial Products—The Use of Proteins and Amino Acids. *Appl. Microbiol. Biotechnol.* **2007**, *75* (4), 751−762.

(47) Choi, S.; Song, C. W.; Shin, J. H.; Lee, S. Y. Biorefineries for the production of top building block chemicals and their derivatives. *Metabolic Engineering* **2015**, *28*, 223−239.

(48) Klatte, S.; Wendisch, V. F. Redox self-sufficient whole cell biotransformation for amination of alcohols. *Bioorg. Med. Chem.* **2014**, *22* (20), 5578−5585.

(49) Sung, S.; Jeon, H.; Sarak, S.; Ahsan, M. M.; Patil, M. D.; Kroutil, W.; Kim, B.-G.; Yun, H. Parallel anti-sense two-step cascade for alcohol amination leading to ω-amino fatty acids and α,ω-diamines. *Green Chem.* **2018**, *20* (20), 4591−4595.

(50) Hajiali, F.; Tajbakhsh, S.; Marić, M. Thermally reprocessable bio-based polymethacrylate vitrimers and nanocomposites. *Polymer* **2021**, *212*, 123126.

(51) Taplan, C.; Guerre, M.; Winne, J. M.; Du Prez, F. E. Fast Processing of Highly Crosslinked, Low-viscosity Vitrimers. *Materials Horizons* **2020**, *7* (1), 104−110.

(52) Guerre, M.; Taplan, C.; Nicolaÿ, R.; Winne, J. M.; Du Prez, F. E. Fluorinated Vitrimer Elastomers with a Dual Temperature Response. *J. Am. Chem. Soc.* **2018**, *140* (41), 13272−13284.

(53) Spiesschaert, Y.; Taplan, C.; Stricker, L.; Guerre, M.; Winne, J. M.; Du Prez, F. E. Influence of the polymer matrix on the viscoelastic behaviour of vitrimers. *Polym. Chem.* **2020**, *11* (33), 5377−5385.

(54) Hong, L. F.; Cheng, L. H.; Lee, C. Y.; Peh, K. K. Characterisation of Physicochemical Properties of Propionylated Corn Starch and Its Application as Stabiliser. *Food Technol. Biotechnol* **2015**, *53* (3), 278−285.

(55) Xu, H.; Wang, H.; Zhang, Y.; Wu, J. Vinylogous Urethane Based Epoxy Vitrimers with Closed-Loop and Multiple Recycling Routes. *Ind. Eng. Chem. Res.* **2022**, *61* (48), 17524−17533.

(56) Majzoobi, M.; Kaveh, Z.; Farahnaky, A. Effect of Acetic Acid on Physical Properties of Pregelatinized Wheat and Corn Starch Gels. *Food Chem.* **2016**, *196*, 720−725.

(57) Pratiwi, M.; Faridah, D. N.; Lioe, H. N. Structural Changes to Starch after Acid Hydrolysis, Debranching, Autoclaving-Cooling Cycles, and Heat Moisture Treatment (HMT): A Review. *Starch - Stärke* **2018**, *70* (1−2), 1700028.

(58) Shen, Y.; Yao, Y.; Wang, Z.; Wu, H. Hydroxypropylation reduces gelatinization temperature of corn starch for textile sizing. *Cellulose* **2021**, *28* (8), 5123−5134.

(59) da Silveira, N.; Zucatti, R.; Vailatti, A.; Leite, D. Acid hydrolysis of regular corn starch under external electric field. *J. Braz. Chem. Soc.* **2019**, *30*, 2567−2574.

(60) Alberta Araújo, M.; Cunha, A. M.; Mota, M. Enzymatic degradation of starch-based thermoplastic compounds used in protheses: identification of the degradation products in solution. *Biomaterials* **2004**, *25* (13), 2687−2693.

(61) Karimi, M.; Biria, D. The promiscuous activity of alpha-amylase in biodegradation of low-density polyethylene in a polymer-starch blend. *Sci. Rep.* **2019**, *9* (1), 2612.

(62) Hamdi, G.; Ponchel, G. Enzymatic Degradation of Epichlorohydrin Crosslinked Starch Microspheres by α-Amylase. *Pharm. Res.* **1999**, *16* (6), 867−875.

(63) van der Maarel, M. J. E. C.; van der Veen, B.; Uitdehaag, J. C. M.; Leemhuis, H.; Dijkhuizen, L. Properties and applications of starch-converting enzymes of the α-amylase family. *J. Biotechnol.* **2002**, *94* (2), 137−155.

(64) Giuberti, G.; Rocchetti, G.; Lucini, L. Interactions Between Phenolic Compounds, Amylolytic Enzymes and Starch: An Updated Overview. *Current Opinion in Food Science* **2020**, *31*, 102−113.

(65) Cochran, B.; Lunday, D.; Miskevich, F. Kinetic Analysis of Amylase Using Quantitative Benedict's and Iodine Starch Reagents. *J. Chem. Educ.* **2008**, *85* (3), 401.

(66) Turner, R. The Starch-Iodide Reaction: Stability and Proportionality of color produced by small amounts of iodine. *J. Am. Chem. Soc.* **1930**, *52* (7), 2768−2773.

(67) Stromeyer. Ein sehr empsindliches Reagens für Jodine, aufgefunden in der Stärke (Amidon). *Annalen der Physik* **1815**, *49* (1−2), 146−153.

(68) Bouchereau, A.; Aziz, A.; Larher, F.; Martin-Tanguy, J. Polyamines and Environmental Challenges: Recent Development. *Plant Science* **1999**, *140* (2), 103−125.

(69) Kusano, T.; Berberich, T.; Tateda, C.; Takahashi, Y. Polyamines: essential factors for growth and survival. *Planta* **2008**, *228* (3), 367−381.

🕮 Recommended by ACS

6 Unpublished Results

6.1 Monomer Syntheses – Reactants and Conditions

This subchapter describes the used raw materials as suitable reactants for the acetoacetylation reaction and further usage as monomers for vinylogous urethane vitrimers. The respective reaction conditions for the acetoacetylation are shown in Table 5 of the experimental section (chapter 6.5.1.2). *Tert*-butylacetoacetate (TBA) and 2,2,6-trimethyl-1,3-dioxin-4-one (TMDO) are readily known as acetoacetylation agents for various alcohols and other nucleophiles in organic chemistry.[74-76] At elevated temperatures above 110 °C the agents split into a reactive acetylketene and *tert*-butanol or acetone as a byproduct. The highly electrophilic acetylketene undergoes fast addition reactions with almost any available nucleophile. In this work, mainly alcohols have been converted into acetoacetates, while incidentally, amines have been reacted to acetoacetamides. The reaction scheme is shown in **Figure 31** and likewise described in the introduction (chapter 3.3.1.).
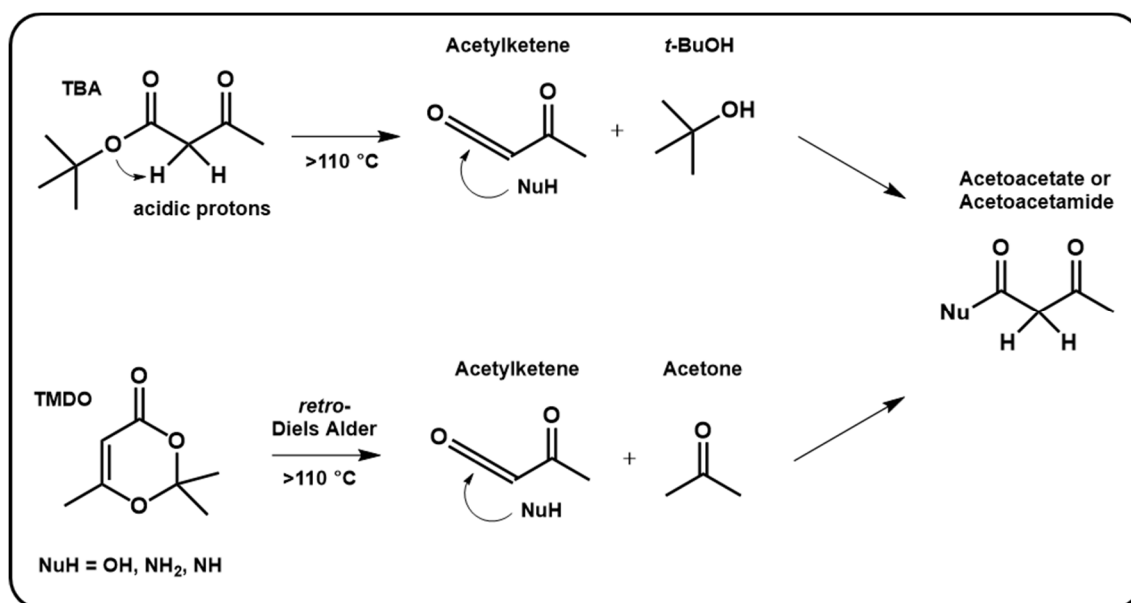
Figure 31: Acetoacetylation agents TBA and TMDO splitting into a reactive acetylketene at elevated temperatures. Nucleophiles, *e.g.* alcohols or amines attack the electrophilic acetylketene and undergo an addition reaction to form acetoacetates or acetoacetamides.

In the scope of this work, several alcohols have been partly or entirely acetoacetylated, while the reaction conditions were set by using one of the acetoacetylation agents, suitable solvents, temperatures, and reaction times. The used conditions strongly depended on the physical and chemical properties of the used alcohols, *e.g.* melting point, boiling point, solubility, reactivity of the nucleophiles, and the desired grade of acetoacetylation. Moreover, it was investigated that the acetoacetylation of several alcohols likewise works without using an additional solvent, utilizing similar reaction conditions. For example, ethylene glycol or glycerol could be easily acetoacetylated without an additional solvent. If a solvent was needed, high boiling solvents like xylene, mesitylene, or dimethylformamide (DMF) were used to reach typical reaction temperatures of 130−140 °C.

Moreover, it was investigated that the acetoacetylation using TMDO works faster than using TBA. Monitoring the conversion of glycerol, a complete conversion was measured already after 1 h at 135 °C when using TMDO, but 4 h at 135 °C when using TBA. Obviously, the *retro*-Diels-Alder reaction of TMDO proceeds more efficiently, the reaction mechanism is different and/or the backward reaction proceeds slower. This behavior is also discussed in publication 2.[23] In both cases, the remaining acetylketenes can dimerize into dehydracetic acid. Usually, all solvents and byproducts of the reaction can efficiently be removed *in vacuo* at 130 °C.

In the following, as an example, the characterization of the acetoacetate products is shown on the raw material ethylene glycol (EG), while the analyses for the other alcohols are shown in the appendix (Figure A1 and Figure A2). The characterization was carried out by ATR-FT-IR spectroscopy, ^{1}H/^{13}C NMR spectroscopy, and ESI-MS spectrometry. The acetoacetylated products were titled as Alcohol$_{AcAc}$ (*e.g.* EG$_{AcAc}$). Since the reaction is robust and reliably supplied the desired products, not all products were additionally analyzed by MS measurements. Moreover, the synthetic routes and the analysis of the used acetoacetate monomers are described in publications 1, 2, and 3. ATR-FT-IR spectra of the acetoacetylated ethylene glycol EG$_{AcAc}$ and the raw ethylene glycol show the disappearance of the O-H bands in the area of 3000−3600 cm^{-1} and the appearance of the characteristic acetoacetate ester (1740 cm^{-1}) and ketone (1711 cm^{-1}) stretching vibrations as well as the C-O stretching vibration (1742 cm^{-1}) in **Figure 32 a/b**. The bands can shift in the range of a few wavenumbers in case another alcohol is used.
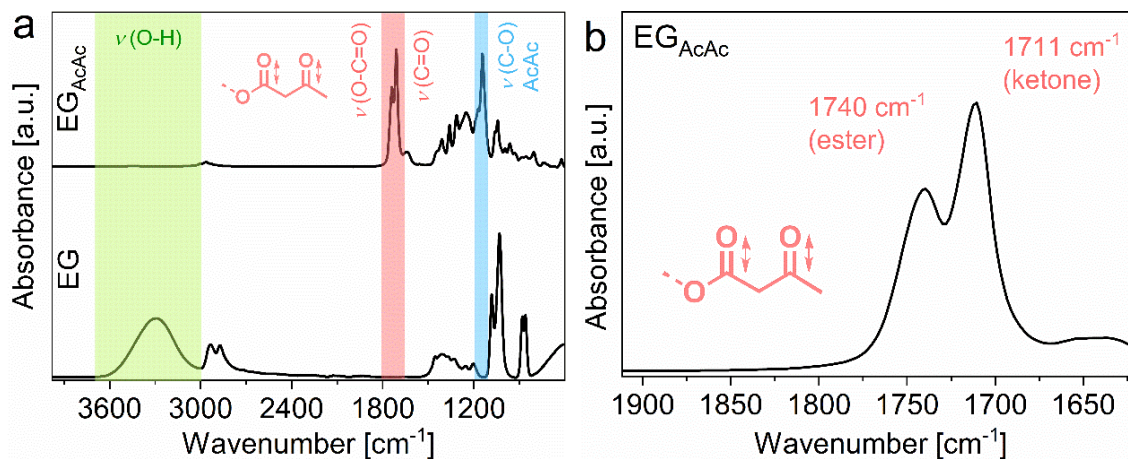
Figure 32: (a) ATR-FT-IR spectra of the acetoacetylated ethylene glycol (EG$_{AcAc}$) and the raw alcohol ethylene glycol showing the disappearance of the O-H band in the area of 3000−3600 cm^{-1} and the characteristic acetoacetate ester (1740 cm^{-1}) and ketone stretching vibrations (1711 cm^{-1}) as well as the C-O stretching vibration (1142 cm^{-1}). **(b)** Cutout of the characteristic acetoacetate bands area.
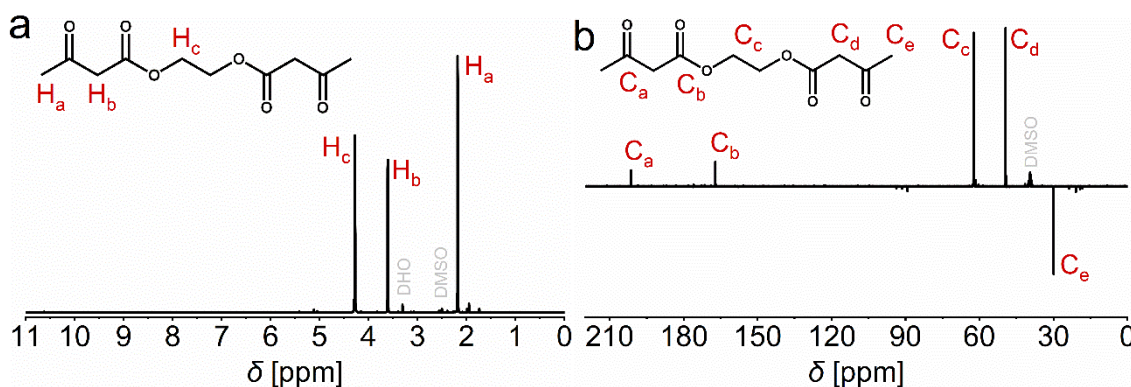
Figure 33: (a) ^{1}H NMR spectrum of the acetoacetylated ethylene glycol monomer EG$_{AcAc}$, showing the characteristic CH$_2$ and CH$_3$ acetoacetate signals and intensities. ^{1}H NMR (300 MHz, DMSO-*d6*, 298 K): 4.27 (2H, s, CH$_2$), 3.61 (2H, s, CH$_2$), 2.18 (3H, s, CH$_3$). **(b)** ^{13}C NMR DEPTQ-135 spectrum of EG$_{AcAc}$, showing the characteristic CH$_2$ and CH$_3$ acetoacetate signals. ^{13}C NMR (75 MHz, DMSO-*d6*, 298 K): 201.38 (q, C=O), 167.14 (q, COO), 62.36 (s, CH$_2$), 49.42 (s, CH$_2$), 29.97 (p, CH$_3$).

^{1}H NMR spectra proved the formation of the acetoacetate by measuring the characteristic chemical shifts (DMSO-*d6*), including the acetoacetate signals at 2.18 ppm (CH$_3$) and 3.61 ppm (CH$_2$) shown in **Figure 33a**. ^{13}C NMR spectra likewise proved the successful synthesis by measuring the characteristic signal of the acetoacetate group at 29.97 ppm (CH$_3$) and 49.42 ppm (CH$_2$), as shown in Figure 33b. The spectra for the other alcohols

are shown in the appendix Figure A2. Supportive to this, mass spectrometry (ESI$^+$) measured the correct *m/z* value with the sodium adduct *m/z* = 253.067 (100%) for EG$_{AcAc}$ as shown in **Figure 34**.
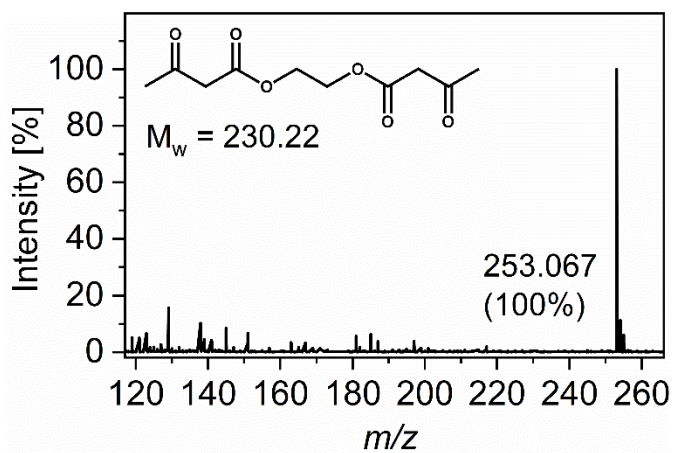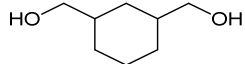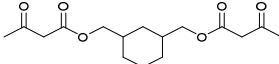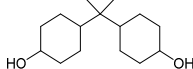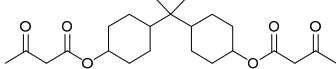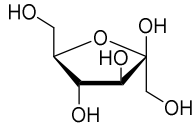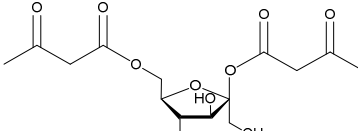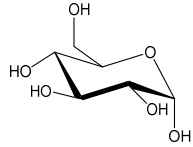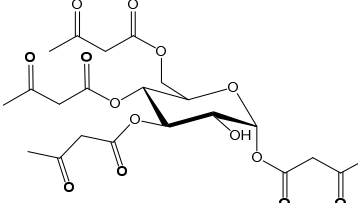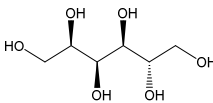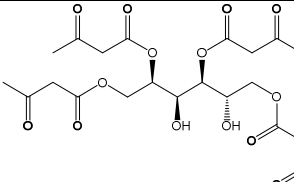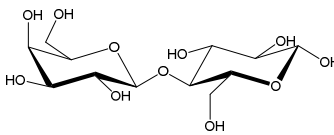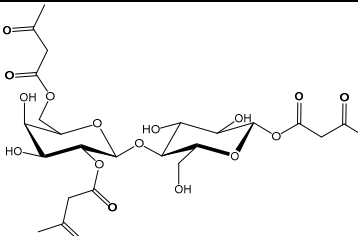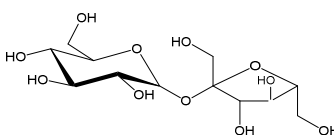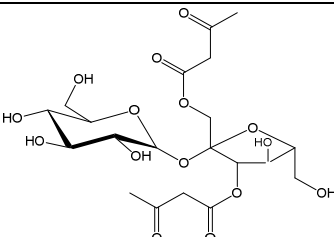
Figure 34: Mass spectrometry (ESI$^+$) measured the correct *m/z* value with the sodium adduct *m/z* = 253.067 (100%) for the acetoacetylated ethylene glycol monomer EG$_{AcAc}$.

Since the backbone structure defines the polymers properties, several bio-based and petroleum-based alcohols were acetoacetylated as suitable monomers for vinylogous urethane vitrimers. **Table 1** shows the abbreviations and structures of the alcohols and the acetoacetates.

Table 1: Abbreviations and structures of the raw alcohols and the acetoacetylated monomers described in this work.

Aromatic Alcohols		Acetoacetates	
PH		PH$_{AcAc}$	
RE		RE$_{AcAc}$	
NDO		NDO$_{AcAc}$	
BPA		BPA$_{AcAc}$	
THPE		THPE$_{AcAc}$	
Aliphatic Alcohols		**Acetoacetates**	
EG		EG$_{AcAc}$	
HM		HM$_{AcAc}$	
DOD		DOD$_{AcAc}$	
PEG300		PEG300$_{AcAc}$	
PEG 4000		PEG 4000$_{AcAc}$	
3-arm PEG		3aPEG$_{AcAc}$	
BZ		BZ$_{AcAc}$	
HT		HT$_{AcAc}$	

CH		CH$_{AcAc}$	
DCH		DCH$_{AcAc}$	
Saccharides and derivates		**Acetoacetates**	
FRU		FRU$_{AcAc}$	
GLU		GLU$_{AcAc}$	
SO		SO$_{AcAc}$	
LAC		LAC$_{AcAc}$	
SAC		SAC$_{AcAc}$	

Polysaccharides represent one of the most natural resources on earth and build several biopolymers and supramolecular structures (Introduction, chapter 3.4). This part investigated whether bio-based polymers, *e.g.,* starch (amylose and amylopectin), chitosan, chitin, and cellulose, can be modified by the described acetoacetylation reaction. It was shown that the functionalization works for dissolved homopolymers (*e.g.,* chitosan) and supramolecular structures (*e.g.,* starch or cellulose nanoparticles). In the scope of publication 3 the modification of starch granules is shown in detail. Moreover, cellulose nanofibers (100 x 7 nm) from bacteria (*Acetobacter aceti subspecies xylinum*) were acetoacetylated and showed a huge grade of acetoacetylation, caused by the large surface

area of the nanoparticles.[149, 150] Moreover, even larger supramolecular structures like common cotton linters (fibers, 10 µm) or milkweed fibers (fibers, 20 µm x 1 cm), mainly consisting of cellulose, could be acetoacetylated.[151] [152]

Table 2: Abbreviations and structures of the raw polysaccharides and the acetoacetylated products (n = repeating units).

Polysaccharides and macromolecular structures		Acetoacetates	
Chitosan		Chs$_{AcAc}$	
Chitin particles		Chi$_{AcAc}$	
Starch (corn, rice, wheat, tapioca)		Starch$_{AcAc}$	
Cellulose – Nanoparticles (bacteria) Cellulose – Cotton Linters Cellulose – Milkweed Fibers		CLBac$_{AcAc}$ CLL$_{AcAc}$ CLMW$_{AcAc}$	

A crucial factor is the used solvent since it should not break the intra- and intermolecular interactions at high temperatures and, thus, the supramolecular structure of the networks during the reaction. For this reason, the reaction was carried out as a bulk reaction or in non-polar solvents like xylene. Afterward, the mixture was washed with xylene or ethanol to remove excess TMDO and byproducts. SEM images show the intact hollow structure

of acetoacetylated milkweed fibers (appendix, Figure A3). **Table 2** shows the structure of the raw polysaccharides and the acetoacetylated monomers. ATR-FT-IR spectra of the acetoacetylated products showed the appearance of the characteristic acetoacetate ester (1740 cm^{-1}) and ketone (1711 cm^{-1}) stretching vibrations (appendix, Figure A4). Detailed NMR analyses are shown exemplified on corn starch in publication 3.

Keto-Enol tautomerism

Furthermore, it is known from literature for many decades that acetoacetates undergo keto-enol tautomerism, forming a 6-membered cyclic structure that is stabilized by intramolecular hydrogen bonds. Usually, the keto form is thermodynamically preferred, while the equilibrium is determined by the surround protic/aprotic polarity (solvent, monomer), temperature and time.[77-80]
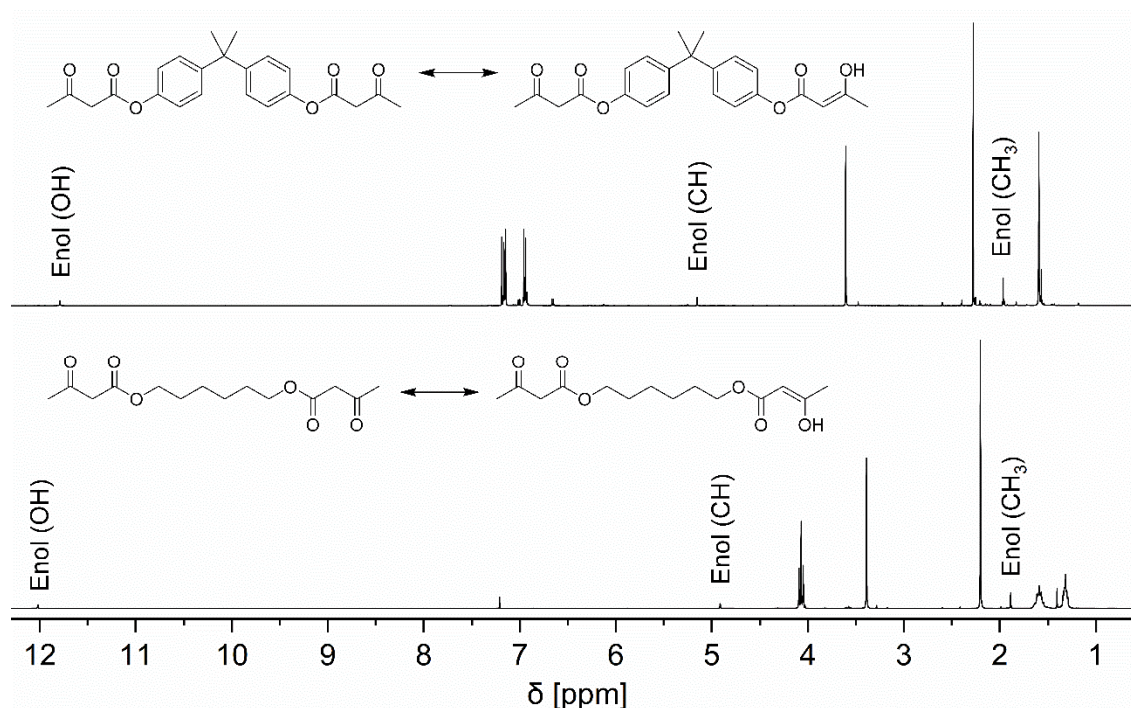
Figure 35: ^{1}H NMR spectra of the acetoacetate monomer BPA$_{AcAc}$ (top) and HM$_{AcAc}$ (bottom) showing keto-enol tautomerism and especially the signals of the few available enol tautomers.

A comparison of acetoacetate monomers derived from aliphatic and aromatic alcohols is shown in **Figure 35**. HM$_{AcAc}$ derived from the aliphatic 1,6-hexanediol showed 7 mol% enol-tautomer after 1 months, while BPA$_{AcAc}$, derived from bisphenol-A showed 13 mol% enol-tautomer after 1 month at room temperature. These results confirm the

formation of the enol-tautomer in both monomers, while the aromatic monomers show a higher preference for the enol-tautomer. Nevertheless, the amount of keto and enol form is not a crucial factor since both tautomers reacted after adding primary amines due to the continued transformation of the tautomers. For this reason, this behavior, already studied in detail, was not further focused in this work but is mentioned for the sake of completeness.

Acetoacetamidation of amines

In 2015 Gama *et al*. reported the acetoacetamidation of anilin derivates in boiling water by using TMDO. [153] Adapting this finding, it was investigated if the acetoacetylation could likewise take place in hot water, which turned out is not possible. This finding offers a selective acetoacetamidation even in the presence of hydroxy groups. The natural biopolymer chitosan was used as a raw material in this reaction to explore that. Chitosan contains hydroxy and amine groups and is a linear polysaccharide made of randomly distributed deacylated *β*-(1-4)-linked *D*-glucosamine and acetylated *N*-acetyl-*D*-glucosamine. The polymer is mainly produced by treating the chitin shells of shrimp and other crustaceans with an alkaline substance, such as sodium hydroxide. Nevertheless, chitosan can also be produced directly from mushrooms and also extracted from mushroom waste.[154]

Chitosan has several commercial and possible biomedical uses. It can be used in agriculture as a seed treatment and biopesticide, helping plants to fight off fungal infections. In winemaking, it can be used as a fining agent, helping prevent spoilage. In industry, it can be used in a self-healing polyurethane paint coating.[155] In medicine, it is helpful in bandages to reduce bleeding and as an antibacterial agent; it can also be used to help deliver drugs through the skin.[155]

First, the reaction was carried out on low molecular chitosan oligomers, which are soluble in water or DMF. When the reaction was carried out in DMF, an acetoacetylation and acetoacetamidation were observed, while in water, only the acetoacetamidation proceeded. This behavior allows a selective reaction by the choice of solvent and enables water as a green and preferable solvent. During the reaction, the highly reactive acetylketene can rarely react with the weak nucleophile water, but the emerging 3-oxobutanoic acid directly splits into acetone and CO_2 at elevated temperatures, which

can be easily removed by distillation.[153] As a reference, an acetoacetamide based on piperazine was prepared according to Denissen *et al.*.[21]

Chitosan, with a high molecular weight, is not soluble in water anymore. Nevertheless, it is soluble in aqueous acetic acid solution (1 wt% AA, 1 wt%). For this reason, it was investigated if the acetoacetamidation likewise proceeds in the acidic medium. Experiments proved that the reaction also works in an acidic aqueous solution, allowing the modification of high molecular weights chitosan chains up to 200 kDa. The possible reaction of acetic acid and the reactive acetylketene leads to the formation of 3-oxobutanoic propionic anhydride, which likewise dissociates into acetic acid, acetone, and CO_2 at elevated temperatures.[153]

With this, a robust, selective, and water-based method for the preparation of monomers for vinylogous urethane vitrimers was explored. The grade of acetoacetamidation and further reaction to the vinylogous urea can be set by the amount of TMDO. ATR-FT-IR spectra of the acetoacetylated polysaccharides show the appearance of the characteristic acetoacetate ester (1740 cm^{-1}) and ketone (1711 cm^{-1}) and the acetoacetamide amide (1623 cm^{-1}) and ketone (1710 cm^{-1}) stretching vibrations (**Figure 36**). ^{1}H NMR spectra are shown in the appendix (Figure A2).
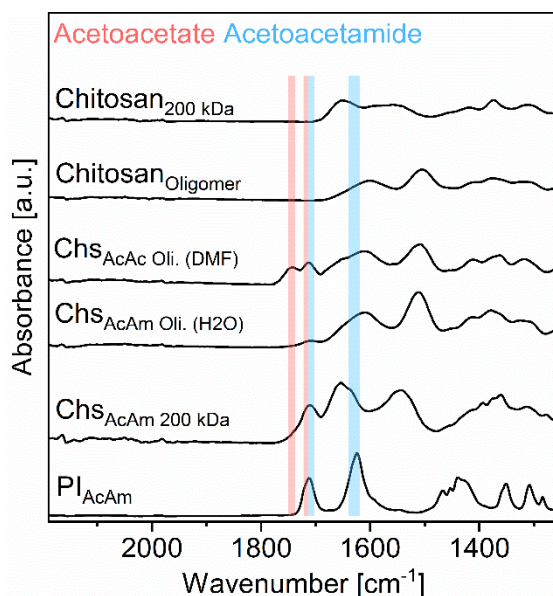
Figure 36: ATR-FT-IR spectra of acetoacetylated (AcAc) and acetoacetamidated (AcAm) chitosan oligomers and chitosan polymers, showing the characteristic ester, amide and C=C bands.

In the following chapters, the monomers were used for polymerizations in specific subprojects. Other monomers were used in the scope of the published publications or outsourced to other cooperation projects or theses and are not part of this work.

6.2   Polymerization – Gelation Times

The condensation reaction of acetoacetates with primary amines is an exothermic reaction and can proceed very fast, even at room temperature. In this chapter, a comparison of different amines cured with the trifunctional acetoacetate GL_{AcAc} is shown in terms of the gelation times and polymerization temperature. The acetoacetate to amine ratio R was set to 0.75 in the case of diamines and R = 0.6 for triamines to obtain fast relaxing networks with a sufficient amount of free amines. Moreover, ethanol (1/4 of the total monomer mass) was used to enable solid amines for the condensation reaction. Most amines can easily be mixed and polymerized with GL_{AcAc} by a bulk reaction. Nevertheless, for the comparison, ethanol was added for all polymerizations. **Figure 37** shows an overview of the gelation times, the applied temperatures, and the used di- and trifunctional amines cured with GL_{AcAc}. The results showed that the rate of the exothermic condensation reaction depends on various factors, and the gelation times vary from a few seconds up to several hours. Moreover, some amines did not lead to gelation at all. The concentration of the relevant functional group (amine) in relation to the backbone, the functionality, and nucleophilicity of the amine were identified as the decisive factors for the polymerization rate. The nucleophilicity of primary amines is known to be lowered with aliphatic chains in *alpha*-position to the amine group, which sterically hinder nucleophilic attacks on electrophiles.[156] The trifunctional amine TREN exhibits a functionality of 3, a small backbone, and sterically not hindered amine groups. For these reasons, the gelation occured readily after a few seconds at room temperature with an extensive heat evolution. Difunctional amines, *e.g.* DAE, DAB, CHDA, m-X and many more, have likewise a relatively small backbone and sterically not hindered amine groups. These vitrimer compositions showed gelation times of a few minutes, while a rising chain length/mass of the diamine increased the gelation times. Therefore, the small DAB gelated after 1 minute, while the priamines® PA1075 and PA1074 gelated after 20 minutes. The poly(oxypropylene)-based amines JD200, JD400, JD2000, JT403 and JT3000 contain primary amine groups with a methyl group in *alpha*-position, which lengthened the gelation times. For example, JD200 gelates 2–3 times slower than DADD or DCM with a comparable molecular mass and chain length.
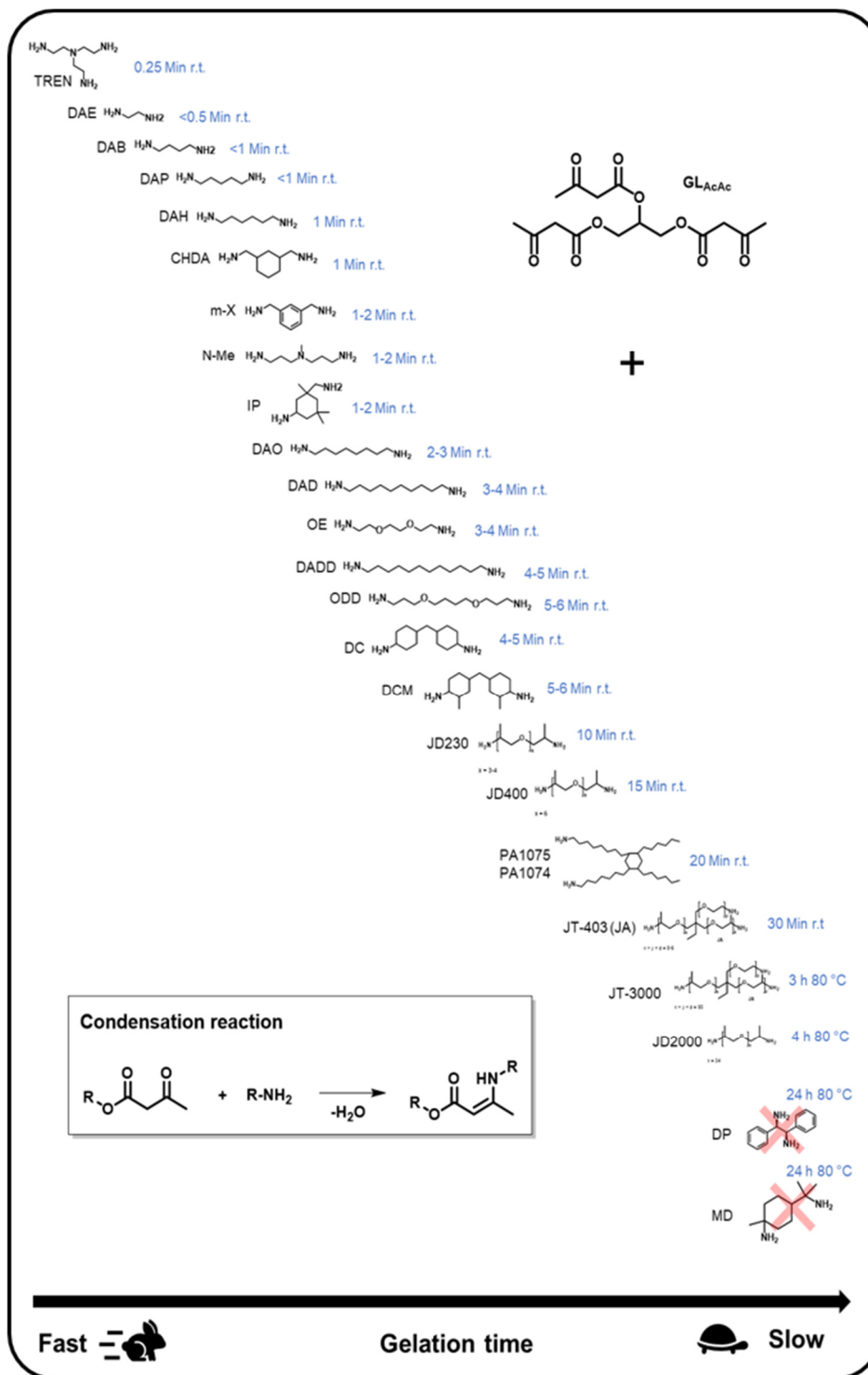
Figure 37: Overview of the gelation times, curing temperatures, and the used di-and trifunctional amines cured with the trifunctional Acetoacetate GL$_{AcAc}$ in a condensation reaction to form a vinylogous urethane vitrimer.

Moreover, the trifunctional amine JT403 gelated slower than PA1075 even if it shows a higher functionality, concentration of amine groups, and a comparable viscosity.

Comparing JT3000 and JD2000, the gelation times were about 3–4 hours even when heating to 80 °C, which the large backbone and the low concentration of amine groups can explain. The low nucleophilicity and concentration of the amines slowed down the reaction by a multiple. Comparing DP and MD, the nucleophilicity of the amines is very low, and no gelation occurred even after heating for 24 h at 80 °C. This is reasonable because the amines are sterically hindered through phenyl-groups or 1–2 methyl groups in *alpha*-position.

This chapter shows that the gelation times vary a lot depending on the monomers. Nevertheless, this offers the potential to adjust the gelation time by choosing suitable monomer compositions for specific processes or applications. Moreover, the speed of the condensation reaction often gives a good impression of the exchange reaction rate in the final vitrimer materials. This is because the vitrimers exchange reaction likewise depends on the nucleophilicity of the amine and the concentration of the relevant functional groups (vinylogous urethane groups and amine groups) compared to the overall monomer backbones. However, other factors also play a major role, and no exact correlation or prediction can be given in general.

Aromatic and secondary di- and trifunctional amines, *e.g.* *m*-phenylendiamine, 4,4′-diaminodiphenylmethane, parafuchsin base, melamine, 3-aminobenzylamine, piperazin, 4,4′-trimethylenedipiperidine and acetalydehyd trimer were also tested as possible reactants for vinylogous urethanes. Unfortunately, the use of secondary amines showed a partial bonding to acetoacetates, but the nucleophilicity and conversion rates were too low to obtain cross-linked materials. Moreover, the low nucleophilicity most likely hinders efficient transamination reactions in the materials at elevated temperatures. Even catalysts like *p*-toluenesulfonic acid could not accelerate the condensation reaction and enable vinylogous urethane vitrimers. Aromatic amines likewise showed low reactivity due to their low nucleophilicity but generated cross-linked materials when using *p*-toluenesulfonic acid as a catalyst. Unfortunately, the materials showed thermal degradation at temperatures above 100 °C. These findings are probably the reasons why there have been almost no publications about secondary or aromatic amines as monomers. Only one publication about photoactivated healable vitrimeric copolymers using aminoantracen and 1,12-diaminododecane for the synthesis of vinylogous urethane vitrimers is reported. However, the authors also stated that the aromatic amines did not bind very well and aromatic amines, therefore are not very suitable.[87]

6.3 Vinylogous Urethane Vitrimers

In this chapter, several different vinylogous urethane vitrimers and vinylogous urea vitrimers are compared in terms of their spectroscopic and thermomechanical properties by using different synthetic routes, monomers, or compositions. The focus was on investigating the thermomechanical properties and, particularly, the reprocessability of the networks. Several factors are explored, summarized and discussed in this chapter. The results are separated into different subchapters, with a short summary given in each.

6.3.1 Impact of Different Amine Monomers

Glycerol was used as a suitable raw material for vinylogous urethane vitrimers, since it is cheap and widely available as a residual byproduct from the continuously growing biodiesel production. Transesterification reactions were used to break the triglyceride structure of oils and fats and release fatty acids and glycerol as residuals. However, for every 100 kg of biodiesel production, approximately 10 kg of crude glycerol is generated, for which use should subsequently be found.[157-159]

As described in detail in publication 3, glycerol can undergo fast and efficient bulk-acetoacetylation reactions with TMDO, producing a trifunctional acetoacetate. The acetoacetate acts as a suitable cross-linker for vinylogous urethane networks and can be cured with various available di- and trifunctional amines, as shown in the chapter "Polymerization" (6.2). This chapter investigated the influence of different amines and their backbones in terms of their thermomechanical properties. For comparison, the trifunctional acetoacetate and an R-value of 0.75 were kept constant.

6.3.1.1 Comparison of Five Diamines with Comparable Molar Mass

In this subchapter five different diamines with a C-8 (N,O) backbone, comparable molecular weights of 136–148 g mol^{-1}, and partly containing heteroatoms were investigated in terms of the thermomechanical properties of the corresponding vitrimers with the triacetoacetate of glycerol. Since the molecular weights, R-values, acetoacetate monomer, chain lengths and the cross-linking density (mass ratios) of the prepared materials were quite similar, different properties can be related to backbone effects

regarding heteroatoms and cyclic backbones. The used monomers are shown in **Figure 38**.
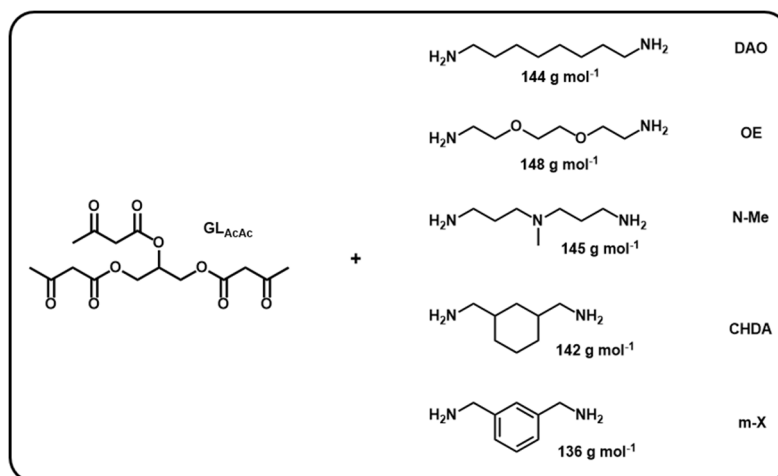
Figure 38: Structure of the acetoacetylated glycerol GL_{AcAc} and different diamines with a C-8 (N, O) backbone and comparable molecular weights of 136–148 g mol^{-1} used for the synthesis of vinylogous urethane vitrimers.

ATR-FT-IR spectra proved the formation of the characteristic C=C band (1595–1597 cm^{-1}) and C=O ester band (1647–1649 cm^{-1}) of the vinylogous urethane groups as shown in **Figure 39**. The vitrimers are abbreviated as VU-Acetoacetate$_{Amine}$ (*e.g.* VU-GL$_{DAO}$).

At this point, it must be addressed that vinylogous urethane vitrimers always contain intramolecular hydrogen bonds, stabilized in a 6-membered cyclic ring of the vinylogous urethane group (**Figure 40**). Consequently, the materials contain a significant amount of free primary amines and secondary amines (vinylogous urethane group). To investigate the behavior of the intra- and inter molecular hydrogen bonds, temperature-dependent FT-IR measurements were carried out on the vitrimer VU-GL$_{DAO}$. Moreover, the transamination reaction proceeds at elevated temperatures and shows aminal structures as an intermediate state (chapter 3.3.4). Nevertheless, it is not clear if IR-measurements can monitor the intermediate states of the exchange reaction itself.
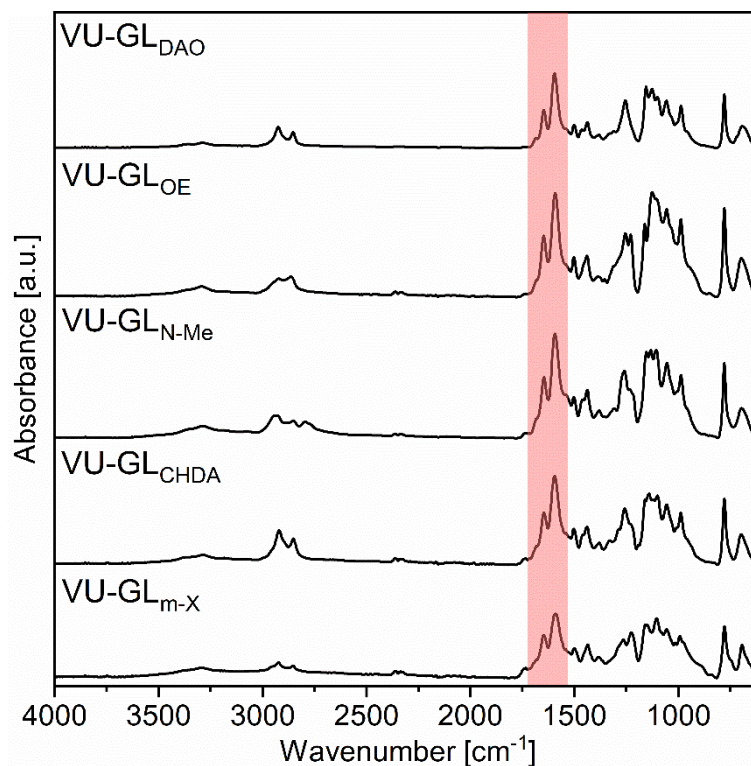
Figure 39: ATR-FT-IR spectra show the formation of the characteristic C=C band (1595–1597 cm^{-1}) and C=O ester band (1647–1649 cm^{-1}) in the prepared vinylogous urethane vitrimers.
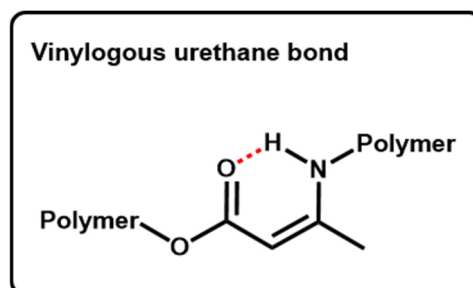
Figure 40: Illustration of the 6-membered ring structure of the vinylogous urethane bond stabilized by intramolecular hydrogen bonds.

The material was heated at 40–160 °C in 20 K steps with a waiting period of 30 minutes. **Figure 41a** shows the heating curves, while Figure 41b shows the cooling curves. Figure 41c shows a cutout of the amine stretching vibration bands in the area of 2800–3550 cm^{-1} and Figure 41d the NH bending, C=C and C=O bands in the area of 1300–1900 cm^{-1}. Comparing the heating and cooling curves, an almost complete, thermoreversible behavior was observed. Moreover, NH/NH$_2$ symmetric (3293 cm^{-1}) and asymmetric stretching vibrations (3357 cm^{-1}) are lowered with rising temperatures and

shift towards higher wavenumbers (3378 cm^{-1}), which indicates the debonding of hydrogen bonds to free amines. In addition, the in-plane bending vibrations of the NH group shift from 1538 to 1516 cm^{-1}, likewise indicating the weakening of the intramolecular hydrogen bond. A shift of the C=O band at 1653 cm^{-1} to higher wavenumbers of 1683 cm^{-1} proves the weakening of the C=O-H hydrogen bond. The results show an expected weakening of the intramolecular hydrogen bonds with rising temperature. Since the shifts already appear at relatively low temperatures below 100 °C, it is questionable if they are related to the transamination reaction, which typically only proceeds at higher temperatures. Nevertheless, the formation of the intermediate states (imine, aminal) should also shift the NH bond vibrations, with the restriction that these intermediates are hardly visible in IR measurements due to their short existence.
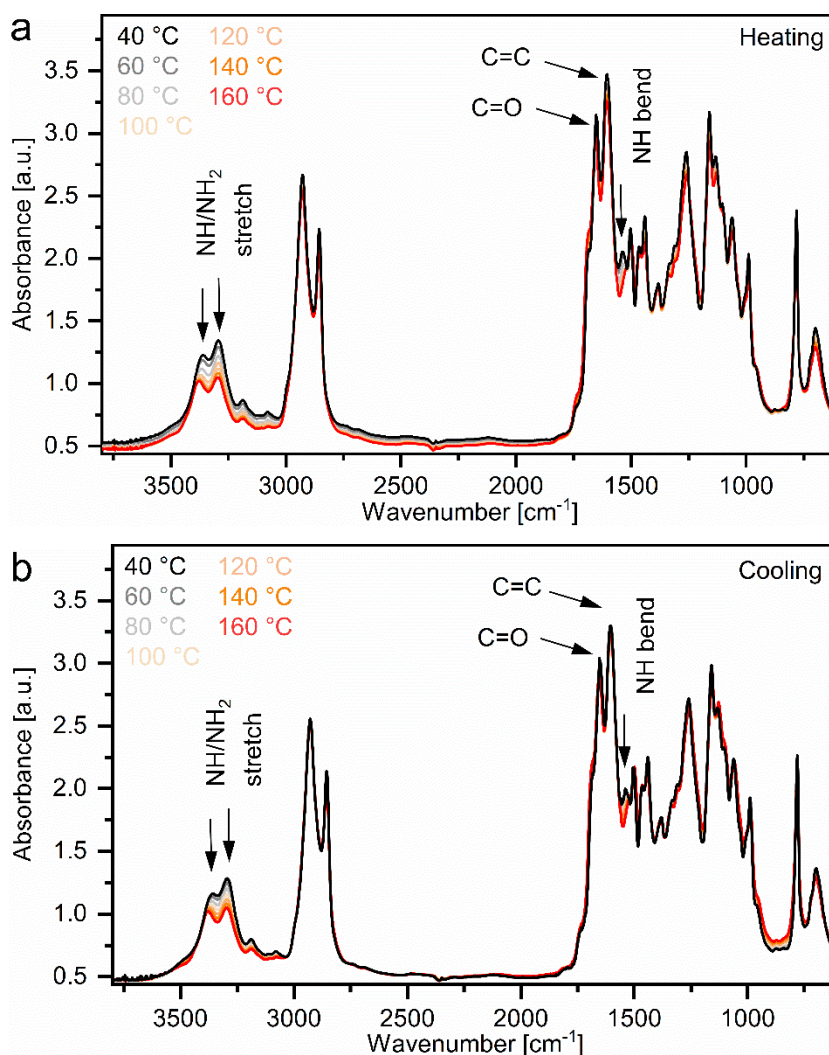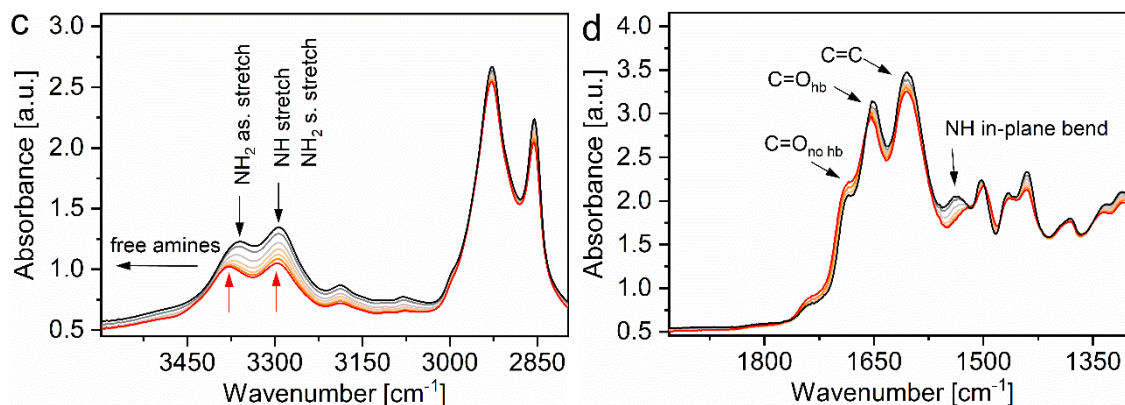
Figure 41: (a) Heating cycle of the temperature-dependent FT-IR measurements of VU-GL$_{DAO}$. **(b)** The cooling cycle of the temperature-dependent FT-IR measurements of VU-GL$_{DAO}$. **(c)** Cutout of the heating cycle showing the amine stretching vibration bands in the area of 2800–3550 cm^{-1} **(d)** Cutout of the heating cycle showing the NH bending, C=C and C=O bands in the area of 1300–1900 cm^{-1}. The spectra were recorded *via* transmission-IR of a thin vitrimer film and transferred into ATR spectra for better comparison to other spectra in this work.

To investigate the thermomechanical properties of a vitrimer, oscillatory and step shear experiments have been carried out. The measurements were carried out within the linear viscoelastic regime. DMTA measurements show cross-linked vitrimers with a characteristic rubbery plateau and different T_gs. In **Figure 42a** only the storage moduli are shown for a better overview, while in Figure 42b the storage and loss moduli are shown. Comparing the results, the cyclohexane-based vitrimer VU-GL$_{CHDA}$ showed the highest stiffness above the glass transition temperature, while the vitrimer VU-GL$_{DAO}$, containing the aliphatic C8-chain, showed the lowest. Comparing the T_gs by plotting the loss factor versus the temperature, the vitrimers with a linear chain (DAO, OE, N-Me) exhibited comparable T_gs in the range of 48–55 °C, while the vitrimers with a cyclic backbone (CHDA and m-X) showed T_gs of 104–105 °C (maximum loss factor, Figure 42c). Using diamines with a linear chain led to lower T_gs than cyclic diamines. The existence of heteroatoms in the chain or the type of cyclic backbone were surprisingly not decisive factors. In fact, the comparable cross-linking density and weight ratio of the acetoacetate to the amine monomers seem to be the essential factors. The differences in using linear or cyclic diamines are caused by the highly different spatial arrangement and mobility of the structural units. Noticeably, VU-GL$_{N-Me}$ shows two transition states in the

DMTA curve, which is discussed later in detail. Frequency sweeps likewise proved the formation of cross-linked materials at 100 °C (Figure 42d).
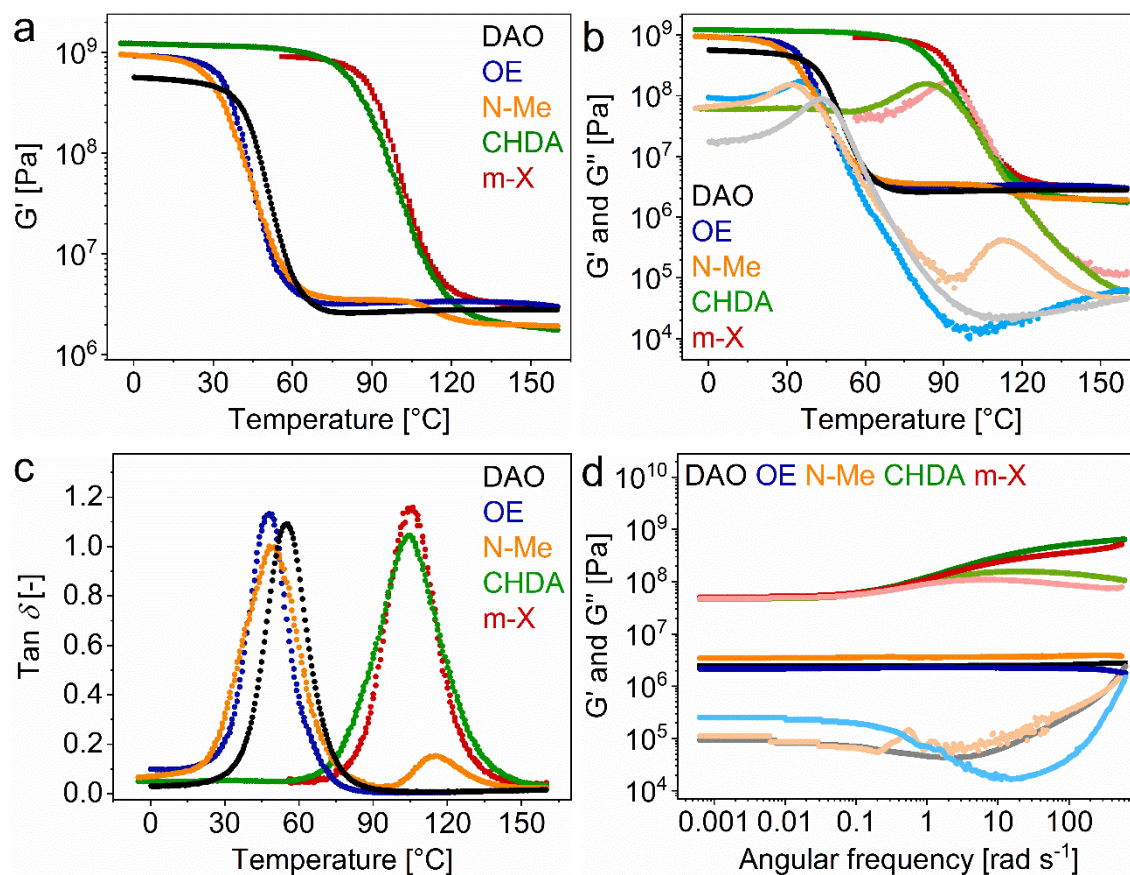
Figure 42: (a) DMTA measurements of the five compared vitrimers (only storage modulus, $\gamma = 0.1\%$, $\omega = 10$ rad s^{-1}). **(b)** DMTA measurements of the compared vitrimers (G' = dark color and G'' = light color). **(c)** Plot of the loss factor versus the temperatures of the compared vitrimers **(d)** Frequency sweeps of the compared vitrimers (G' = dark color and G'' = light color, $\gamma = 0.1\%$, $\omega = 0.000628–628$ rad s^{-1}).

To prove the reprocessability of the networks, stress-relaxation measurements in the temperature range of 110–180 °C were carried out. In **Figure 43a** a comparison of the stress-relaxation curves at 150 °C is shown. The curves show that the polyether-based vitrimer VU-GL$_{OE}$ exhibited the fastest stress-relaxation of 19 s, followed by the N-methyl-based vitrimer VU-GL$_{N-Me}$ with 32 s. In comparison, the vitrimer with the aliphatic carbon chain (VU-GL$_{DAO}$) shows a stress-relaxation time of 63 s, which is more than three times longer than the one measured for VU-GL$_{OE}$. VU-GL$_{CHDA}$ and VU-GL$_{m-X}$ showed much slower stress-relaxation times of 115 and 103 s. These results show that

heteroatoms accelerate the transamination reaction in the vitrimer, with the polar polyether-backbone showing the strongest effect. In Figure 43b/44c, the stress-relaxation curves of VU-GL$_{OE}$ and VU-GL$_{DAO}$ are shown at 110–160 °C, while the curves of the other vitrimers are shown in the appendix (Figure A5–A7). This behavior can also be attributed to a neighboring group participation (NGP) of the heteroatoms. Nishimura *et al.* described that a secondary amine, which is located three CH$_2$ groups next to the reactive center, accelerated the stress-relaxation times and lowered the activation energies. The diamines OE and N-Me exhibit the heteroatoms in a similar position and can possibly show the same effect. Nevertheless, this was observed for silyl ethers and therefore represent another covalent dynamic chemistry.[66] Moreover, Cromwell *et al.* described a similar behavior for a tertiary amine in boronic esters.[65] NGP is decribed in the introduction (chapter 3.2.3, Figure 18) and was not subject for an in-depth investigation on vinylogous urethane vitrimers so far, while accelerating effects have been measured for poly(propylene glycol) vitrimers.[70]

Next, the activation energies of the transamination reaction were determined by plotting the stress-relaxation time at 37% of the normalized stress-relaxation modulus versus the reciprocal temperature to calculate the E_a from the slope of the linear fit. Doing that, E_as of 78–120 kJ mol^{-1} were calculated (Figure 43d). The vitrimer VU-GL$_{DAO}$, which showed the shortest stress-relaxtion time, showed also the lowest E_a of 78 kJ mol^{-1}. Next, VU-GL$_{N-Me}$ followed with 86 kJ mol^{-1} and the second fastest stress-relaxation. The vitrimer VU-GL$_{CHDA}$ showed a relatively slow stress-relaxation but showed a surprisingly low E_a of 86 kJ mol^{-1}. The vitrimers VU-GL$_{DAO}$ and VU-GL$_{m-X}$ exhibited relatively high activation energies of 114 and 120 kJ mol^{-1}. As known from the literature, short stress-relaxation times are not generally accompanied by low activation energies. Spiesschaert *et al.* presented a comparison between vinylogous urethane vitrimers synthesized by fourteen different diol-derived materials with backbones ranging from silicones (poly(dimethylsiloxane), PDMS), to polyethers (poly(tetrahydrofuran) (PTHF), poly(ethylene glycol) (PEG) and poly(propylene glycol) (PPG)) as well as more hydrophobic backbone spacers (1,10-decanediol, pripol® 2033).[70] To investigate the influence of the cross-linking density on the stress-relaxation times, the focus was on two different polyethers used with different molecular weights: PTHF (M_n: 250, 650, 1000, 2000, and 2900 g mol^{-1}) and PPG (M_n: 400, 725 and 2000 g mol^{-1}). The trifunctional

amine TREN was used as a cross-linker. The materials showed activation energies in the range of 68–117 kJ mol^{-1}, stress-relaxation times of 2–345 s at 140 °C and T_{gs} of -120–31 °C. The results show that the influences are very complex, and precise correlations and trends are difficult to identify. Nevertheless, a trend of a lower activation energy with faster stress relaxation was observed, especially when comparing the vitrimers with linear diamines VU-GL$_{OE}$, VU-GL$_{N-Me}$ and VU-GL$_{DAO}$.
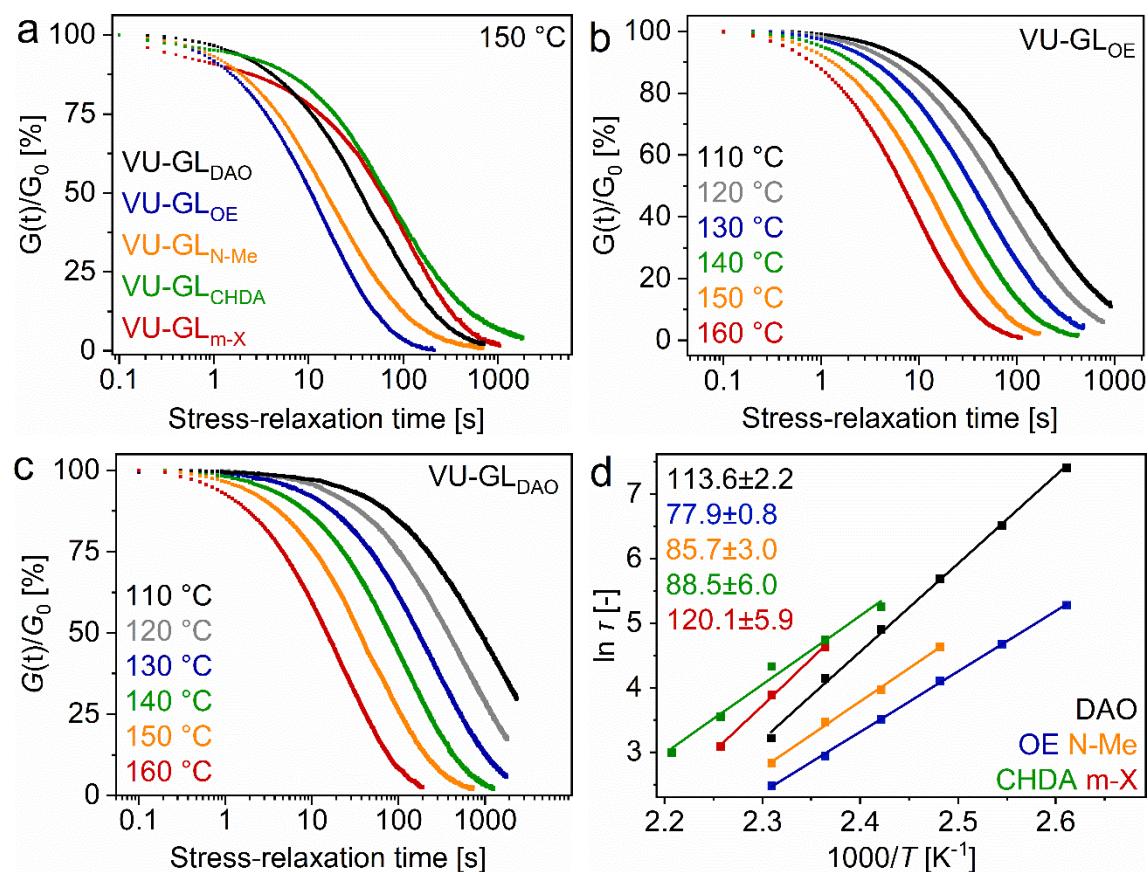
Figure 43: **(a)** Comparison of the stress-relaxation curves of the five compared vitrimers at 150 °C ($\gamma = 1\%$). **(b/c)** Stress-relaxation curves of VU-GL$_{DAO}$ and VU-GL$_{OE}$ in the range of 110–160 °C ($\gamma = 1\%$). **(d)** Plot of ln τ versus the reciprocal temperature to determine the activation energy from the slope of the linear fit.

DSC measurement proved DMA results by measuring similar T_gs of 41, 48, and 53 °C for VU-GL$_{N-Me}$, VU-GL$_{OE}$ and VU-GL$_{DAO}$ as well as 92 and 100 °C for VU-GL$_{CHDA}$ and VU-GL$_{m-X}$ (mid) as shown in **Figure 44**.
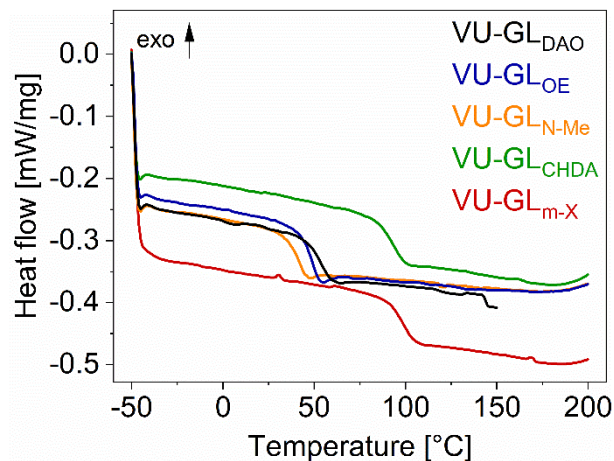
Figure 44: DSC measurements of the vitrimers VU-GL$_{N-Me}$, VU-GL$_{OE}$, VU-GL$_{DAO}$, VU-GL$_{CHDA}$ and VU-GL$_{m-X}$ showing the glass transition temperatures.

Tensile tests were carried out in order to investigate the mechanical properties. **Figure 45a/b** show the stress-strain curves of the five compared vitrimers, measured with 3–4 specimen each. Thermosetting vitrimers with averaged E-moduli of 815–1410 MPa (Figure 45c), tensile strengths of 40–65 MPa (Figure 45d), and elongations at break of 3.3–6.4% (Figure 45e) were measured. The results show that the vitrimers with cyclic backbone show a significantly higher stiffness than the vitrimers based on linear diamines. Accordingly, the latter vitrimers appeared much softer and showed a large plastic deformation, especially in the case of VU-GL$_{N-Me,}$ with ultimate strains of averaged 102%. VU-GL$_{N-Me}$ also showed a significantly higher toughness than the other vitrimers (Figure 45f).
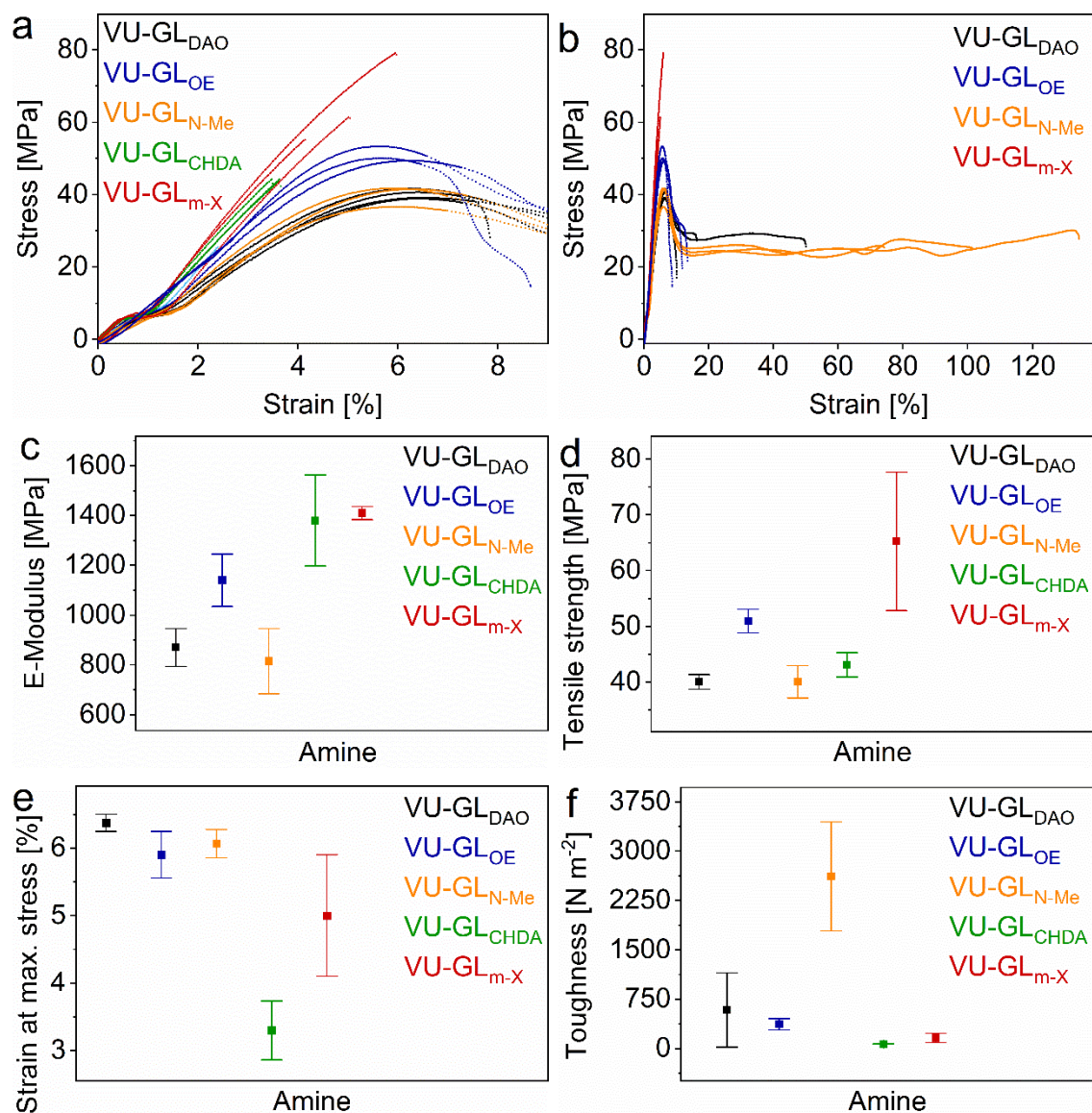
Figure 45: (**a/b**) Stress-strain curves of the vitrimers VU-GL$_{DAO}$, VU-GL$_{OE,}$ VU-GL$_{N-Me,}$ VU-GL$_{CHDA}$ and VU-GL$_{m-X}$ with a cutout from 0–1% and 0–140% strain. (**c**) E-Moduli of the five compared vitrimers with error bars. (**d**) Tensile strengths of the five compared vitrimers with error bars. (**e**) Elongations at ultimate strength of the five compared vitrimers with error bars. (**f**) Toughness of the five compared vitrimers with error bars.

Dual temperature response of VU-GL$_{N-Me}$

The vitrimer VU-GL$_{N-Me}$ (**Figure 46a**) showed a dual temperature response with two reversible transitions in the DMTA measurements. The first one is located at 49 °C and attributed to the normal glass-transition of the vitrimer. However, a second, smaller one was observed at a higher temperature of 115 °C (Figure 46b/c). This behavior is quite unusual and was not observed for countless other synthesized vitrimers with different backbones. At this point, it must be noted that the vitrimers were measured a few weeks after the synthesis, which may cause relaxation, crystallization, aging, or other effects. Nevertheless, the only difference in this composition is the tertiary N-methyl group in the middle of the diamine chain. Obviously, the tertiary amine is responsible for a stabilized rubbery plateau in the area of 75–100 °C. At higher temperatures, the effect is no longer present and resulted in another slightly lower rubbery plateau in the range of 130–160 °C. The storage modulus in the glassy state was measured with 955 MPa, the first rubbery plateau with 3.6 MPa and the second rubbery plateau with 1.9 MPa. The glass transition shows a decrease of 951 MPa, while the second transition only shows a low decrease of 1.7 MPa. Nevertheless, the first rubbery plateau exhibits almost double the value of the second. Repeatedly measured DSC measurements showed only the glass transition and no other transition in the range of 100–130°C (Figure 46d). The results from the tensile test were already presented and compared to the other vitrimers in the previous chapter. As an outstanding result, the vitrimer VU-GL$_{N-Me}$ showed higher ultimate strains than the other vitrimers with a similar T_g. This additional stability might be caused by another contributing interaction (*e.g.*, non-covalent bonds).
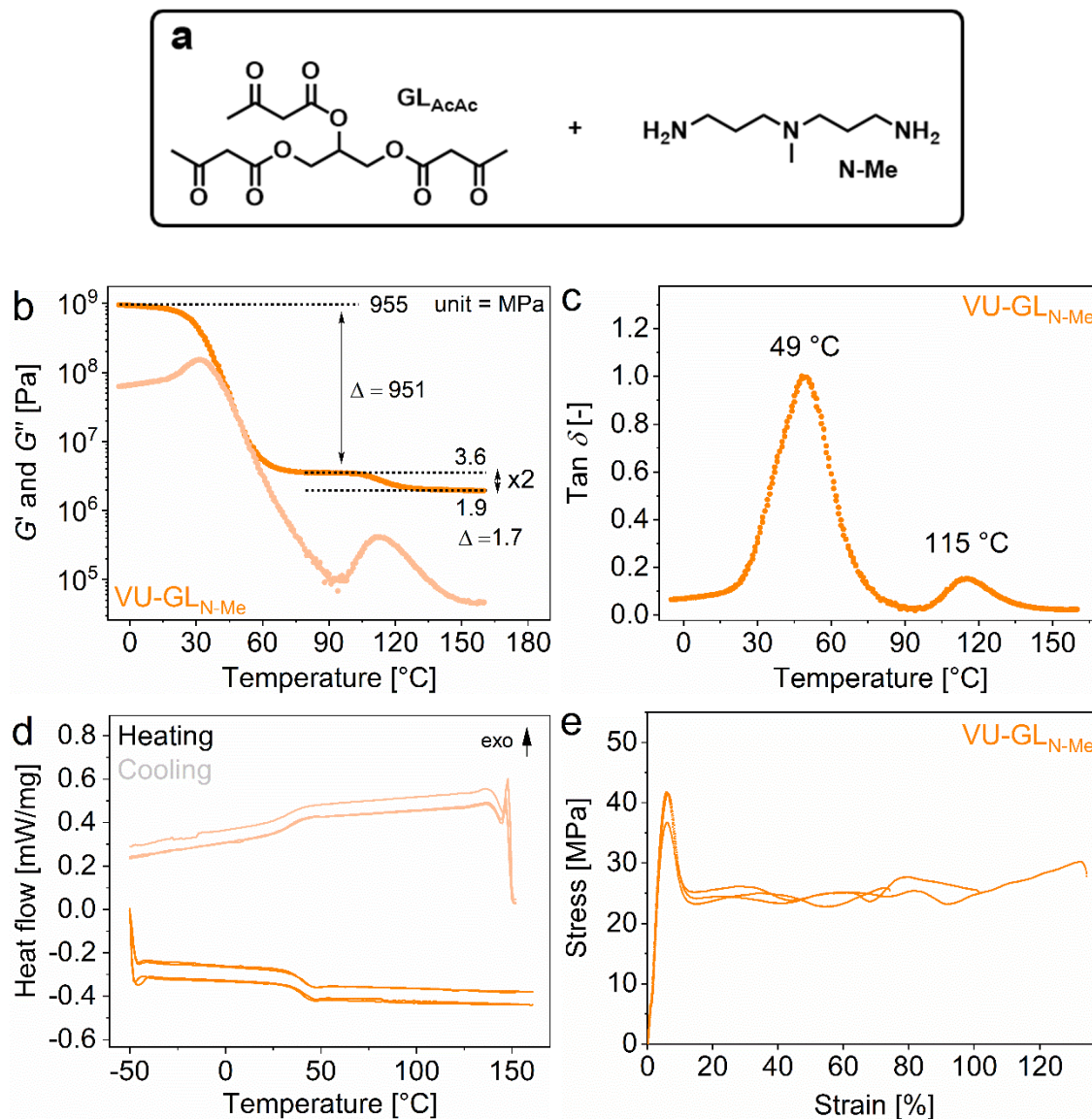
Figure 46: (a) Structure of the used monomers for the synthesis of VU-GL$_{N-Me}$ **(b)** DMTA measurements of the vitrimer VU-GL$_{N-Me}$ showing two temperature transitions (G' = dark color and G" = light color, γ = 0.1%, ω = 10 rad s^{-1}). **(c)** Plot of the loss factor versus the temperatures of the vitrimer VU-GL$_{N-Me}$ **(d)** DSC heating and cooling curves of the vitrimer VU-GL$_{N-Me}$ showing the glass transition temperature. **(e)** Stress-strain curves of the vitrimer VU-GL$_{N-Me}$.

An explanation for this phenomenon could be intermolecular hydrogen bonds between the tertiary amines and primary or secondary amines in the network, which have a strengthened effect up to 100 °C (**Figure 47**). This behavior is already described for several thermoreversible polymer systems in the literature.[160] The vitrimer VU-GL$_{N-Me}$ shows a significantly higher toughness than the other vitrimers. Hydrogen bonds can provide additional toughness to the network when the chains align through tensile stress.
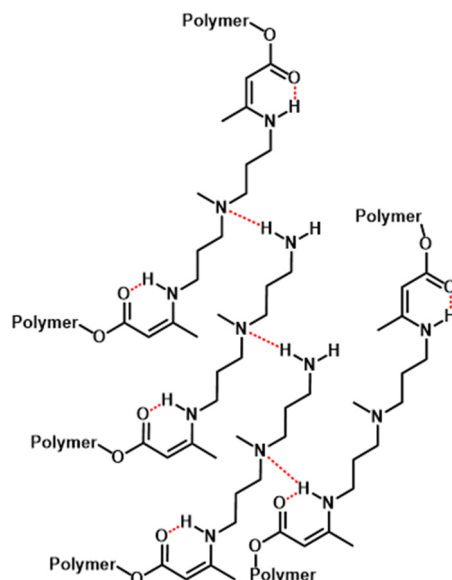
Figure 47: Structure of the vinylogous urethane bond stabilized by intramolecular hydrogen bonds, which can also be considered as 6-membered ring. Moreover, the vitrimer VU-GL$_{N-Me}$ contains tertiary amines, which may undergo intermolecular hydrogen bonding with primary or secondary amines (hydrogen bonds marked in red).

Temperature-dependent IR measurements were carried out to evaluate this hypothesis according to the same procedure as shown for VU-GL$_{DAO}$ (**Figure 48**). Comparing the spectra of the temperature-dependent measurements, which contain an additional *N*-methyl group, the characteristic C-H vibration of the CH$_3$ group can be identified at a wavenumber of 2796 cm^{-1}. The spectra likewise showed the thermoreversible weakening of the intramolecular hydrogen bonds, but no further differences to the spectra of VU-GL$_{DAO}$ could be observed. The C-N bond of tertiary amines is very weak and cannot be identified in the fingerprint area. No additional N-H$_2$N hydrogen bonds can be identified from these spectra, which the other intramolecular hydrogen bonds might cover. No evidence for a different behavior was found in the spectra, while the measurements at least confirm a similar behavior of the different vitrimers. In here, only the heating curves are shown.
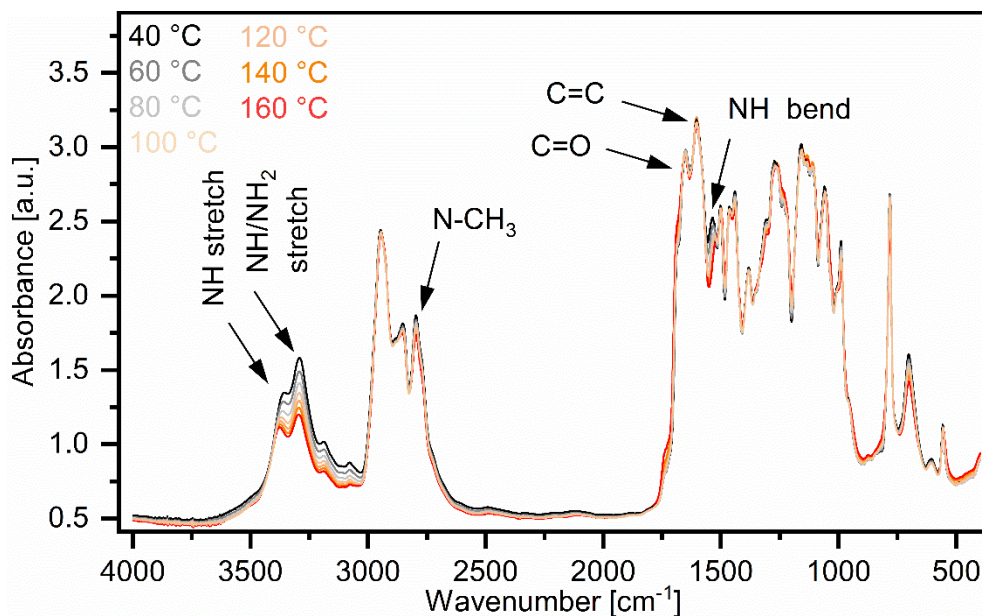
Figure 48: Heating cycle of the temperature-dependent FT-IR measurements of VU-GL$_{\text{N-Me}}$.

The unique behavior of VU-GL$_{\text{N-Me}}$ was unexpectedly found while testing various amine monomers, but it could not completely be clarified what causes this effect. Possible reasons could be the formation of non-covalent interactions, *e.g.* hydrogen bonds or ionic interactions as well as aging reactions or side reactions initiated by the tertiary amines. Nevertheless, it was already clear that this behavior only appeared a few weeks after the synthesis, while the other vitrimers stayed constant. However, the results showed that, as known for many polymers, the networks can rearrange themselves over time and thus change their properties. Since vitrimers are dynamic polymers, effects similar to those of classic thermoplastics could occur over time (creep, crystallization). Unfortunately, this result was generated at the end of the Ph.D. period and could not be studied further.

6.3.1.2 Impact of Different Triamine Backbones

In this subchapter, three different amines were cured with GL_{AcAc} and compared in terms of their properties. J403 with a molecular weight of 440 g mol^{-1}, J3000 with a molecular weight of 3000 g mol^{-1} and the small TREN with a molecular weight of 146 g mol^{-1} (**Figure 49**). Similar R-values of 0.6 were set for the vitrimers.
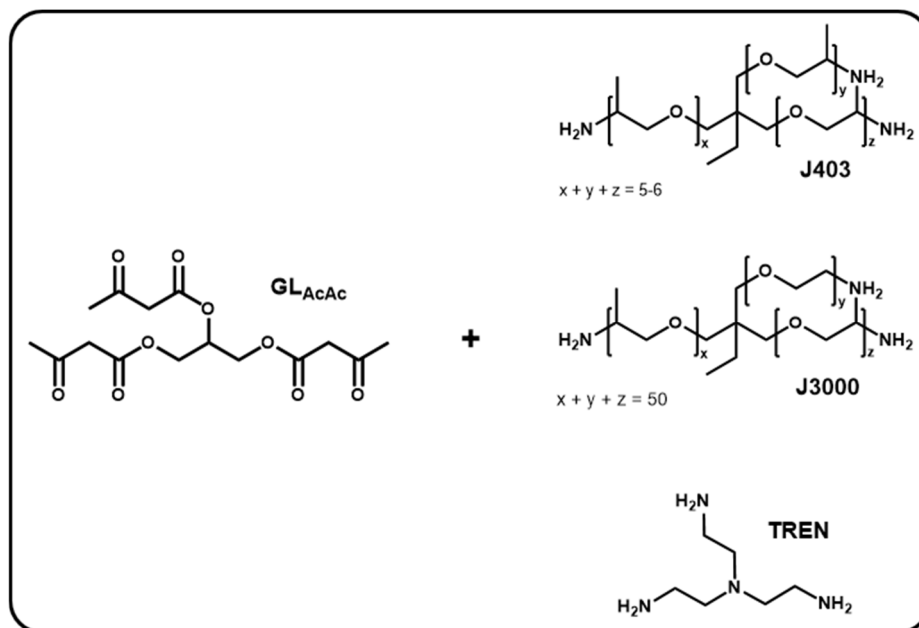
Figure 49: Structure of the acetoacetylated GL_{AcAc} and different trifunctional amines J403, J3000 and TREN.

DMTA measurements proved cross-linked materials with different rubbery plateaus. The vitrimer VU-GL$_{J3000}$ shows the lowest cross-linking density, while GL$_{TREN}$ shows the highest with more than one magnitude higher (**Figure 50a**). The T_gs of the materials were measured by DMTA and DSC measurements and were determined in the range of -58–82 °C (Figure 50b). DSC measured the Tg of VU-GL$_{J3000}$ and the measurement is shown in the appendix (Figure A8). Comparing the stress-relaxation times at 160 °C, VU-GL$_{TREN}$ showed very short stress-relaxation times of 4.8 s, followed by VU-GL$_{J3000}$ (42 s) and VU-GL$_{J403}$ (632 s) (Figure 50c). This is remarkable since VU-GL$_{TREN}$ exhibits the highest cross-linking density with the highest storage modulus at the rubbery plateau and the highest T_g of the materials. This behavior can be explained by the higher nucleophilicity of the amine-groups and the higher concentration of the relevant functional groups (vinylogous urethane bonds and amines), which lead to fast

transamination reactions. As already described in the chapter "Polymerization" (6.2), the nucleophilicity of sterically hindered primary amines with a methyl group in *alpha*-position is lowered compared to terminal amines. Comparing VU-GL$_{J403}$ and VU-GL$_{J3000}$, VU-GL$_{J3000}$ showed much shorter stress-relaxation times because of the low cross-linking density. The chain mobility is very high in this material, and the very low cross-linking density outweighs the higher concentration of amine groups in the vitrimer VU-GL$_{J403}$. Stress-relaxation measurements were carried out at 110–160 °C to determine the activation energies. The stress-relaxation curves are shown in the appendix (Figure A9 and A10).
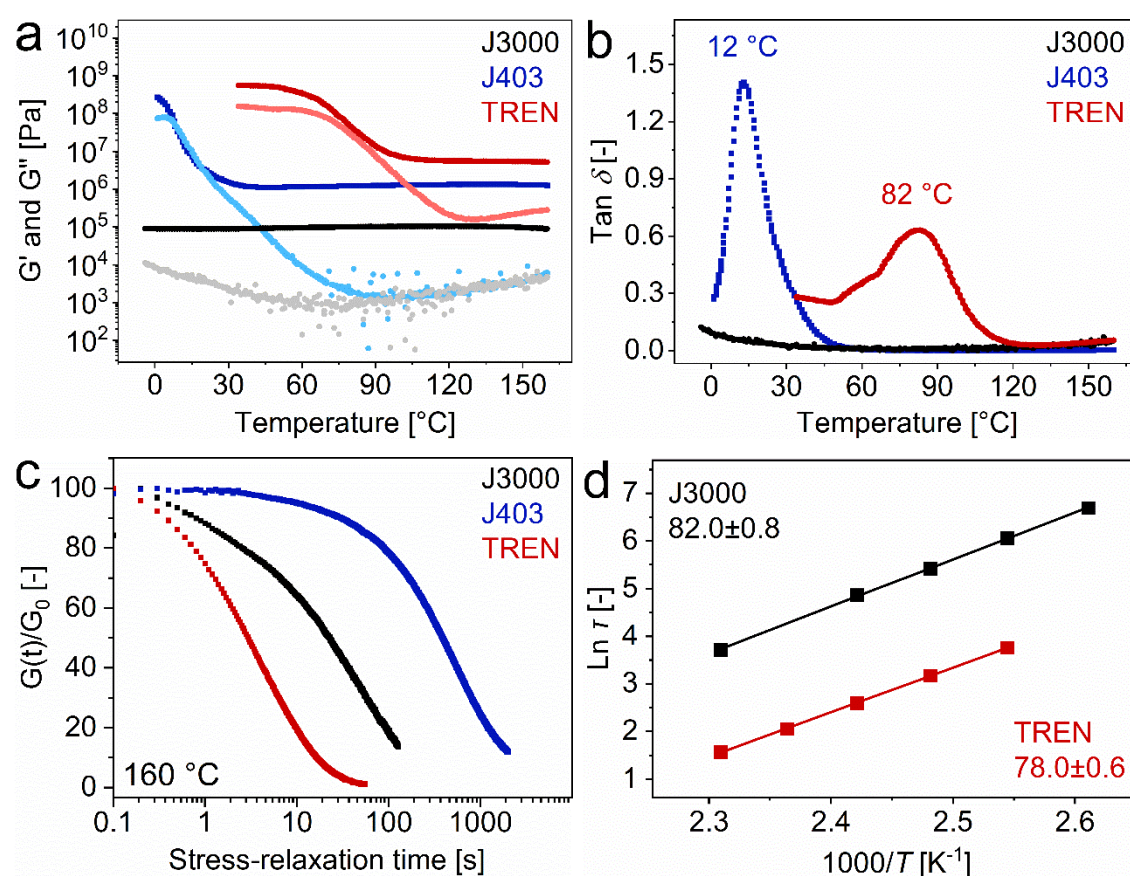
Figure 50: (a) DMTA measurements of the vitrimers VU-GL$_{J403}$, VU-GL$_{J3000}$ and VU-GL$_{TREN}$ (G' = dark color and G'' = light color, $\gamma = 0.1\%$, $\omega = 10$ rad s^{-1}). **(b)** Plot of the loss factor versus the temperature of the vitrimers. **(c)** Comparison of the stress-relaxation curves of the vitrimers at 160 °C. **(d)** Plot of ln τ versus the reciprocal temperature. The activation energies were calculated from the slope of the linear fit (unit in kJ mol^{-1}).

The activation energies were calculated to 78.0±0.6 kJ mol^{-1} for VU-GL$_{TREN}$ and 82.0±0.8 kJ mol^{-1} for VU-GL$_{J3000}$ (Figure 50d). For VU-GL$_{J403}$ a calculation was not reasonable since the stress-relaxation time at 160 °C was already very long. Comparing the activation energies, somewhat similar values were obtained.

This subchapter impressively shows that the ability for complete and fast stress-relaxation (reprocessibility) is not compulsory related to a low T_g or a low cross-linking density. Other factors, like a high nucleophilicity and a high concentration of the functional groups, can accelerate the relaxation rate and proceed much faster than a low T_g, slightly cross-linked and flexible vitrimer-elastomer. This behavior was likewise investigated in the scope of publication 2 with different monomers.

6.3.2 Impact of Different Acetoacetate Monomers

As shown in chapter 6.1 several alcohols can be used as raw materials for vinylogous urethane vitrimers. The monomers were prepared according to the synthetic procedures described in the experimental section 6.5.1.2. This chapter presents and discusses the influence of using different acetoacetate monomers on the thermomechanical properties.

6.3.2.1 Impact of Trifunctional Acetoacetate Backbones

Different vitrimers derived from trifunctional acetoacetates, cured with the same diamines, were compared in terms of their properties. GL_{AcAc}, HT_{AcAc} and $3aPEG_{AcAc}$ were cured with CHDA and DCM (R = 0.75). The structures are shown in **Figure 51**. ATR-FT-IR spectra showed the formation of the characteristic C=C band (1595–1597 cm^{-1}) and C=O ester band (1647–1649 cm^{-1}) of the vinylogous urethane bonds (all spectra in appendix, Figure A11).
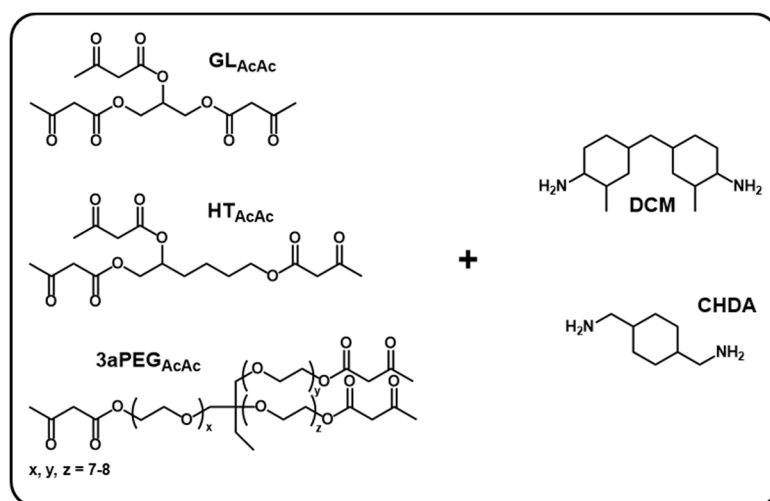
Figure 51: Structure of acetoacetylated, trifunctional monomers GL_{AcAc}, HT_{AcAc} and $3aPEG_{AcAc}$ and the diamines CHDA and DCM utilized for the synthesis of vinylogous urethane vitrimers.

DMTA measurements show cross-linked materials with a characteristic rubbery plateau and different glass transition temperatures. VU-GL$_{CHDA}$ and VU-HT$_{CHDA}$ showed high storage moduli of 1 GPa in the glassy state (20 °C), while VU-3aPEG$_{CHDA}$ showed no glassy state in the measured temperature range (**Figure 52a/c**). Comparing the differences between the monocyclic diamine CHDA and the dicyclic diamine DCM, higher T_gs were

observed when using DCM. VU-HT$_{DCM}$ showed a storage modulus of 1 GPa, while VU-GL$_{DCM}$ and 3aPEG$_{DCM}$ showed lower values. Comparing the maximum loss factors, T_gs of 5–147 °C were measured, exhibiting a broad range when using different monomers. The use of DCM leads to higher T_gs than CHDA, while long polyether chains of the triacetoacetate 3aPEG$_{AcAc}$ lowered the T_g (Figure 52b/d).
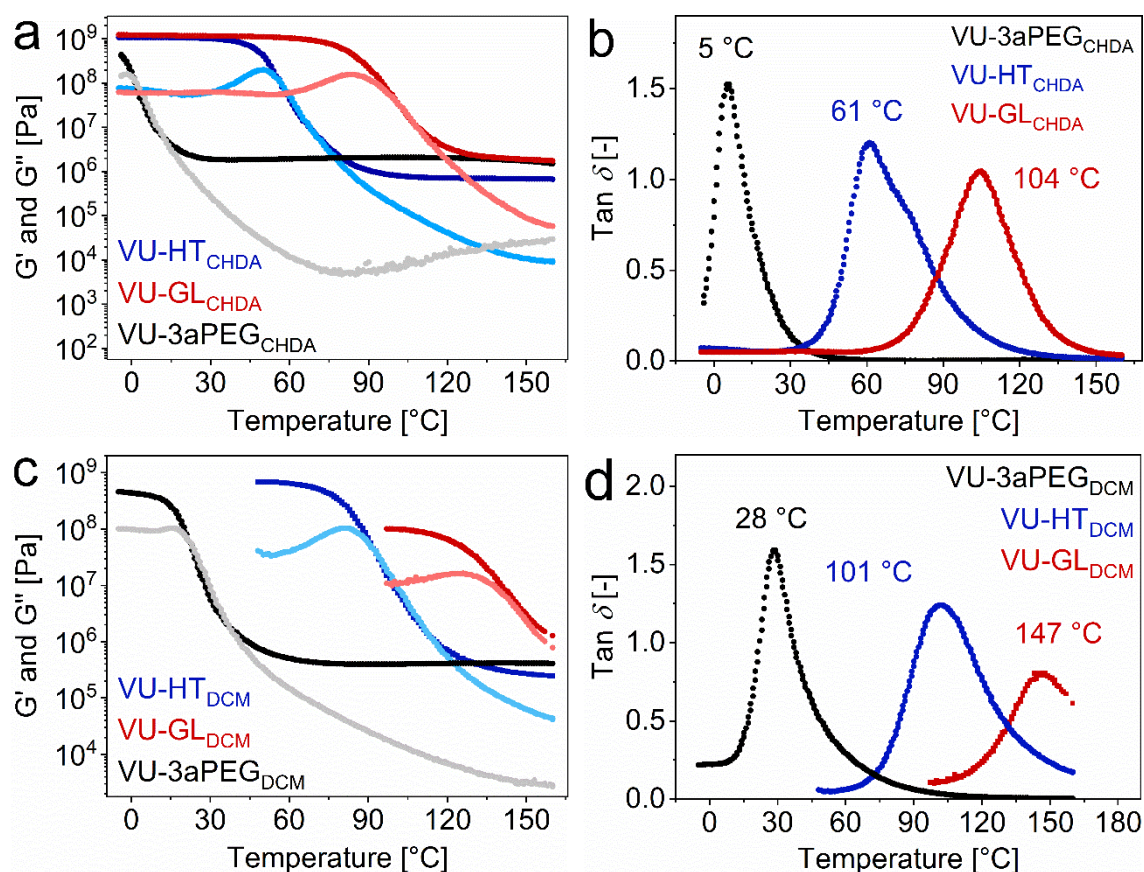
Figure 52: (a/c) DMTA measurements of the vitrimers VU-GL$_{J403,}$ VU-GL$_{J3000}$ and VU-GL$_{TREN}$ (G'= dark color and G''= light color, γ= 0.1%, ω= 10 rad s^{-1}). **(b/d)** Plot of the loss factor versus the temperature of the vitrimers, showing the glass transition temperatures.

Stress-relaxation measurements at 160 °C were carried out to compare the reprocessability of the networks. Comparing the different amines CHDA and DCM cured with the same acetoacetate, significantly longer stress-relaxation times were observed in case of DCM (**Figure 53a**). This behavior can be attributed to the sterical hindrance of the amine, which lowers its nucleophilicity. Moreover, the bulky dicyclohexane backbone may hinder the mobility of the chains. Furthermore, the vitrimers cured with 3aPEG$_{AcAc}$ showed always shorter stress-relaxation times than HT$_{AcAc}$. This behavior is probably due

to the lower cross-linking density and the polarity of the ether-chains of the PEG-based vitrimers. As explored in chapter 6.3.1, ether bridges accelerate the exchange reaction in the vitrimers. Nevertheless, comparing the three acetoacetates cured with CHDA showed comparable short stress-relaxation times, while 3aPEG showed the shortest stress-relaxation time. The low T_g, in combination with a low cross-linking density and additional ether groups, enables high chain mobility and fast stress-relaxation (Figure 53b). In this comparison, the stress-relaxation times increase with a theoretically lower cross-linking density of the low molecular acetoacetates. Comparing the activation energies of the vitrimers, the acetoacetates cured with CHDA show comparable activation energies of 67–76 kJ mol^{-1}, which are typical values for VUs (Figure 53c).
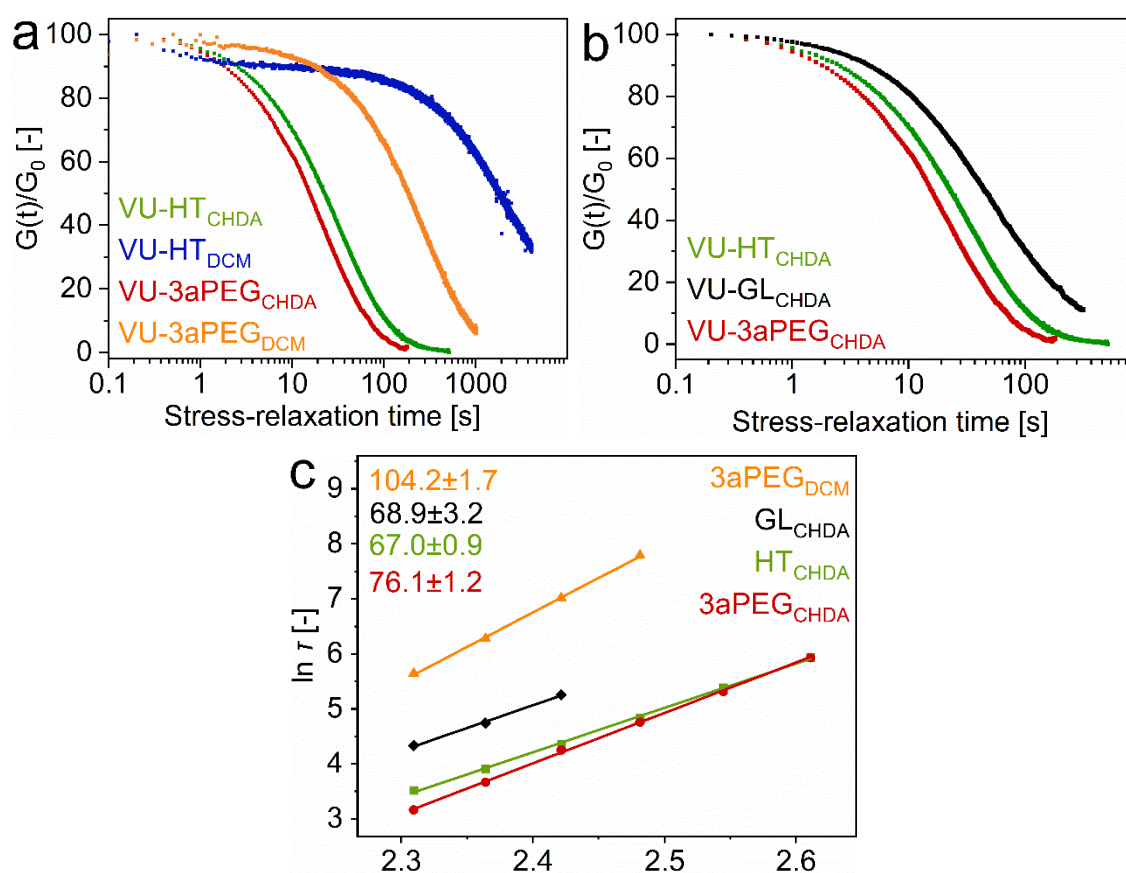
Figure 53: (**a**) Comparison of the stress-relaxation curves of the vitrimers VU-HT$_{CHDA}$, VU-HT$_{DCM}$, VU-3aPEG$_{CHDA}$ and VU-3aPEG$_{DCM}$ at 160 °C. (**b**) Comparison of the stress-relaxation curves of the vitrimers VU-GL$_{CHDA}$, VU-HT$_{CHDA}$ and VU-3aPEG$_{CHDA}$ at 160 °C. Plot of ln τ versus the reciprocal temperature. The activation energies were calculated from the slope of the linear fit (unit in kJ mol^{-1}).

The vitrimer VU-3aPEG$_{DCM}$ showed very slow stress-relaxation and higher activation energies of 103 kJ mol^{-1}, while exhibiting a low T_g of 28 °C. The higher activation energy might be attributed to the different intermediate states of the sterically hindered amine DCM. Moreover, longer chain lengths of *e.g.*, PPG increase the E_a according to literature.[70]

6.3.2.2 Impact of difunctional acetoacetate backbones

For another comparison, different difunctional acetoacetates were polymerized with the trifunctional J403. This amine is typically used as a hardener for conventional polymers, *e.g.,* epoxy resins. Moreover, most available trifunctional amines are highly toxic (*e.g.,* TREN) and, therefore, not necessarily preferred as reactants for plastics. J403 represents a less toxic alternative. In this comparison, the nucleophilicity of the amine and the content of free amines stays constant, while the mass ratio and backbone change due to the influence of the different acetoacetates.
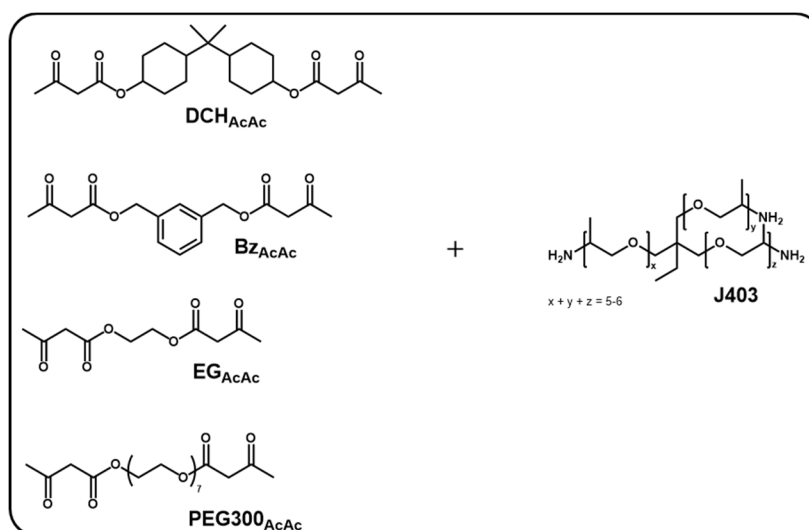
Figure 54: Structure of acetoacetylated, trifunctional monomers DCH$_{AcAc}$, Bz$_{AcAc}$, EG$_{AcAc}$ and PEG300$_{AcAc}$ as well as J403 utilized for the synthesis of vinylogous urethane vitrimers.

ATR-FT-IR spectra proved the formation of the characteristic C=C band (1595–1597 cm^{-1}) and C=O ester band (1647–1649 cm^{-1}) of the vinylogous urethane bonds (all spectra in appendix, Figure A11). DMTA measurements show cross-linked materials with a stable rubbery plateau, while the plateaus of the cyclic backbones (DCH and Bz) appear a little higher (**Figure 55a**). The poly(oxypropylen)-based backbone of J403 produces

materials with a relatively low T_g of -26–45 °C (maximum loss factor). The T_g of VU-PEG300$_{J403}$ was measured by DSC measurements (appendix, Figure A12). The PEG-based vitrimer showed the lowest T_g, followed by the EG-based vitrimer, the BZ-based vitrimer and the DCH-based vitrimer (Figure 55b). Comparing the stress-relaxation times, the VU-PEG$_{J403}$ and VU-DCH$_{J403}$ show relatively short stress-relaxation times, while VU-EG$_{J403}$ and VU-BZ$_{J403}$ showed much longer times (Figure 55c). This effect is most likely attributed to the lower cross-linking density of the materials with the bigger PEG and DCH-backbone, but especially surprising for the DCH-backbone. As discussed earlier in chapter 6.3.1, the polyether-backbone shows the fastest stress-relaxation, while the effect is not that pronounced due to the poly(oxypropylen)-backbone of the amine in each of the vitrimers. Comparing the activation energies, VU-PEG$_{J403}$ showed the lowest with 74 kJ mol^{-1}, followed by VU-BZ$_{J403}$ with 83 kJ mol^{-1} and VU-DCH$_{J403}$ with 105 kJ mol^{-1} (Figure 55d). This trend proved a lower activation energy when using the PEG-based monomer, while likewise the low cross-linking density might influence this behavior. Remarkably, VU-BZ$_{J403}$ showed a relatively high activation energy, which might be caused by the aromatic backbone. Effects like π–π stacking might change the structural arrangement of the vitrimer. This could also explain the long stress-relaxation times.
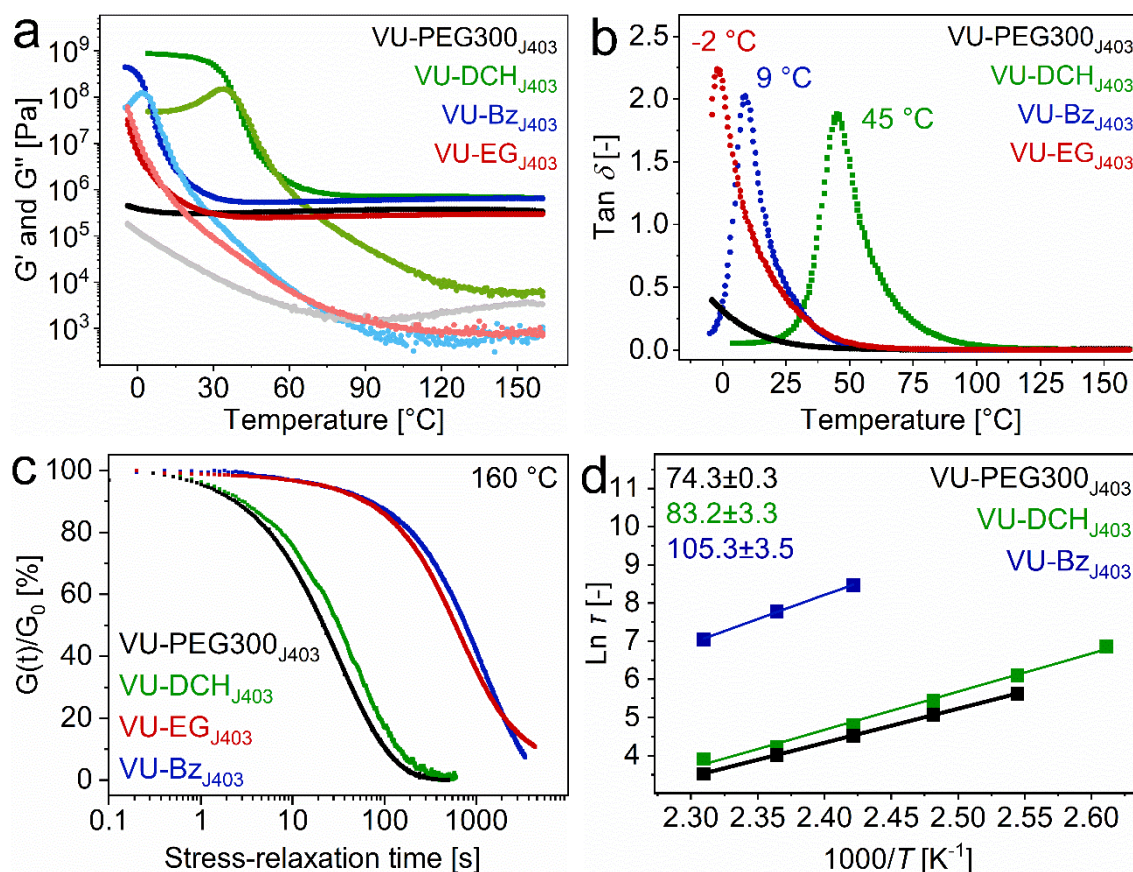
Figure 55: (a) DMTA measurements of the vitrimers VU-DCH$_{J403}$, VU-Bz$_{J403}$, VU-EG$_{J403}$ and VU-PEG300$_{J403}$ (G'= dark color and G''= light color, $\gamma = 0.1\%$, $\omega = 10$ rad s^{-1}). **(b)** Plot of the loss factors versus the temperature of the vitrimers, showing the glass transition temperatures. **(c)** Comparison of the stress-relaxation curves of the vitrimers at 160 °C ($\gamma = 1\%$). **(d)** Plot of ln τ versus the reciprocal temperature. The activation energies were calculated from the slope of the linear fit (unit in kJ mol^{-1}).

6.3.2.3 Comparison of a similar backbone with amine or acetoacetate

This subchapter compared vitrimers with a similiar backbone structure based on a dicyclohexane and poly(oxypropylen) or poly(oxyethylene) backbone. The key is that in VU-DCH$_{J403}$ the acetoacetate carried the dicyclic backbone, while in VU-3aPEG$_{DCM}$ the amine carried the dicyclic backbone (**Figure 56**).
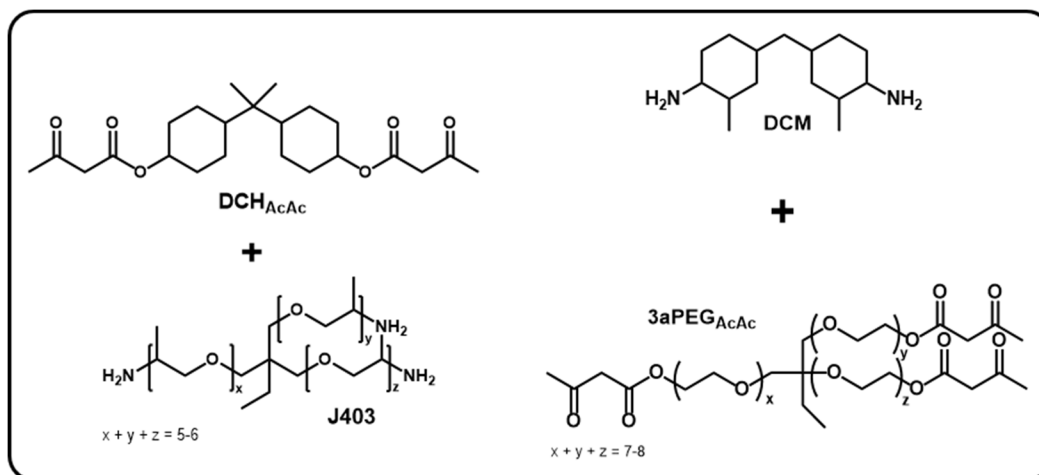
Figure 56: Structure of acetoacetate monomers DCH$_{AcAc}$ and 3aPEG$_{AcAc}$ as well as the amines DCM and J403.

Both vitrimers were already described in previous chapters, while the focus is only on a direct comparison and differences. The rubbery plateau of VU-DCH$_{J403}$ is higher than VU-3aPEG$_{DCM}$. Correlating this with a potential cross-linking density, this finding is reasonable, since the molecular mass of the repeating unit is a little higher in the case of VU-3aPEG$_{DCM}$. Moreover, the non-stoichiometric cross-linking with an R-value of 0.75 led to a higher cross-linking density in case of using a trifunctional amine instead of a trifunctional acetoacetate (**Figure 57a**). The T_gs of the materials were measured by DMTA measurements and determined by the maximum loss factor at 28 °C and 45 °C (Figure 57b). Comparing the stress-relaxation times, the network with the higher nucleophilicity of the amine shows shorter stress-relaxation times (VU-DCH$_{J403}$). As described in previous chapters, this is a crucial factor that outweighed other influences, e.g., the polyether backbone or the cross-linking density (Figure 57c). Comparing the activation energies, VU-DCH$_{J403}$ shows a lower value, which might also be attributed to the sterically hindered type of amine (Figure 57d). This chapter shows that the vitrimers represent polymers with a relatively low T_g, which differ not too much in terms of their

properties, except for the stress-relaxation times. Due to the different monomers, VU-DCH$_{J403}$ almost ten times faster stress-relaxation than VU-3aPEG$_{J403}$.
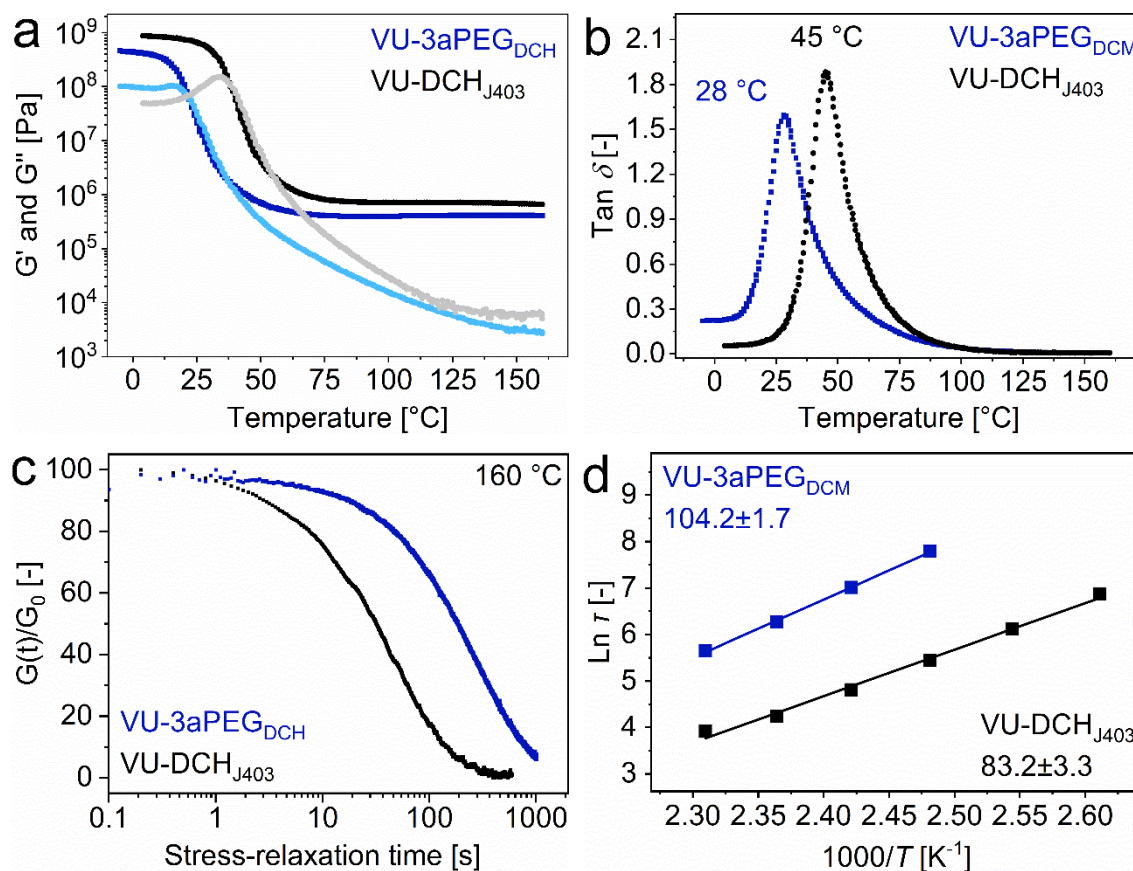
Figure 57: (a) DMTA measurements of the vitrimers VU-DCH$_{J403}$ and VU-3aPEG300$_{DCM}$ (*G'*= dark color and *G''*= light color, γ = 0.1%, ω = 10 rad s^{-1}). **(b)** The plot of the loss factors versus the temperature shows the glass transition temperatures. **(c)** Comparison of the stress-relaxation curves of the vitrimers at 160 °C (γ = 1%). **(d)** Plot of ln τ versus the reciprocal temperature. The activation energies were calculated from the slope of the linear fit (unit in kJ mol^{-1}).

6.3.3   Vinylogous Urethane Vitrimers – Properties, Correlations and Trends

In summary, this chapter shows the influence of the different monomers and monomer backbones on the thermomechanical properties. In particular, the stress-relaxation times, activation energies, oscillatory shear experiment, glass transition temperatures and mechanical properties (tensile tests) are compared and discussed. The results are shown in **Table 3**.

Table 3: The following table shows the prepared vitrimer compositions and their properties. The shown properties include the glass transition temperature (maximum loss factor), the stress-relaxation times at 150 and 160 °C, the activation energies, the storage moduli at 20 and 150 °C as well as the E-moduli, tensile strengths and strains at maximum stress. The highest value in a row is always marked in green, while the lowest value is marked in red.

Vitrimer	T_g [°C]	τ_{150} [s]	τ_{160} [s]	E_a [kJ mol⁻¹]	$G'_{20\,°C}$ [GPa]	$G'_{150\,°C}$ [MPa]	$E_{t\,\varnothing\,r.t.}$ [MPa]	$\sigma_{m\varnothing\,r.t.}$ [MPa]	$\varepsilon_{m\varnothing\,r.t.}$ [%]
VU-GL$_{DAO}$	55	63	25	113.6±2.2	0.52	2.81	870±75	40.0±1.3	6.4±0.1
VU-GL$_{OE}$	48	19	11	77.9±0.8	0.86	3.18	1140±105	51.0±2.1	5.9±0.4
VU-GL$_{N-Me}$	49	32	17	85.7±3.0	0.78	1.97	815±131	40.0±2.9	6.1±0.2
VU-GL$_{m-X}$	105	103	49	120.1±5.9	0.92 [1]	3.00	1410±182	43.1±2.2	3.3±0.4
VU-GL$_{CHDA}$	104	115	76	88.5±6.0	1.19	1.89	1380±26	65.2±12.4	5.0±0.9
VU-GL$_{TREN}$	82	7.8	4.8	78.0±0.6	0.59 [2]	5.4	1467±58	63.3±2.6	5.83±0.3
VU-GL$_{J403}$	12	5500#	632	-	0.003	1.32	-	-	-
VU-GL$_{T3000}$	-58*	-	42	82.0±0.8	0.090	0.097	-	-	-
VU-HT$_{CHDA}$	61	50	33.8	67.0±1.0	1.1	0.71	1466±95	52.4±5.2	4±0.5
VU-HT$_{DCM}$	101	-	331	-	0.67 [3]	0.27	1148±136	15.8±6.8	1.5±0.4
VU-3aPEG$_{DCM}$	28	531	282	104.2±1.7	0.089	0.43	14.8±3.6	4.3±1.0	216±25
VU-3aPEG$_{CHDA}$	5	39	23.7	76.1±1.2	0.0026	1.78	4.9±0.4	3.6±0.8	140±28
VU-DCH$_{J403}$	45	69	50	83.2±3.3	0.75	0.7	1187±29	40.6±5.8	4.3±1.0
VU-Bz$_{J403}$	9	2409	115	74.3±0.3	0.0014	0.66	-	-	-
VU-PEG300$_{J403}$	-26*	56	34	105.3±3.5	0.0003	0.37	-	-	-
VU-EG$_{J403}$	-2	-	948	-	0.0043	0.3	-	-	-
VU-GL$_{DAB}$	85	30	-	83.9±2.4	0.6 [4]	2.6	1100±46	65.9±1.6	7.83±0.2
VU-GL$_{DAP}$	67*	-	-	-	-	-	1050±17	56.6±1.6	7.36±0.2
VU-GL$_{DAH}$	55*	51	-	74.5±5.0	0.62	1.9	961±124	50.8±2.7	6.83±0.2
VU-GL$_{DAD}$	41*	-	-	-	-	-	548±35	25.8±1.2	6.18±0.1
VU-GL$_{DADD}$	33	108	-	101.3±2.2	0.23	2.4	300±14	15.5±1.8	6.82±0.2
VU-GL$_{PA}$	-18*	4.9	4.0	62.1±1.5	0.007	0.63	4.2±2.6	0.16±0.01	134±8.50
VU-GL$_{ODD}$	11	136	79	78.3±0.62	0.004	2.44	4.6±1.1	3.6±1.1	124±28
VU-GL$_{DCM}$	147	-	-	-	0.1 [5]	3.23	-	-	-
VU-HT$_{N-Me}$	21	296	153	90.1±1.6	0.026	1.95	52.5±30.4	8.35±2.1	160±20
VU-GL$_{BAP}$	56	54	-	71.7±2.6	0.59	1.36	1263±34.0	54.7±1.8	5.83±0.05

extrapolated *DSC [1] 55 °C [2] 33°C [3] 47°C [4] 45°C [5] 96°C

Activation energies: The calculated activation energies differ in the range of 62–120 kJ mol^{-1} for all investigated vinylogous urethane vitrimers (composites excluded). Comparing the results to reported values for vinylogous urethane vitrimers, the values were in between the reported values of 60–150 kJ mol^{-1}.[55, 56, 70] Nevertheless, it was already shown in the literature that the activation energies were often not that accurate and can also vary quite a lot, even when using the identical monomers. For this reason, it is hard to identify significant trends. One reason is that a bit of change in the stress-relaxation time has a massive influence on the linear fit of the slope to calculate the activation energies.[56, 70] For these reasons, trends and discussions are only described in the context of hypotheses and should be considered critically in the literature as well as in this work.

Stress relaxation (Reprocessability): Since this work explores the behavior of vitrimers, the ability for reprocessing is of major interest and influencing factors were investigated and discussed. It was shown that heteroatoms (O, N) in aliphatic chains accelerate the transamination reaction. Moreover, aliphatic chains led to faster stress-relaxation than cyclic backbones due to lower sterical hindrance. The nucleophilicity of the amines plays a major role in the exchange reaction, since the amines initiate the transamination reaction by a nucleophilic attack. The nucleophilicity is determined by the sterical hindrance in *alpha*-position of the amine and/or the electronic configuration. The cross-linking density and concentration of the relevant functional groups often generate an opposite effect. On the one hand, a lower cross-linking density facilitates exchange reactions because a less amount of cross-linking points have to be reacted, but on the other hand, a low crosslinking density means a low concentration of the reacting functional groups, which is necessary for the exchange reaction to proceed. Depending on the used monomers, these factors can outweigh each other, as shown in publications 2 and 3 or chapter 6.3.1. and 6.3.2. In addition, it was shown in publication 1 and several other publications that a higher amount of excess amines or the use of a catalyst accelerates the exchange reaction.[56] The identified effects are shown schematically in **Figure 58.**
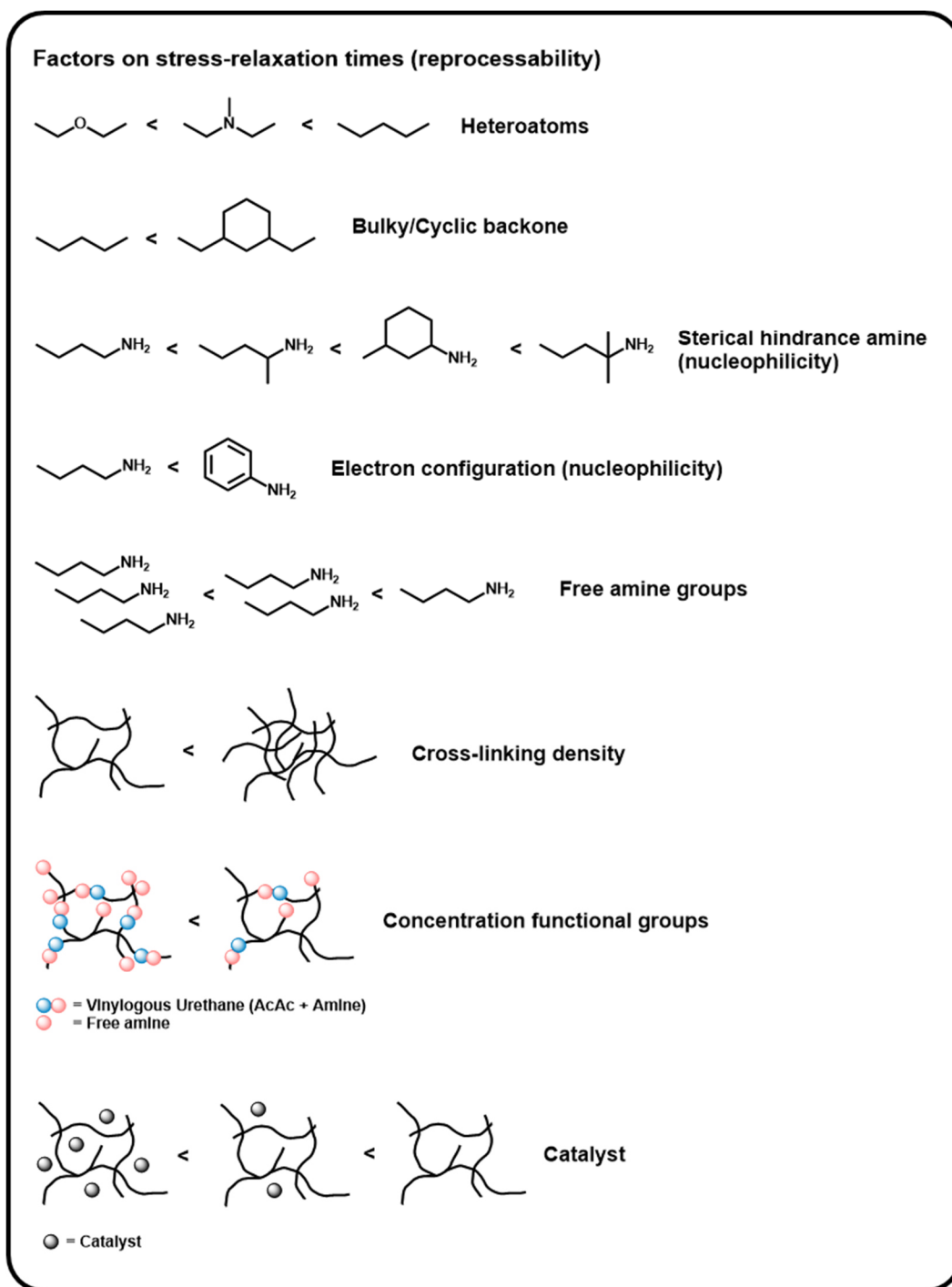
Figure 58: Factors influencing the stress-relaxation times. Heteroatoms in the backbone (O, N), the structure of the backbone (aliphatic or cyclic), the amines nucleophilicity in terms of the sterical hindrance (*alpha*-position), the amines nucleophilicity in terms of the electron configuration (aliphatic, aromatic), the amount of free amine groups, the concentration of the relevant functional groups, the cross-linking density and the amount of catalyst were identified as relevant factors.

Tensile test: Tensile test measurements show the formation of elastomeric and thermosetting vitrimers with E-moduli of 5–1466 MPa, tensile strengths of 0.2–66 MPa and elongations and maximum stress of 3–216% (Table 3). The combination of flexible or rigid and stiff monomer backbones determines the mechanical properties and can be chosen according to various available monomers. With this, a toolbox was enabled to prepare suitable vitrimers with a broad range of mechanical properties. Moreover, polymers like VU-GL$_{DADD}$ and VU-$_{GLN-Me}$ showed a high toughness of 2549 N m^{-2} and 2624 N m^{-2}, which may be caused by their specific glass transition temperature or intermolecular interactions, *e.g.,* hydrogen bonds or non-covalent interactions causing strain-hardening.

Storage modulus and cross-linking density

One standard analysis method for the characterization of cross-linked materials are DMA measurements. From the classic rubber elasticity theory, the rubbery area's storage modulus can be used to evaluate network parameters like the molecular weight between cross-links. It is assumed that the elastic modulus is independent of the network structure and mainly depends on the tightness of the network. This approach can be used to determine the cross-link density, the molecular weight between the cross-linking points and the number of repeating units between cross-linking points.

Equation 1a describes the calculation of molecular weight in between cross-links (M$_c$) by multiplying the gas constant R$_g$, the absolute temperature and the density of the polymer at that temperature divided through the storage modulus of the rubbery plateau at 150 °C. Since the exact Poisson ratio and the densities were unavailable, the Poisson ratio was considered 0.5 and the density 1 g cm^{-3}. Moreover, the cross-linking density q was calculated by dividing the average mass of the repeating unit (M$_{RU}$) through the average molecular mass between the cross-links (**Equation 1b**).[161-163]

$$M_c = \frac{R_g T d}{G'_{Rubbery}} \tag{1a}$$

$$q = \frac{M_{RU}}{M_c} \tag{1b}$$

Equation 1: (a) Equation to calculate the molecular weight between cross-links by the rubbery plateau of the storage modulus at 150 °C (M_c = molecular weight between cross-links, R_g = gas constant, T = temperature, d = density, G' = rubbery plateau). **(b)** The cross-linking density q was calculated by dividing the average mass of the monomers repeating unit (M_{RU}) through the average mass between the cross-links (M_c).

Figure 59a shows a plot of the calculated molecular weights between the cross-linking points versus the rubbery plateau calculated with equation 1a. Higher average molecular weights between the cross-links were obtained from lower rubbery plateaus, with the vitrimer VU-GL$_{J3000}$ showing the highest value of 36 260 g mol^{-1} and VU-GL$_{TREN}$ the lowest with 650 g mol^{-1}. Since the networks were synthesized in non-stoichiometric ratios with an R-value of 0.75, it is reasonable that the masses are higher than the respective repeating units. Nevertheless, the ratio of chains within the network and dangling, free side chains is unknown but plays a significant role for the average molecular mass and cross-linking density. Figure 59b shows a plot of the cross-linking density versus the rubbery plateau and exhibits a vague linear trend of a higher cross-linking density with a higher rubbery plateau, which was expected due to the used theoretical model. Figure 59c, Figure 59d and Figure 59e show different plots of the cross-linking density versus the glass transition temperature, the stress relaxation time versus the glass transition temperature, and the stress-relaxation time versus the cross-linking density. As shown for the individual vitrimers in the previous chapters there a no trends or correlations in respect to these properties. The stress-relaxation is not dependent on the cross-linking density, the rubbery plateau, or the glass transition temperature. Figure 59f plots the number of repeating units between cross-links (NRU) versus the rubbery plateau, which shows a trend to a higher number of repeating units with a lower rubbery plateau. The values in the graphics are additionally shown in **Table 4**.
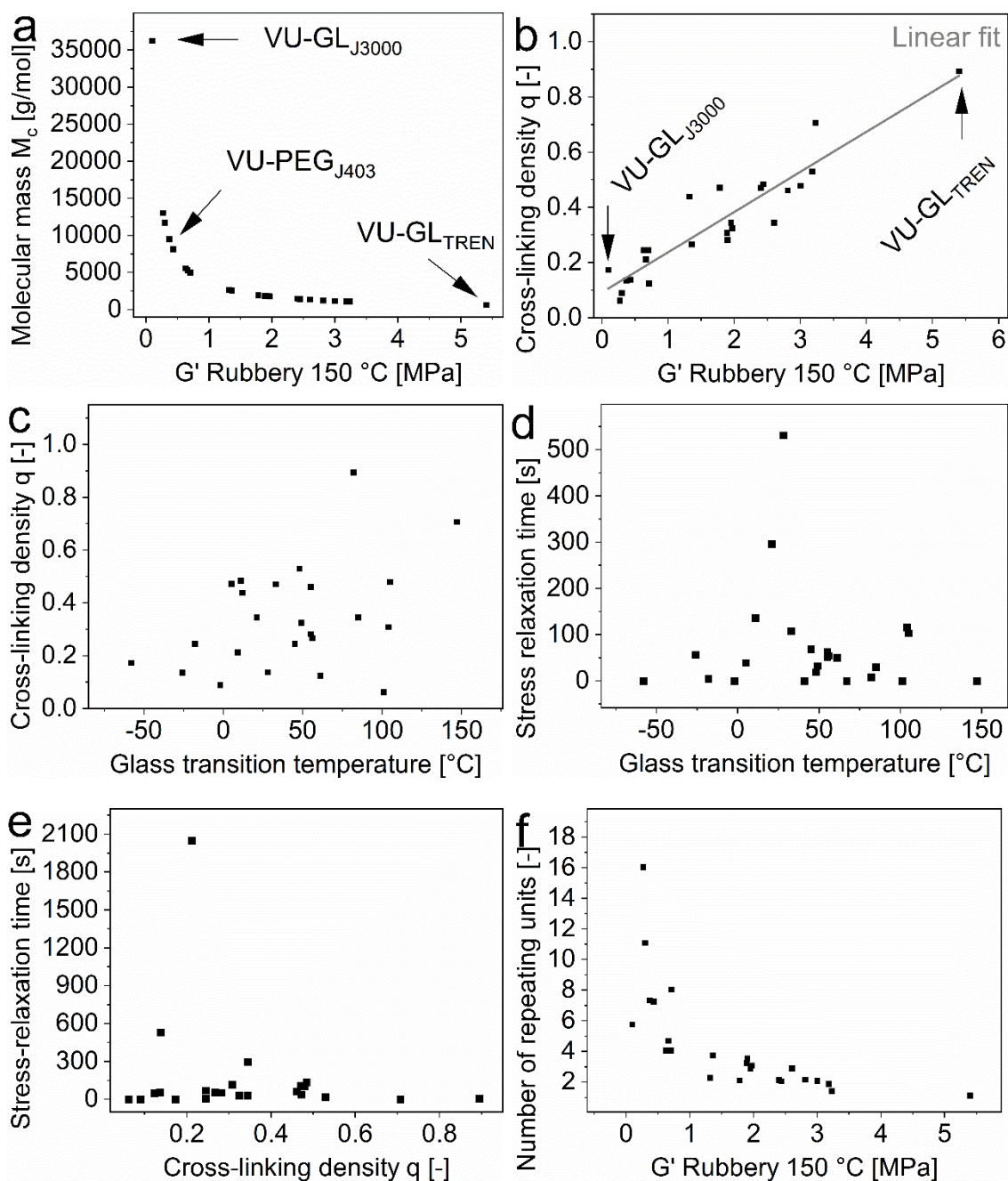
Figure 59: **(a)** Plot of the molecular weight between cross-links versus the storage modulus (rubbery plateau). **(b)** Plot of the cross-linking density versus the storage modulus (rubbery plateau). **(c)** Plot of the cross-linking density versus the glass transition temperature. **(d)** Plot of the stress relaxation time at 150 °C versus the glass transition temperature. **(e)** Plot of the stress relaxation time at 150 °C versus the cross-linking density. **(f)** Plot of the repeating units versus the storage modulus of the rubbery plateau at 150°C. Each point represents one individual vitrimer from Table 3.

Table 4: The table shows the prepared vitrimer compositions and their properties. The shown properties include the glass transition temperature (T_g, maximum loss factor), the stress-relaxation times at 150 °C (τ_{150}), the storage moduli at 150 °C ($G'_{150\,°C}$), the mass of the average repeating unit (M_{RU}), the calculated molecular weight in between the cross-links (M_c), the cross-linking density (q), the number of repeating units (NRU) and the R-value.

Vitrimer	T_g [°C]	τ_{150} [s]	$G'_{150\,°C}$ [MPa]	M_{RU} [g mol^{-1}]	M_c [g mol^{-1}]	q [-]	NRU [-]	R [-]
VU-GL$_{DAO}$	55	63	2.81	578	1251	0.46	4.1	0.75
VU-GL$_{OE}$	48	19	3.18	586	1105	0.53	4.7	0.75
VU-GL$_{N-Me}$	49	32	1.97	580	1785	0.32	7.3	0.75
VU-GL$_{m-X}$	105	103	3.00	562	1172	0.48	11.1	0.75
VU-GL$_{CHDA}$	104	115	1.89	574	1860	0.31	2.9	0.75
VU-GL$_{TREN}$	82	7.8	5.4	485	651	0.75	-	0.75
VU-GL$_{J403}$	12	5500	1.32	876	2664	0.33	3.5	0.75
VU-GL$_{T3000}$	-58	-	0.097	4290	36254	0.12	-	0.75
VU-HT$_{CHDA}$	61	50	0.71	616	4953	0.12	2.1	0.75
VU-HT$_{DCM}$	101	-	0.27	812	13024	0.06	4.1	0.75
VU-3aPEG$_{DCM}$	28	531	0.43	1128	8178	0.14	2.1	0.75
VU-3aPEG$_{CHDA}$	5	39	1.78	932	1975	0.47	1.4	0.75
VU-DCH$_{J403}$	45	69	0.7	1234	5023	0.25	2.9	0.75
VU-Bz$_{J403}$	9	2409	0.66	1132	5328	0.21	3.7	0.75
VU-PEG300$_{J403}$	-26	56	0.37	1294	9504	0.14	4.1	0.75
VU-EG$_{J403}$	-2	-	0.3	1056	11722	0.09	4.7	0.75
VU-GL$_{DAB}$	85	30	2.6	466	1352	0.34	7.3	0.75
VU-GL$_{DAP}$	67	-	-	494	-	-	11.1	0.75
VU-GL$_{DAH}$	55	51	1.9	522	1850	0.28	2.9	0.75
VU-GL$_{DAD}$	41	-	-	634	-	-	-	0.75
VU-GL$_{DADD}$	33	108	2.4	690	1465	0.47	3.5	0.75
VU-GL$_{PA}$	-18	4.9	0.63	1370	5582	0.25	-	0.75
VU-GL$_{ODD}$	11	136	2.44	698	1441	0.48	2.1	0.75
VU-GL$_{DCM}$	147	-	3.23	770	1088	0.71	4.1	0.75
VU-HT$_{N-Me}$	21	296	1.95	622	1803	0.34	2.1	0.75
VU-GL$_{BAP}$	56	54	1.36	690	2585	0.27	1.4	0.75

Glass transition temperature: This chapter shows that the T_g of the vitrimers can be easily set from -58–147 °C by choosing the monomers in terms of their backbone. Aliphatic chains with ether bonds lead to low T_gs, followed by aliphatic carbon chains, monocyclic backbones and dicyclic backbones (**Figure 60)**. One decisive factor is the mass ratio of these compounds, while it did not matter if the acetoacetate or amine carried the respective backbone. If both monomers, the acetoacetate and the amine carry, *e.g.* a polyether backbone, the factors can overlap or average out. In addition, it was shown that the T_g is generally not correlated to the stress-relaxation or the activation energies. Nevertheless, when the T_g is very high and appears in the temperature range where the exchange reaction typically proceeds (>100 °C), it hindered the stress-relaxation ability. At T_gs above 100 °C, the rubbery plateau is usually not reached and the movement of the chains is hindered. In this case, a measurement of the stress-relaxation or the calculation of the activation energies at different temperatures should not be considered.
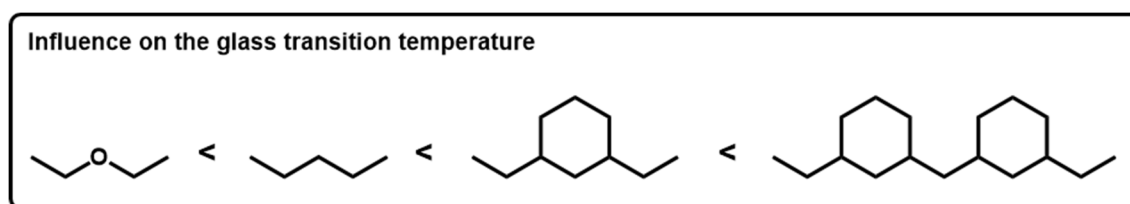
Figure 60: Influence of the backbone on the glass transition temperatures of the vitrimers. Aliphatic chains with ether bonds lead to low T_gs, followed by aliphatic carbon chains, monocyclic backbones and dicyclic backbones.

6.3.4 Vipoxy – Epoxy-Vitrimers Derived from Aromatic Alcohols

Epoxy resins belong to the class of thermosetting polymers which are used for many applications, *e.g.* wind turbine blades, various other fiber-reinforced composites, construction-adhesives, insulation of electronics, fabrication of components in casting processes, coatings and many more. The resins are used due to their simple handling by easily mixing the liquid monomers in an addition reaction, outstanding thermomechanical properties, chemical resistance, and long-time stability. Various different epoxy-monomers and hardeners (amines, carboxylic acids, thiols) are used nowadays and represent their own subclasses of thermosetting polymers.[164] However, typical epoxy resins are not recyclable/reprocessable due to their permanent cross-linked nature. In publication 2 it was shown that aromatic alcohols, *e.g.* bisphenol-A, which are typically used as raw material for epoxy resins, undergo an actoacetylation reaction and act as a suitable monomer for vinylogous urethane vitrimers. Moreover, Jeffamine® T403 (J403 or JA) was used as a commercially established, trifunctional amine-cross-linker for epoxy resins. In this chapter, a comparison between the vitrimers derived from aromatic acetoacetates, a reference epoxy resin and an epoxy-vitrimer network is shown. The objectives were to show the miscibility of the permanent and the dynamic networks on the one hand and to mimic the desirable properties of epoxy resins by using a similar backbone (BPA, JA) at the other hand. The overall goal was always to maintain the reprocessability of the materials.

The epoxy resin, prepared by the addition reaction of bisphenol-A diglycidylether (BADGE) derivates, and JA was investigated for almost 50 years.[165] However, the chemical reactions of epoxy- and acetoacetate groups with primary amines differ significantly, while the backbone structures, the stoichiometric ratio of the functional groups, and the mass ratio of the used monomers are pretty similar (**Figure 61**).
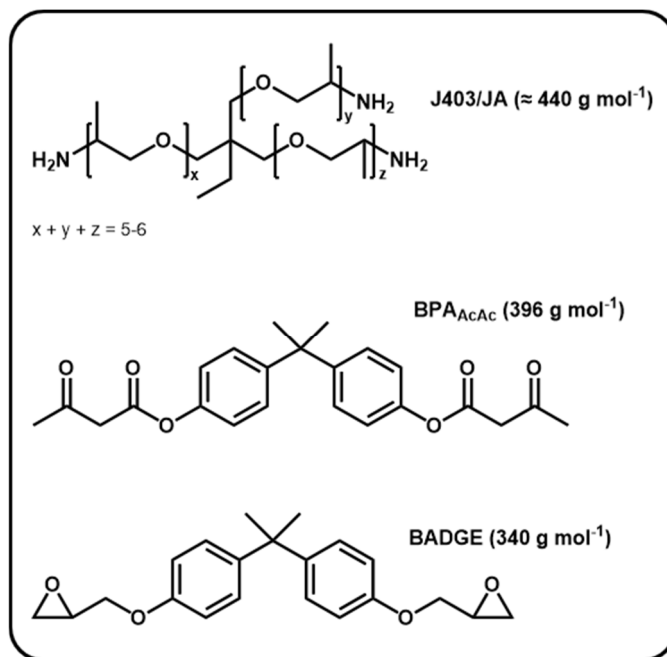
Figure 61: Structure and molecular mass of the used monomers J403/JA, BPA$_{AcAc}$ and BADGE.

Primary amines react with epoxy groups in an addition reaction. The nucleophilic amine attacks the electrophilic epoxy group (mainly the terminal end) and generates a secondary amine and a hydroxy group. The generated secondary amines and hydroxy groups can likewise undergo an addition reaction with remaining epoxy groups, while the amount of this reaction depends on the used stoichiometric ratio of the monomers. Depending on the desired mechanical properties, epoxy resins are mostly cured with a specific, non-stoichiometric ratio, which can also represent an excess of amines.[165] In this work, an excess of amine groups was used for all materials. The condensation reaction of aromatic acetoacetates and primary amines to form vinylogous urethane vitrimers was explained in detail in the introduction and publication 2. **Figure 62** shows the major reactions in the investigated epoxy resin and the vitrimer.
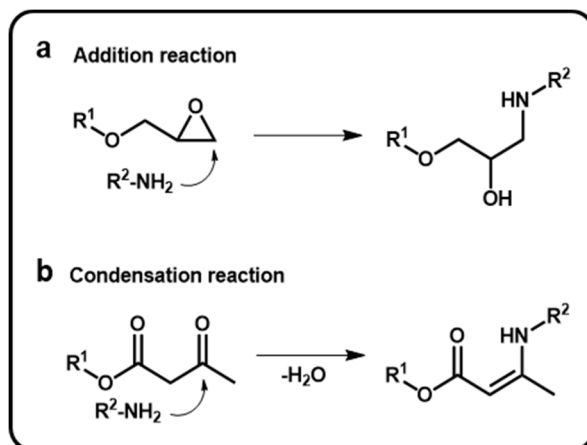
Figure 62: (a) Addition reaction of epoxy groups with primary amines. **(b)** Condensation reaction of acetoacetate groups with primary amines to prepare vinylogous urethanes. Secondary amines and hydroxy groups can likewise undergo an addition reaction with epoxy groups (R = residue).

In this work, polymer networks with R-values of 0.7 and 0.9 were synthesized, which makes the first addition reaction the major reaction for the epoxy resin. The R-value is determined by the ratio of epoxy groups and/or acetoacetate groups to amine groups. For a comparison, a similar R-value was set for all materials. Comparing the final structure of the polymers, **Figure 63** shows that most of the backbone structure stays the same, while only the small linkage-part (marked in red) is different.
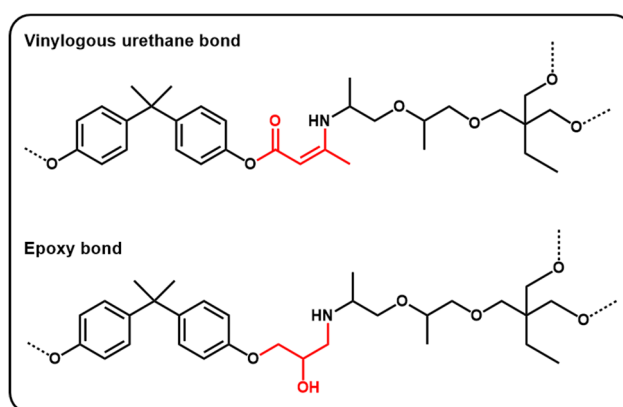
Figure 63: Structure of the resulting epoxy resin bonds and the vinylogous urethane bond marked in black in case of similarities and in red for differences. Only the main products derived from the condensation reaction of the acetoacetates and the first addition reaction of the epoxy groups with the primary amine are shown.

In the following, the vitrimer BPA$_{JA, 0.9}$ and the epoxy resin BADGE$_{JA, 0.9}$ (abbreviation: Acetoacetate/epoxide$_{Amine, R-value}$) are compared. To investigate the mechanical properties of the materials, oscillatory and step shear experiments were carried out. DMTA measurements show cross-linked polymers with the typical rubbery plateau (**Figure 64a**). In comparison to the epoxy resin, the storage and loss moduli of BPA$_{JA,0.9}$ show higher values obove the T_g and lower values below the T_g, indicating a higher stiffness in the glassy state and a lower stiffness and cross-linking density in the rubbery state. However, the T_gs of the materials appear in quite the same range of 30 °C (epoxy resin) and 37 °C (vitrimer) (Figure 64b).
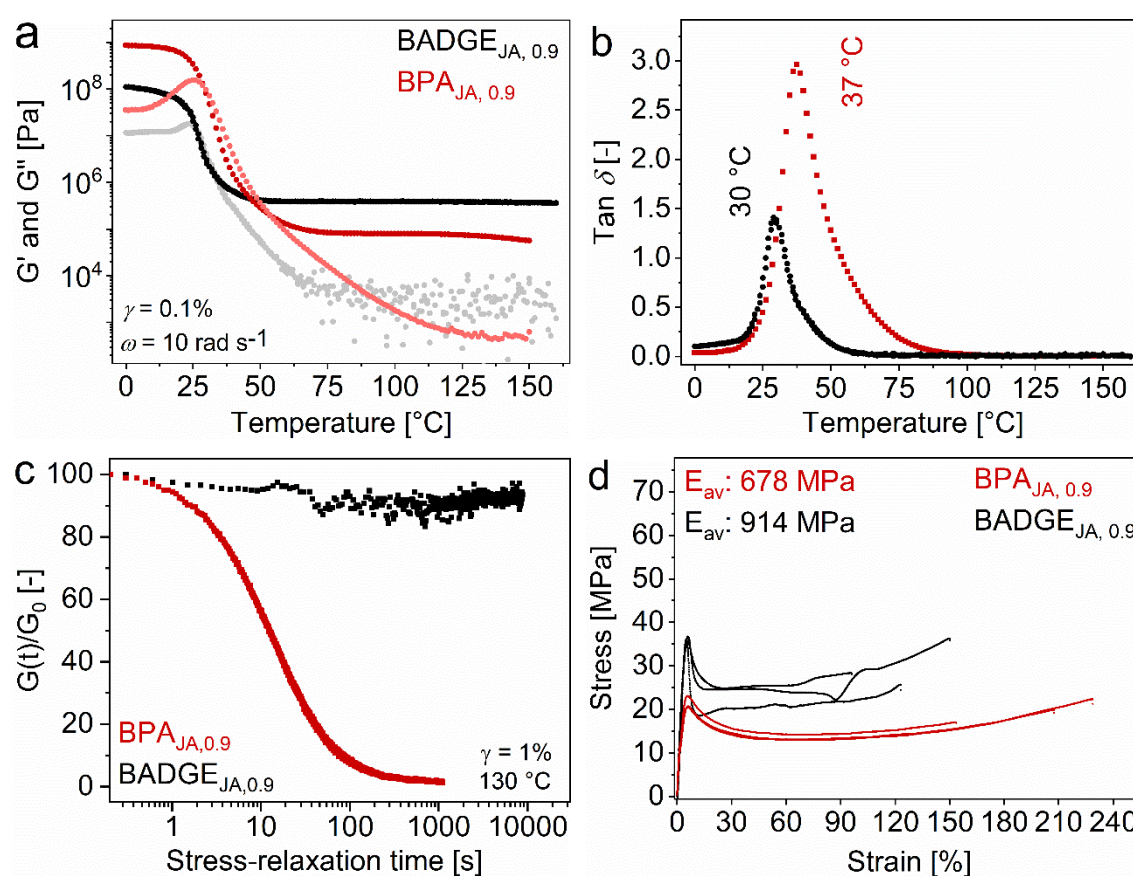
Figure 64: DMTA and tensile test measurements of the epoxy resin BADGE$_{JA,0.9}$ and vitrimer BPA$_{JA,0.9}$. (**a**) DMTA measurements show cross-linked materials with a rubbery plateau up to 150 °C. (**b**) The glass transition temperatures (tan δ) appear in a similar range of 30 °C and 37 °C. (**c**) Stress-relaxation measurements at 130 °C show fast stress-relaxation in case of the vitrimer, while the epoxy resin shows no stress-relaxation. (**d**) Stress-strain curves of the materials (20 °C).

To confirm the reprocessability of the networks, stress-relaxation measurements were carried out at 130 °C. The vitrimer shows a short stress-relaxation time of 20 s, while the cross-linked epoxy resin shows no stress-relaxation (Figure 64c). Tensile tests (20 °C) of BADGE$_{JA,\,0.9}$ and BPA$_{JA,\,0.9}$ show soft materials with averaged E-moduli of 914 and 678 MPa, tensile strengths of 36.2 and 21.4 MPa, elongations and maximum stress of 5.6 and 5.8% as well as ultimate strains of 122 and 197% (Figure 64d).

Another objective of this work was to explore if epoxy-vitrimer networks with particular implemented covalent dynamic bonds can be synthesized and adjusted to show reprocessability, while maintaining a large part of the original epoxy network. Therefore, BADGE was mixed with BPA$_{AcAc}$ in a ratio of 67 wt% BADGE and 33 wt% BPA$_{AcAc}$, representing an epoxide to acetoacetate ratio of 70:30 mol%. Afterward, JA was added (R = 0.7) and mixed until a homogeneous mass was obtained. The reaction rate (gelation) was significantly slower than using only acetoacetates since the addition reaction of epoxides and amines is typically slower. After curing for 20 h at 100 °C and 1 h at 150 °C (*in vacuo*), the material was heat pressed at 150 °C to a 1 mm thick film. The epoxy-vitrimer was named as Vipoxy$_{JA,\,0.7}$.

ATR-FT-IR spectra of BPA$_{JA,0.7}$ (publication 2), BADGE$_{JA,0.7}$ and Vipoxy$_{JA,0.7}$ were measured to prove the formation of the characteristic bonds of the materials. After curing, the characteristic asymmetric C-O-C stretching vibration bands of the epoxy group (910 cm^{-1}) was no longer present and the N-H/O-H stretching vibration bands of secondary amines/hydroxy groups appeared (3000–3600 cm^{-1}). The vitrimer shows the characteristic C=C and C=O ester stretching vibration bands (1593 cm^{-1} and 1664 cm^{-1}) as well as C=C and C=O amide stretching vibration bands (1580 cm^{-1} and 1614 cm^{-1}) of the vinylogous urethane/urea co-networks (VUT/VUA) in the area of 1560–1690 cm^{-1}. Moreover, several other bands, *e.g.* primary amines (1590 cm^{-1}) and C=C bands or the aromatic backbone of bisphenol-A (1580 cm^{-1} and 1606 cm^{-1}) are present as shown in **Figure 65**. Detailed information are also shown in publication 2. Comparing the epoxy-vitrimer (vipoxy) with the other networks, the characteristic bands of both materials were observed, proving the formation of the co-network.
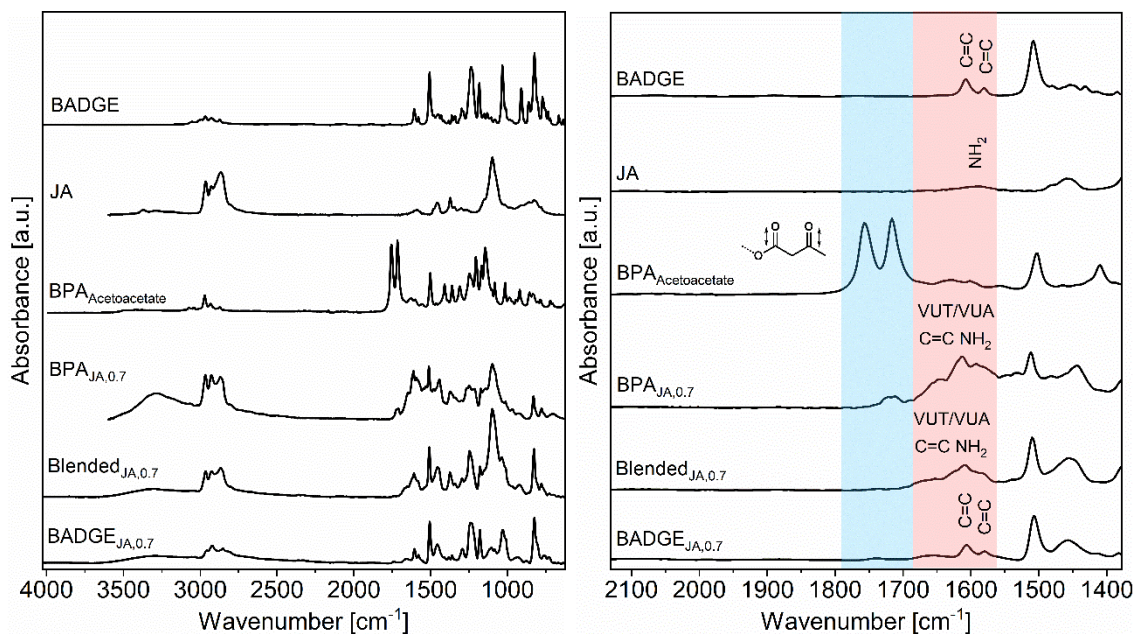
Figure 65: ATR-FT-IR spectra of BPA$_{JA,0.7}$, BADGE$_{JA,0.7}$ and Vipoxy$_{JA,0.7}$ with full spectra (left) and cut out spectra (right).

DMTA measurements show cross-linked polymers with the typical rubbery plateaus and comparable storage and loss moduli (**Figure 65a**). Surprisingly, Vipoxy showed a higher storage modulus in the glassy state and in the rubbery state, which is a promising result. Nevertheless, this result is hard to explain and can be caused by the complex combination of the undergoing reactions of two different polymer types. The materials show low T_gs in the area of 14–37 °C, with the epoxy-vitrimer exhibiting a value of 21 °C within the middle of that range (Figure 66b). Since epoxy resins are typically not reprocessable, stress-relaxation measurements were carried out to compare the dynamic behavior of the epoxy resin, Vipoxy and the vitrimer at elevated temperatures. As expected, the epoxy resin showed no stress-relaxation, while the pure vitrimer and Vipoxy showed full stress-relaxation. Vipoxy shows longer stress-relaxation times than the pure vitrimer, which can be explained by the lower amount of dynamic cross-links (Figure 66c). Tensile tests at 20 °C show soft materials with the epoxy-vitrimer exhibiting averaged values in between the pure networks, according to a rule of mixture (Figure 66d). The stress-strain curves show E-moduli of 12–422 MPa, tensile strengths of 15.5–17.6 MPa, elongations at maximum stress of 5.2%, and ultimate strains of 155–305%. All materials appear soft and flexible, which is caused by the low T_gs in the transition to the rubbery state.
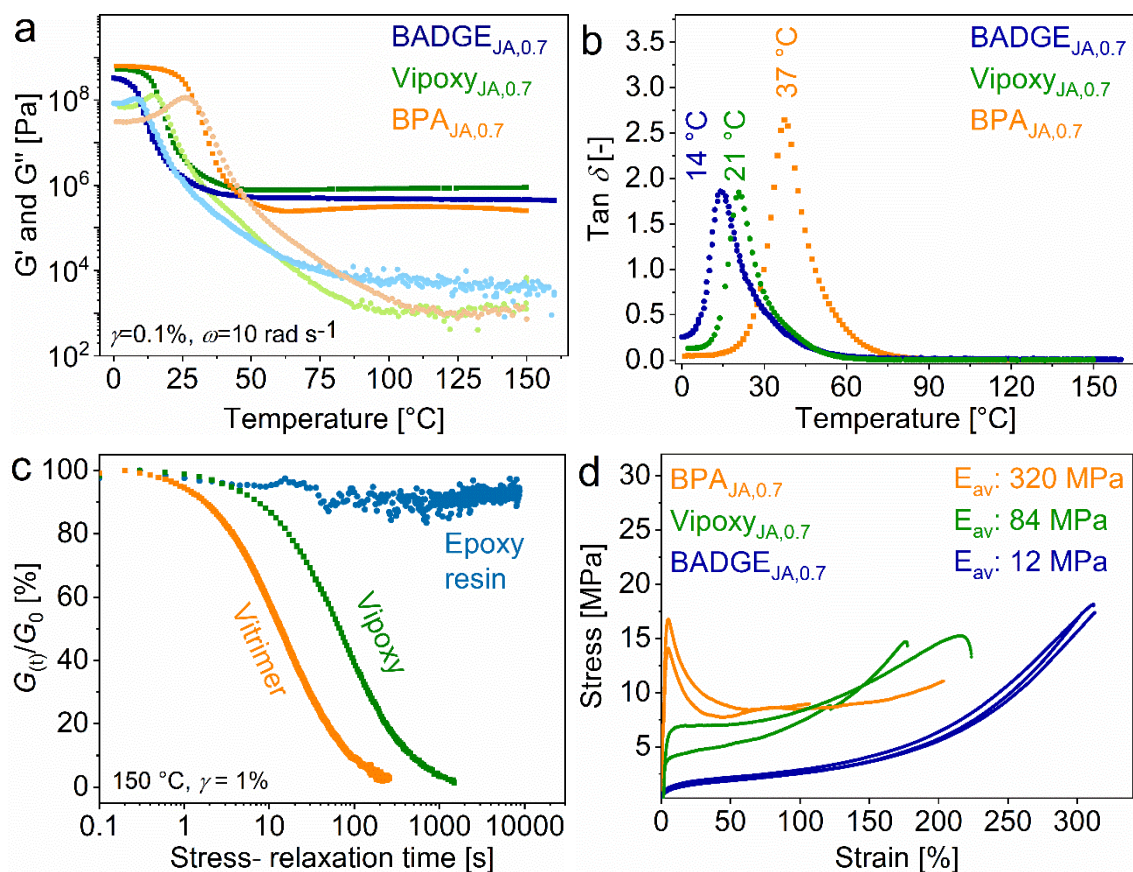
Figure 66: (a) DMTA measurements of the epoxy resin BADGE$_{JA,0.7}$, Vipoxy$_{JA,0.7}$ and BPA$_{JA, 0.7}$. The measurements show cross-linked materials with a rubbery plateau up to 150 °C. **(b)** The glass transition temperatures appear in a similar range of 14–37 °C (loss factor). **(c)** Stress relaxation measurements at 130 °C, showing stress-relaxation in case of the vitrimers and no stress-relaxation in terms of the epoxy resin. **(d)** Stress-strain curves show soft materials with E-moduli of 12–422 MPa, tensile strengths of 15.5–17.6 MPa, elongations at maximum stress of 5.2% and ultimate strains of 155–305%.

This chapter shows that vinylogous urethane/urea vitrimers derived from aromatic alcohols show not the same but comparable properties to epoxy resins derived from similar backbones, with the benefit that vitrimers are fully recyclable. Moreover, it was shown that epoxy-monomers and acetoacetate monomers could be easily mixed and cured with amines to give epoxy-vitrimer co-networks with 70 mol% (67 wt%) initial epoxy groups. Comparing the mechanical properties, the vipoxy exhibits properties by mainly following a rule of mixtures and showing values between the range of the pure networks (T_g, stress-relaxation, tensile test). Nevertheless, the overall thermomechanical properties of all the compared materials were quite comparable, with the benefit that the vitrimer

and the vipoxy networks showed full stress-relaxation and are, therefore, reprocessable. Further experiments can clarify the limits regarding the cross-linking density, the maximum amount of epoxy resin, and the excess of amines. These findings offer future potential for the use of vitrimers, or the partly implementation of covalent dynamic bonds into established thermosetting materials, *e.g.* epoxy resins, and turn them into recyclable/reprocessable materials, while maintaining their excellent thermomechanical and physical properties. Nevertheless, it has to be noted that the prepared materials showed a low glass transition temperature. Usually, mixtures or prepolymerized epoxy monomers derived from aromatic alcohols are used and the resulting epoxy resins exhibit thermosetting materials with a high glass transition temperature above 70 °C. However, for commercial epoxy resins, the exact composition of the mixtures is often unknown and consists of different types of epoxy monomers and different purities. Moreover, the course of hydrolysis reactions has not been definitively clarified and might be a major problem for high-end applications.

Just recently, a publication from Xu *et al.* showed epoxy-vitrimers with the implementation of the diglycidylether of bisphenol-F (DGEBF) cured with EG_{AcAc} or Gl_{AcAc} and the diamine m-X. Obviously, the published work and this work were performed simultaneously. The study proved the discussed findings of this chapter and underlined the scientific interest in the effort to make established thermosets reprocessable.[29]

Initially, the development of vinylogous urethane vitrimers and epoxy-vitrimers derived from aromatic alcohols was related to a cooperation project with subproject A6. Within the project, A6 developed hierarchical composites made of super-crystalline iron-oxide particles, a commercial phosphonic acid ligand and a commercial epoxy resin. The super-crystalline particles were modified by ligand exchange, and the epoxy resin was incorporated into the sedimented, compressed inorganic *via* the infiltration method. By this method, a liquid is sucked into a porous material by applying a vacuum. With this method, high inorganic contents can be achieved in composite materials. After curing the epoxy resin within the composite, the material showed a high bending strength and fracture toughness due to a multi-hierarchical arrangement of self-similar, hard filler particles connected by soft organic interfaces.[166]

After developing the individual methods and materials in both projects, the goal was to combine the findings to create a thermoreversible hierarchical composite. The

tailor-made phosphonic acid ligand (chapter 6.4.1) and the vinylogous urethane/urea co-networks described in this chapter should be used instead of the commercial alternatives. Using the vitrimers instead of a rigid epoxy network should enable a hierarchical, thermoreversible composite that might be postmodificated by heat compression to a nacre-like brick-and-mortar structure with outstanding properties, according to the overall goal of project area A (SFB986). Unfortunately, the project could not be continued within the given time frame of this thesis.

6.3.5 Porous and Dense Vitrimer Films Based on Sugars

In another project, sugars were used as green, cheap, and widely available raw materials for the synthesis of vinylogous urethane vitrimers. It was found that glucose, lactose, sucrose and sorbitol can be partly and fully acetoacetylated with TMDO by bulk reaction. The acetoacetylation reaction is described in detail in chapter 6.1. In the course of the bachelor thesis of Jannik Winter, the objective of the work was to investigate *D*-glucose as a suitable reactant for vinylogous urethane vitrimers and explore the condensation reaction of acetoacetylated glucose with different bio-based and fossil-based amines. Moreover, different synthetic routes should be investigated, enabling the synthesis of vinylogous urethanes in water and exploring the possibility of producing porous vitrimer films by sintering precipitated vinylogous urethane fragments. This work was inspired by a publication of Loos *et al*., where a super amphiphilic membrane with a closed-loop life cycle was explored. A porous membrane was prepared by grinding and sintering an epoxy/carboxylic acid-based vitrimer, which could be used for oil/water separation.[28] Porous, water-permeable materials offer possible applications to separate/clean water from oil, dirt, bacteria, capturing metals (*e.g.,* lithium), and many more. The benefit of using vitrimers for such applications is that the porous structure can be achieved by simple sintering of cross-linked polymer fragments, which is not possible with common thermosets or elastomers. The fragments will slowly react at the touching points and react to a cross-linked, porous network. Moreover, vitrimers offer mechanical and chemical recycling routes, which enable reprocessing, purifying, or re-usage of the dense films and porous materials (*e.g.* when pores are filled).

Depending on the gelation rate, solubility and viscosity of the used monomers, different synthetic routes for the condensation reaction were investigated. The stabilization as enamine-one tautomer allows the synthesis of vinylogous urethanes even in water because the equilibrium of the condensation reaction is shifted widely to the products. This behavior is different from regular polyimine networks, which are stabilized in the electrophilic imine form and significantly more affected by the backward reaction (hydrolysis). In the first part of the chapter, two vitrimers are compared. It is shown that acetoacetylated glucose can likewise be polymerized in a bulk reaction with the low viscous amine J403 or by precipitation in water at room temperature. The first vitrimer VU1-Glu$_5$JA$_{0.5}$ (VinylogousUrethane-Glucose$_{functionalityAcAc}$Amine$_{R-value}$) was prepared with an acetoacetate functionality of 4–5 and mixed with the trifunctional amine J403 in a bulk reaction. An excess of amines (R = 0.5) was chosen to ensure a sufficient amount of amines in the network for reprocessing. To prove that the polymerization also works in water at room temperature, the vitrimer VU2-Glu$_2$JA$_{0.5}$ was synthesized. In this case, only a partly acetoacetylated glucose monomer (average f ≈ 2) was used to ensure solubility in water at room temperature through the remaining OH groups. The amine was added to the aqueous solution, and the vitrimer started to precipitate after a few minutes. The mixture was continued stirred for another 24 h and afterward washed with water. Both vitrimers were dried for 20 h at 100 °C *in vacuo* and heat-pressed for 10 minutes at 150 °C to a 1 mm thick film.

ATR-FTR-IR spectra proved the formation of the characteristic vinylogous urethane bands in both materials, proving that the reaction works as a bulk reaction and in water (**Figure 67a**). DMTA measurements showed cross-linked materials with a rubbery plateau at elevated temperatures (Figure 67b/c). VU1-Glu$_5$JA$_{0.5}$ shows a low T_g of 32 °C and, compared to VU2-Glu$_2$JA$_{0.5}$, higher storage and loss moduli above the glassy and rubbery states. VU2 shows a higher T_g of 67 °C and exhibits a softer material with a lower stiffness in the glassy state. The higher weight ratio of the flexible monomer J403 can explain the lower T_g of VU1. VU1 contains 72 wt% of J403, while VU2 contains only 61 wt%, determined by the R-value. Stress-relaxation measurements at 110–150 °C showed shorter stress-relaxation times for the less cross-linked VU2 with comparable activation energies of 73–81 kJ mol^{-1} (Figure 67d/e). Tensile tests were carried out at 20 °C to investigate the mechanical properties of the materials.
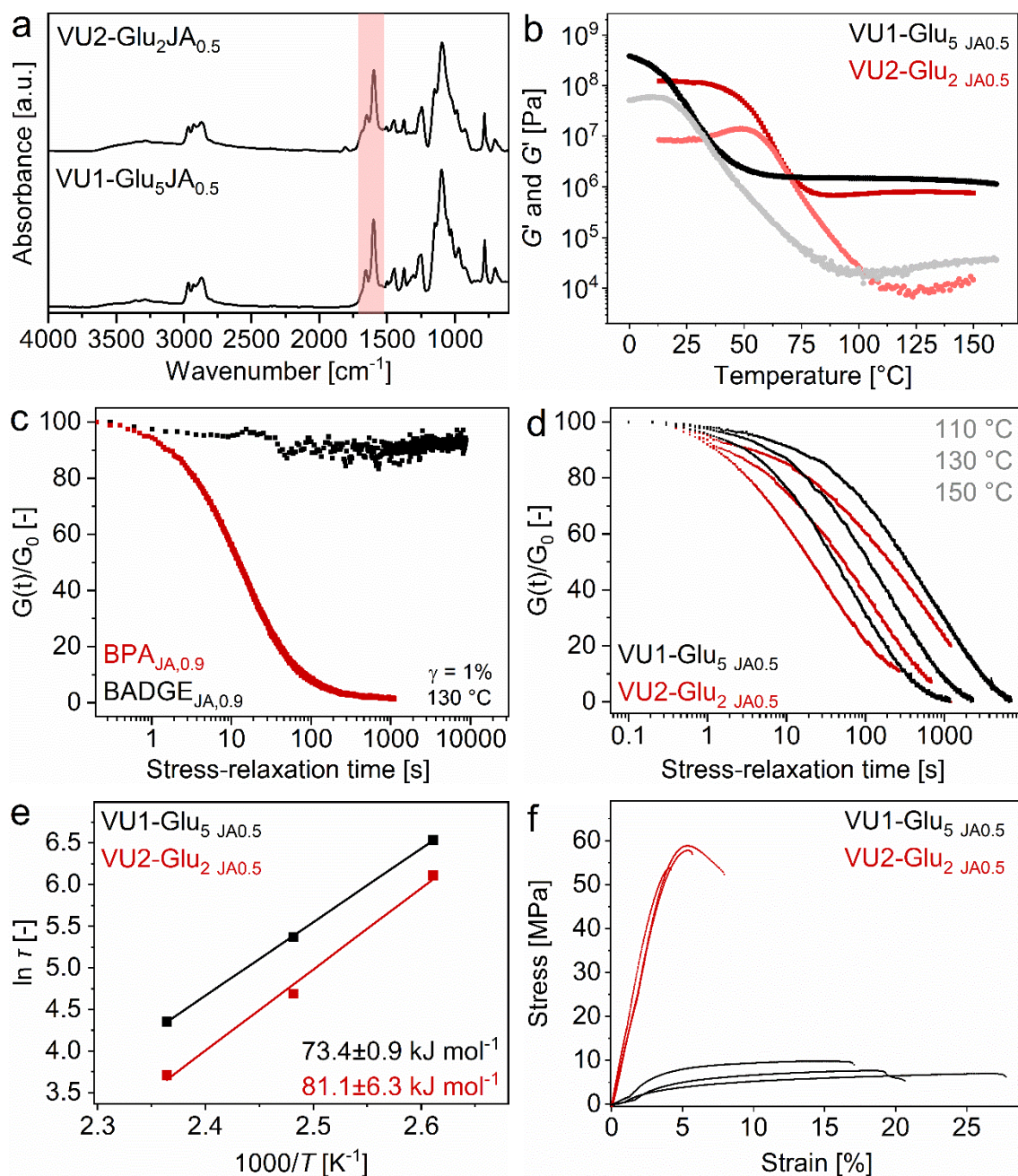
Figure 67: Measurements of the vinylogous urethane vitrimers, synthesized by bulk reaction or in aqueous solution. (**a**) ATR-FT-IR spectra of VU1 and VU2. (**b**) DMTA measurements of the vitrimers show cross-linked materials with a rubbery plateau (G'= dark color and G''= light color, (ω = 10 rad s^{-1}, γ = 0.1%). (**c**) Plot of the loss factors showing the T_g of the vitrimers. (**d**) Stress-relaxation measurements of the vitrimers at different temperatures proved their reprocessability. (**e**) Activation energies of the vitrimers exhibiting comparable values of 70–80 kJ mol^{-1} (**f**) Stress-strain curves of the vitrimers show a soft vitrimer in case of VU1 and hard vitrimer in case of VU2.

The vitrimer VU2 showed an averaged E-modulus of 1567 MPa, an averaged tensile strength of 56.5 MPa, and an averaged elongation at maximum stress of 5%. VU1 showed an averaged E-modulus of 104 MPa, a tensile strength of 8.2 MPa, and an elongation at maximum stress of 22% (Figure 67f). The results show that VU1 appears as a soft material, since the glass transition temperature is below 20 °C. VU2 shows a higher T_g and already reached the glassy state at 20 °C.

This subchapter shows that D-glucose is a suitable raw material for vinylogous urethane vitrimers and can be cured with the poly(oxypropylene)-based triamine J403. Moreover, the synthesis can be carried out at room temperature in water since the partly acetoacetylated D-glucose with remaining OH groups and J403 are water-soluble. Nevertheless, a sintering process to obtain porous materials was not possible with these vitrimers. For an efficient sintering process, the temperature has to be in a suitable range for the exchange reaction to proceed, which is usually above 100 °C for vinylogous urethane vitrimers. Moreover, sintering works better if the materials are not yet in the rubbery state at the sintering temperature, which means a high T_g is usually beneficial. For these reasons, a vitrimer cured with fully acetoacetylated glucose and cadaverine (DAP) was developed. Cadaverine is a bio-based/biogenic amine and is generated from the amino acid lysine by an enzymatic decarboxylation reaction.[167] Unfortunately, the reaction could not be carried out as a bulk reaction because the condensation reaction with the small diamine proceeds very fast and no homogeneous materials could be obtained. However, it was explored that fully acetoacetylated D-glucose is partly soluble in water at 80 °C. Moreover, when adding amines to the aqueous acetoacetate solution, the condensation starts, and the mixture turns into a clear and transparent solution before cross-linked vitrimer fragments start to precipitate. The reaction temperature was lowered after 30 minutes to room temperature and stirred for another 24 hours. The precipitated fragments were washed several times and isolated as white powder. The unique, dynamic behavior of vitrimers allows the materials to be compressed as a film again under heat compression. With this, either a porous material or a dense vitrimer film could be synthesized (VU3). **Figure 68** shows pictures of the bulk reaction as gel and film as well as the solvent-based route.
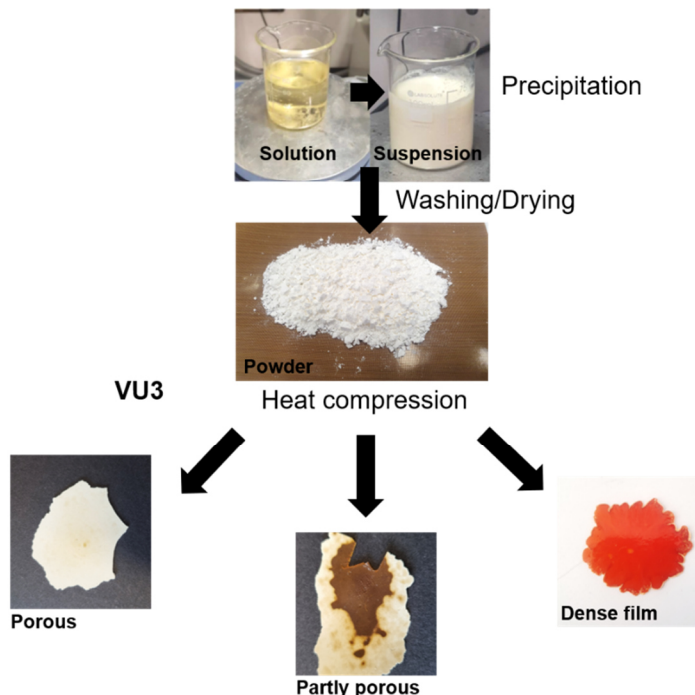
Figure 69: Pictures of the bulk reaction of vinylogous urethane, showing the gelation and the compressed film (left). Pictures of the water-based synthetic route showing the clear solution, the precipitated vitrimer in the solvent, the dried powder, and the compressed porous and dense films (right).

SEM images show the porous material sintered for 10 minutes at 130 °C and 20 kN, while compressing at 160 °C at 40 kN led to dense films, as shown in **Figure 69a**. ATR-FT-IR spectra show similar results in the case of the dense and porous films by measuring the characteristic vinylogous urethane bands as shown in Figure 69b.
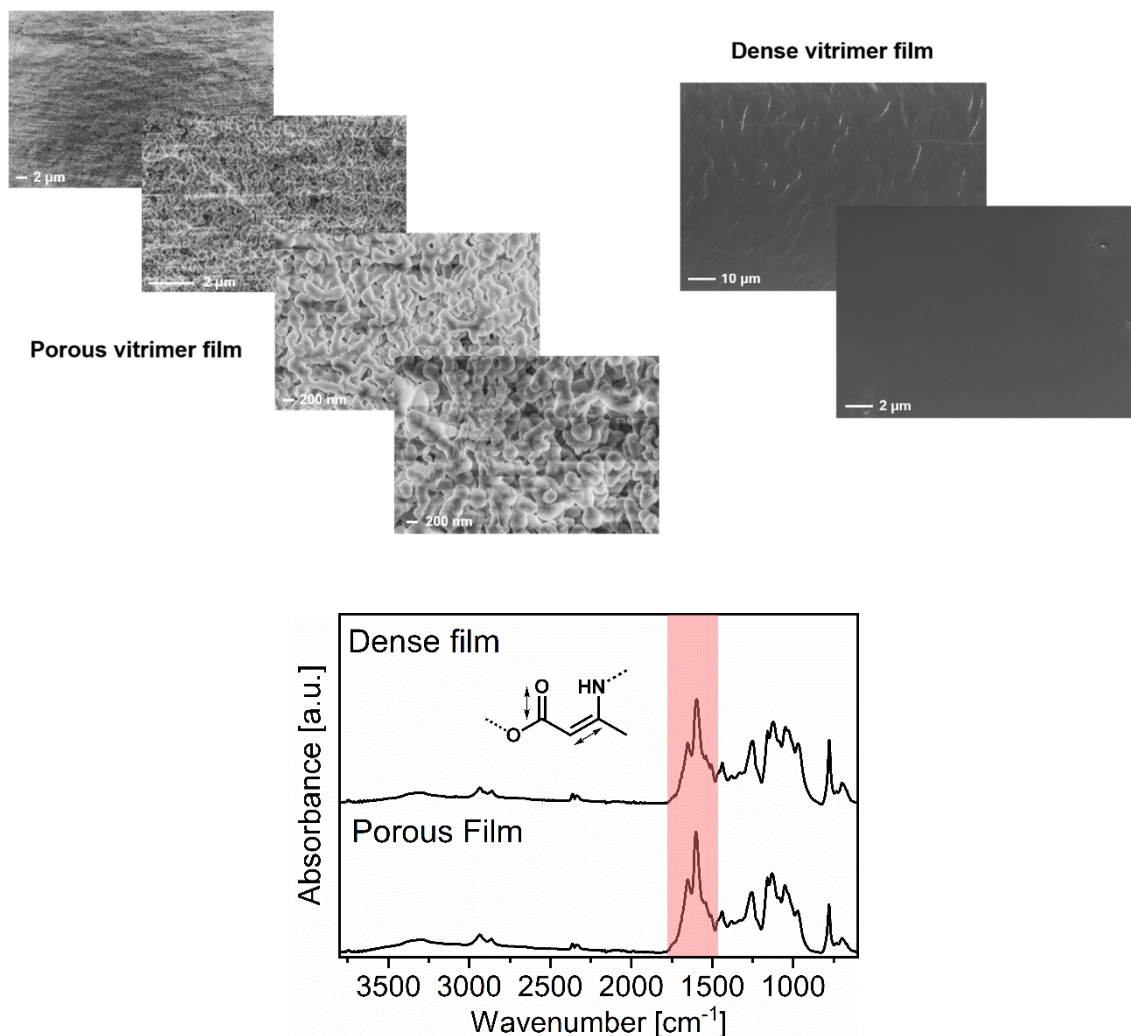
Figure 69: (a) SEM images showing the porous film with worm-like structures compared to a dense film. **(b)** ATR-FT-IR spectra of the dense film and a porous film show the characteristic vinylogous urethane bands and similar spectra in both cases.

At this point, it must be noted that a high glass transition temperature is crucial for sintering porous films because it prevents the material from melting directly into a dense film. The vitrimer made of acetoacetylated *D*-glucose and cadaverine exhibited a high glass transition temperature above 120 °C, as shown by DSC measurements (**Figure 70**). Compared to the previous vitrimers VU1 and VU2 the use of cadaverin led to a lot higher T_g than using the poly(oxypropylene)-based J403.
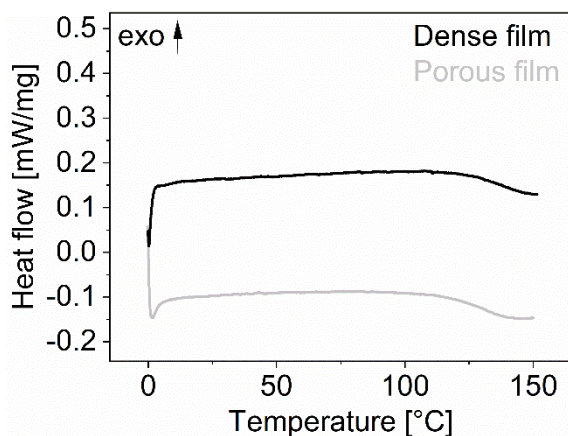
Figure 70: DSC measurements of the dense and porous films show comparable T_gs of 115–120 °C (on-set).

To determine the thermomechanical properties, oscillatory and step shear experiments were carried out. Amplitude sweeps showed yield points below 0.1% at 150 °C, proving both material's high-crosslinking density and stiffness, even at high temperatures (**Figure 71a**). Frequency sweeps at 150 °C proved the formation of cross-linked materials in a broad frequency range (Figure 71b). The dense film always showed a slightly higher storage modulus, while the trend was not very pronounced. Stress-relaxation measurements were carried out at 160 °C and proved the reprocessability of both networks (Figure 71c). Nevertheless, it must be addressed that the low yield points and the high stiffness of materials gave problems for the DMA measurements. These properties often led to measurement errors and reached the limits of the device. For these reasons, DMTA measurements and the determination of the activation energies were not possible. Tensile tests were carried out to compare the dense vitrimer films and the porous materials (**Figure 72**). The results show brittle materials in both cases, while the dense film shows a higher mechanical stability and stiffness than the porous film (E-modulus: ≈1800 MPa and 800 MPa). This result was expected due to the porous network structure. Moreover, the vitrimer powder was compressed at room temperature in another experiment. The compressed material disintegrated immediately when applying any force, indicating that the fragments were not connected.
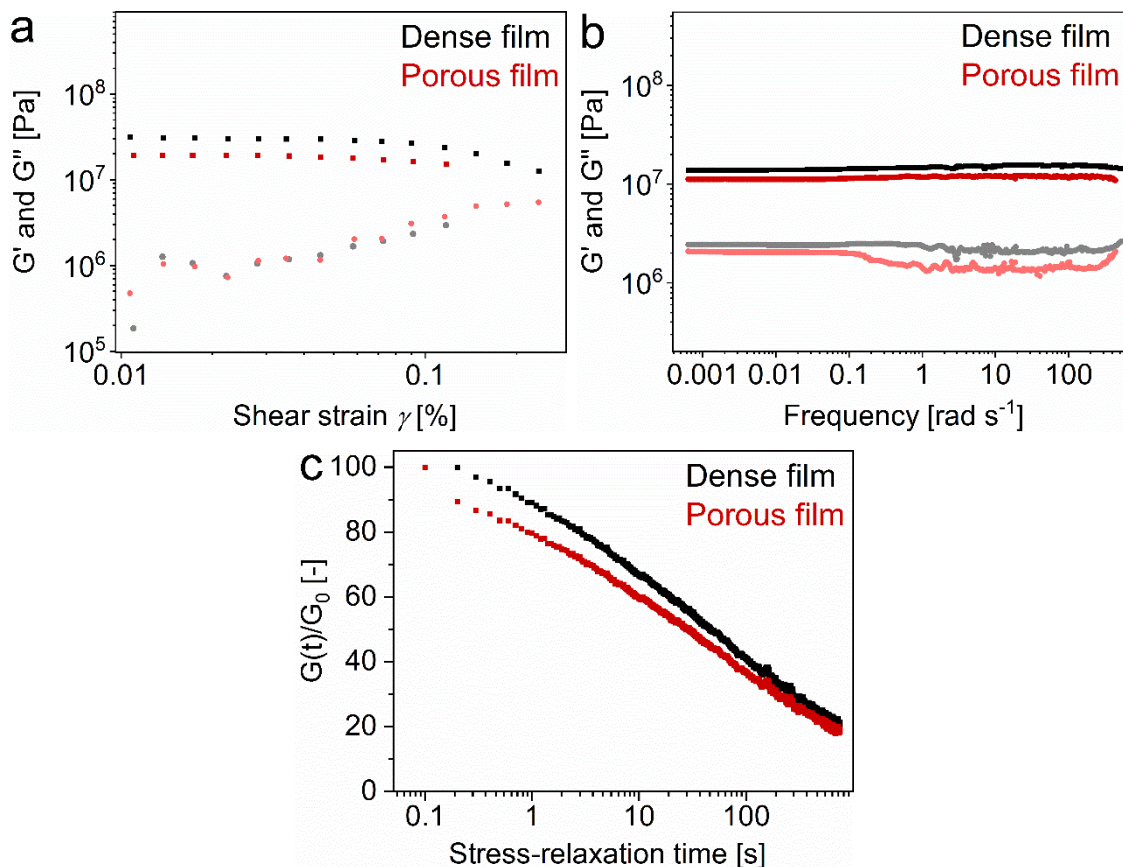
Figure 71: (**a**) Amplitude sweeps of the dense and the porous vitrimer films (G' = dark color and G'' = light color, ω = 10 rad s^{-1}, 150 °C) (**b**) Frequency sweeps of the dense and the porous vitrimer films (G' = dark color and G'' = light color, γ = 0.01 , 150 °C). (**c**) Stress-relaxation measurements of the dense and the porous vitrimer films (γ = 0.1).

This is reasonable because the exchange reaction to connect the particles cannot proceed at room temperature and prevents the fragments to connect to each other. First experiments showed that water can slowly penetrate through the porous film, while this behavior was not observed for the dense film. This behavior is necessary to allow the application of a rough filter membrane. For a detailed picture, further investigations regarding the pore size and the polarity of the surface have to be carried out.
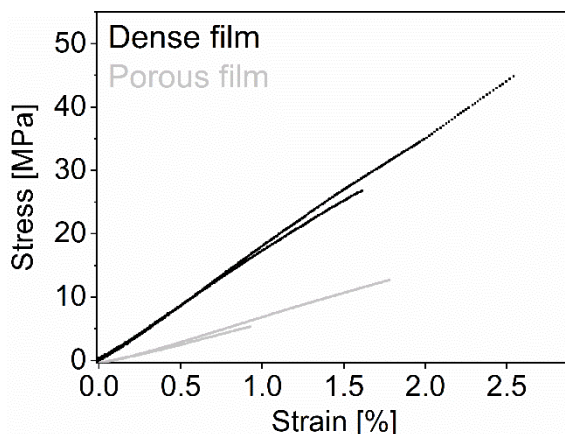
Figure 72: Stress-strain curves of the dense and porous vitrimers films.

This chapter showed, that *D*-glucose can be used to prepare acetoacetate monomer for vinylogous urethane vitrimers in a water-born polymerization. The cross-linked vinylogous urethane fragments precipitate in water and could be sintered into porous films with a worm-like structure. The unique nature of vitrimers enables a fusion of the vitrimer fragments at the touching points. These networks can possibly be used for applications, *e.g.,* water/oil separation or the implementation of other functional units, *e.g.,* crown ethers for lithium filtration, silver particles for antiviral and antibacterial filtering or many other functional modifications. To also contribute critical thoughts, it is questionable whether energy-intensive chemical and physical recycling methods can reprocess the membranes/pores sufficiently well and techno-economical calculations must show whether such applications are possible.

The research on this subject was continued in the scope of the master thesis of Gloria Signorato.[168]

6.3.6 Vinylogous Urea Vitrimers – One-pot Pulk Polymerization

Since the first introduction of vinylogous urethane vitrimers (VU) by Du Prez and coworkers in 2015, countless works have been published based on various alcohols as basis for acetoacetate monomers and a broad band of mechanical properties have been developed.[55, 70] However, vinylogous urea vitrimers (V-UREA) have attracted less attention withonly one reported publication in 2018. In this work, V-UREAs based on different acetoacetamide monomers derived from primary aliphatic, primary aromatic and secondary amines were cured with trifunctional TREN and DAH (**Figure 73**). The vitrimers were discovered in terms of their mechanical properties, exchange mechanism, and their application in fiber-reinforced composites. Comparing the results to VUs, slightly lower activation energies of 49–54 kJ mol^{-1} were calculated, with remarkably short stress-relaxation times.[21] Moreover, V-UREAs with comparable mechanical properties were reported, showing that vinylogous urea vitrimers can compete with reported VU-vitrimers properties.[55]
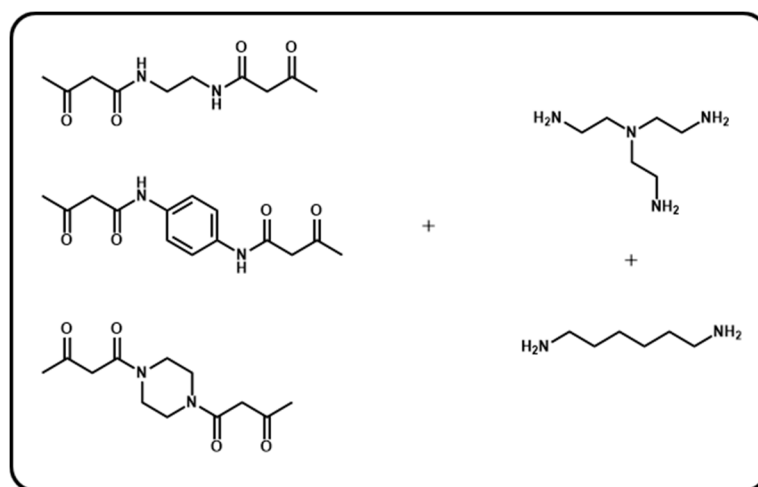
Figure 73: Acetoacetamide monomer structures for the synthesis of vinylogous urea vitrimers based on aliphatic ethylendiamine, 1,4-benzenediamine and piperazin according to Denissen *et al.*.[21]

Nevertheless, this type of vitrimer did not receive much attention afterward, with only one further publication, which is included in this thesis, reporting about "blended vinylogous urethane/urea vitrimers derived from aromatic alcohols" (publication 2). Reasons for that might be the enormous availability and interest in alcohol-based raw

materials for vinylogous urethane vitrimers, the higher affinity to hydrolysis, or the more complex synthetic route to acetoacetamide monomers. Nevertheless, vinylogous urea vitrimers show similar reaction behavior to vinylogous urethanes with fast, catalyst-free exchange reactions. Moreover, the availability of countless different di- and trifunctional primary and secondary amines offers the potential for a variety of material properties. As established for vinylogous urethanes, the acetoacetamide monomers for vinylogous urea vitrimers were typically synthesized by the reactant TBA at 135 °C.[21] The reactive acetylketene undergoes a fast addition reaction with the nucleophilic amine to form the acetoacetamide. A disadvantage, in contrast to acetoacetates, is that amines likewise react with the TBA or acetoacetamides during the reaction, giving a mixture of different compounds, which have to be extensively separated and purified.

To turn this weakness into a strength, the acetoacetamidation agent TBA was substituted with TMDO. Furthermore, the usually two step synthetic route, with the monomer synthesis first and the polymerization step second, was combined to a simple one-pot polymerization.

With this, a new synthetic route of vinylogous urea vitrimers was developed. As example, the trifunctional amine J403 was mixed in a stoichiometric ratio with TMDO (**Figure 74a**). The stoichiometric ratio was set to two amine groups per TMDO unit plus an excess of amines in the network. This ratio is equal to a R-value of 0.7 in the final material (R = acetoacetamide to amine ratio). After stirring for 20 minutes at 135 °C a homogeneous gel was obtained and post cured for 40 minutes at 135 °C, followed by 20 h at 100 °C and 1 h at 150 °C *in vacuo.* At elevated temperatures, the amines react fastly with the electrophilic acetylketene to form the acetoacetamide, followed by a fast condensation reaction to form a vinylogous urea bond (Figure 74b). For the network formation the use of a trifunctional amine and a suitable R-value is crucial in order to obtain a cross-linked polymer network. Two materials were synthesized by this synthetic route and named as V-UREA1 and V-UREA2
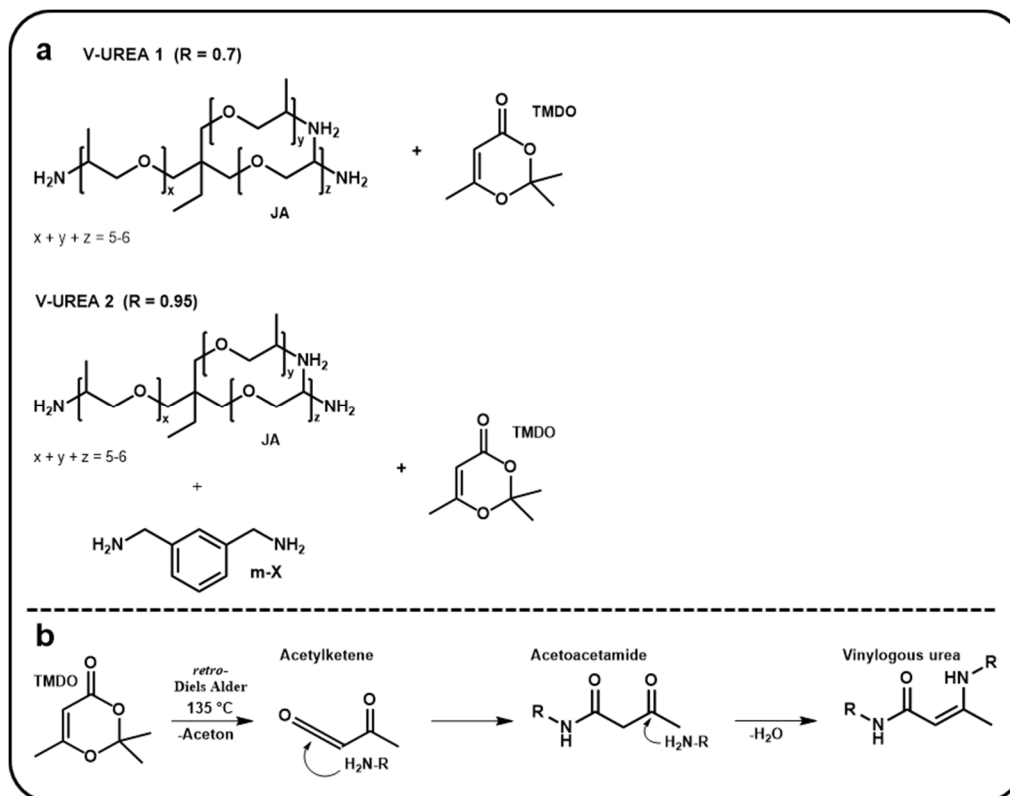
Figure 74: (**a**) Used monomers for the one-pot bulk reaction of TMDO, T403 and m-X. (**b**) TMDO dissociated into a reactive acetylketene, which undergoes a fast addition reaction with a primary amine, followed by the condensation reaction of the emerged acetoacetamide to form the vinylogous urea vitrimer.

V-UREA1 was only synthesized with J403 and TMDO (R = 0.7), while V-UREA2 was synthesized with a mixture of J403 (40 mol% NH_2 groups) and *m*-X (60 mol% NH_2 groups) (R = 0.95). After curing, the dried gels were heat pressed at 150 °C to a 1 mm thick films as shown in **Figure 75**.
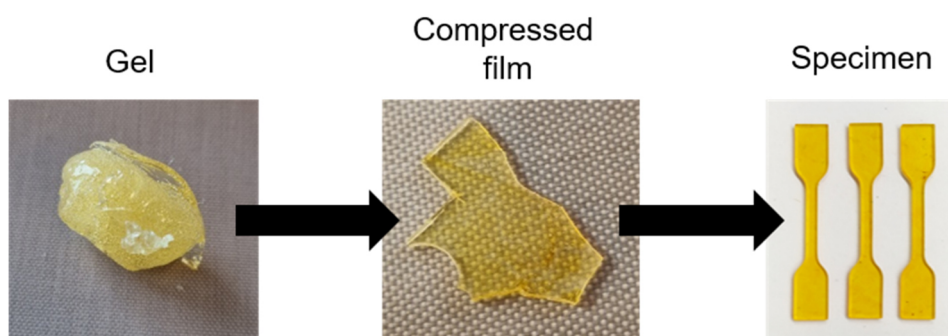
Figure 75: Pictures of the synthesized gel, the compressed film and the specimen of the synthesized vinylogous urea vitrimers.

ATR-FT-IR spectra show the formation of the characteristic vinylogous urea bonds compared to vinylogous urethane bonds (**Figure 76**). The C=C band in VU and V-UREA appears at a similar wavenumber of 1590-1600 cm^{-1}, while the C=O amide bands appear at 1622–1624 cm^{-1} and the C=O ester bands at higher wavenumbers around 1650 cm^{-1}. As shown in publications 2 and 3, these bands can shift up to 9 cm^{-1} for different VU networks depending on the used monomers backbones. Nevertheless, the conjugated amide bands of V-UREA appear at significantly lower wavenumbers than the conjugated ester bands of VU.
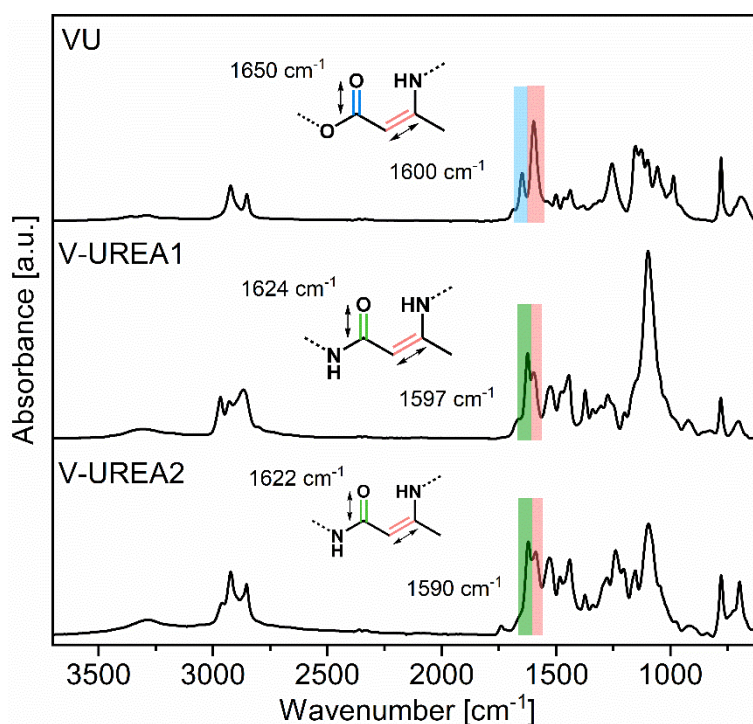
Figure 76: ATR-FT-IR spectra of a reference vinylogous urethane vitrimer showing the characteristic C=O ester (blue) and C=C (red) bands (VU-DADD, publication 3). Besides, the synthesized vinylogous urea vitrimers V-UREA1 and V-UREA2, show the characteristic C=C (red), C=O amide (green) and C=O bands.

To investigate the mechanical properties of the vitrimers, oscillatory and step shear experiments were carried out. The measurements were carried out within the viscoelastic regime so that the storage and loss modulus were independent of strain. Amplitude sweeps were measured at 100 °C and showed yield stresses >20% (**Figure 77a**). DMTA measurements show cross-linked polymers with a characteristic rubbery plateau, while the plateau of V-UREA2 is lower than V-UREA1. This can be explained by the lower

cross-linking density when the linear diamine *m*-X was implemented (Figure 77b). The loss factors indicate a low T_g of the poly(oxypropylen)-based V-UREA1 (1 °C) and a higher T_g (45 °C) in the case of the mixed V-UREA2 (Figure 77c). Frequency sweeps likewise prove the formation of cross-linked materials at 100 °C (Figure 77d). To prove the reprocessability of the networks, stress-relaxation measurements in the temperature range of 100–160 °C were carried out (Figure 77e) (stress-relaxation curves of V-UREA2 are shown in appendix Figure A13). Next, the activation energies of the chemical exchange reaction (transamination) were determined by plotting the stress-relaxation time at 37% of the normalized stress-relaxation modulus versus the reciprocal temperature to calculate the E_a from the slope of the linear fit. Doing that, similar activation energies of 66–68 kJ mol^{-1} were calculated for both materials (Figure 77f). Comparing this result to reported values of 49–54 kJ mol^{-1} for vinylogous urea vitrimers, the values are significantly higher. This can be attributed to the different molecular structure of the networks or a more accurate determination. Inhere 7 measurement points were used in a broad temperature range, while in the publication described at the beginning only 3 points were used in a shorter temperature range.[21] However, also for vinylogous urethane vitrimers, a broad range of activation energies between 68–149 kJ mol^{-1} have been reported for different polymers, which leads to the assumption that this can also be the case for vinylogous urea vitrimers.[70]

Tensile tests were carried out at 20 °C to investigate the mechanical properties of the materials. The elastomeric V-UREA1 shows an averaged low E-modulus of 2 MPa, a tensile strength of 0.9 MPa and a tensile strain of 136%. V-UREA2 shows an averaged E-modulus of 850 MPa, a tensile strength of 33 MPa and a tensile strain of 4.3% (**Figure 78**). The results show that the use of *m*-X with the aromatic backbone enhance the stiffness and T_g of the vitrimer. Moreover, it proves that the developed one-pot polymerization also works for V-UREAs with different amines and likewise linear diamines can be implemented.
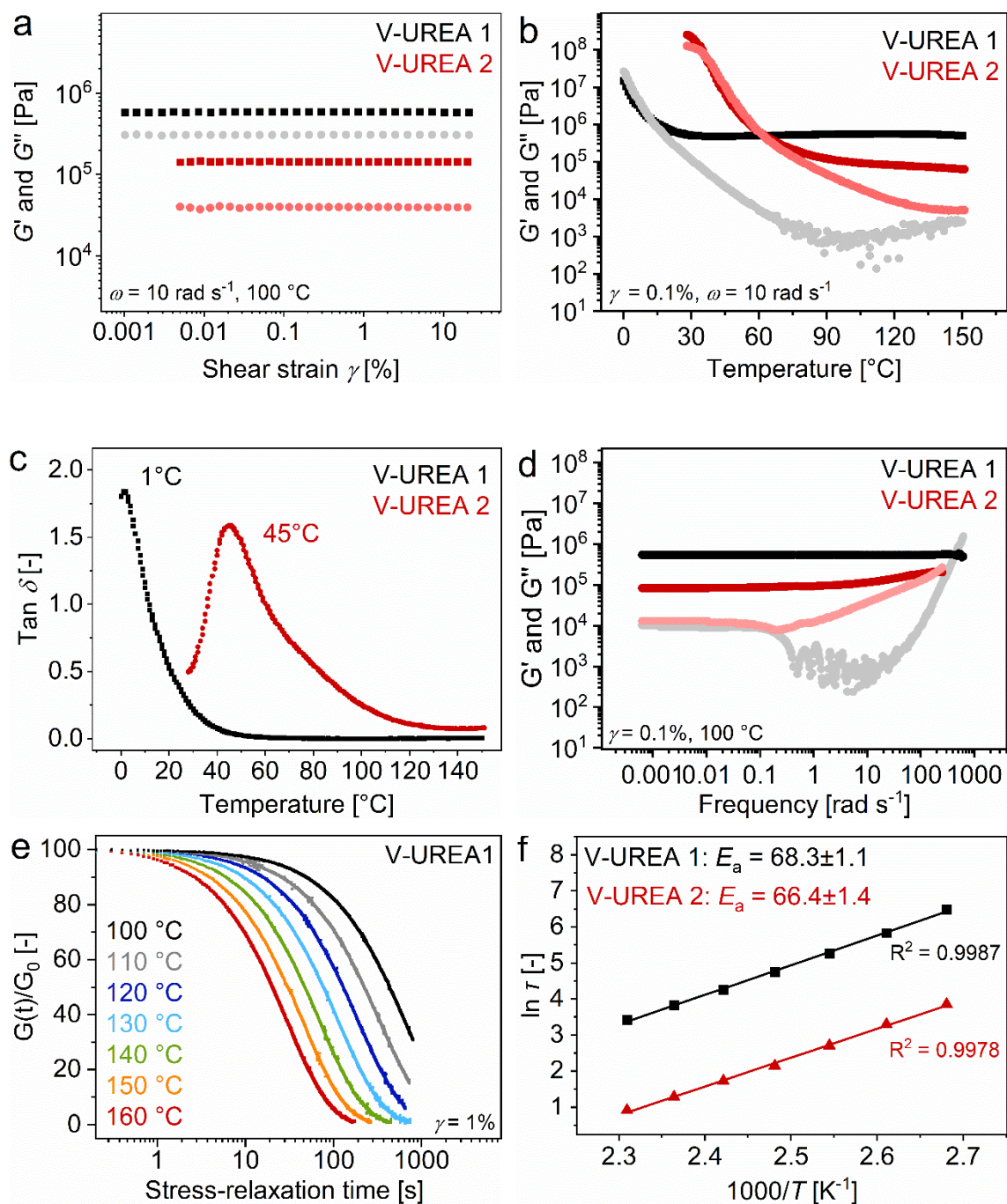
Figure 77: (a) Amplitude sweeps of V-UREA1 and V-UREA2 (*G'* = dark color and *G''* = light color). **(b)** DMTA measurements of V-UREA1 and V-UREA2. **(c)** Plot of the loss factor versus the temperatures of V-UREA1 and V-UREA2. **(d)** Frequency sweeps of V-UREA1 and V-UREA2 **(e)** Stress-relaxation measurements of V-UREA1. **(f)** Plot of ln τ versus the reciprocal temperature to determine the activation energy from the slope of the linear fit.
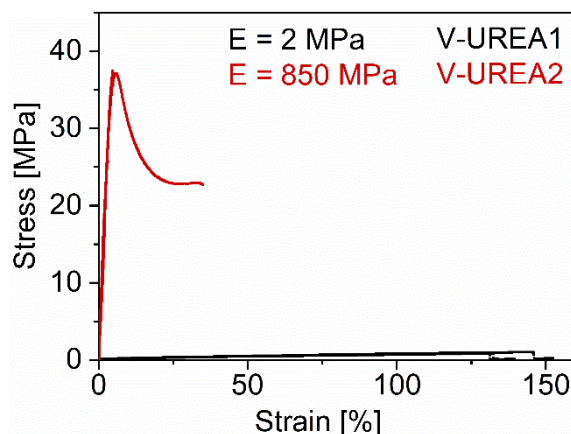
Figure 78: Stress-strain curves of the vitrimers V-UREA1 and V-UREA2 at 20 °C.

This chapter introduced an easy pathway for the one-pot bulk synthesis of vinylogous urethane vitrimers networks, exemplified shown by mixing TMDO with J403 and using the diamine *m*-X as a hardener due to its aromatic backbone. The synthetic route implies the acetoacetamidation and condensation reaction simultaneously, which lowers the effort and energetic costs for the fabrication of this type of vitrimer. As described in chapter 6.1, acetoacetamides and vinylogous urea vitrimers can likewise be synthesized in water, which offers another green synthetic route and expands the choice of possible monomers. As an outlook, the method can possibly be expanded by various other di- and trifunctional aliphatic, aromatic and secondary amines, as well as mixtures of these and different R-values. With this, the materials dynamic behavior and the thermomechanical properties can be tuned and various tailor-made vitrimers can be synthesized.

6.4 Composites

6.4.1 Iron-oxide Nanocomposites

This chapter describes the synthesis and characterization of different vitrimer-composites made of iron-oxide nanoparticles and a vitrimer matrix. Furthermore, a phosphonic acid ligand/linker was developed to bind the iron-oxide surface to the vinylogous urethane vitrimers.

6.4.1.1 Synthesis of a phosphonic acid ligand with an acetoacetate endgroup

Phosphonic acid ligands are known to bind very well to iron-oxides surfaces, *e.g.*, iron-oxide nanoparticles. In order to prepare thermoreversible vitrimer nanocomposites, a ligand was synthesized to connect the interface of the nanoparticles to the polymer matrices.[169-171] 11-Hydroxyundecylphosphonic acid (HUPA) was modified by an acetoacetylation reaction using TMDO to form the corresponding acetoacetate ligand HUPA$_{AcAc}$ (**Figure 79a**). ATR-FT-IR spectra proved the formation of HUPA$_{AcAc}$ by measuring the characteristic acetoacetate C=O ester (1739 cm^{-1}) and C=O ketone (1714 cm^{-1}) bands, while the O-H band (3000–3500 cm^{-1}) of HUPA disappeared. Furthermore, the spectra showed the typical P-OH (2200–2450 cm^{-1} and 1000–1070 cm^{-1}) and P=O (1253 cm^{-1}) bands of the phosphonic acid moiety (Figure 79b). ^{1}H NMR spectroscopy confirmed the results by measuring the characteristic CH$_3$ (2.16 ppm) and CH$_2$ (3.58 ppm) signals of the acetoacetate group together with the typical signals and intensities of HUPA$_{AcAc}$ (Figure 79c). ^{13}C NMR spectroscopy likewise proves the structure by measuring the characteristic CH$_3$ (30.1 ppm), CH$_2$ (49.6 ppm) and the emerging quaternary signals (167.3 ppm, 201.6 ppm) of the acetoacetate group together with the corresponding CH$_2$ groups of the backbone (Figure 79d). ESI-MS confirmed the formation by measuring *m/z* values of M$^+$ = 337.177 and M^{Na+} = 359.158 (M$_w$ = 336.176 g mol^{-1}) (Figure 79e).
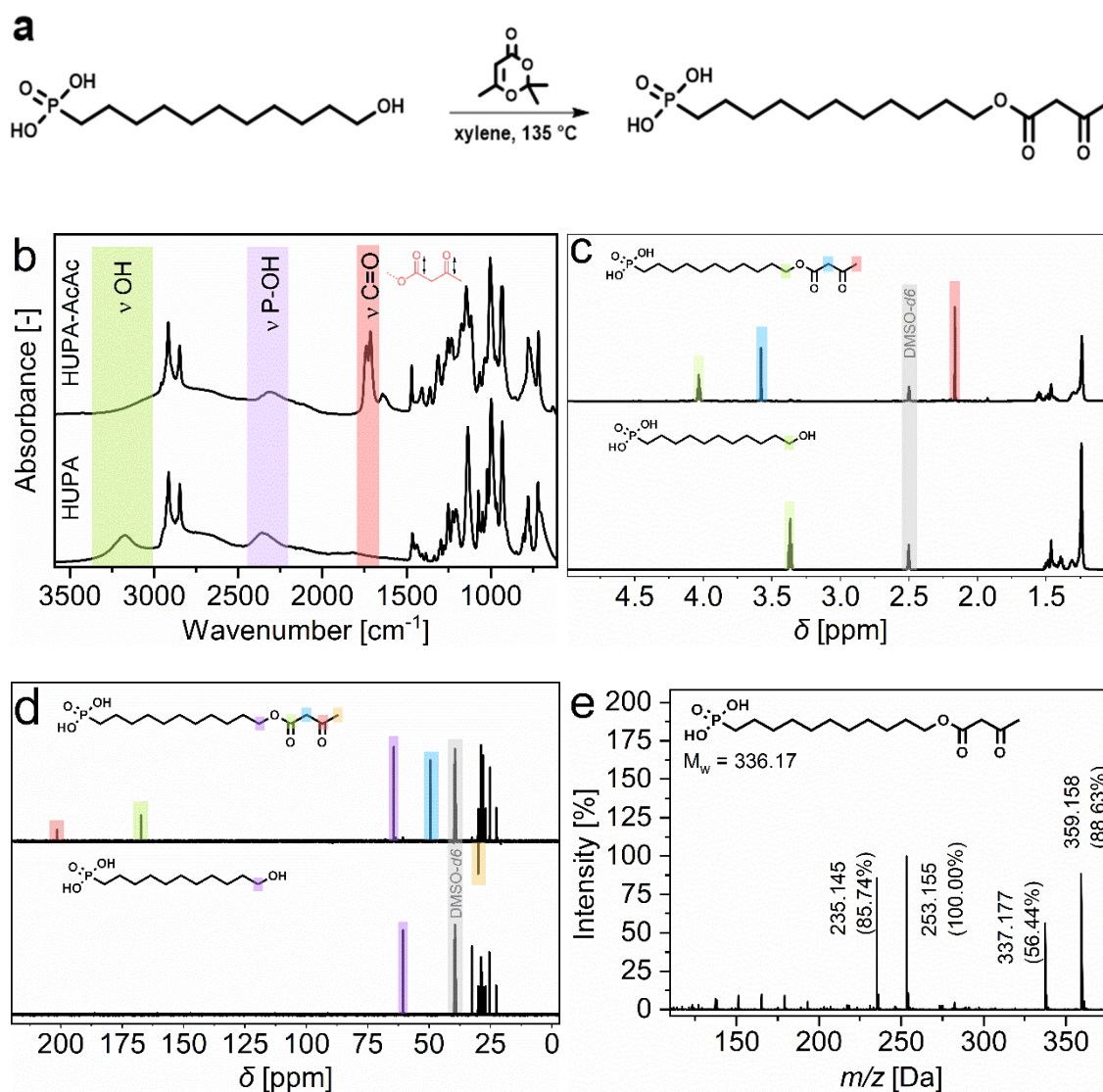
Figure 79: (a) Scheme of the acetoacetylation reaction of HUPA. **(b)** ATR-FT-IR spectra of the raw ligand HUPA and the acetoacetylated ligand HUPA$_{AcAc}$ **(c)** ^{1}H NMR spectra of HUPA and HUPA$_{AcAc}$, showing the characteristic CH$_3$ (2.16 ppm) and CH$_2$ (3.58 ppm) signals of the acetoacetate group **(d)** ^{13}C NMR spectra of HUPA and HUPA$_{AcAc}$ proving the formation by measuring the characteristic CH$_3$ (30.1 ppm) and CH$_2$ (49.6 ppm) signals **(e)** ESI$^+$-MS measurement of HUPA$_{AcAc}$.

6.4.1.2 Ligand exchange on cubic and spherical iron-oxide nanoparticles

In order to bind the ligands to the surface of the particles, a ligand exchange was carried out, where oleic acid was substituted with HUPA$_{AcAc}$. Michael Kampferbeck and Lea Klauke developed and carried out the particle syntheses and the ligand exchanges in the scope of the SFB986 project A1. Cubic and spherical nanoparticles with a diameter of 12–18 nm were synthesized. Subproject A2 developed and delivered the ligand to subproject A1 and returned modified nanoparticles solutions, which were used by A2 for the synthesis of composite materials. ATR-FT-IR proved the ligand exchange by measuring the characteristic C=O ester (1739 cm^{-1}), C=O ketone (1714 cm^{-1}) stretching vibration bands and the P-O stretching vibration band in the area of 920–1100 cm^{-1}. In addition, monofunctional hexylamine was added to the modified particles, proving the formation of the characteristic vinylogous urethane bonds prepared by the condensation reaction of the acetoacetate group and hexylamine. The vinylogous urethane bands show the characteristic C=O ester (1650 cm^{-1}) and C=C (1605 cm^{-1}) stretching vibrations together with decreasing acetoacetate bands (**Figure 80**).
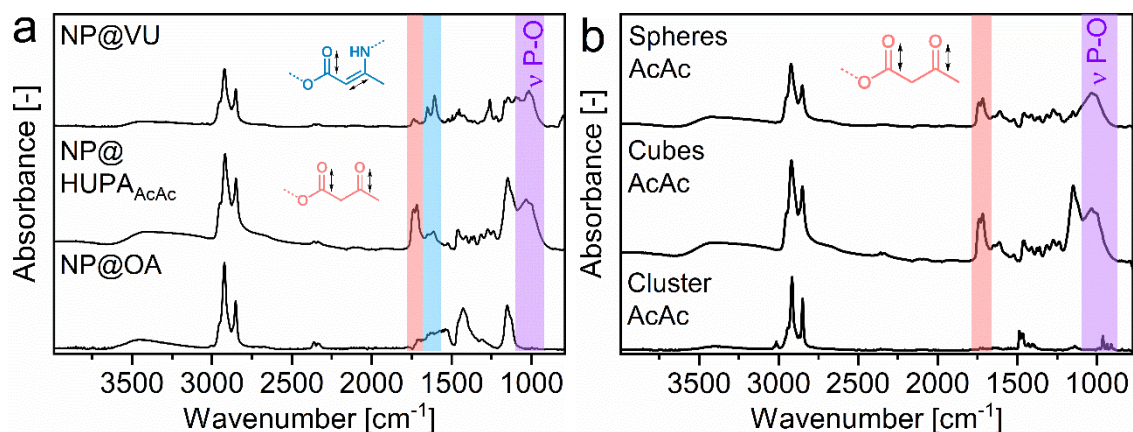
Figure 80: (a) ATR-FT-IR spectra of the iron-oxide nanoparticles (NP) with oleic acid (OA), the nanoparticles with HUPA$_{AcAc}$ after the ligand exchange (marked in red) and after adding hexylamineto form the characteristic vinylogous urethane bonds (marked in blue). The P-O vibration of HUPA$_{AcAc}$ is marked in purple. **(b)** ATR-FT-IR spectra showing spherical, cubic and clustered iron-oxide nanoparticles after the ligand exchange with HUPA$_{AcAc}$, showing the characteristic carbonyl bands of the acetoacetate (marked in red). The P-O vibration of HUPA$_{AcAc}$ is marked in purple.

6.4.1.3 Magneto-responsive elastomeric composites

In this chapter, the synthesis and characterization of magneto-responsive elastomers is described. As mentioned earlier, the SFB986 area-A aims for the development of hierarchical, thermoreversible composite materials. As a milestone, it was investigated if the modified particles could be homogeneously distributed into a vitrimer matrix with a relatively low amount of particles. Besides this test, the synthesis of magneto-responsive elastomers offers potential applications in the field of robotics and sensors by using the unique, self-healing, and shape-memory properties of vitrimers, combined with the magnetic properties of iron-oxide. Properties such as the deformation of soft materials in a magnetic field *via* contraction or deflection, orientation and alignment of particles in a magnetic field, or a magnetic field-induced shape memory are just a few interresting properties for smart materials. Even medical applications, *e.g.*, nanoparticle guidance, cell guidance, molecular separation, or controlled drug delivery, are possible.[172] In combination with vitrimers, possible properties such as reprocessing, self-healing, or solid-state alignment of the particles in a magnetic field are conceivable. One example of a magneto-responsive elastomeric vitrimer doped with iron-oxide microparticles was already published. The elastomeric vitrimer was synthesized by a thioplast with the epoxy-terminated monomer (EPS25), which were mixed in a stoichiometric ratio of two sulfhydryls (2,2′-(ethylenedioxy)diethanethiol (EDDET) and pentaerythritol tetrakis (3-mercaptopropionate) (PETMP)). (Dimethylamino)pyridine (DMAP) was chosen as a catalyst and iron-oxide particles in the micrometer range were added. The vitrimer showed viscoelastic properties under thermal treatment/UV-light by disulfide metathesis. The material exhibited shape-memory, remolding, reprocessing, and self-healing properties, while the focus was on various options of weldability and malleability. The material could be moved by magnetic fields and pass through small tunnels due to the flexibility of the elastomeric network. Also, precise reprogramming of the shape by lasers was shown.[133]

In this work, the vitrimer VU-EG$_{J403}$ (R = 0.75) was used and the composite synthesized with additional 10 wt% of functionalized, 18 nm cubic iron-oxide nanoparticles with a surface density of 1.65 ligands nm^{-1} and 42 mol% of exchanged HUPA$_{AcAc}$ (provided and measured by subproject A1). The average functionality of one nanoparticle was calculated to 1700 acetoacetate groups. The prepared composite was named as

VUC-EG$_{J403}$. The use of the ligand HUPA$_{AcAc}$ stabilized the nanoparticles in chloroform very well, since the polarity of the aprotic, polar acetoacetate group interacts very well with the solvent. The use of J403 enabled slow gelation, which hindered early agglomeration and precipitation of the material. Pictures show the gelation process and the resulting black material as well as SEM images, showing a homogenous distribution of the particles in the vitrimer composite (**Figure 81).**
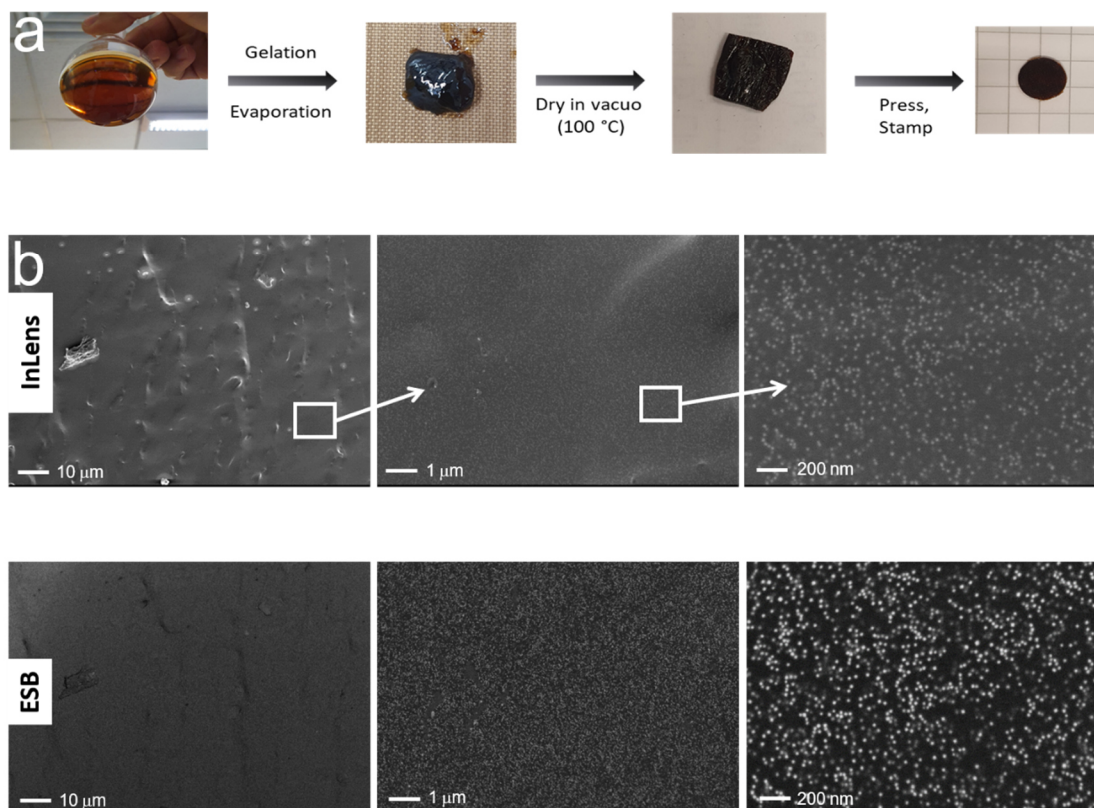
Figure 81: (a) Pictures of the gelation process of the elastomeric, magneto-responsive composite material. (**b**) SEM images of the composite VUC-EG$_{J403}$, showing a homogeneous particle distribution in different magnifications and detectors (cross-fracture).

ATR-FT-IR spectra proved the formation of the characteristic C=C band (1597 cm^{-1}) and C=O ester band (1650 cm^{-1}) of the vinylogous urethane bonds, as shown in the appendix (Figure A14). Since the mass content of the inorganic particles is only 10 wt%, the matrix and composite spectra appear pretty similar, while the particle bands can barely be identified. DMTA measurements of the composite and the matrix vitrimer without particles show cross-linked materials with a characteristic rubbery plateau (**Figure 82a**). The rubbery plateau of the composite appears slightly higher than the matrix, which is

caused by the addition of the multifunctional cross-linker (nanoparticles). Nevertheless, it is reasonable that the curves do not differ significantly since the load of particles is only 10 wt%. The loss factors showed elastomers with T_gs of 0 °C in the matrix and 2 °C in the composite (loss factor maximum, Figure 82b). Stress relaxation experiments were carried out in order to investigate the reprocessability of the networks. Interestingly, the composite showed five times shorter stress-relaxation times at 160 °C (Figure 82c). Since the particle load is quite low, similar relaxation times are generally expected but the experimental results showed huge differences. Exploring the differences, a phosphonic acid ligand was added to the composite. Brønsted acids are known to efficiently catalyze the transamination reaction, which can explain the shorter relaxation times. The phosphonic acid provides additional protons and acted not only as a cross-linker but also as a catalyst. With this, the relatively slowly relaxating VU-EG$_{J403}$ matrix vitrimer, became a fastly relaxating vitrimer as a composite VUC-EG$_{J403}$. This behavior is quite unusual since composites usually show longer relaxation times than the pure matrix vitrimer. For the composite, stress-relaxation measurements at 130–160 °C were carried out (Figure 82d). An activation energy of 104±0.4 kJ mol^{-1} was determined (Figure 82e). Since the matrix vitrimer relaxated very slowly, no activation energy could be determined.

The stress-relaxation experiments show that the composites are fully reprocessable and can be remolded and reshaped several times by heat compression. Furthermore, it was investigated if the functional vitrimers could be combined with other vitrimers by adding defined shapes and fusing the materials. As shown in **Figure 83**, a zig-zag shape and a dot were put onto a vitrimer film and were slowly compressed at 150 °C until the composite was embedded into the pure vitrimer matrix. This experiment showed that vitrimer units and films could be easily fused, and even defined shapes of functional, modified vitrimers could be implemented.
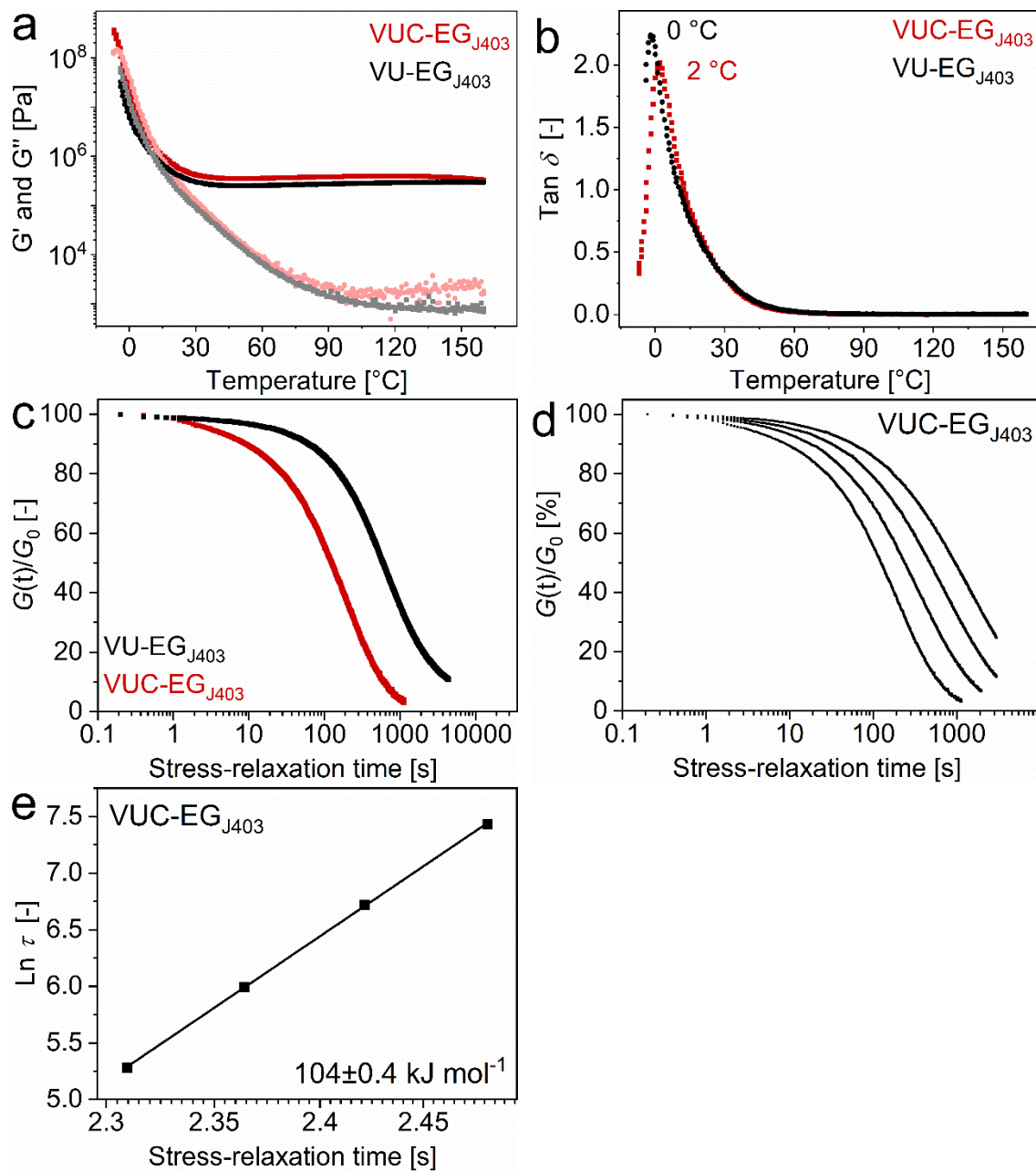
Figure 82: (a) DMTA measurements of VU-EG$_{J403}$ and the composite VUC-EG$_{J403}$ with 10 wt% nanoparticles (G' = dark color and G'' = light color, ω = 10 rad s^{-1}, γ = 0.01%). **(b)** DMTA measurements showing the loss factor and T_gs of the materials. **(c)** Stress-relaxation measurements of the matrix vitrimer and the composite at 160 °C. **(d)** Stress-relaxation measurements of the composite at 130, 140, 150 and 160 °C **(e)** Plot of ln τ versus the reciprocal temperature to determine the activation energy of the composite from the slope of the linear fit.
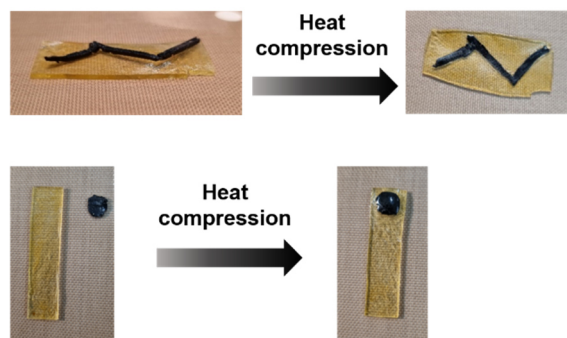
Figure 83: Pictures of the matrix vitrimer VU-EG$_{J403}$ and the composite material VUC-EG$_{J403}$ in different shapes before and after fusion through heat compression at 150 °C.

Moreover, the material showed magnetic field-induced deflection of the fused material, while the small dot is enough to bend the whole material (**Figure 84**). Especially in the case of magneto-responsive composites, this behavior can offer the potential for specific applications in terms of thermoresponsive or mechanical-responsive materials, as mentioned in the introduction of this chapter. Moreover, benefits are the lower amount of needed functional material and the ability to control the shape and pathway of the functional layer/unit.
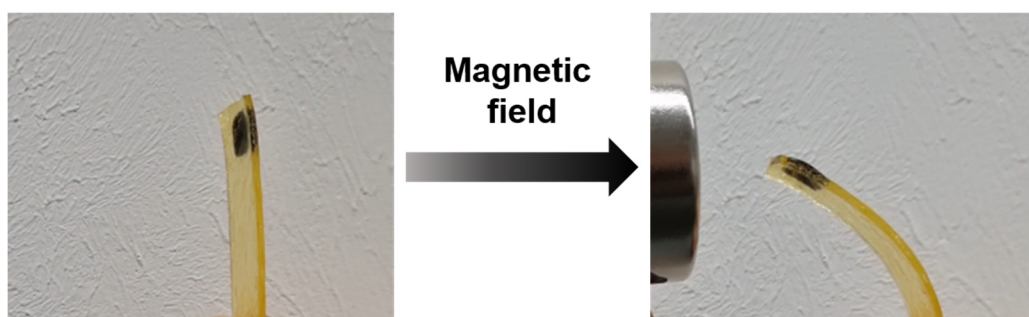
Figure 84: Bending of the fused elastomeric vitrimer-composite in a magnetic field.

This chapter shows that iron-oxide nanoparticles can be easily implemented into a vitrimer matrix. Moreover, the catalyzing effect of the phosphonic acid ligand HUPA$_{AcAc}$ on the exchange reaction was described. At least, the fusion of different vitrimers was explored together with a deflecting effect in a magnetic field, which offers possible applications and research fields for the prepared magneto-responsive vitrimers.

6.4.1.4 Composites with a high load of inorganic particles

In this subchapter, a composite with a high load of 70 wt% of inorganic iron-oxide nanoparticles was prepared. HUPA$_{AcAc}$-modified, 12 nm cubic nanoparticles were dispersed in chloroform and mixed with GL$_{AcAc}$ and DAO. Since the desired composite materials with a high load of inorganic particles should exhibit a rigid material with a high elastic modulus, a thermosetting matrix vitrimer was chosen. **Figure 85a/b** show the resulting black material and SEM images show a highly packed material with a partly ordered and random distribution of the cubic nanoparticles. Because of the particle's different packing, the composite showed different phases and was not totally homogeneous. The main goal was to investigate if composites with such a high load of particles were still reprocessable because the close packing of the nanoparticle cross-linkers may hinder an efficient stress-relaxation process.
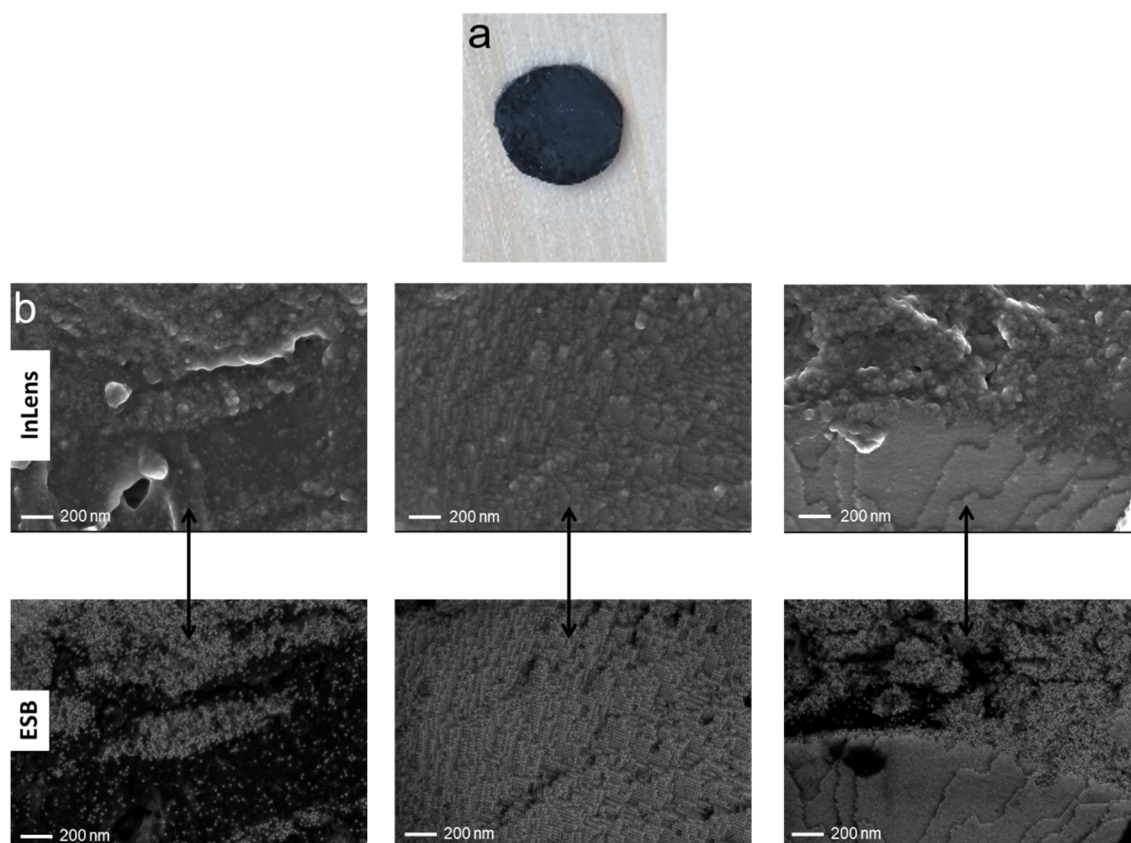
Figure 85: (a) Picture of the composite material **(b)** SEM images of the composite VUC-GL$_{DAO}$, showing a homogeneous particle distribution in different magnifications (cross-fracture).

ATR-FT-IR spectra proved the formation of the characteristic C=C band (1597 cm^{-1}) and C=O ester band (1650 cm^{-1}) of the vinylogous urethane bonds (appendix, Figure A14). DMTA measurements show a significant change in the properties in comparison of the pure matrix vitrimer VU-GL$_{DAO}$ and the composite material VUC-GL$_{DAO}$ with 70 wt% modified nanoparticle load. Both materials exhibit cross-linked materials with a characteristic rubbery plateau, while the rubbery plateau of the composite is more than one magnitude higher (**Figure 86a**). In addition, the T_g of the composite is significantly higher than the matrix vitrimer. Plotting the loss factor versus the temperature T_gs of 33 °C for the matrix and 65 °C for the composite were measured (Figure 86b). These results show the reinforcing effect of the nanoparticles, which act as an additional polyfunctional cross-linker due to the HUPA$_{AcAc}$ bearing ligand with a functionality of approximately 1600 acetoacetate groups per nanoparticle ($f = 1600$). Moreover, the relatively low amount of vitrimer between the particles can no longer be considered an actual polymer since the number of repeating units is theoretically in the range of oligomers.

Stress-relaxation experiments were carried out in the range of 90–130 °C to explore the composites reprocessing ability. This was especially interesting since the high load of particles may hinder efficient stress-relaxation, which is a typical label for vitrimers. Figure 86c shows the normalized stress-relaxation curves and complete stress relaxation of the composite VUC-GL$_{DAO}$. Remarkably, the stress-relaxation times of the composite were much shorter than the pure matrix vitrimer. This behavior was already investigated for the magneto-responsive elastomers in the previous chapter and can be attributed to the presence of the HUPA$_{AcAc}$ ligand, which acted as a Brønsted catalyst. Moreover, a comparison of the activation energies shows comparable values of 107 (matrix) and 102 kJ mol^{-1} (composite), with the composite even showing a slightly lower activation energy (Figure 86d). This behavior is also quite unusual since the activation energies of composites are usually higher than the pure matrix.[22] Since the amounts of material were consistently low for composites with high loads of particles, nanoindentation measurements were carried out to gain results about the mechanical properties. For VU-GL$_{DAO}$, an averaged E-modulus and an averaged hardness of 1.1 ±0.1 GPa and 0.05±0.01 GPa were measured. For VUC-GL$_{DAO}$, an averaged E-modulus and an averaged hardness of 2.2 ±0.2 GPa and 0.16±0.02 GPa were measured, doubling the E-modulus

and a tripling of the hardness. The results pointed out that implementing the particles can greatly strengthen the material while simultaneously improving the reprocessability due to the phosphonic acid catalyst.
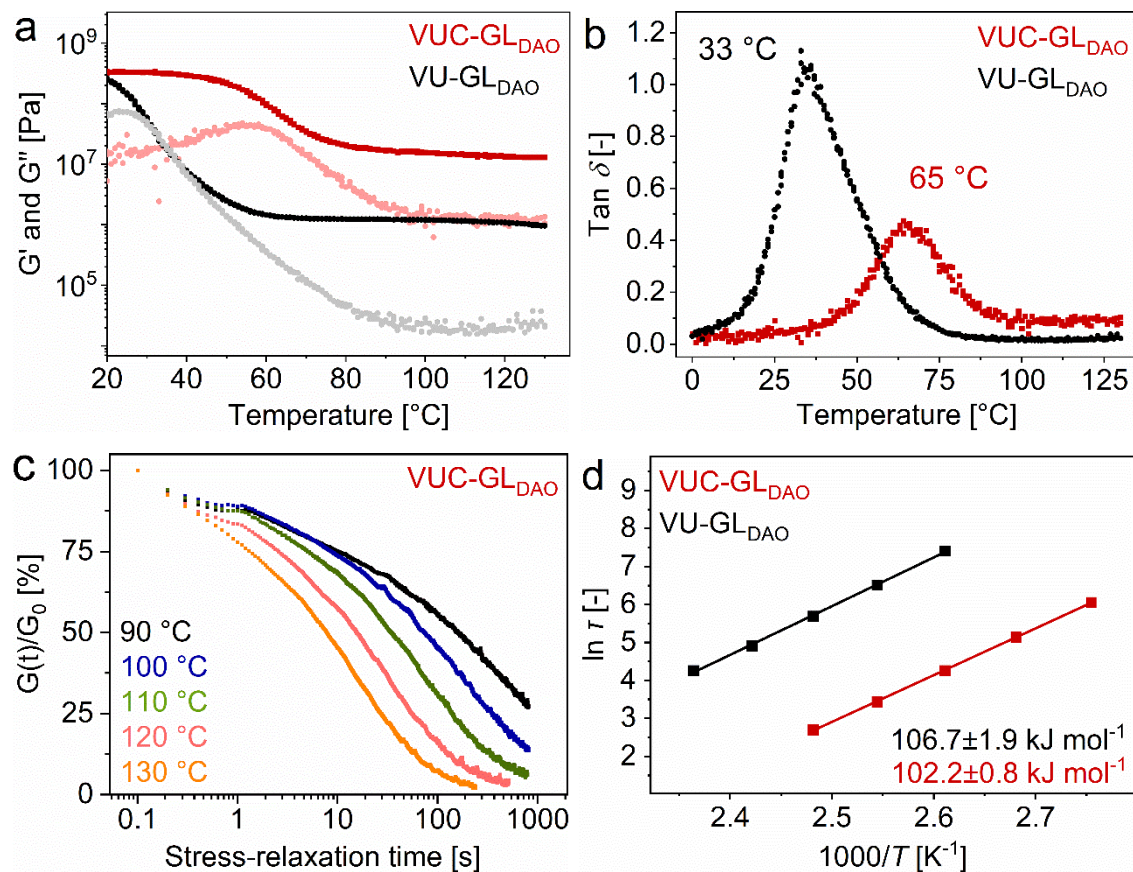
Figure 86: (a) DMTA measurements of VU-GL$_{DAO}$ and the composite VUC-GL$_{DAO}$ with 70wt% nanoparticles (G'= dark color and G''= light color, ω = 10 rad s^{-1}, γ = 0.01%). **(b)** DMTA measurements show the loss factor and T_gs of the materials. **(c)** Stress-relaxation measurements of the composite at 90–130 °C (γ = 1%). **(d)** Plot of ln τ versus the reciprocal temperature to determine the activation energy of the matrix vitrimer and composite from the slope of the linear fit.

6.4.1.5 Hierarchical composites

In the scope of the project SFB986 area A, the goal was to develop hierarchical materials with different length scales, a high content of inorganic particles and a thermoreversible polymer matrix (**Figure 87)**. Several milestones had to be reached to achieve this goal, from the development of the nanoparticles, the nanoparticle clustering, the ligand/linker, the vitrimers, and a route to combine everything (project A1 and A2). This subchapter shows a first trial in which clustered spherical nanoparticles (15 nm) were functionalized with HUPA$_{AcAc}$ and incorporated into a vitrimer matrix (VU-EG$_{J403}$), followed by a heat compression step. The vitrimer was chosen since it usually stabilized the nanoparticles very well and prevented agglomeration and sedimentation. A weight ratio of approximately 50 wt% polymer was used. SEM images show intact nanoparticle clusters of 200–400 nm embedded in a vitrimer matrix of VUHC-EG$_{J403}$ (Figure 87). Heat compression at 150 °C showed that the composite can be remolded without destroying the clusters, which showed a reasonably good stability of the clusters. Nevertheless, the process has to be improved since the composite showed inhomogeneities due to relatively fast agglomeration and sedimentation of the large and not well dispersible clusters in toluene. Further research has to be done to stabilize the clusters and embed them into a vitrimer matrix. Mechanical tests were not conducted on this material since the synthesized amount was very low.

This chapter describes that a simple acetoacetylation reaction can synthesize a suitable phosphonic acid ligand with an acetoacetate-bearing group. Moreover, it was investigated that the ligand can easily substitute oleic acid ligands and formate stable solutions in chloroform. The modified nanoparticles can be used for magneto-responsive elastomers and acted as an additional polyfunctional cross-linker in the material. Magneto-responsive elastomers are attractive for applications such as robotics or sensors. In the scope of SFB986 it was also shown that the particles could be used in high amounts to prepare highly loaded composites with 70 wt% of particles, which significantly changed the thermomechanical properties. Remarkably, it was found that adding the ligand HUPA$_{AcAc}$ provided additional protons to the material and acted as a Brønsted catalyst, which accelerates the transamination reaction.
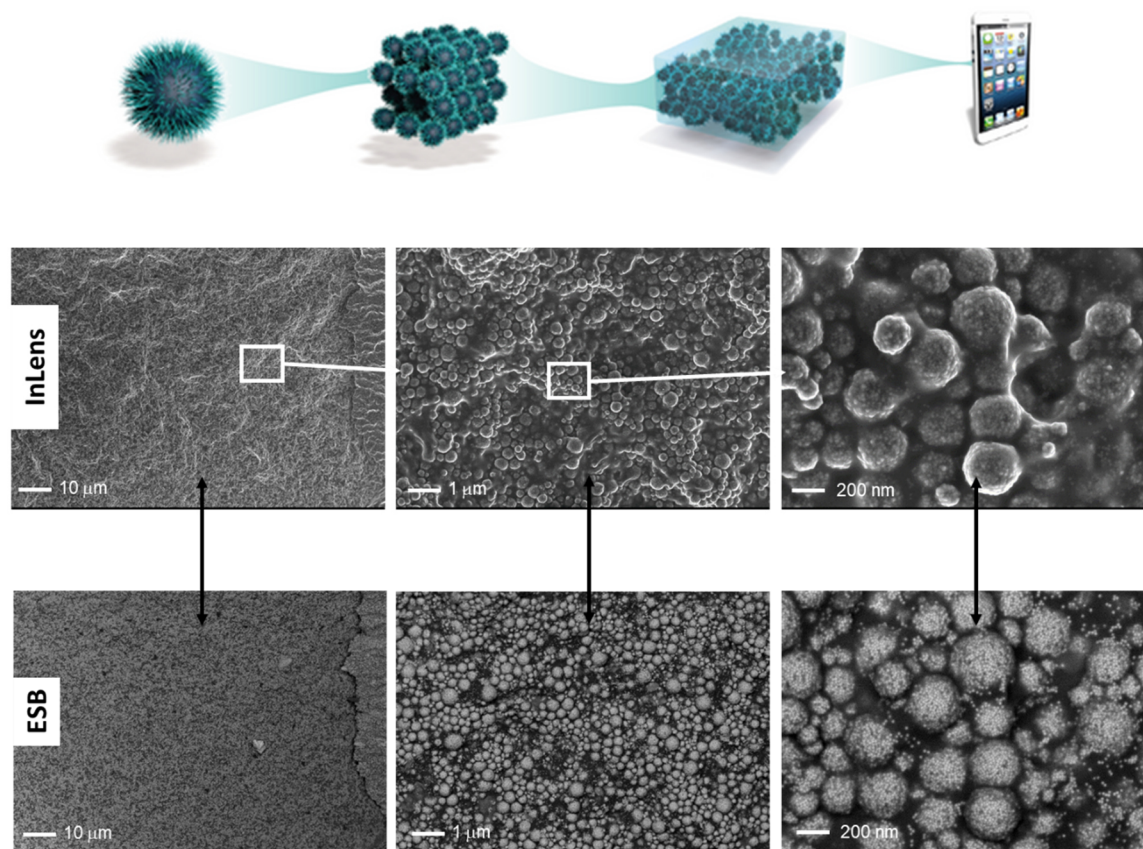
Figure 87: SEM images of the hierarchical composite VUHC-EG$_{J403}$, showing 200–400 nm nanoparticle clusters prepared of 15 nm spherical nanoparticles embedded into a vitrimer matrix at different magnifications. Reproduced with permission of SFB986.

As an outlook, it is shown that nanoparticle clusters could be modified by the ligand HUPA$_{AcAc}$ and implemented into a vitrimer matrix to form a hierarchical composite on different length scales.

6.4.2 Nacre-inspired, Polymer-ceramic Vitrimer Composites

In this chapter, a nacre-inspired, thermoreversible polymer-ceramic vitrimer composite based on surface-modified aluminaoxide platelets, acetoacetylated glycerol and a poly(ethylene glycol)-based diamine (2,2′-(ethylendioxy)diethylamino, OE) is explored. The project was carried out in collaboration with subproject A6 (TUHH). The central part of the results was published by Winhard *et al.* in Elsevier – Additive Manufacturing with the title "Direct write 4D-printing of smart, nacre-inspired, organic-ceramic composites" (DOI:10.1016/j.addma.2023.103776). Benedikt Winhard and co-workers (A6) prepared the modified aluminaoxide platelets, developed, processed and optimized the *in-situ* polymerization *via* 3D-printing and characterized the polymers/composites. This work focused on a single-step printing process, in which micron-sized alumina-platelets were printed as suspensions with a trifunctional acetoacetate and an amine. After printing, the solvent evaporates quickly, which enables a fast polycondensation reaction of the acetoacetates and the amines to align the platelets and form the composite material.
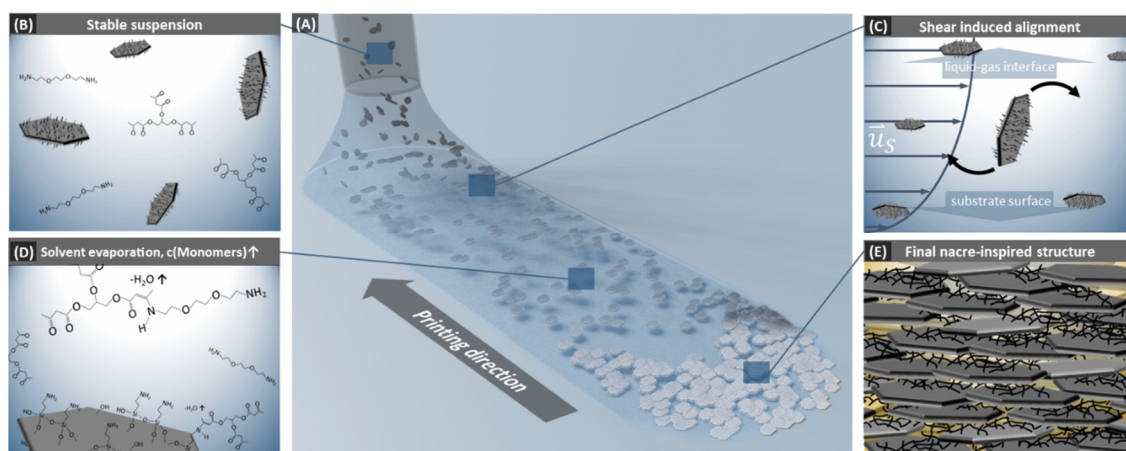
Figure 88: (**a**) Scheme of the direct write 4D-printing process. (**b**) Scheme of the used monomers: APTMS-functionalized alumina platelets, trifunctional acetoacetates, diamines and ethanol as solvent. (**c**) The platelets align after extrusion due to shear flow induced by suspension spreading. (**d**) The solvent evaporation induces the polycondensation reaction of the acetoacetates and diamines to form a vinylogous urethane vitrimer. (**e**) Scheme of the synthesized polymer-inorganic composite material. Reprinted from Winhard *et al.*[173] with permission of Elsevier, ©2023, licensed under CC-BY-4.0

The unique properties of vitrimers enable self-healing, reprocessing, reshaping, and rearrangement of the alumina platelets within the cross-linked composite material. Detailed information is shown in the publication, while the overall process is shown schematically in **Figure 88**.[173]

Besides 4D-printing, the used materials were also synthesized by simple bulk reaction and investigated in terms of their thermomechanical properties. This project was conducted in the scope of this thesis and the results are shown in the following part. The goal was to implement the alumina-platelets homogeneously into a vitrimer matrix and enable a thermal- and pressure-induced alignment of the anisotropic platelets in the final, cross-linked composites. The ethanolic aluminaoxide-aminopropyltrimethoxysilane (Al_2O_3-APTMS) solution was provided by subproject A6. Ethanol was slowly evaporated until the mixture became highly viscous. The ratio of inorganic particles to vitrimer matrix was also set to 40:60 wt%, as carried out for the 4d-printing project. The acetoacetate monomer GL_{AcAc} and the diamine OE were added and mixed until gelation occurred (R = 0.8). Afterward, the composite was post-cured to ensure complete conversion and remove excess water and ethanol. ATR-FT-IR spectra proved the formation of the vinylogous urethane vitrimer by measuring the characteristic C=C (1592 cm^{-1}) and C=O ester stretching vibration bands (1646 cm^{-1}) of the vinylogous urethane bonds. Moreover, N-H bands (3000–3700 cm^{-1}), C-N (1230 cm^{-1}), and C-O (1164 cm^{-1}) bands were measured and characterized the vinylogous urethane vitrimer matrix in the pure reference vitrimer and the vitrimer composite (**Figure 89**).
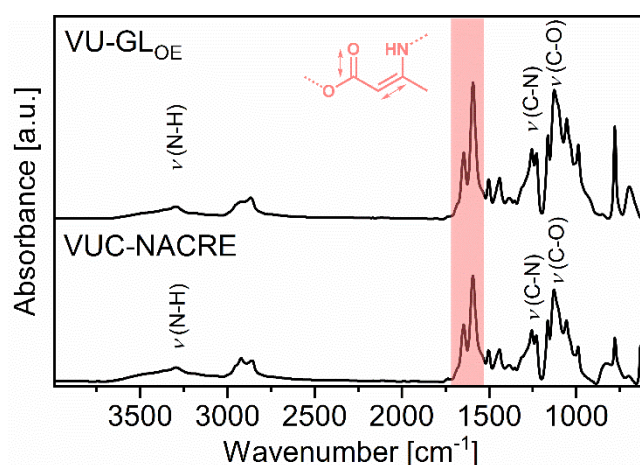
Figure 89: ATR-FT-IR of the reference matrix vitrimer VU-GL$_{OE}$ and VU-NACRE showing the characteristic C=C band (1592 cm^{-1}) and C=O ester band (1646 cm^{-1}) of the vinylogous urethane bonds together with N-H bands (3000–3700 cm^{-1}), C-N (1230 cm^{-1}) and C-O (1164 cm^{-1}) bands.

DMA measurements were carried out to investigate the material's mechanical properties and reprocessability by oscillatory and step shear experiments. Amplitude sweeps of the matrix vitrimer at 100 °C show a high yield point at 30%, while for the composite material, 1% was measured. Due to the additional amine-bearing surface, the Al_2O_3 particles acted as a filler and polyfunctional cross-linker and increased the cross-linking density, which led to a decrease in flexibility with a higher stiffness of the composite (**Figure 90a**). Frequency sweeps of the matrix vitrimer and composite material at 100 °C indicate cross-linked materials in a broad frequency range (Figure 90b). DMTA measurements in the range of 0–150 °C displayed maximal storage moduli of 810 MPa (VU-GL$_{OE}$) and 1180 MPa (VUC-NACRE) and rubbery plateaus of 0.3 MPa (VU-GL$_{OE}$) and 1.5 MPa (VUC-NACRE), indicating cross-linked materials and a higher stiffness of the composite material (Figure 90c). The loss factors (maximum) indicate rather similar glass transition temperatures of 32 °C (VU-GL$_{OE}$) and 34 °C (VUC-NACRE). This is reasonable since the composite consists mainly of the matrix vitrimer (60 wt%) (Figure 90d).
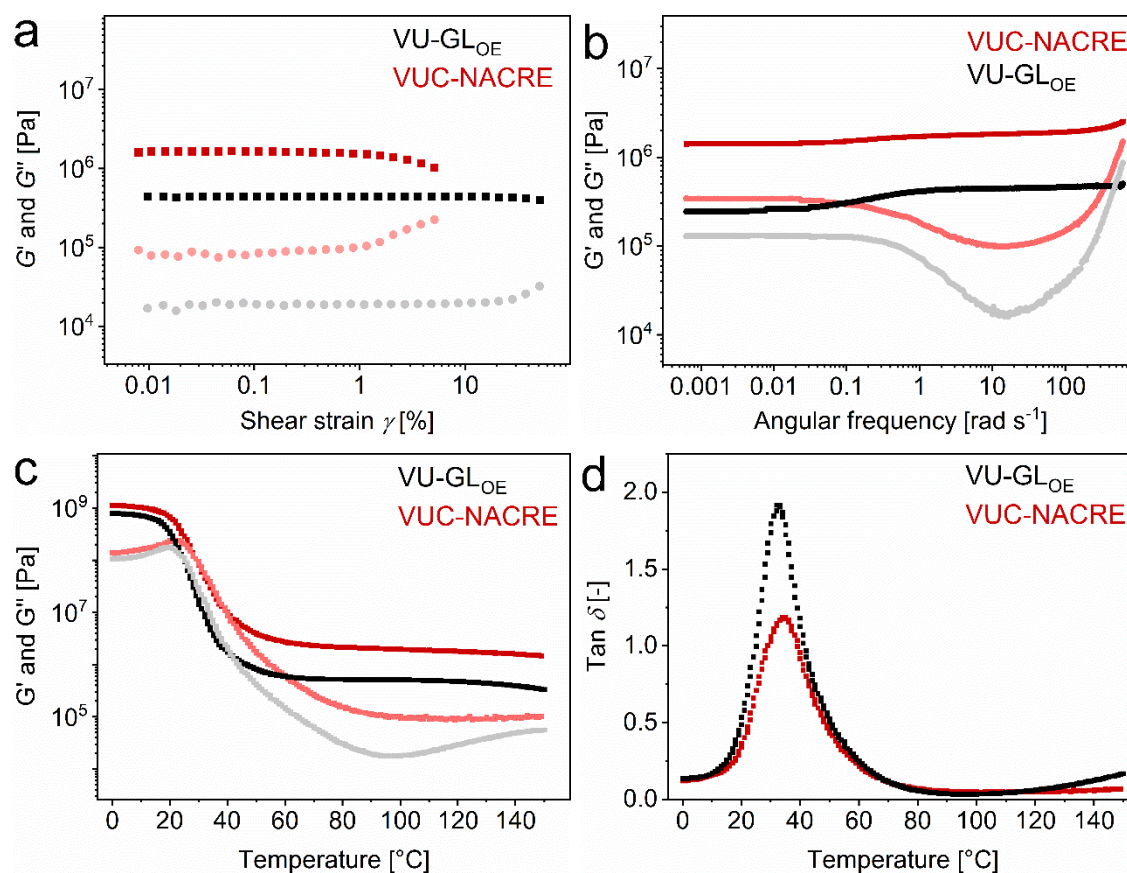
Figure 90: (a) Amplitude sweeps of the matrix vitrimer and composite material at 100 °C (ω = 10 rad s^{-1}). **(b)** Frequency sweep of the materials at 100 °C (ω = 0.00062–620 rad s^{-1}, γ = 0.1%). **(c)** DMTA measurements of the matrix vitrimer and composite material at 0–150 °C, showing the storage and loss moduli (ω = 10 rad s^{-1}, γ = 0.01%). **(d)** DMTA measurements show the loss factors and the glass transition temperatures of the materials *(ω = 10 rad s^{-1}, γ = 0.1%)*.

Stress relaxation measurements were carried out at different temperatures of 90–150 °C, with the matrix vitrimer showing shorter stress relaxation times than the composite. The vitrimer shows a fast stress-relaxation time of 1.3 s at 150 °C, while the composite shows 10 s **(Figure 91a/b)**. Comparing the activation energies, the composite material shows a higher activation energy of 86.0±6.9 kJ mol^{-1} than the matrix vitrimer with 66.2±1.5 kJ mol^{-1}, which fit reported values for vinylogous urethane vitrimers (Figure 91c).[55, 70]
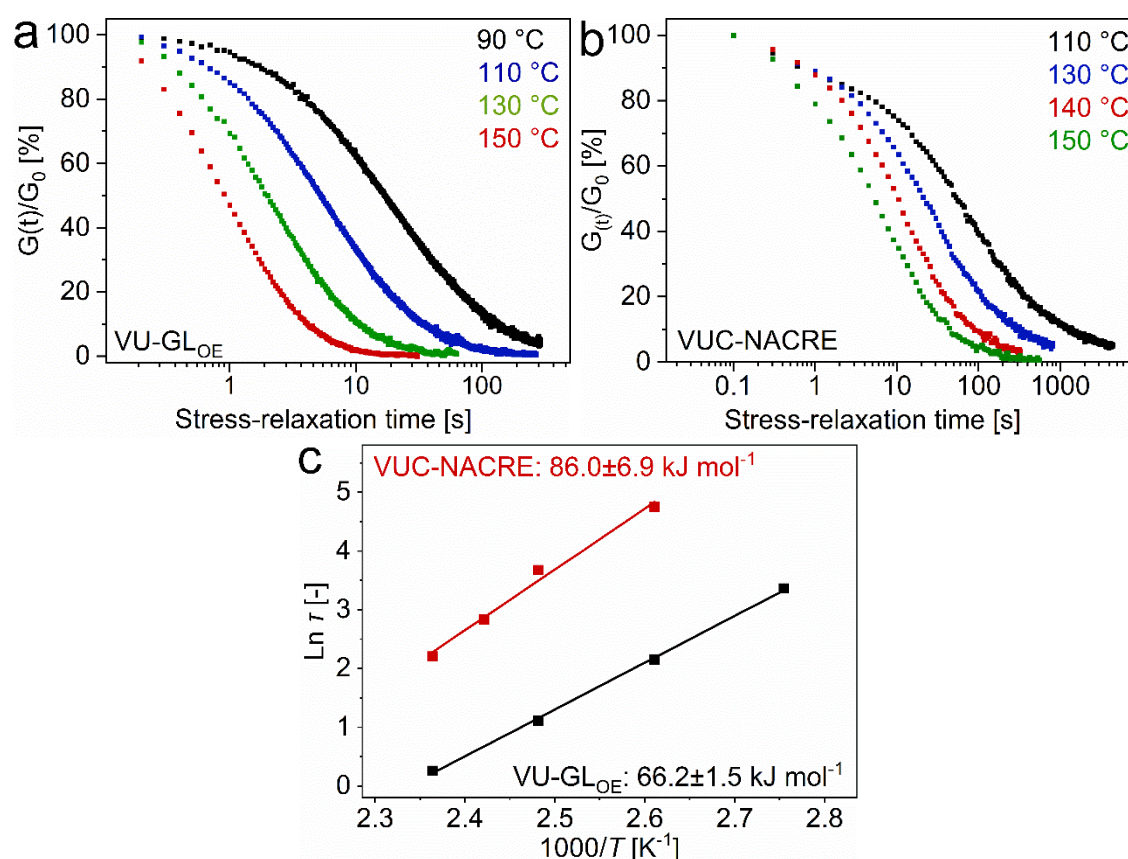
Figure 91: (a) Stress-relaxation measurements of the matrix vitrimer VU-GL$_{OE}$ in the temperature range of 90–150 °C (γ = 1%). **(b)** Stress relaxation measurements of VUC-NACRE in the temperature range of 110–150 °C (γ = 1%). **(c)** Plot of ln τ against the reciprocal temperature. The slope of the linear fit determines the activation energies of the materials VU-GL$_{OE}$ and VUC-NACRE.

Typically, composites show higher activation energies than pure matrix vitrimers, which is also shown in publication 3.[22]

In order to investigate the mechanical properties of the materials, tensile tests have been carried out at room temperature (20 °C). The comparison of the matrix vitrimer and the composite material shows a dramatic increase in the elastic modulus ($E_\emptyset$) from 130 to 1725 MPa and tensile strengths ($\sigma_{m\emptyset}$) from 5.8 to 29.9 MPa, while the elongations at maximum stress ($\varepsilon_{m\emptyset}$) decreased from 7.5 to 2.5% (**Figure 92).** The aluminaoxide platelets increase the stiffness of the materials by a multiple and lead to a resilient yet reprocessable composite material.
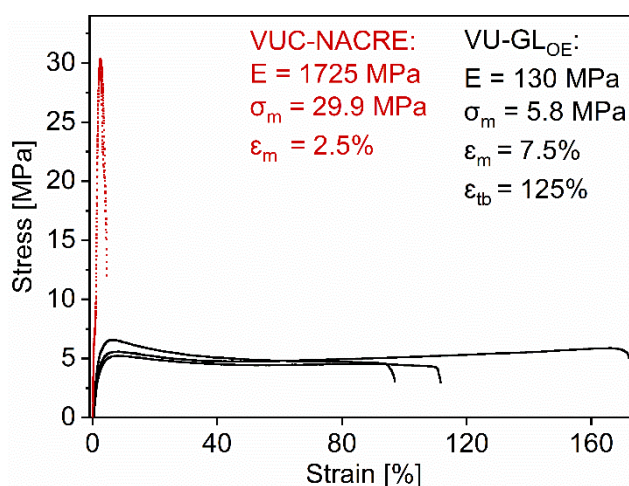
Figure 92: Stress-strain curves of the materials VU-GL$_{OE}$ and VUC-NACRE derived from tensile test measurements at 20 °C, showing the averaged E-modulus ($E_\emptyset$), tensile strength ($\sigma_{m\emptyset}$) and strain at break ($\varepsilon_{m\emptyset}$ and $\varepsilon_{tb\emptyset}$).

Pictures and SEM images of the composite material before and after compression molding showed homogeneously distributed particles within the composite material. Most interestingly, before heat compression, the orientation of the anisotropic aluminaoxide platelets was not ordered, while after heat compression, the platelets were ordered to a nacre-like, layered structure (**Figure 93**). This behavior showed that the thermoreversible vitrimer enables the reorganization and the alignment of the hard and inorganic platelets within the polymer matrix. This outstanding property allows a postmodification of the composite structure by heat and pressure. Showing this property was a major goal of SFB 986, as it shows the possibility of subsequently rearranging

particle clusters in the composite and thus generating defined structures such as brick and mortar structures.
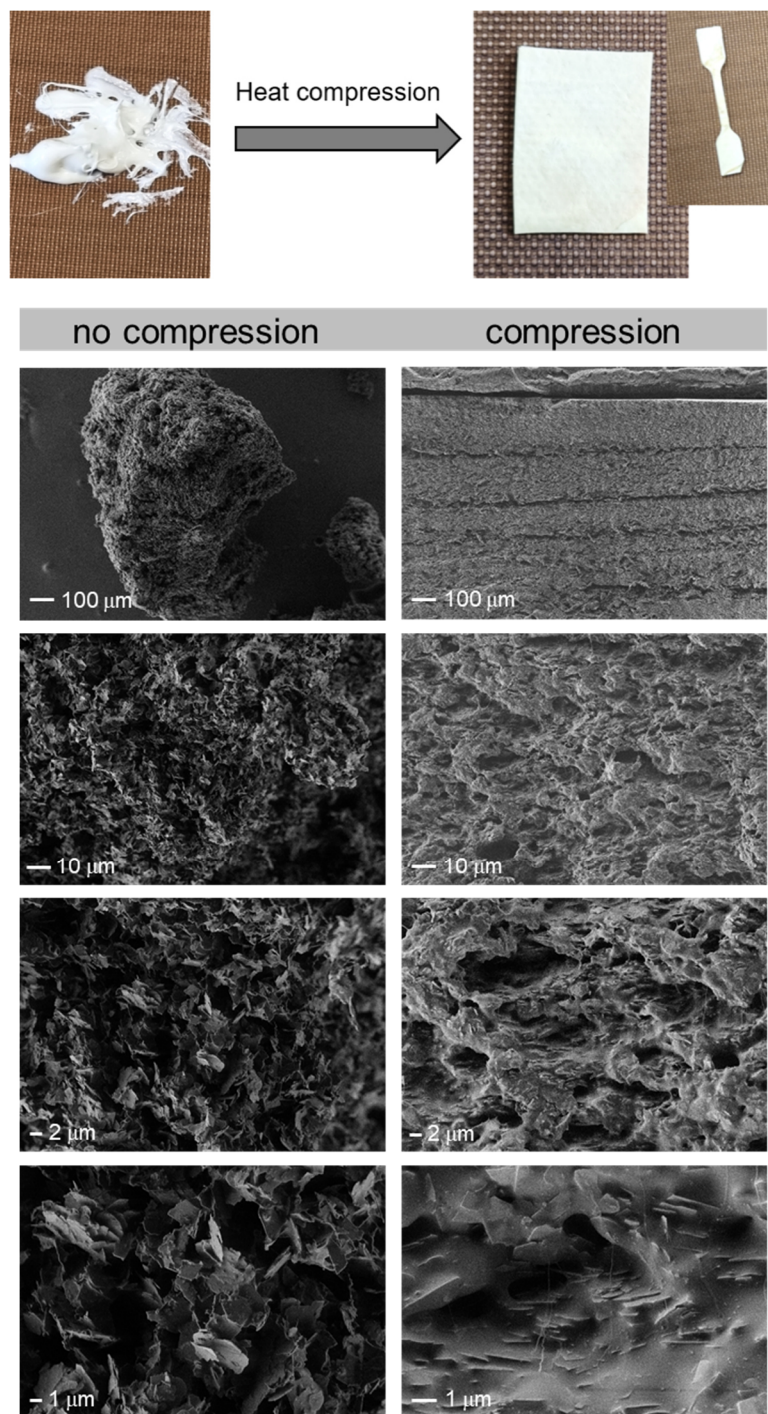
Figure 93: Pictures of the composite material VUC-NACRE before and after heat compression at 150 °C for 2 minutes and 10 kN pressure. The composite was pressed into a 1 mm thick film. SEM pictures of the composite material before and after heat compression with different magnifications show a random distribution of the platelets before compression and a layered, more ordered structure afterward.

Comparing the results to the composites obtained by 4d-printing, the properties were comparable and showed the same trends but were not precisely the same. Both composites show low glass transition temperatures of 20–35 °C (on-set) and cross-linked materials. Moreover, tensile tests show comparable trends. The E-moduli and tensile strengths of the composited were always increased in both processing methods, while the elongation at break was decreased dramatically due to the higher cross-linking density. Nevertheless, a direct comparison is not shown here because the measurement devices, sample preparation, and measurement parameters were different.

6.5 Experimental Section

6.5.1.1 Materials

This chapter shows the used raw materials, their purities and the suppliers.

Hexylamine (99%), para-toluene sulfonic acid monohydrate (99%), trifluoroacetic acid (99%), *tert*-butyl-acetoacetate (≥98%), 2,2'-(ethylenedioxy)diethylamine (98%), *m*-Xylylendiamine (98%), 3,3-N-methyl propyl diamine (98%), Bispenol-A diglycidylether, PEG 300 (98%), PEG 4000 (98%), 3-armPEG (98%), 1,2,6-Hexantriol (98%), 1,4-Cyclohexandimethanol (98%), 1,12 Dodecanediol (98%), 1,3-Benzoldimethanol (98%), Mentane diamine (98%), Ethylenediamine (98%), 11-hydroxyundecylphosphonic acid (95%), and Cellulose cotton linters or fibers were purchased from Sigma-Aldrich. Benzylamine (≥99%) and benzylacetoacetate (≥95%), D-Fructose (98%), D-Glucose (98%), D-Sorbitol (98%), D-Laktose (98%) and D-Saccharose (98%), Chitosan (95-98%) different molecular weights, Chitin particles (98%), Cellulose were obtained from TCI. Methylacetoacetate (≥99%), and Tris(2-aminoethyl)amine (97%) were purchased from Alfa Aesar. Ethylacetoacetate (98%) and 1,6-hexanediol (≥97%) were purchased from MERCK KG aA. Acetic acid (95%) was obtained by VWR and dodecylamine (≥98%) was purchased from Fluka. Sodiumacetate (99%) was purchased from pro analysis. Xylene (99%, isomeric mixture) and MgSO4 (99%) were purchased from Grüssing. Benzene-*d*6, DMSO-*d*6, methanol-*d*4, and CDCl₃ were purchased from Deutero GmbH. Acetic acid and chloroform were purchased from VWR chemicals. Bisphenol-A (97%), 2,7-naphthalenediol (98%), and hexylamine (99%) were purchased from Sigma-Aldrich. 2,2,6-Trimethyl-1,3-dioxin-4-one (95%), benzylamine (99%), aniline (98%), *tert*-butylacetoacetate (98%) and 1,1,1-tris(4-hydroxyphenyl)ethane (98%) were obtained from TCI. Tris(2-aminoethyl)amine (97%) was purchased from Alfa Aesar. Phenol (99.5%) was purchased from MERCK. Xylene (99%, isomeric mixture) and resorcin (98%) were purchased from Grüssing. CDCl₃, benzene-*d*6 and DMSO-*d*6 were purchased from Deutero GmbH. Jeffamine® T-403 Jeffamine® D230, Jeffamine® D400, Jeffamine® D2000, Jeffamine® T403, Jeffamine® T3000 were purchased from Huntsman. Starch (corn), starch (wheat), starch (rice), hexylamine (99%), alpha-amylase (aspergillus oryzae, 30 U mg-1), iodine (99.5%) and

ethanol (99%) were purchased from Sigma-Aldrich. 2,2,6-trimethyl-1,3-dioxin-4-one (95%), tert-butylacetoacetate (98%), 1,5-diaminopentane (98%), 1,4-diaminobutane (98%), 1,6-diaminohexane (98%), 1,8-diaminooctane (98%), 1,10-diaminodecan (98%), 1,12-diaminododecane (98%) and 1,6-hexanediol (98%) were obtained from TCI. Ethylene glycol (99.5%) was purchased from Honeywell. Acetic acid (100%) and tetrahydrofuran (HPLC-grade) were purchased from VWR. Glycerol (99.5%) was purchased from ROTH. Isobutylamine (99%) was purchased from Alfa Aesar. DMSO-$_d$6 was purchased from Deutero GmbH. Priamine® 1075 and Priamine® 1074 were provided from Croda International. α-alumina platelets were purchased from Kinsei Matec Co.,LTD (Japan). (3-aminopropyl)trimethoxysilane (APTMS) was purchased from Merck KGaA.

6.5.1.2 Monomer Syntheses – Acetoacetylation and Acetoacetamidation

Acetoacetylation

Propane-1,2,3-triyl tris(3-oxobutanoate) (GL$_{AcAc}$): The crude, brownish 2,2,6-trimethyl-1-3-dioxin-4-one (TMDO) was purified by vacuum distillation at 60 °C and 0.1 mbar to obtain the pure colorless product. Glycerol (10.0 g, 0.108 mol) and the purified TMDO (or TBA) (48.6 g, 0.342 mol) were mixed in a 250 mL flask. The mixture was heated at 135 °C for 3 h, while the byproduct acetone was removed by distillation during the reaction. The temperature in the distill head was usually between 75–90 °C. When the temperature dropped to 35 °C in the still head, the remaining acetone, TMDO, and dehydroacetic acid were removed in *vacuo* at 130 °C and 0.1 mbar. The residue represented the desired product in a high degree of purity (99%), appearing as a slightly yellowish liquid. The reaction was carried out as a bulk reaction or in the high boiling solvents xylene or DMF, depending on the solubility and viscosity of the reactants. The following **Table 5** shows the reaction conditions from the respective monomer syntheses. Usually, an excess of 5% TMDO (in relation to OH groups) was used. The syntheses of the used monomers in the publications 1, 2 and 3 may differ a little and are described in the experimental section of the respective publication.

Acetoacetamidation

The crude, brownish 2,2,6-trimethyl-1-3-dioxin-4-one (TMDO) was purified by vacuum distillation at 60 °C and 0.1 mbar to obtain the pure colorless product. Chitosan (10.0 g, 0.108 mol) and the purified TMDO (48.6 g, 0.342 mol) were mixed in a 250 mL flask with water (concentration = 3M, all compounds). The mixture was refluxed for 3 h and the remaining mixture was washed with water and precipitated in ethanol. **Table 5** shows the reaction conditions from the respective monomer syntheses.

Table 5: Conditions for the acetoacetylation reaction of the different acetoacetate monomers.

Monomer	Agent	Solvent	Temp [°C]	Time [h]	Purification
EG_{AcAc}	TMDO	-	135	2	Oil pump, 130°C
GL_{AcAc}	TMDO	-	135	2	Oil pump, 130°C
HM_{AcAc}	TBA	Xylene (3M)	135	3	Oil pump, 130°C
DOD_{AcAc}	TBA	Xylene (3M)	135	3	Oil pump, 130°C
$PEG300_{AcAc}$	TBA	Xylene (3M)	135	3	Oil pump, 130°C
$PEG4000_{AcAc}$	TBA	Xylene (3M)	135	3	Oil pump, 130°C
$3aPEG_{AcAc}$	TBA	Xylene (3M)	135	3	Oil pump, 130°C
BZ_{AcAc}	TBA	Xylene (3M)	135	3	Oil pump, 130°C
HT_{AcAc}	TBA	Xylene (3M)	135	3	Oil pump, 130°C
CH_{AcAc}	TBA	Xylene (3M)	135	3	Oil pump, 130°C
DCH_{AcAc}	TBA	Xylene (3M)	135	3	Oil pump, 130°C
FRU_{AcAc}	TMDO	-	135	1	Oil pump, 130°C
GLU_{AcAc}	TMDO	-	135	1	Oil pump, 130°C
SO_{AcAc}	TMDO	-	135	1	Oil pump, 130°C
LAC_{AcAc}	TMDO	-	135	1	Oil pump, 130°C

SAC$_{AcAc}$	TMDO	-	135	1	Oil pump, 130°C
Chi$_{AcAc}$	TBA	-	135	3	Washing EtOH, H_2O
Starch$_{AcAc}$	TMDO	-	135	1	Washing EtOH
CLBac$_{AcAc}$	TBA	-	135	3	Washing EtOH, H_2O
CLLint$_{AcAc}$	TMDO	Xylene (1M)	135	1	Oil pump, 130°C
CLMW$_{AcAc}$	TMDO	Xylene (1M)	135	1	Washing Xylene
Chitosan (Oligomer)	TMDO	DMF (3M)	130	1	Oil pump, 130°C
Chitosan (Oligomer)	TMDO	H_2O (3M)	100	4	Washing EtOH, H_2O
Chitosan 200 kDa	TMDO	H_2O (AA) (3M)	100	4	Washing EtOH, H_2O

6.5.1.3 Polymerization – Condensation Reaction and Gelation Times

All vitrimers were prepared by the following exemplary synthesis route: GL$_{AcAc}$ (1.42 g, 4.12 mmol) and 1/4 of the total monomers mass of ethanol (0.6 g) were mixed with a diamine/triamine, *e.g.*, DAH (0.960.6 g, 8.4 mmol) and stirred with a spatula. The acetoacetate (GL$_{AcAc}$) to amine ratio was set to R = 0.75 when using a diamine and R = 0.6 when using a triamine. After a few minutes, a homogeneous, opaque, and cross-linked gel was obtained and the gelation times were monitored for each amine. The gel was filled onto a PTFE (poly(tetrafluoroethylene)) sheet and cured for 18 h at 100 °C in a vacuum oven (oil pump). Afterward, the vitrimer was postcured for 1 h at 150 °C in *vacuo* to ensure complete conversion and removal of remaining reaction water. Next, the samples were pressed for 5−10 min at 160 °C with a pressure of 500−1000 N cm^{-2} into a 1 mm thick film. The products were obtained as yellowish films.

6.5.1.4 Polymerization – Impact of Different Acetoacetate Backbones

All vitrimers were prepared by the following exemplary synthesis route: HT_{AcAc} (2.45 g, 6.34 mmol) or another acetoacetate was mixed with a diamine/triamine, *e.g.*, CHDA (1.802 g, 12.68 mmol) and stirred with a spatula. The acetoacetate to amine ratio was set to R = 0.75. After a few minutes, a homogeneous, opaque, and cross-linked gel was obtained. The gel was filled onto a PTFE (poly(tetrafluoroethylene)) sheet and cured for 18 h at 100 °C in a vacuum oven (oil pump). Afterward, the vitrimer was post-cured for 1 h at 150 °C in *vacuo* to ensure complete conversion and removal of remaining reaction water. Next, the samples were pressed for 5−10 min at 160 °C with a pressure of 500−1000 N cm^{-2} into a 1 mm thick film. The products were obtained as yellowish films.

6.5.1.5 Vipoxy – Epoxy-vitrimers

All materials were prepared by the following exemplary synthetic route: Propane-2,2-diylbis(4,1-phenylene)bis(3-oxobutanoate) (BPA_{AcAc}) (1.38 g, 3.48 mmol) was provided in a rolled rim glass and heated up in an oil bath at 100 °C. JT403 (2.05 g, 6.96 mmol) was added under constant stirring. As soon as a homogeneous, opaque gel was obtained, the vitrimer-gel was filled onto a Teflon sheet and cured for 20 h at 100 °C in vacuo (oil pump). Afterward, the vitrimer was post-cured for 1 h at 150 °C in vacuo, in order to ensure full conversion and the removal of the remaining reaction water. Next, the samples were pressed for 5−10 min at 150 °C with a pressure of 500−1000 N cm^{-2} into a 1 mm thick film. The synthetic route follows the same protocol for the synthesis of the epoxy resins and the epoxy-vitrimer materials. BPA_{AcAc} and BADGE were mixed at 100 °C to a homogeneous mass. The amine was added, according to the described synthetic procedure. The products were obtained as yellowish films.

6.5.1.6 Water-based Polymerization − Porous and Dense Vitrimer Films

The acetoacetylated D-glucose-based monomers were dissolved in demineralized water at room temperature (water-soluble, partly acetoacetylated monomers) or at 80 °C (fully acetoacetylated monomers) with a concentration of 5 g/L. The amines were calculated through the determined acetoacetate to amine value R and dissolved in demineralized water with a concentration of 20 g/L (*e.g.* Gly$_{2eq}$: 1.00 g, 0.0029; J403: 1.68 g, 0.0038 mol). Afterward, the solutions were combined and stirred. After 30−60 seconds,

the mixtures became cloudy, and the cross-linked polymer fragments began to precipitate. The condensation reaction of amines also assists the desolvation of the acetoacetate monomers by adding polar amine groups to the molecule. After 30 minutes, the temperature was set to room temperature and the mixture was then stirred for about 24 hours to allow the complete formation and precipitation of the vinylogous urethane vitrimer fragments. The product was filtered and washed with demineralized water three times using a Buchner funnel. The resulting product was stored in a drying oven at 50 °C for about 24 hours. The product was obtained as a white powder.

6.5.1.7 Vinylogous Urea Vitrimers – One-pot Bulk Polymerization

The crude, brownish 2,2,6-trimethyl-1-3-dioxin-4-one (TMDO) was purified by vacuum distillation at 60 °C and 0.1 mbar to obtain the pure colorless product. TMDO (3.20 g, 0.0225 mol) and JT403 (7,69 g, 0.0174 mol) were mixed in a 100 mL flask. The mixture was stirred and heated to 135 °C. After 20 minutes a gel was formed, which was postcured for another 40 minutes at 135 °C. The gel was filled onto a PTFE (poly(tetrafluoroethylene)) sheet and cured for 20 h at 100 °C in a vacuum oven (oil pump). Afterwards, the vitrimer was postcured for 1 h at 150 °C in *vacuo* to ensure complete conversion and removal of remaining reaction water. Next, the samples were pressed for 5−10 min at 150 °C with a pressure of 500−1000 N cm^{-2} into a 1 mm thick film. The products were obtained as yellowish films.

6.5.1.8 Iron-oxide Nanocomposites

Synthesis of (11-((3-oxobutanoyl)oxyundecyl)phosphonic acid (HUPA$_{AcAc}$)

(11-((3-oxobutanoyl)oxyundecyl)phosphonic acid (HUPA$_{AcAc}$): The crude, brownish 2,2,6-trimethyl-1,3-dioxin-4-one (TMDO) was purified by vacuum distillation at 60 °C and 0.1 mbar to obtain the purified colorless product. **(**11-hydroxyundecyl) phosphonic acid (1.96 g, 7.8 mmol), the purified TMDO (1.18 g, 8.3 mmol), and 11 mL xylene were mixed in a 50 mL flask. The mixture was heated at 130 °C for 1 h, while the byproduct acetone was removed by distillation during the reaction. The temperature in the distill head was usually between 75–90 °C. When the temperature dropped to 35 °C in the still head, the remaining acetone, TMDO, and dehydroacetic acid were removed in *vacuo* at 130 °C and 0.1 mbar. The residue represented the desired product in a high degree of

purity, appearing as a slightly yellowish solid after cooling. ^{1}H NMR (600 MHz, DMSO-*d6*, 298 K): 4.03 (2H, m, CH_2), 3.57 (2H, s, CH_2), 2.16 (3H, s, CH_3), 1.58 –1.40 (6H, m, CH_2), 1.34 –1.20 (14H, m, CH_2). ^{13}C NMR (DEPTQ-135, 75 MHz, DMSO-*d6*, 298 K): 201.5 (q, C=O), 169.3 (q, COO), 64.4 (s, CH_2), 49.6 (s, CH_2), 30.1 (s, CH_2), 30.1 (p, CH_3) 30.0 (s, CH_2), 29.0 (s, CH_2), 28.9 (s, CH_2), 28.7 (s, CH_2), 28.6 (s, CH_2), 28.0 (s, CH_2), 27.9 (s, CH_2), 27.0 (s, CH_2) 25.3 (s, CH_2). ESI-MS: m/z = 359.158 [M^{Na+}].

Synthesis of iron oxide nanoparticles

The syntheses of iron-oxide particles were conducted by Lea Klauke or Michael Kampferbeck (SFB986-A1). Spherical iron oxide nanoparticles were synthesized according to the approach by Yu *et al.*[174] Iron oxide hydroxide (2.09 g, goethite) was dispersed in oleic acid (47.1 g) and 1-octadecene (100 mL). The reaction mixture was heated to 320 °C for three hours, before cooling the dispersion to room temperature. The obtained nanoparticles were precipitated with acetone, centrifugated and redispersed in toluene several times. The procedure was repeated until the grafting density of the oleic acid ligand was close to a monolayer. The synthesis of cubic iron oxide nanoparticles was carried out according to the method of Kampferbeck *et al..*[175] The protocol is based on the synthesis of spherical iron oxide nanoparticles. Parts of oleic acid were substituted with sodium oleate to achieve shape control. The mixture was heated to 325 °C and after the nucleation, the dispersion was cooled to room temperature and diluted with toluene (1:1 vol.). Afterward, the particles were precipitated with acetone and after centrifugation, the nanocubes were dispersed in toluene. The washing procedure was repeated two times with methanol/acetone (3:1 vol.). and than with pure acetone. The procedure was repeated until the grafting density of the oleic acid ligand was close to a monolayer. Detailed masses, volumes of the reactants and the synthesis time are shown in **Table 6**.

Table 6: Masses and volumes of reactants used for the synthesis of differently sized cubic iron oxide nanoparticles.

Size [nm]	FeOOH [g]	OA [g]	NaOL [g]	ODE [mL]	Time [min]
12	2.00	19.1	6.90	75	145
18	3.00	38.2	10.3	75	230

All iron oxide nanoparticle samples were characterized via dynamic light scattering, transmission electron microscopy, TGA and IR measurements by the cooperation partner of subproject A1 (Lea Klauke and Michael Kampferbeck).

Ligand exchange

The ligand exchange of the oleic acid substituted with PA_{AcAc} was carried out by Lea Klauke (subproject A1) and conducted in chloroform. The nanoparticles were precipitated with acetone (1:1 vol.), centrifugated (10000 G, 8 min), and redispersed in chloroform to form a colloidal solution (10–20 mg mL^{-1}). A solution of PA_{AcAc} ligand in chloroform was prepared, and the amount was calculated to a 5 to 6 times excess of the amount, which is necessary to form a monolayer of PA_{AcAc} on iron oxide nanoparticles (size depending). The weight in masses and volumes are shown in **Table 7**. Afterward, the prepared nanoparticle dispersion and the e PA_{AcAc} solution were mixed overnight.

Table 7: Masses and volumes used for the ligand exchange of PA_{AcAc}.

Nanoparticle size [nm], shape	Nanoparticle mass [mg]	Desired PA_{AcAc} excess	PAAcAc [mg]	Total solvent volume [mL]
12, cubes	1100	6	966.7	120
18, cubes	230	1	39.3	11

After the exchange, the nanoparticles were precipitated with methanol, centrifugated (12000 G, 10 min), and redispersed in chloroform to remove the excess ligands. The

washing steps were repeated several times until the organic fraction of the ligand was constant in TGA measurements.

Synthesis of the iron-oxide nanocomposites

The iron-oxide nanoparticles were obtained in chloroform solutions with a concentration of 14–16 mg mL^{-1}. The solution was dried until a concentration of 100 mg mL^{-1} was reached, and the vitrimer monomers were added to the solution. The ratio of inorganic particles to vitrimer and the respective R-value changed according to the synthesized composites and is shown in **Table 8**.

Table 8: Masses and volumes used for the composite materials.

Nanoparticle size [nm], shape	Vitrimer	R-value	Wt% Inorganic
12, cubes	VU-EG$_{J403}$	0.75	70
18, cubes	VU-GL$_{DAO}$	0.75	10
15 nm spheres, 200–400 nm cluster	VU-EG$_{J403}$	0.75	50

As soon as a homogeneous, vitrimer-composite-gel was obtained, the gel was filled onto a Teflon sheet and cured for 24 h at 100 °C in vacuo (oil pump) to ensure complete conversion and the removal of the remaining reaction water. Next, the samples were pressed for 5–10 min at 130 °C into a 1 mm thick film.

6.5.1.9 Nacre-inspired Polymer-ceramic Composites

α-alumina platelets with d50 = 2 μm and thickness of ~0.04 μm (determined by supplier), resulting in an aspect ratio of ~50, were purchased from Kinsei Matec Co., LTD (Japan). The functionalization of the alumina platelets with the APTMS-ligand was carried out according to the procedure of G. Pandey *et al.*[176] and A. Yamaguchi *et al.*[177] and delivered by subproject A6. The provided ethanolic APTMS-alumina solution was dried until a viscous mass was obtained (1/3 of the total monomer mass ethanol). The ratio of inorganic

particles to polymer was set to 40:60 wt%, as carried out in 4d printing as well. GL_{AcAc} was prepared according to the synthesis route in chapter 6.5.1.1 with a conversion of 90%. GL_{AcAc} (2.0 g, 5.8 mmol) and OE (1.61 g, 10.9 mmol) were added to the solution under constant stirring (R = 0.8). As soon as a homogeneous, opaque and cross-linked mass was obtained, the vitrimer-composite-gel was filled onto a Teflon sheet and cured for 24 h at 100 °C in vacuo (oil pump) in order to ensure complete conversion and the removal of the remaining reaction water. Next, the samples were pressed for 5–10 min at 150 °C into a 1 mm thick film. The pure matrix vitrimer was synthesized by the same synthetic route.

6.5.1.10   Instrumentation

Nuclear magnetic resonance: ^{1}H NMR and ^{13}C NMR (DEPTQ-135) spectra were recorded on a Bruker AVANCEII (Bruker BioSpin GmbH, Ettlingen, Germany) at 300 or 600 MHz with deuterated dimethylsulfoxide (DMSO-*d6*) as a solvent. Sample concentrations were between 20–40 mg mL^{-1}, and measurements were recorded at 298 K. Data processing was carried out with MestReNova (Version 14.1.0, Mestrelab Research S.L., Santiago de Compostela, Spain).

Mass spectrometry (MS): Electrospray ionization (ESI) was measured on an Agilent 6224 ESI-TOF device coupled with an Agilent HPLC 1200 Series and direct injection (110–3200 m/z). Electron ionization (EI-DIP) was measured on a Thermo ISQ LT EI device coupled with a Thermo Trace 1300 and direct injection (40–800 m/z). Data processing was carried out by MestReNova (Version 14.1.0, Mestrelab Research S.L., Santiago de Compostela, Spain).

Attenuated Total Reflection-Fourier Transformation Infrared (ATR-FT-IR): Spectra were recorded on a Bruker FT-IR Vertex 70 (Bruker BioSpin GmbH, Ettlingen, Germany) with a diamond ATR-probe. All samples were measured in the range of 4000–600 cm^{-1} with a resolution of 2 cm^{-1} and 32 scans. Measurements and data processing was carried out with Opus 8.7.

Thermogravimetric analysis (TGA): A TG 209 F1 Libra (NETZSCH-Gerätebau GmbH, Selb, Germany) was used to determine the mass loss during heat treatment. A temperature range of 25–600 °C with a heating rate of 10 K min^{-1} under ambient atmosphere (oxygen) was used with a flow rate of 20 mL min^{-1}. About 5–10 mg of polymer was weighed into a ceramic crucible. Data processing was performed with Proteus analysis 8.0.3 (NETZSCH-Gerätebau GmbH, Selb, Germany).

Differential scanning calorimetry (DSC): A differential scanning calorimeter DSC 204 F1 Phoenix (NETZSCH-Gerätebau GmbH, Selb, Germany) was used. 5–10 mg polymer was weighed into an aluminum crucible. The measurements were performed in nitrogen atmosphere with a flow rate of 20 mL min^{-1} in the temperature range between (-50)–180 °C. The heating and cooling rates were set to 10 K min^{-1} and the thermal properties were analyzed using the DSC data of the second and third heating curve. Data processing was performed by Proteus analysis 8.0.3 (NETZSCH-Gerätebau GmbH, Selb, Germany).

Dynamic-mechanical analysis (DMA): For oscillatory and step shear experiments, a rotational rheometer MCR 502 (Anton Paar GmbH, Graz, Austria) with an 8 mm plate-plate geometry and a heat chamber with a flooded nitrogen atmosphere was used. The temperature was controlled by a Peltier plate. The gap between the lower and the upper plate was usually set to 1 mm, and a normal force of 1 N was applied. Amplitude sweeps were carried out between 0.001% and 30% shear strain (γ) at a constant angular frequency (ω) of 10 rad s^{-1} at 100 °C. This should ensure that the chosen strain amplitude γ_0 was within the linear viscoelastic regime, so that the storage modulus G$^{'}$ and the loss modulus G$^{''}$ were independent of strain. Frequency sweeps were carried out between 0.001 Hz and 100 Hz angular frequency (ω) at a constant shear strain (γ) of 0.1% at 100 °C. Temperature-dependent measurements were usually carried out with an angular frequency of 10 rad s^{-1} at a constant shear strain of 0.1% in the temperature range of 0–160 °C. Stress relaxation experiments were carried out with a shear strain of 1%, and the relaxation modulus was recorded as a function of time in the temperature range of 90–160 °C. Data processing was performed by RheoCompass 1.30 (Anton Paar GmbH, Graz, Austria). Specimens for the DMA were pushed out with an 8 mm punch. The vitrimer

films were previously placed in a drying chamber at 100 °C for 1 minute in order to heat them above the glass transition temperature to prevent splintering during processing.

Tensile test: Stress-strain curves were recorded at room temperature (20 °C) on a universal testing machine type Z020 (Zwick Roell GmbH & Co. KG, Ulm, Germany) using a 5 kN load cell. The measurements were carried out in accordance with the test standard DIN EN ISO 527-1. The initial force was 0.1 MPa, and the clamping length was 13.24 mm. The elastic modulus was determined at a speed of 1 mm min^{-1} (0.025–0.2%) and the test speed was carried out at 10 mm min^{-1}. Data processing was performed by TestXpert *II V3.71*. The test specimens for the tensile test were punched out with a cutting press type ZCP020 (Zwick Roell). The attachment was used for test specimens of type 5B (according to DIN EN ISO 527-2). The vitrimer films were placed in a drying cabinet at 100 °C for one minute in order to heat them above the glass transition temperature, to prevent splintering during processing.

Powder X-Ray diffraction (XRD) measurements were conducted on a Panalytical MPD X`Pert Pro (Malvern Panalytical, Malvern, Great Britain) with Cu Kα radiation (λ_1 = 1.5405980 Å, λ_2 = 1.5444260 Å) at a scan step size of 0.0131°.

Scanning electron microscopy (SEM) images were recorded on a LEO Gemini 1550 (Carl Zeiss, Oberkochen, Germany). Secondary electrons were detected with an Everhart-Thornley detector, operating with 1–5 kV and 50–100 pA.

Optical microscope images were recorded with a Zeiss AX10 Observer A1 (Carl Zeiss, Oberkochen, Germany) microscope with EC EPIPLAN 10x/0.2 HD and EC EPIPLAN 20x/0.2 HD lenses.

Elemental analysis was carried out on a CHN-Element analyzer Vario EL III (Fa. Elementar Analysensysteme GmbH, Langenselbold, Germany).

Nanoindentation was performed in an Agilent Nano Indenter G200 (Agilent, USA) system using the continuous stiffness measurement method, with a constant strain target of 0.05 s^{-1}, a harmonic displacement target of 2 nm, and a harmonic frequency of 45 Hz. The system was equipped with a Berkovich tip. A number of 30 indents per sample were performed. The nanoindenter conducted the measurements in displacement-control mode. After the desired indentation depth was reached, the load was held constant for 10 s before withdrawing the tip from the sample.

7   Discussion

This work presents several approaches in terms of the base reaction behavior and the thermomechanical properties of vinylogous urethane vitrimers and composites. The goal was to build an in-depth understanding of this type of vitrimer and further optimize it for the usage of smart, recyclable materials.

Various influences on the polymerization and exchange rate were investigated and gave a detailed insight for the development of the next vitrimer generations. Within three publications and unpublished results, numerous different vitrimers were explored to determine the influence of synthetic parameters on the cross-linking chemistry, the mechanical properties and, in particular, the reprocessability of the vitrimers. Factors such as the stereoisomerism of the vinylogous urethane bond in different solvents, the use of different acetoacetate to amine ratios, catalysts, different monomers with respect to the backbone and the nucleophilicity of the amine, cross-linking densities and additional heteroatoms in the network were explored (publication 1, chapter 6.3). Through in-depth characterization of these networks, crucial trends and correlations were identified. In particular, heteroatoms in the monomer backbone, a high excess of amines, highly nucleophilic amines, a high concentration of functional groups, low cross-linking densities, the use of long-chained monomers and the use of catalysts were identified as accelerating factors for the transamination exchange reaction. Especially the choice of the amine is a crucial factor since sterically hindered primary amines (*e.g.,* Jeffamines[®] or 1,8-diamino-*p*-menthan) demonstrated a lower nucleophilicity and, therefore, lower exchange rates than terminal primary amines.

In addition, a one-pot bulk polymerization to obtain vinylogous urea vitrimers derived from only amines was developed and offered a great alternative to the widely used and researched vinylogous urethane vitrimers by showing similar properties (chapter 6.3.6).

The choice of solvents and raw materials was led by a strong focus on utilizing bio-based, non-toxic alternative substances to improve and simplify the established synthetic routes to reduce the carbon footprint and enhance the applicability.

To mention some disadvantages of vitrimers, it has to be noted that vinylogous urethane vitrimers contain a high amount of free primary amine groups. Primary amines undergo oxidation reactions at elevated temperatures, which is the main reason for the yellowish

color of the materials and may limit the infinite reprocessability due to this side reaction. Moreover, many amines are toxic, and truly bio-based and non-toxic amines can rarely be found, limiting the range of green and price-compatible applications. However, the advantages of this type of vitrimer are the catalyst-free, fast proceeding exchange reactions, the large availability of (bio-based) alcohols for acetoacetate monomers, and the prospect of a growing field of industrial, bio-based production methods of amines, *e.g.* cadaverine and putrescin.

Epoxy resins are used for many applications due to their easy handling and outstanding properties in terms of chemical resistance and mechanical properties. Moreover, epoxy resins are often used in combination with fibers to obtain composite materials such as wind turbine blades, boats, airplanes, constructions, and many more. The benefit of composites is their lightweight in combination with good flexibility and fracture toughness while maintaining high strength. However, the many advantages cannot outweigh the fact that these highly cross-linked, epoxy resins cannot be recycled very well. Therefore, recyclable alternatives that maintain the unique properties and handling of epoxy resins are of great importance in achieving a circular economy.

This work showed that typical raw alcohols used for epoxy resins could be likewise acetoacetylated and cured with primary amines to give vinylogous urethane/urea vitrimers (Publication 2). The materials exhibited not the same but comparable properties to epoxy resins derived from similar backbones, with the benefit that vitrimers are fully recyclable. Moreover, it was shown that these acetoacetylated monomers could be likewise implemented into epoxy resins. The liquid acetoacetate and epoxy monomers were easily mixed to a homogeneous blend and then cured with amines, while the curing occurred in a reasonable time frame at room temperature, as known from typical epoxy resins. With this, epoxy-vitrimer co-networks with 70 mol% (67 wt%) initial epoxy groups were prepared (chapter 6.5.1.5). Comparing the mechanical properties, the vipoxy exhibited properties by mainly following a rule of mixtures and showed values between the range of the pure networks (T_g, stress-relaxation, tensile test). Nevertheless, the overall thermomechanical properties of all the compared materials were quite comparable, with the benefit that the vitrimer and the vipoxy networks showed full stress-relaxation and were, therefore, reprocessable. Further experiments can clarify the limits regarding the cross-linking density, the maximum amount of epoxy resin, and the excess

of amines. These findings offer future potential for the use of vitrimers, or the partly implementation of covalent dynamic bonds into established thermosetting materials, *e.g.* epoxy resins, and turn them into recyclable/reprocessable materials while maintaining their excellent thermomechanical and physical properties.

The preparation of porous vitrimer films aimed to investigate *D*-glucose as a suitable reactant for green vinylogous urethane vitrimers and explore the condensation reaction of acetoacetylated glucose with different bio-based and fossil amines (Chapter 6.3.5). Moreover, different synthetic routes were established, enabling the synthesis of vinylogous urethanes in water and exploring the possibility of producing porous vitrimer films by sintering precipitated vinylogous urethane fragments. Porous, water-permeable materials offer possible applications to separate/clean water from oil, dirt, bacteria, capturing metals (*e.g.,* lithium), and many more. The benefit of using vitrimers for such applications is that the porous structure can be achieved by simple sintering of cross-linked polymer fragments, which is not possible with common thermosets or elastomers. The fragments slowly react at the touching points and form a cross-linked, porous network. Moreover, vitrimers offer mechanical and chemical recycling routes, which enable reprocessing, purifying, or re-usage of the dense films and porous materials (*e.g.* when pores are filled).

Composites represent an important class of materials used in many fields requiring high-performance materials. These composites are by no means only man-made, but nature also produces incredibly strong composites, which researchers are using as a guide nowadays. Examples are natural hybrid materials like nacre, cuttlebone, or bones. Moreover, composites are used in numerous future-oriented applications, *e.g.*, rotor blades consisting of glass fiber-reinforced epoxy resins, balsa wood, copper, iron and lacquers. The benefit of composites is their lightweight in combination with good flexibility and fracture toughness while maintaining a high strength. However, the many advantages cannot outweigh the fact that these highly cross-linked, artificial materials cannot be recycled very well, which is increasingly causing environmental problems, leading to wasted resources and scarcity. Using vitrimers represents one possible solution and offers several chemical or mechanical recycling methods. Nevertheless, complicated and costly separation methods cannot be totally excluded. Moreover, most of the recent

studies only face small scales and did not take into consideration the challenges of bigger scales in applied materials and industry. Properties such as impact resistance, correction of gauche defects, polymerization and gelation rates, or standard production methods were rarely investigated. Studies in these fields will follow up soon and can show the real potential of vitrimers for widespread and large-scale high-performance materials and their possible use in a circular economy.

This work shows several approaches in terms of combining vitrimers with organic and inorganic fillers, some of which represent hierarchical, supramolecular structures. The final goal was to mimic nature's complex structures, while the focus was first to take partial steps in the development and combination of individual hierarchical levels of the complex, hierarchical composite.

Vitrimer-composites of biodegradable polymer-polymer composites with starch (publication 3), nacreous inorganic-organic composites with alumina oxide (chapter 6.4.2), and magnetic inorganic-organic nanocomposites with iron-oxide particles (chapter 6.4.1) were prepared. Moreover, a phosphonic acid ligand, bearing an acetoacetate group, was developed and used to bind the interface of iron-oxide nanoparticles to the vitrimers. It was found that the mechanical properties of the composites, *e.g.* the elastic moduli and tensile strengths, significantly increased while maintaining the characteristic reprocessability of the vitrimers. Furthermore, it was shown that the particles could be aligned within the material by heat compression, enabling a solid-state postmodification within the anisotropic material. Magnetic, elastomeric or thermosetting composites, on the other hand, offer potential opportunities in the fields of high-performance sensors or robotic technologies. Furthermore, the first hierarchical vitrimer composites were successfully synthesized by using iron-oxide nanoparticle clusters.

Nevertheless, it must be noted that the preparation of a hierarchical structure with a well-defined periodic structure on several hierarchical levels from the nano to the microscale is a very demanding task and was not ultimately achieved in this work. The in here presented composite materials showed hierarchical elements, but the particles, cluster or supramolecular structures were mostly randomly distributed in a vitrimer matrix and more work must be done to embed the fillers in a very defined manner. However, several steps from the synthesis of the linker-ligand, the matrix vitrimers, nanoparticles, nanoparticle clusters and homogeneous composite materials with a high load of single

nanoparticles were achieved. The materials showed astonishing properties in terms of mechanical properties, high cross-linking densities combined with fast reprocessing rates.

7.1   Outlook

For an overview, this chapter describes further research topics, applications, and cooperations in a dense format. The publications and unpublished results increased the understanding of various influences on the properties of vitrimer networks. Especially, the knowledge about polymerization rates, reprocessability, and thermomechanical properties can be adapted to prepare second-generation, fast reprocessable materials using the provided toolbox. Nevertheless, the desired properties are strongly dependent on the aspired application. For a robust, rigid and reprocessable network, the amine should show a high nucleophilicity and the amine groups should appear in a close spatial arrangement of 2–4 CH_2 groups, which enables fast transamination reaction. Using a di- and triamine with short chains leads to a high cross-linking density and usually a high brittleness. For this reason, the acetoacetate monomer should be flexible, soft and contain linear chains. In addition, heteroatoms, *e.g.,* ether or tertiary amines in the backbone, accelerate the exchange rates and can lower the activation energy. For an application where a slow polymerization rate is necessary (*e.g.,* infiltration, spouted bed) the acetoacetate should be adjusted by a longer linear chain length, which slows down the polymerization by simply lowering the concentration of the functional groups. Moreover, adding a weak base can also slow down the reaction, while the amount should be well controlled to prevent side reactions. The glass transition temperature and the mechanical properties can be chosen in a broad range and adjusted for several synthetic procedures and processing routes like 3D-printing, infiltration method, and spouted bed granulation. Cooperations in this field have been already started and can be continued in a promising manner. In this context, the use of epoxy-vitrimers (vipoxy), as a substitute for conventional resins is a highly relevant topic for current challenges in research and industry. Especially, the recyclability of fiber composites such as rotor blades is of major interest to the industry due to the enormous recycling problems with these cross-linked composites.

In addition, this work showed promising green protocols by using bio-based raw materials and water as a solvent, which reduce the carbon footprint and lead to materials with good thermomechanical properties. Starch was used as a reinforcing, cross-linking agent, while likewise the acetoacetylation of other biopolymers and supramolecular networks has been shown. Implementing these structures into a bio-based, metabolizable vitrimer matrix gives the perspective for further resilient and strong bio-based and/or biodegradable

materials. Likewise, porous vitrimers films were developed in this scope, which can carry functional units like crown ethers, silver particles, magnetic particles, or other units as a functional filter for different applications. The benefit is the reprocessability to regain and reactivate blocked pores of the films.

Magnetic composites can be used for sensors, robotics or highly resilient performance materials with outstanding strength and toughness. Using vitrimers enabled a thermally induced solid-state rearrangement of the particles inside the matrix, allowing an alignment as postmodification. Moreover, aligning magnetic nano-particles in a magnetic field might be possible, which gives the basis for magneto-mechanical responsive composites. Anisotropic particles, *e.g.* alumina oxide platelets or nanoparticle clusters, can be aligned to nacre-like structures and the properties investigated in terms of the resulting anisotropic composite material. The layered structure mimics natural solid materials and can enable outstanding composites with high mechanical strength and fracture toughness.

8   References

(1) Baekeland, L. H. The synthesis, constitution, and uses of Bakelite. *Industrial & Engineering Chemistry* **1909**, *1* (3), 149-161.

(2) Grellmann, W.; Seidler, S. *Polymer testing*; Carl Hanser Verlag GmbH Co KG, 2022.

(3) Patterson, G. D. Materia Polymerica: Bakelite. In *100+ Years of Plastics. Leo Baekeland and Beyond*, ACS Symposium Series, Vol. 1080; American Chemical Society, 2011; pp 21-29.

(4) Brydson, J. A. *Plastics materials*; Elsevier, 1999.

(5) Geyer, R.; Jambeck, J. R.; Law, K. L. Production, use, and fate of all plastics ever made. *Science Advances* **2017**, *3* (7), 1700782.

(6) Krishnakumar, B.; Pucci, A.; Wadgaonkar, P. P.; Kumar, I.; Binder, W. H.; Rana, S. Vitrimers based on bio-derived chemicals: Overview and future prospects. *Chemical Engineering Journal* **2022**, *433*, 133261.

(7) Koltzenburg, S.; Maskos, M.; Nuyken, O.; Mülhaupt, R. *Polymere: Synthese, Eigenschaften und Anwendungen*; Springer, 2014.

(8) Olabisi, O.; Adewale, K. *Handbook of thermoplastics*; CRC press, 2016.

(9) Williams, R. J. *Thermosetting Polymers*; 2002.

(10) McNaught, A. D.; Wilkinson, A. *Compendium of chemical terminology*; Blackwell Science Oxford, 1997.

(11) Winne, J. M.; Leibler, L.; Du Prez, F. E. Dynamic covalent chemistry in polymer networks: a mechanistic perspective. *Polymer Chemistry* **2019**, *10* (45), 6091-6108.

(12) Yang, L.; Tan, X.; Wang, Z.; Zhang, X. Supramolecular polymers: historical development, preparation, characterization, and functions. *Chemical reviews* **2015**, *115* (15), 7196-7239.

(13) Wasserfall, L. Synthesis and characterization of vinylogous urethane vitrimers. Universität Hamburg, 2019 (unpublished).

(14) Burattini, S.; Greenland, B. W.; Merino, D. H.; Weng, W.; Seppala, J.; Colquhoun, H. M.; Hayes, W.; Mackay, M. E.; Hamley, I. W.; Rowan, S. J. A Healable Supramolecular Polymer Blend Based on Aromatic π−π Stacking and Hydrogen-Bonding Interactions. *Journal of the American Chemical Society* **2010**, *132* (34), 12051-12058.

(15) Lange, R.; Van, M. Gurp and EW Meijer. *J. Polym. Science: Part A,. Polym. Chem* **1999**, *37*, 3657-3670.

(16) Hilger, C.; Stadler, R. New multiphase thermoplastic elastomers by combination of covalent and association-chain structures. *Die Makromolekulare Chemie: Macromolecular Chemistry and Physics* **1990**, *191* (6), 1347-1361.

(17) Müller, M.; Dardin, A.; Seidel, U.; Balsamo, V.; Iván, B.; Spiess, H. W.; Stadler, R. Junction dynamics in telechelic hydrogen bonded polyisobutylene networks. *Macromolecules* **1996**, *29* (7), 2577-2583.

(18) Kunz, M. J.; Hayn, G.; Saf, R.; Binder, W. H. Hydrogen-bonded supramolecular poly (ether ketone) s. *Journal of Polymer Science Part A: Polymer Chemistry* **2004**, *42* (3), 661-674.

(19) Montarnal, D.; Capelot, M.; Tournilhac, F.; Leibler, L. Silica-like malleable materials from permanent organic networks. *Science* **2011**, *334* (6058), 965-968.

(20) Guerre, M.; Taplan, C.; Nicolaÿ, R.; Winne, J. M.; Du Prez, F. E. Fluorinated Vitrimer Elastomers with a Dual Temperature Response. *Journal of the American Chemical Society* **2018**, *140* (41), 13272-13284.

(21) Denissen, W.; De Baere, I.; Van Paepegem, W.; Leibler, L.; Winne, J.; Du Prez, F. E. Vinylogous urea vitrimers and their application in fiber reinforced composites. *Macromolecules* **2018**, *51* (5), 2054-2064.

(22) Schenk, V.; Labastie, K.; Destarac, M.; Olivier, P.; Guerre, M. Vitrimer composites: current status and future challenges. *Materials Advances* **2022**, *3* (22), 8012-8029.

(23) Haida, P.; Signorato, G.; Abetz, V. Blended vinylogous urethane/urea vitrimers derived from aromatic alcohols. *Polymer Chemistry* **2022**, *13* (7), 946-958.

(24) Krishnakumar, B.; Sanka, R. V. S. P.; Binder, W. H.; Parthasarthy, V.; Rana, S.; Karak, N. Vitrimers: Associative dynamic covalent adaptive networks in thermoset polymers. *Chemical Engineering Journal* **2020**, *385*, 123820.

(25) Zhang, H.; Cui, J.; Hu, G.; Zhang, B. Recycling strategies for vitrimers. *International Journal of Smart and Nano Materials* **2022**, *13* (3), 367-390.

(26) Zheng, J.; Png, Z. M.; Ng, S. H.; Tham, G. X.; Ye, E.; Goh, S. S.; Loh, X. J.; Li, Z. Vitrimers: Current research trends and their emerging applications. *Materials Today* **2021**, *51*, 586-625.

(27) Chen, F.; Gao, F.; Zhong, J.; Shen, L.; Lin, Y. Fusion of biobased vinylogous urethane vitrimers with distinct mechanical properties. *Materials Chemistry Frontiers* **2020**, *4* (9), 2723-2730.

(28) Ye, C.; Voet, V. S. D.; Folkersma, R.; Loos, K. Robust Superamphiphilic Membrane with a Closed-Loop Life Cycle. *Advanced Materials* **2021**, *33* (15), 2008460.

(29) Xu, H.; Wang, H.; Zhang, Y.; Wu, J. Vinylogous Urethane Based Epoxy Vitrimers with Closed-Loop and Multiple Recycling Routes. *Industrial & Engineering Chemistry Research* **2022**, *61* (48), 17524-17533.

(30) Taynton, P.; Yu, K.; Shoemaker, R. K.; Jin, Y.; Qi, H. J.; Zhang, W. Heat- or Water-Driven Malleability in a Highly Recyclable Covalent Network Polymer. *Advanced Materials* **2014**, *26* (23), 3938-3942.

(31) Kloxin, C. J.; Scott, T. F.; Adzima, B. J.; Bowman, C. N. Covalent Adaptable Networks (CANs): A Unique Paradigm in Cross-Linked Polymers. *Macromolecules* **2010**, *43* (6), 2643-2653.

(32) Engle, L.; Wagener, K. A review of thermally controlled covalent bond formation in polymer chemistry. *Journal of Macromolecular Science, Part C: Polymer Reviews* **1993**, *33* (3), 239-257.

(33) Esen, C.; Kumru, B. Photocatalyst-Incorporated Cross-Linked Porous Polymer Networks. *Industrial & Engineering Chemistry Research* **2022**, *61* (30), 10616-10630.

(34) Kamplain, J. W.; Bielawski, C. W. Dynamic covalent polymers based upon carbene dimerization. *Chemical communications* **2006**, (16), 1727-1729.

(35) Higaki, Y.; Otsuka, H.; Takahara, A. A thermodynamic polymer cross-linking system based on radically exchangeable covalent bonds. *Macromolecules* **2006**, *39* (6), 2121-2125.

(36) Craven, J. M. Cross-linked thermally reversible polymers produced from condensation polymers with pendant furan groups cross-linked with maleimides. Google Patents: 1969.

(37) Nagata, M.; Yamamoto, Y. Synthesis and characterization of photocrosslinked poly (ε-caprolactone) s showing shape-memory properties. *Journal of Polymer Science Part A: Polymer Chemistry* **2009**, *47* (9), 2422-2433.

(38) Lendlein, A.; Jiang, H.; Jünger, O.; Langer, R. Light-induced shape-memory polymers. *Nature* **2005**, *434* (7035), 879-882.

(39) Connal, L. A.; Vestberg, R.; Hawker, C. J.; Qiao, G. G. Fabrication of reversibly crosslinkable, 3-dimensionally conformal polymeric microstructures. *Advanced Functional Materials* **2008**, *18* (20), 3315-3322.

(40) Imai, Y.; Ogoshi, T.; Naka, K.; Chujo, Y. Formation of IPN organic-inorganic polymer hybrids utilizing the photodimerization of thymine. *Polymer bulletin* **2000**, *45*, 9-16.

(41) Pezron, E.; Ricard, A.; Leibler, L. Rheology of galactomannan-borax gels. *Journal of Polymer Science Part B: Polymer Physics* **1990**, *28* (13), 2445-2461.

(42) Belowich, M. E.; Stoddart, J. F. Dynamic imine chemistry. *Chemical Society Reviews* **2012**, *41* (6), 2003-2024.

(43) Skene, W. G.; Lehn, J.-M. P. Dynamers: polyacylhydrazone reversible covalent polymers, component exchange, and constitutional diversity. *Proceedings of the National Academy of Sciences* **2004**, *101* (22), 8270-8275.

(44) Chakma, P.; Digby, Z. A.; Shulman, M. P.; Kuhn, L. R.; Morley, C. N.; Sparks, J. L.; Konkolewicz, D. Anilinium salts in polymer networks for materials with mechanical stability and mild thermally induced dynamic properties. *ACS Macro Letters* **2019**, *8* (2), 95-100.

(45) Denissen, W.; Winne, J. M.; Du Prez, F. E. Vitrimers: permanent organic networks with glass-like fluidity. *Chemical Science* **2016**, *7* (1), 30-38.

(46) Dyre, J. C. Colloquium: The glass transition and elastic models of glass-forming liquids. *Reviews of modern physics* **2006**, *78* (3), 953.

(47) Angell, C. A. Formation of glasses from liquids and biopolymers. *Science* **1995**, *267* (5206), 1924-1935.

(48) Van Zee, N. J.; Nicolaÿ, R. Vitrimer Chemistry and Applications. In *Macromolecular Engineering*, pp 1-38.

(49) Urbain, G.; Bottinga, Y.; Richet, P. Viscosity of liquid silica, silicates and alumino-silicates. *Geochimica et cosmochimica acta* **1982**, *46* (6), 1061-1072.

(50) Plazek, D. J.; O'Rourke, V. M. Viscoelastic behavior of low molecular weight polystyrene. *Journal of Polymer Science Part A-2: Polymer Physics* **1971**, *9* (2), 209-243.

(51) Elling, B. R.; Dichtel, W. R. Reprocessable Cross-Linked Polymer Networks: Are Associative Exchange Mechanisms Desirable? *ACS Central Science* **2020**, *6* (9), 1488-1496.

(52) Guerre, M.; Taplan, C.; Winne, J. M.; Du Prez, F. E. Vitrimers: directing chemical reactivity to control material properties. *Chemical Science* **2020**, *11* (19), 4855-4870.

(53) Hajikarimi, P.; Moghadas Nejad, F. Chapter 3 - Mechanical models of viscoelasticity. In *Applications of Viscoelasticity*, Hajikarimi, P., Moghadas Nejad, F. Eds.; Elsevier, 2021; pp 27-61.

(54) Mezger, T. *Das Rheologie Handbuch: Für Anwender von Rotations-und Oszilla-tions-Rheometern. 5., vollständig überarbeitete Auflage*; 2016.

(55) Denissen, W.; Rivero, G.; Nicolaÿ, R.; Leibler, L.; Winne, J. M.; Du Prez, F. E. Vinylogous urethane vitrimers. *Advanced Functional Materials* **2015**, *25* (16), 2451-2457.

(56) Taplan, C.; Guerre, M.; Winne, J. M.; Du Prez, F. E. Fast processing of highly crosslinked, low-viscosity vitrimers. *Materials Horizons* **2020**, *7* (1), 104-110.

(57) Stern, M.; Tobolsky, A. Stress-time-temperature relations in polysulfide rubbers. *Rubber Chemistry and Technology* **1946**, *19* (4), 1178-1192.

(58) Osthoff, R.; Bueche, A.; Grubb, W. Chemical stress-relaxation of polydimethylsiloxane elastomers1. *Journal of the American Chemical Society* **1954**, *76* (18), 4659-4663.

(59) Tobolsky, A. V. Stress relaxation studies of the viscoelastic properties of polymers. *Journal of Applied Physics* **1956**, *27* (7), 673-685.

(60) Sperling, L. H.; Cooper, S. L.; Tobolsky, A. V. Elastomeric and mechanical properties of poly-m-carboranylenesiloxanes. *Journal of Applied Polymer Science* **1966**, *10* (11), 1725-1735.

(61) Lee, T.; Sperling, L.; Tobolsky, A. Thermal stability of elastomeric networks at high temperatures. *Journal of Applied Polymer Science* **1966**, *10* (12), 1831-1836.

(62) Demongeot, A.; Mougnier, S.; Okada, S.; Soulié-Ziakovic, C.; Tournilhac, F. Coordination and catalysis of Zn2+ in epoxy-based vitrimers. *Polymer Chemistry* **2016**, *7* (27), 4486-4493.

(63) Self, J. L.; Dolinski, N. D.; Zayas, M. S.; Read de Alaniz, J.; Bates, C. M. Brønsted-acid-catalyzed exchange in polyester dynamic covalent networks. *ACS Macro Letters* **2018**, *7* (7), 817-821.

(64) Altuna, F. I.; Pettarin, V.; Williams, R. J. Self-healable polymer networks based on the cross-linking of epoxidised soybean oil by an aqueous citric acid solution. *Green Chemistry* **2013**, *15* (12), 3360-3366.

(65) Cromwell, O. R.; Chung, J.; Guan, Z. Malleable and self-healing covalent polymer networks through tunable dynamic boronic ester bonds. *Journal of the American Chemical Society* **2015**, *137* (20), 6492-6495.

(66) Nishimura, Y.; Chung, J.; Muradyan, H.; Guan, Z. Silyl ether as a robust and thermally stable dynamic covalent motif for malleable polymer design. *Journal of the American Chemical Society* **2017**, *139* (42), 14881-14884.

(67) Delahaye, M.; Winne, J. M.; Du Prez, F. E. Internal catalysis in covalent adaptable networks: phthalate monoester transesterification as a versatile dynamic cross-linking chemistry. *Journal of the American Chemical Society* **2019**, *141* (38), 15277-15287.

(68) Martin, R.; Rekondo, A.; de Luzuriaga, A. R.; Cabañero, G.; Grande, H. J.; Odriozola, I. The processability of a poly (urea-urethane) elastomer reversibly crosslinked with aromatic disulfide bridges. *Journal of Materials Chemistry A* **2014**, *2* (16), 5710-5715.

(69) Chen, Y.; Tang, Z.; Liu, Y.; Wu, S.; Guo, B. Mechanically robust, self-healable, and reprocessable elastomers enabled by dynamic dual cross-links. *Macromolecules* **2019**, *52* (10), 3805-3812.

(70) Spiesschaert, Y.; Taplan, C.; Stricker, L.; Guerre, M.; Winne, J. M.; Du Prez, F. E. Influence of the polymer matrix on the viscoelastic behaviour of vitrimers. *Polymer Chemistry* **2020**, *11* (33), 5377-5385.

(71) Wang, S.; Ma, S.; Li, Q.; Yuan, W.; Wang, B.; Zhu, J. Robust, fire-safe, monomer-recovery, highly malleable thermosets from renewable bioresources. *Macromolecules* **2018**, *51* (20), 8001-8012.

(72) Hendriks, B.; Waelkens, J.; Winne, J. M.; Du Prez, F. E. Poly (thioether) vitrimers via transalkylation of trialkylsulfonium salts. *ACS Macro Letters* **2017**, *6* (9), 930-934.

(73) Obadia, M. M.; Mudraboyina, B. P.; Serghei, A.; Montarnal, D.; Drockenmuller, E. Reprocessing and recycling of highly cross-linked ion-conducting networks through

transalkylation exchanges of C–N bonds. *Journal of the American Chemical Society* **2015**, *137* (18), 6078-6083.

(74) Witzeman, J. S.; Nottingham, W. D. Transacetoacetylation with tert-butyl acetoacetate: synthetic applications. *The Journal of Organic Chemistry* **1991**, *56* (5), 1713-1718.

(75) Carroll, M. F.; Bader, A. R. The Reactions of Diketene with Ketones1. *Journal of the American Chemical Society* **1953**, *75* (21), 5400-5402.

(76) Clemens, R. J.; Hyatt, J. A. Acetoacetylation with 2, 2, 6-trimethyl-4H-1, 3-dioxin-4-one: a convenient alternative to diketene. *The Journal of Organic Chemistry* **1985**, *50* (14), 2431-2435.

(77) Ruggiero, S. J.; Luaces, V.-M. Determination of the equilibrium constant for keto-enol tautomerism of ethyl acetoacetate. *Journal of Chemical Education* **1988**, *65* (7), 629.

(78) Moriyasu, M.; Kato, A.; Hashimoto, Y. Kinetic studies of fast equilibrium by means of high-performance liquid chromatography. Part 11. Keto–enol tautomerism of some β-dicarbonyl compounds. *Journal of the Chemical Society, Perkin Transactions 2* **1986**, (4), 515-520.

(79) Ward, C. Keto-enol tautomerism of ethyl acetoacetate: Experiment in homogeneous equilibrium. *Journal of Chemical Education* **1962**, *39* (2), 95.

(80) Folkendt, M. M.; Weiss-Lopez, B. E.; Chauvel Jr, J. P.; True, N. S. Gas-phase proton NMR studies of keto-enol tautomerism of acetylacetone, methyl acetoacetate, and ethyl acetoacetate. *The Journal of Physical Chemistry* **1985**, *89* (15), 3347-3352.

(81) Martínez, R. F.; Ávalos, M.; Babiano, R.; Cintas, P.; Jiménez, J. L.; Light, M. E.; Palacios, J. C. Tautomerism in Schiff bases. The cases of 2-hydroxy-1-naphthaldehyde and 1-hydroxy-2-naphthaldehyde investigated in solution and the solid state. *Organic & Biomolecular Chemistry* **2011**, *9* (24), 8268-8275.

(82) Ahlbrecht, H. Zum problem der imin-enamin-tautomerie. *Tetrahedron Letters* **1968**, *9* (42), 4421-4424.

(83) Clark, R. A.; Parker, D. C. Imine-enamine tautomerism. I. 2-(N-Cyclohexylimino)-1, 3-diphenylpropane. *Journal of the American Chemical Society* **1971**, *93* (26), 7257-7261.

(84) Shin, C.-g.; Masaki, M.; Ohta, M. The Independent Isolation of a Primary Enamine and the Tautomeric Imine. *Bulletin of the Chemical Society of Japan* **1971**, *44* (6), 1657-1660.

(85) Scheutz, G. M.; Lessard, J. J.; Sims, M. B.; Sumerlin, B. S. Adaptable crosslinks in polymeric materials: resolving the intersection of thermoplastics and thermosets. *Journal of the American Chemical Society* **2019**, *141* (41), 16181-16196.

(86) Denissen, W.; Droesbeke, M.; Nicolaÿ, R.; Leibler, L.; Winne, J. M.; Du Prez, F. E. Chemical control of the viscoelastic properties of vinylogous urethane vitrimers. *Nature communications* **2017**, *8* (1), 14857.

(87) Wright, T.; Tomkovic, T.; Hatzikiriakos, S. G.; Wolf, M. O. Photoactivated Healable Vitrimeric Copolymers. *Macromolecules* **2019**, *52* (1), 36-42.

(88) Lessard, J. J.; Scheutz, G. M.; Hughes, R. W.; Sumerlin, B. S. Polystyrene-based vitrimers: inexpensive and recyclable thermosets. *ACS Applied Polymer Materials* **2020**, *2* (8), 3044-3048.

(89) Lessard, J. J.; Garcia, L. F.; Easterling, C. P.; Sims, M. B.; Bentz, K. C.; Arencibia, S.; Savin, D. A.; Sumerlin, B. S. Catalyst-free vitrimers from vinyl polymers. *Macromolecules* **2019**, *52* (5), 2105-2111.

(90) Chinthapalli, R.; Skoczinski, P.; Carus, M.; Baltus, W.; de Guzman, D.; Käb, H.; Raschka, A.; Ravenstijn, J. Biobased building blocks and polymers—global capacities, production and trends, 2018–2023. *Industrial Biotechnology* **2019**, *15* (4), 237-241.

(91) Lucherelli, M. A.; Duval, A.; Avérous, L. Biobased vitrimers: towards sustainable and adaptable performing polymer materials. *Progress in Polymer Science* **2022**, 101515.

(92) Geyer, R.; Jambeck, J. R.; Law, K. L. Production, use, and fate of all plastics ever made. *Science advances* **2017**, *3* (7), e1700782.

(93) Mohanty, A.; Misra, M. a.; Hinrichsen, G. Biofibres, biodegradable polymers and biocomposites: An overview. *Macromolecular materials and Engineering* **2000**, *276* (1), 1-24.

(94) Vink, E. T.; Rábago, K. R.; Glassner, D. A.; Springs, B.; O'Connor, R. P.; Kolstad, J.; Gruber, P. R. The sustainability of NatureWorks™ polylactide polymers and Ingeo™ polylactide fibers: an update of the future. *Macromolecular Bioscience* **2004**, *4* (6), 551-564.

(95) Oliveira, C. C.; Rochedo, P. R.; Bhardwaj, R.; Worrell, E.; Szklo, A. Bio-ethylene from sugarcane as a competitiveness strategy for the Brazilian chemical industry. *Biofuels, Bioproducts and Biorefining* **2020**, *14* (2), 286-300.

(96) Furtwengler, P.; Avérous, L. Renewable polyols for advanced polyurethane foams from diverse biomass resources. *Polymer Chemistry* **2018**, *9* (32), 4258-4287.

(97) Vidil, T.; Llevot, A. Fully Biobased Vitrimers: Future Direction toward Sustainable Cross-Linked Polymers. *Macromolecular Chemistry and Physics* **2022**, *223* (13), 2100494.

(98) Lligadas, G.; Ronda, J. C.; Galia, M.; Cadiz, V. Renewable polymeric materials from vegetable oils: a perspective. *Materials today* **2013**, *16* (9), 337-343.

(99) Mutlu, H.; Meier, M. A. Castor oil as a renewable resource for the chemical industry. *European Journal of Lipid Science and Technology* **2010**, *112* (1), 10-30.

(100) Galià, M.; de Espinosa, L. M.; Ronda, J. C.; Lligadas, G.; Cádiz, V. Vegetable oil-based thermosetting polymers. *European journal of lipid science and technology* **2010**, *112* (1), 87-96.

(101) Llevot, A. Sustainable synthetic approaches for the preparation of plant oil-based thermosets. *Journal of the American Oil Chemists' Society* **2017**, *94*, 169-186.

(102) Savaliya, M. L.; Dhorajiya, B. D.; Dholakiya, B. Z. Current trends in separation and purification of fatty acid methyl ester. *Separation & Purification Reviews* **2015**, *44* (1), 28-40.

(103) El Fray, M.; Skrobot, J.; Bolikal, D.; Kohn, J. Synthesis and characterization of telechelic macromers containing fatty acid derivatives. *Reactive and Functional Polymers* **2012**, *72* (11), 781-790.

(104) Ogunniyi, D. S. Castor oil: a vital industrial raw material. *Bioresource technology* **2006**, *97* (9), 1086-1091.

(105) Jiang, L.; Tian, Y.; Wang, X.; Zhang, J.; Cheng, J.; Gao, F. A fully bio-based Schiff base vitrimer with self-healing ability at room temperature. *Polymer Chemistry* **2023**, *14* (7), 862-871.

(106) Isikgor, F. H.; Becer, C. R. Lignocellulosic biomass: a sustainable platform for the production of bio-based chemicals and polymers. *Polymer Chemistry* **2015**, *6* (25), 4497-4559.

(107) Jang, Y. S.; Kim, B.; Shin, J. H.; Choi, Y. J.; Choi, S.; Song, C. W.; Lee, J.; Park, H. G.; Lee, S. Y. Bio-based production of C2–C6 platform chemicals. *Biotechnology and bioengineering* **2012**, *109* (10), 2437-2459.

(108) Becker, J.; Lange, A.; Fabarius, J.; Wittmann, C. Top value platform chemicals: bio-based production of organic acids. *Current opinion in biotechnology* **2015**, *36*, 168-175.

(109) Sternberg, J.; Sequerth, O.; Pilla, S. Green chemistry design in polymers derived from lignin: review and perspective. *Progress in Polymer Science* **2021**, *113*, 101344.

(110) Fache, M.; Boutevin, B.; Caillol, S. Vanillin, a key-intermediate of biobased polymers. *European polymer journal* **2015**, *68*, 488-502.

(111) Xu, C.; Arancon, R. A. D.; Labidi, J.; Luque, R. Lignin depolymerisation strategies: towards valuable chemicals and fuels. *Chemical Society Reviews* **2014**, *43* (22), 7485-7500.

(112) Dawoud, M. M.; Saleh, H. M. Introductory chapter: Background on composite materials. *Characterizations of Some Composite Materials* **2018**.

(113) Wegst, U. G.; Bai, H.; Saiz, E.; Tomsia, A. P.; Ritchie, R. O. Bioinspired structural materials. *Nature materials* **2015**, *14* (1), 23-36.

(114) Clancy, A. J.; Anthony, D. B.; De Luca, F. Metal Mimics: Lightweight, Strong, and Tough Nanocomposites and Nanomaterial Assemblies. *ACS Applied Materials & Interfaces* **2020**, *12* (14), 15955-15975.

(115) Nepal, D.; Kang, S.; Adstedt, K. M.; Kanhaiya, K.; Bockstaller, M. R.; Brinson, L. C.; Buehler, M. J.; Coveney, P. V.; Dayal, K.; El-Awady, J. A.; et al. Hierarchically structured bioinspired nanocomposites. *Nature Materials* **2023**, *22* (1), 18-35.

(116) Sun, J.; Bhushan, B. Hierarchical structure and mechanical properties of nacre: a review. *Rsc Advances* **2012**, *2* (20), 7617-7632.

(117) Ratna, D. Recent advances and applications of thermoset resins. **2022**.

(118) Oliveux, G.; Bailleul, J.-L.; Gillet, A.; Mantaux, O.; Leeke, G. A. Recovery and reuse of discontinuous carbon fibres by solvolysis: Realignment and properties of remanufactured materials. *Composites Science and Technology* **2017**, *139*, 99-108.

(119) Pakdel, E.; Kashi, S.; Varley, R.; Wang, X. Recent progress in recycling carbon fibre reinforced composites and dry carbon fibre wastes. *Resources, Conservation and Recycling* **2021**, *166*, 105340.

(120) Verma, S.; Balasubramaniam, B.; Gupta, R. K. Recycling, reclamation and re-manufacturing of carbon fibres. *Current opinion in green and sustainable chemistry* **2018**, *13*, 86-90.

(121) Ruiz de Luzuriaga, A.; Martin, R.; Markaide, N.; Rekondo, A.; Cabañero, G.; Rodríguez, J.; Odriozola, I. Epoxy resin with exchangeable disulfide crosslinks to obtain reprocessable, repairable and recyclable fiber-reinforced thermoset composites. *Materials Horizons* **2016**, *3* (3), 241-247.

(122) Yang, Y.; Pei, Z.; Zhang, X.; Tao, L.; Wei, Y.; Ji, Y. Carbon nanotube–vitrimer composite for facile and efficient photo-welding of epoxy. *Chemical Science* **2014**, *5* (9), 3486-3492.

(123) Zhang, J.; Lei, Z.; Luo, S.; Jin, Y.; Qiu, L.; Zhang, W. Malleable and recyclable conductive mwcnt-vitrimer composite for flexible electronics. *ACS Applied Nano Materials* **2020**, *3* (5), 4845-4850.

(124) Chen, J.; Huang, H.; Fan, J.; Wang, Y.; Yu, J.; Zhu, J.; Hu, Z. Vitrimer chemistry assisted fabrication of aligned, healable, and recyclable graphene/epoxy composites. *Frontiers in Chemistry* **2019**, *7*, 632.

(125) Niu, Z.; Wu, R.; Yang, Y.; Huang, L.; Fan, W.; Dai, Q.; Cui, L.; He, J.; Bai, C. Recyclable, robust and shape memory vitrified polyisoprene composite prepared through a green methodology. *Polymer* **2021**, *228*, 123864.

170

(126) Chabert, E.; Vial, J.; Cauchois, J.-P.; Mihaluta, M.; Tournilhac, F. Multiple welding of long fiber epoxy vitrimer composites. *Soft Matter* **2016**, *12* (21), 4838-4845.

(127) Yue, L.; Guo, H.; Kennedy, A.; Patel, A.; Gong, X.; Ju, T.; Gray, T.; Manas-Zloczower, I. Vitrimerization: converting thermoset polymers into vitrimers. *ACS Macro Letters* **2020**, *9* (6), 836-842.

(128) Huang, B.; He, H.; Dufresne, A.; He, X.; Wang, S. Enhancing toughness, healing and reprocessability of sustainable epoxy vitrimer composites by PEG-assisted regenerated cellulose. *Industrial Crops and Products* **2021**, *170*, 113804.

(129) Legrand, A. l.; Soulié-Ziakovic, C. Silica–epoxy vitrimer nanocomposites. *Macromolecules* **2016**, *49* (16), 5893-5902.

(130) Bai, L.; Zheng, J. Robust, reprocessable and shape-memory vinylogous urethane vitrimer composites enhanced by sacrificial and self-catalysis Zn (II)–ligand bonds. *Composites Science and Technology* **2020**, *190*, 108062.

(131) Liu, X.; Li, Y.; Xing, X.; Zhang, G.; Jing, X. Fully recyclable and high performance phenolic resin based on dynamic urethane bonds and its application in self-repairable composites. *Polymer* **2021**, *229*, 124022.

(132) Hajiali, F.; Tajbakhsh, S.; Marić, M. Thermally reprocessable bio-based polymethacrylate vitrimers and nanocomposites. *Polymer* **2021**, *212*, 123126.

(133) Dong, G.; He, Q.; Cai, S. Magnetic vitrimer-based soft robotics. *Soft Matter* **2022**, *18* (39), 7604-7611.

(134) Dhers, S.; Vantomme, G.; Avérous, L. A fully bio-based polyimine vitrimer derived from fructose. *Green Chemistry* **2019**, *21* (7), 1596-1601.

(135) Lei, Z. Q.; Xie, P.; Rong, M. Z.; Zhang, M. Q. Catalyst-free dynamic exchange of aromatic Schiff base bonds and its application to self-healing and remolding of crosslinked polymers. *Journal of Materials Chemistry A* **2015**, *3* (39), 19662-19668.

(136) Ciaccia, M.; Cacciapaglia, R.; Mencarelli, P.; Mandolini, L.; Di Stefano, S. Fast transimination in organic solvents in the absence of proton and metal catalysts. A key to imine metathesis catalyzed by primary amines under mild conditions. *Chemical Science* **2013**, *4* (5), 2253-2261.

(137) Ciaccia, M.; Pilati, S.; Cacciapaglia, R.; Mandolini, L.; Di Stefano, S. Effective catalysis of imine metathesis by means of fast transiminations between aromatic–aromatic or aromatic–aliphatic amines. *Organic & Biomolecular Chemistry* **2014**, *12* (20), 3282-3287.

(138) Miyasaka, M.; Takazoe, T.; Kudo, H.; Nishikubo, T. Synthesis of hyperbranched polycarbonate by novel polymerization of di-tert-butyl tricarbonate with 1,1,1-tris(4-hydroxyphenyl)ethane. *Polymer Journal* **2010**, *42* (11), 852-859.

(139) Domininghaus, H.; Eyerer, P. P. Elsner i T. Hirth, Die Kunststoffe und ihre Eigenschaften, 6., neu bearbeitete und erweiterte Auflage. Berlin: Springer-Verlag: 2005.

(140) Irfan, M. *Chemistry and technology of thermosetting polymers in construction applications*; Springer Science & Business Media, 2012.

(141) Mishnaevsky Jr, L.; Branner, K.; Petersen, H. N.; Beauson, J.; McGugan, M.; Sørensen, B. F. Materials for wind turbine blades: An overview. *Materials* **2017**, *10* (11), 1285.

(142) Ahmadi, Z. Epoxy in nanotechnology: A short review. *Progress in Organic Coatings* **2019**, *132*, 445-448.

(143) Botelho, E. C.; Silva, R. A.; Pardini, L. C.; Rezende, M. C. A review on the development and properties of continuous fiber/epoxy/aluminum hybrid composites for aircraft structures. *Materials Research* **2006**, *9*, 247-256.

(144) Wan, J.; Li, C.; Bu, Z.-Y.; Xu, C.-J.; Li, B.-G.; Fan, H. A comparative study of epoxy resin cured with a linear diamine and a branched polyamine. *Chemical Engineering Journal* **2012**, *188*, 160-172.

(145) Burton, B.; Alexander, D.; Klein, H. Epoxy formulations using Jeffamine polyether-amines. **2004**.

(146) Zhang, Y.; Rempel, C.; Liu, Q. Thermoplastic Starch Processing and Characteristics—A Review. *Critical Reviews in Food Science and Nutrition* **2014**, *54* (10), 1353-1370.

(147) Laycock, B. G.; Halley, P. J. Chapter 14 - Starch Applications: State of Market and New Trends. In *Starch Polymers*, Halley, P. J., Avérous, L. Eds.; Elsevier, 2014; pp 381-419.

(148) Ribba, L.; Garcia, N. L.; D'Accorso, N.; Goyanes, S. Chapter 3 - Disadvantages of Starch-Based Materials, Feasible Alternatives in Order to Overcome These Limitations. In *Starch-Based Materials in Food Packaging*, Villar, M. A., Barbosa, S. E., García, M. A., Castillo, L. A., López, O. V. Eds.; Academic Press, 2017; pp 37-76.

(149) Moniri, M.; Boroumand Moghaddam, A.; Azizi, S.; Abdul Rahim, R.; Bin Ariff, A.; Zuhainis Saad, W.; Navaderi, M.; Mohamad, R. Production and status of bacterial cellulose in biomedical engineering. *Nanomaterials* **2017**, *7* (9), 257.

(150) Huang, Y.; Zhu, C.; Yang, J.; Nie, Y.; Chen, C.; Sun, D. Recent advances in bacterial cellulose. *Cellulose* **2014**, *21*, 1-30.

(151) Hassanzadeh, S.; Hasani, H. A Review on Milkweed Fiber Properties as a High-Potential Raw Material in Textile Applications. *Journal of Industrial Textiles* **2017**, *46* (6), 1412-1436.

(152) Sczostak, A. Cotton linters: an alternative cellulosic raw material. In *Macromolecular Symposia*, 2009; Wiley Online Library: Vol. 280, pp 45-53.

(153) Gama, F. H.; de Souza, R. O.; Garden, S. J. An efficient green protocol for the preparation of acetoacetamides and application of the methodology to a one-pot synthesis of Biginelli dihydropyrimidines. Expansion of dihydropyrimidine topological chemical space. *RSC advances* **2015**, *5* (87), 70915-70928.

(154) Poverenov, E.; Arnon-Rips, H.; Zaitsev, Y.; Bar, V.; Danay, O.; Horev, B.; Bilbao-Sainz, C.; McHugh, T.; Rodov, V. Potential of chitosan from mushroom waste to enhance quality and storability of fresh-cut melons. *Food Chemistry* **2018**, *268*, 233-241.

(155) Kumari, S.; Kishor, R. Chitin and chitosan: origin, properties, and applications. In *Handbook of chitin and chitosan*, Elsevier, 2020; pp 1-33.

(156) Henderson, W. A., Jr.; Schultz, C. J. The Nucleophilicity of Amines. *The Journal of Organic Chemistry* **1962**, *27* (12), 4643-4646.

(157) Domingos, A. M.; Pitt, F. D.; Barros, A. A. C. Purification of residual glycerol recovered from biodiesel production. *South African Journal of Chemical Engineering* **2019**, *29* (1), 42-51.

(158) Santibáñez, C.; Varnero, M. T.; Bustamante, M. Residual glycerol from biodiesel manufacturing, waste or potential source of bioenergy: a review. *Chilean journal of agricultural research* **2011**, *71* (3), 469.

(159) Monteiro, M. R.; Kugelmeier, C. L.; Pinheiro, R. S.; Batalha, M. O.; da Silva César, A. Glycerol from biodiesel production: Technological paths for sustainability. *Renewable and Sustainable Energy Reviews* **2018**, *88*, 109-122.

(160) Rahmstorf, E.; Abetz, V. Supramolecular networks from block copolymers based on styrene and isoprene using hydrogen bonding motifs—Part 1: Synthesis and characterization. *Materials* **2018**, *11* (9), 1608.

(161) Barszczewska-Rybarek, I. M.; Korytkowska-Wałach, A.; Kurcok, M.; Chladek, G.; Kasperski, J. DMA analysis of the structure of crosslinked poly (methyl methacrylate) s. *Acta of bioengineering and biomechanics* **2017**, *19* (1).

(162) Flory, P. J. Molecular Theory of Rubber Elasticity. *Polymer Journal* **1985**, *17* (1), 1-12.

(163) Menard, K. P.; Menard, N. *Dynamic mechanical analysis*; CRC press, 2020.

(164) Pham, H. Q.; Marks, M. J. Epoxy Resins. In *Ullmann's Encyclopedia of Industrial Chemistry*.

(165) Morgan, R. J.; Kong, F.-M.; Walkup, C. M. Structure-property relations of polyethertriamine-cured bisphenol-A-diglycidyl ether epoxies. *Polymer* **1984**, *25* (3), 375-386.

(166) Plunkett, A.; Temiz, K.; Warren, C.; Wisniewski, V.; Furlan, K. P.; Garay, J.; Giuntini, D.; Domènech, B.; Schneider, G. A. Bridging Nanocrystals to Robust, Multifunctional, Bulk Materials through Nature-Inspired, Hierarchical Design. **2022**.

(167) Morris, D. R.; Fillingame, R. H. Regulation of amino acid decarboxylation. *Annual Review of Biochemistry* **1974**, *43* (1), 303-321.

(168) Signorato, G. Sugar-based vinylogous urethane vitrimers films and membranes. Universität Hamburg, 2023 (not published).

(169) Yee, C.; Kataby, G.; Ulman, A.; Prozorov, T.; White, H.; King, A.; Rafailovich, M.; Sokolov, J.; Gedanken, A. Self-assembled monolayers of alkanesulfonic and-phosphonic acids on amorphous iron oxide nanoparticles. *Langmuir* **1999**, *15* (21), 7111-7115.

(170) Andrews, B.; Almahdali, S.; James, K.; Ly, S.; Crowder, K. N. Copper oxide surfaces modified by alkylphosphonic acids with terminal pyridyl-based ligands as a platform for supported catalysis. *Polyhedron* **2016**, *114*, 360-369.

(171) Kampferbeck, M.; Vossmeyer, T.; Weller, H. Cross-linked polystyrene shells grown on iron oxide nanoparticles via surface-grafted AGET–ATRP in microemulsion. *Langmuir* **2019**, *35* (26), 8790-8798.

(172) Thevenot, J.; de Oliveira, H.; Sandre, O.; Lecommandoux, S. Magnetic responsive polymer composite materials. *Chemical Society Reviews* **2013**, *42* (17), 7099-7116.

(173) Winhard, B. F.; Haida, P.; Plunkett, A.; Katz, J.; Domènech, B.; Abetz, V.; Furlan, K. P.; Schneider, G. A. 4D-printing of smart, nacre-inspired, organic-ceramic composites. *Additive Manufacturing* **2023**, *77*, 103776.

(174) Yu, W. W.; Falkner, J. C.; Yavuz, C. T.; Colvin, V. L. Synthesis of monodisperse iron oxide nanocrystals by thermal decomposition of iron carboxylate salts. *Chemical Communications* **2004**, (20), 2306-2307.

(175) Kampferbeck, M.; Klauke, L. R.; Weller, H.; Vossmeyer, T. Little Adjustments Significantly Simplify the Gram-Scale Synthesis of High-Quality Iron Oxide Nanocubes. *Langmuir* **2021**, *37* (32), 9851-9857.

(176) Pandey, G.; Tharmavaram, M.; Phadke, G.; Rawtani, D.; Ranjan, M.; Sooraj, K. Silanized halloysite nanotubes as 'nano-platform' for the complexation and removal of Fe (II) and Fe (III) ions from aqueous environment. *Separation and Purification Technology* **2022**, *293*, 121141.

(177) Yamaguchi, A.; Uejo, F.; Yoda, T.; Uchida, T.; Tanamura, Y.; Yamashita, T.; Teramae, N. Self-assembly of a silica–surfactant nanocomposite in a porous alumina membrane. *Nature Materials* **2004**, *3* (5), 337-341.

9   Appendix

9.1   Author Contributions to the Publications

Acid-Mediated Autocatalysis in Vinylogous Urethane Vitrimers

<u>Philipp Haida</u> and Volker Abetz
Macromol. Rapid Commun., **2020**, *41*(14), 2000273
doi.org/10.1002/marc.202000273

P.H. and V.A. designed the project, P.H. performed, examined, and evaluated the analytical data. V.A. supervised the project and provided the resources. P.H. wrote the original draft. P.H. and V. A. reviewed and edited the original draft. All authors have read and agreed to the published version of the manuscript.

Blended vinylogous urethane/urea vitrimers derived from aromatic alcohols

<u>Philipp Haida</u>, Gloria Signorato and Volker Abetz
Polym. Chem., **2022**, *13*, 946-958
doi.org/10.1039/D1PY01237A

P.H. and V.A. designed the project, P.H. and Gloria Signorato (G.S.) performed, examined, and evaluated the analytical data. V.A. supervised the project and provided the resources. P.H. wrote the original draft. P.H. and V. A. reviewed and edited the original draft. All authors have read and agreed to the published version of the manuscript.

Starch-Reinforced Vinylogous Urethane Vitrimer Composites: An Approach to Biobased, Reprocessable, and Biodegradable Materials

<u>Philipp Haida</u>, Suwabun Chirachanchai and Volker Abetz
Sustain. Chem. Eng., **2023**, *11*, 22, 8350–8361
doi.org/10.1021/acssuschemeng.3c01340

P.H., S.C. and V.A. designed the project, P.H. performed, examined, and evaluated the analytical data. S.C. and V.A. supervised the project and provided the resources. P.H. wrote the original draft. P.H., S.C. and V.A. reviewed and edited the original draft. All authors have read and agreed to the published version of the manuscript.

9.2   Publication 1 – Supporting Information

The Publication is reprinted with permission from P. Haida and V. Abetz, *Macromol. Rapid Commun.*, **2020**, *41*(14), 2000273 - published by Wiley.

Supporting Information

Acid-Mediated Autocatalysis in Vinylogous Urethane Vitrimers

Philipp Haida and Volker Abetz*

Supporting Information

Acid-Mediated Autocatalysis in Vinylogous Urethane Vitrimers

Philipp Haida, Volker Abetz*
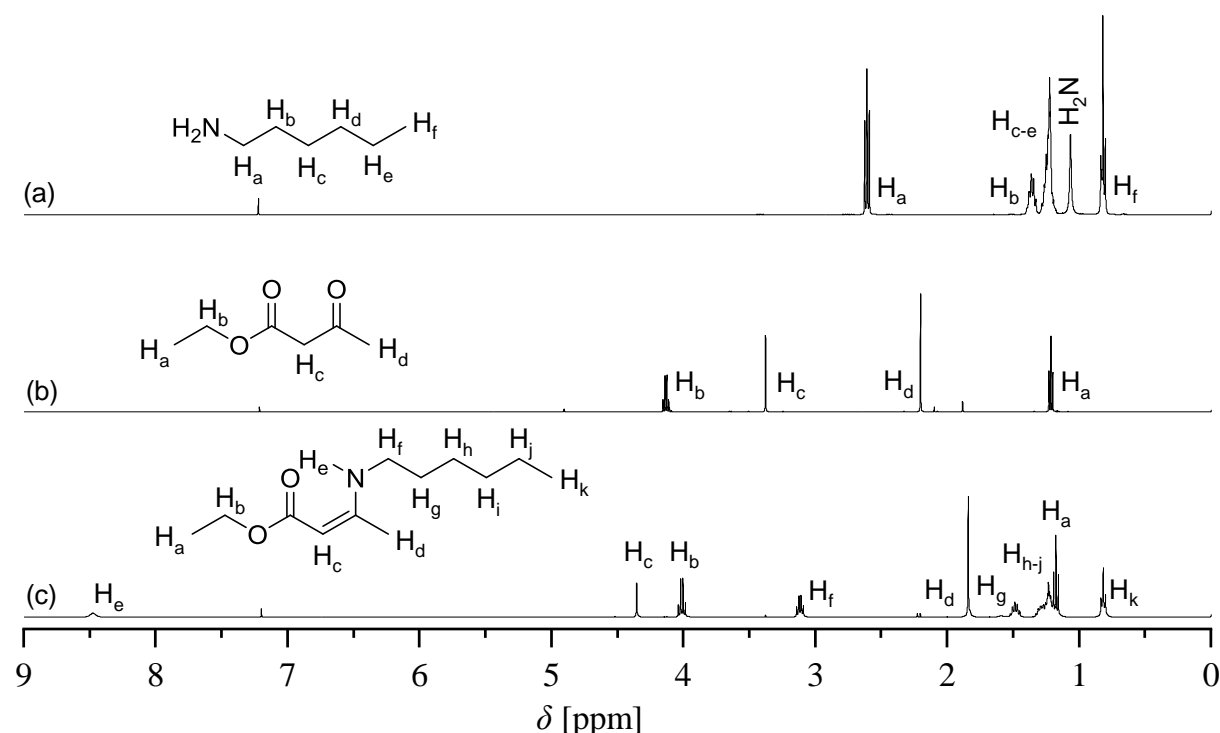
Figure S 1: ^{1}H NMR spectra (CDCl₃) of the condensation reaction of hexylamine (a) and ethylacetoacetate (b), yielding the *cis-* and *trans-*enamine-ones, with the *cis-*enamine-one representing the predominant stereoisomer (c). *Ethyl(cis)-3-(hexylamino)but-2-enoate:* ^{1}H NMR (500 MHz, CDCl₃, δ): 8.50 (t, 1H; NH), 4.36 (s, 1H; CH), 4.14 (q, *J* = 6.62 Hz, 2H; CH₂), 3.12 (q, *J* = 6.41 Hz,2H; CH₂), 1.84 (s, 3H; CH₃), 1.53−1.43 (m, 2H; CH₂), 1.33−1.13 (m, 6H; CH₂), 1.18 (t, *J* = 7.08 Hz, 3H; CH₃), 0.82 (t, *J* = 7.50 Hz, 3H; CH₃).

Ethyl(trans)-3-(hexylamino)but-2-enoate: ^{1}H NMR (500 MHz, CDCl₃, δ): 5.35 (t, 1H; NH), 4.52 (s, 1H; CH), 4.01 (q, *J* = 7.24 Hz, 2H; CH₂), 2.93 (q, *J* = 5.00 Hz, 2H; CH₂), 2.20 (s, 3H; CH₃), 1.53−1.42 (m, 2H; CH₂), 1.33−1.13 (m, 6H; CH₂), 1.18 (t, *J* = 7.08 Hz, 3H; CH₃), 0.82 (t, *J* = 7.50 Hz, 3H; CH₃).

Figure S 2: ^{1}H NMR spectra (DMSO-d_6) of the *cis-* and *trans-*enamine-ones, with the *cis*-enamine-one representing the predominant stereoisomer. *Ethyl(cis)-3-(hexylamino)but-2-enoate*: ^{1}H NMR (600 MHz, DMSO-d_6, δ): 8.50 (t, $J = 5.37$ Hz, 1H; CH), 4.32 (s, 1H), 3.95 (q, $J = 7.10$ Hz, 2H; CH$_2$), 3.18 (q, $J = 6.92$ Hz, 2H; CH$_2$), 1.88 (s, 3H; CH$_3$), 1.52−1.43 (m, 2H, CH$_2$), 1.33−1.22 (m, 6H; CH$_2$), 1.13 (t $J = 7.54$ Hz, 3H; CH$_3$), 0.87 (t, $J = 7.10$ Hz, 3H; CH$_3$).

ethyl(trans)-3-(hexylamino)but-2-enoate: ^{1}H NMR (600 MHz, DMSO-d_6, δ): 6.64 (t, $J = 5.37$ Hz, 1H; NH), 4.34 (s, 1H; CH), 3.90 (q, $J = 7.02$ Hz, 2H; CH$_2$), 2.87 (q, $J = 6.71$ Hz, 2H; CH$_2$), 2.16 (s, 3H; CH$_3$), 1.52−1.42 (m, 2H ; CH$_2$), 1.33−1.22 (m, 6H; CH$_2$), 1.12 (t, $J = 7.54$ Hz, 3H; CH$_3$), 0.87 (t, $J = 7.10$ Hz, 3H; CH$_3$).

Figure S 3: ^{13}C NMR (DEPTQ) spectrum of the stereoisomeric mixture of the *cis*-en and *trans*-en measured in DMSO-d_6.

ethyl(cis)-3-(hexylamino)but-2-enoate: ^{13}C NMR (600 MHz, DMSO-d_6, δ): 169.9 (C=O), 162.6 (C4), 81.5 (C3), 57.9 (C2), 42.7 (C2), 31.5 (C2), 30.5 (HNC2), 26.9 (C2), 22.6 (C2), 19.4 (C1), 15.1 (C1), 14.4 (C1). *ethyl(trans)-3-(hexylamino)but-2-enoate:* ^{13}C NMR (600 MHz, DMSO-d_6, δ): 168.4 (C=O), 162.6 (C4), 80.5 (C3), 57.5 (C2), 43.1 (C2), 31.5 (C2), 28.2 (NC2), 26.9 (C2), 22.6 (C2), 19.4 (C1), 15.1 (C1), 14.4 (C1).
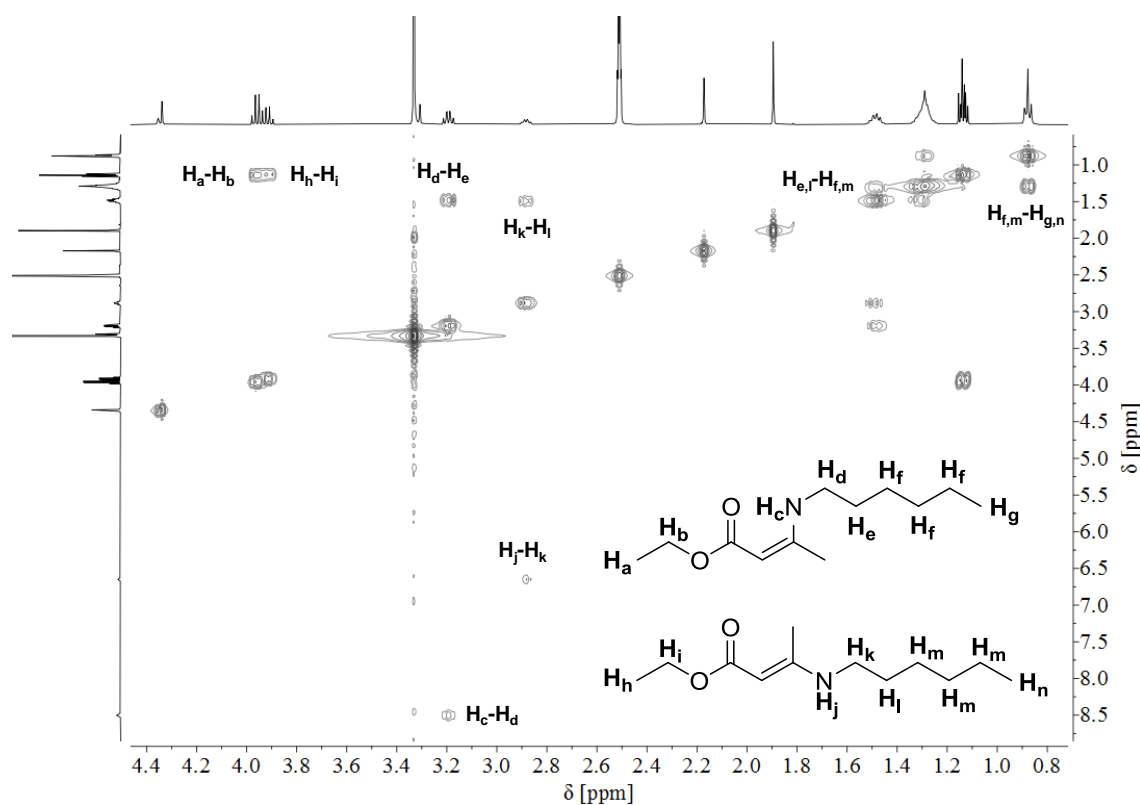
Figure S 4: COSY-NMR spectrum of the stereoisomeric mixture of the *cis*-en and *trans*-en measured in DMSO-d_6.

3
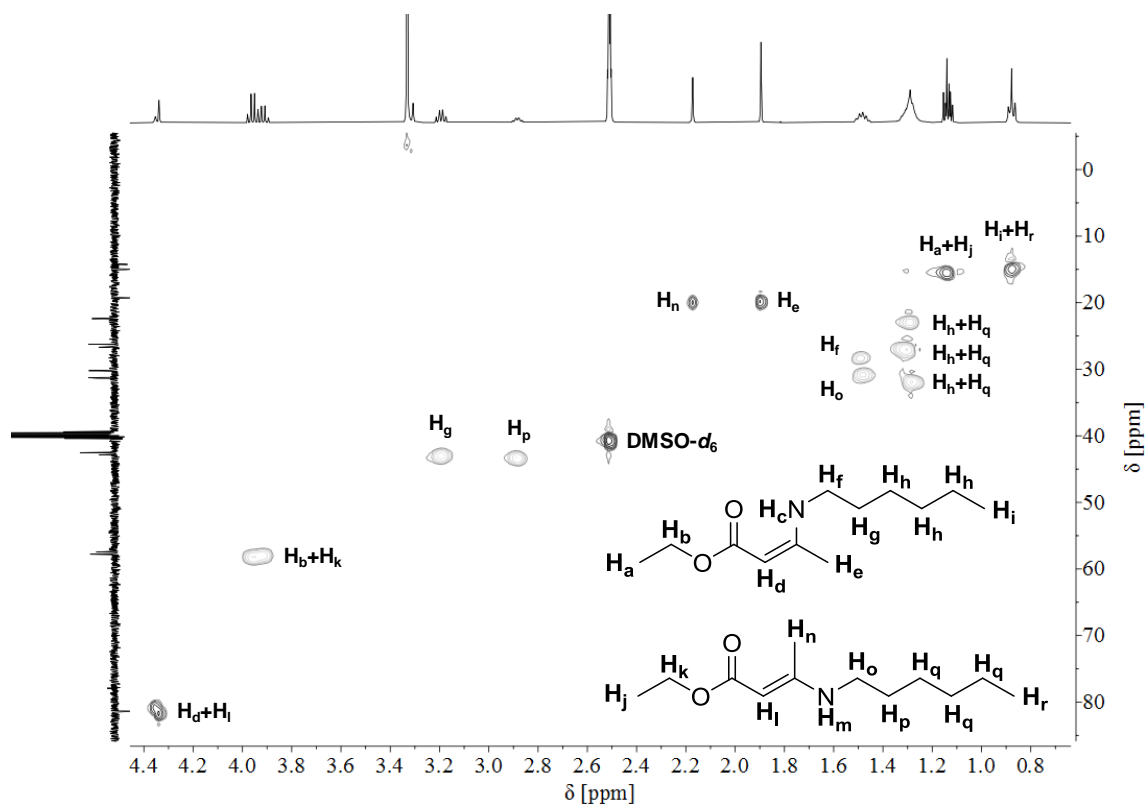
Figure S 5: HSQC-NMR spectrum of the stereoisomeric mixture of the *cis*-en and *trans*-en measured in DMSO-*d6*.
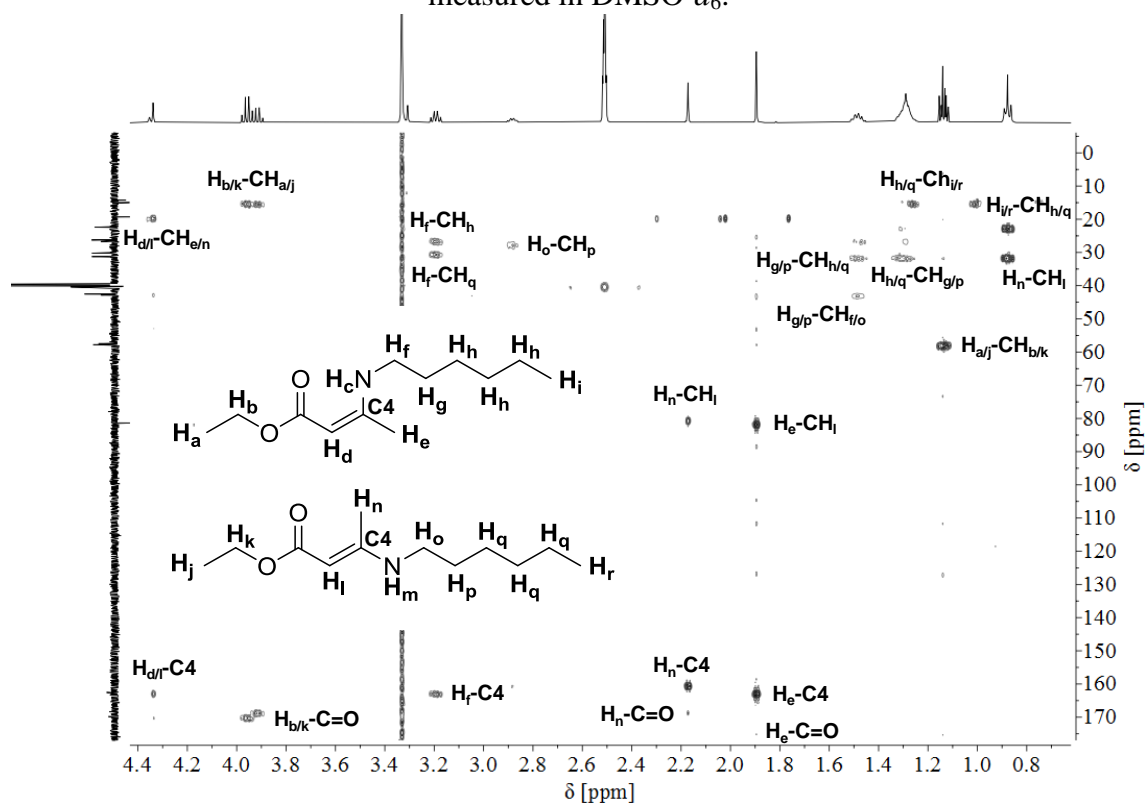
Figure S 6: HMBC-NMR spectrum of the stereoisomeric mixture with the *cis*-en and *trans*-en measured in DMSO-*d6*.
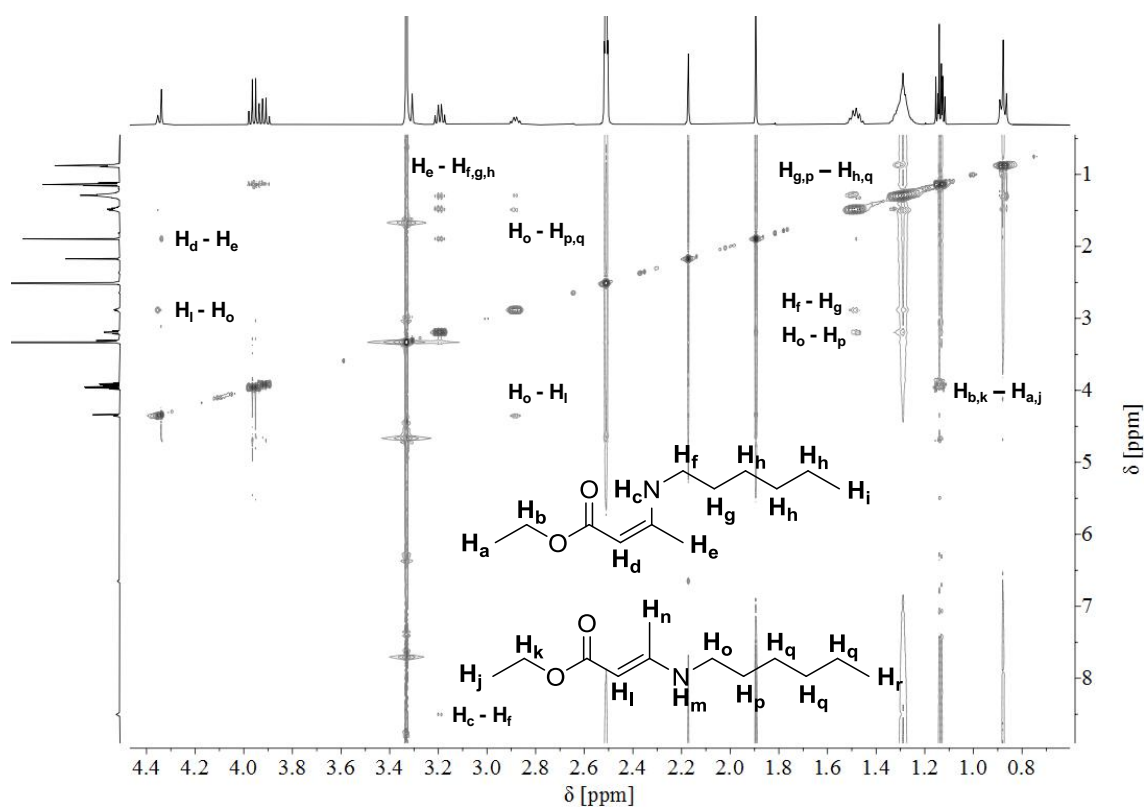
Figure S 7: NOESY-NMR spectrum of the stereoisomeric mixture with the *cis*-en and *trans*-en measured in DMSO-d_6.
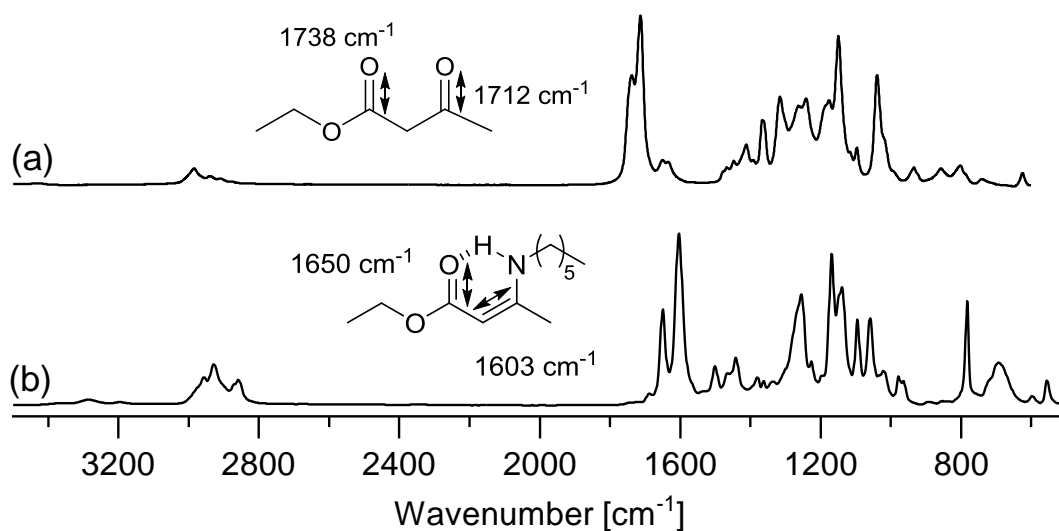
Figure S 8: ATR-FT-IR spectra of ethylacetoacetate (a) and the resulting enamine-one (b). The spectra show the characteristic absorption bands of ethylacetoacetate with the C=O ester (1738 cm^{-1}) and C=O ketone (1712 cm^{-1}) as well as the C=O ester (1650 cm^{-1}) and C=C band (1603 cm^{-1}) of the enamine-one product.
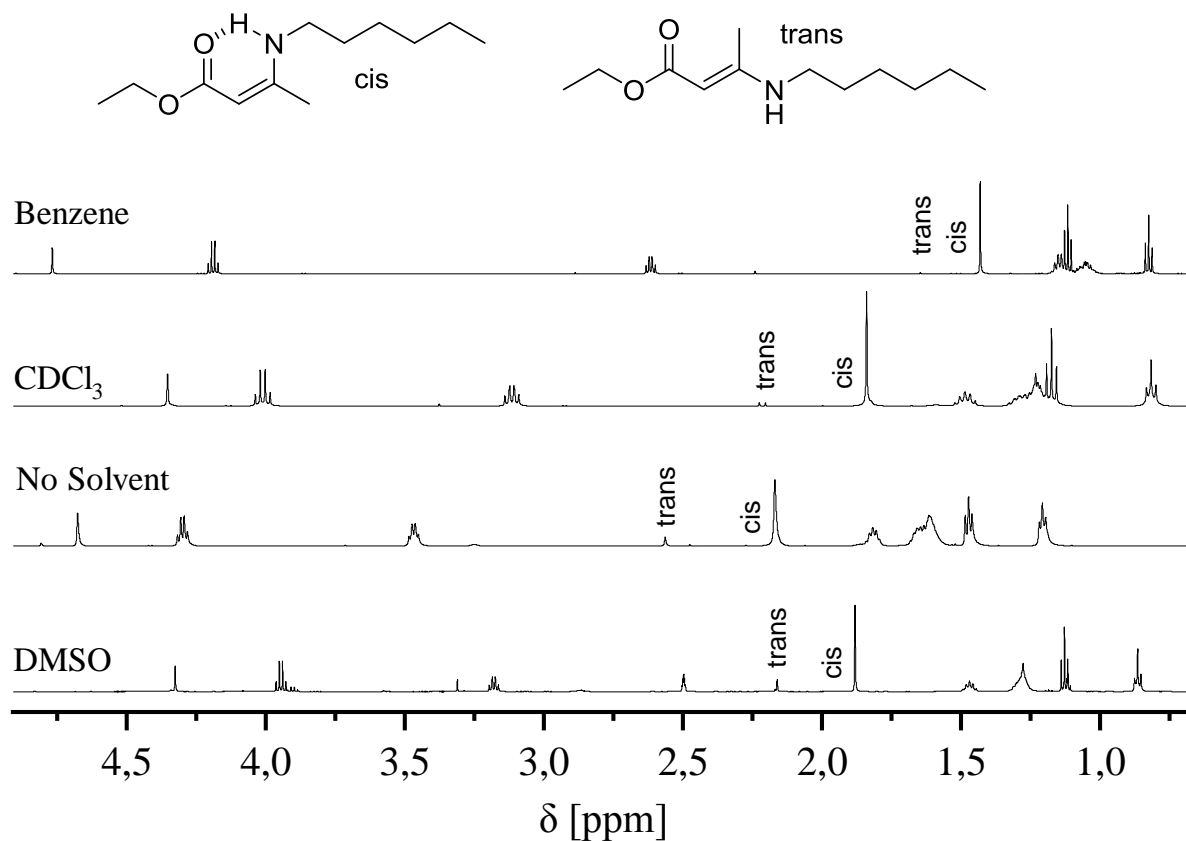
Figure S 9: ^{1}H NMR spectra of the *cis-* and *trans*-enamine-one stereoisomers measured in benzene-d_6, chloroform-d_1, DMSO-d_6 and without solvent.
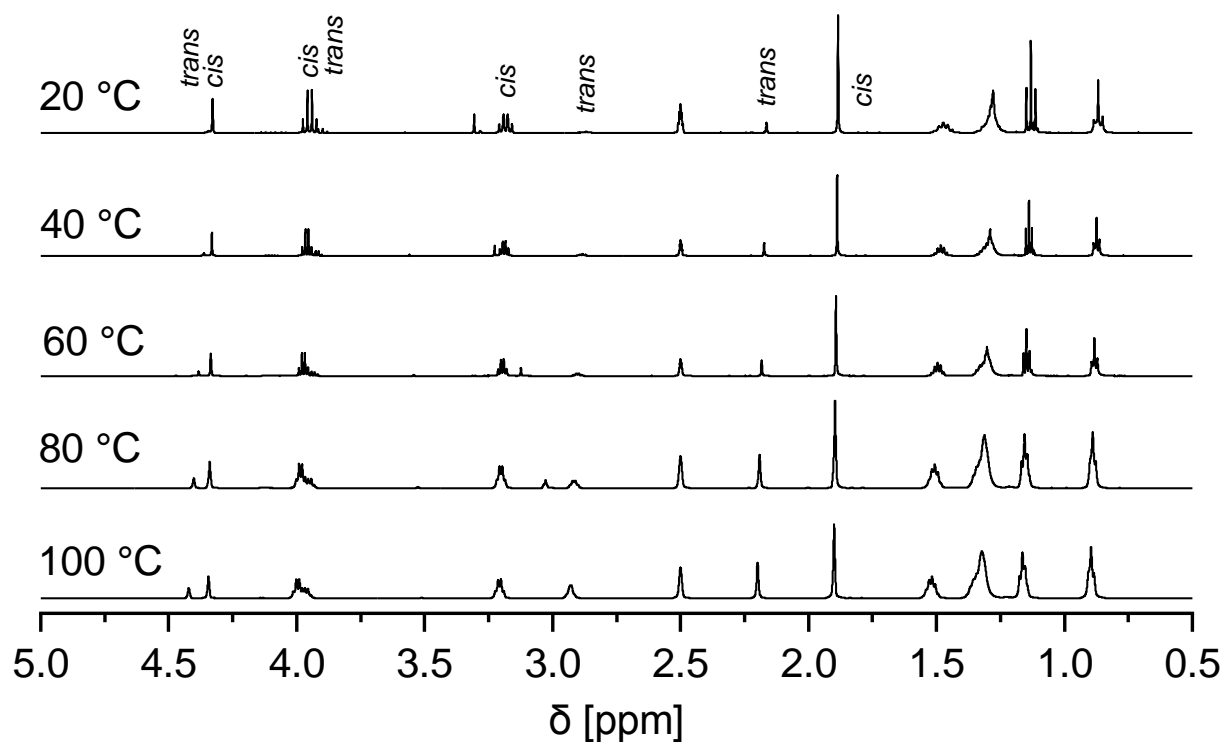
Figure S 10: Temperature dependent ^{1}H NMR spectra of the *cis-* and *trans*-enamine-one stereoisomers measured in DMSO-d_6 in the range of 20–100 °C.

Table S1: *Cis-trans* stereoisomerism determined by temperature dependent ^{1}H NMR measurements in deuterated benzene, DMSO and without solvent in a temperature range of 20–110 °C. With increasing temperature, the preference for the *cis*-enamine-one slowly disappears through equilibration.

	20	25	30	35	40	45	50	55	60	70	80	90	100	110	[°C]
Benzene-*d6*															[mol%]
cis-en	99	99	99	99	98	98	98	98	98	-	-	-	-	-	
trans-en	1	1	1	2	2	2	2	3	3	-	-	-	-	-	
No Solvent															[mol%]
cis-en	91	-	91	-	91	-	91	-	90	90	89	89	-	-	
trans-en	9	-	9	-	9	-	9	-	10	10	11	12	-	-	
DMSO-*d6*															[mol%]
cis-en	87	-	87	-	86	-	86	-	85	83	74	69	65	60	
trans-en	13	-	13	-	14	-	14	-	15	17	26	31	35	40	
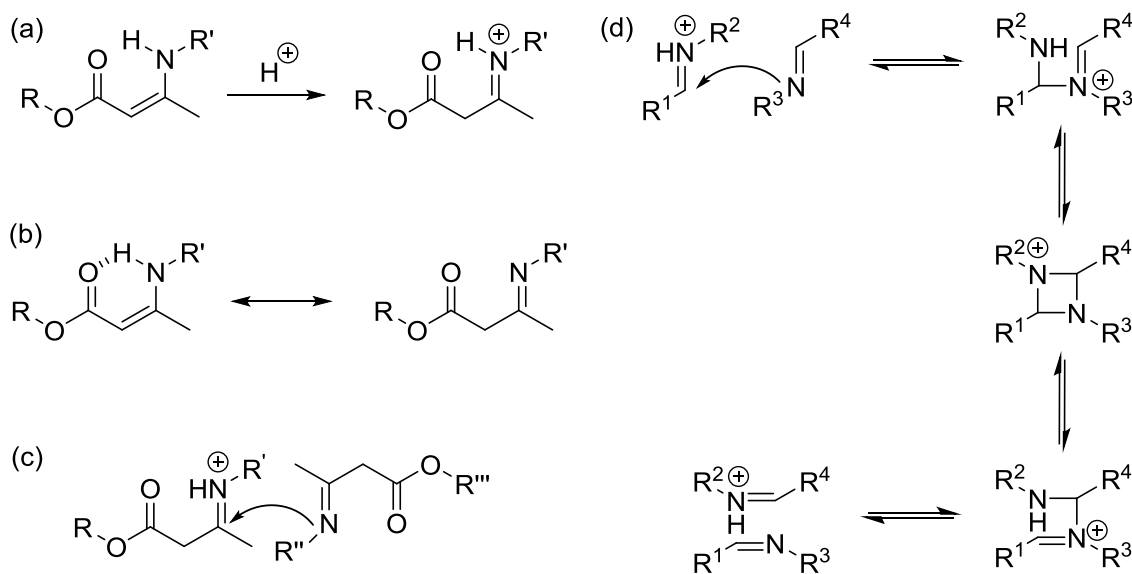
Figure S11: (a) Protonation of the enamine-one. (b) Structures of the imine/enamine tautomerism. (c) Assumed mechanism of the polar imine metathesis (d) Polar mechanism of the acid catalysed imine metathesis (literature).
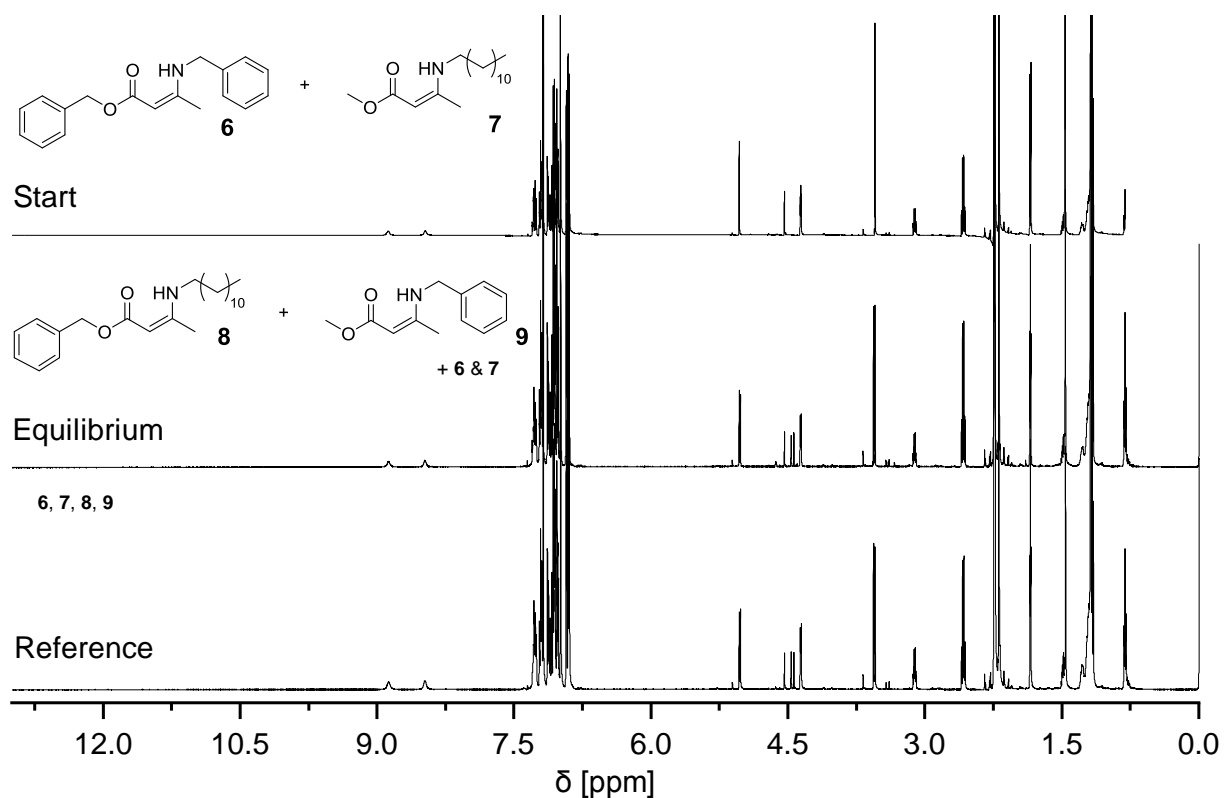
Figure S 12: ^{1}H NMR-spectra of the model compound experiment of the acid-mediated autocatalysis in vinylogous urethanes. Spectra of the two reactants **6** and **7** before heating (start), the equilibrium state (**6**, **7**, **8**, **9**) and the reference mixture (**6**, **7**, **8**, **9**).
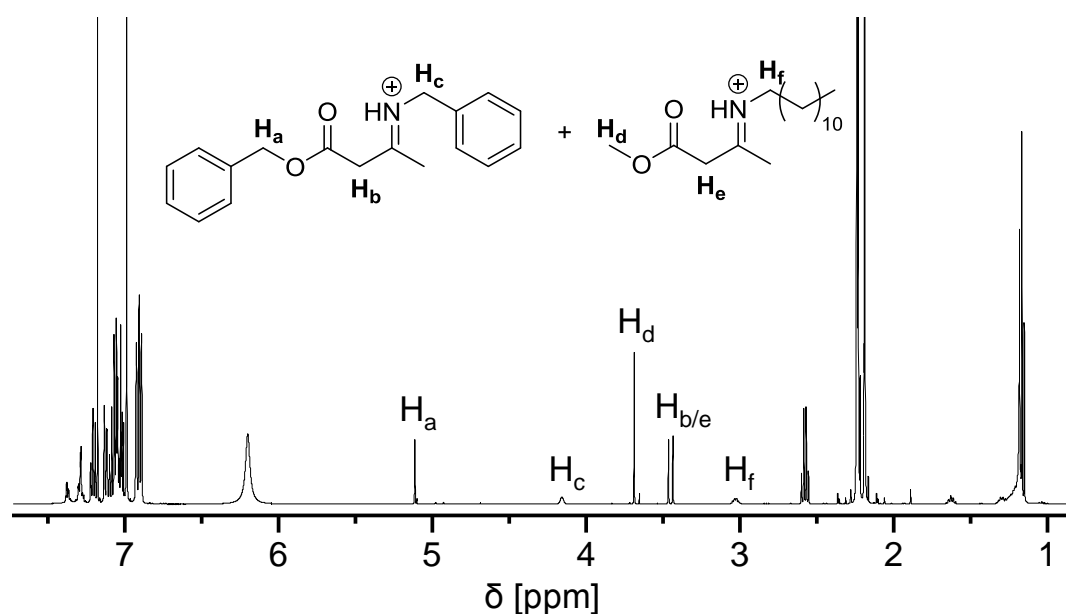
Figure S 13: Addition of a mixture of enamine-ones to an excess of trifluoracetic acid. All enamine-ones were instantly protonated as iminium-ones and remaining water as oxonium-ion , thus quenching the exchange reactions.
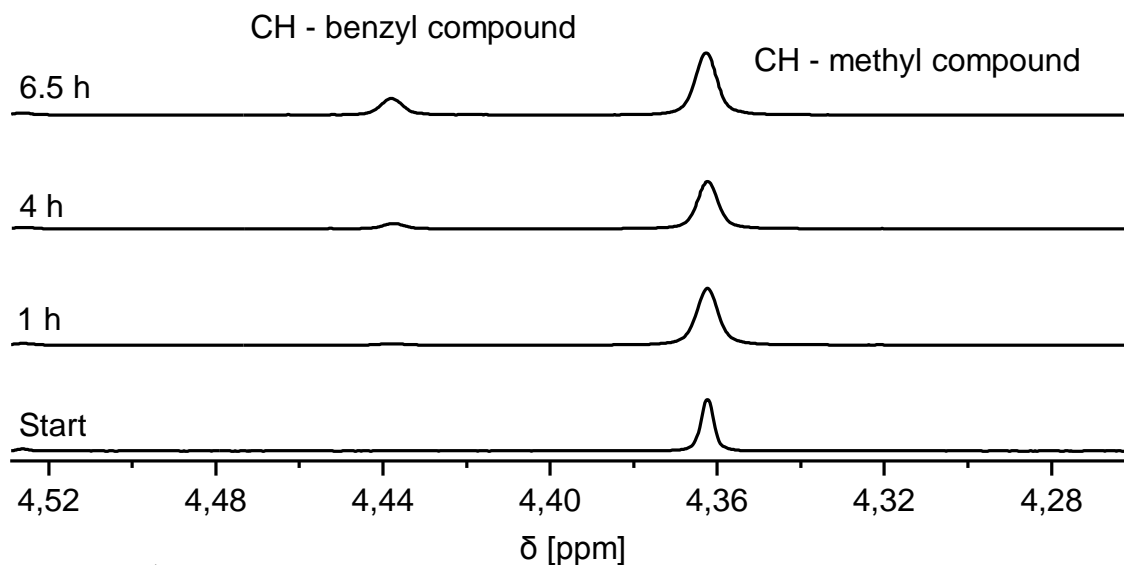
Figure S 14: ^{1}H NMR spectra of the model compound reaction to determine the backward reaction of enamine-ones with water. The signal (CH) of the benzyl compound appeared at 4.44 ppm.
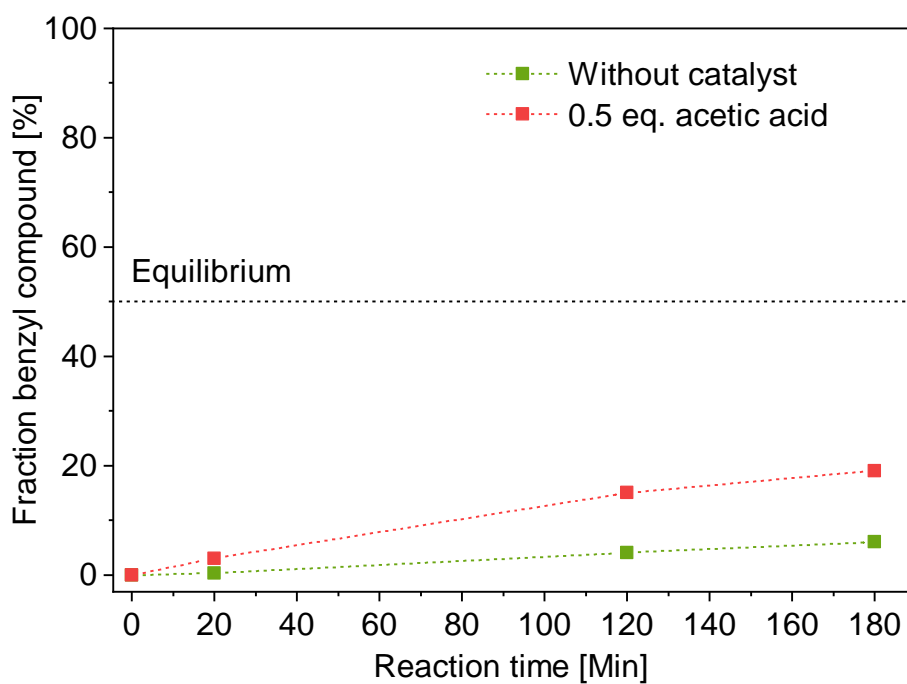
Figure S 15: Model compound reaction to investigate the backward reaction of protonated iminium-ones and water with and without acetic acid as catalyst.
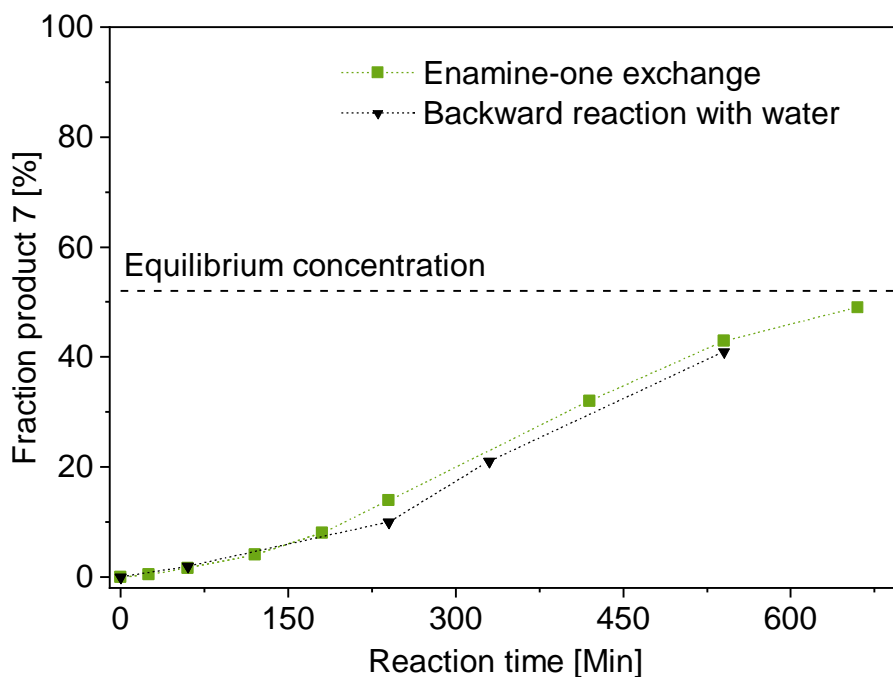
Figure S 16: Sigmoidal conversion curves in comparison of the enamine-one exchange (Figure 3) and experiment to directly determine the dissociation of enamine-one with water (Figure 6) under almost dry conditions. The curves show the autocatalysed reactions, which lead to renewed condensation reactions and dynamic transimination reactions.
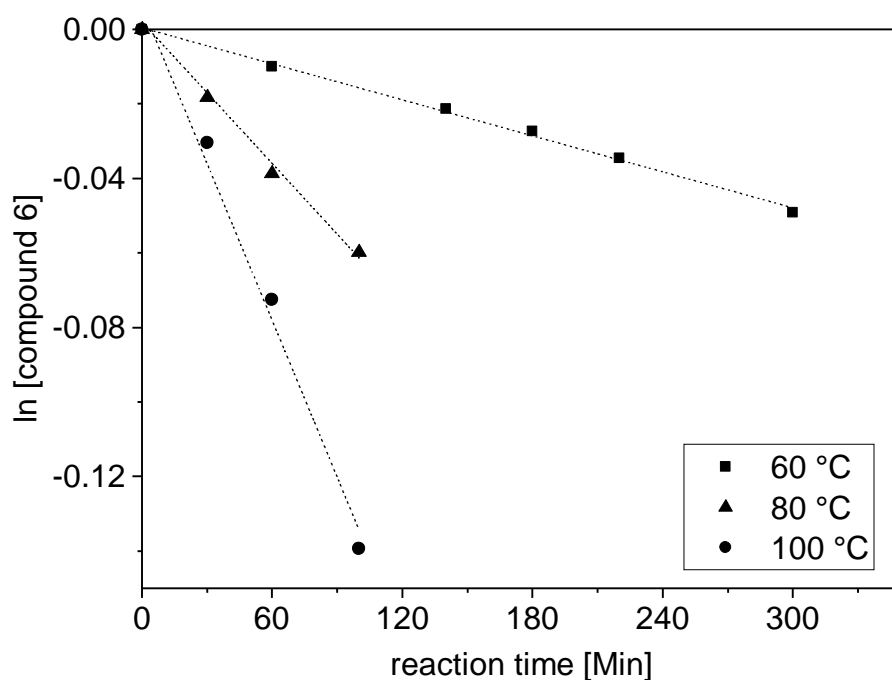
Figure S 17: First order plot of the conversions of compound 6 during the enamine-one exchange model reaction (Figure 3). A linear decay is observed for at least 100 minutes reaction time. Afterwards the backward reaction of the equilibrium has a significant influence on the reaction order.

Calculation of the activation energy (E_a) via an Arrhenius law:

The decrease of the reactant concentration as a function of time is described by:[33]

$$[R] = 1 - c_P + c_P * e^{\frac{-kt}{c_P}}$$

$[R]$	concentration reactant
c_P	equilibrium ratio of the products ($\frac{4}{5}$)
k	initial rate (fitted)
t	reaction time [s]

Equation S1: Exponential fit for the conversion of the reactant to determine the initial rate k.

The activation energy was calculated by plotting ln k versus 1000/T.

$$y(x) = \frac{54x}{R} \pm 0.7$$
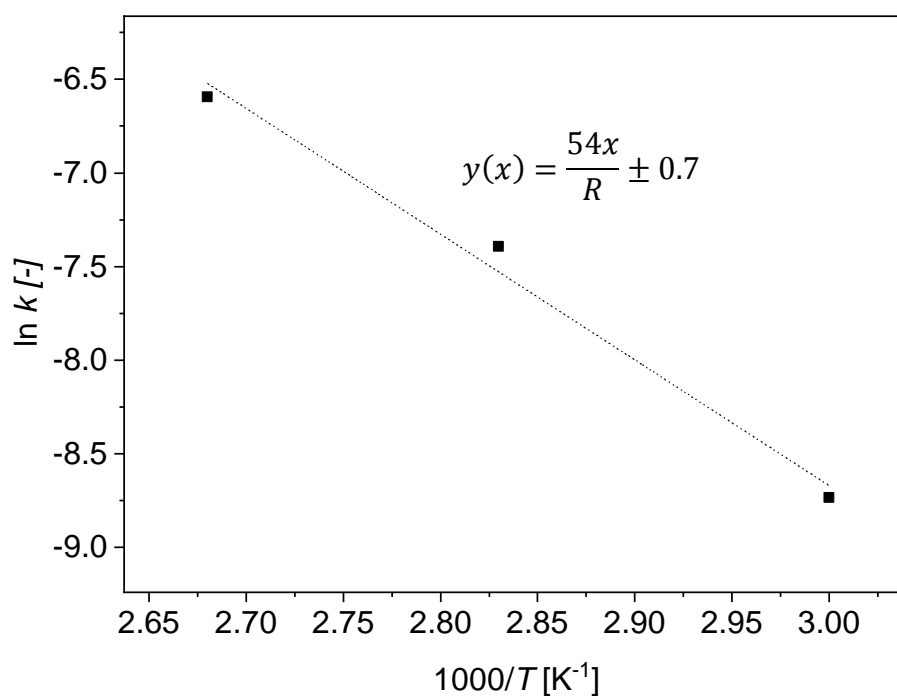
Figure S 18: Investigation of the activation energy for the imine metathesis reaction by plotting ln k versus 1000/T and fitting the gradient. An activation energy of 54 kJ mol^{-1} was calculated.
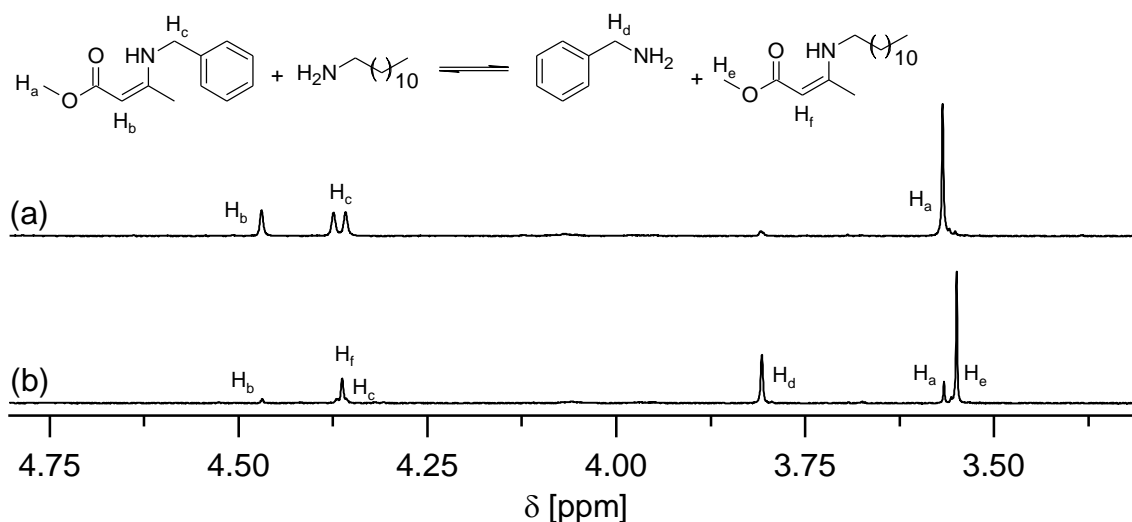
Figure S 19: ^{1}H NMR-spectra of the transimination model compound reaction in vinylogous urethanes. Spectra of the two reactants **11** and **12** before heating and the equilibrium state after stirring for 2 h (**11**, **12**, **13**, **14**).
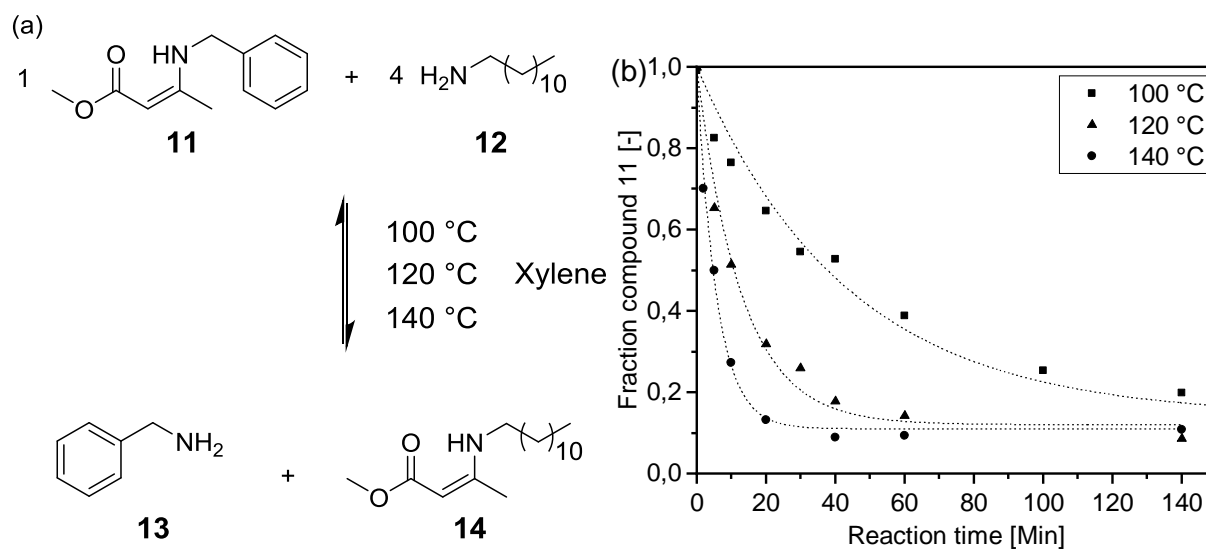
Figure S20: (a) Schematic representation of the transimination model reaction of compounds **11** and **12** with an excess of primary amines measured in xylene. (b) Conversion of **11** (yielding 14) at 100 °C, 120 °C and 140 °C plotted versus the reaction time.

12
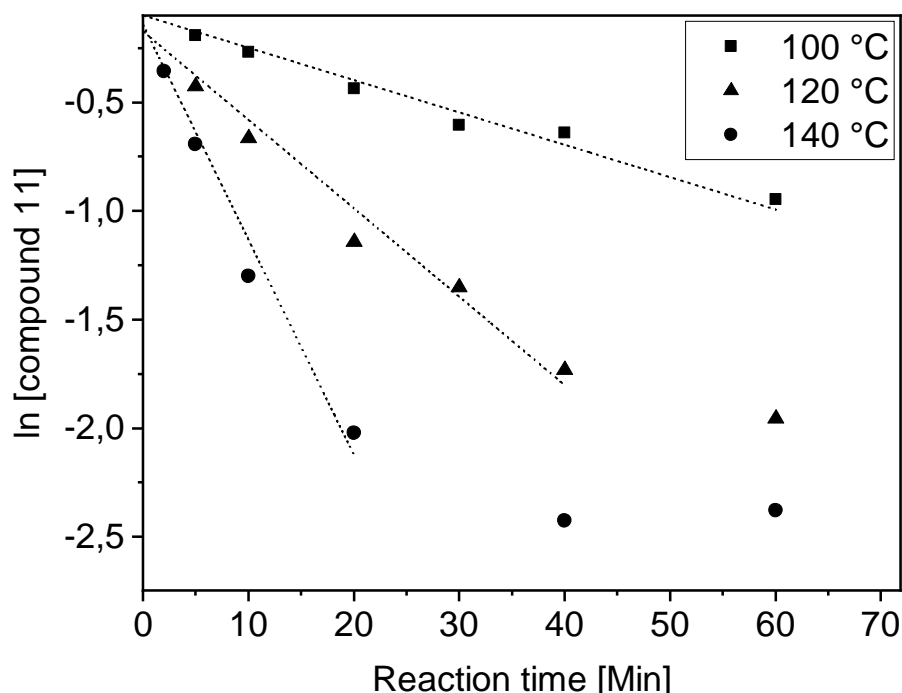
Figure S 21: First order plots of the compound 11 conversions at different temperatures. A linear decay can be observed for 60 minutes at 100°C, 40 minutes at 120 °C and 20 minutes at 140 °C reaction time. At higher conversions the backward reaction of the equilibrium has a significant influence on the reaction order.
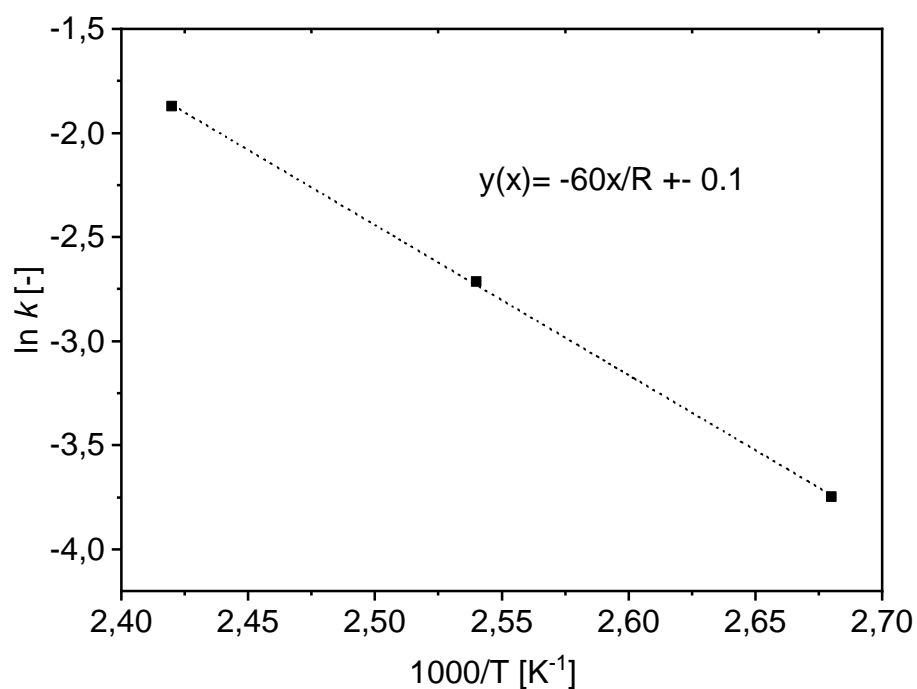
Figure S 22: Investigation of the activation energy for the transimination reaction by plotting ln k against 1000/T and fitting the gradient. An activation energy of 60 kJ mol^{-1} was calculated.

Calculation of the activation energy (E_a) by stress relaxation experiments:

The stress relaxation times as a function of temperature can be described by an Arrhenius law:

$$\tau(T) = \tau_0\, e^{\frac{E_a}{RT}}$$

Equation S2: Arrhenius law for calculating the activation energy by stress-relaxation times according to Maxwell law for visoelastic fluids (37%, 1/e)) as a function of temperature.

τ	stress relaxation time (37 %)	[s]
τ_0	Stress relaxation time (normalized 0,1)	[s]
E_a	activation energy	[kJ mol^{-1}]
R	gas constant	[J K^{-1} mol^{-1}]
T	temperature	[K]

Figure S23: ATR-FT-IR measurements of the vinylogous urethane vitrimers VU-A, VU-A$_{H+}$, VU-E$_{H+}$, VU-NA, VU-NA$_{H+}$. The measurements show the respective C=O (1650 cm^{-1}) ester and C=C band (1602 cm^{-1}) of the vinylogous urethanes as well as the C=O (1650 cm^{-1}) ester and C=O ketone band of the acetoacetate monomer in networks with an excess of acetoacetates
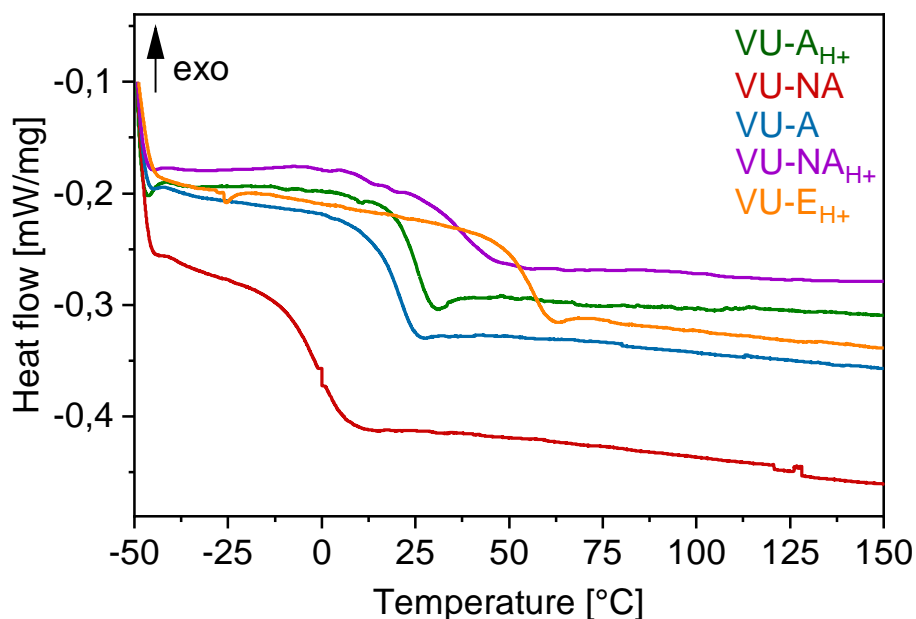
Figure S24: Differential scanning calorimetry (DSC) measurements to determine the glass transition temperatures T_g of the vinylogous urethane vitrimers VU-A (13 °C), VU-NA (-8 °C), VU-A$_{H+}$ (17 °C), VU-NA$_{H+}$ (29 °C).and VU-E$_{H+}$ (51 °C) (on-set).
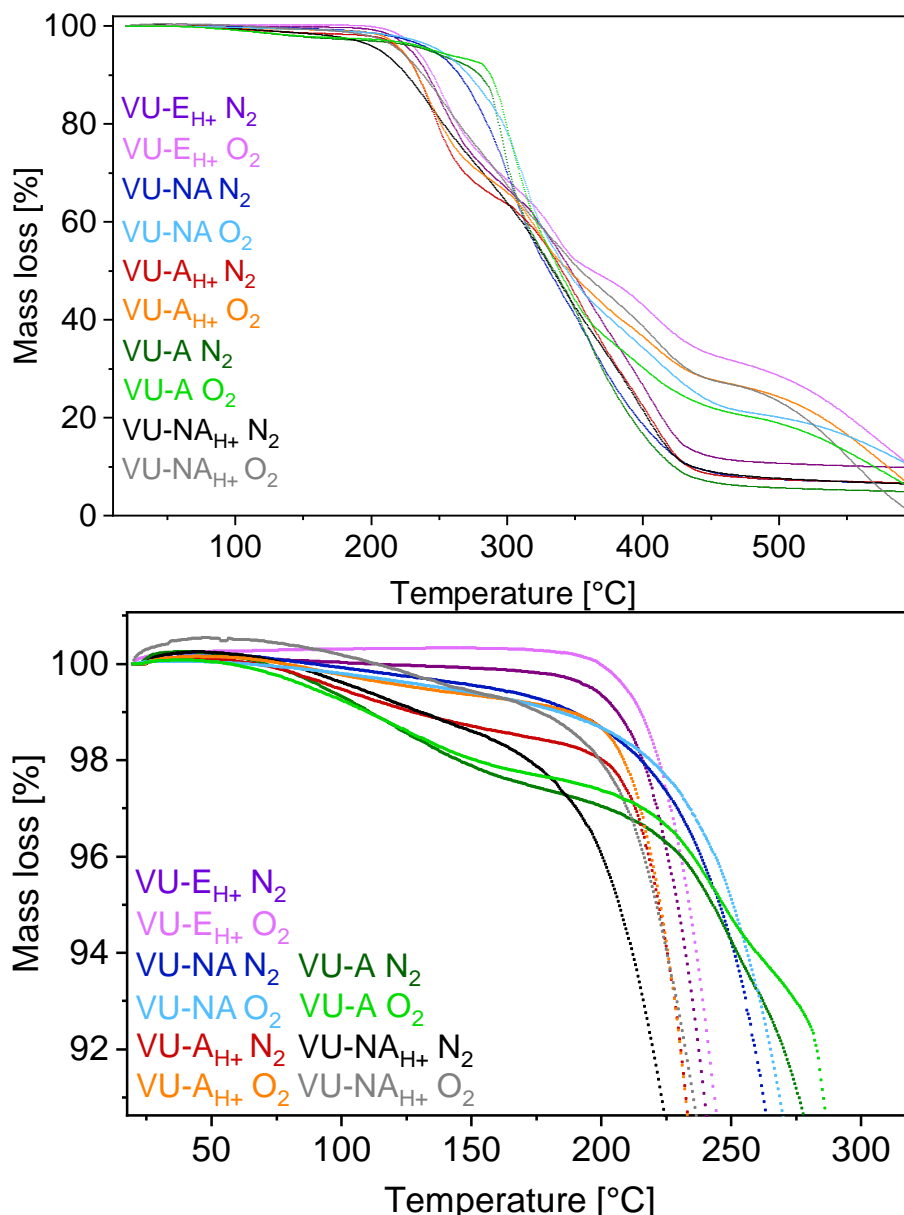
Figure 25: Thermal gravimetric analysis (DMA) measurements to determine the thermal degradation points of the vinylogous urethane vitrimers with degradation points of 281 °C (VU-A), 226 °C (VU-A$_{H+}$), 222 °C (VU-E$_{H+}$), 251 °C (VU-NA) and 220 °C (VU-NA$_{H+}$) under oxygen atmosphere with no significant change by measuring under nitrogen atmosphere. Until the degradation point the full cured vitrimer VU-E$_{H+}$ (R =1.0) is the most stable.
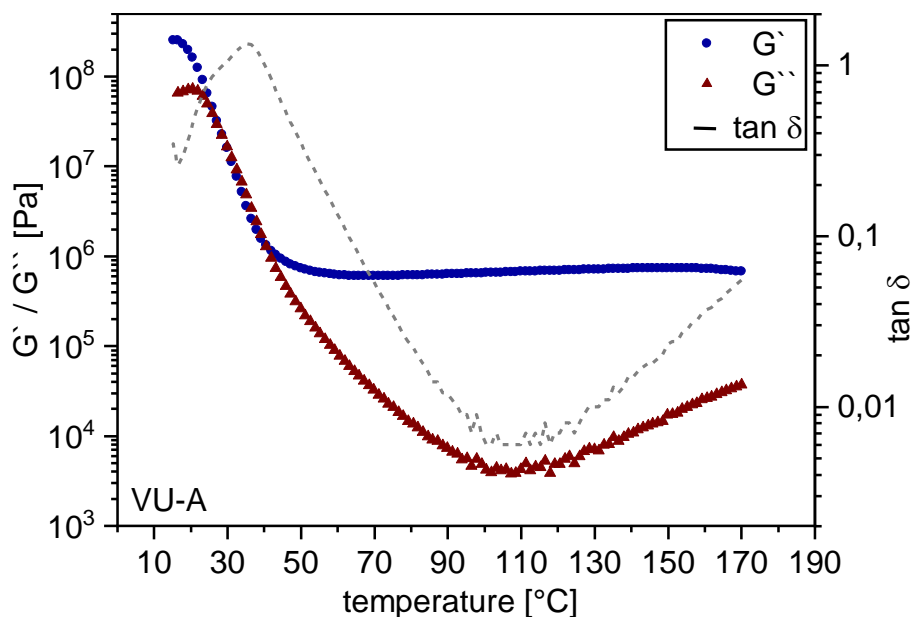
Figure S26: Temperature dependent dynamical-mechanical analysis (DMA) measurement of **VU-A**. A storage modulus of 0.25 GPa and a rubbery plateau of 0.7 MPa was obtained using G`. In addition, the loss modulus G`` and tan δ are shown in the diagram.
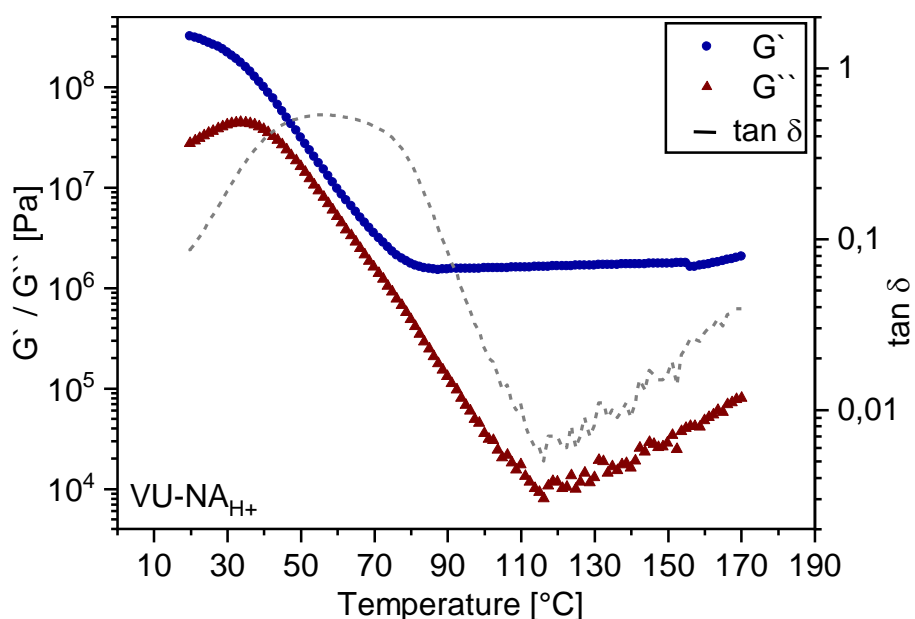
Figure S27: Temperature dependent dynamical-mechanical analysis (DMA) measurement of **VU-NA$_{H+}$**. A storage modulus of 0.5 GPa and a rubbery plateau of 0.4 MPa was obtained using G`. In addition, the loss modulus G`` and tan δ are shown in the diagram.
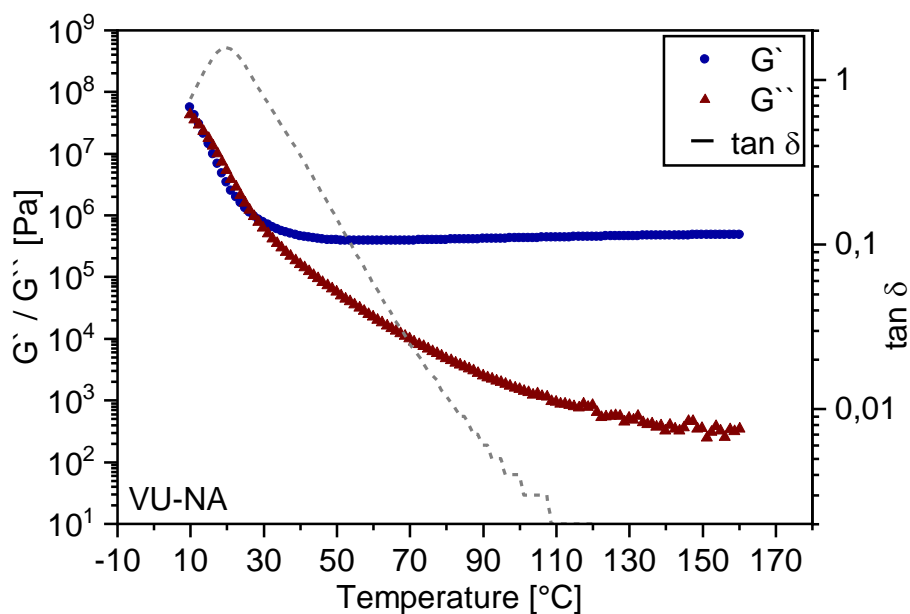
Figure S28: Temperature dependent dynamical-mechanical analysis (DMA) measurement of **VU-NA**. A storage modulus of 0.3 GPa and a rubbery plateau of 1.5 MPa was obtained using G`. In addition, the loss modulus G`` and tan δ are shown in the diagram.
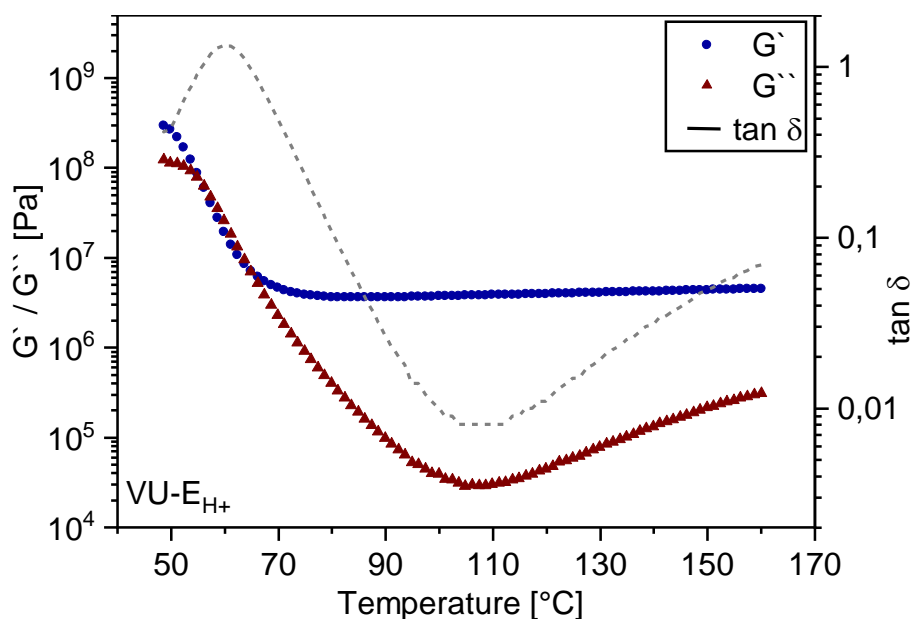
Figure S29: Temperature dependent dynamical-mechanical analysis (DMA) measurement of **VU-E$_{H+}$**. A storage modulus of 0.3 GPa and a rubbery plateau of 4 MPa was obtained using G`. In addition, the loss modulus G`` and tan δ are shown in the diagram.
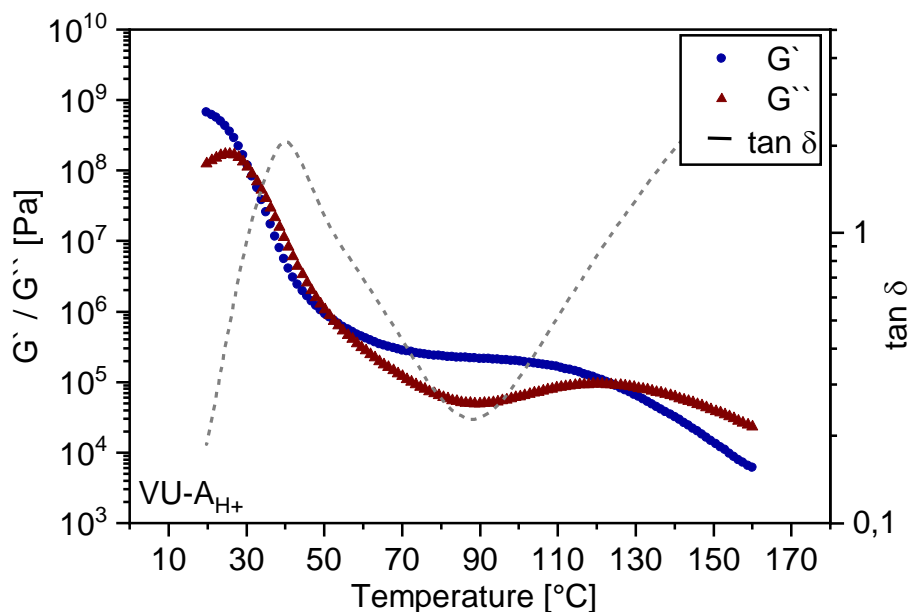
Figure S30: Temperature dependent dynamical-mechanical analysis (DMA) measurement of **VU-A$_{H+}$**. A storage modulus of 0.7 GPa was obtained using G`. In addition, the loss modulus G`` and tan δ are shown in the diagram.
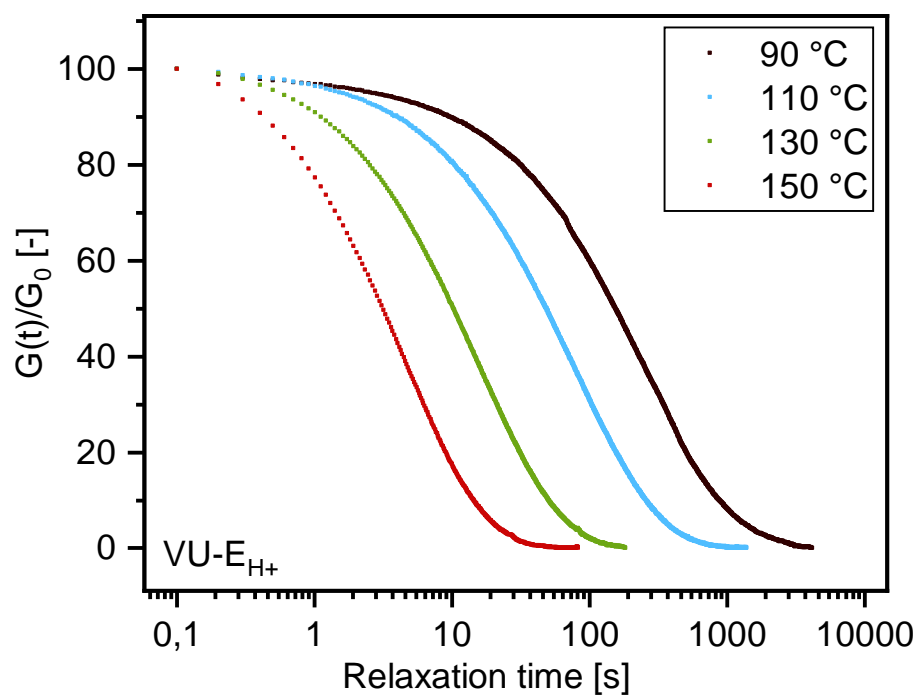
Figure S31: Normalized stress relaxation curves of VU-E$_{H+}$, measured at 90 °C–150 °C with a torsional deformation of 1%.
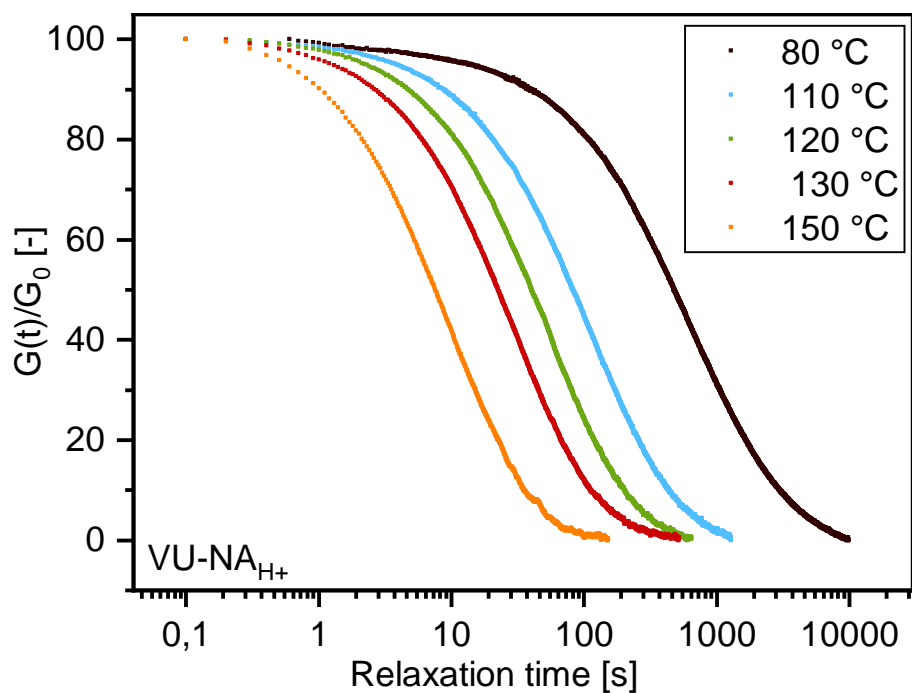
Figure S32: Normalized stress relaxation curves of VU-NA$_{H+}$, measured at 80 °C–150 °C with a torsional deformation of 1%.
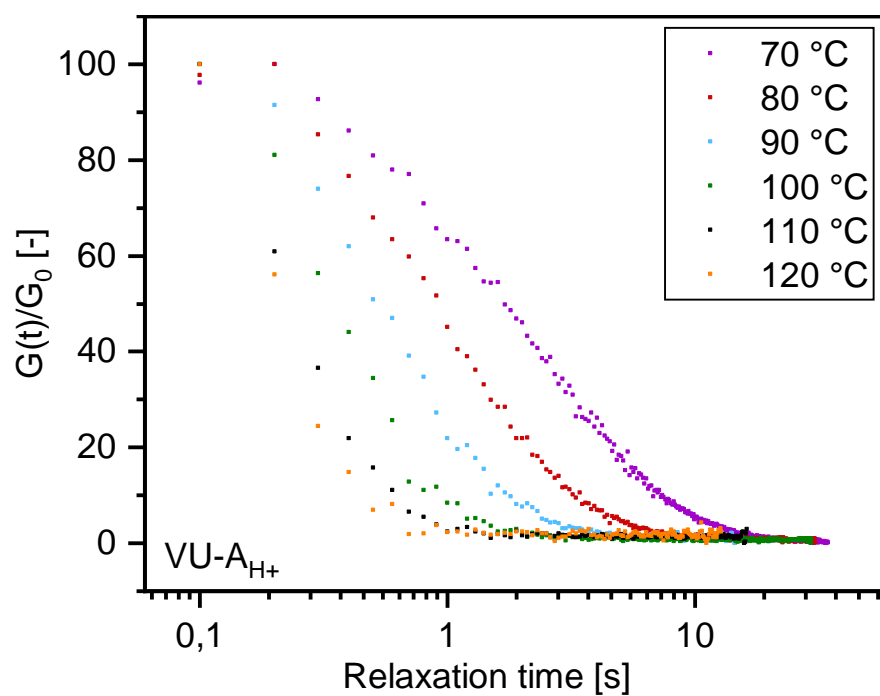
Figure S33: Normalized stress relaxation curves of VU-A$_{H+}$, measured at 70 °C–120 °C with a torsional deformation of 1%.
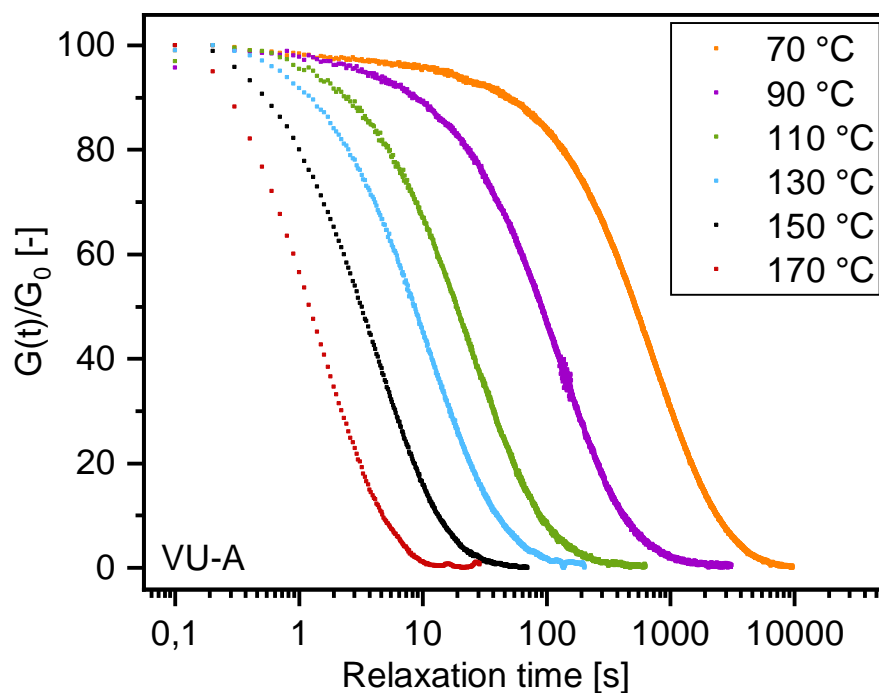
Figure S34: Normalized stress relaxation curves of VU-A, measured at 70 °C–170 °C with a torsional deformation of 1%.
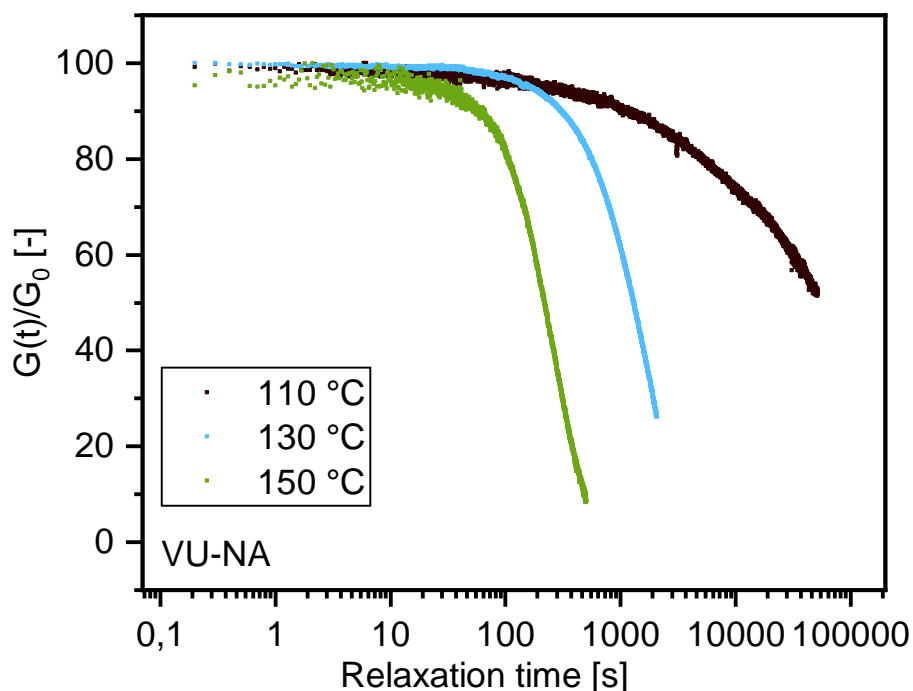
Figure S35: Normalized stress relaxation curves of VU-NA$_{H+}$, measured at 110 °C–150 °C with a torsional deformation of 1%.

9.3   Publication 2 – Supporting Information

Electronic Supplementary Information (ESI) for:

Blended Vinylogous Urethane/Urea Vitrimers Derived from Aromatic Alcohols

Philipp Haida,[a]

Gloria Signorato,[a] and Volker Abetz[a,b*]

[a]Institute of Physical Chemistry, Universität Hamburg, Martin-Luther-King-Platz 6, 20146 Hamburg, Germany

[b]Helmholtz-Zentrum Hereon, Institute of Membrane Research, Max-Planck-Straße 1, 21502 Geesthacht, Germany.

E-Mail: volker.abetz@hereon.de
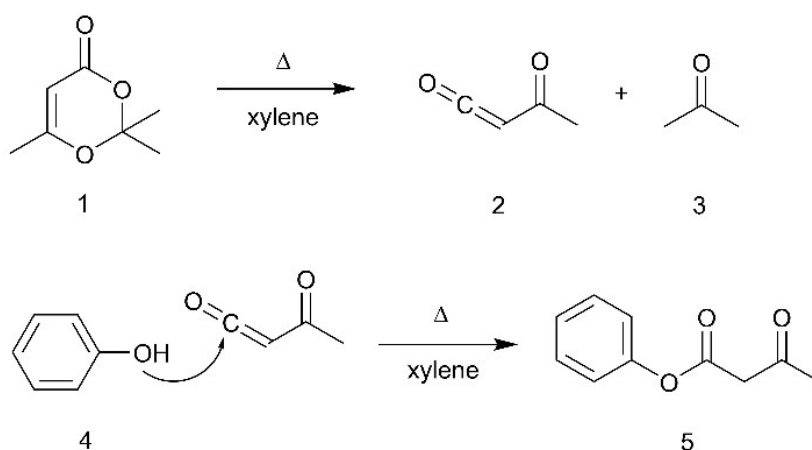
Fig. S1 Schematic representation of the synthesis route for the acetoacetylation of aromatic alcohols using TMDO (**1**). TMDO undergoes a retro-Diels Alder reaction at temperatures above 110 °C, releasing a reactive acetylketene (**2**) and acetone (**3**), while the acetylketene undergoes a fast addition reaction with the aromatic alcohol (**4**) to give the desired aromatic acetoacetate (**5**).
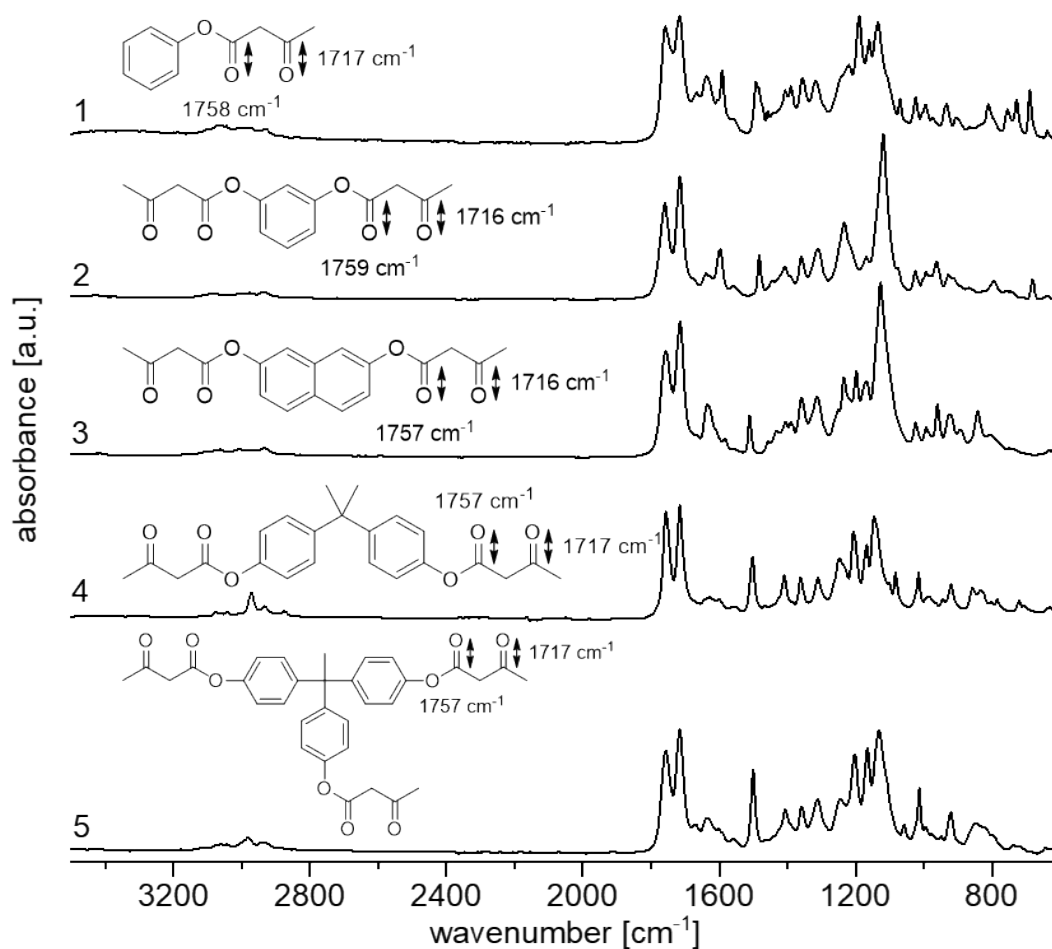
Fig. S2a Full ATR-FT-IR spectra of the synthesized acetoacetate monomers pheny-3-oxobutanoate (PH)(1), 1,3-phenylene bis(3-oxobutanoate) (RE)(2), naphthalene-2,7-diyl bis(3-oxobutanoate) (NDO)(3), propane-2,2-diylbis(4,1-phenylene) bis(3-oxobutanoate) (BPA)(4) and ethane-1,1,1-triyltris(benzene-4,1-diyl) tris(3-oxobutanoate) (THPE)(5).
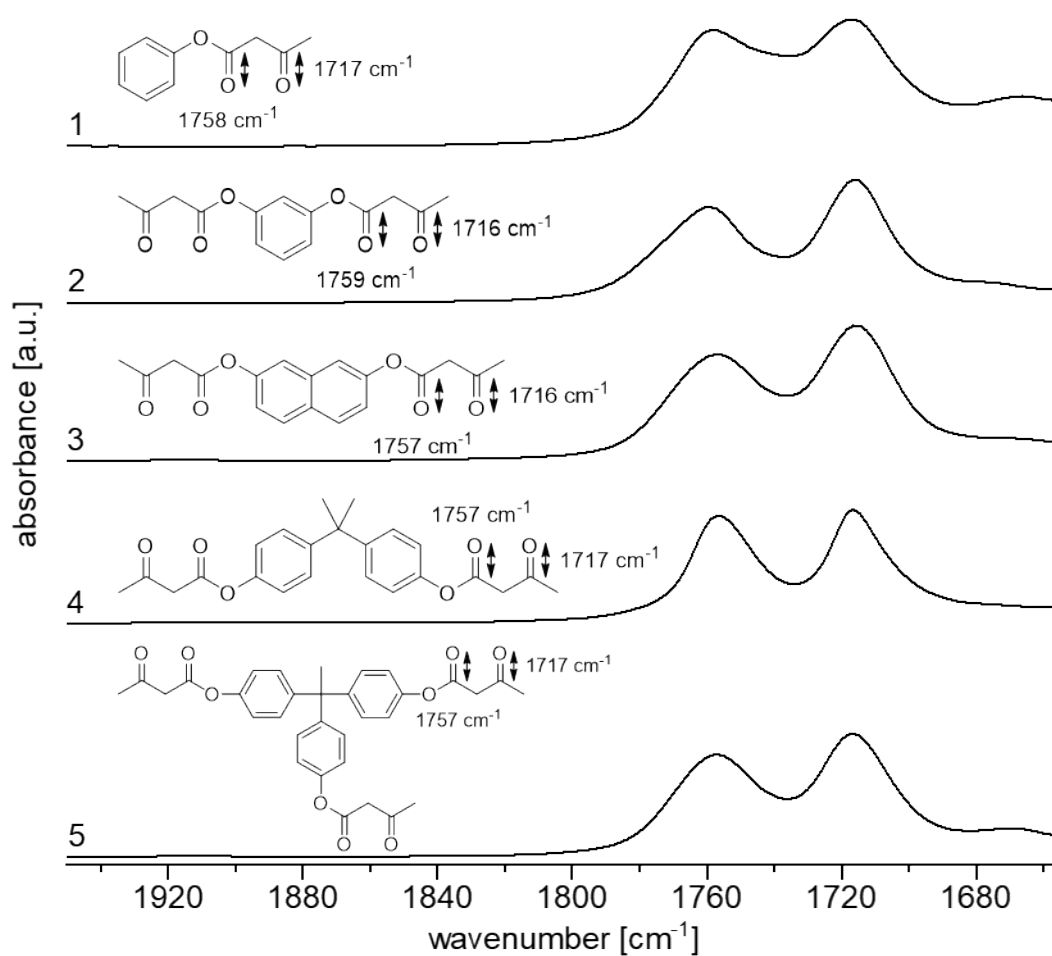
Fig. S2b ATR-FT-IR spectra of the synthesized acetoacetate-monomers PH (1), RE (2), NDO (3), BPA (4) and THPE (5) with the focus on the characteristic C=O ester (1757–1759 cm^{-1}) and C=O ketone bands (1716–1717 cm^{-1}).
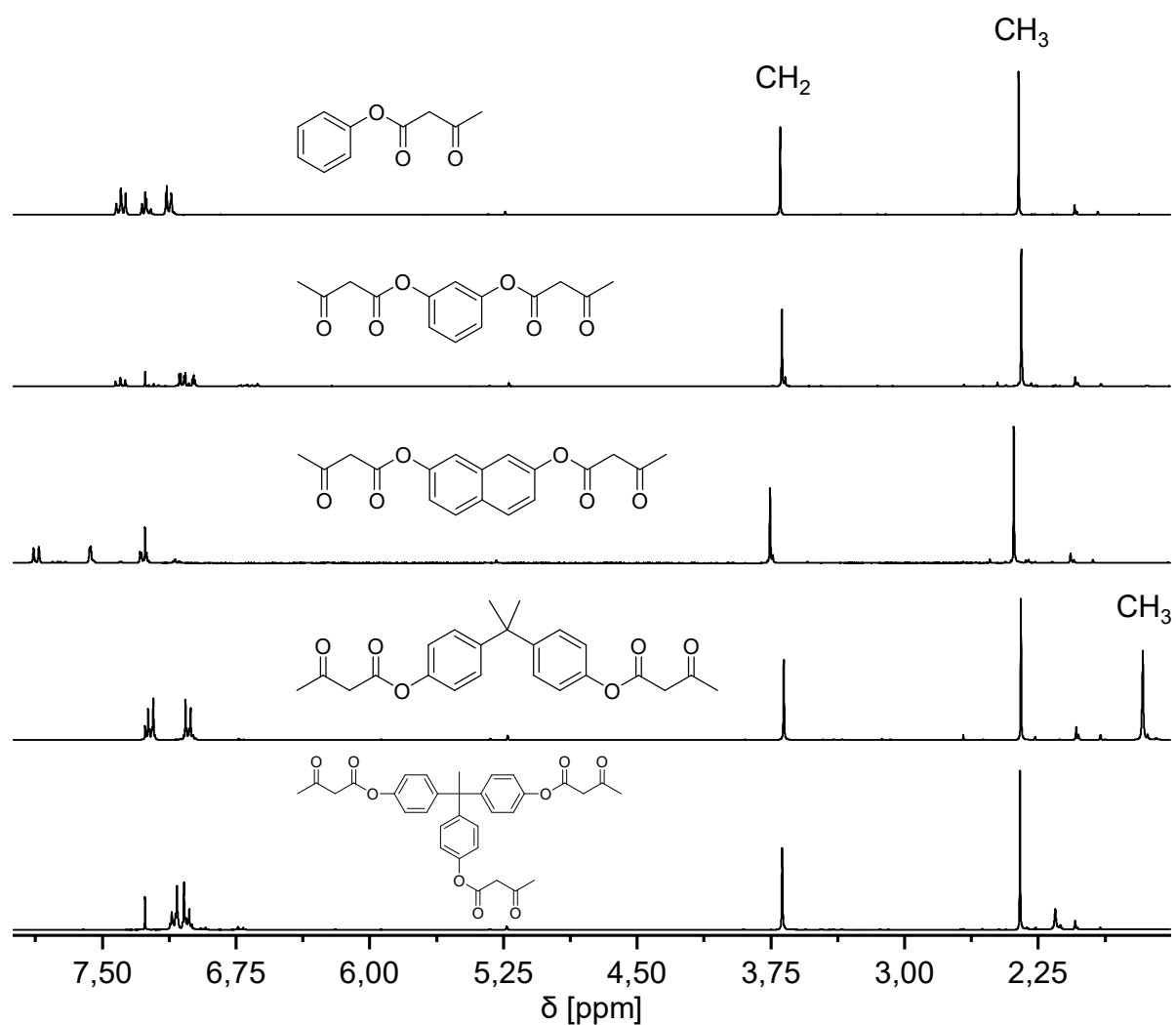
Fig. S3a ^{1}H NMR (CDCl$_3$, 25 °C) spectra of the synthesized acetoacetate monomers PH, RE, NDO, BPA and THPE (from top to bottom). The characteristic CH$_2$ and CH$_3$ signals appear at similar chemical shifts. A detailed list of all signals is provided in the experimental section.
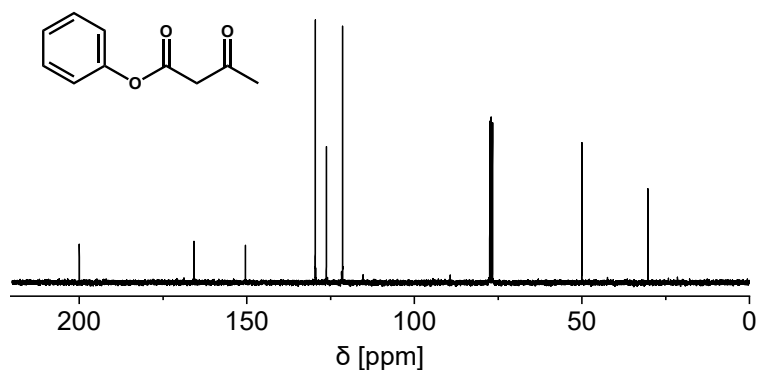
Fig. S3b ^{13}C NMR (broadband decoupled, CDCl$_3$, 25 °C) spectrum of the synthesized acetoacetate monomer phenyl-3-oxobutanoate (PH). δC (75 MHz, CDCl$_3$, Me$_4$Si): 200.06 (q, C=O), 165.83 (q, COO), 150.49 (q, Ph), 129.63 (t, Ph), 126.33 (t, Ph), 121.15 (t, Ph), 50.09 (s, CH$_2$), 30.37 (p, CH$_3$).
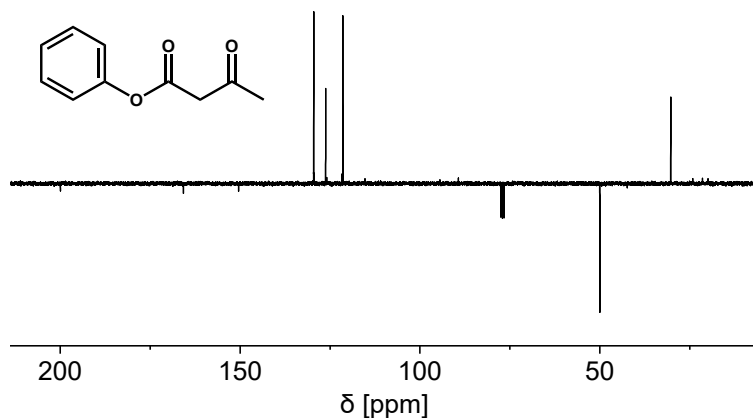
Fig. S3c ^{13}C NMR (DEPTQ-135, CDCl$_3$, 25 °C) spectrum of the synthesized acetoacetate monomer phenyl-3-oxobutanoate (PH). δC (75 MHz, CDCl$_3$, Me$_4$Si): 200.06 (q, C=O), 165.83 (q, COO), 150.49 (q, Ph), 129.63 (t, Ph), 126.33 (t, Ph), 121.15 (t, Ph), 50.09 (s, CH$_2$), 30.37 (p, CH$_3$).
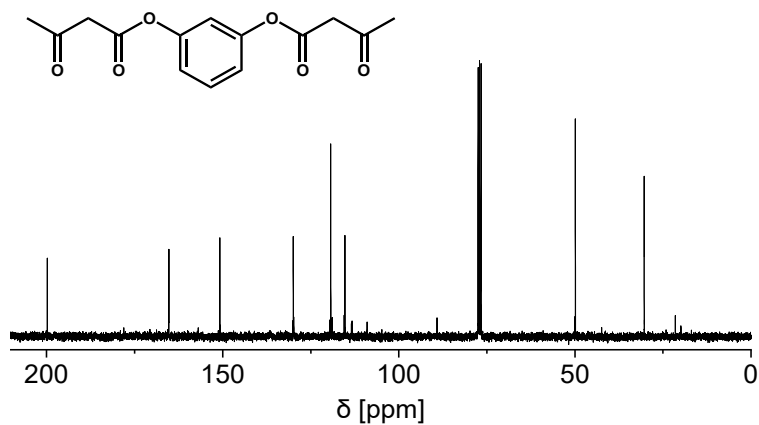
Fig. S3d ^{13}C NMR (broadband decoupled, CDCl$_3$, 25 °C) spectrum of the synthesized acetoacetate monomer 1,3-phenylene bis(3-oxobutanoate) (RE). δC (75 MHz, CDCl$_3$, Me$_4$Si): 199.97 (q, C=O), 165.38 (q, COO), 150.90 (q, Ph-O), 130.05 (t, Ph), 119.42 (t, Ph), 115.38 (t, Ph), 49.46 (s, CH$_2$), 30.41 (p, CH$_3$).
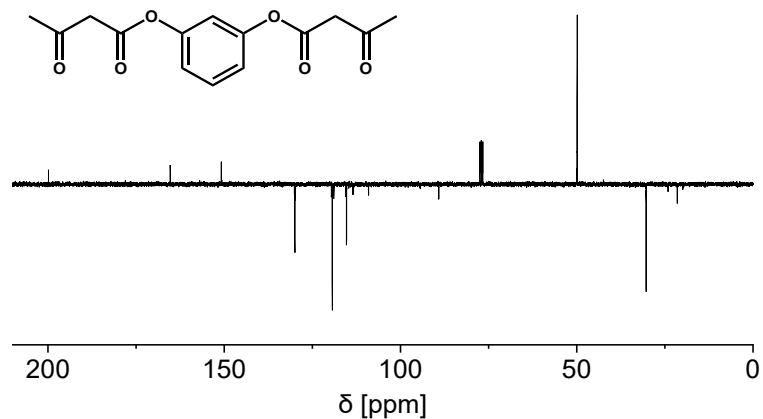
Fig. S3e ^{13}C NMR (DEPTQ-135, CDCl$_3$, 25 °C) spectrum of the synthesized acetoacetate monomer 1,3-phenylene bis(3-oxobutanoate) (RE). δC (75 MHz, CDCl$_3$, Me$_4$Si): 199.97 (q, C=O), 165.38 (q, COO), 150.90 (q, Ph-O), 130.05 (t, Ph), 119.42 (t, Ph), 115.38 (t, Ph), 49.46 (s, CH$_2$), 30.41 (p, CH$_3$).
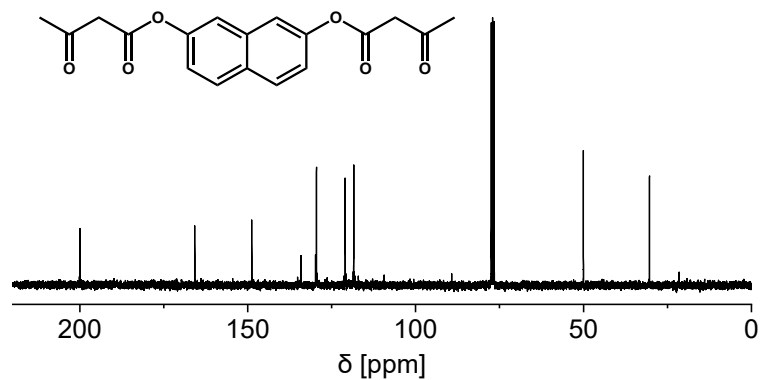
Fig. S3f ^{13}C NMR (broadband decoupled, CDCl$_3$, 25 °C) spectrum of the synthesized acetoacetate monomer naphthalene 2,7 diyl bis(3 oxobutanoate) (NDO). δC (75 MHz, CDCl$_3$, Me$_4$Si): 200.03 (q, C=O), 165.86 (q, COO), 148.89 (q, Ph-O), 134.25 (q, Ph), 129.86 (q, Ph), 129.63 (t, Ph), 121.08 (t, Ph), 118.53 (t, Ph), 50.13 (s, CH$_2$), 30.47 (p, CH$_3$).
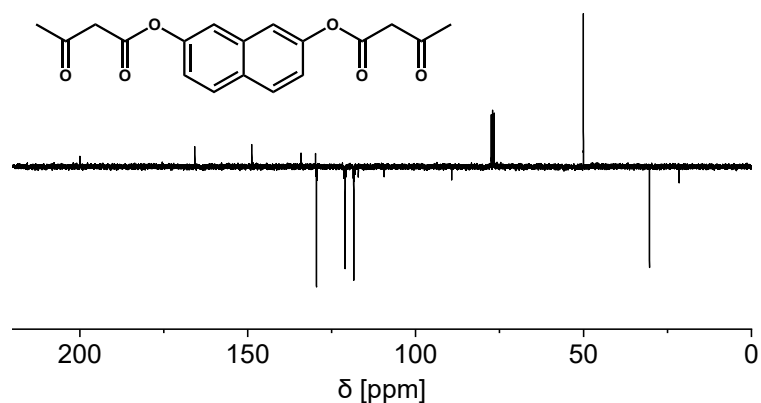
Fig. S3g ^{13}C NMR (DEPTQ-135, CDCl$_3$, 25 °C) spectrum of the synthesized acetoacetate monomer naphthalene 2,7 diyl bis(3 oxobutanoate) (NDO). δC (75 MHz, CDCl$_3$, Me$_4$Si): 200.03 (q, C=O), 165.86 (q, COO), 148.89 (q, Ph-O), 134.25 (q, Ph), 129.86 (q, Ph), 129.63 (t, Ph), 121.08 (t, Ph), 118.53 (t, Ph), 50.13 (s, CH$_2$), 30.47 (p, CH$_3$).
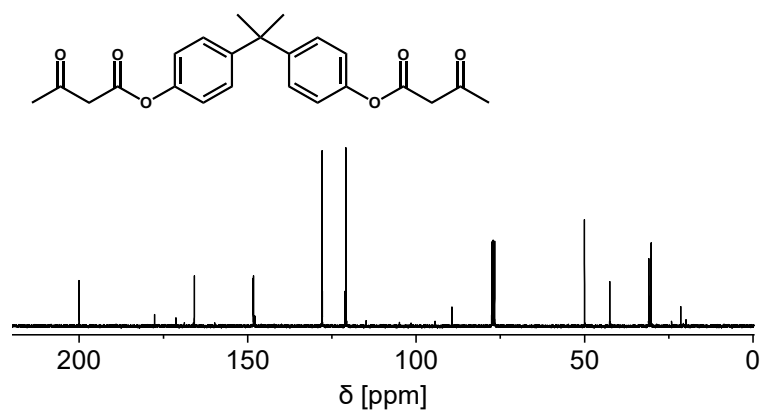
Fig. S3h ^{13}C NMR (broadband decoupled, CDCl$_3$, 25 °C) spectrum of the synthesized acetoacetate monomer propane-2,2-diylbis(4,1-phenylene)bis(3-oxobutanoate) (BPA). δC (75 MHz, CDCl$_3$, Me$_4$Si): 200.06 (q, C=O), 165.87 (q, COO), 148.37 (q, Ph), 148.28 (q, Ph-O), 127.96 (t, Ph), 120.86 (t, Ph), 50.06 (s, CH$_2$), 42.57 (q, C-CH$_3$), 30.95 (p, CH$_3$), 30.31 (p, O=C-CH$_3$).
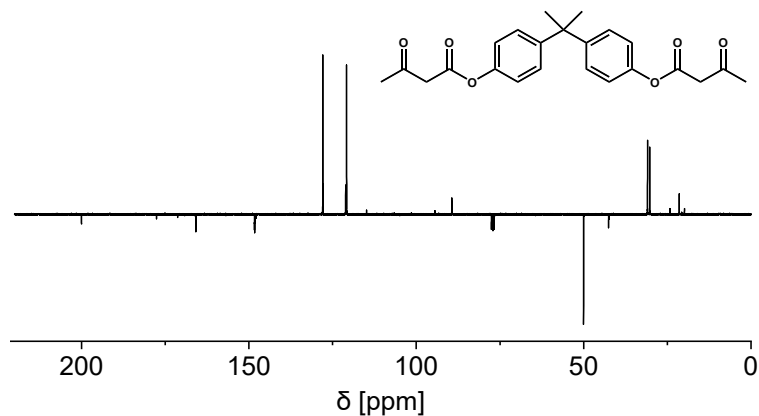
Fig. S3i ^{13}C NMR (DEPTQ-135, CDCl$_3$, 25 °C) spectrum of the synthesized acetoacetate monomer propane-2,2-diylbis(4,1-phenylene)bis(3-oxobutanoate) (BPA). δC (75 MHz, CDCl$_3$, Me$_4$Si): 200.06 (q, C=O), 165.87 (q, COO), 148.37 (q, Ph), 148.28 (q, Ph-O), 127.96 (t, Ph), 120.86 (t, Ph), 50.06 (s, CH$_2$), 42.57 (q, C-CH$_3$), 30.95 (p, CH$_3$), 30.31 (p, O=C-CH$_3$).
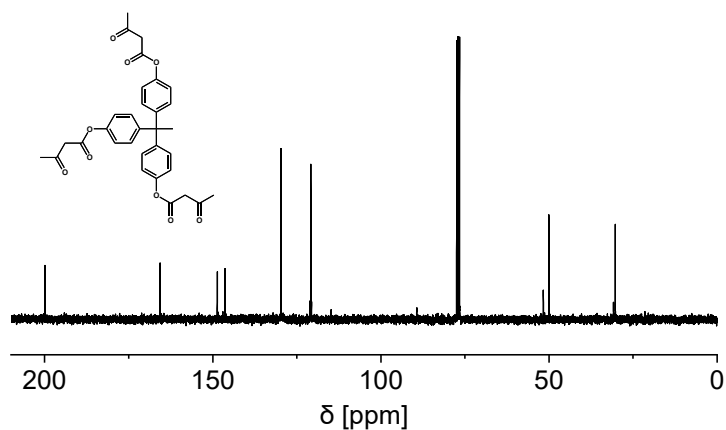
Fig. S3j ^{13}C NMR (broadband decoupled, CDCl$_3$, 25 °C) spectrum of the synthesized acetoacetate monomer ethane-1,1,1-triyltris(benzene-4,1-diyl) tris(3-oxobutanoate) (THPE). δC (75 MHz, CDCl$_3$, Me$_4$Si): 200.01 (q, C=O), 165.81 (q, COO), 148.77 (q, Ph-O), 146.48 (q, Ph-C), 129.86 (t, Ph), 120.93 (t, Ph), 51.80 (q, C-CH$_3$) 50.15 (s, CH$_2$), 30.95 (p, C-CH$_3$), 30.40 (p, O=C-CH$_3$).
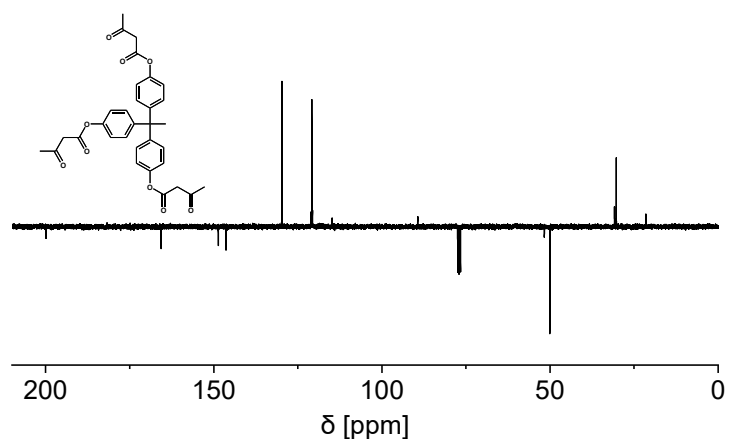
Fig. S3k ^{13}C NMR (DEPTQ-135, CDCl$_3$, 25 °C) spectrum of the synthesized acetoacetate monomer ethane-1,1,1-triyltris(benzene-4,1-diyl) tris(3-oxobutanoate) (THPE). δC (75 MHz, CDCl$_3$, Me$_4$Si): 200.01 (q, C=O), 165.81 (q, COO), 148.77 (q, Ph-O), 146.48 (q, Ph-C), 129.86 (t, Ph), 120.93 (t, Ph), 51.80 (q, C-CH$_3$) 50.15 (s, CH$_2$), 30.95 (p, C-CH$_3$), 30.40 (p, O=C-CH$_3$).
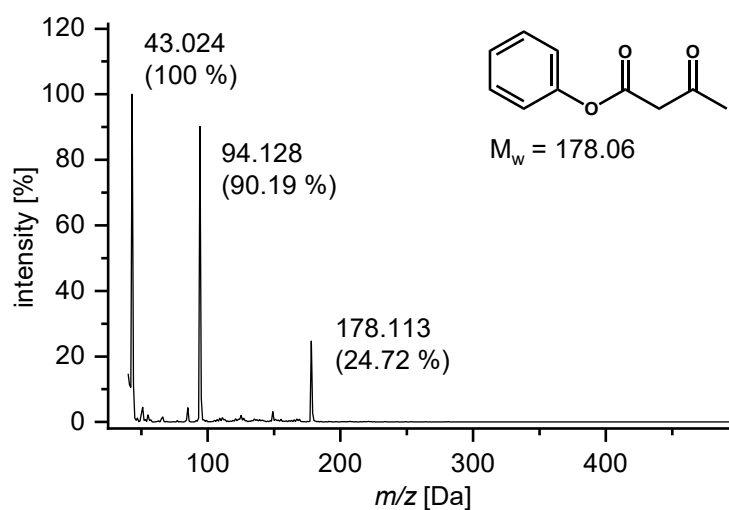
Fig. S4a EI-DIP measurement of phenyl-3-oxobutanoate (PH), showing the characteristic molecule-ion peak and fragmentations. EI-DIP: *m/z* 179.152 (M$^+$ + 1, 2.73 %) 178.113 (M$^+$, 24.72), 94.128 (90.19), 43.024 (100). Calculated for C$_{10}$H$_{10}$O$_3$ (M$^+$) 178.063, found 178.113.
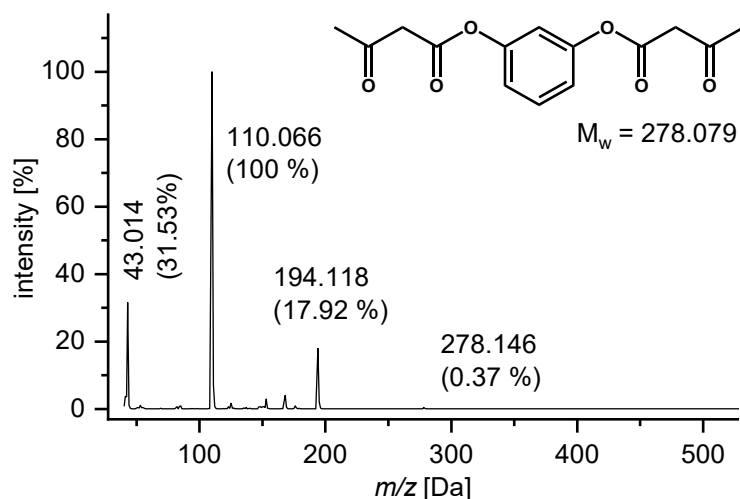
Fig. S4b EI-DIP measurement of 1,3-phenylene bis(3-oxobutanoate) (RE), showing the characteristic molecule-ion peak and fragmentations. EI-DIP: m/z 278.146 (M⁺, 0.37%), 194.118 (17.92), 110.066 (100) 43.014 (31.53). Calculated for $C_{14}H_{14}O_6$ (M⁺) 278.079, found 278.146.
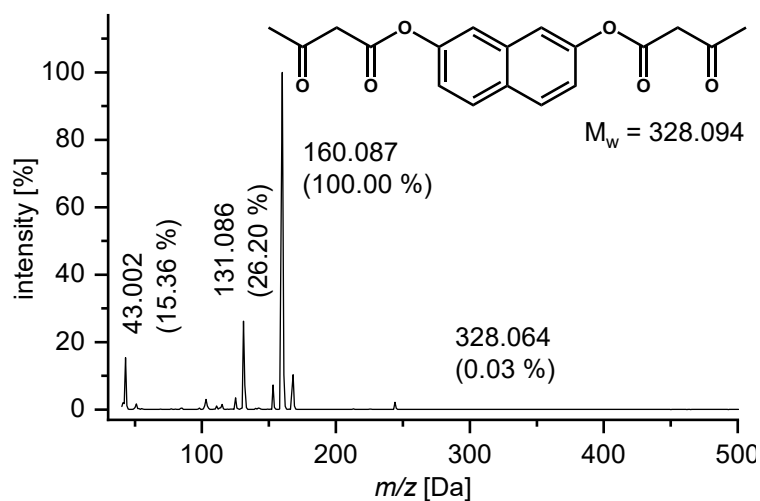
Fig. S4c EI-DIP measurement of naphthalene 2,7 diylbis(3 oxobutanoate)(NDO), showing the characteristic molecule-ion peak and fragmentations. EI-DIP: m/z 178.113 (M, 24.72 %), 94.128 (90.19), 43.024 (100). EI-DIP: m/z 328.064 (M⁺, 0.03%), 160.087 (100.00), 131.086 (26.20), 43.002 (15.06). Calculated for $C_{18}H_{16}O_6$ (M⁺) 328.094, found 328.064.
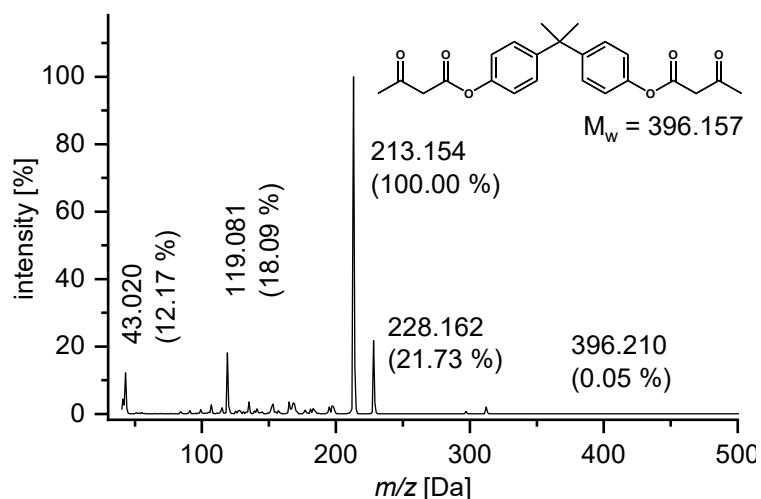
Fig. S4d EI-DIP measurement of propane-2,2-diylbis(4,1-phenylene)bis(3-oxobutanoate) (BPA), showing the characteristic molecule-ion peak and fragmentations. EI-DIP: *m/z* 396.210 (M$^+$, 0.05%), 228.162 (21.73), 213.154 (100.00), 119.081 (18.09), 43.020 (12.17). Calculated for $C_{23}H_{24}O_6$ (M$^+$) 396.157, found 396.210.
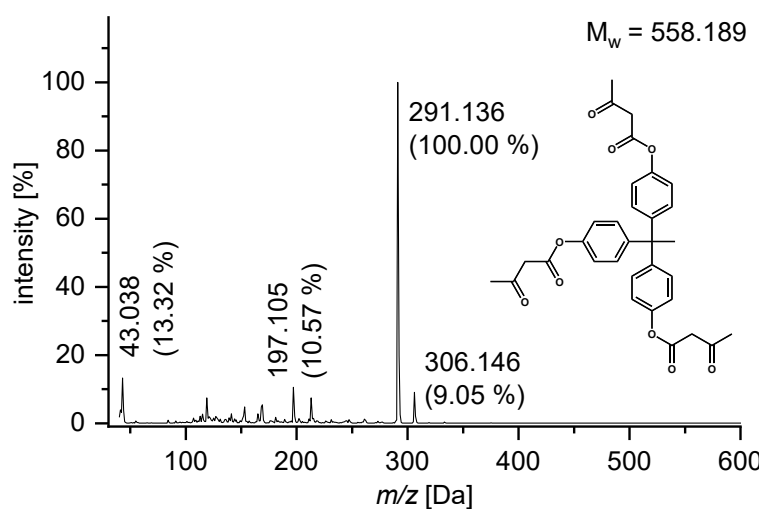
Fig. S4e EI-DIP measurement of ethane-1,1,1-triyltris(benzene-4,1-diyl) tris(3-oxobutanoate) (THPE), showing the characteristic molecule-ion peak and fragmentations. EI-DIP: m/z 558.271 (0.01 %) 306.146 (9.05), 291.136 (100.00), 197.105 (10.57) 43.038 (13.32) (O=C-CH$_3^+$). Calculated for $C_{32}H_{30}O_9$ (M$^+$) 558.189, found 558.271.
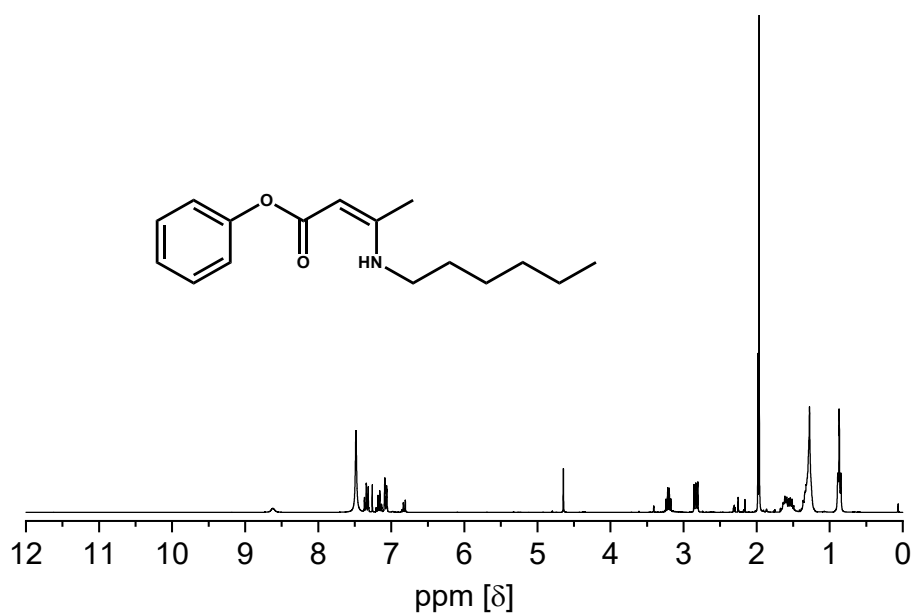
Fig. S5a ¹H NMR spectra (CDCl₃, 25 °C) of spectrum of the synthesized vinylogous urethane reference compound Phe-VUT-Hex. δH (300 MHz, CDCl₃, 298 K): 8.62 (1H, s, NH), 7.40–7.30 (2 H, m, Ph), 7.23–7.12 (1H, m, Ph), 7.11–7.05 (2H, m, Ph), 4.65 (s, 1H; CH), 3.20 (2H, m, CH₂) 1.98 (3H, s, CH₃), 1.68–1.47 (2H, m, CH₂), 1.40–1.18 (6H, m, CH₂), 0.93–0.79 (3H, t, CH₃). Acetic acid: 1.97 (3H, s, CH₃)
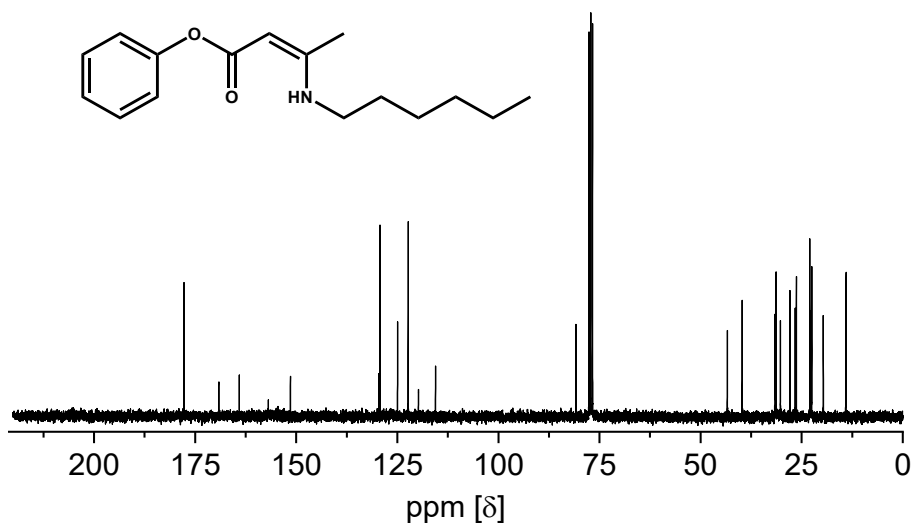
Fig. S5b ¹³C NMR (broadband decoupled, CDCl₃, 25 °C) spectrum of the synthesized vinylogous urethane reference compound Phe-VUT-Hex. δC (75 MHz, CDCl₃, Me₄Si, 298 K): 169.16 (q, COO), 164.08 (q, C=C), 151.54 (q, Ph-O), 129.28 (t, Ph), 124.96 (t, Ph), 122.32 (t, Ph), 80.82 (t, CH), 43.38 (s, CH₂), 31.59 (s, CH₂), 31.32 (s, CH₂), 26.62 (s, CH₂), 22.49 (s, CH₂), 31.6 (p, C-CH₃) 14.11 (p, CH₂-CH₃). Acetic acid: 177.74 (q, COOH), 22.99 (p, CH₃).
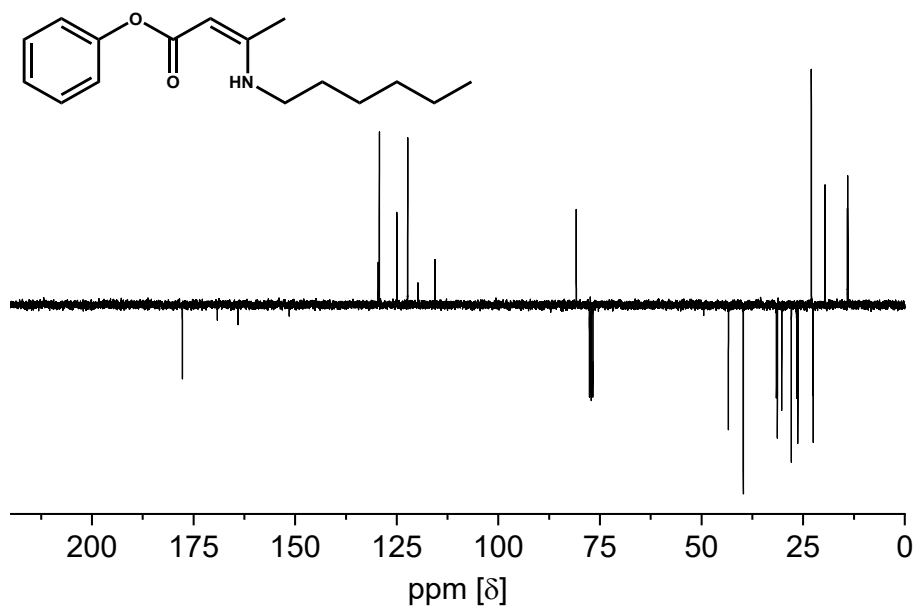
Fig. S5c ^{13}C NMR (DEPTQ-135, CDCl$_3$, 25 °C) spectrum of the synthesized vinylogous urethane reference compound Phe-VUT-Hex. δC (75 MHz, CDCl$_3$, Me$_4$Si, 298 K): 169.16 (q, COO), 164.08 (q, C=C), 151.54 (q, Ph-O), 129.28 (t, Ph), 124.96 (t, Ph), 122.32 (t, Ph), 80.82 (t, CH), 43.38 (s, CH$_2$), 31.59 (s, CH$_2$), 31.32 (s, CH$_2$), 26.62 (s, CH$_2$), 22.49 (s, CH$_2$), 31.6 (p, C-CH$_3$) 14.11 (p, CH$_2$-CH$_3$). Acetic acid: 177.74 (q, COOH), 22.99 (p, CH$_3$).
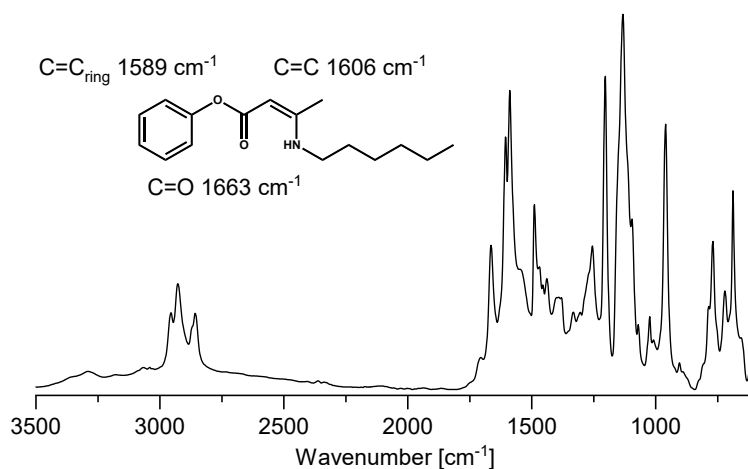
Fig. S6a ATR-FT-IR spectrum of the vinylogous urethane reference compound Phe-VUT-Hex with the characteristic C=O ester band at 1663 cm^{-1}, C=C band at 1606 cm^{-1} and C=C at 1589 cm^{-1} stretching vibrations of the phenylic unit.
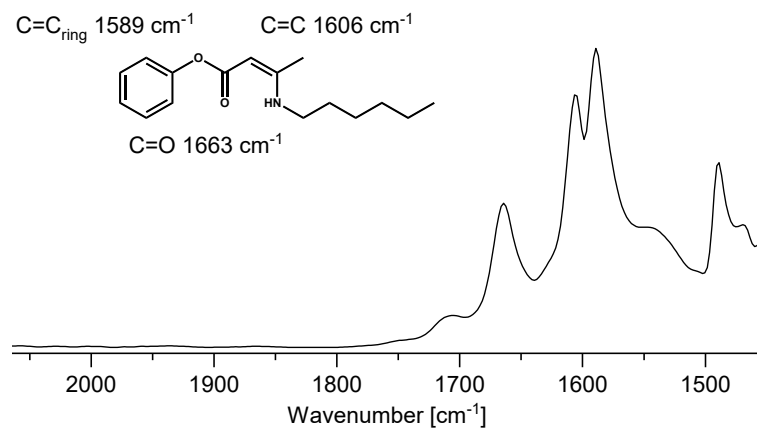
Fig. S6b ATR-FT-IR spectrum of the vinylogous urethane reference compound Phe-VUT-Hex with the characteristic C=O ester band at 1663 cm⁻¹, C=C band at 1606 cm⁻¹ and C=C at 1589 cm⁻¹ stretching vibrations of the phenylic unit proved by measuring ATR-FT-IR-spectra of Phenol (C=C at 1591 cm⁻¹).
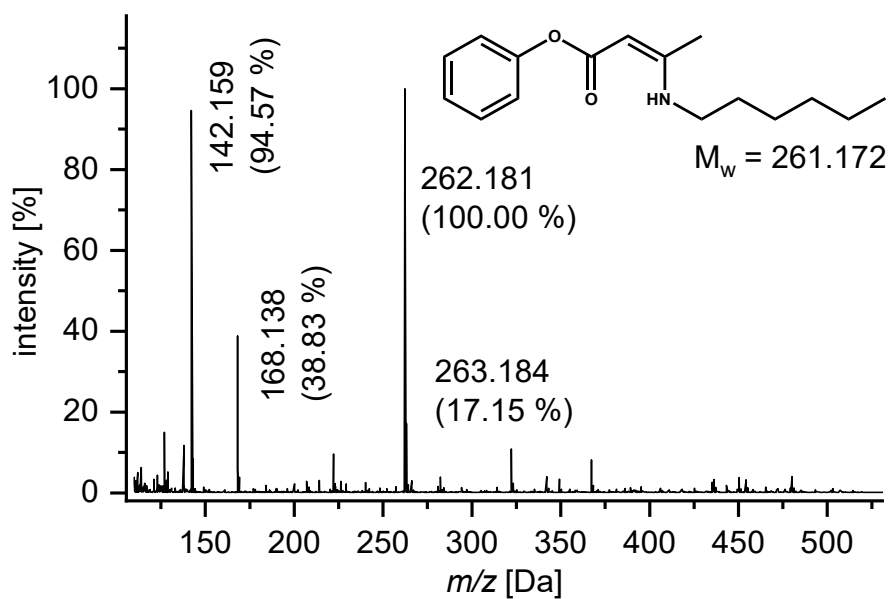
Fig. S7 ESI-MS spectrum of the synthesized vinylogous urethane reference Phe-VUT-Hex showing the characteristic molecule ion peaks 262.181 (M⁺ + 1) and 263.184 (M⁺ + 2).
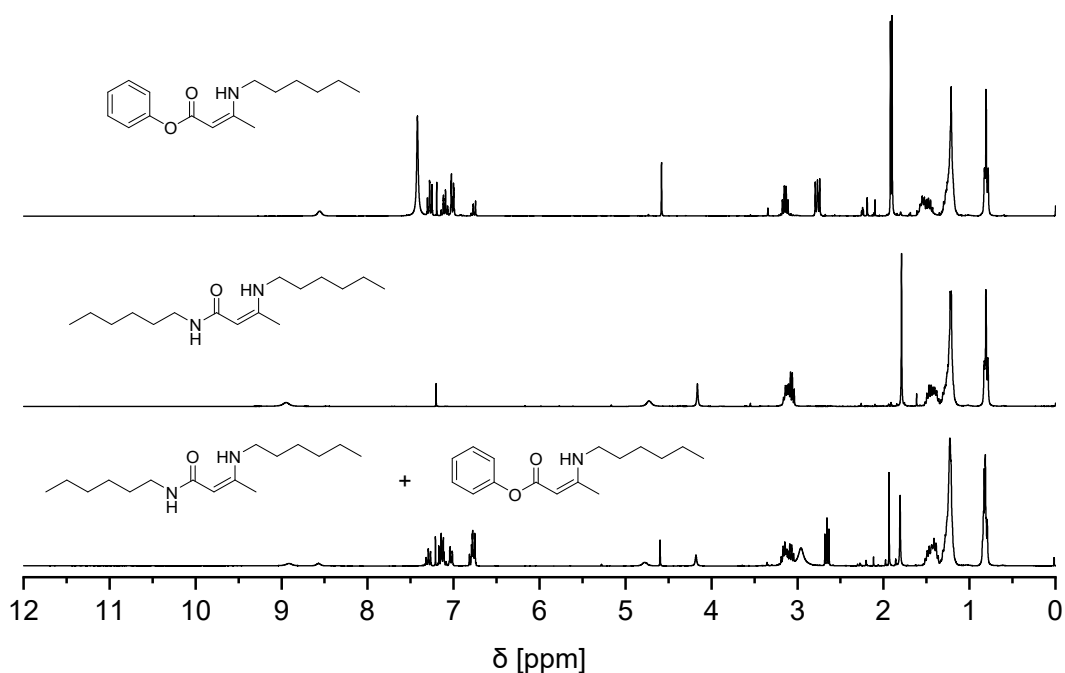
Fig. S8 ^{1}H NMR spectra (CDCl$_3$, 25 °C) of the reference Phe-VUT-Hex (top), Hex-VUA-Hex (middle) and the mixture of both compounds during the synthesis in chloroform (bottom). Hex-VUA-Hex: δH (300 MHz, CDCl$_3$): 9.00 (1H, s, NH), 4.78 (1H, s, NH), 4.22 (1H, s, CH), 3.18 (2H, d, CH$_2$), 3.13 (2H, d, CH$_2$), 1.85 (3H, s, CH$_3$), 1.60–1.42 (4H, m, CH$_2$), 1.40–1.20 (12H, m, CH$_2$), 0.87 (3H, t, CH$_3$), 0.86 (3H, t, CH$_3$). Phe-VUT-Hex: δH (300 MHz, CDCl$_3$, 298 K): 8.62 (1H, s, NH), 7.40–7.30 (2 H, m, Ph), 7.23–7.12 (1H, m, Ph), 7.11–7.05 (2H, m, Ph), 4.65 (s, 1H; CH), 3.20 (2H, m, CH$_2$) 1.98 (3H, s, CH$_3$), 1.68–1.47 (2H, m, CH$_2$), 1.40–1.18 (6H, m, CH$_2$), 0.93–0.79 (3H, t, CH$_3$).
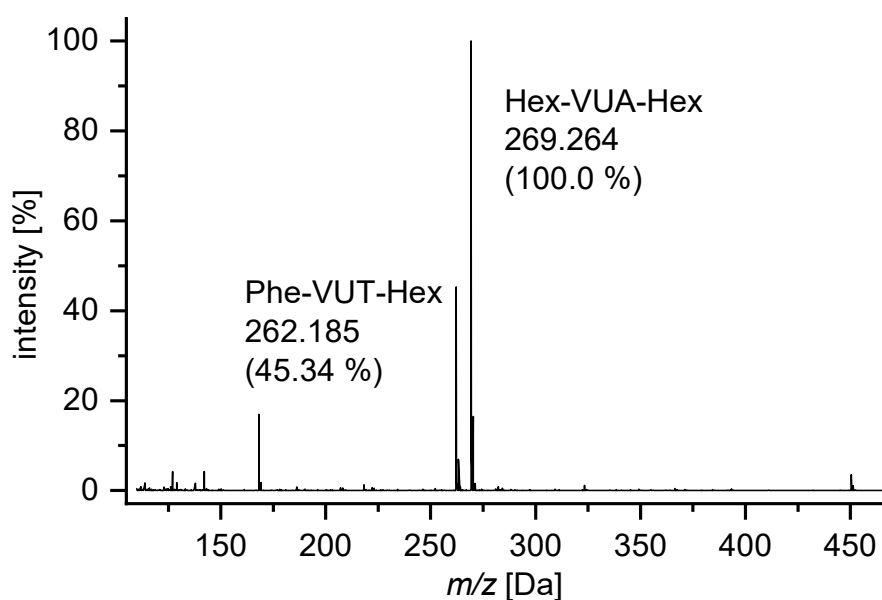
Fig. S9 ESI-MS spectrum of the synthesized mixture of vinylogous urethane Phe-VUT-Hex and Hex-VUA-Hex showing the characteristic molecule ion peaks 269.264 (M$^+$ + 1) and 262.185 (M$^+$ + 1).
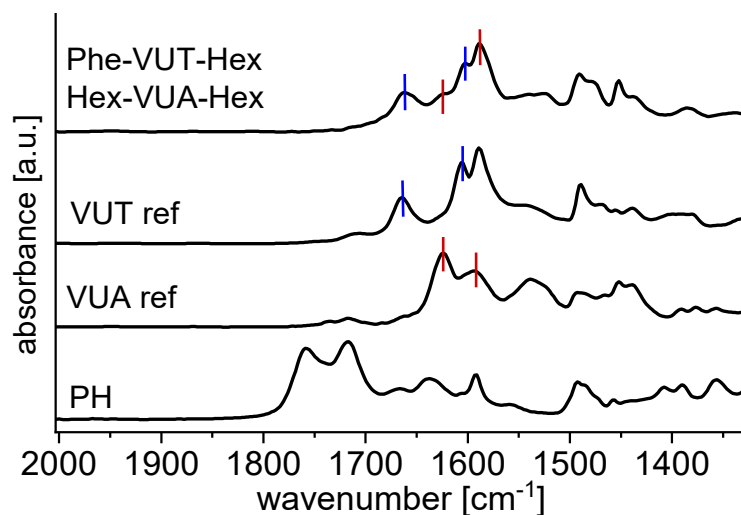
Fig. S10 ATR-FT-IR spectra of the vinylogous urethane and vinylogous urea reference compounds in comparison to the mixture resulted from the condensation/substitution reaction of PH and hexylamine in chloroform. The spectra show the characteristic C=O ester band (1663 cm^{-1}), C=C$_{VUT}$ band (1606 cm^{-1}), C=O amide band (1623 cm^{-1}) and C=C$_{VUA}$ band (1590 cm^{-1}
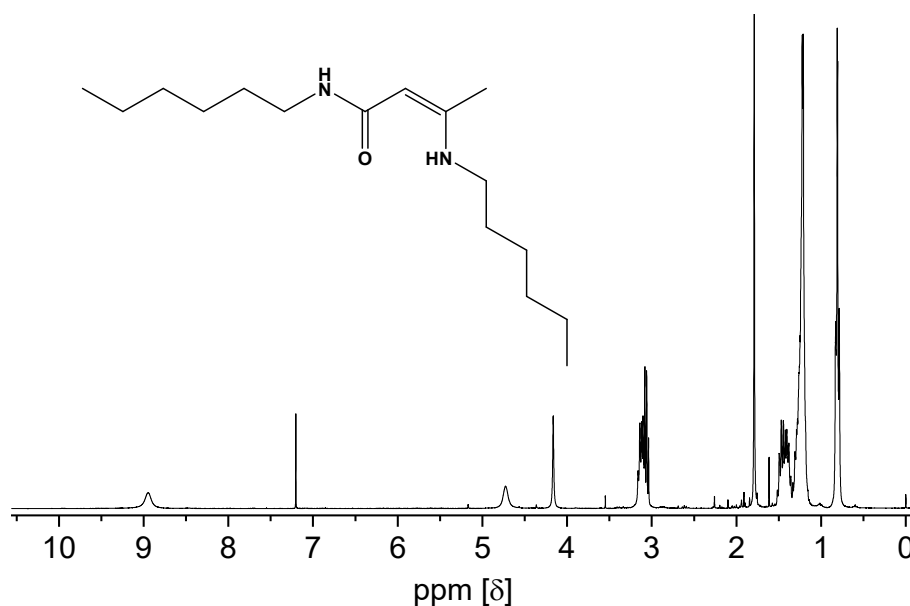
Fig. 11a ^{1}H NMR spectra (CDCl$_3$, 25 °C) of spectrum of the synthesized vinylogous urea reference compound N-hexyl-3-(hexylamino)but-2-enamide (Hex-VUA-Hex). δH (300 MHz, CDCl$_3$): 9.00 (1H, s, NH), 4.78 (1H, s, NH), 4.22 (1H, s, CH), 3.18 (2H, d, CH$_2$), 3.13 (2H, d, CH$_2$), 1.85 (3H, s, CH$_3$), 1.60–1.42 (4H, m, CH$_2$), 1.40–1.20 (12H, m, CH$_2$), 0.87 (3H, t, CH$_3$), 0.86 (3H, t, CH$_3$).
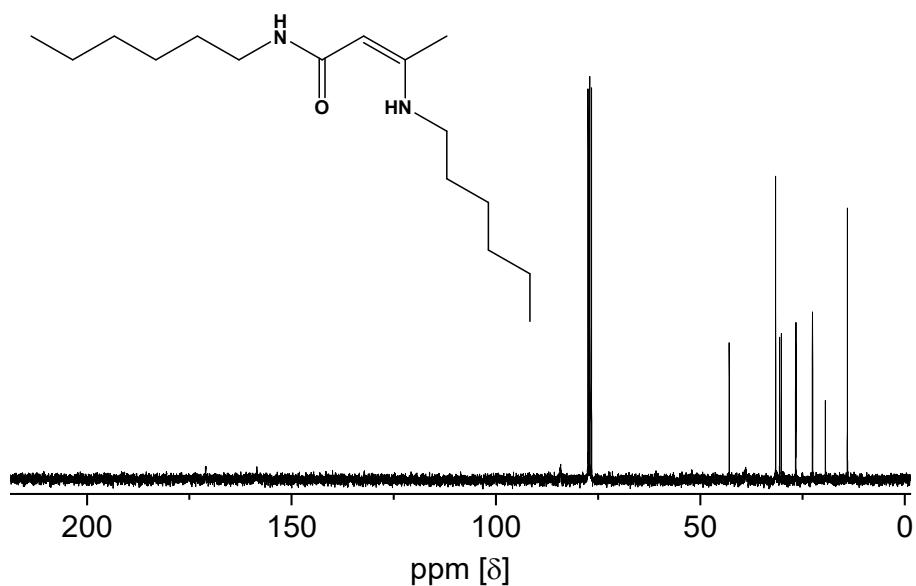
Fig. S11b ^{13}C NMR (broadband decoupled, CDCl$_3$, 25 °C) spectrum of the synthesized vinylogous urea reference compound N-hexyl-3-(hexyllamino)but-2-enamide (Hex-VUA-Hex). δC (75 MHz, CDCl3, 25°C): 171.10 (q, C=O), 158.61 (q, C-CH$_3$), 84.32 (t, CH), 43.04 (s, CH$_2$), 31.07 (s, CH$_2$), 30.73 (s, CH$_2$), 30.31 (s, CH$_2$), 26.83 (s, CH$_2$), 26.75 (s, CH$_2$), 22.72 (s, CH$_2$), 22.66 (s, CH$_2$), 19.53 (p, CH$_3$). 14.15 (p, CH$_3$).
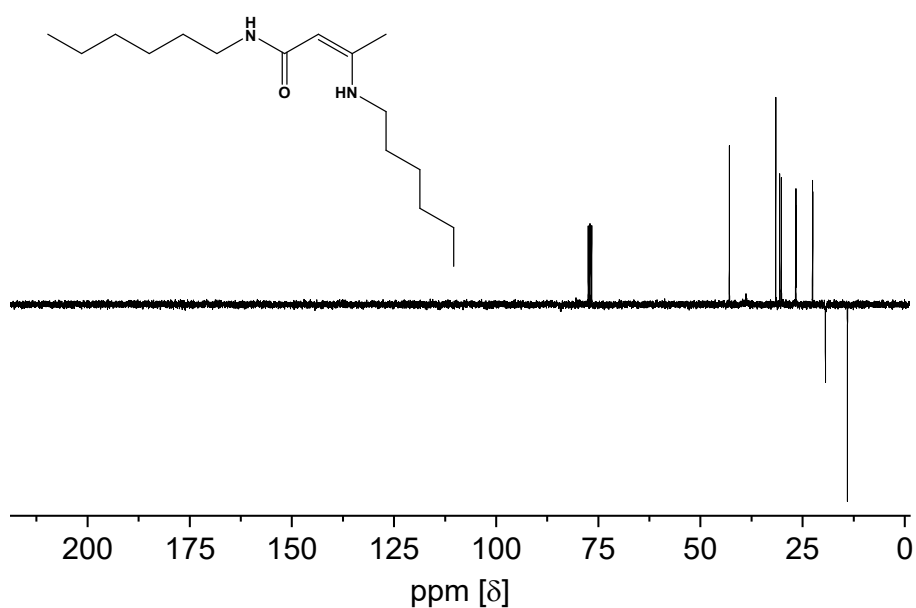
Fig. S11c ^{13}C NMR (DEPTQ-135, CDCl$_3$, 25 °C) spectrum of the synthesized vinylogous urea reference compound N-hexyl-3-(hexylamino)but-2-enamide (Hex-VUA-Hex). δC (75 MHz, CDCl3, 25°C): 171.10 (q, C=O), 158.61 (q, C-CH$_3$), 84.32 (t, CH), 43.04 (s, CH$_2$), 31.07 (s, CH$_2$), 30.73 (s, CH$_2$), 30.31 (s, CH$_2$), 26.83 (s, CH$_2$), 26.75 (s, CH$_2$), 22.72 (s, CH$_2$), 22.66 (s, CH$_2$), 19.53 (p, CH$_3$). 14.15 (p, CH$_3$).
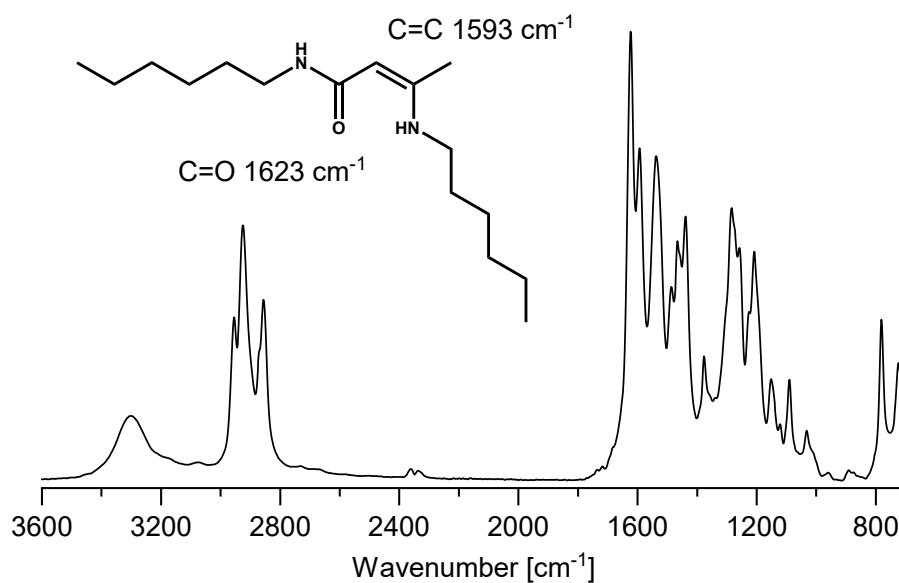
Fig. S12 ATR-FT-IR spectrum of the vinylogous urea reference compound Hex-VUA-Hex with the characteristic C=O amid band at 1623 cm^{-1} and C=C band at 1593 cm^{-1}.
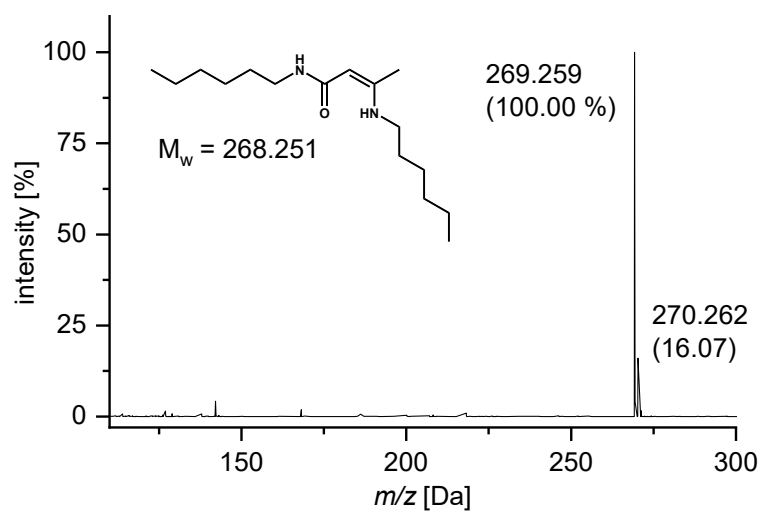
Fig. S13 ESI-MS spectrum of the synthesized vinylogous urea reference compound Hex-VUA-Hex showing the characteristic molecule ion peaks 269.264 (M$^+$ + 1) and 270.262 (M$^+$ + 2).
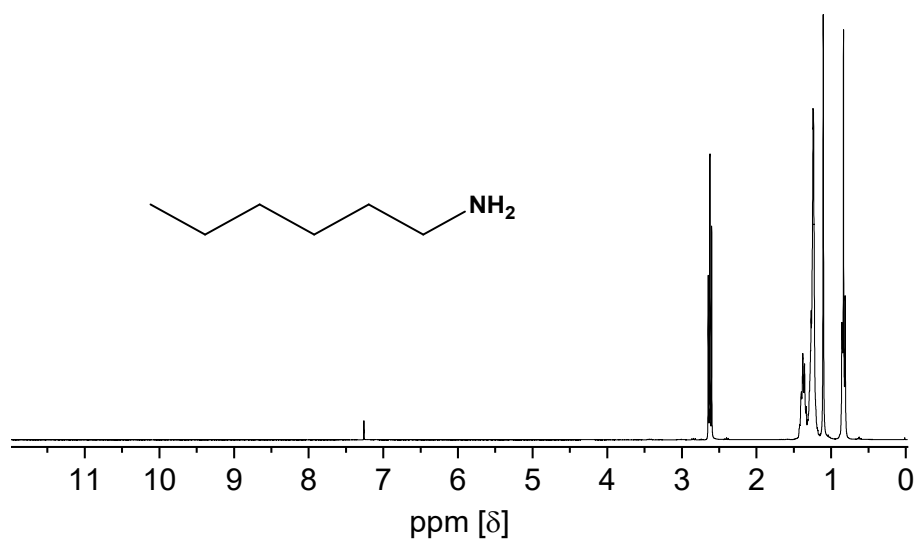
Fig. S14a ^{1}H NMR spectra (CDCl$_3$, 25 °C) of spectrum of hexylamine. δH (300 MHz, CDCl$_3$): δH (300 MHz, CDCl$_3$, 25°C): 2.62 (2H, t, N-CH$_2$), 1.43–1.32 (2H, m, CH$_2$), 1.32–1.17 (6H, m, CH$_2$), 1.11 (2H, s, NH$_2$), 0.83 (3H, t, CH$_3$).
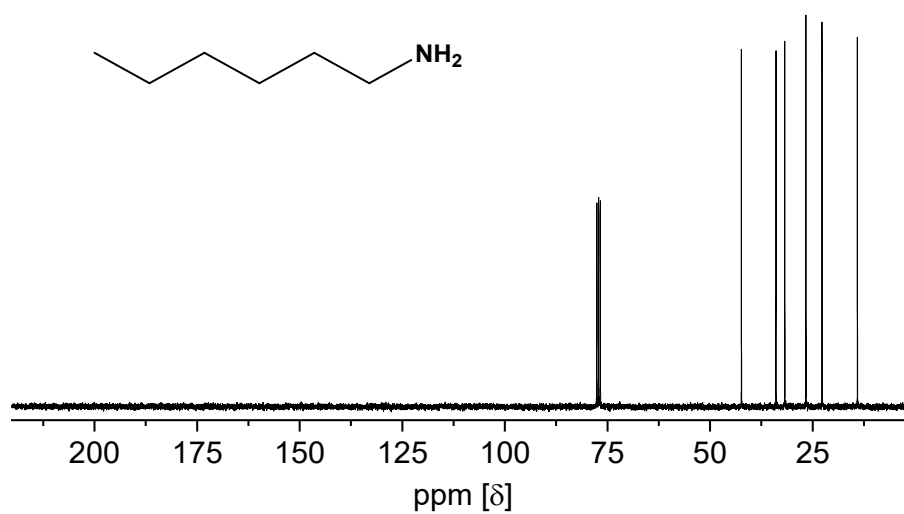
Fig. S14b ^{13}C NMR (broadband decoupled, CDCl$_3$, 25 °C) spectrum of hexylamine. δC (75 MHz, CDCl$_3$): 42.35 (s, CH$_2$), 33.93 (s, CH$_2$), 31.78 (s, CH$_2$), 26.63 (s, CH$_2$), 22.70 (s, CH$_2$), 14.08 (s, CH$_3$).
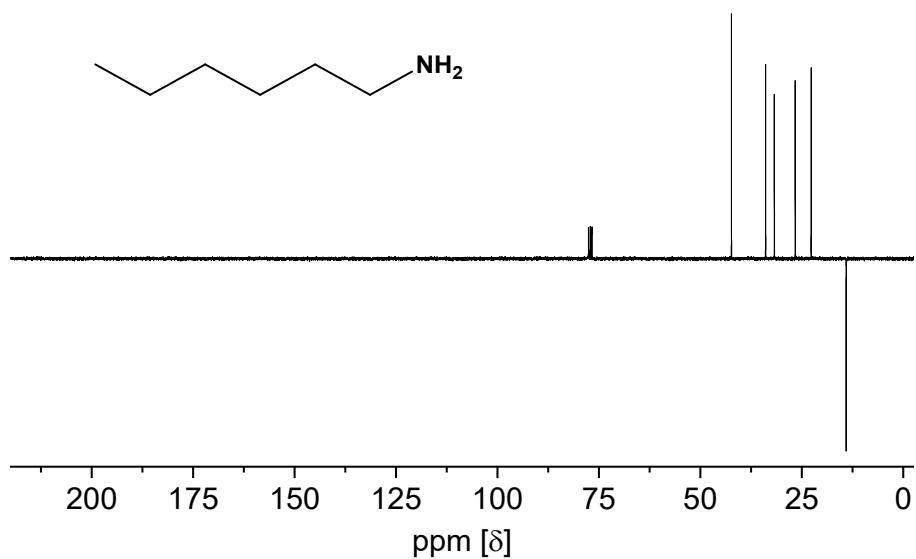
Fig. S14c ^{13}C NMR (DEPTQ-135, CDCl$_3$, 25 °C) spectrum of hexylamine. δC (75 MHz, CDCl$_3$): 42.35 (s, CH$_2$), 33.93 (s, CH$_2$), 31.78 (s, CH$_2$), 26.63 (s, CH$_2$), 22.70 (s, CH$_2$), 14.08 (s, CH$_3$).
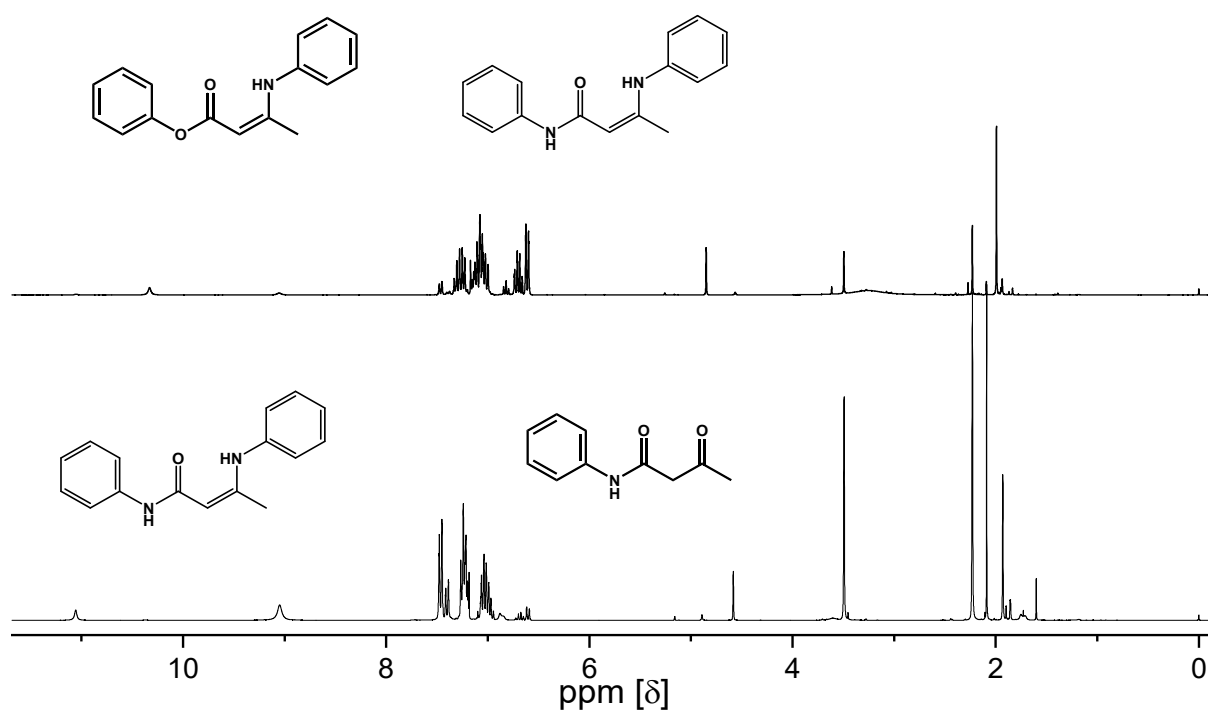
Fig. S15 ^{1}H NMR spectra (CDCl$_3$, 25 °C) of the condensation reaction product Phenyl-3-(phenylamino)but-2-enoate (Phe-VUT-Phe) synthesized by mixing phenylacetoacetate and aniline, producing mainly the vinylogous urethane product (67%) (top). ^{1}H NMR reference spectra of the vinylogous urea compound N-phenyl-3-(phenylamino)but-2-enamide Phe-VUA-Phe, showing the vinylogous urea compound and the acetoacetamide intermediate product (bottom). Phe-VUA-Phe: δH (300 MHz, CDCl$_3$): 11.06 (1H, s, NH), 7.43–7.34 (2H, d, Ph), 7.26–7.15 (4H, m, Ph), 7.08–6.91 (4H, m, Ph), 6.85 (1H, s, NH), 4.57 (1H, s, CH), 1.91 (3H, s,

CH$_3$). Phe-VUT-Phe: δH (300 MHz, CDCl$_3$, 298 K): 10.33 (1H, t, NH), 7.50–6.97 (10H, m, Ph), 4.87 (1H, s, CH), 2.02 (3H, s, CH$_3$).
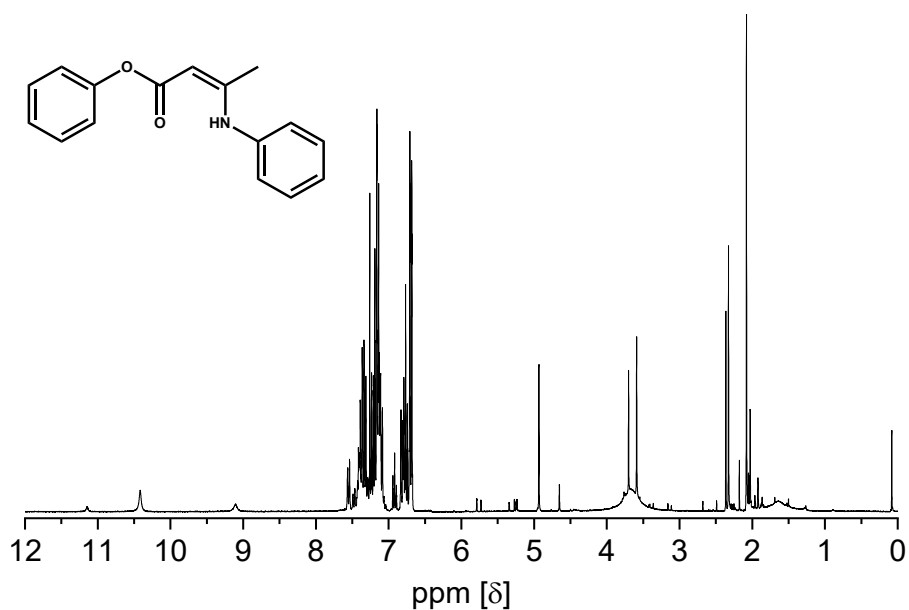
Fig. S16a ^{1}H NMR spectra (CDCl$_3$, 25 °C) of spectrum of the synthesized vinylogous urethane mixture of Phe-VUT-Phe and Phe-VUA-Phe. Phe-VUA-Phe: δH (300 MHz, CDCl$_3$): 11.06 (1H, s, NH), 7.43–7.34 (2H, d, Ph), 7.26–7.15 (4H, m, Ph), 7.08–6.91 (4H, m, Ph), 6.85 (1H, s, NH), 4.57 (1H, s, CH), 1.91 (3H, s, CH$_3$). Phe-VUT-Phe: δH (300 MHz, CDCl$_3$, 298 K): 10.33 (1H, t, NH), 7.50–6.97 (10H, m, Ph), 4.87 (1H, s, CH), 2.02 (3H, s, CH$_3$).
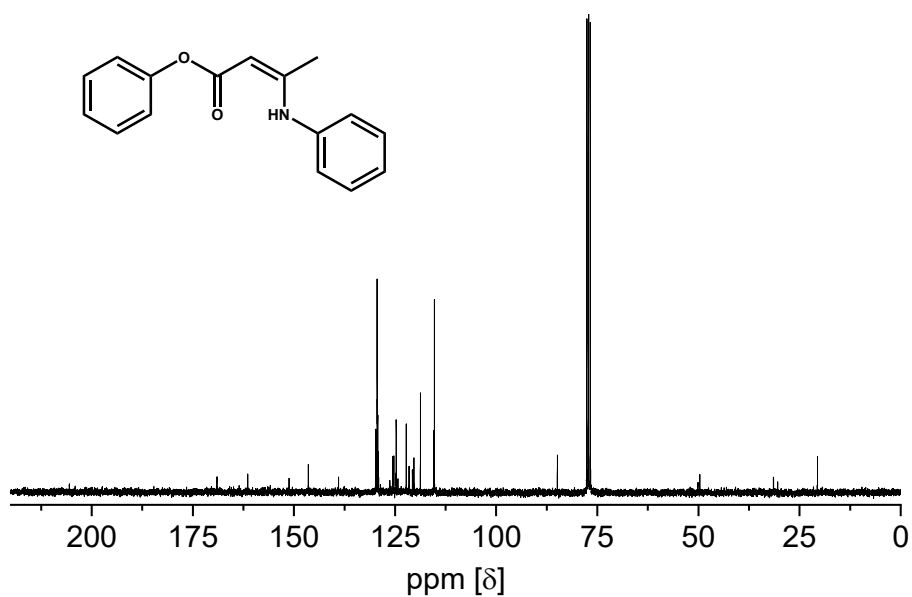
Fig. S16b ^{13}C NMR (broadband decoupled, CDCl$_3$, 25 °C) of the synthesized vinylogous urethane mixture of Phe-VUT-Phe and Phe-VUA-Phe. Phe-VUT-Phe: δC (75 MHz, CDCl$_3$, Me$_4$Si): 169.04 (q, COO), 161.42 (q, C=C), 151.21 (q, Ph-O), 129.45 (t, Ph), 129.10 (t, Ph), 124.74 (t, Ph), 122.24 (t, Ph), 118.72 (t, Ph), 84.86 (t, CH), 20.74 (p, CH$_3$). Phe-VUA-Phe: δC (75 MHz, CDCl$_3$): 168.85 (q, C=O), 157.38 (q, C-CH$_3$), 139.71 (q, Ph), 138.91 (q, Ph), 129.08 (t, Ph), 129.00 (t, Ph), 124.56 (t, Ph), 124.18 (t, Ph), 123.37 (t, Ph), 120.11 (t, Ph), 88.66 (t, CH), 20.57 (p, CH$_3$).
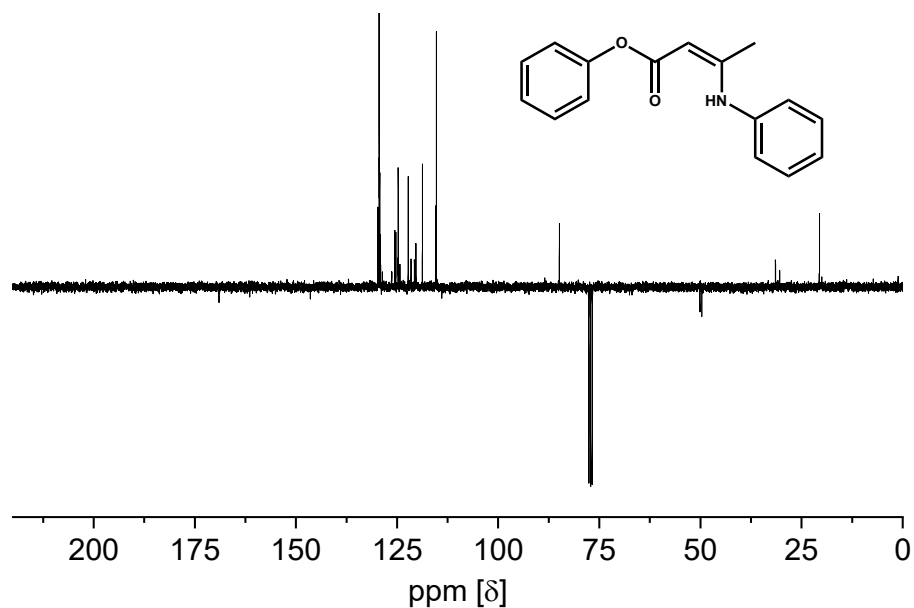
Fig. S16c ^{13}C NMR (DEPTQ-135, CDCl$_3$, 25 °C) of the synthesized vinylogous urethane mixture of Phe-VUT-Phe and Phe-VUA-Phe. Phe-VUT-Phe: δC (75 MHz, CDCl$_3$, Me$_4$Si): 169.04 (q, COO), 161.42 (q, C=C), 151.21 (q, Ph-O), 129.45 (t, Ph), 129.10 (t, Ph), 124.74 (t, Ph), 122.24 (t, Ph), 118.72 (t, Ph), 84.86 (t, CH), 20.74 (p, CH$_3$). Phe-VUA-Phe: δC (75 MHz, CDCl$_3$): 168.85 (q, C=O), 157.38 (q, C-CH$_3$), 139.71 (q, Ph), 138.91 (q, Ph), 129.08 (t, Ph), 129.00 (t, Ph), 124.56 (t, Ph), 124.18 (t, Ph), 123.37 (t, Ph), 120.11 (t, Ph), 88.66 (t, CH), 20.57 (p, CH$_3$).
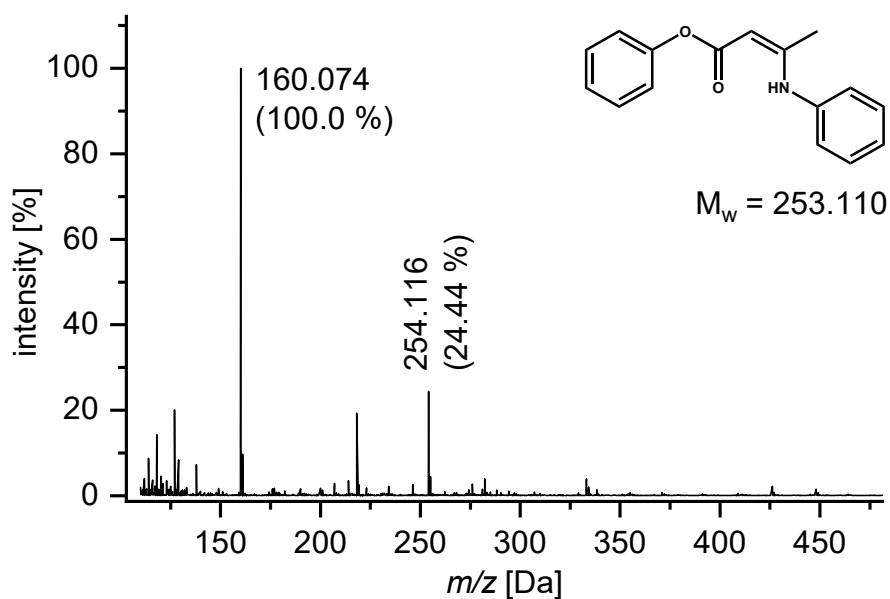
Fig. S17 ESI-MS spectrum of the synthesized vinylogous urethane compound Phe-VUT-Phe showing the characteristic molecule ion peak 254.116 (M$^+$ + 1).
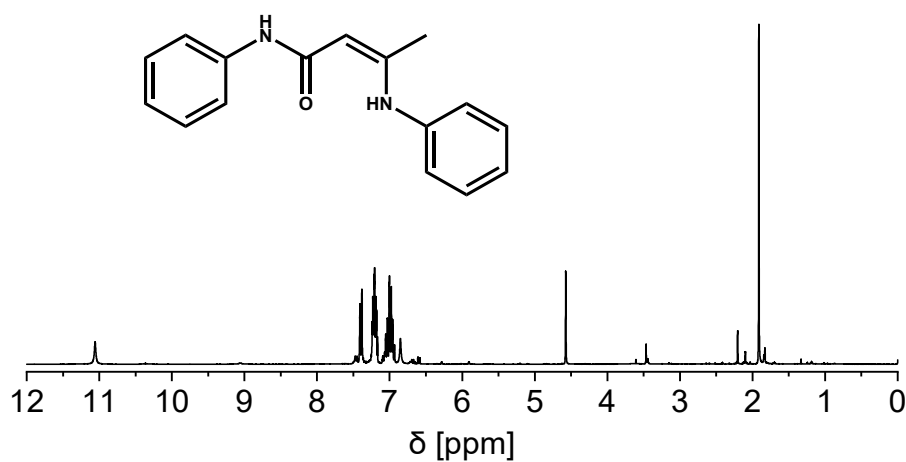
Fig. S18a ^{1}H NMR spectra (CDCl$_3$, 25 °C) of spectrum of the synthesized vinylogous urea reference compound N-phenyl-3-(phenylamino)but-2-enamide (Phe-VUA-Phe). δH (300 MHz, CDCl$_3$): 11.06 (1H, s, NH), 7.43–7.34 (2H, d, Ph), 7.26–7.15 (4H, m, Ph), 7.08–6.91 (4H, m, Ph), 6.85 (1H, s, NH), 4.57 (1H, s, CH), 1.91 (3H, s, CH$_3$).
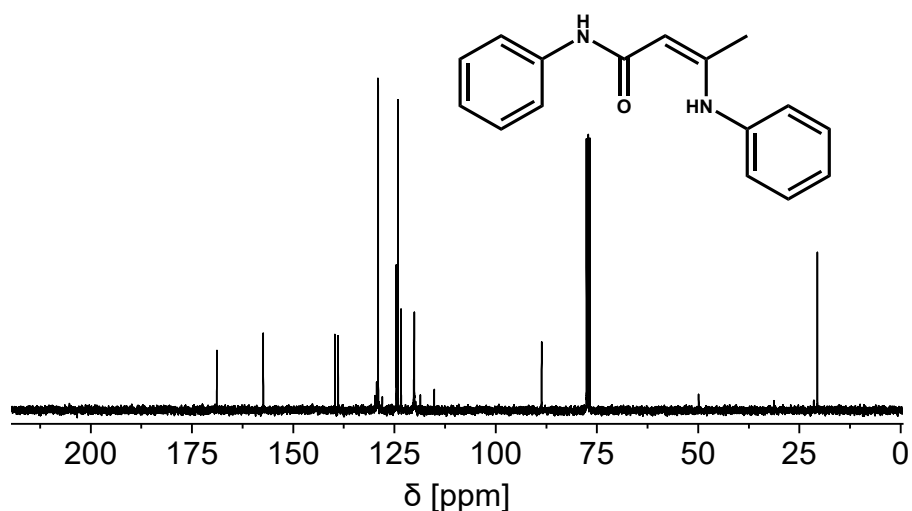
Fig. S18b ^{13}C NMR (broadband decoupled, CDCl$_3$, 25 °C) spectrum of the synthesized vinylogous urea reference compound N-phenyl-3-(phenylamino)but-2-enamide (Phe-VUA-Phe). δC (75 MHz, CDCl$_3$): 168.85 (q, C=O), 157.38 (q, C-CH$_3$), 139.71 (q, Ph), 138.91 (q, Ph), 129.08 (t, Ph), 129.00 (t, Ph), 124.56 (t, Ph), 124.18 (t, Ph), 123.37 (t, Ph), 120.11 (t, Ph), 88.66 (t, CH), 20.57 (p, CH$_3$).
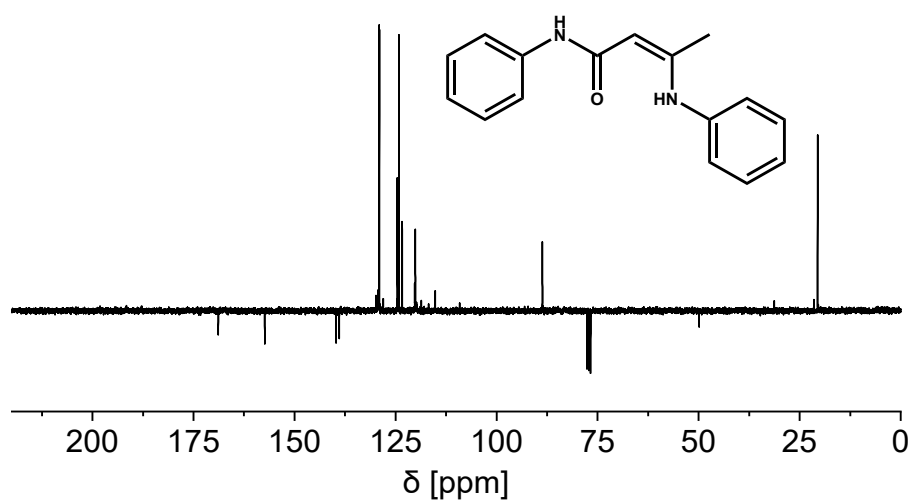
Fig. S18c ^{13}C NMR (DEPTQ-135, CDCl$_3$, 25 °C) spectrum of the synthesized vinylogous urea reference compound N-phenyl-3-(phenylamino)but-2-enamide (Phe-VUA-Phe). δC (75 MHz, CDCl$_3$): 168.85 (q, C=O), 157.38 (q, C-CH$_3$), 139.71 (q, Ph), 138.91 (q, Ph), 129.08 (t, Ph), 129.00 (t, Ph), 124.56 (t, Ph), 124.18 (t, Ph), 123.37 (t, Ph), 120.11 (t, Ph), 88.66 (t, CH), 20.57 (p, CH$_3$).
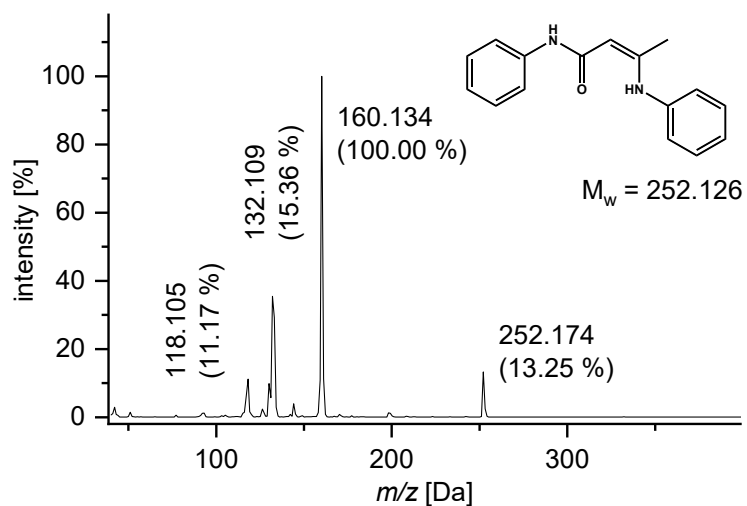
Fig. S19 EI-DIP measurement of N-phenyl-3-(phenylamino)but-2-enamide (Phe-VUA-Phe), showing the characteristic molecule-ion peak and fragmentations. EI-DIP: m/z 252.174 (M⁺, 13.25 %), 160.134 (100.00), 132.109 (15.36), 118.105 (11.17). Calculated for $C_{16}H_{16}N_2O_6$ (M+) 252.126, found 252.174.
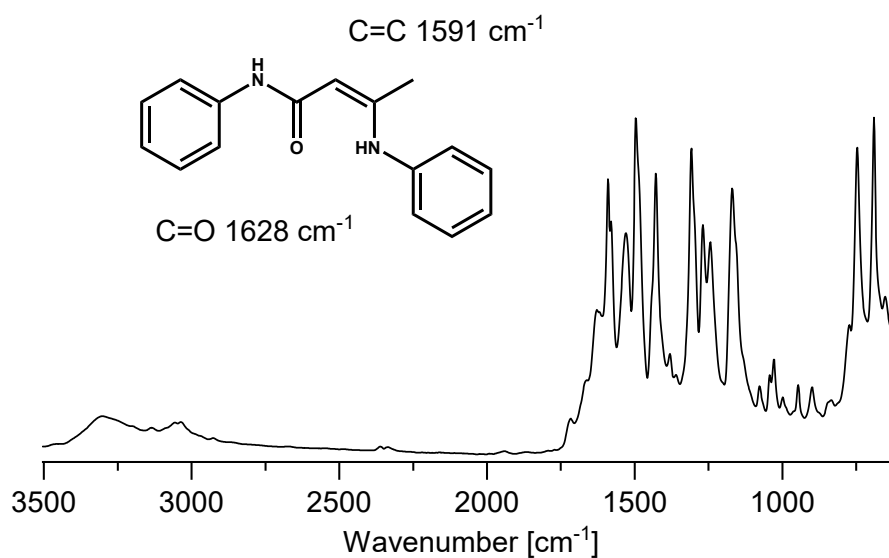
Fig. S20 ATR-FT-IR spectrum of the vinylogous urea compound Phe-VUA-Phe showing the characteristic C=O amid band at 1628 cm⁻¹ and C=C band at 1591 cm⁻¹.
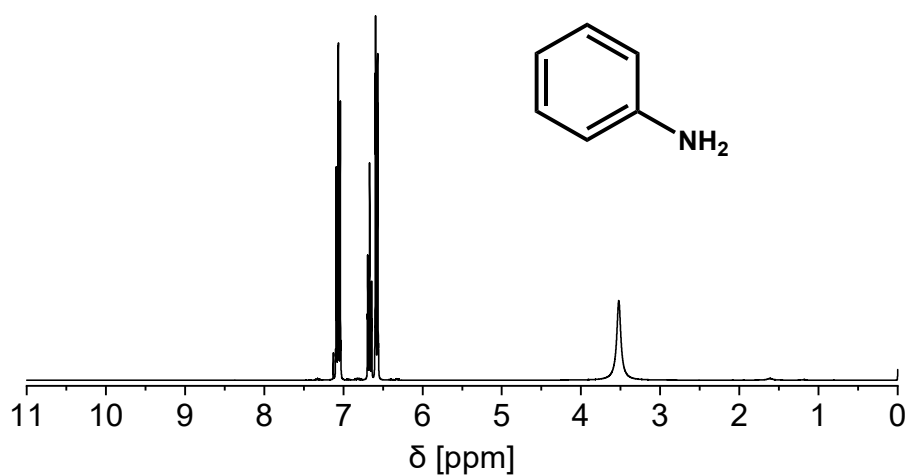
Fig. S21a ^{1}H NMR spectra (CDCl$_3$, 25 °C) of spectrum of aniline. δH (300 MHz, CDCl$_3$, 25°C): 7.06 (2H, t, Ph), 6.66 (1H, t, Ph), 6.57 (2H, d, Ph), 3.52 (2H, s, NH$_2$).
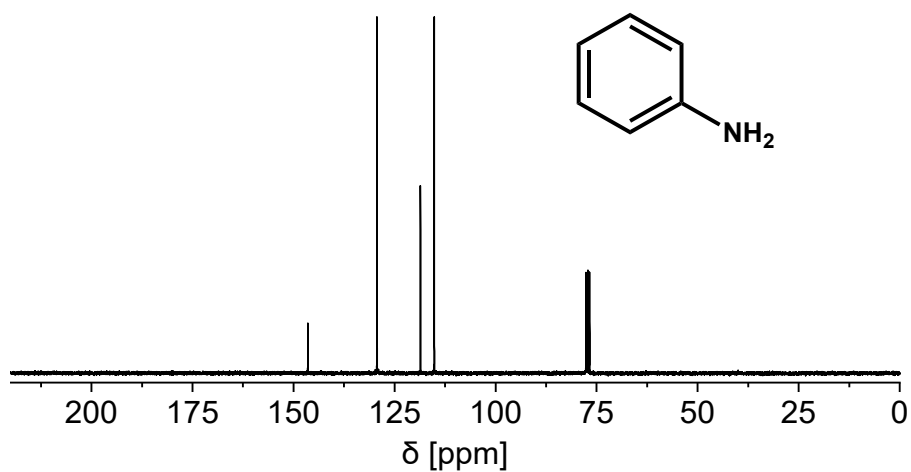
Fig. S21b ^{13}C NMR (broadband decoupled, CDCl$_3$, 25 °C) spectrum of aniline. δC (75 MHz, CDCl$_3$): 146.47 (q, Ph), 129.35 (t, Ph), 118.59 (t, Ph), 115.17 (t, Ph).
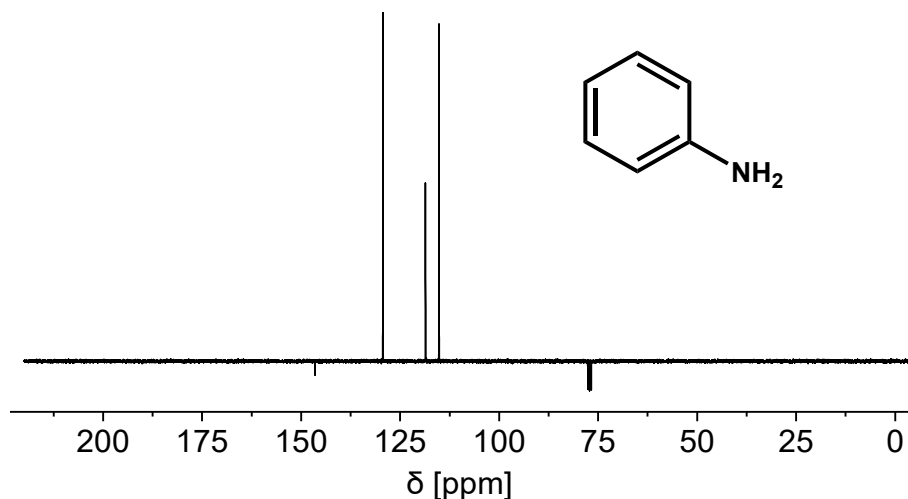
Fig. S21c ^{13}C NMR (DEPTQ-135, CDCl$_3$, 25 °C) spectrum of aniline.
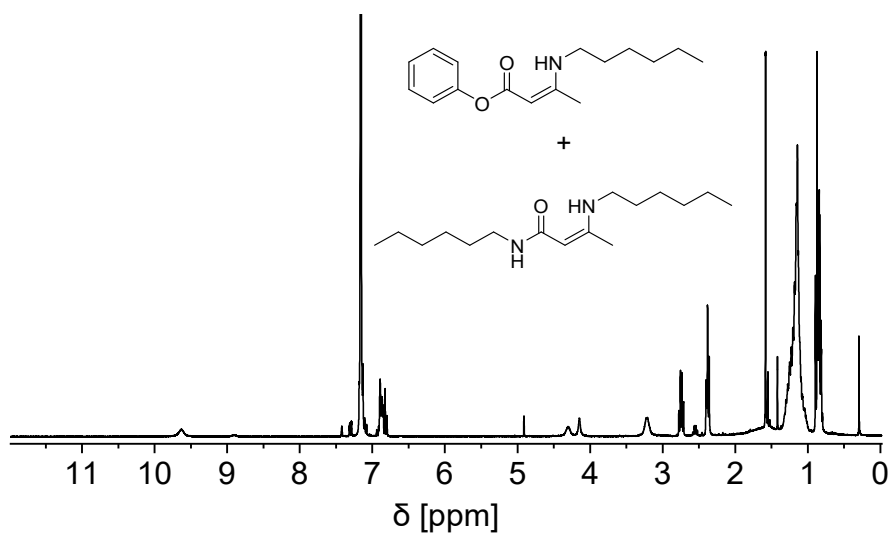
Fig. S22a ^{1}H NMR spectra (benzene-d6, 25 °C) of spectrum of the synthesized mixture of Phe-VUT-Hex and Hex-VUA-Hex. Phenyl-3-(hexylamino)but-2-enoate (Phe-VUT-Hex) δH (300 MHz, benzene-d6, 298 K): 8.90 (1H, s, NH), 4.90 (1H, s, CH), 2.54 (2H, dd, CH$_2$) 1.41 (3H, s, CH$_3$), 1.33–1.03 (8H, m, CH$_2$), 0.89–0.78 (6H, t, CH$_3$). N-hexyl-3-(hexylamino)but-2-enamide (Hex-VUA-Hex) δH (300 MHz, benzene-d6, 298 K): 9.68 (1H, s, NH), 4.63 (1H, t, NH), 4.25 (1H, s, CH), 3.26 (2H, d, CH$_2$), 2.77 (2H, dd, CH$_2$), 1.61 (3H, s, CH$_3$), 1.42–1.02 (16H, m, CH$_2$, 0.84 (3H, t, CH$_3$), 0.83 (3H, t, CH$_3$).
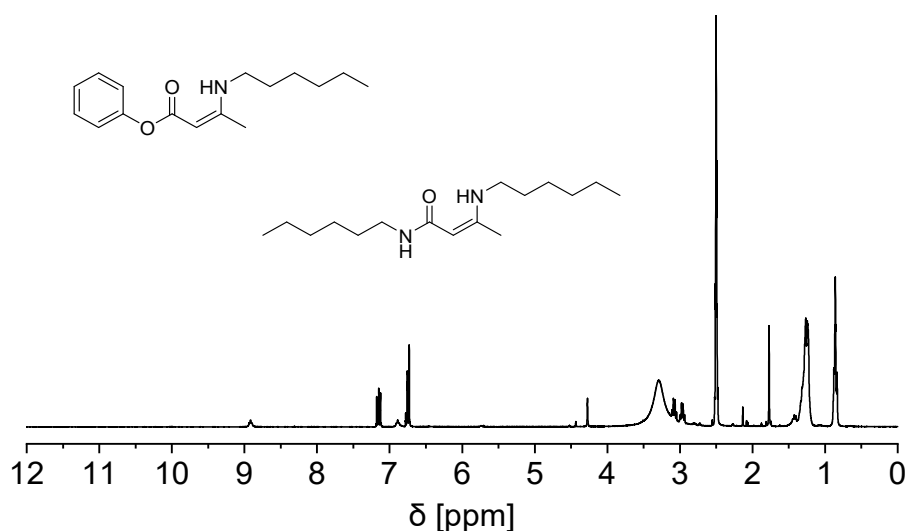
Fig. S22b ¹H NMR spectra (DMSO-d6, 25 °C) of spectrum of the synthesized mixture of Phe-VUT-Hex and Hex-VUA-Hex. Hex-VUA-Hex: δH (300 MHz, DMSO-d6, 298 K): δH (300 MHz, DMSO-d6. 298 K): 8.92 (1H, t, NH), 6.89 (1H, t, NH), 4.28 (1H, s, CH), 3.08 (2H, dd, CH$_2$), 2.97 (2H, dd, CH$_2$), 1.77 (3H, s, CH$_3$), 1.51–1.05 (16H, m, CH$_2$), 0.86 (3H, t, CH$_3$), 0.85 (3H, t, CH$_3$). Phe-VUT-Hex: δH (300 MHz, DMSO-d6, 298 K): 8.52 (1H, s, NH), 7.19–7.06 (2 H, m, Ph), 6.79–6.66 (3H, m, Ph), 4.57 (s, 1H; CH), 3.23 (2H, m, CH$_2$) 1.77 (3H, s, CH$_3$), 1.57–1.40 (2H, m, CH$_2$), 1.35–1.14 (6H, m, CH$_2$), 0.90–0.78 (3H, t, CH$_3$). Acetic acid: 8.8 (COOH), 1.77 (3H, s, CH$_3$).
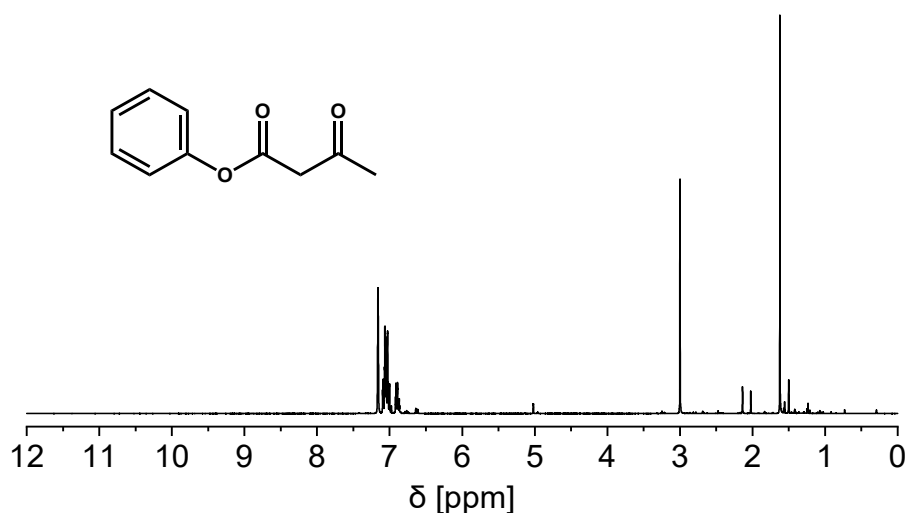
Fig. S22c ¹H NMR spectra (benzene-d6, 25 °C) of spectrum of the synthesized monomer PH.

δH (300 MHz, benzene-d6, 298 K): 7.11–6.97 (4H, m, Ph), 6.92–6.85 (1H, m, Ph), 3.00 (2H, s, CH$_2$), 1.62 (3H, s, CH$_3$).
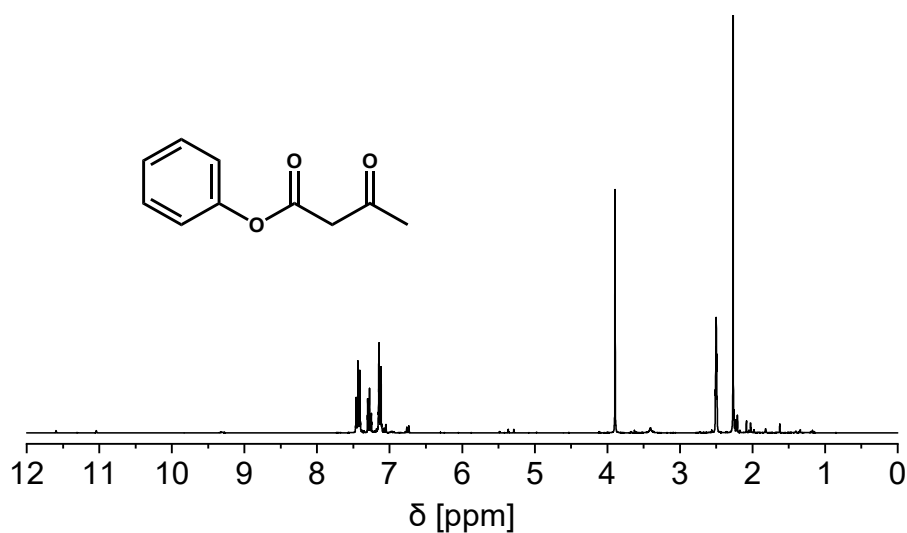
Fig. S22d ¹H NMR spectra (DMSO-d6, 25 °C) of spectrum of the synthesized monomer PH. δH (300 MHz, DMSO-d6, 298K): 7.47–7.39 (2H, m, Ph), 7.31–7.24 (1H, m, Ph), 7.16–7.10 (2H, m, Ph), 3.89 (2H, s, CH₂), 2.27 (3H, s, CH₃).
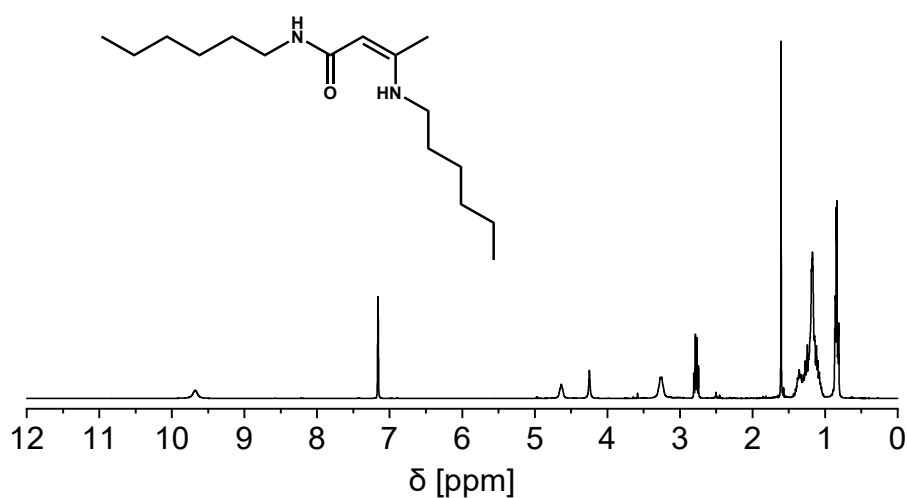
Fig. S22e ¹H NMR spectra (benzene-d6, 25 °C) of spectrum of the synthesized vinylogous urea reference compound N-hexyl-3-(hexylamino)but-2-enamide (Hex-VUA-Hex). δH (300 MHz, benzene-d6, 298 K): 9.68 (1H, s, NH), 4.63 (1H, t, NH), 4.25 (1H, s, CH), 3.26 (2H, d, CH₂), 2.77 (2H, dd, CH₂), 1.61 (3H, s, CH₃), 1.42–1.02 (16H, m, CH₂, 0.84 (3H, t, CH₃), 0.83 (3H, t, CH₃).
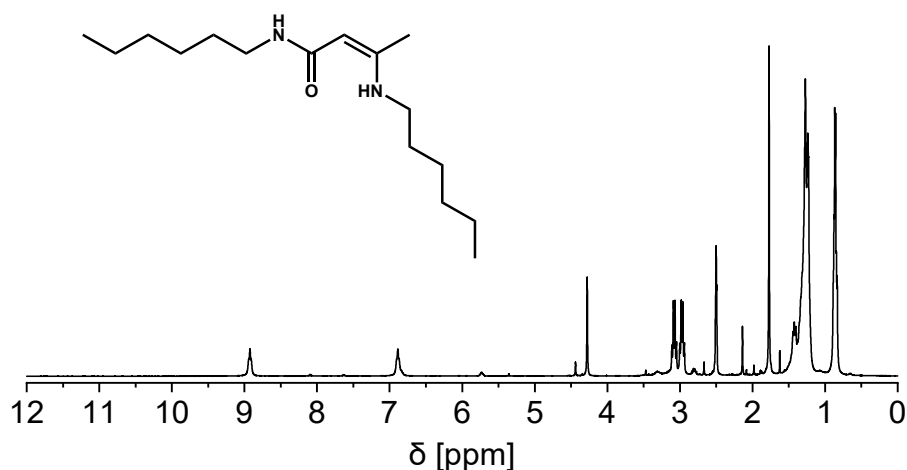
Fig. S22f ^{1}H NMR spectra (DMSO-d6, 25 °C) of spectrum of the synthesized vinylogous urea reference compound N-hexyl-3-(hexylamino)but-2-enamide (Hex-VUA-Hex). δH (300 MHz, DMSO-d6, 298 K): δH (300 MHz, DMSO-d6. 298 K): 8.92 (1H, t, NH), 6.89 (1H, t, NH), 4.28 (1H, s, CH), 3.08 (2H, dd, CH_2), 2.97 (2H, dd, CH_2), 1.77 (3H, s, CH_3), 1.51–1.05 (16H, m, CH_2), 0.86 (3H, t, CH_3), 0.85 (3H, t, CH_3).
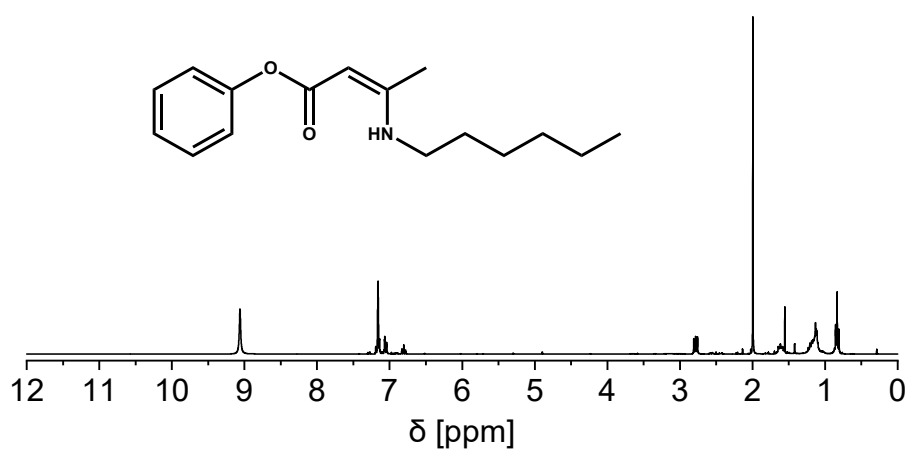
Fig. S22g ^{1}H NMR spectra (benzene-d6, 25 °C) of spectrum of the synthesized vinylogous urethane reference compound Phe-VUT-Hex. δH (300 MHz, benzene-d6, 298 K): 8.90 (1H, s, NH), 4.90 (1H, s, CH), 2.54 (2H, dd, CH_2) 1.41 (3H, s, CH_3), 1.33–1.03 (8H, m, CH_2), 0.89–0.78 (6H, t, CH_3).
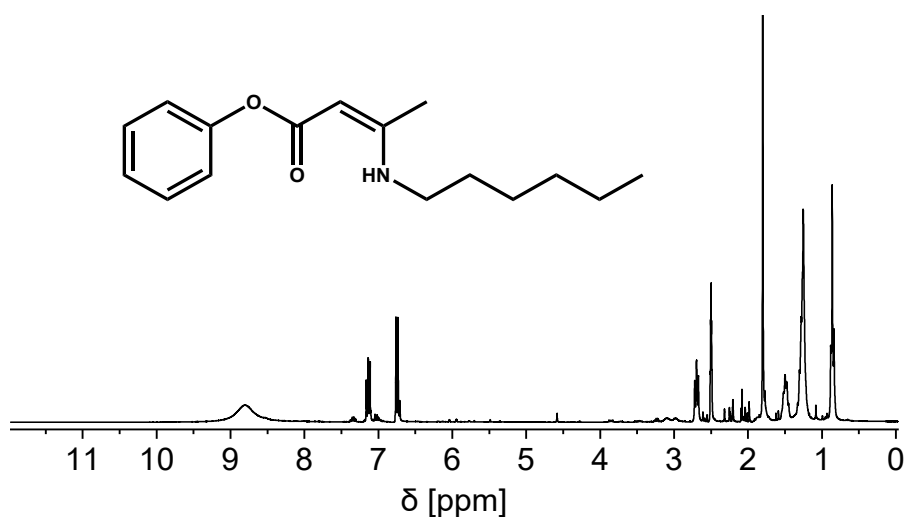
Fig. S22h ¹H NMR spectra (DMSO-d6, 25 °C) of spectrum of the synthesized vinylogous urethane reference compound (Phe-VUT-Hex). δH (300 MHz, DMSO-d6, 298 K): 8.52 (1H, s, NH), 7.19–7.06 (2 H, m, Ph), 6.79–6.66 (3H, m, Ph), 4.57 (s, 1H; CH), 3.23 (2H, m, CH₂) 1.77 (3H, s, CH₃), 1.57–1.40 (2H, m, CH₂), 1.35–1.14 (6H, m, CH₂), 0.90–0.78 (3H, t, CH₃). Acetic acid: 8.8 (COOH), 1.77 (3H, s, CH₃).
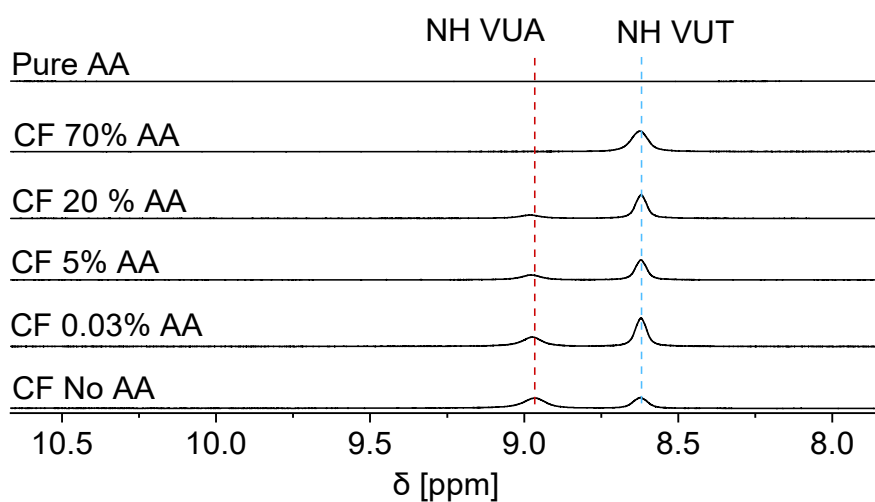
Fig. S23a ¹H NMR spectra (CDCl₃, 25 °C) showing the final ratio of the VUA und VUT compounds by using different amounts of acetic acid (mol %). The ratio was determined by the characteristic NH chemical shifts at 8.98 (VUA) and 8.62 ppm (VUT).
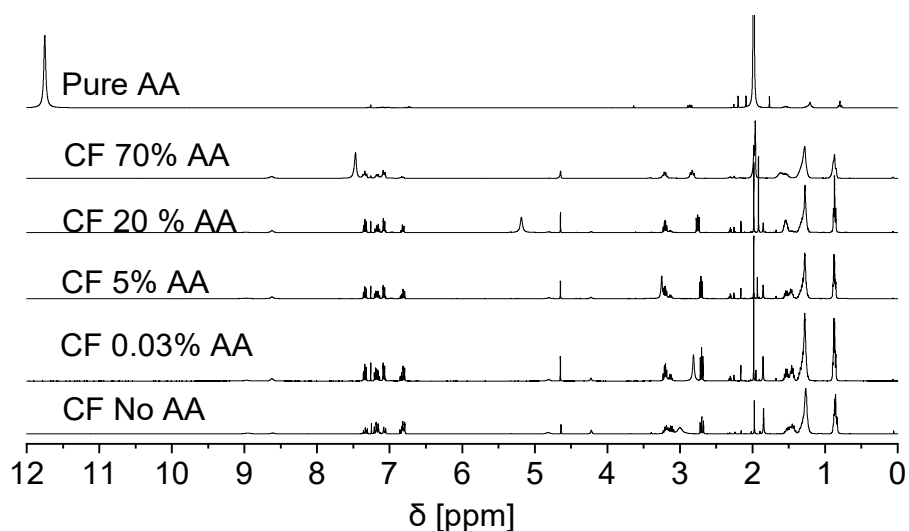
Fig. S23b ^{1}H NMR spectra (CDCl$_3$, 25 °C) showing the final ratio of the VUA und VUT compounds by using different amounts of acetic acid (mol %).
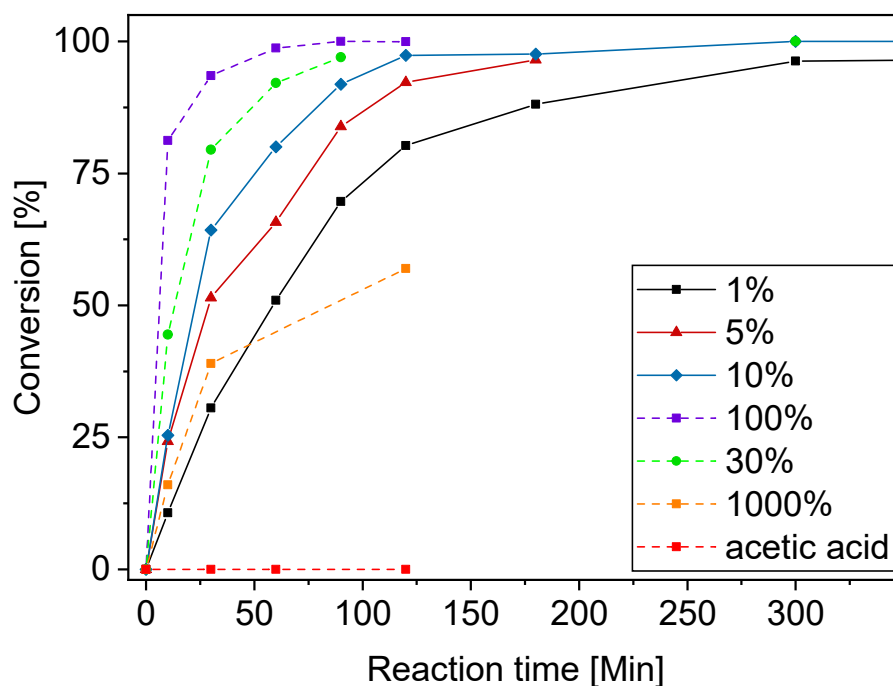
Fig. S24 Conversions of the reaction of phenylacetoacetate (PH) and 2 equivalents of hexylamine in chloroform with different amounts of acetic acid (mol %). The conversion rates are highly increased by using the catalyst, while with higher amount the reaction is slowed down and finally totally inhibited due to protonation of all nucleophilic amines in pure acetic acid.
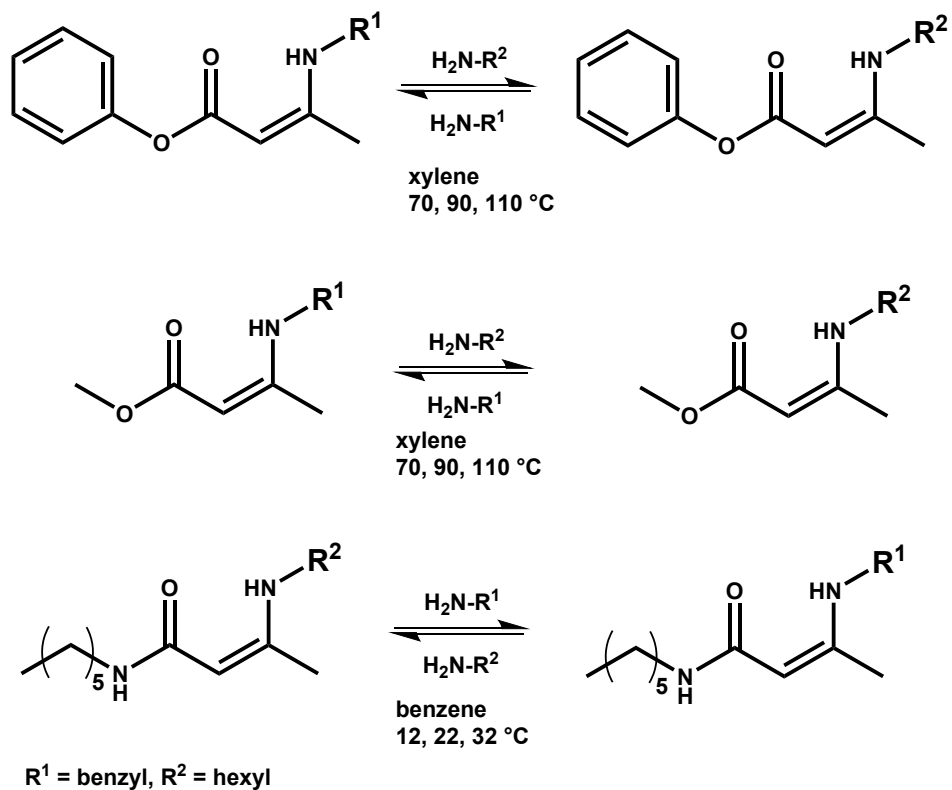
Fig. S25 Overview of the conducted exchange reactions. The transamination reaction of the aromatic vinylogous urethane compounds (top), the aliphatic vinylogous urethane compounds (middle) and the vinylogous urea compounds were investigated (bottom).
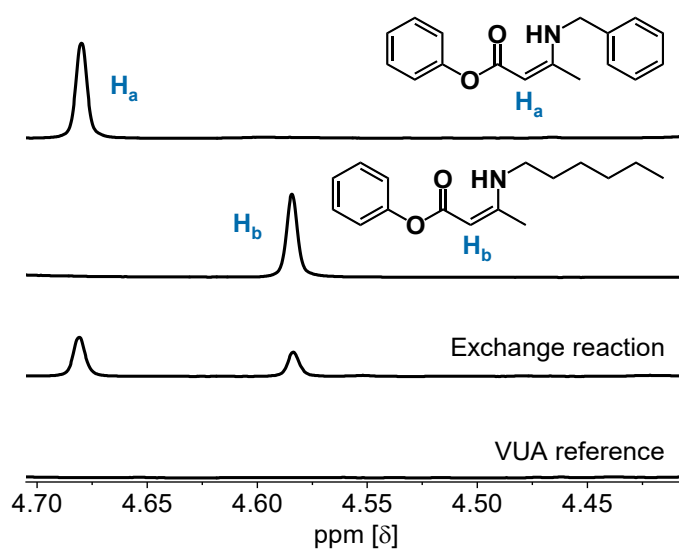
Fig. S26a ^{1}H NMR spectra (CDCl$_3$, 25 °C) showing the characteristic vinylic protons of the reference compounds Phe-VUT-Hex and Phe-VUT-Bz in comparison to the spectrum after the exchange reaction. The signals clearly show the appearance of both signals.

Phe-VUT-Hex
Hex-VUA-Hex

Phe-VUT-Bz
Bz-VUA-Bz

Exchange
reaction

VUT reference

VUA reference

ppm [δ]
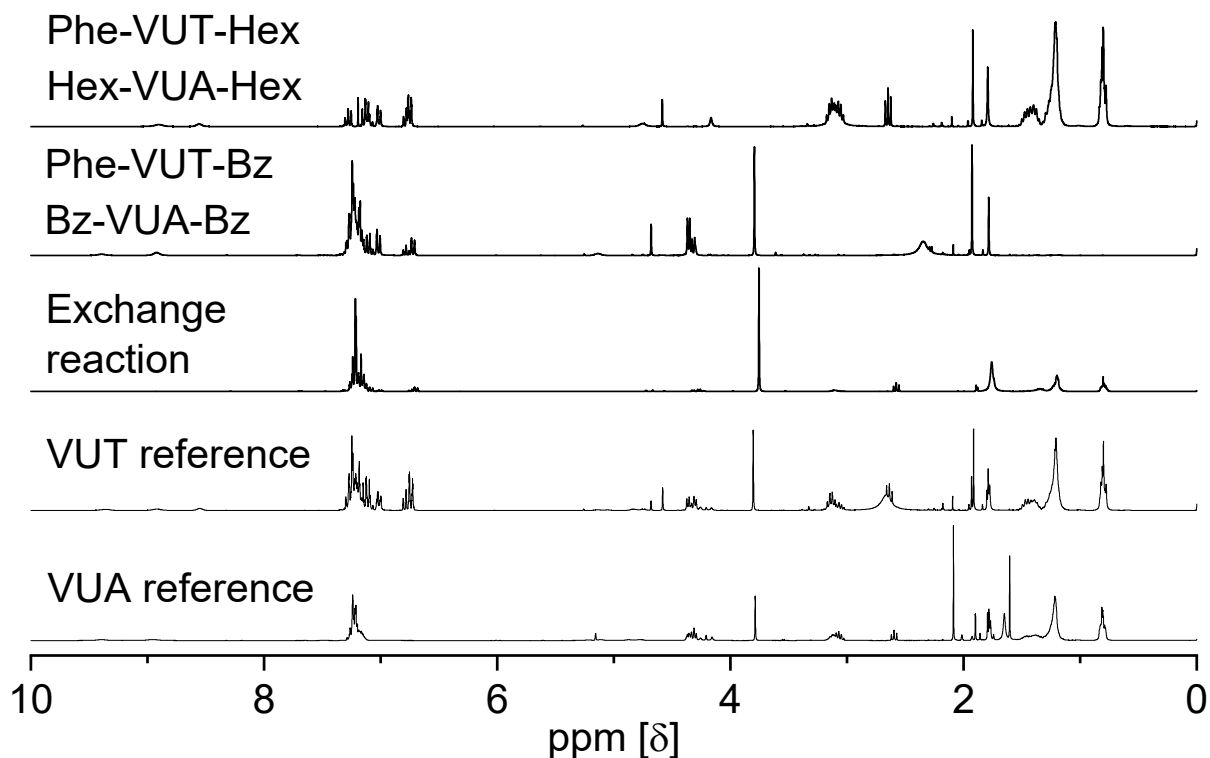
Fig. S26b ^{1}H NMR spectra (CDCl$_3$, 25 °C) showing the signals of the vinylogous urethane compounds Phe-VUT-Hex and Phe-VUT-Bz and the resulting spectra after the exchange reaction, proving the exchange reaction by showing the presence of both signals. ^{1}H NMR spectra of the characteristic NH protons before and after the exchange reaction in comparison to the vinylogous urethane and urea compounds Phe-VUT-Hex, Phe-VUT-Bz, Hex-VUA-Hex and Hex-VUA-Bz, proving the exchange reaction of the vinylogous urea compounds.

Exchange reaction

VUA reference (both)

ppm [δ]
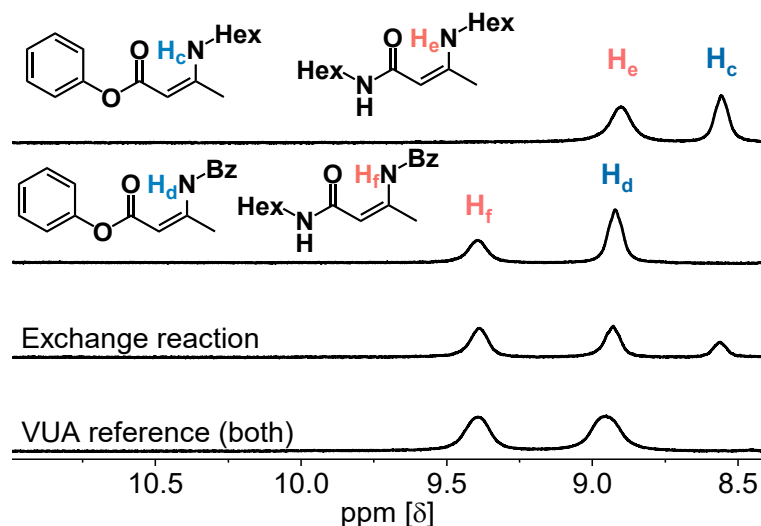
Fig. S27 ^{1}H NMR spectra (CDCl$_3$, 25 °C) of the characteristic NH protons before and after the exchange reaction in comparison to the vinylogous urethane and urea compounds Phe-VUT-Hex, Phe-VUT-Bz, Hex-VUA-Hex and Hex-VUA-Bz, proving the exchange reaction of the vinylogous urea compounds.
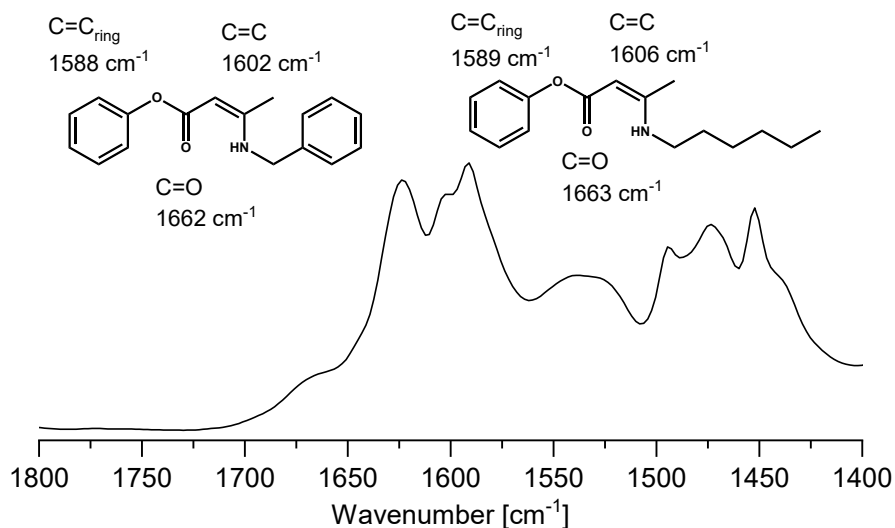
Fig. 28 ATR-FT-IR spectra did not show a visible significant shift in the C=O ester or C=C bands after the exchange reaction.

Calculation of the activation energy (E_a) via an Arrhenius law:

The decrease of the reactant concentration as a function of time is described by:[33]

$$[R] = 1 - c_P + c_P * e^{\frac{-kt}{c_P}}$$

$[R]$	concentration reactant
c_P	equilibrium ratio of the products ($\frac{4}{5}$)
k	initial rate (fitted)
t	reaction time [s]

Equation S1: Exponential fit for the conversion of the reactant to determine the initial rate k.
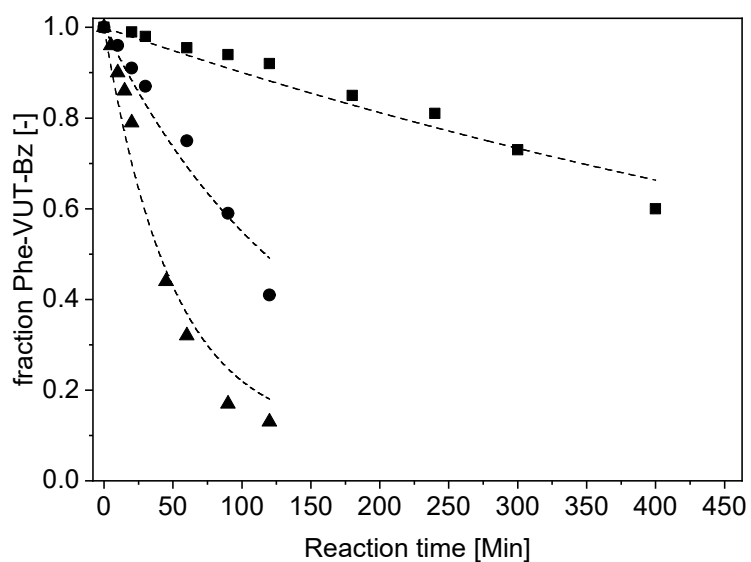
Fig. S29a Monitoring the decay of the vinylogous urethane compound Phe-VUT-Bz at 70, 90 and 110 °C during the exchange reaction with hexylamine.
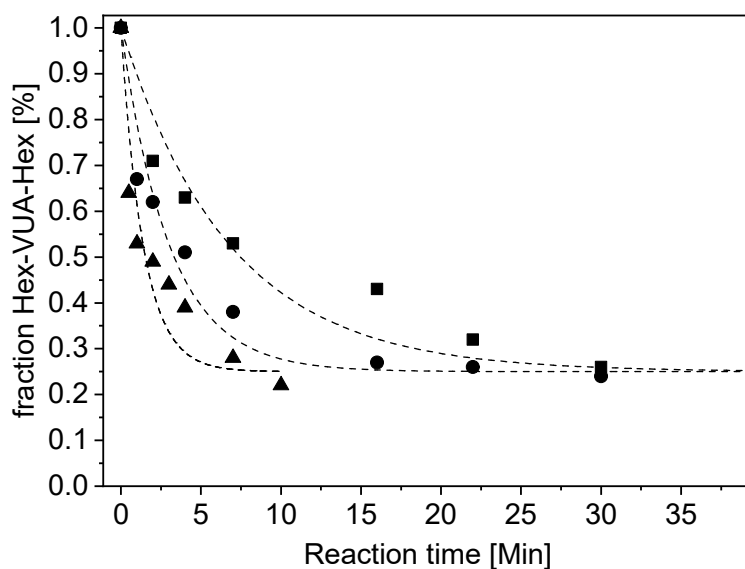
Fig. S29b Monitoring the decay of the vinylogous urea compound Hex-VUA-Hex at 12, 22 and 32 °C during the exchange reaction with benzylamine.
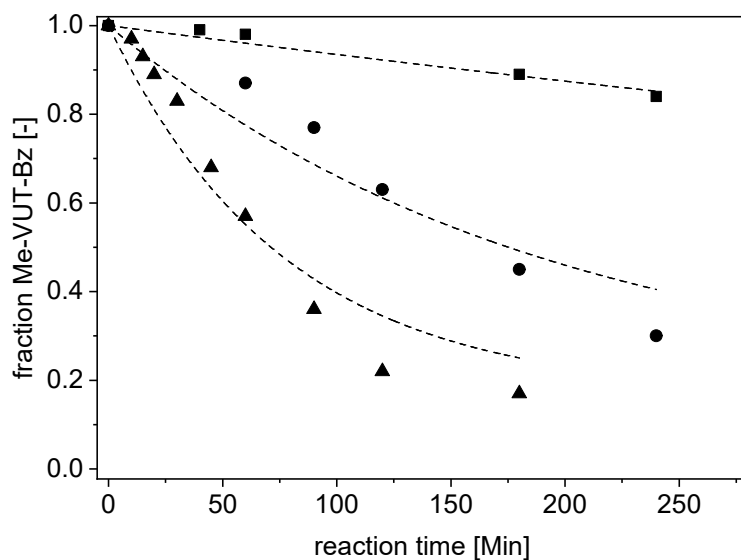
Fig. S29c Monitoring the decay of the vinylogous urethane compound Methyl-VUT-Bz at 70, 90 and 110 °C during the exchange reaction with hexylamine.
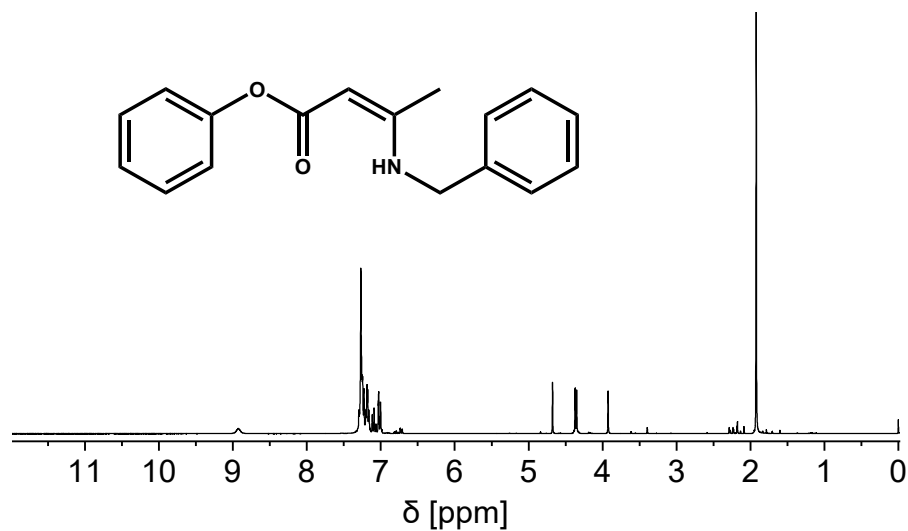
Fig. S30a ^{1}H NMR spectra (CDCl$_3$, 25 °C) of spectrum of the synthesized vinylogous urethane reference compound (Phe-VUT-Bz). δH (300 MHz, CDCl$_3$, 298 K): 8.98 (1H, t, NH), 7.33–7.03 (10H, m, Ph), 4.72 (1H, s, CH), 4.36 (2H, d, CH$_2$), 1.94 (s, 3H, CH$_3$).
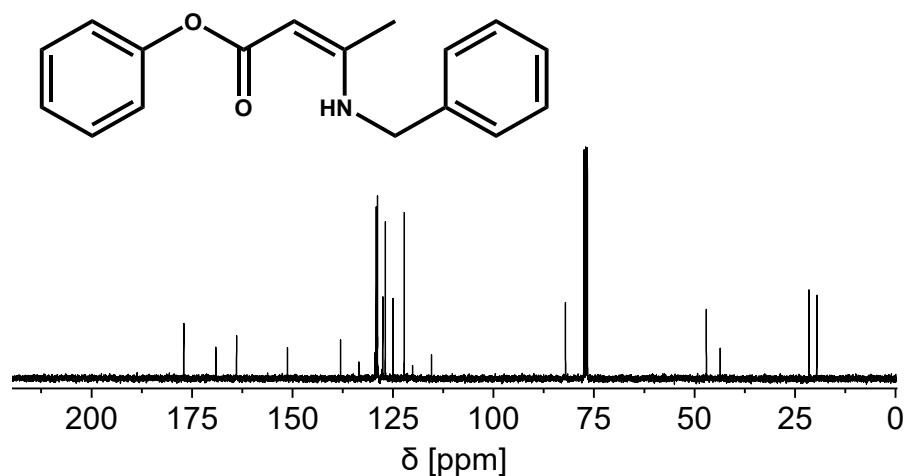
Fig. S30b ^{13}C NMR (broadband decoupled, CDCl$_3$, 25 °C) spectrum of the synthesized vinylogous urethane reference compound Phe-VUT-Bz. δC (75 MHz, CDCl$_3$, Me$_4$Si): 169.16 (q, COO), 164.08 (q, C=C), 151.54 (q, Ph-O), 129.28 (t, Ph), 124.96 (t, Ph), 122.32 (t, Ph), 80.82 (t, CH), 43.38 (s, CH$_2$), 31.59 (s, CH$_2$), 31.32 (s, CH$_2$), 26.62 (s, CH$_2$), 22.49 (s, CH$_2$), 31.6 (p, C-CH$_3$) 14.11 (p, CH$_2$-CH$_3$).
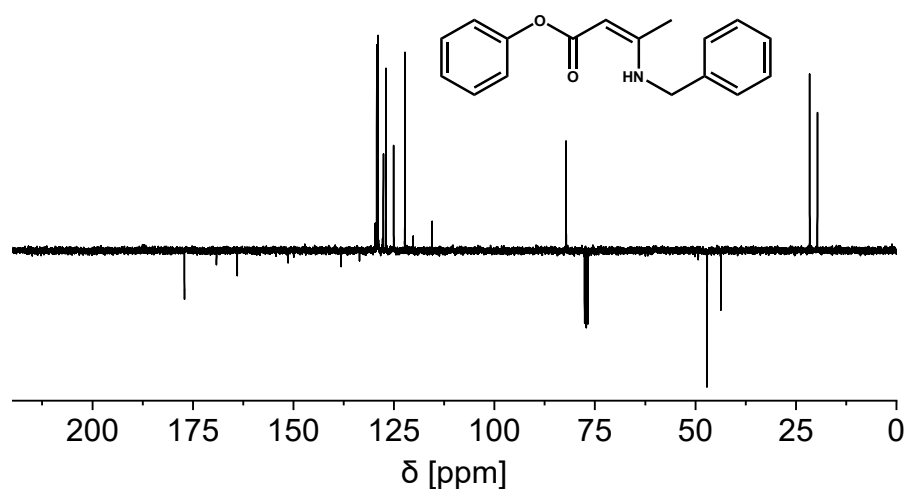
Fig. S30c ^{13}C NMR (DEPTQ-135, CDCl$_3$, 25 °C) spectrum of the synthesized vinylogous urethane reference compound Phe-VUT-Bz. δC (75 MHz, CDCl$_3$, Me$_4$Si): 169.16 (q, COO), 164.08 (q, C=C), 151.54 (q, Ph-O), 129.28 (t, Ph), 124.96 (t, Ph), 122.32 (t, Ph), 80.82 (t, CH), 43.38 (s, CH$_2$), 31.59 (s, CH$_2$), 31.32 (s, CH$_2$), 26.62 (s, CH$_2$), 22.49 (s, CH$_2$), 31.6 (p, C-CH$_3$) 14.11 (p, CH$_2$-CH$_3$).
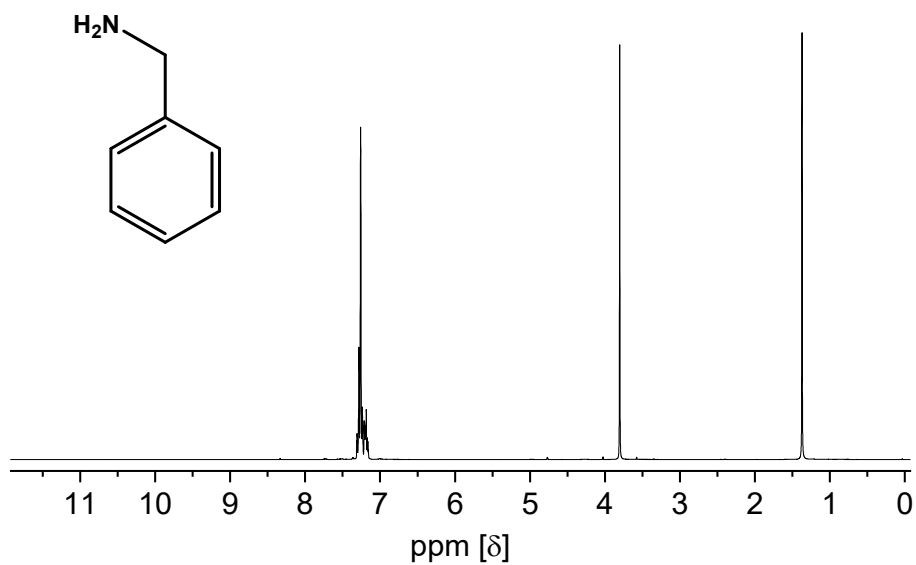
Fig. S30d ^{1}H NMR spectra (CDCl$_3$, 25 °C) of spectrum of benzylamine. δH (300 MHz, CDCl$_3$): δH (300 MHz, CDCl$_3$, 25°C): 7.31–7.15 (5H, m, Ph), 3.80 (2H, s, CH$_2$), 1.37 (2H, s, NH$_2$).
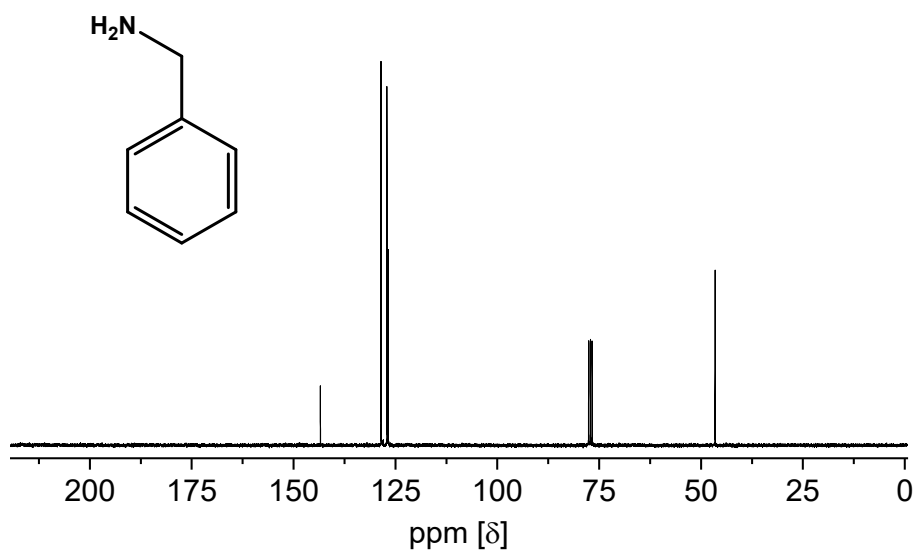
Fig. S30e ^{13}C NMR (broadband decoupled, CDCl$_3$, 25 °C) spectrum of benzylamine. δC (75 MHz, CDCl$_3$): 143.42 (q, Ph), 128.56 (t, Ph), 127.08 (t, Ph), 126.79 (t, Ph), 46.56 (s, CH$_2$).
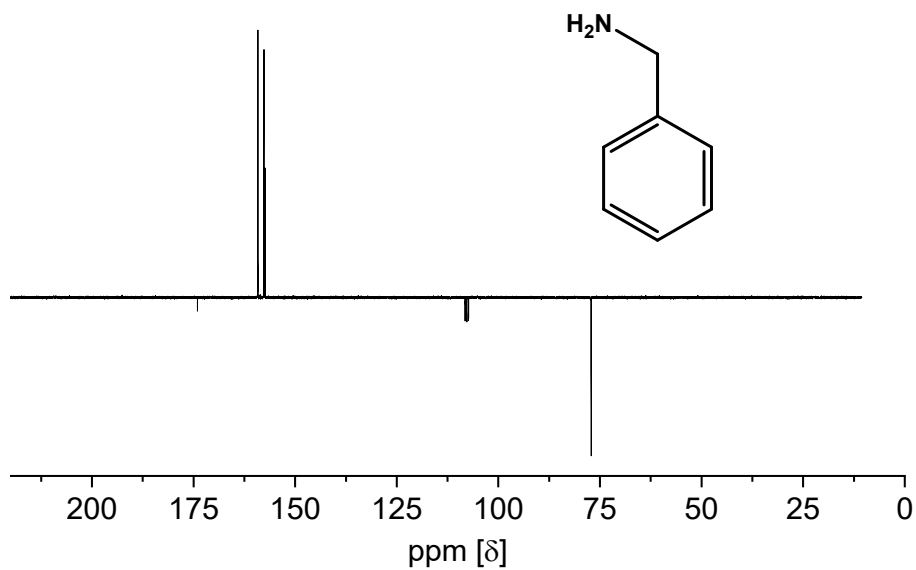
Fig. S30f ^{13}C NMR (DEPTQ-135, CDCl$_3$, 25 °C) spectrum of benzylamine. δC (75 MHz, CDCl$_3$): 143.42 (q, Ph), 128.56 (t, Ph), 127.08 (t, Ph), 126.79 (t, Ph), 46.56 (s, CH$_2$).
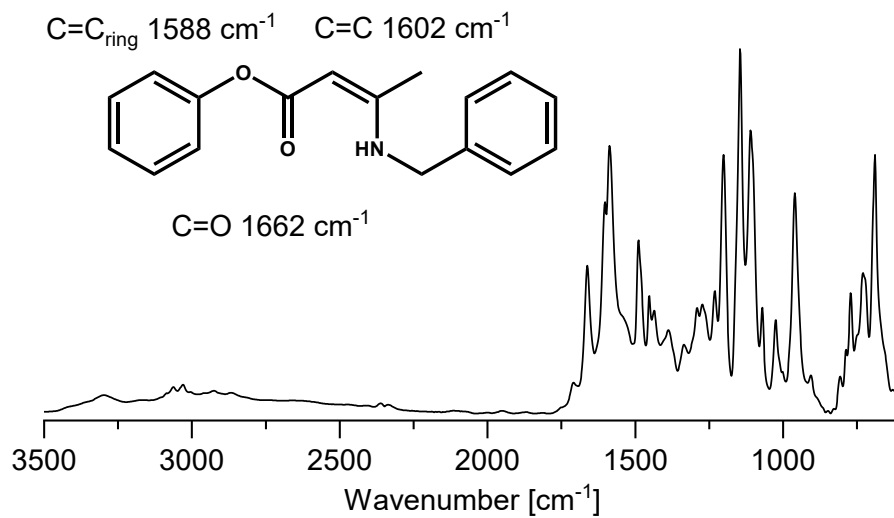
Fig. S31 ATR-FT-IR spectrum of the vinylogous vinylogous urethane reference compound Phe-VUT-Bz with the characteristic C=O ester band at 1662 cm^{-1} and C=C band at 1602 cm^{-1}.
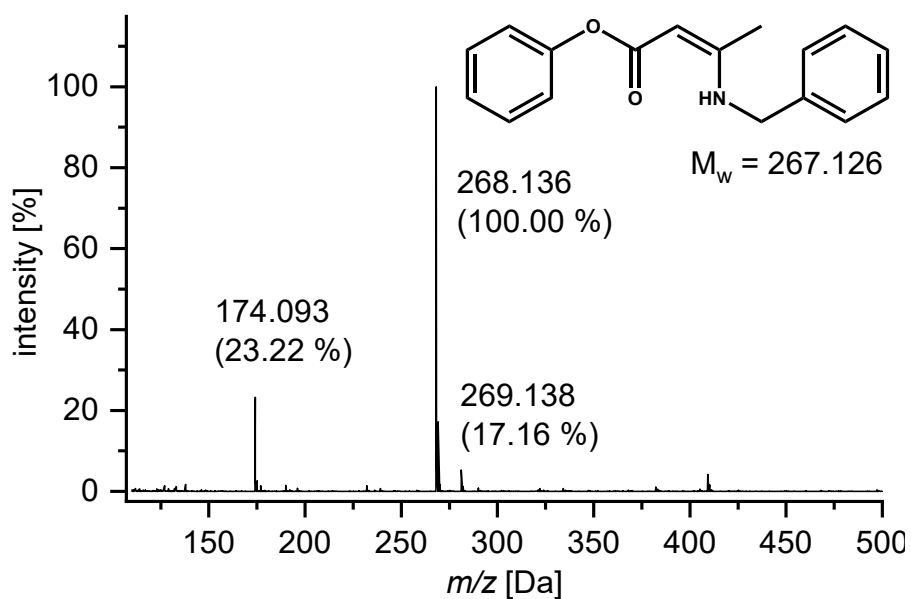
Fig. S32 ESI-MS spectrum of the synthesized vinylogous urethane compound Phe-VUT-Bz showing the characteristic molecule ion peak m/z = 268.136 (M$^+$ + 1) and m/z = 269.138 (M$^+$ + 2).
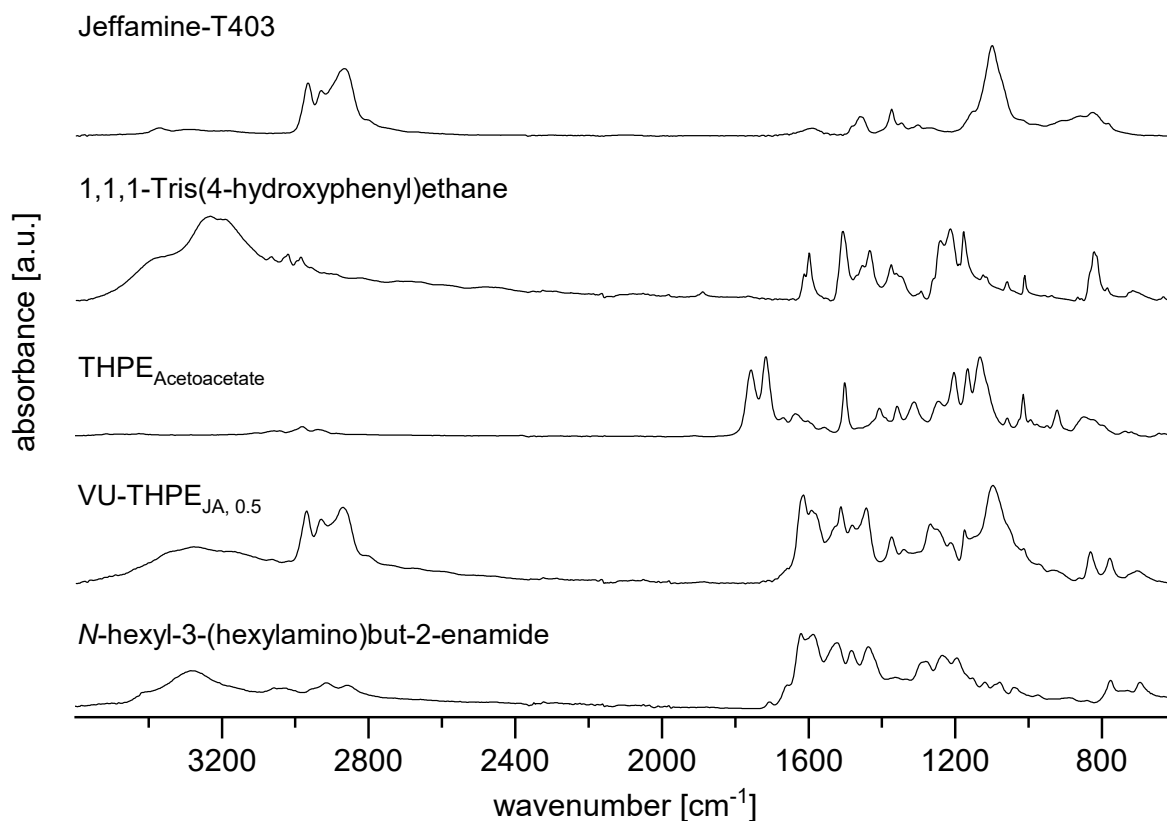
Fig. S33 ATR-FT-IR spectra of the reactants Jeffamine-T403, 1,1,1-Tris(4-hydroxyphenyl)ethane, the acetoacetate monomer THPE$_{AcAc}$, the vinylogous urea reference N-hexyl-3-(hexylamine)but-2-enamide and the product VU-THPE$_{JA, 0.5}$.
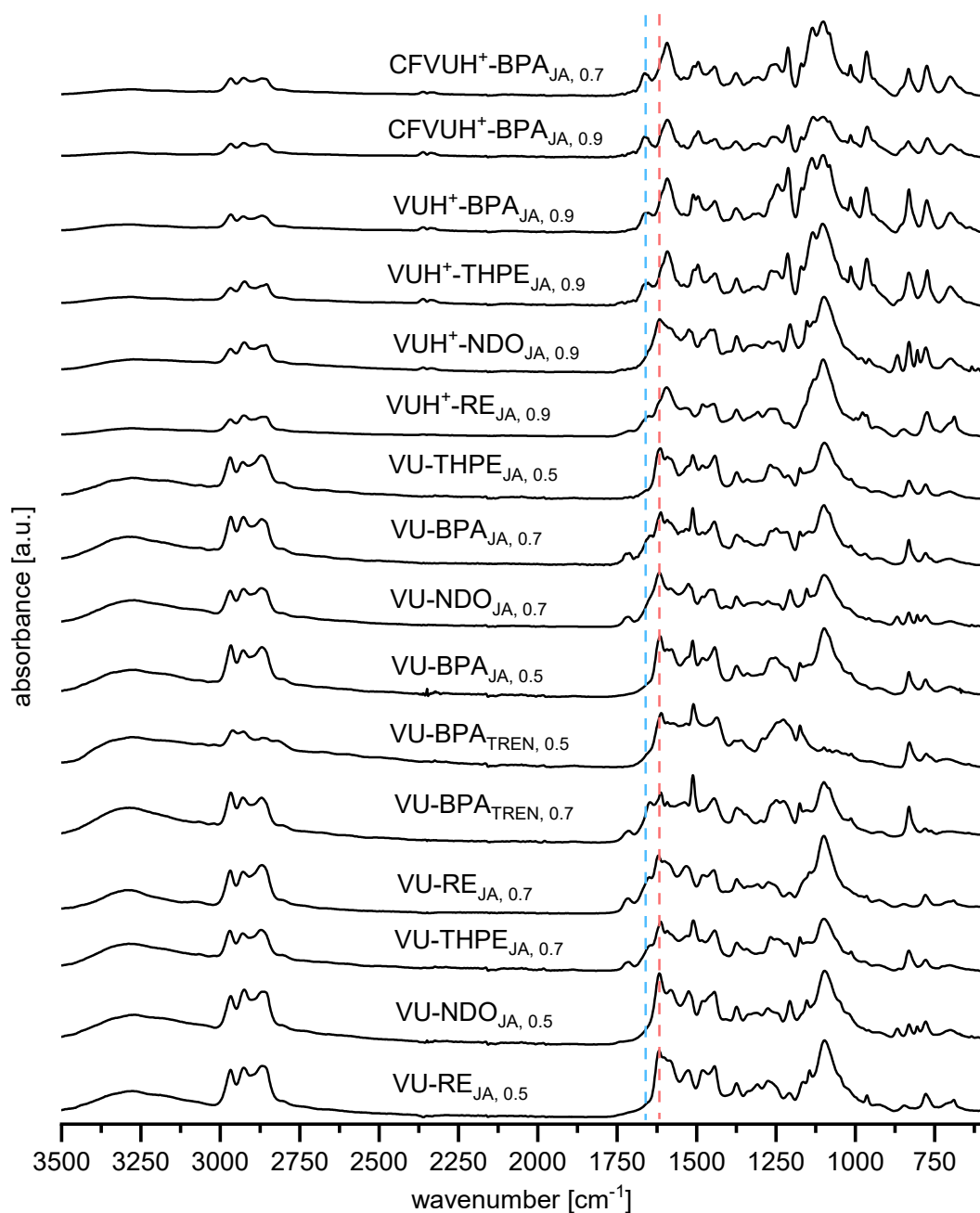
Fig. S34a ATR-FT-IR spectra of all synthesized blended poly (vinylogous urethane/urea) vitrimer networks derived from RE, NDO, BPA and THPE cured with JA or TREN with and without acetic acid in a bulk or solvent-based polymerization. The blue line marks the

characteristic VUT C=O ester band, while the red line marks the characteristic VUA C=O amid band.
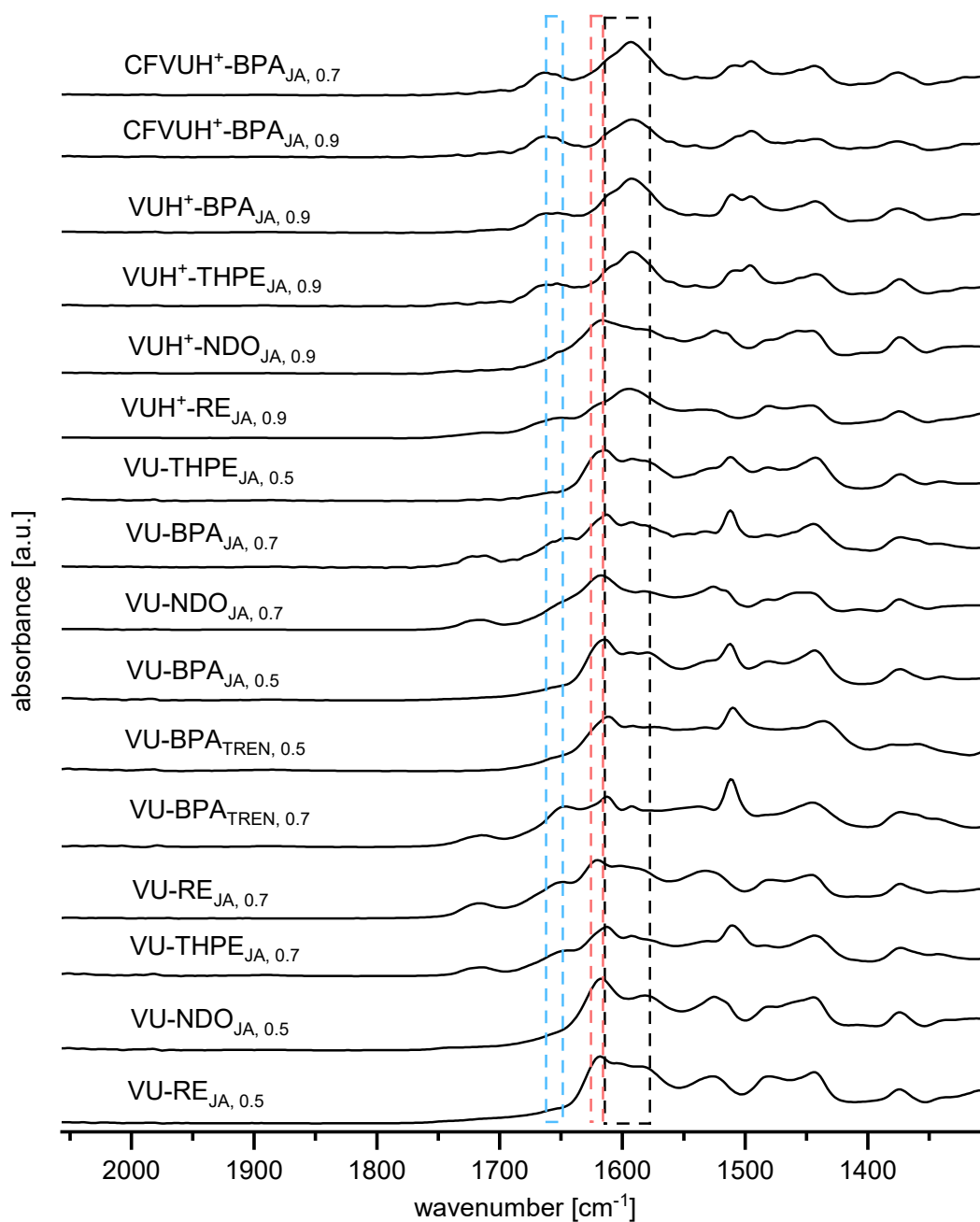
Fig. S34b ATR-FT-IR spectra of all synthesized blended poly (vinylogous urethane/urea) vitrimer networks derived from RE, NDO, BPA and THPE cured with JA or TREN with and without acetic acid in a bulk or solvent-based polymerization. The blue line marks the

characteristic VUT C=O ester band, while the red line marks the characteristic VUA C=O amid band. The black line marks the are of C=C stretching bands.
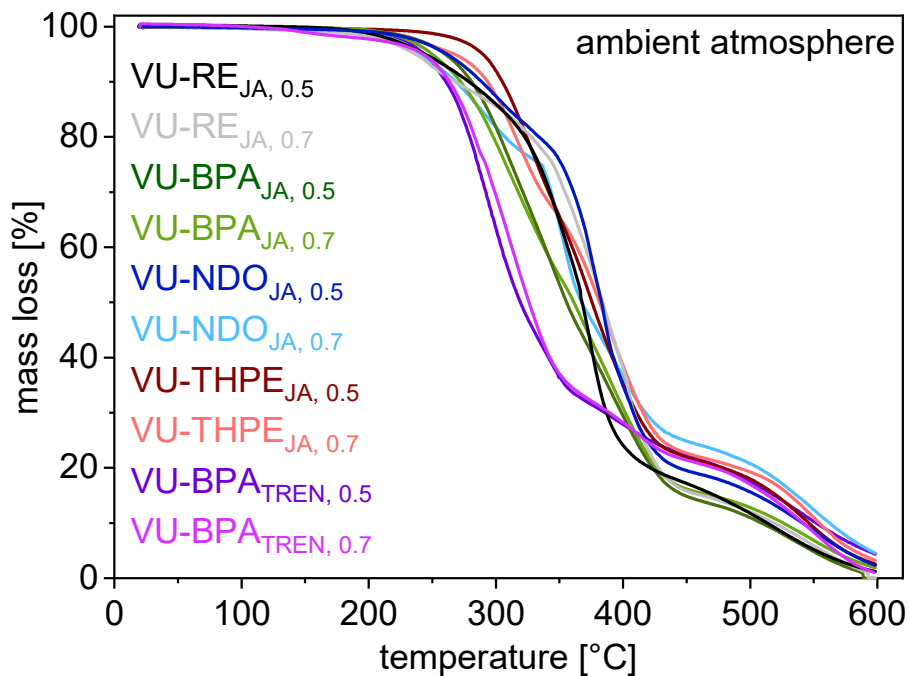
Fig. S35a Thermogravimetric analysis (TGA) measurements of the vitrimers cured without additional catalyst and acetoacetate to amine ratios of 0.5 and 0.7. The thermal degradation points were determined at 5 % mass loss.
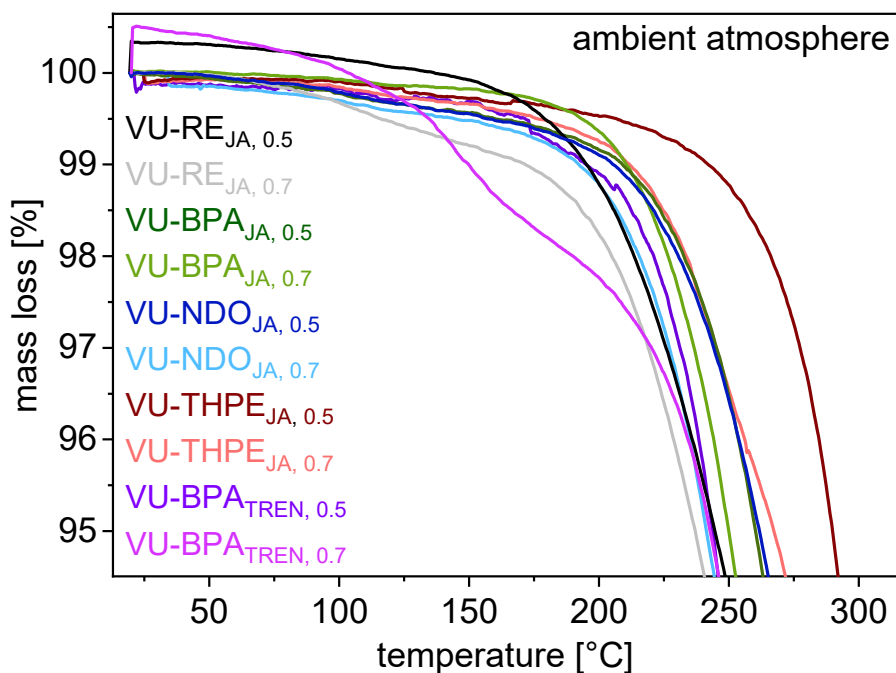
Fig. S35b Details of the thermogravimetric analysis (TGA) measurements of the vitrimers cured without additional catalyst and acetoacetate to amine ratios of 0.5 and 0.7. The thermal degradation points were determined at 5 % mass loss.
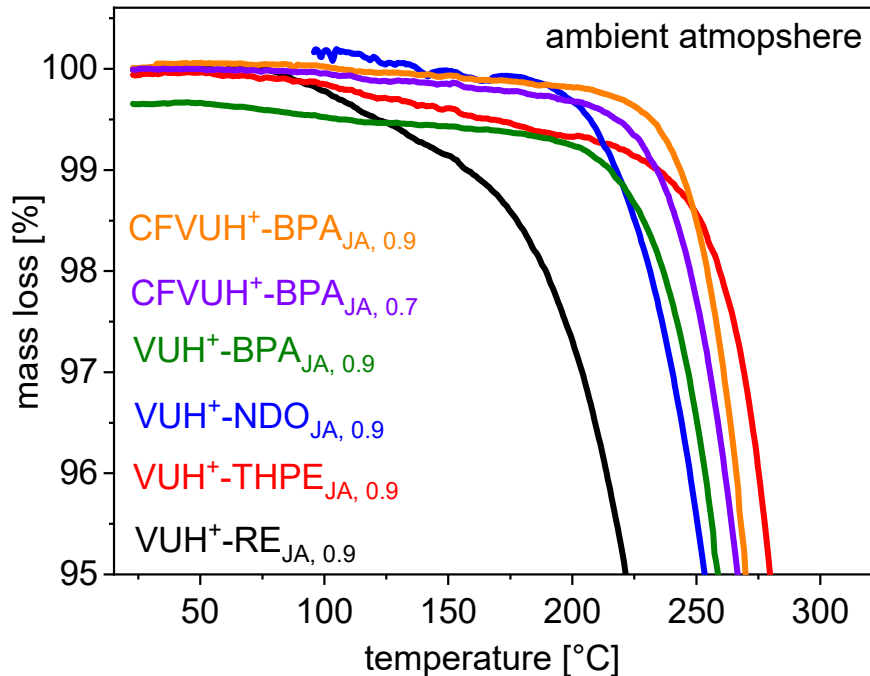
Fig. S35c Details of the thermogravimetric analysis (TGA) measurements of the vitrimers cured with additional acetic acid and/or chloroform as solvent. The thermal degradation points were determined at 5 % mass loss.
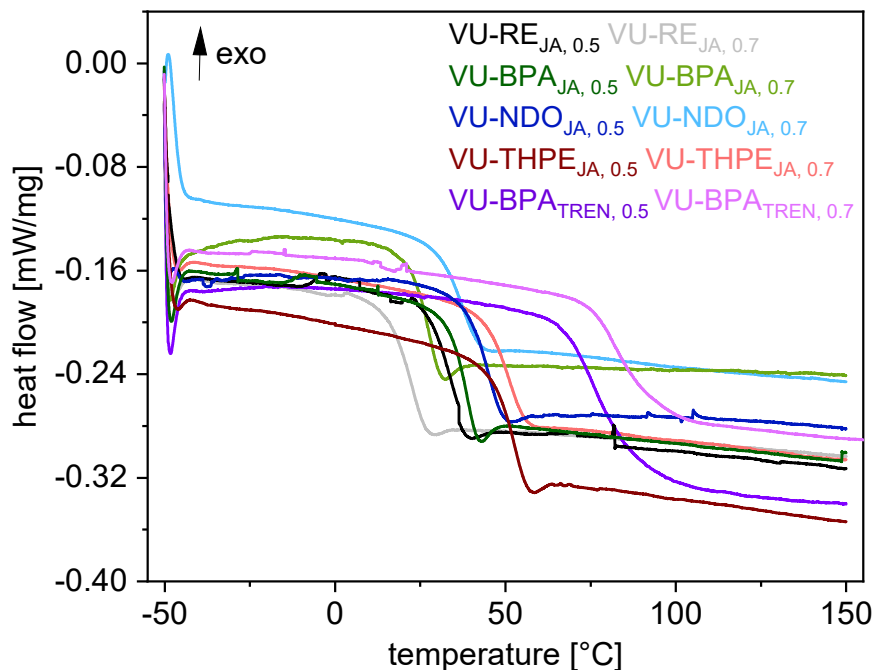
Fig. S36a Differential scanning calorimetrie (DSC) measurements of the vitrimers polymerized with JA or TREN and acetoacetate to amine ratios of 0.5 or 0.7 and without catalyst.
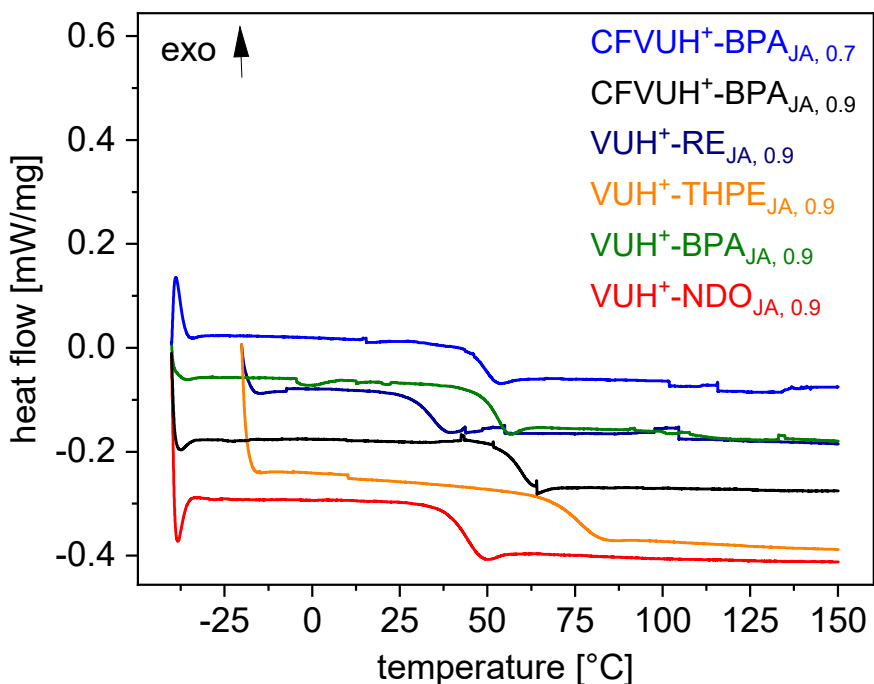
Fig. S36b Differential scanning calorimetrie (DSC) measurements of the vitrimers polymerized with JA and an acetoacetate to amine ratios of 0.7 or 0.9 with acetic acid as catalyst.

Calculation of the activation energy (E_a) by stress relaxation experiments:[1]

The stress relaxation times as a function of temperature can be described by an Arrhenius law:

$$\tau(T) = \tau_0\, e^{\frac{E_a}{RT}}$$

τ	stress relaxation time (37 %)	[s]
τ_0	Stress relaxation time (normalized 0,1)	[s]
E_a	activation energy	[kJ mol^{-1}]
R	gas constant	[J K^{-1} mol^{-1}]
T	temperature	[K]

Equation S2: Arrhenius law for calculating the activation energy by stress-relaxation times according to Maxwell law for viscoelastic fluids (37%, 1/e)) as a function of temperature.

The activation energy was calculated by plotting ln k versus 1000/T.
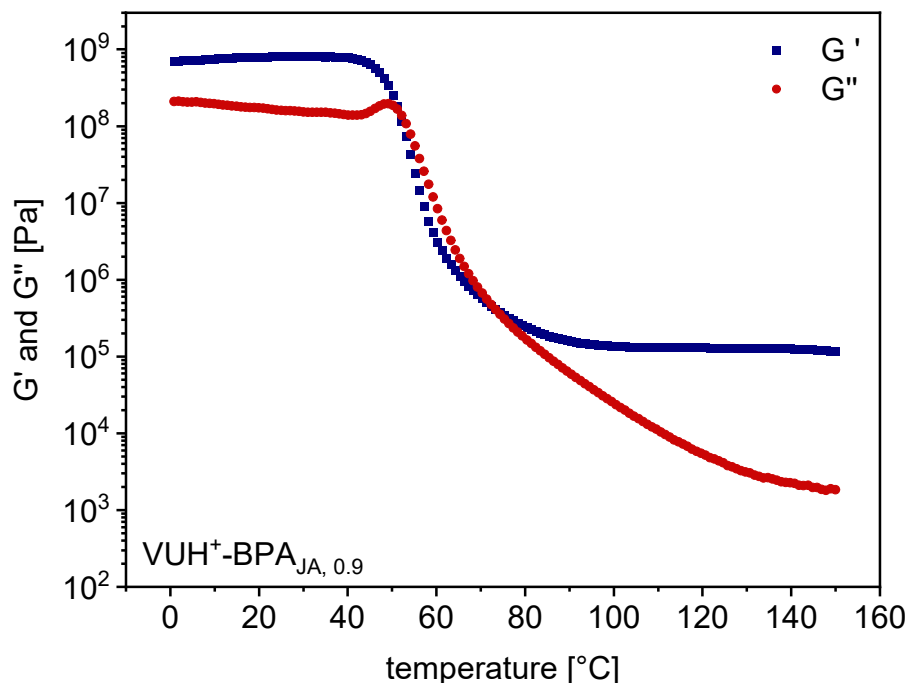
Fig. S37a Temperature-dependent DMA measurement (ω = 10 rad/s, y = 0.1 %) of VUH$^+$-BPA$_{JA,\,0.9}$ in the temperature range of 0–150 °C, showing the storage- and loss modulus (G' and G'') with the characteristic rubbery plateau of the cross-linked material at elevated temperatures up to 150 °C.
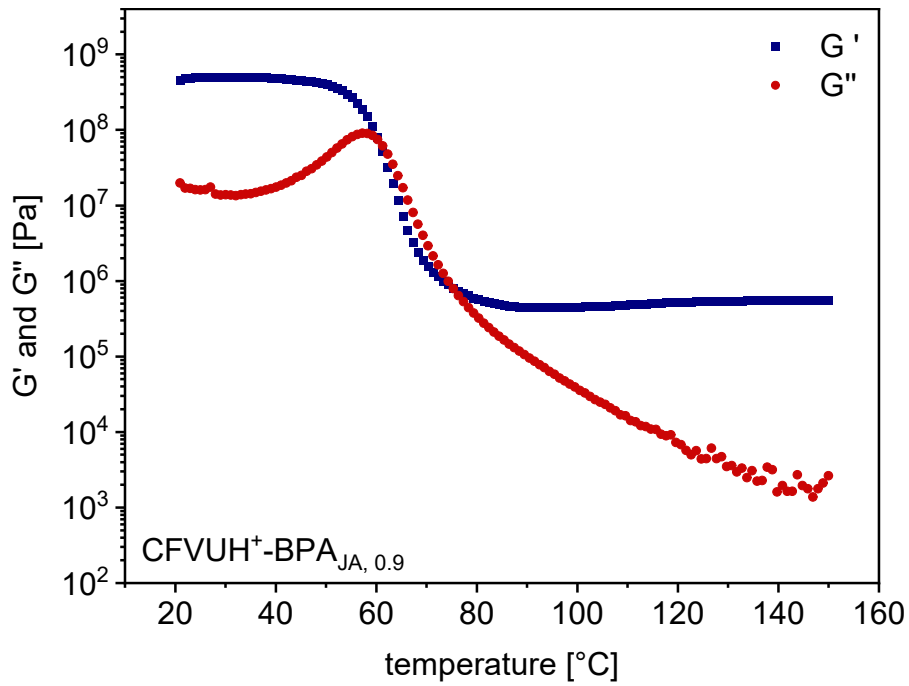
Fig. S37b Temperature-dependent DMA measurement (ω = 10 rad/s, y = 0.1 %) of CFVUH⁺-BPA$_{JA, 0.9}$ in the temperature range of 20–150 °C, showing the storage- and loss modulus (G' and G'') with the characteristic rubbery plateau of the cross-linked material at elevated temperatures up to 150 °C.
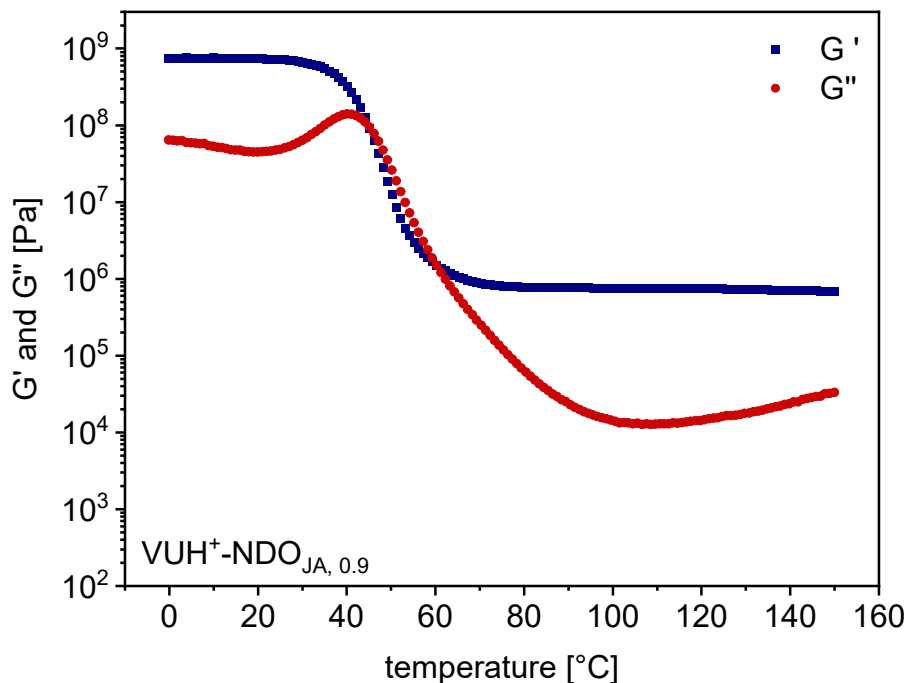
Fig. S37c Temperature-dependent DMA measurement (ω = 10 rad/s, y = 0.1 %) of VUH⁺-NDO$_{JA, 0.9}$ in the temperature range of 0–150 °C, showing the storage- and loss modulus (G' and G'') with the characteristic rubbery plateau of the cross-linked material at elevated temperatures up to 150 °C.
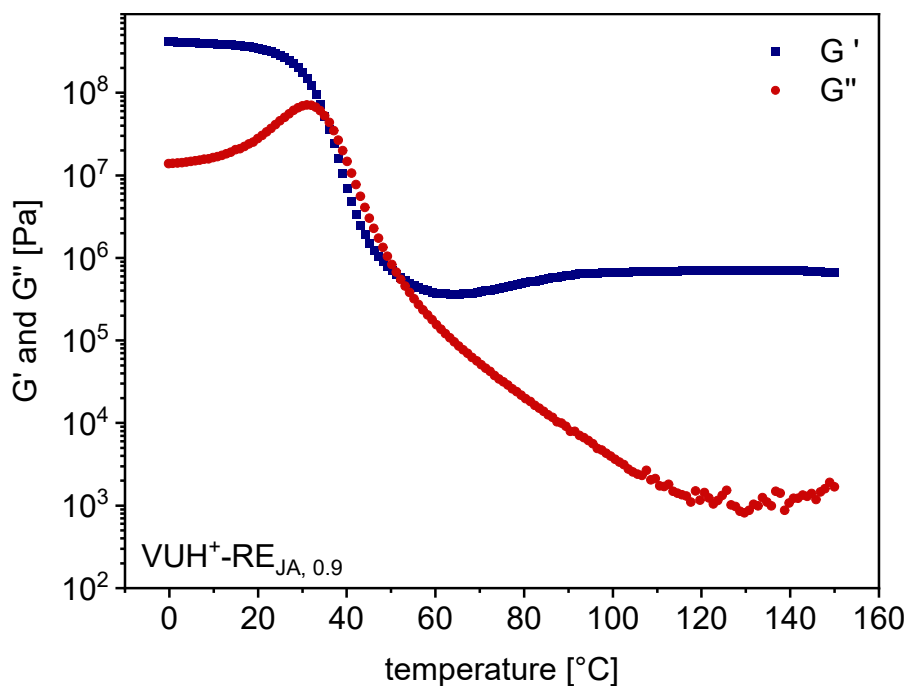
Fig. S37d Temperature-dependent DMA measurement ($\omega = 10$ rad/s, $y = 0.1$ %) of VUH$^+$-RE$_{JA, 0.9}$ in the temperature range of 0–150 °C, showing the storage- and loss modulus (G' and G'') with the characteristic rubbery plateau of the cross-linked material at elevated temperatures up to 150 °C.
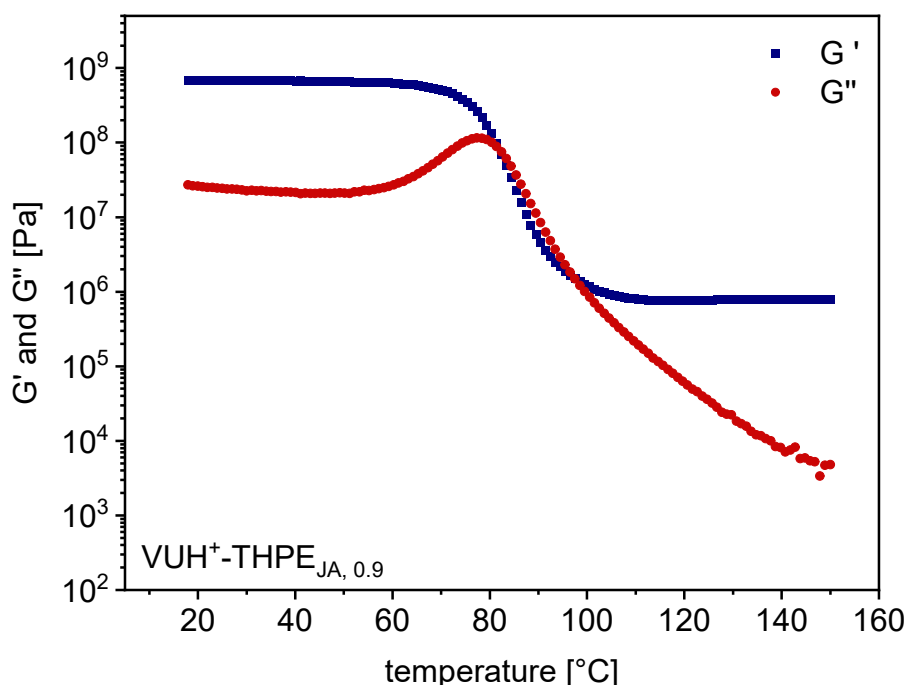
Fig. S37e Temperature-dependent DMA measurement ($\omega = 10$ rad/s, $y = 0.1$ %) of VUH$^+$-THPE$_{JA, 0.9}$ in the temperature range of 20–150 °C, showing the storage- and loss modulus (G' and G'') with the characteristic rubbery plateau of the cross-linked material at elevated temperatures up to 150 °C.
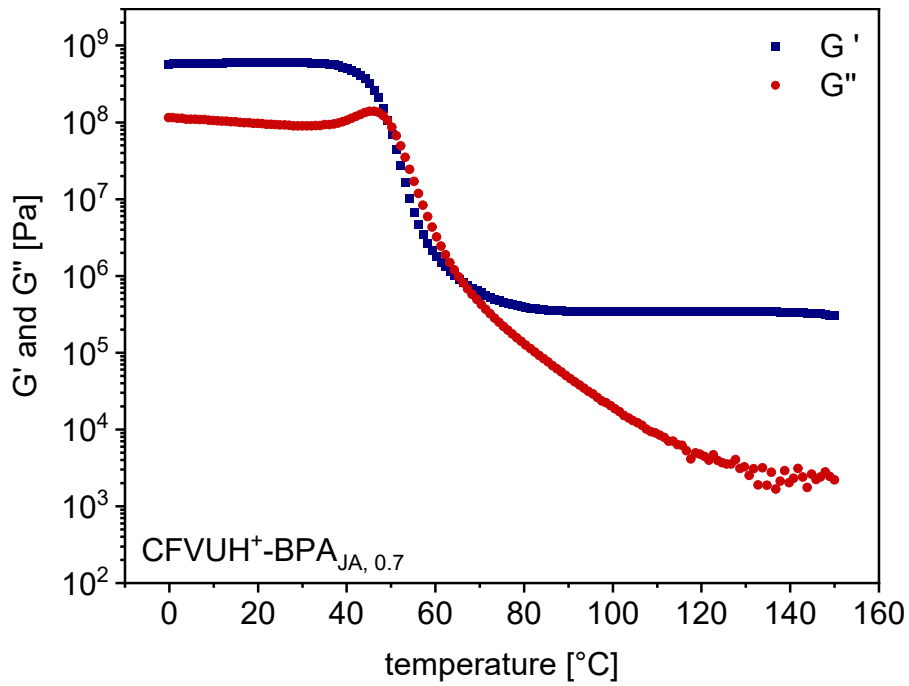
Fig. S37f Temperature-dependent DMA measurement ($\omega = 10$ rad/s, $y = 0.1\,\%$) of VUH$^+$-BPA$_{JA, 0.7}$ in the temperature range of 0–150 °C, showing the storage- and loss modulus (G′ and G′′) with the characteristic rubbery plateau of the cross-linked material at elevated temperatures up to 150 °C.
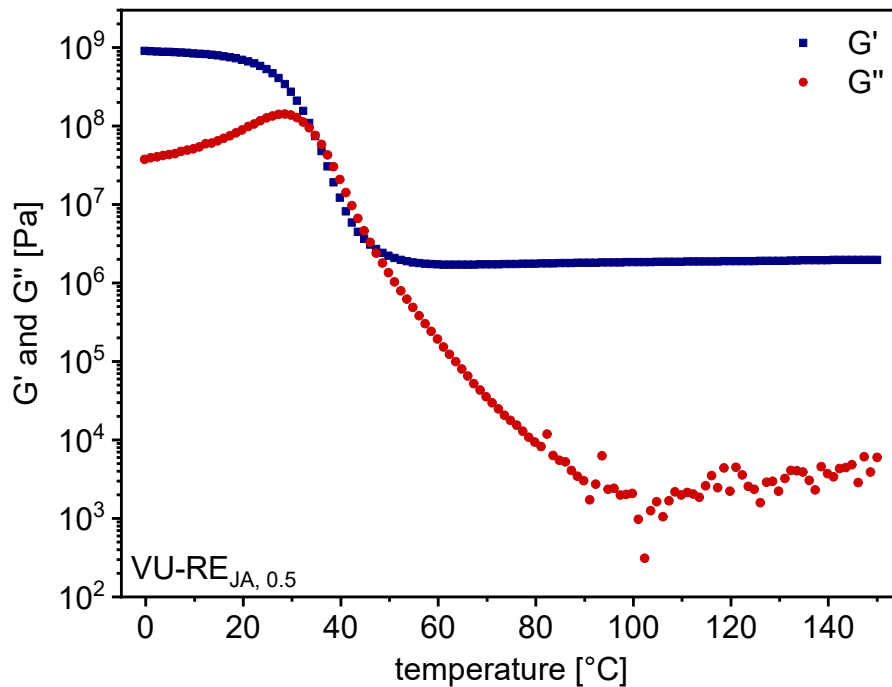
Fig. S37g Temperature-dependent DMA measurement ($\omega = 10$ rad/s, $y = 0.1\,\%$) of VU-RE$_{JA, 0.5}$ in the temperature range of 0–150 °C, showing the storage- and loss modulus (G′ and G′′) with the characteristic rubbery plateau of the cross-linked material at elevated temperatures up to 150 °C.
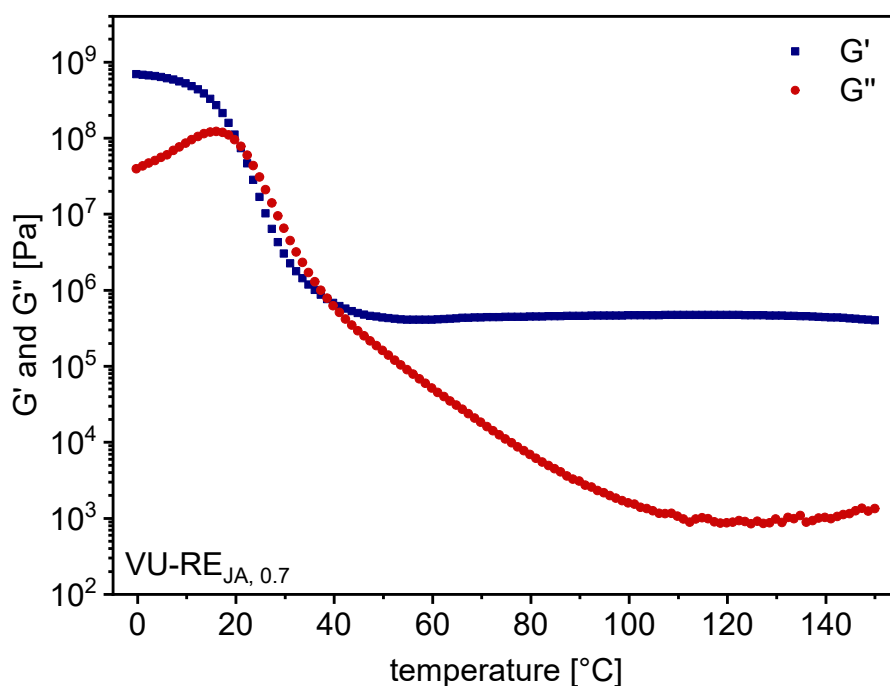
Fig. S37h Temperature-dependent DMA measurement (ω = 10 rad/s, y = 0.1 %) of VU-RE$_{JA, 0.7}$ in the temperature range of 0–150 °C, showing the storage- and loss modulus (G' and G'') with the characteristic rubbery plateau of the cross-linked material at elevated temperatures up to 150 °C.
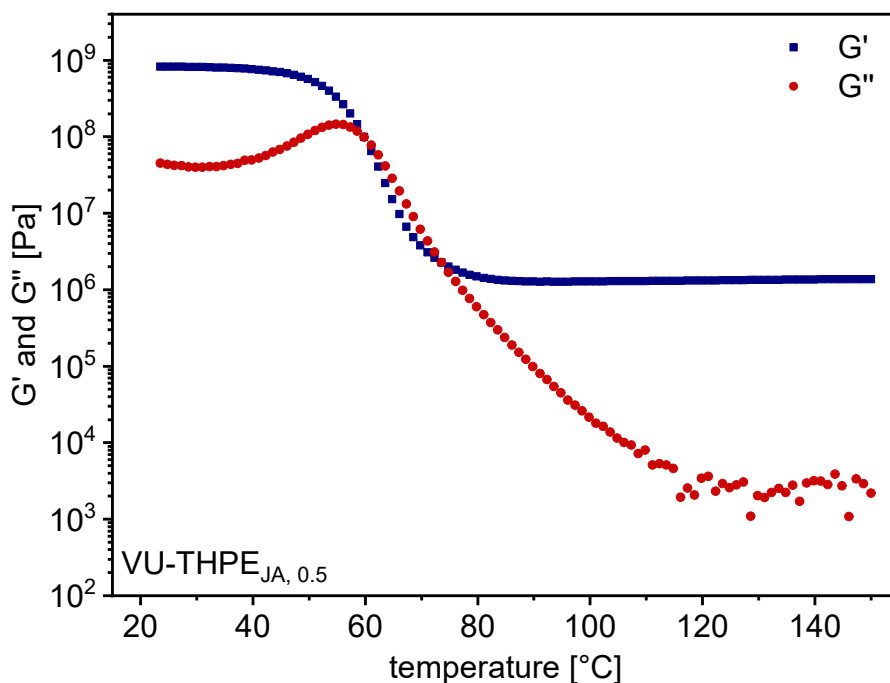
Fig. S37i Temperature-dependent DMA measurement (ω = 10 rad/s, y = 0.1 %) of VU-THPE$_{JA, 0.5}$ in the temperature range of 20–150 °C, showing the storage- and loss modulus (G' and G'') with the characteristic rubbery plateau of the cross-linked material at elevated temperatures up to 150 °C.
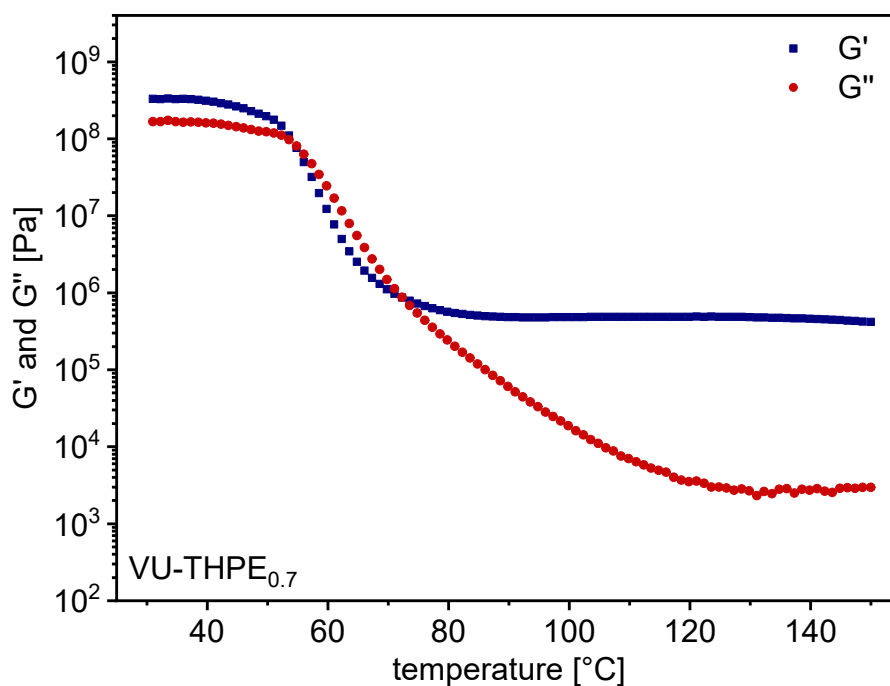
Fig S37j Temperature-dependent DMA measurement (ω = 10 rad/s, *y* = 0.1 %) of VU-THPE$_{JA, 0.7}$ in the temperature range of 20–150 °C, showing the storage- and loss modulus (G' and G'') with the characteristic rubbery plateau of the cross-linked material at elevated temperatures up to 150 °C.
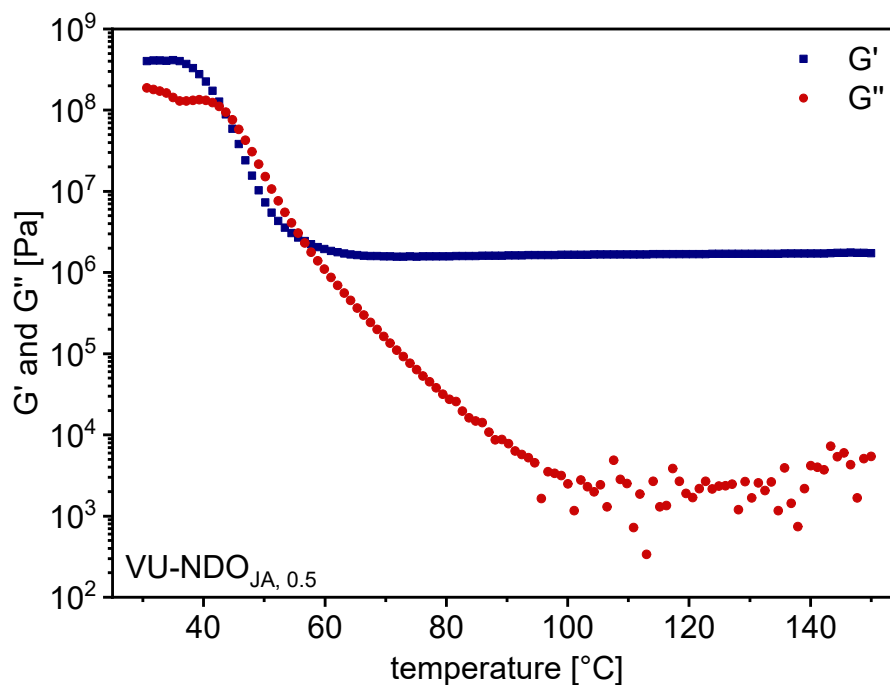
Fig. S37k Temperature-dependent DMA measurement *(ω = 10 rad/s,* y *= 0.1 %)* of VU-NDO$_{JA, 0.5}$ in the temperature range of 30–150 °C, showing the storage- and loss modulus *(G' and G'')* with the characteristic rubbery plateau of the cross-linked material at elevated temperatures up to 150 °C.
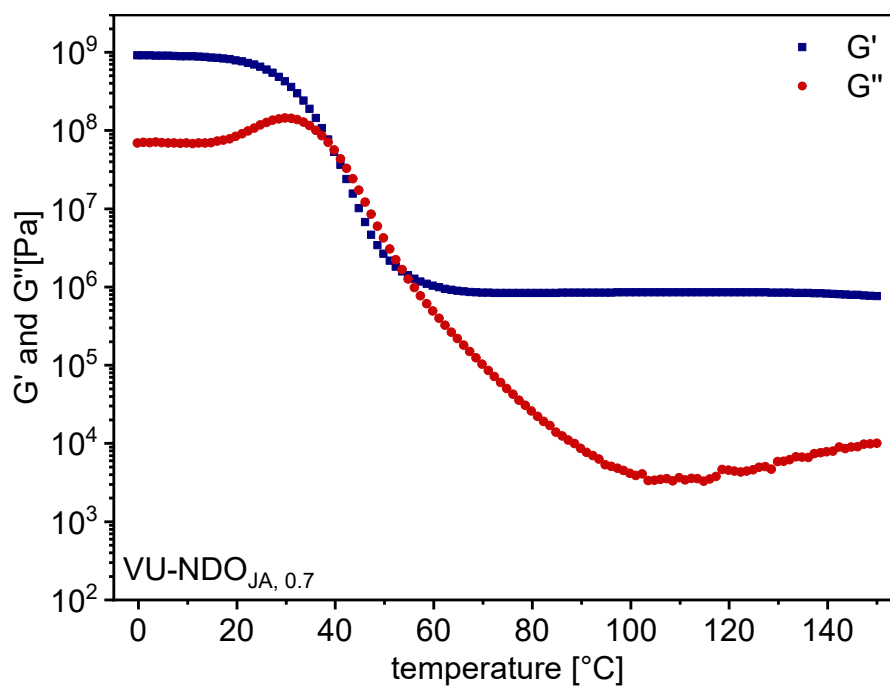
Fig. S37l Temperature-dependent DMA measurement (ω = 10 rad/s, y = 0.1 %) of VU-NDO$_{JA, 0.7}$ in the temperature range of 0–150 °C, showing the storage- and loss modulus (G' and G'') with the characteristic rubbery plateau of the cross-linked material at elevated temperatures up to 150 °C
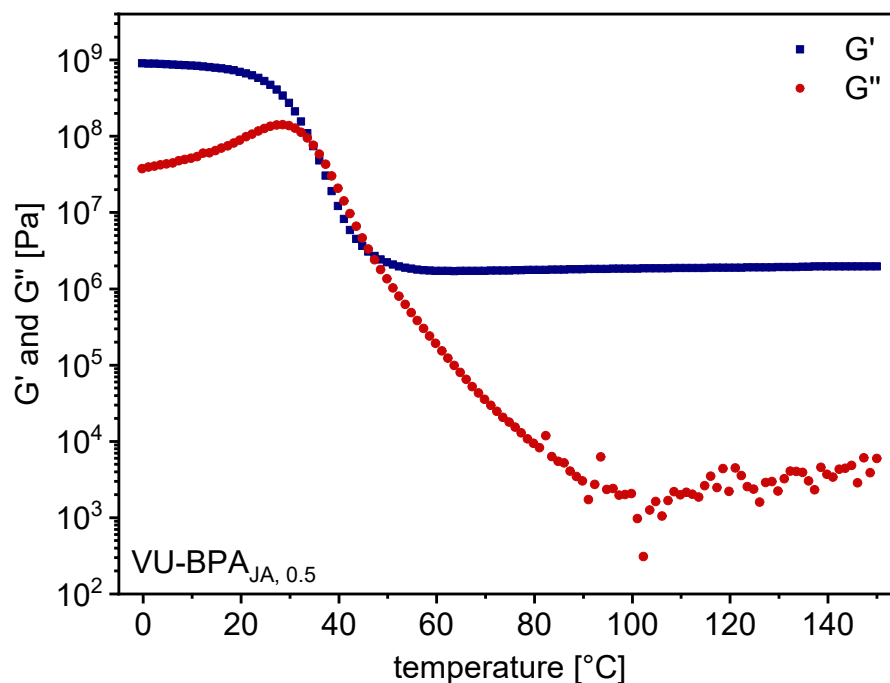
Fig. S37m Temperature-dependent DMA measurement *(ω = 10 rad/s,* y *= 0.1 %)* of VU-BPA$_{JA, 0.5}$ in the temperature range of 0–150 °C, showing the storage- and loss modulus *(G' and G'')* with the characteristic rubbery plateau of the cross-linked material at elevated temperatures up to 150 °C.
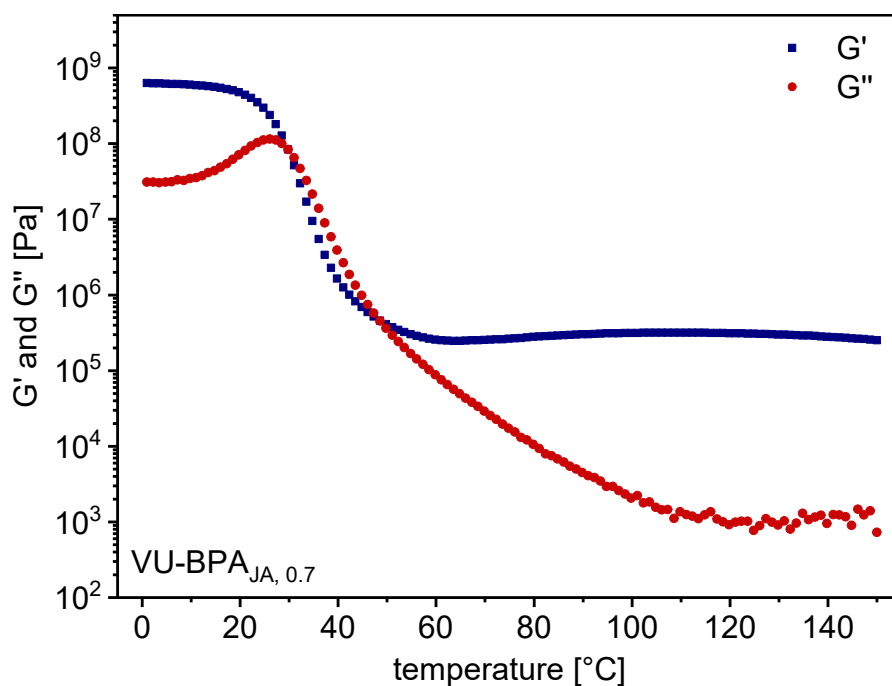
Fig. S37n Temperature-dependent DMA measurement (ω = 10 rad/s, y = 0.1 %) of VU-BPA_{JA, 0.7} in the temperature range of 0–150 °C, showing the storage- and loss modulus (G' and G'') with the characteristic rubbery plateau of the cross-linked material at elevated temperatures up to 150 °C.
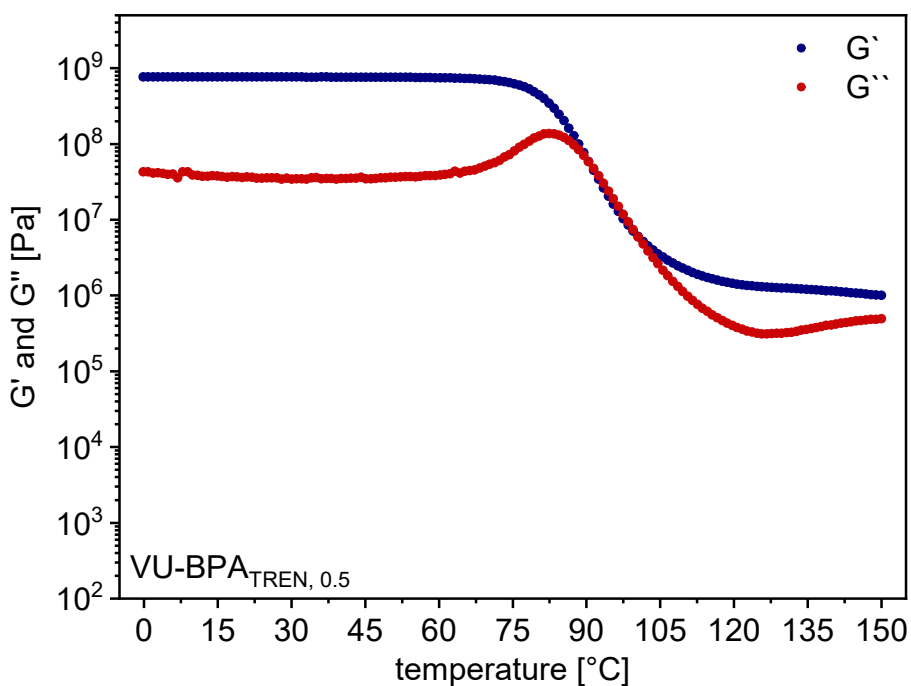
Fig. S37o Temperature-dependent DMA measurement (ω = 10 rad/s, y = 0.1 %) of VU-BPA_{TREN, 0.5} in the temperature range of 75–150 °C, showing the storage- and loss modulus (G' and G'') with the characteristic rubbery plateau of the cross-linked material at elevated temperatures up to 150 °C.
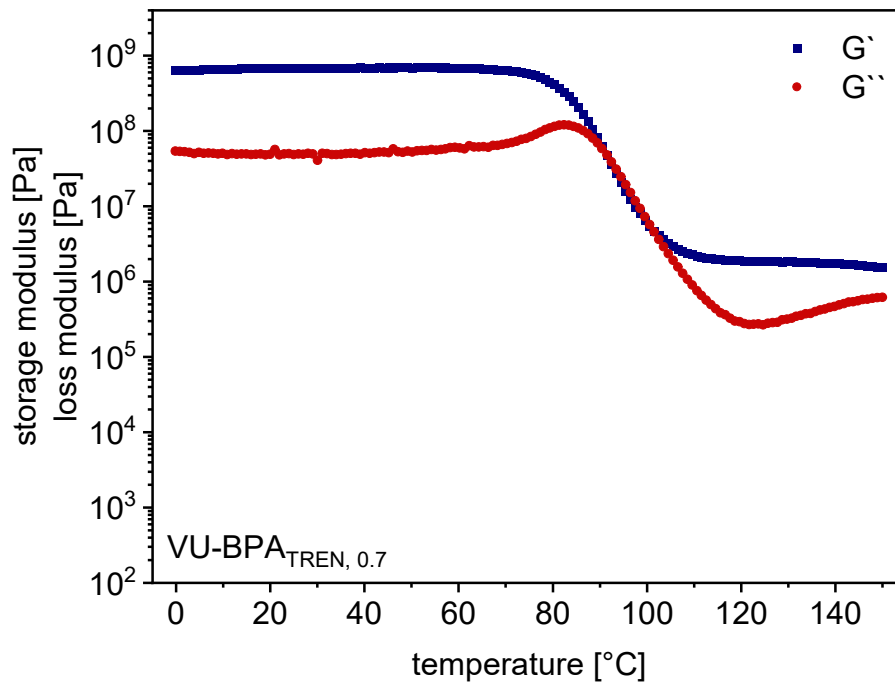
Fig. S37p Temperature-dependent DMA measurement ($\omega = 10$ rad/s, $y = 0.1$ %) of VU-BPA$_{\text{TREN, 0.7}}$ in the temperature range of 75–150 °C, showing the storage- and loss modulus (G' and G'') with the characteristic rubbery plateau of the cross-linked material at elevated temperatures up to 150 °C.
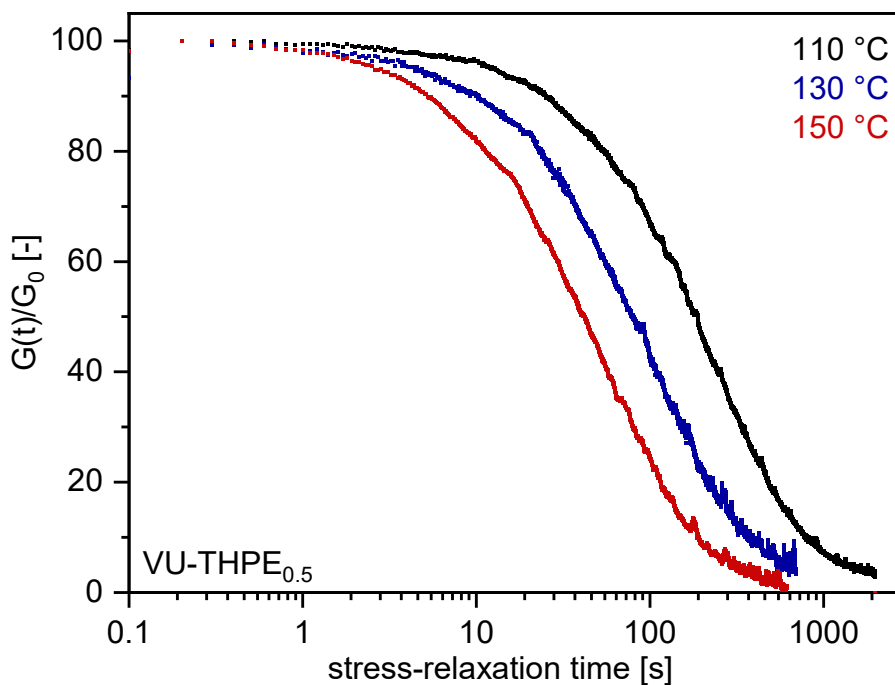
Fig. S38a Stress relaxation experiment of VU-THPE$_{\text{JA, 0.5}}$, plotting the normalized stress relaxation against the stress-relaxation time (DMA) measured at temperatures of 110, 130 and 150 °C.
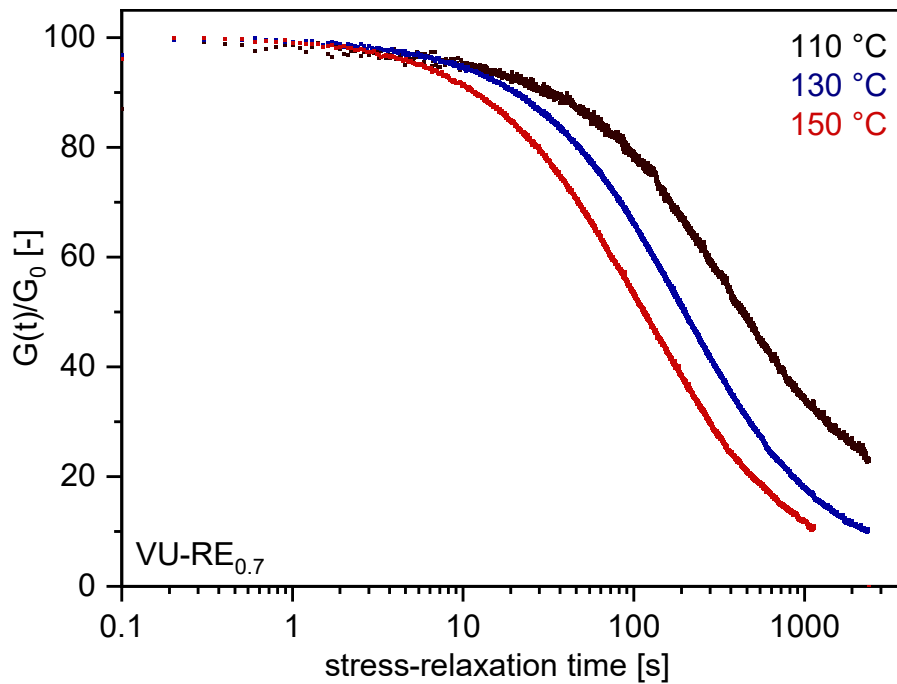
Fig. S38b Stress relaxation experiment of VU-RE$_{JA, 0.7}$, plotting the normalized stress relaxation against the stress-relaxation time (DMA) measured at temperatures of 110, 130 and 150 °C.
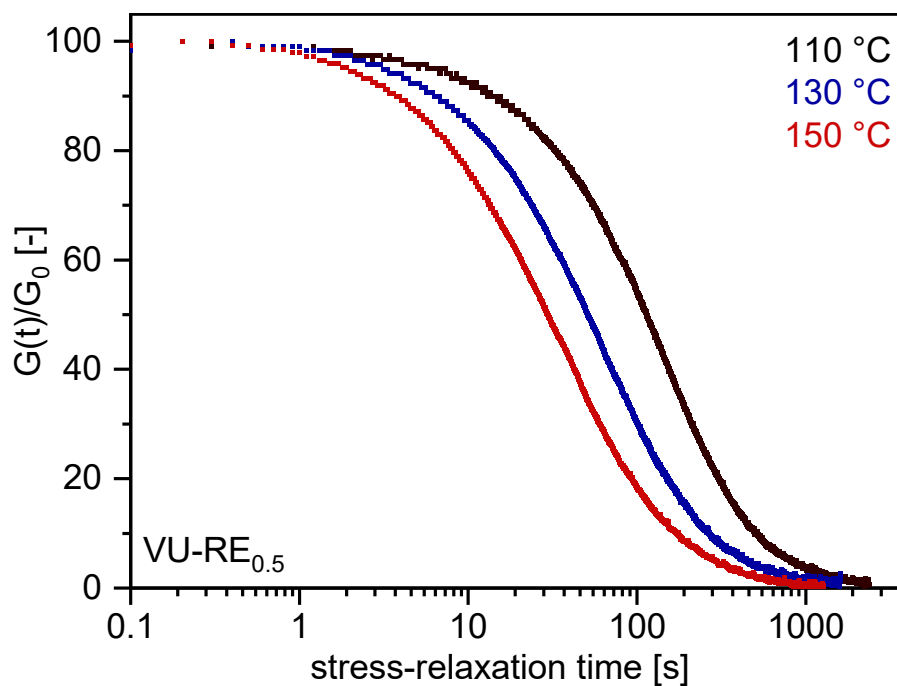
Fig. S38c Stress relaxation experiment of VU-RE$_{JA, 0.5}$, plotting the normalized stress relaxation against the stress-relaxation time (DMA) measured at temperatures of 110, 130 and 150 °C.
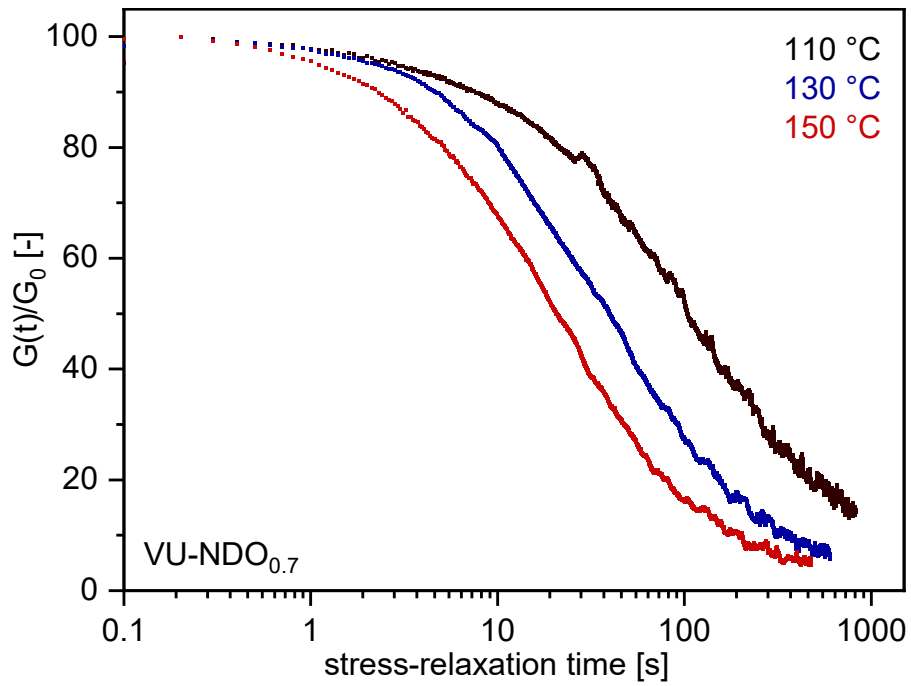
Fig. S38d Stress relaxation experiment of VU-NDO_{JA, 0.7}, plotting the normalized stress relaxation against the stress-relaxation time (DMA) measured at temperatures of 110, 130 and 150 °C.
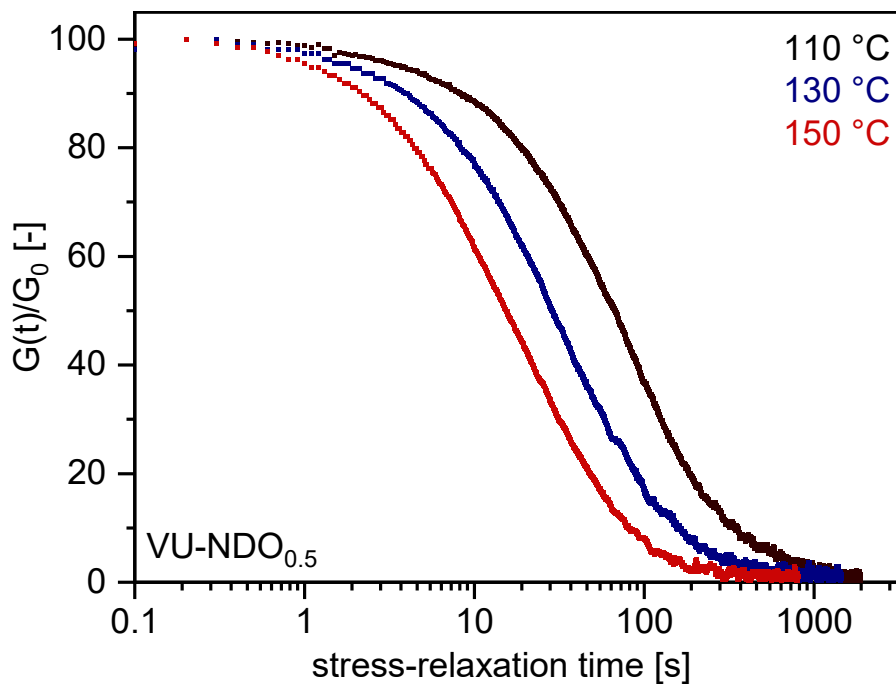
Fig. S38e Stress relaxation experiment of VU-NDO_{JA, 0.5}, plotting the normalized stress relaxation against the stress-relaxation time (DMA) measured at temperatures of 110, 130 and 150 °C.
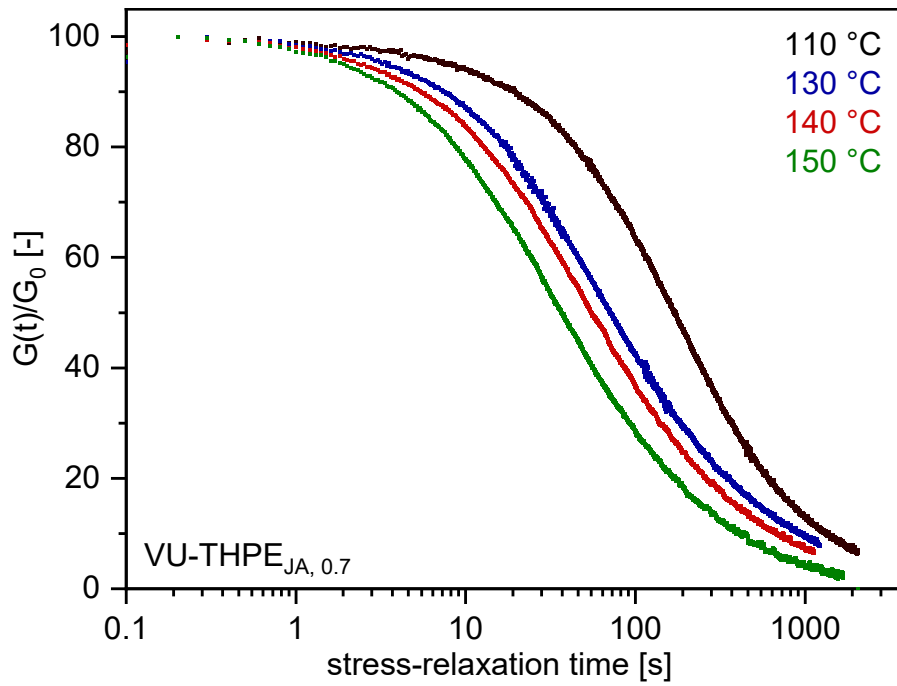
Fig. S38f Stress relaxation experiment of VU-THPE_JA, 0.7, plotting the normalized stress relaxation against the stress-relaxation time (DMA) measured at temperatures of 110, 130, 140 and 150 °C.
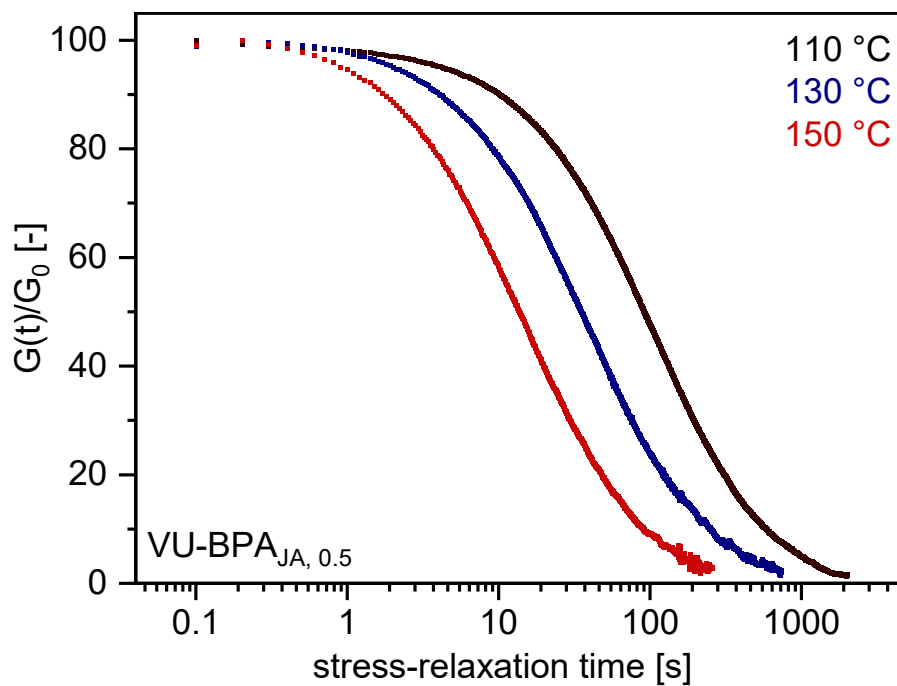
Fig. S38g Stress relaxation experiment of VU-BPA_JA, 0.5, plotting the normalized stress relaxation against the stress-relaxation time (DMA) measured at temperatures of 110, 130 and 150 °C.
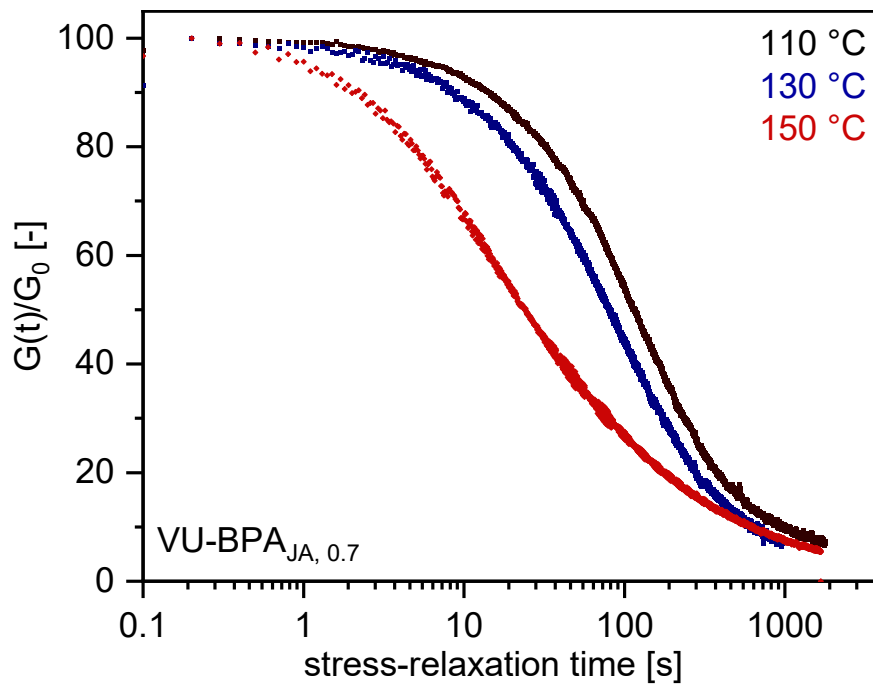
Fig. S38h Stress relaxation experiment of VU-BPA$_{JA, 0.7}$, plotting the normalized stress relaxation against the stress-relaxation time (DMA) measured at temperatures of 110, 130 and 150 °C
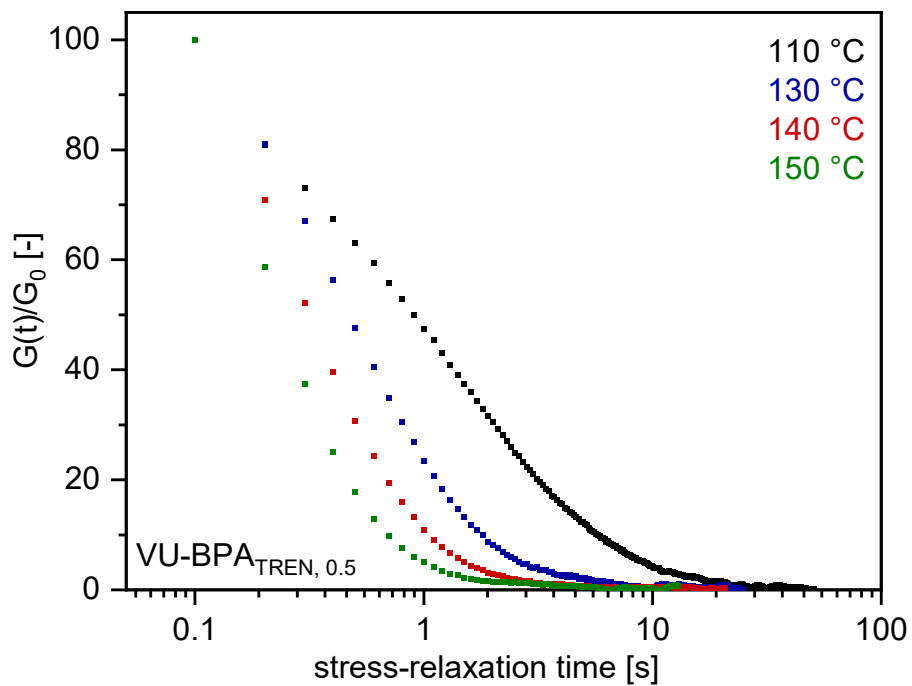
Fig. S38i Stress relaxation experiment of VU-BPA$_{TREN, 0.5}$, plotting the normalized stress relaxation against the stress-relaxation time (DMA) measured at temperatures of 110, 130 and 150 °C.
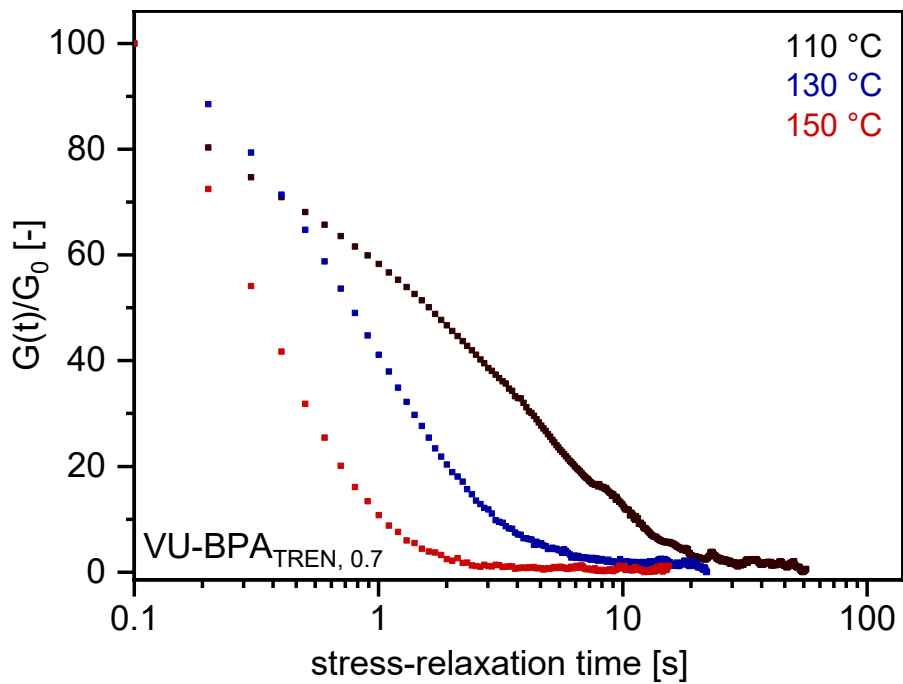
Fig. S38j Stress relaxation experiment of VU-BPA$_{TREN, 0.7}$, plotting the normalized stress relaxation against the stress-relaxation time (DMA) measured at temperatures of 110, 130 and 150 °C.
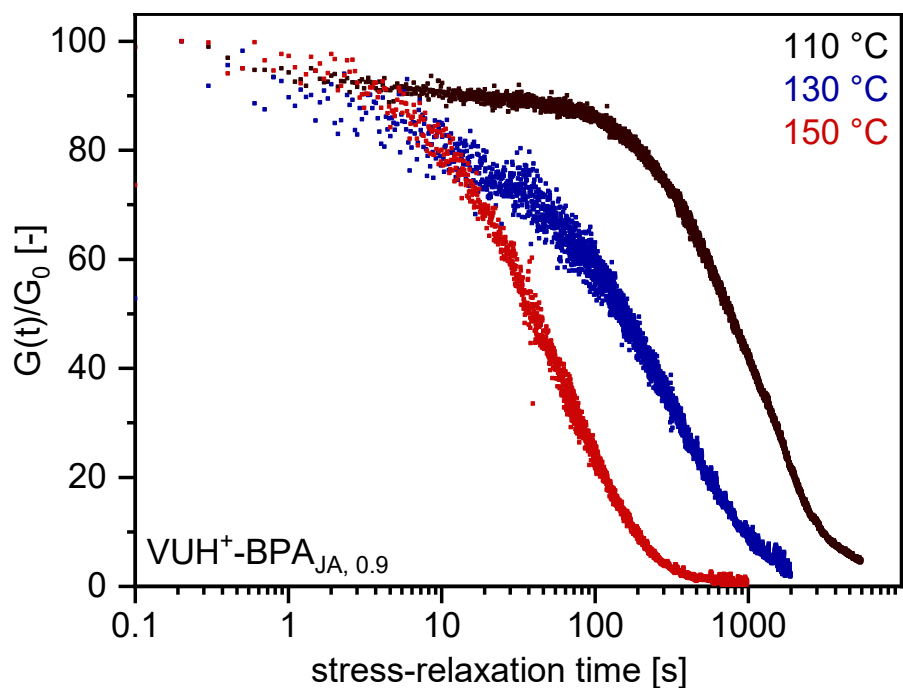
Fig. S38k Stress relaxation experiment of VUH$^+$-BPA$_{JA, 0.9}$, plotting the normalized stress relaxation against the stress-relaxation time (DMA) measured at temperatures of 110, 130 and 150 °C.
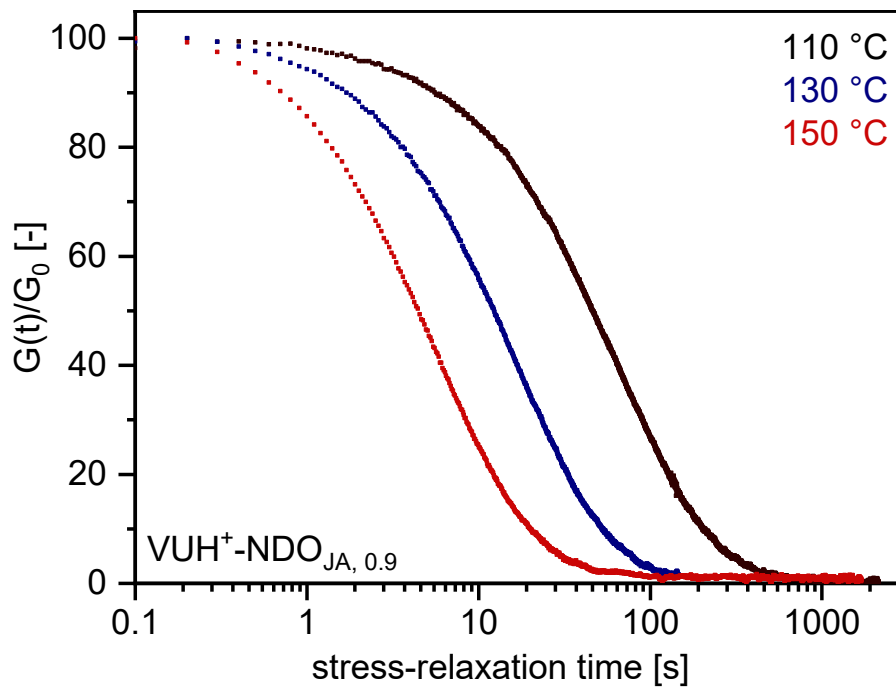
Fig. S38l Stress relaxation experiment of VUH+-NDO$_{JA, 0.9}$, plotting the normalized stress relaxation against the stress-relaxation time (DMA) measured at temperatures of 110, 130 and 150 °C.
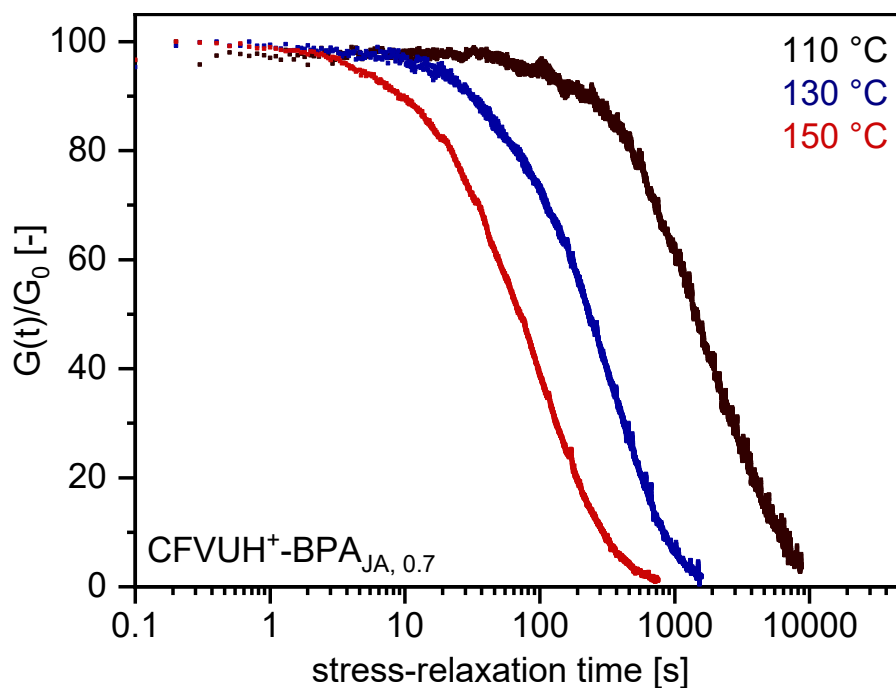
Fig. S38m Stress relaxation experiment of CFVUH+-BPA$_{JA, 0.7}$, plotting the normalized stress relaxation against the stress-relaxation time (DMA) measured at temperatures of 110, 130 and 150 °C.
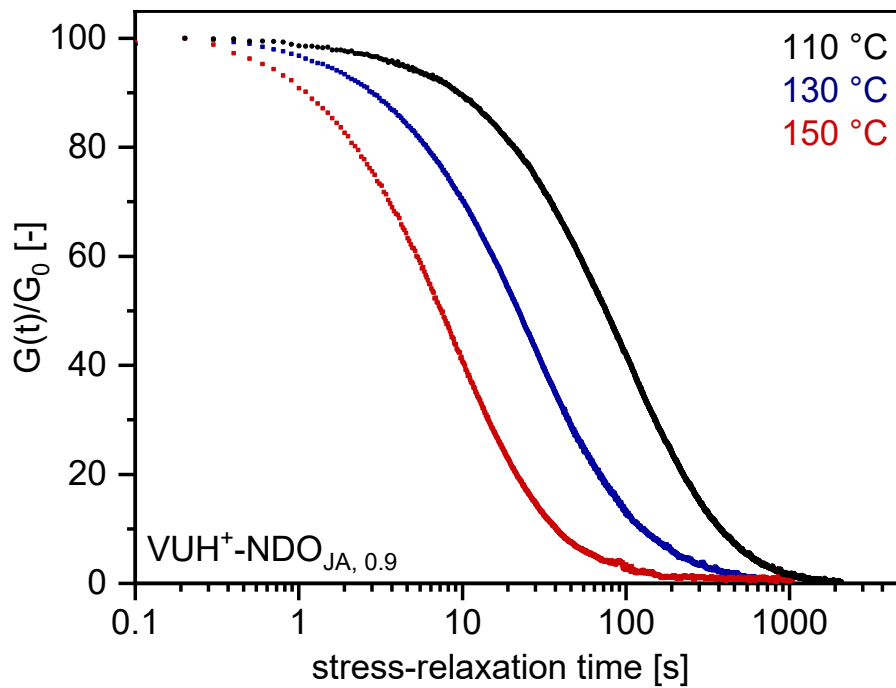
Fig. S38n Stress relaxation experiment of VUH⁺-NDO$_{JA, 0.9}$, plotting the normalized stress relaxation against the stress-relaxation time (DMA) measured at temperatures of 110, 130 and 150 °C.
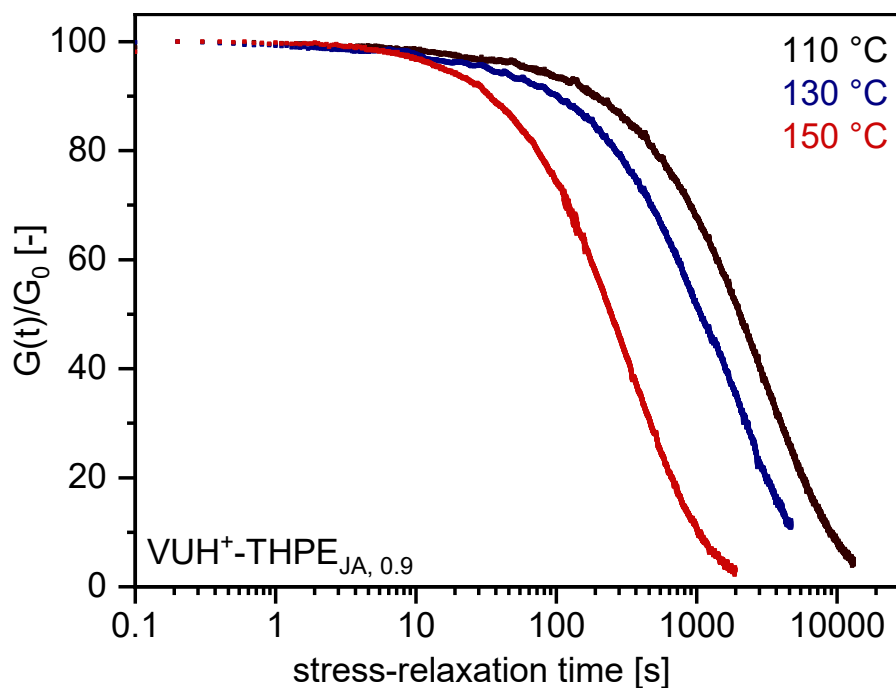
Fig. S38o Stress relaxation experiment of VUH⁺-THPE$_{JA, 0.9}$, plotting the normalized stress relaxation against the stress-relaxation time (DMA) measured at temperatures of 110, 130 and 150 °C.
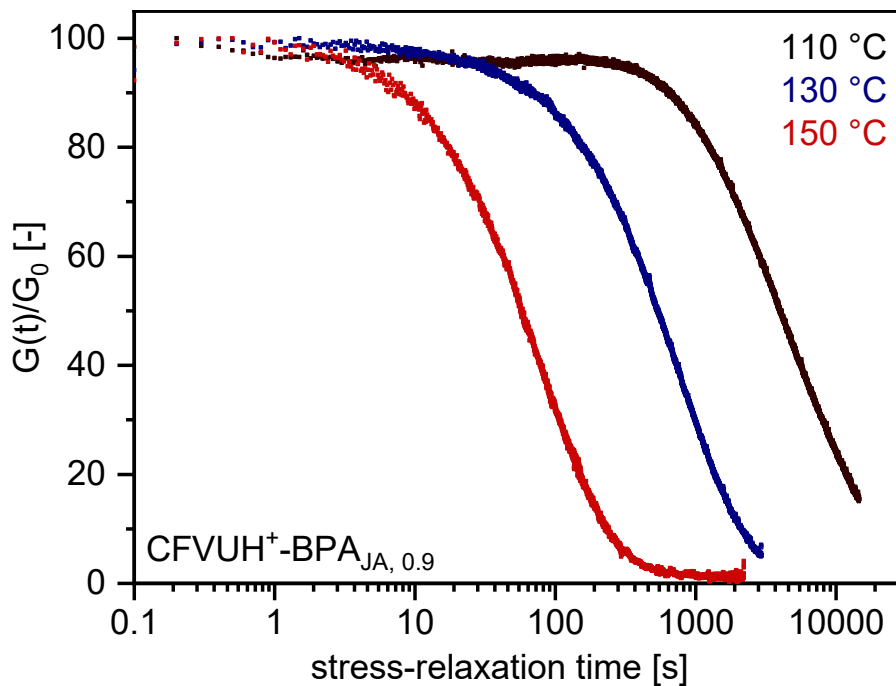
Fig. S38p Stress relaxation experiment of CFVUH⁺-BPA_{JA, 0.9}, plotting the normalized stress relaxation against the stress-relaxation time (DMA) measured at temperatures of 110, 130 and 150 °C.
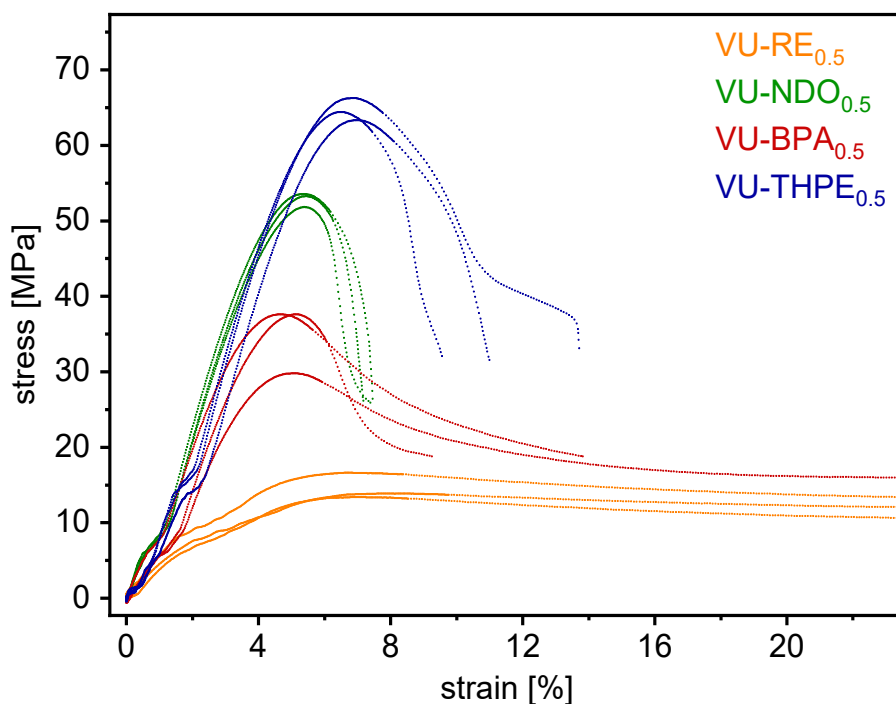
Fig. S39a Stress-strain measurements of the vitrimers VU-RE_{JA, 0.5}, VU-NDO_{JA, 0.5}, VU-BPA_{JA, 0.5} and VU-THPE_{JA, 0.5} with an acetoacetate to amine ratio of 0.5 at room temperature (the test was carried out at 10 mm min^{-1}).
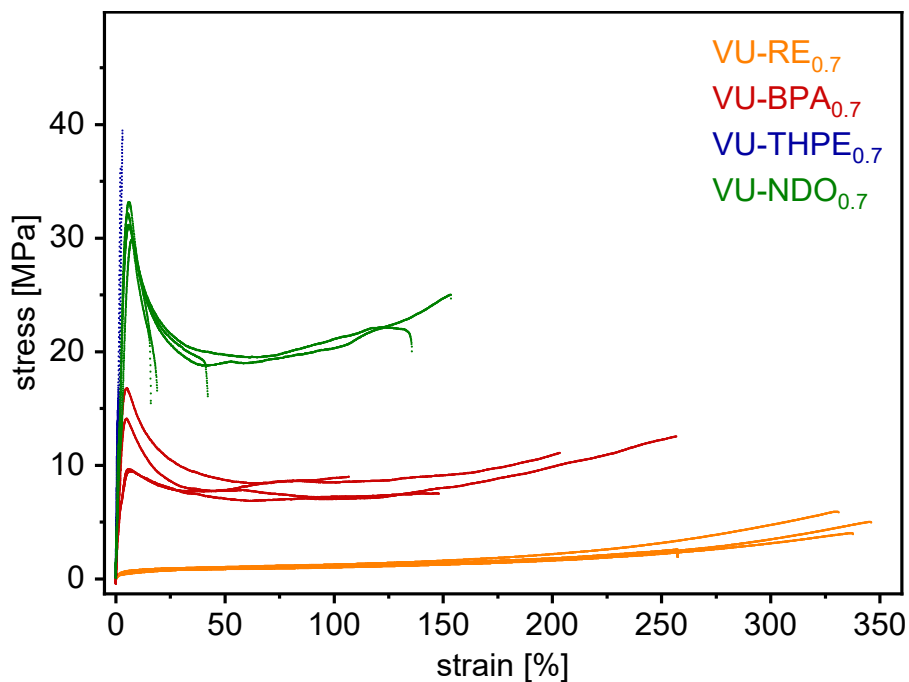
Fig. S39b Stress-strain measurements of the vitrimers VU-RE$_{JA, 0.5}$, VU-NDO$_{JA, 0.5}$, VU-BPA$_{JA,0.5}$ and VU-THPE$_{JA, 0.5}$ with an acetoacetate to amine ratio of 0.7 at room temperature (the test was carried out at 10 mm min^{-1}).
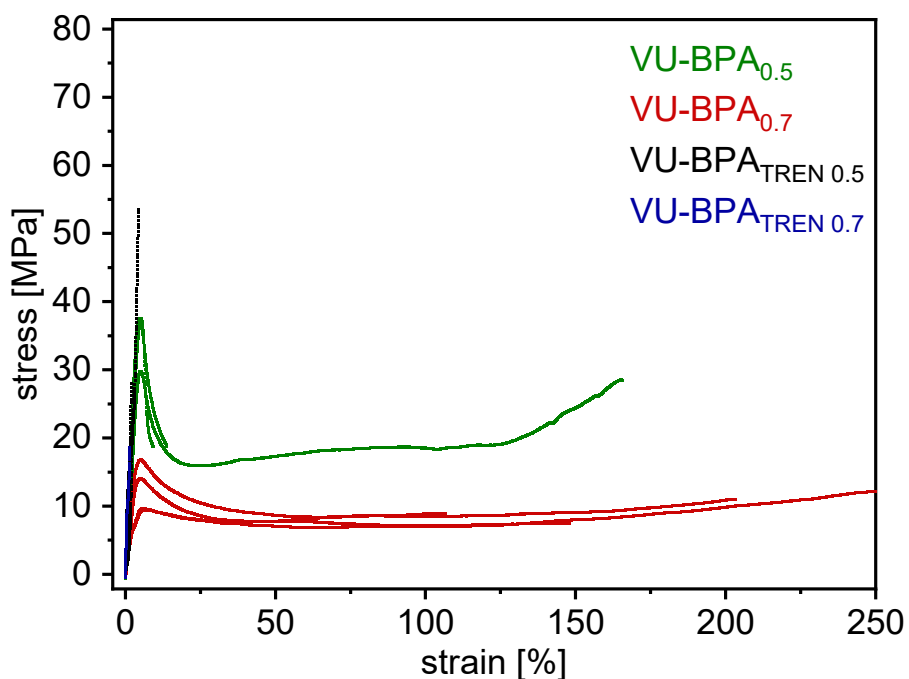
Fig. S39c Stress-strain measurements of the vitrimers VU-BPA cured with JA or TREN and acetoacetate to amine ratio of 0.5 or 0.7 at room temperature (the test was carried out at 10 mm min^{-1}).
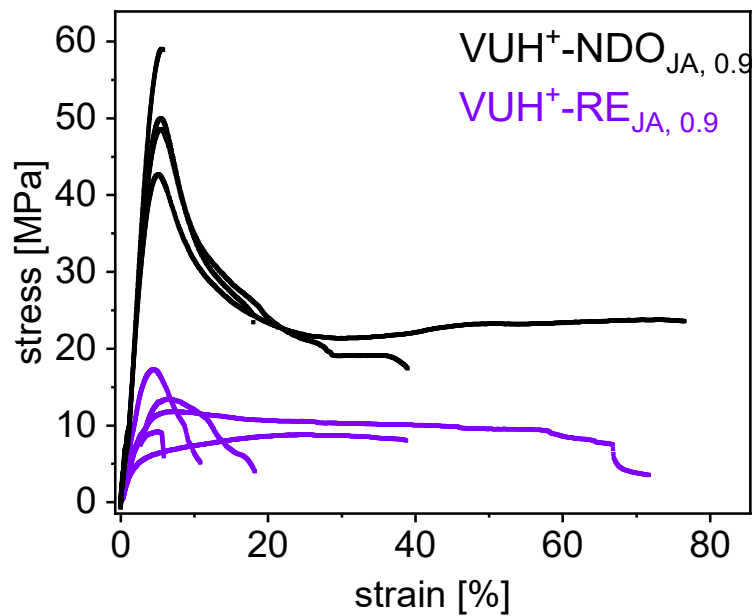
Fig. S39d Stress-strain measurements of the vitrimers VUH$^+$-NDO$_{JA,\,0.9}$ and VUH$^+$-RE$_{JA,\,0.9}$.
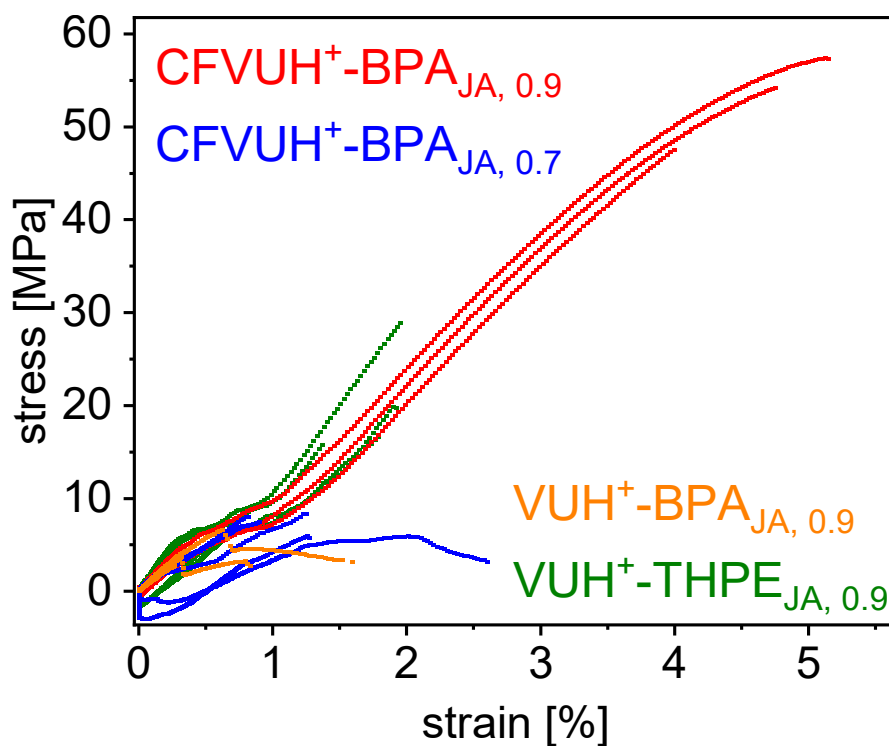
Fig. S39e Stress-strain measurements of the vitrimers CFVUH$^+$-BPA$_{JA,\,0.9}$, CFVUH$^+$-BPA$_{JA,\,0.7}$ VUH$^+$-BPA$_{JA,\,0.9}$ and VUH$^+$-THPE$_{JA,\,0.9}$.
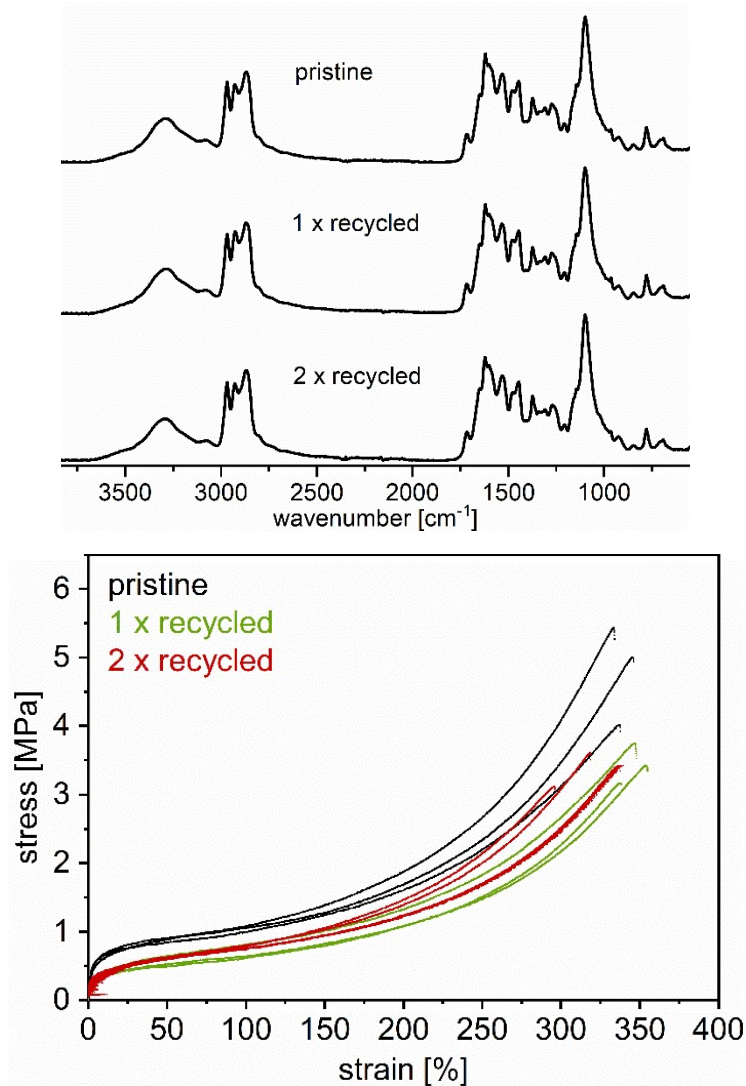
Fig. S40 Reprocessing cycles of the vitrimers by consecutive grinding and compression molding (150 °C, 300 s), generating homogeneous, transparent, and bubble-free films (specimen) (top). Repetitive ATR-FT-IR spectra of the exemplary reprocessing cycles of the elastomeric vitrimer VU-RE$_{0.7}$, showing similar spectra after each cycle (middle). Repetitive stress-strain measurements of the exemplary reprocessing cycles of the elastomeric vitrimer VU-RE$_{0.7}$, showing a stable stress and strain behavior after a slight decrease after the first cycle (bottom).
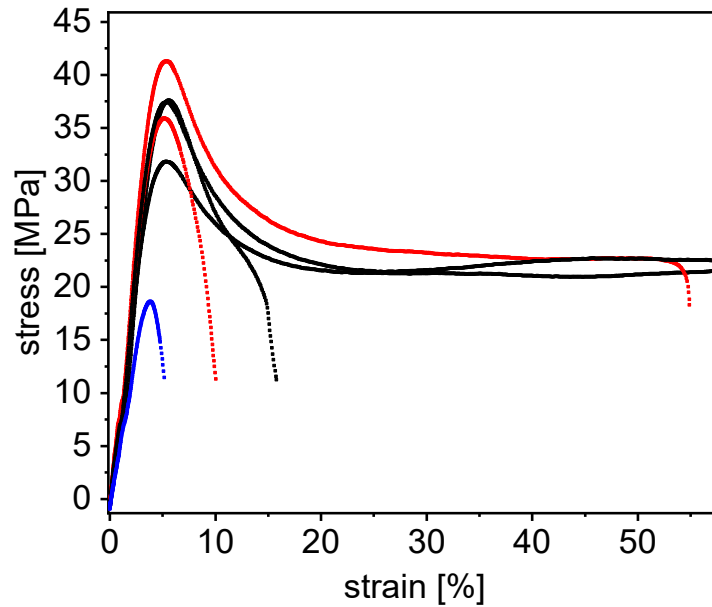
Fig. S41 Self-healing, exemplary showed for VU-RE$_{JA, 0.5}$. The DIN 5B bones were cut half and put into the oven for 30 minutes at 150 °C. Tensile tests show almost full recovery after the self-healing process (black: original, red: self-healed). The blue curve represents a sample which was not cured after cutting, showing significantly lower stress resistant.

References

[1]   W. Denissen, G. Rivero, R. Nicolaÿ, L. Leibler, J. M. Winne, F. E. Du Prez, *Advanced Functional Materials* **2015**, 25, 2451.

9.4 Publication 3 – Supporting Information

Reprinted with permission from *Sustain. Chem. Eng.*, **2023**, *11*, 22, 8350–8361 (DOI:10.1021/acssuschemeng.3c01340). Copyright 2023 American Chemical Society.

Supporting Information

Starch-reinforced Vinylogous Urethane Vitrimer Composites: An Approach to Biobased, Reprocessable and Biodegradable Materials

Philipp Haida[a], Suwabun Chirachanchai[b] and Volker Abetz*[c,a]

[a] Institute of Physical Chemistry, Universität Hamburg, Grindelallee 117, 20146 Hamburg, Germany

[b] Center of Excellence in Bioresources to Advanced Materials, The Petroleum and Petrochemical College, Chulalongkorn University, 254 Soi Chula 12, Wangmai, Pathumwan, Bangkok 10330, Thailand

[c] Institute of Membrane Research, Helmholtz-Zentrum Hereon, Max-Planck-Straße 1, 21502 Geesthacht, Germany

volker.abetz@hereon.de

The supporting information contains 36 pages with 57 figures and 3 tables.

Materials: Starch (corn), starch (wheat), starch (rice), hexylamine (99%), *alpha*-amylase (aspergillus oryzae, 30 U mg^{-1}), iodine (99.5%) and ethanol (99%) were purchased from Sigma-Aldrich. 2,2,6-trimethyl-1,3-dioxin-4-one (95%), *tert*-butylacetoacetate (98%), 1,5-diaminopentane (98%), 1,4-diaminobutane (98%), 1,6-diaminohexane (98%), 1,8-diaminooctane (98%), 1,10-diaminodecan (98%), 1,12-diaminododecane (98%) and 1,6-hexanediol (98%) were obtained from TCI. Ethylene glycol (99.5%) was purchased from Honeywell. Acetic acid (100%) and tetrahydrofuran (HPLC-grade) were purchased from VWR. Glycerol (99.5%) was purchased from ROTH. Isobutylamine (99%) was purchased from Alfa Aesar. DMSO-*d6* was purchased from Deutero GmbH. Priamine 1075 was provided from Croda International.

Methods: Nuclear magnetic resonance: ^{1}H NMR and ^{13}C NMR (DEPTQ-135) spectra were recorded on a Bruker AVANCEII (Bruker BioSpin GmbH, Ettlingen, Germany) at 300 or 600 MHz with deuterated dimethylsulfoxide (DMSO-*d6*) as a solvent. Sample concentrations were between 20–40 mg mL^{-1}, and measurements were recorded at 298 K. Data processing was carried out with MestReNova (Version 14.1.0, Mestrelab Research S.L., Santiago de Compostela, Spain). **Mass spectrometry (MS):** Electrospray ionization (ESI) was measured on an Agilent 6224 ESI-TOF device coupled with an Agilent HPLC 1200 Series and direct injection (110–3200 m/z). Electron ionization (EI-DIP) was measured on a Thermo ISQ LT EI device coupled with a Thermo Trace 1300 and direct injection (40–800 m/z). Data processing was carried out by MestReNova (Version 14.1.0, Mestrelab Research S.L., Santiago de Compostela, Spain). **Attenuated Total Reflection-Fourier Transformation Infrared (ATR-FT-IR):** Spectra were recorded on a Bruker FT-IR Vertex 70 (Bruker BioSpin GmbH, Ettlingen, Germany) with a diamond ATR-probe. All samples were measured in the range of 4000–600 cm^{-1} with a resolution of 2 cm^{-1} and 32 scans. Measurements and data processing was carried out with Opus 8.7. **Thermogravimetric analysis (TGA):** A TG 209 F1 Libra

(NETZSCH-Gerätebau GmbH, Selb, Germany) was used to determine the mass loss during heat treatment. A temperature range of 25–600 °C with a heating rate of 10 K min^{-1} under ambient atmosphere (oxygen) was used with a flow rate of 20 mL min^{-1}. About 5–10 mg of polymer was weighed into a ceramic crucible. Data processing was performed with Proteus analysis 8.0.3 (NETZSCH-Gerätebau GmbH, Selb, Germany).

Differential scanning calorimetry (DSC): A differential scanning calorimeter DSC 204 F1 Phoenix (NETZSCH-Gerätebau GmbH, Selb, Germany) was used. 5–10 mg polymer was weighed into an aluminum crucible. The measurements were performed in nitrogen atmosphere with a flow rate of 20 mL min^{-1} in the temperature range between (-50)–180 °C. The heating and cooling rates were set to 10 K min^{-1} and the thermal properties were analyzed using the DSC data of the second and third heating curve. Data processing was performed by Proteus analysis 8.0.3 (NETZSCH-Gerätebau GmbH, Selb, Germany).

Dynamic-mechanical analysis (DMA): For oscillatory and step shear experiments, a rotational rheometer MCR 502 (Anton Paar GmbH, Graz, Austria) with an 8 mm plate-plate geometry and a heat chamber with a flooded nitrogen atmosphere was used. The temperature was controlled by a Peltier plate. The gap between the lower and the upper plate was usually set to 1 mm, and a normal force of 1 N was applied. Amplitude sweeps were carried out between 0.001% and 30% shear strain (γ) at a constant angular frequency (ω) of 10 rad s^{-1} at 100 °C. This should ensure that the chosen strain amplitude γ_0 was within the linear viscoelastic regime, so that the storage modulus G' and the loss modulus G'' were independent of strain. Frequency sweeps were carried out between 0.001 Hz and 100 Hz angular frequency (ω) at a constant shear strain (γ) of 0.1% at 100 °C. Temperature-dependent measurements were usually carried out with an angular frequency of 10 rad s^{-1} at a constant shear strain of 0.1% in the temperature range of 0–160 °C. Stress relaxation experiments were carried out with a shear strain of 1%, and the relaxation modulus was recorded as a function of time in the temperature range of 90–

160 °C. Data processing was performed by RheoCompass 1.30 (Anton Paar GmbH, Graz, Austria). Specimens for the DMA were pushed out with an 8 mm punch. The vitrimer films were previously placed in a drying chamber at 100 °C for 1 minute in order to heat them above the glass transition temperature to prevent splintering during processing. **Tensile test:** Stress-strain curves were recorded at room temperature (20 °C) on a universal testing machine type Z020 (Zwick Roell GmbH & Co. KG, Ulm, Germany) using a 5 kN load cell. The measurements were carried out in accordance with the test standard DIN EN ISO 527-1. The initial force was 0.1 MPa, and the clamping length was 13.24 mm. The elastic modulus was determined at a speed of 1 mm min^{-1} (0.025–0.2%) and the test speed was carried out at 10 mm min^{-1}. Data processing was performed by TestXpert *II V3.71*. The test specimens for the tensile test were punched out with a cutting press type ZCP020 (Zwick Roell). The attachment was used for test specimens of type 5B (according to DIN EN ISO 527-2). The vitrimer films were placed in a drying cabinet at 100 °C for one minute in order to heat them above the glass transition temperature, to prevent splintering during processing. **Powder X-Ray diffraction (XRD)** measurements were conducted on a Panalytical MPD X'Pert Pro (Malvern Panalytical, Malvern, Great Britain) with Cu Kα radiation (λ_1=1.5405980 Å, λ_2=1.5444260 Å) at a scan step size of 0.0131 °. **Scanning electron microscopy (SEM)** images were recorded on a LEO Gemini 1550 (Carl Zeiss, Oberkochen, Germany). Secondary electrons were detected with an Everhart-Thornley detector, operating with 1–5 kV and 50–100 pA. **Optical microscope** images were recorded with a Zeiss AX10 Observer A1 (Carl Zeiss, Oberkochen, Germany) microscope with EC EPIPLAN 10x/0.2 HD and EC EPIPLAN 20x/0.2 HD lenses. **Elemental analysis** was carried out on a CHN-Element analyser Vario EL III (Fa. Elementar Analysensysteme GmbH, Langenselbold, Germany).

Synthetic procedures:

The synthesis route was adapted from Witzemann et al. and customized in terms of reaction conditions and acetoacetylation agent.[1] Propane-1,2,3-triyl tris(3-oxobutanoate) (GlyAcAc): The crude, brownish 2,2,6-trimethyl-1-3-dioxin-4-one (TMDO) was purified by vacuum distillation at 60 °C and 0.1 mbar to obtain the pure colorless product. Glycerol (10.0 g, 0.108 mol) and the purified TMDO (48.6 g, 0.342 mol) were mixed in a 250 mL flask. The mixture was heated at 135 °C for 1 h, while the byproduct acetone was removed by distillation during the reaction. The temperature in the distill head was usually between 75–90 °C. When the temperature dropped to 35 °C in the still head, the remaining acetone, TMDO, and dehydroacetic acid were removed in *vacuo* at 135 °C and 0.1 mbar. The residue represented the desired product in a high degree of purity, appearing as a slightly yellowish liquid. Yield = 98%. ^{1}H NMR (300 MHz, DMSO-*d6*, 298 K): 5.23 (1H, m, CH), 4.26 (2H, s, CH_2), 4.24 (2H, s, CH_2), 3.63 (2H, s, CH_2), 3.61 (2H, s, CH_2), 2.17 (3H, s, CH_3). ^{13}C NMR (DEPTQ-135, 75 MHz, DMSO-*d6*, 298 K): 201.32 (q, C=O), 201.10 (q, C=O), 166.92 (q, COO), 166.62 (q, COO), 69.22 (t, CH), 62.20 (s, CH_2), 49.44 (s, CH_2), 49.30 (s, CH_2), 30.03 (p, CH_3), 29.95 (p, CH_3). EI-DIP: m/z = 344.107 (M$^+$, 0.05%), 43.033 ([O=C-CH_3]$^+$, 100%). Calculated for $C_{15}H_{20}O_9$ 344.110, found 344.107. ESI-MS: m/z = 367.101 (M^{Na+}, 100%). Ethane-1,2-diyl bis(3-oxobutanoate) (EgAcAc): The synthetic route follows the same conditions for the acetoacetylation as the synthesis of GlyAcAc. Yield = 99%. ^{1}H NMR (300 MHz, DMSO-*d6*, 298 K): 4.27 (2H, s, CH_2), 3.61 (2H, s, CH_2), 2.18 (3H, s, CH_3). ^{13}C NMR (DEPTQ-135, 75 MHz, DMSO-*d6*, 298 K): 201.38 (q, C=O), 167.14 (q, COO), 62.36 (s, CH_2), 49.42 (s, CH_2), 29.97 (p, CH_3). ESI-MS*: m/z* = 53.067 (M^{Na+}, 100%). Hexane-1,6-diyl bis(3-oxobutanoate) (HexAcAc): The synthetic route follows the same conditions for the acetoacetylation as the synthesis of GlyAcAc. Yield = 99%. ^{1}H NMR (300 MHz, DMSO-*d6*, 298 K): 4.05 (2H, s, CH_2), 3.58 (2H, s, CH_2), 2.17 (3H, s, CH_3), 1.64−1.48 (2H, m, CH_2), 1.36−1.26 (2H, m, CH_2). ^{13}C NMR (75 MHz, DMSO-*d6*, 298 K): 201.55 (q, C=O), 167.29 (q, COO), 64.33 (s,

CH$_2$), 49.56 (s, CH$_2$), 30.02 (p, CH$_3$), 28.01 (s, CH$_2$), 24.88 (s, CH$_2$). ESI-MS: m/z = 309.113 (M^{Na+}, 100%), 287.148 (M$^+$, 1.22%). Acetoacetylated corn starch (CsAcAc): Corn starch (15.00 g, 0.093 mol) and the purified TMDO (31.55 g, 0.222 mol) were mixed in a 250 mL flask until a homogeneous dispersion was obtained. The mixture was heated at 135 °C for 45 min, while the byproduct acetone was removed by distillation during the reaction. The brownish residue was decanted and washed 5 times with 200 mL ethanol until a colorless dispersion with white powder was obtained. The residue represented the desired product in a high degree of purity, appearing as a white powder. Alternatively, *tert*-butylacetoacetate (*t*-BuAcAc) can be used for the acetoacetylation instead of TMDO, but a higher temperature of 160 °C for 2 h is required for an equal conversion. The synthetic procedure works also for other types of starch. Acetoacetylated anhydrous glucose unit (CsAcAc): Yield = 76%. ^{1}H NMR (300 MHz, DMSO-*d6*, 298 K): 5.50 (OH-3), 5.40 (OH-2), 5.11 (H-1), 4.59 (OH-6), 3.80−3.2 (H-2,3,4,5,6) 3.62 (s, CH$_2$), 2.17 (p, CH$_3$). ^{13}C NMR (75 MHz, DMSO-*d6*, 298 K): 100.21 (C-1), 78.86 (C-4), 73.36 (C-3), 71.08 (C-2), 71.71 (C-5), 60.60 (C-6), 49.42 (s, CH$_2$), 30.11 (p, CH$_3$).

Table S6-T1: Equations to determine the swelling ratio, gel fraction and soluble fractions of the materials.

Swelling ratio (SR)	= (S$_{swollen}$(g)-S$_{dry\ before}$(g)/ S$_{dry\ before}$ (g))*100%
Gel fraction	=(S$_{dry\ after}$(g)/ S$_{dry\ before}$(g))*100%
Soluble fraction	=(S$_{sol}$(g)/ S$_{dry\ before}$(g))*100%

S = sample
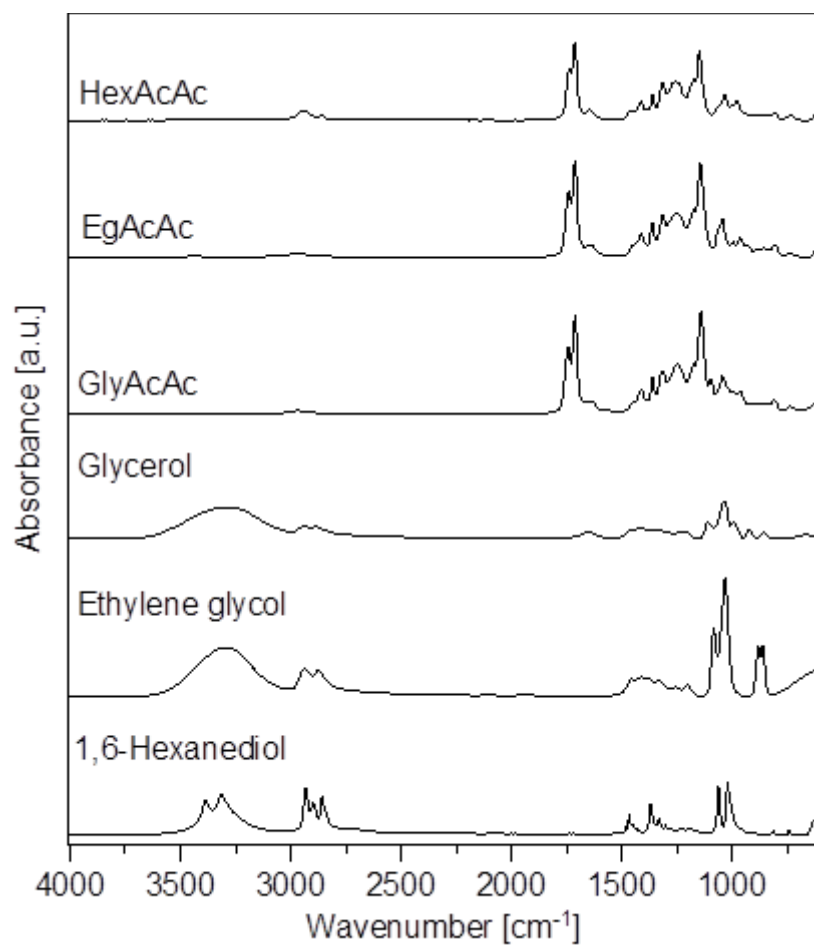
Figure S7-S1. ATR-FT-IR spectra of the acetoacetylated glycerol (GlyAcAc), ethylene glycol (EgAcAc), 1,6-hexanediol (HexAcAc) and the raw alcohols, showing the disappearance of the O-H band in the area of $3000-3600$ cm^{-1} and the characteristic acetoacetate bands (ester (1740 cm^{-1}), ketone (1711 cm^{-1})).
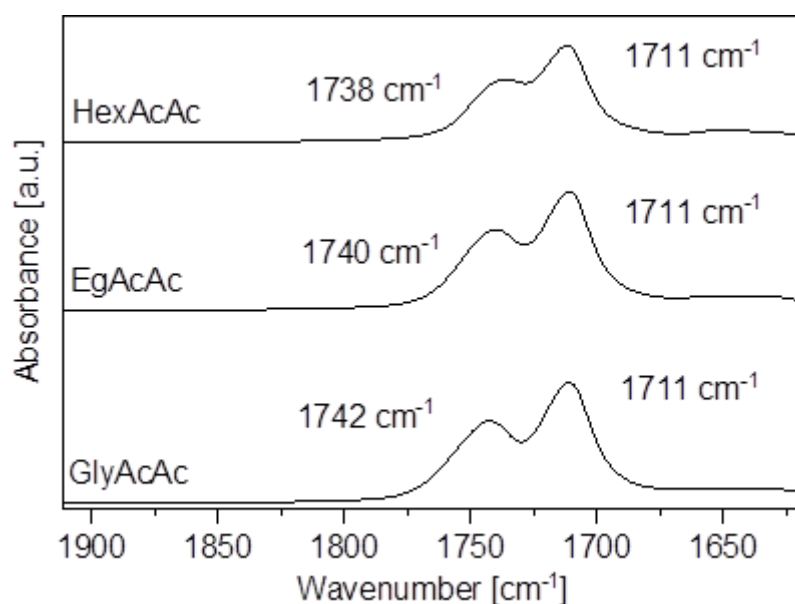
Figure S7-S2. Cutout ATR-FT-IR spectra of GlyAcAc, EgAcAc and HexAcAc, showing the characteristic acetoacetate bands of the ester (1738–1742 cm^{-1}) and ketone bands (1711 cm^{-1}).
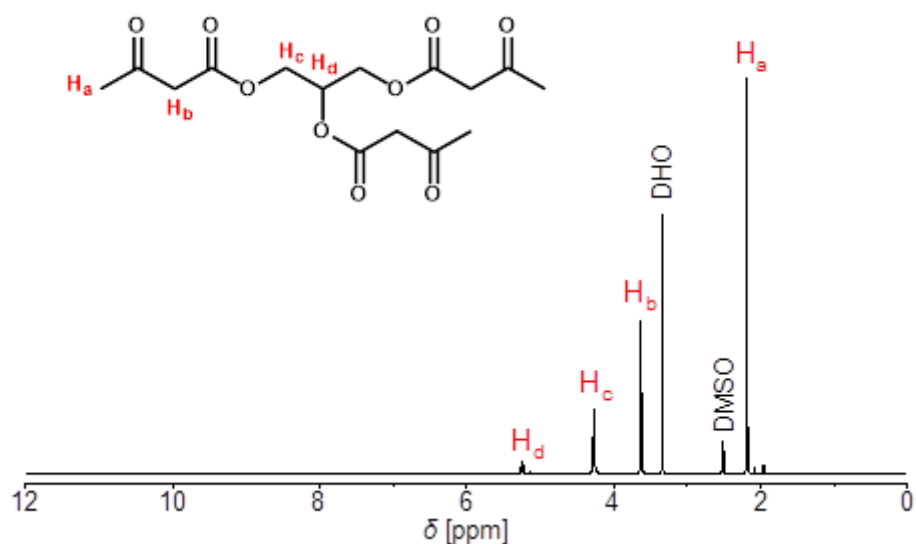
Figure S8-S1. ¹H NMR spectrum of the acetoacetylated glycerol monomer GlyAcAc, showing the characteristic signals and intensities. ¹H NMR (300 MHz, DMSO-*d6*, 298 K): 5.23 (1H, m, CH), 4.26 (2H, s, CH₂), 4.24 (2H, s, CH₂), 3.63 (2H, s, CH₂), 3.61 (2H, s, CH₂), 2.17 (3H, s, CH₃).
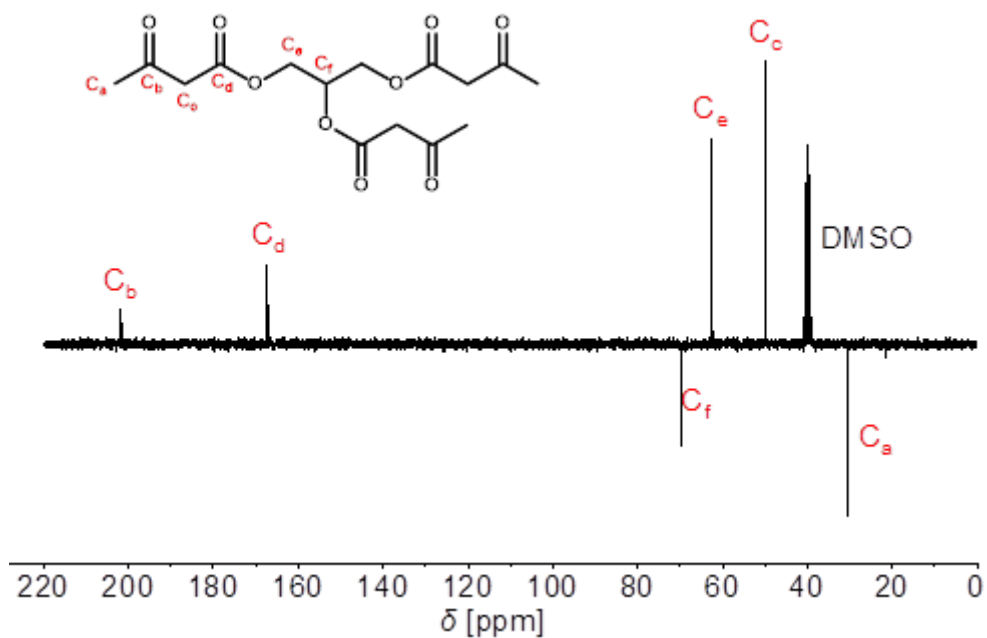
Figure S8-S2. ¹³C NMR DEPTQ-135 spectrum of the acetoacetylated glycerol monomer GlyAcAc, showing the characteristic signals and intensities. ¹³C NMR (75 MHz, DMSO-d6, 298K): 201.32 (q, C=O), 201.10 (q, C=O), 166.92 (q, COO), 166.62 (q, COO), 69.22 (t, CH), 62.20 (s, CH₂), 49.44 (s, CH₂), 49.30 (s, CH₂), 30.03 (p, CH₃), 29.95 (p, CH₃).
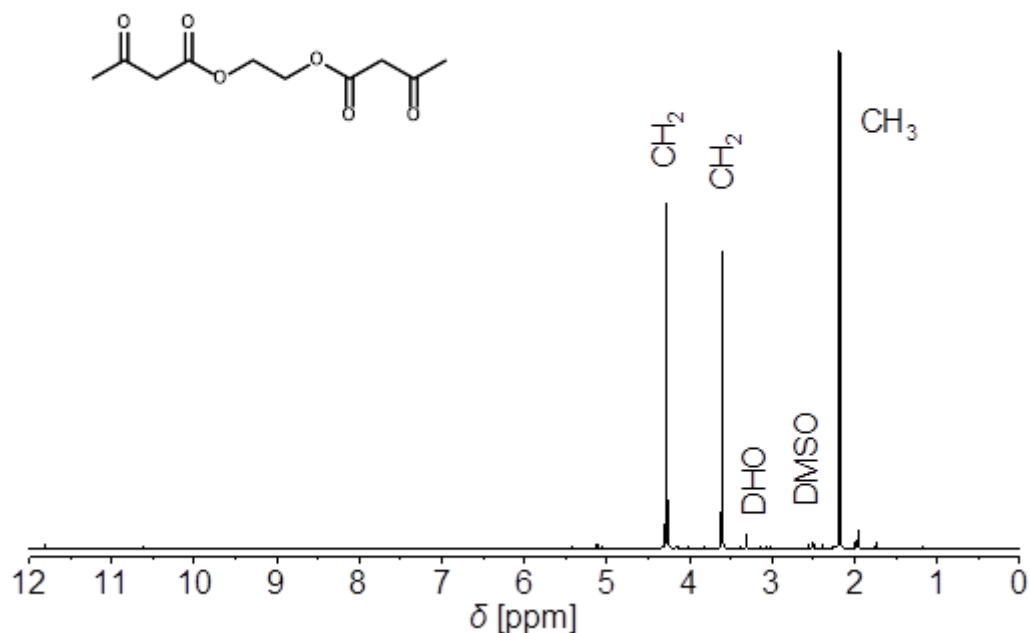
Figure S9-S1. ^{1}H NMR spectrum of the acetoacetylated ethylene glycol monomer EgAcAc, showing the characteristic signals and intensities. ^{1}H NMR (300 MHz, DMSO-*d6*, 298 K): 4.27 (2H, s, CH$_2$), 3.61 (2H, s, CH$_2$), 2.18 (3H, s, CH$_3$).
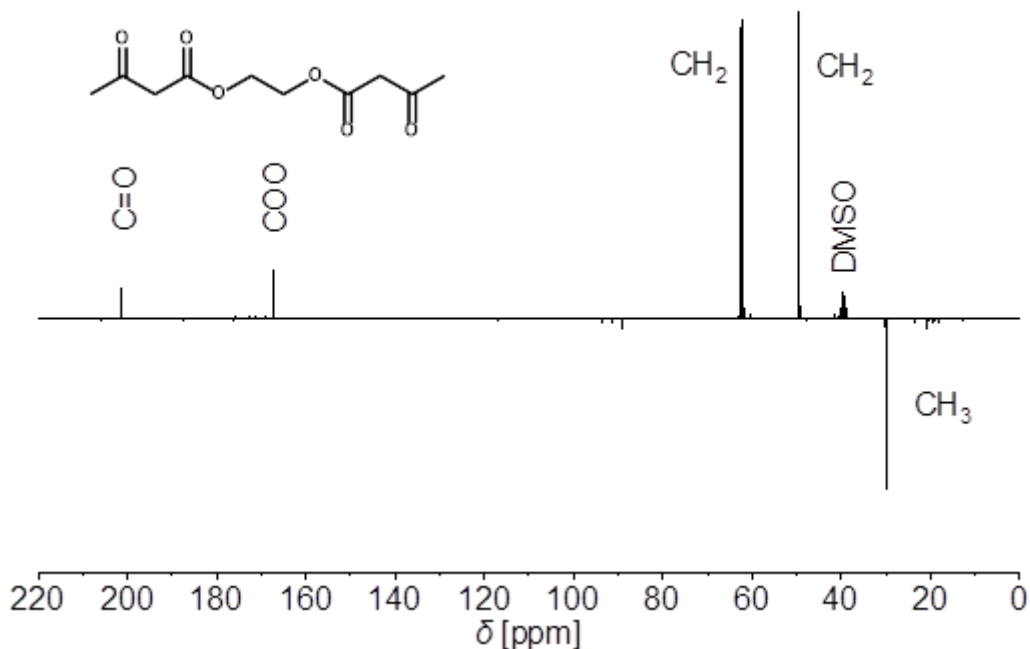
Figure S9-S2. ^{13}C NMR DEPTQ-135 spectrum of the acetoacetylated ethylene glycol monomer EgAcAc, showing the characteristic signals and intensities. ^{13}C NMR (75 MHz, DMSO-*d6*, 298 K): 201.38 (q, C=O), 167.14 (q, COO), 62.36 (s, CH$_2$), 49.42 (s, CH$_2$), 29.97 (p, CH$_3$).
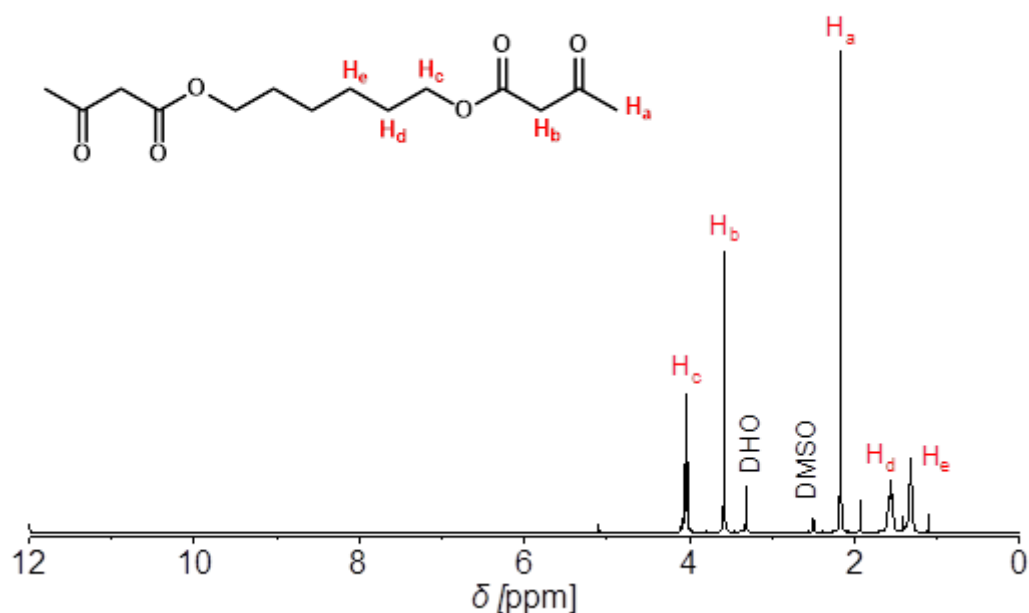
Figure S10-S1. ^{1}H NMR spectrum of the acetoacetylated 1,6-hexanediol monomer HexAcAc, showing the characteristic signals and intensities. ^{1}H NMR (300 MHz, DMSO-*d6*, 298 K): 4.05 (2H, s, CH$_2$), 3.58 (2H, s, CH$_2$), 2.17 (3H, s, CH$_3$), 1.64−1.48 (2H, m, CH$_2$), 1.36−1.26 (2H, m, CH$_2$).
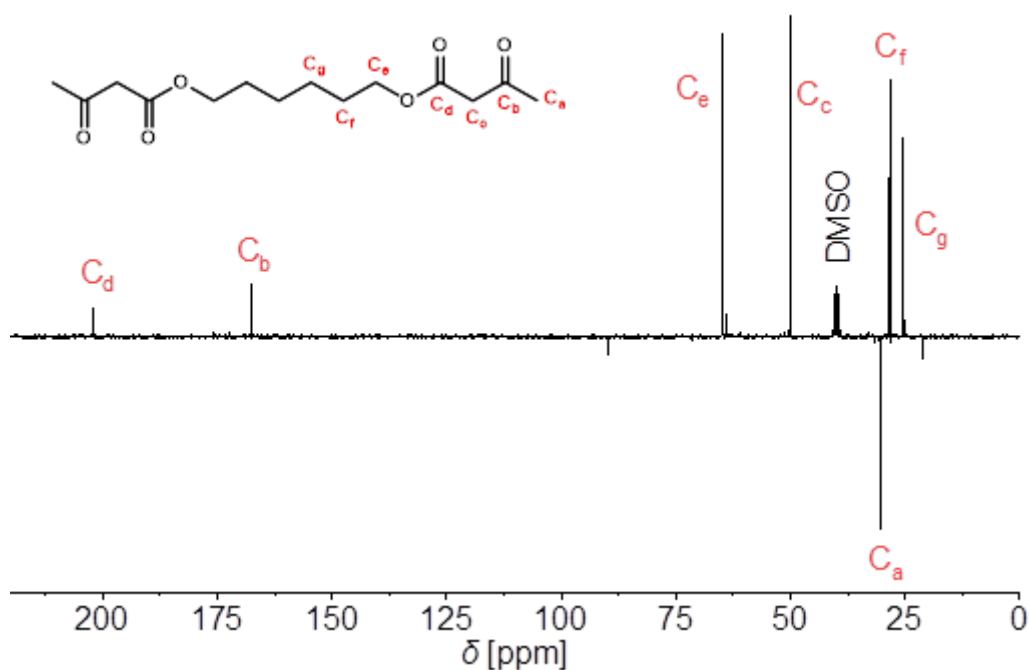
Figure S10-S2. ^{13}C NMR DEPTQ-135 spectrum of the acetoacetylated 1,6-hexanediol monomer HexAcAc, showing the characteristic signals and intensities. ^{13}C NMR (75 MHz, DMSO-*d6*, 298K): 201.55 (q, C=O), 167.29 (q, COO), 64.33 (s, CH$_2$), 49.56 (s, CH$_2$), 30.02 (p, CH$_3$), 28.01 (s, CH$_2$), 24.88 (s, CH$_2$).
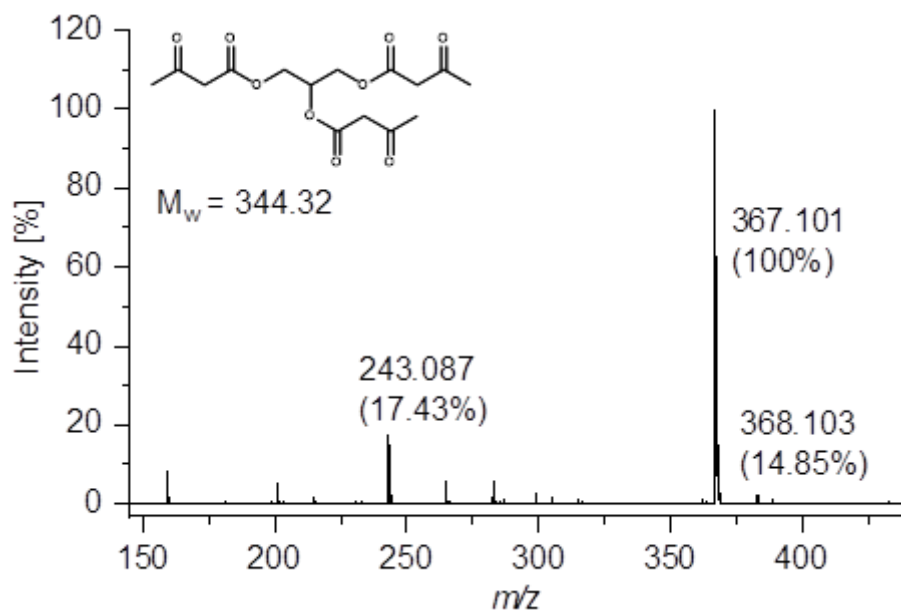
Figure S11-S1. ESI-MS (+) spectrum showing the characteristic peak of M^{Na+} with *m/z* = 367.101.
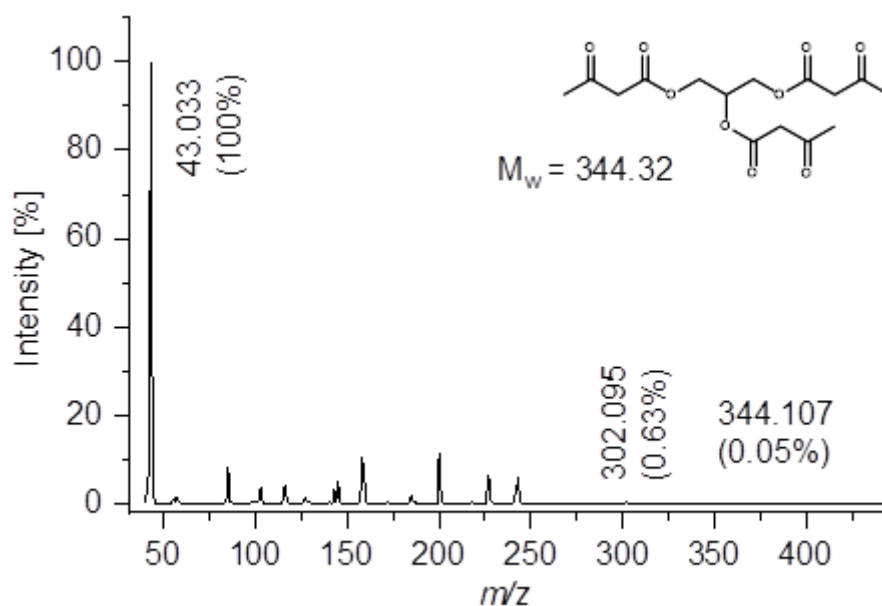
Figure S11-S2. EI-MS spectrum showing the molecule-ion peak of *m/z* = 344.107 (GlyAcAc) and the characteristic fragmentation of the ketone group ([CH_3-C=O], *m/z* = 43).
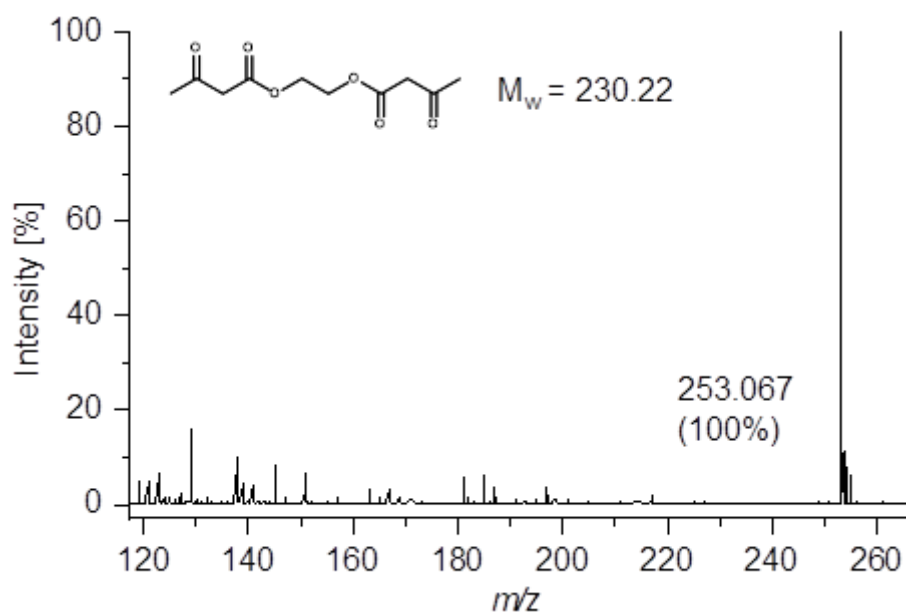
Figure S12-S1. ESI-MS (+) spectrum showing the characteristic peak of M^{Na+} with m/z = 253.067 (GlyAcAc).
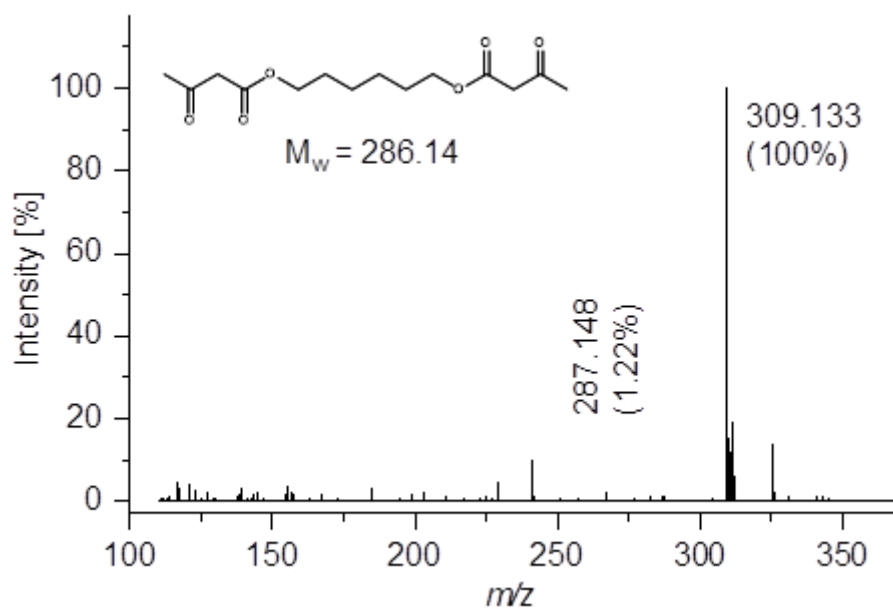
Figure S12-S2. ESI-MS (+) spectrum showing the characteristic peak of M^{Na+} with m/z = 309.133.
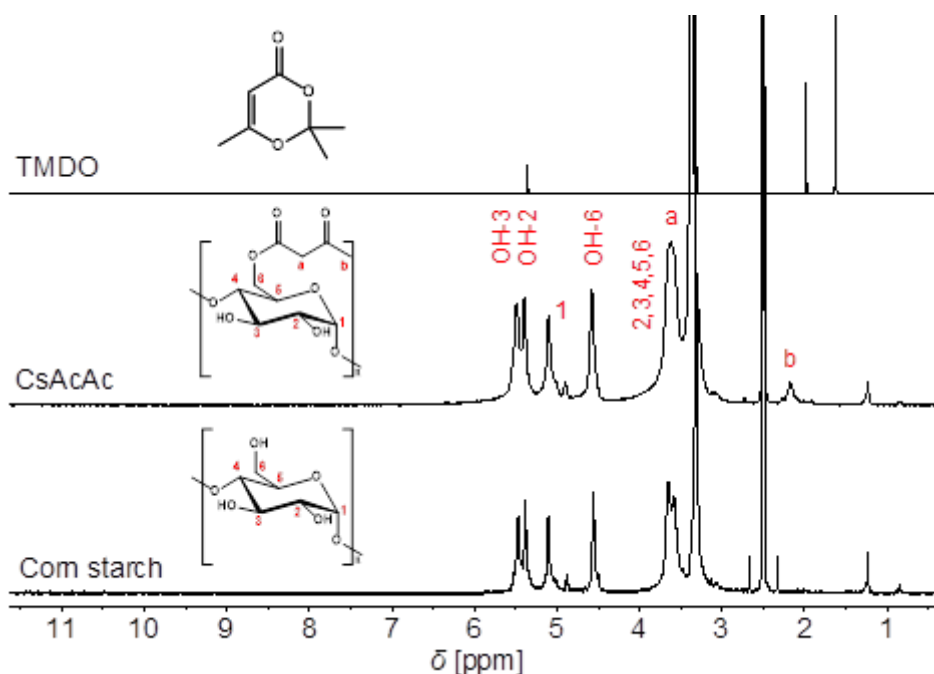
Figure S13-S1. ^{1}H NMR spectra of the acetoacetylated starch monomer (CsAcAc), showing the characteristic signals and intensities at 2.17 ppm (CH$_3$) and 3.62 ppm (CH$_2$) in comparison to raw corn starch and the reactant TMDO. CsAcAc: ^{1}H NMR (300 MHz, DMSO-*d6*, 298 K): 5.50 (OH-3), 5.40 (OH-2), 5.11 (H-1), 4.59 (OH-6), 3.80 - 3.2 (H-2,3,4,5,6), 3.62 (2H, s, CH$_2$), 2.17 (3H, s, CH$_3$). AGU (corn starch): ^{1}H NMR (300 MHz, DMSO-*d6*, 298 K): 5.50 (OH-3), 5.40 (OH-2), 5.11 (H-1), 4.59 (OH-6), 3.80 - 3.2 (H-2,3,4,5,6). TMDO: ^{1}H NMR (300 MHz, DMSO-*d6*, 298K): 5.36 (1H, s, CH$_2$), 1.97 (3H, s, CH$_3$), 1.63 (6H, s, CH$_3$).
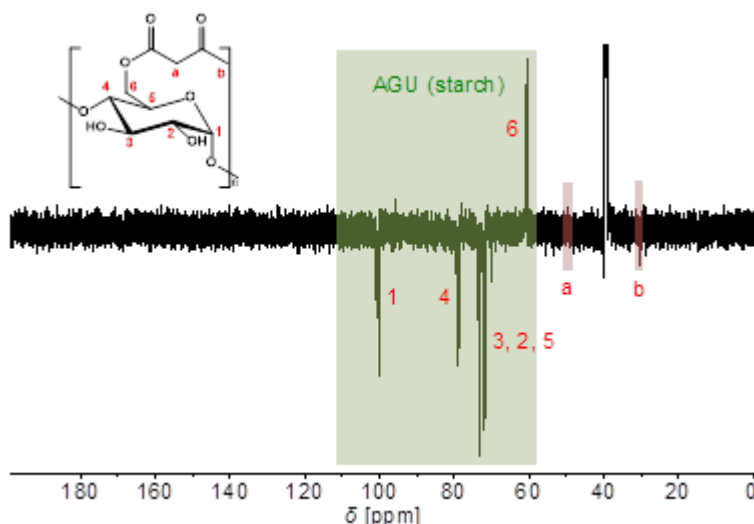
Figure S13-S2. ^{13}C-NMR DEPTQ-135 spectrum of CsAcAc, showing the characteristic CH$_3$ and CH$_2$ signals of the acetoacetate group. Due to the low concentration of the acetoacetate group, the signal-to-noise ratio is bad. ^{13}C NMR (75 MHz, DMSO-*d6*, 298 K): 100.21 (C-1), 78.86 (C-4), 73.36 (C-3), 71.08 (C-2), 71.71 (C-5), 60.60 (C-6), 49.42 (s, CH$_2$), 30.11 (p, CH$_3$). Marked in green, the typical ^{13}C signals of the AGU of corn starch.

Table S14-T1. Results of elementary analysis (NCHS) in comparison of pure corn starch, corn starch treated with isobutylamine and CsAcAc treated with isobutylamine.

Sample	N wt%	C wt%	H wt%	S wt%
Corn starch	0.15	44.43	6.71	0.00
Corn starch	0.17	44.63	6.79	0.00
Corn starch + Isobutylamine	0.12	44.26	6.61	0.00
Corn starch + Isobutylamine	0.13	44.51	6.62	0.00
CsAcAc + Isobutylamine	0.56	45.03	6.61	0.00
CsAcAc + Isobutylamine	0.57	44.62	6.66	0.00
CsAcAc + Isobutylamine	0.58	44.83	6.71	0.00
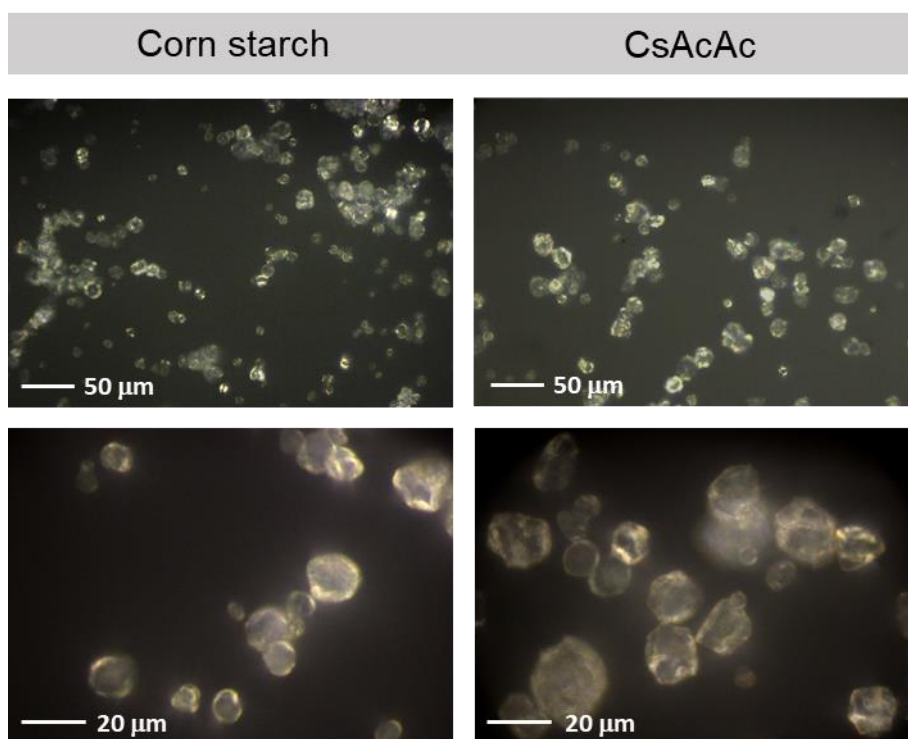
Figure S14-S1. Optical microscope (OM) images of the raw corn starch and the modified corn starch CsAcAc, showing polyhedron-shaped granules with a diameter of 5–20 μm without any significant difference of the granules.
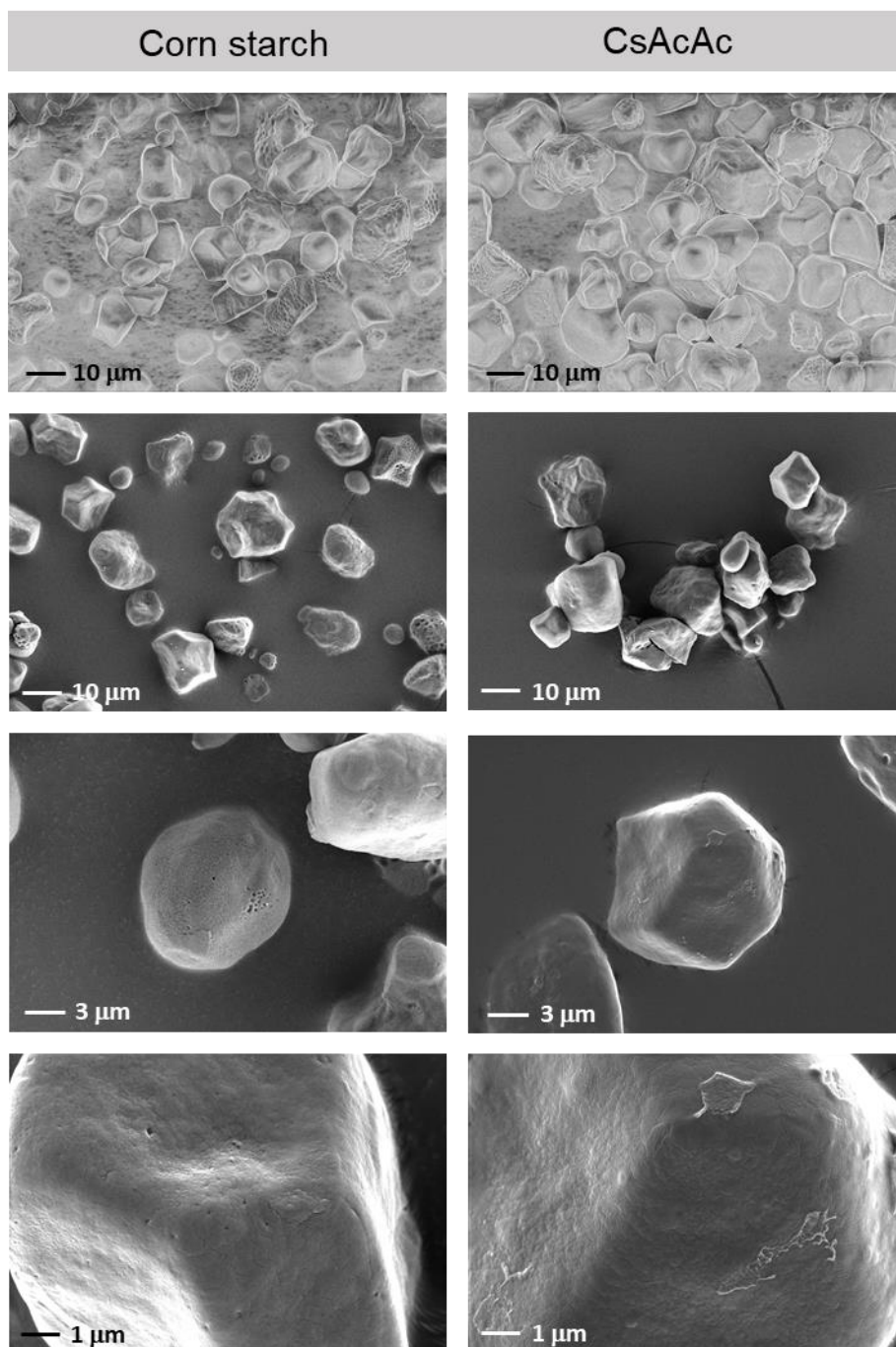
Figure S15-S1. SEM images of the raw corn starch and CsAcAc, showing polyhedron-shaped granules with a diameter of 5–20 µm with a magnification of 1–10 µm and no significant difference before and after the modification.
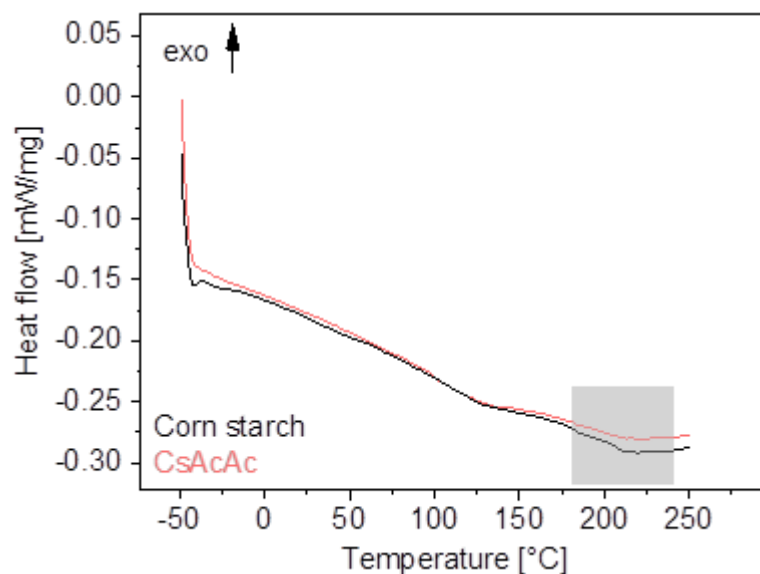
Figure S16-S1. DSC measurements showed no significant difference in comparison of the pure corn starch and CsAcAc. Since the measurements were carried out with dried samples, the melting points were identified at temperatures above 200 °C, indicating the low amount of water according to literature.[2]
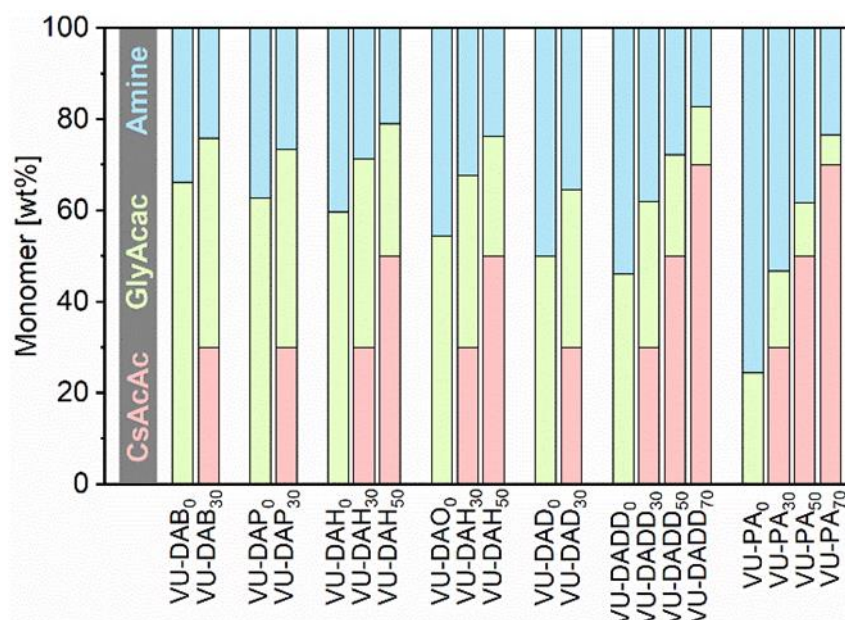
Figure S16-S2. Acronyms and monomer ratios (wt%) of the fabricated material compositions, pointing out that with increasing chain length of the diamine and constant R value, the monomer ratios shift notably. The materials were labelled as VU-Amine$_{wt\%CsAcAc}$ (*e.g.,* VU-DAO$_{30}$).

It was found that vitrimers with relatively long alkyl chains of the diamine (VU-DADD, VU-PA) and low cross-linking density allow the synthesis of vitrimer composites with a high share of CsAcAc up to 70 wt%. Regarding VU-DAB, VU-DAH, VU-DAO, and VU-DAD the highest amount was 30–50 wt%, since reprocessing did not work sufficiently well and led to brittle and cracked materials without efficient reprocessing during heat compression. The acetoacetate (GlyAcAc) to amine ratio was set to R = 0.75 for 0 wt% CsAcAc, R = 0.73 for 30 wt%, R = 0.7 for 50 wt% and R = 0.65 for 70 wt%.
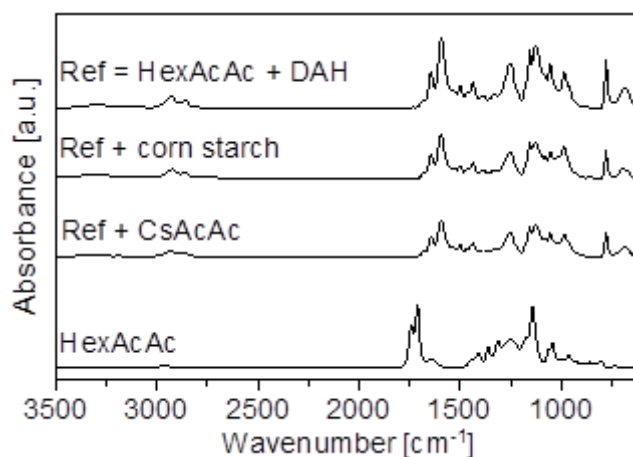
Figure S17-S1. Full ATR-FT-IR spectra of the acetoacetylated HexAcAc before and after the conversion with DAH, showing the disappearance of the characteristic acetoacetate bands of the ester (1740 cm^{-1}) and ketone stretching vibrations (1711 cm^{-1}) as well as the formation of the conjugated C=C (1593 cm^{-1}) and C=O ester (1644 cm^{-1}) stretching vibrations bands of the vinylogous urethane.
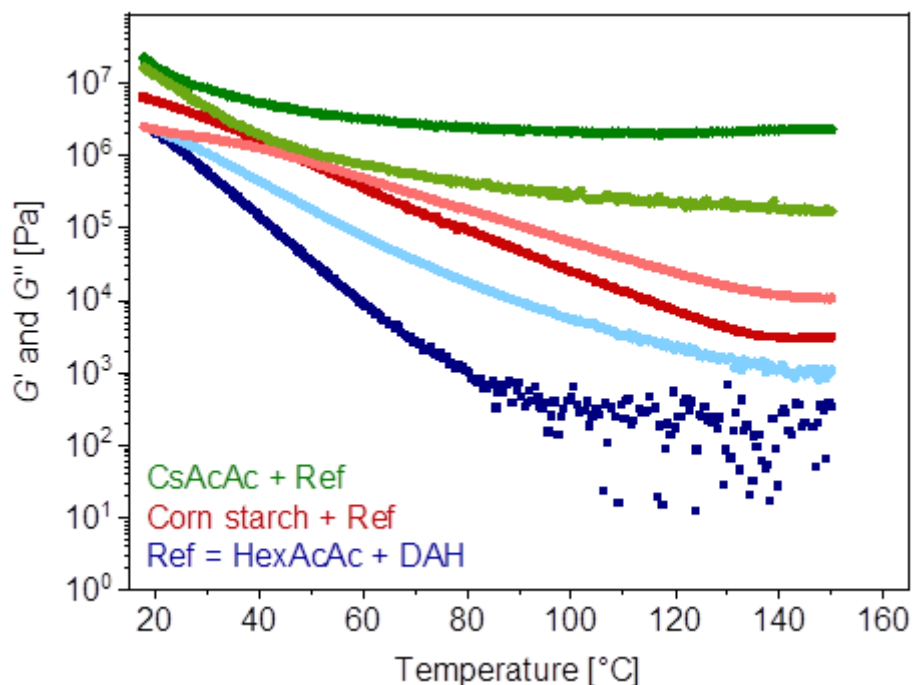
Figure S17-S2. Temperature-dependent DMA measurement of the linear, thermoplastic polymer synthesized by HexAcAc and DAH (G' = dark blue, G" = light blue), a composite synthesized by the linear polymer and 50 wt% of native corn starch (G' = dark red, G" = light red) and the cross-linked polymer synthesized by the linear polymer and 50 wt% CsAcAc (G' = dark green, G" = light green).

S17
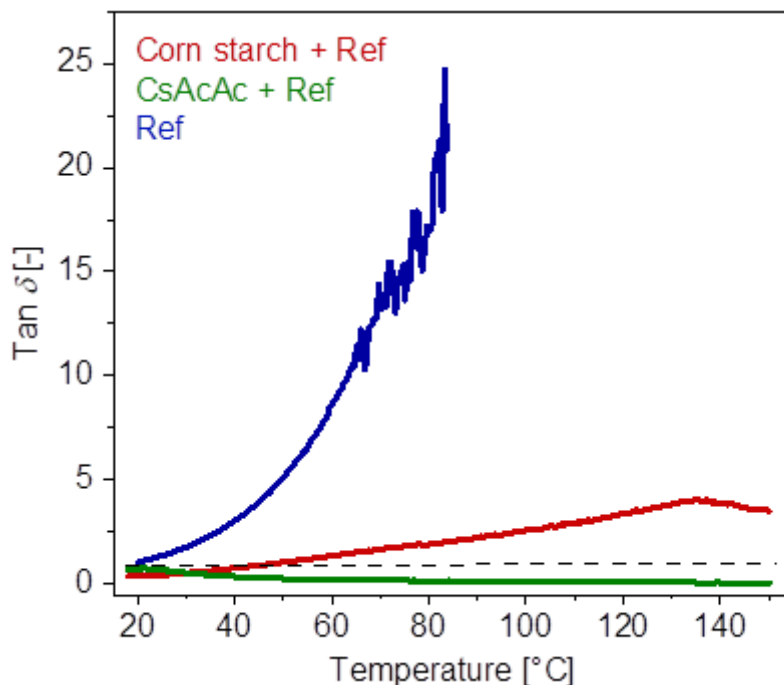
Figure S18-S1. Temperature-dependent DMA measurement (tan δ) of a composite synthesized by the linear polymer and 50 wt% of native corn starch (red), the cross-linked polymer synthesized by the linear polymer and 50 wt% CsAcAc (green) and only the linear reference vitrimer (blue). The device had problems to measure the storage modulus of the linear reference at high temperatures. Therefore, the loss modulus is only shown up to temperatures of 85 °C.
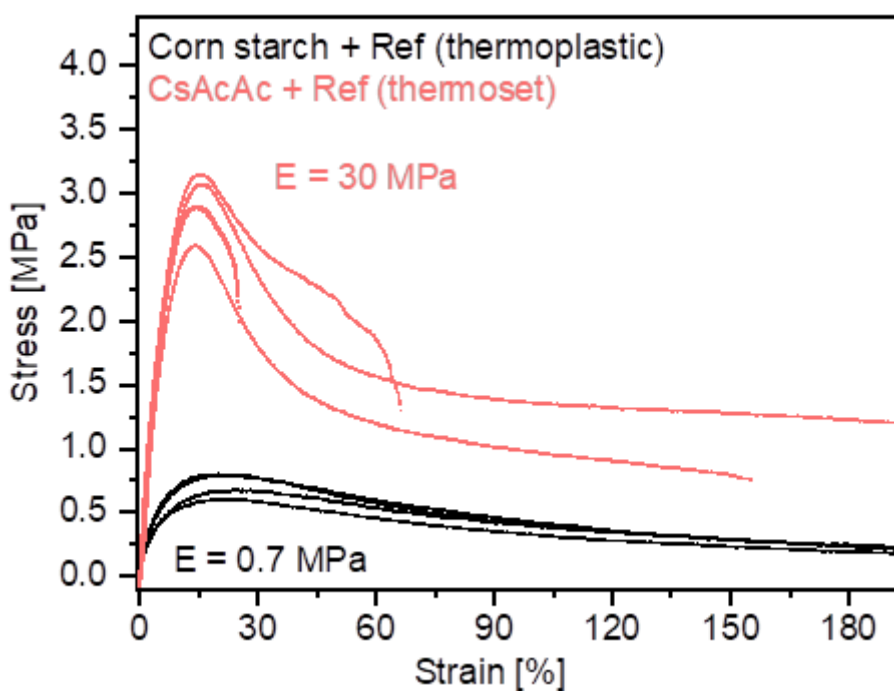
Figure S18-S2. Comparing the measured stress-strain curves of the thermoplastic composite material synthesized by natural corn starch and the thermosetting composite synthesized with the modified corn starch CsAcAc.
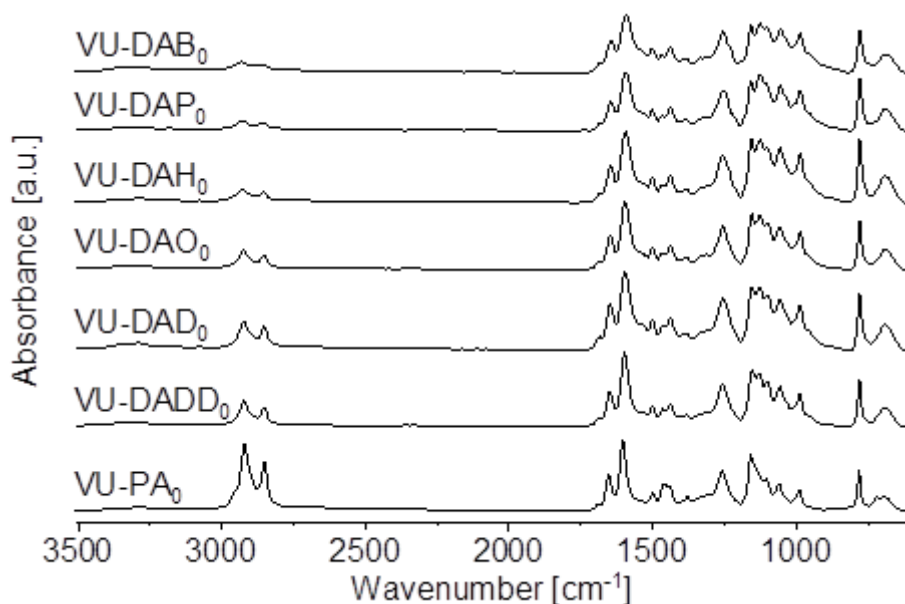
Figure S19-S1. ATR-FT-IR spectra show the characteristic C=C (1592–1604 cm^{-1}) and C=O ester (1644–1654 cm^{-1}) bands of the vinylogous urethane bonds, comparing the seven matrix vitrimers synthesized by GlyAcAc and different diamines.
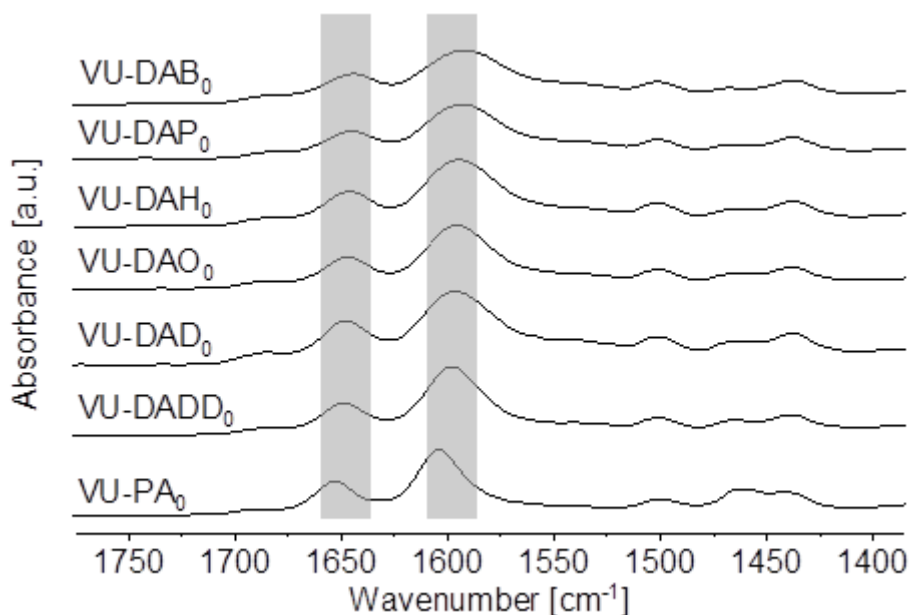
Figure S19-S2. Close up ATR-FT-IR spectra show the characteristic C=C (1592–1604 cm^{-1}) and C=O ester (1644–1654 cm^{-1}) bands of the vinylogous urethane bonds, showing a declining wavenumber with increasing length of the alkyl chain of the diamine.
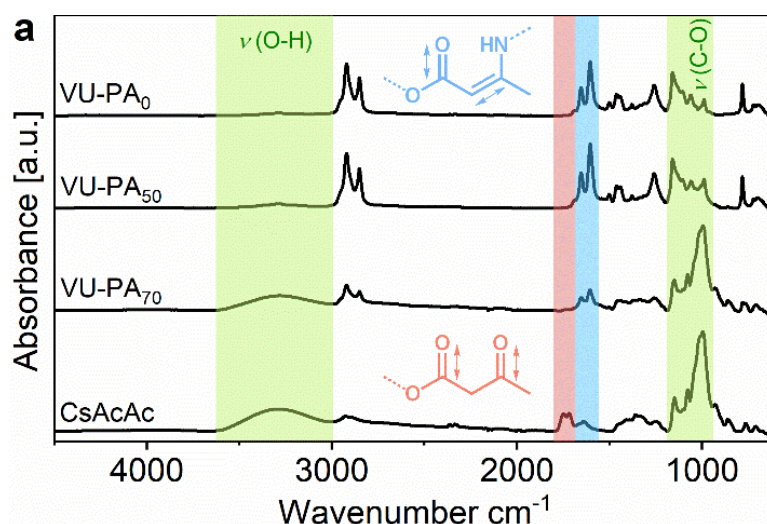
Figure S20-S1 ATR-FT-IR spectra show the disappearance of the C=O ester and C=O ketone stretching vibrations bands of the acetoacetate monomer CsAcAc (red), the formation of the characteristic C=C (1598 cm^{-1}) and C=O ester bands (1650 cm^{-1}) of the vinylogous urethane bonds (blue). Furthermore, the characteristic O-H (3000–3600 cm^{-1}) and C-O stretching vibrations of the AGU (995 cm^{-1}, 1078 cm$^{-1,}$ and 1148 cm^{-1}) are pronounced with a rising amount of CsAcAc in the materials VU-PA$_0$, VU-PA$_{50}$ and VU-PA$_{70}$ (green).
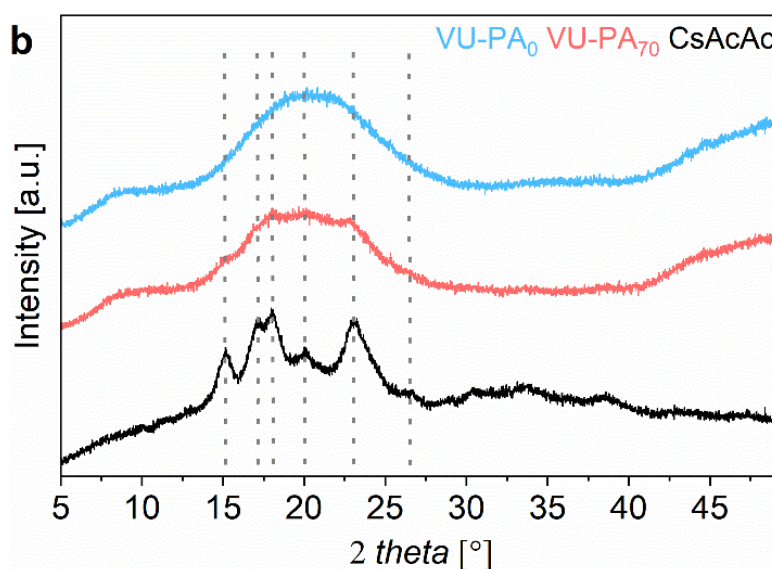
Figure S20-S2 ATR-FT-IR spectra show the disappearance of the C=O ester and C=O ketone stretching vibrations bands of the acetoacetate monomer CsAcAc (red), the formation of the characteristic C=C (1598 cm^{-1}) and C=O ester bands (1650 cm^{-1}) of the vinylogous urethane bonds (blue). Furthermore, the characteristic O-H (3000–3600 cm^{-1}) and C-O stretching vibrations of the AGU (995 cm^{-1}, 1078 cm$^{-1,}$ and 1148 cm^{-1}) are pronounced with a rising amount of CsAcAc in the materials VU-PA$_0$, VU-PA$_{50}$ and VU-PA$_{70}$ (green). XRD diffractograms of CsAcAc (black), the composite VU-PA$_{70}$ with CsAcAc embedded into a vitrimer matrix (red) and the amorphous matrix vitrimer VU-PA$_0$ without any starch (blue).
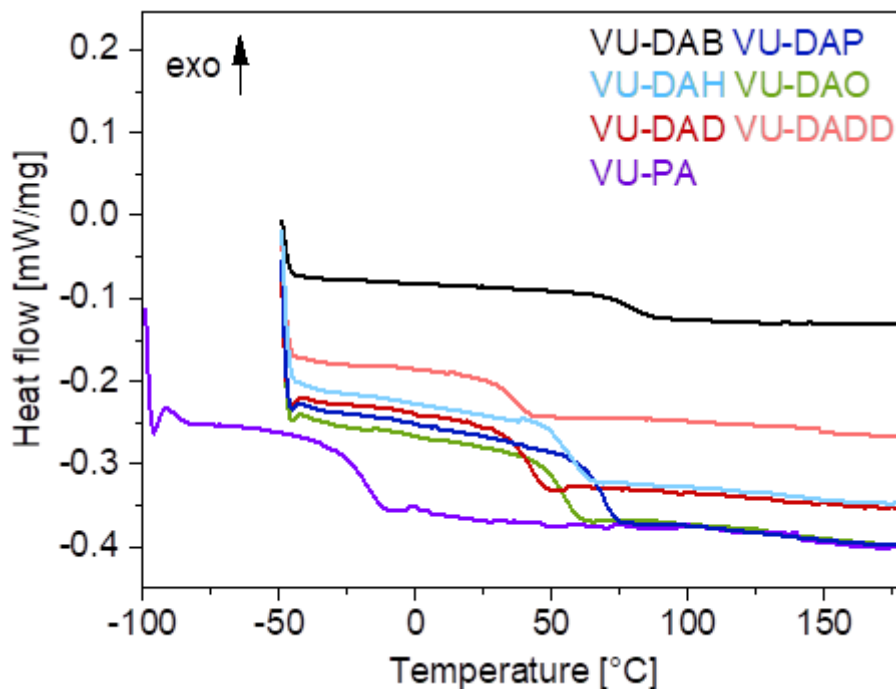
Figure S21-S1. DSC-heating curves of the seven matrix vitrimers. Glass transition temperatures of (-26)–70 °C (on-set) have been measured (VU-DAB: 71 °C, VU-DAP: 63 °C, VU-DAH: 54 °C, VU-DAO: 47 °C, VU-DAD: 36 °C, VU-DADD: 30 °C, VU-PA:(-26) °C).
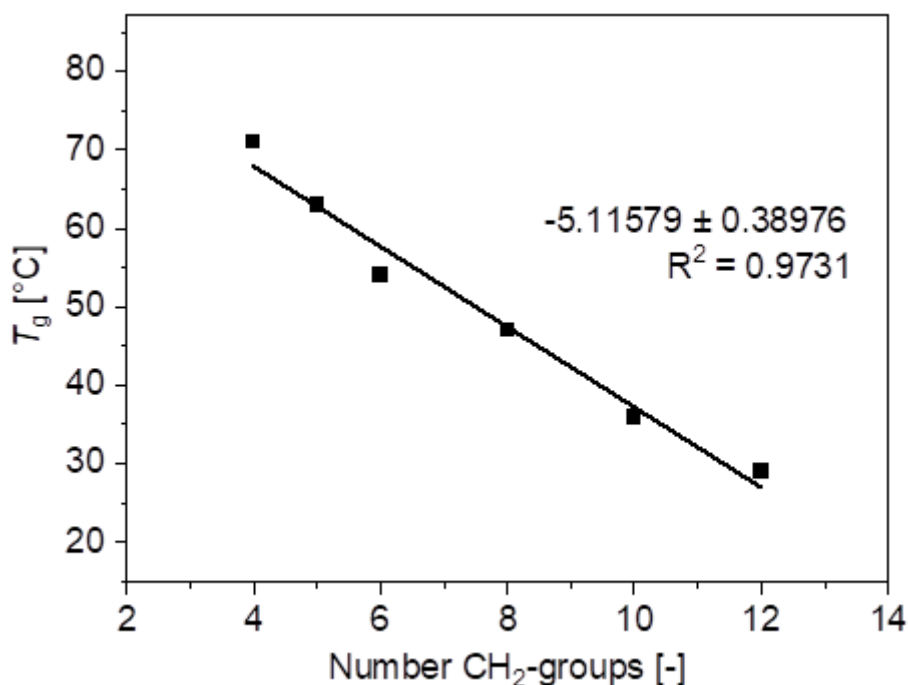
Figure S21-S2. The glass transition temperatures increase with a declining chain length of the diamine and show a linear dependency of CH_2-groups (molecular weight of the aliphatic diamines) and the corresponding T_g, with a calculated value of 5 °C per CH_2-group (slope). Consequently, VU-DAB$_0$ shows the highest T_g, while VU-PA$_0$ exhibits the lowest (VU-DAB$_0$: 71 °C, VU-DAP$_0$: 63 °C, VU-DAH$_0$: 54 °C, VU-DAO$_0$: 47 °C, VU-DAD$_0$: 36 °C, VU-DADD$_0$: 29 °C, VU-PA$_0$: (-26) °C).
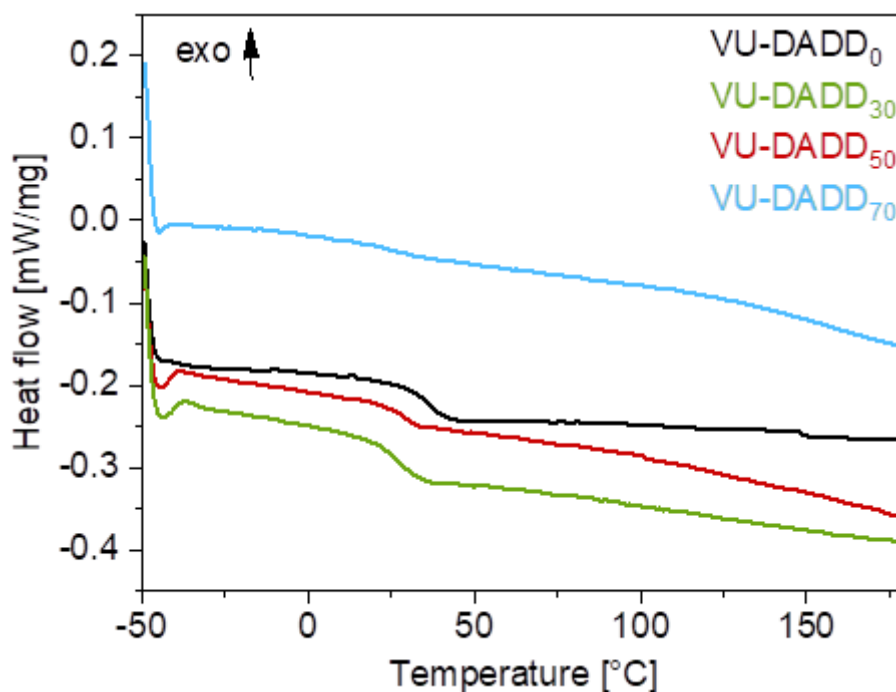
Figure S22-S1. DSC-heating curves of VU-DADD$_0$ with 30, 50 and 70 wt% of CsAcAc. Glass transition temperatures of 20–29 °C (on-set) have been measured.
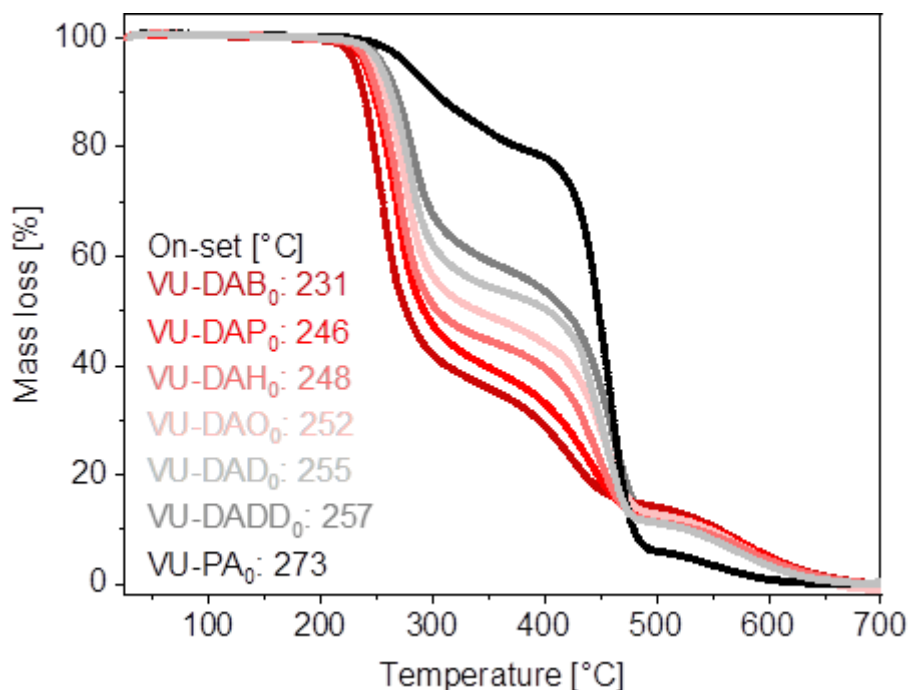
Figure S22-S2. Thermogravimetric analysis measurements of the seven matrix vitrimers carried out under ambient atmosphere. The thermal degradation temperatures were measured to 231–273 °C (on-set) and increase with a rising length of the alkyl chain of the diamine.
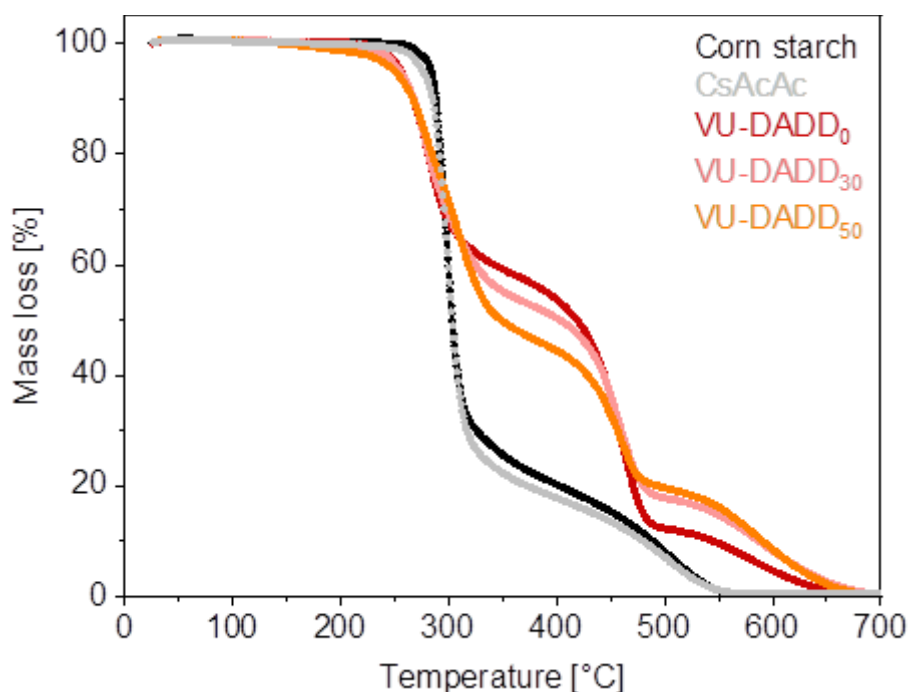
Figure S23-S1. TGA measurements of pure corn starch and CsAcAc, showing degradation temperatures of 287 °C and 290 °C (on-set) under ambient atmosphere. The thermal degradation temperatures of the composite materials were measured within the same range as the corresponding vitrimer matrix and are exemplified shown on the materials VU-DADD$_0$, VU-DADD$_{30}$ and VU-DADD$_{50}$ (250–255 °C (on-set)).
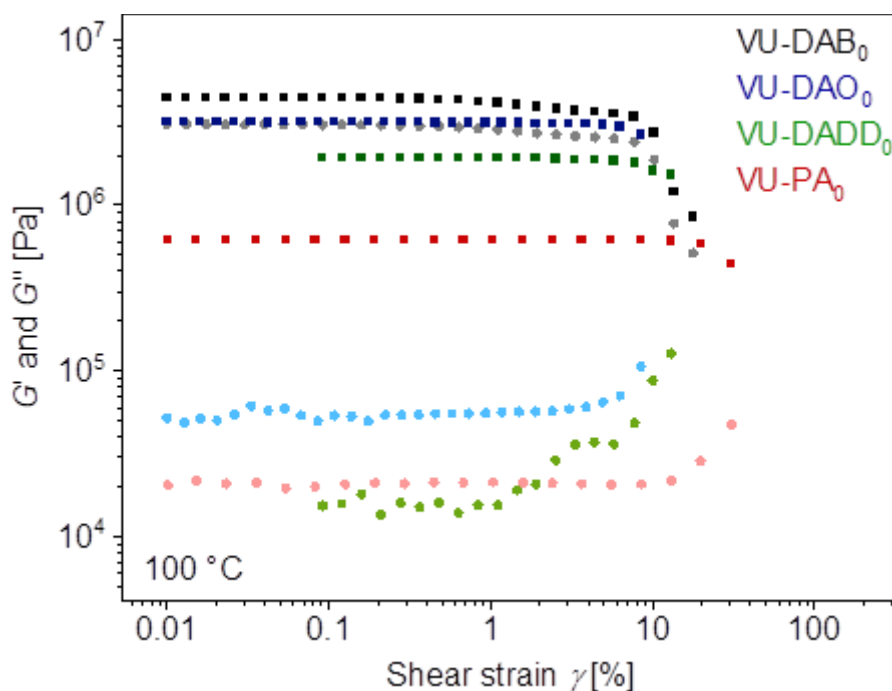
Figure S23-S2. Amplitude sweeps of the matrix vitrimers VU-DAB$_0$, VU-DAO$_0$, VU-DADD$_0$ and VU-PA$_0$, showing yield points of 1–20%, increasing with rising length of the alkyl chain of the diamine (100 °C, ω = 10 rad s^{-1}) (G' = dark color, G''= light color).

S23

Table S24-T1. Results of the swelling experiments in THF, determining the swelling ratio, gel content and soluble fraction of the materials.

Sample	Swelling ratio [%] THF	Gel content [%] THF	Sol. fraction [%] THF
VU-DAB$_0$	49	97.1	3.2
VU-DAB$_{30}$	16	96.3	3.4
VU-DAB$_{50}$	3	97.8	3.5
VU-DAP$_0$	79	96.8	3.2
VU-DAH$_0$	80	94.7	4.7
VU-DAO$_0$	94	97.2	4.1
VU-DAD$_0$	112	92.9	5.0
VU-DADD$_0$	148	91.9	5.5
VU-DADD$_{30}$	80	97.1	2.6
VU-DADD$_{50}$	55	93.6	4.2
VU-PA$_0$	325	84.0	15.0
VU-PA$_{30}$	122	93.2	4.9
VU-PA$_{50}$	43	95.3	1.5
VU-PA$_{70}$	42	92.9	2.8
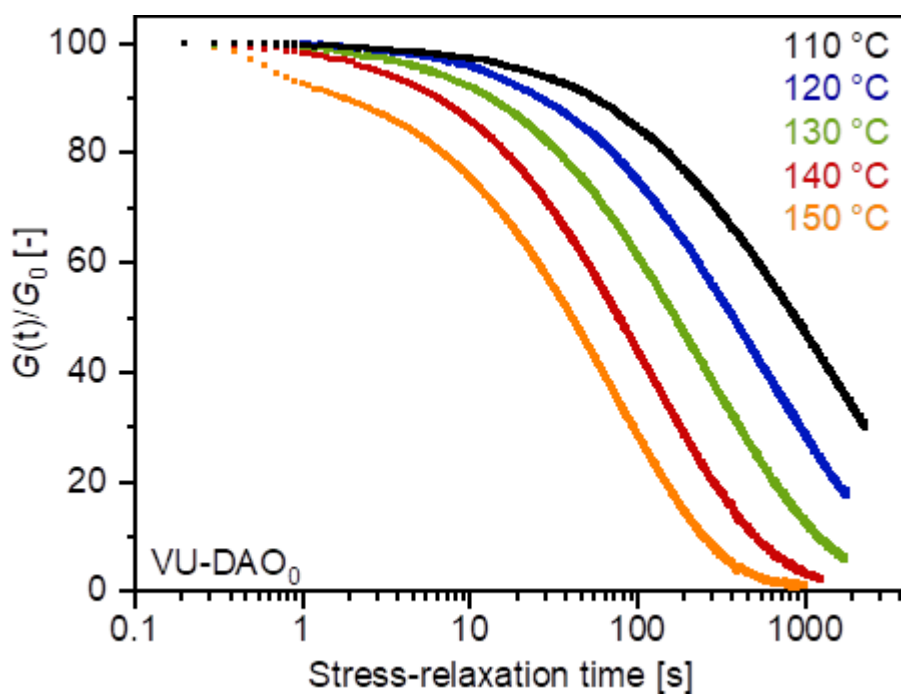
Figure S24-S1. Normalized stress relaxation measurements of the vitrimer VU-DAO$_0$ in the temperature range of 110–150 °C ($\gamma = 1\%$).
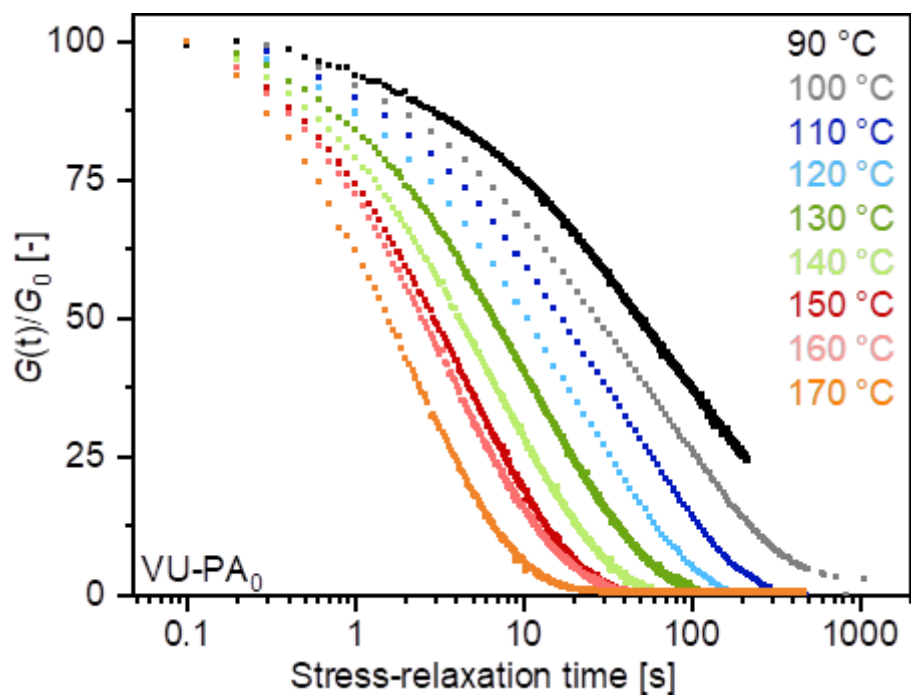
Figure S25-S1. Normalized stress relaxation measurements of the vitrimer VU-PA$_0$ in the temperature range of 90–170 °C (γ = 1%).
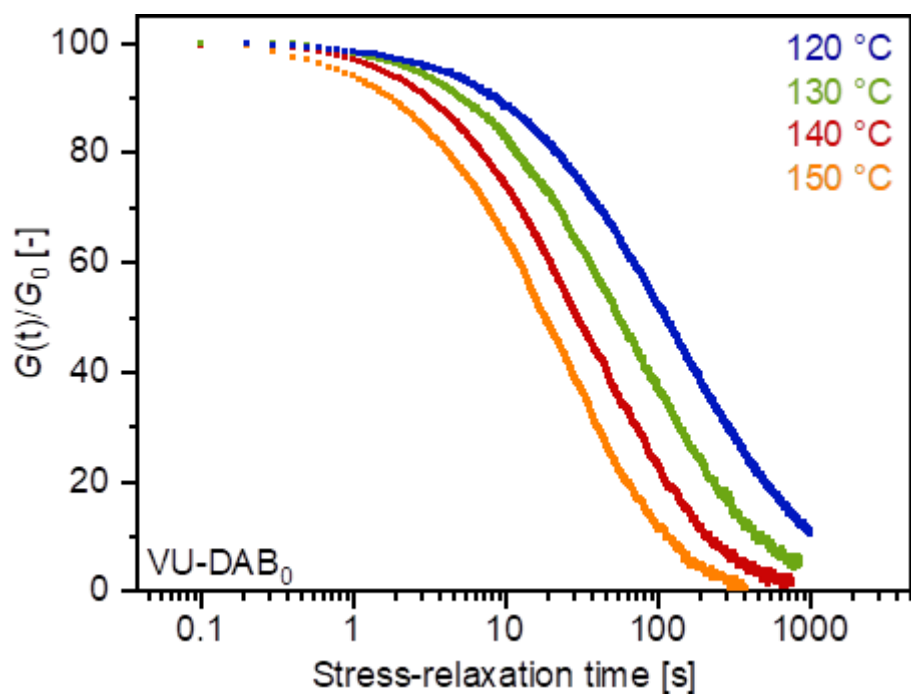
Figure S25-S2. Normalized stress relaxation measurements of the vitrimer VU-DAB$_0$ in the temperature range of 120–150 °C (γ = 1%).
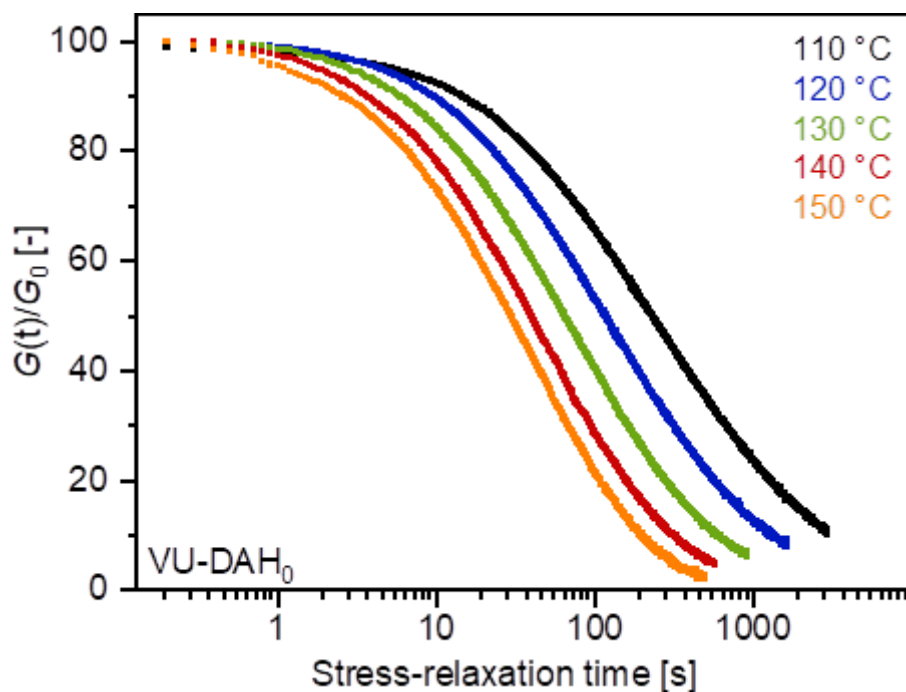
Figure S26-S1. Normalized stress relaxation measurements of the vitrimer VU-DAH$_0$ in the temperature range of 110–150 °C ($\gamma = 1\%$).
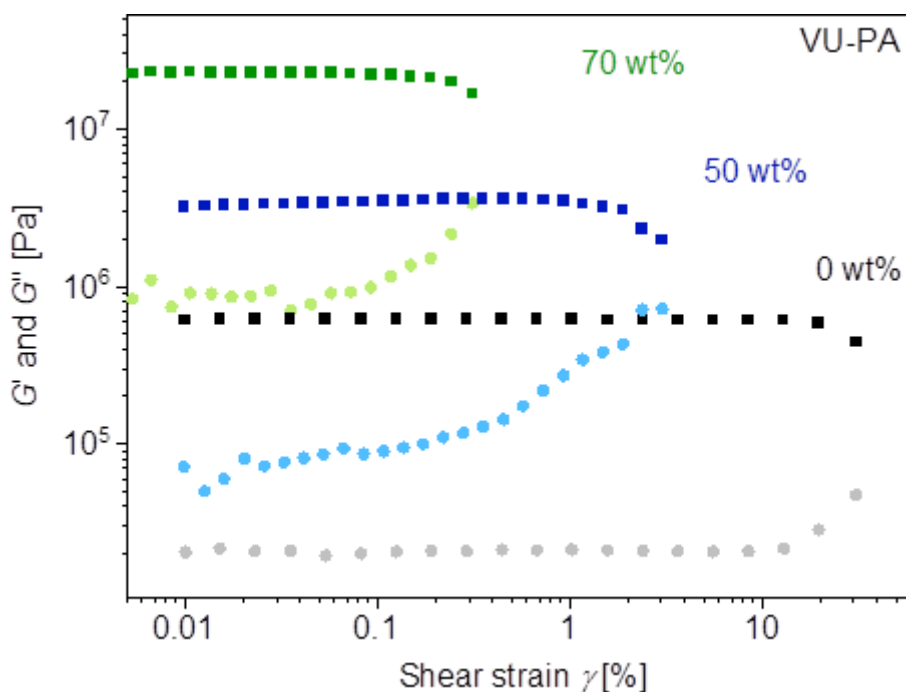
Figure S26-S2. Amplitude sweeps of VU-PA$_0$, VU-PA$_{50}$ and VU-PA$_{70}$, showing a massive shift of the yield point from $\gamma = 20\%$ to $\gamma = 1\%$ to $\gamma = 0.1\%$ shear strain. ($\omega = 10$ rad s^{-1}, 100 °C).
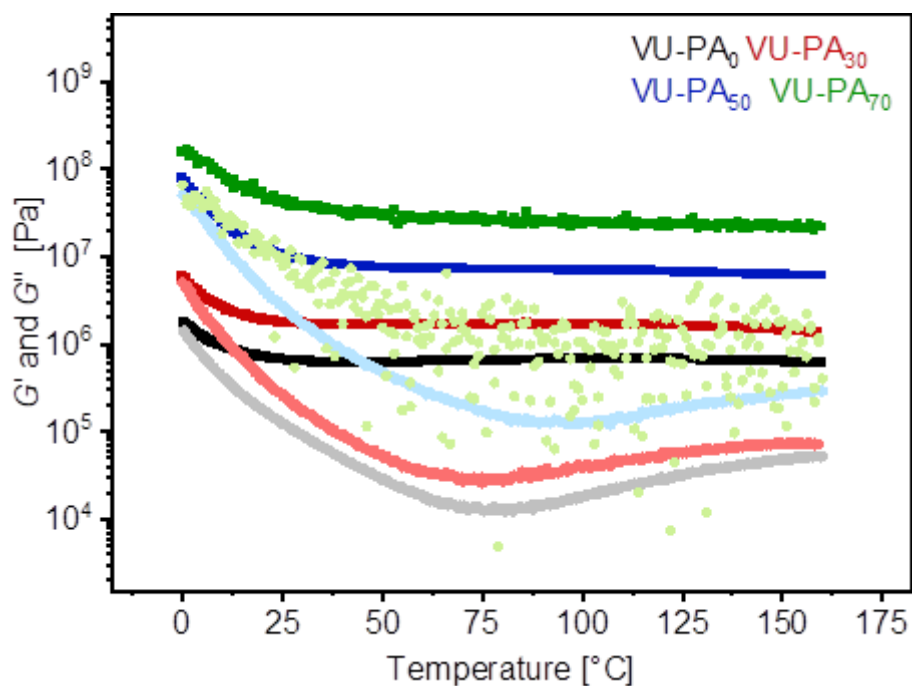
Figure S27-S1. Temperature-dependent DMA measurements of exemplary matrix and composite vitrimers VU-PA$_0$, VU-PA$_{30}$, VU-PA$_{50}$ and VU-PA$_{70}$ carried out at 0–160 °C ($\gamma = 0.1\%$, $\omega = 10$ rad s^{-1}), showing cross-linked materials (because of a low yield point VU-PA$_{70}$ was measured with a different shear strain $\gamma = 0.01\%$)
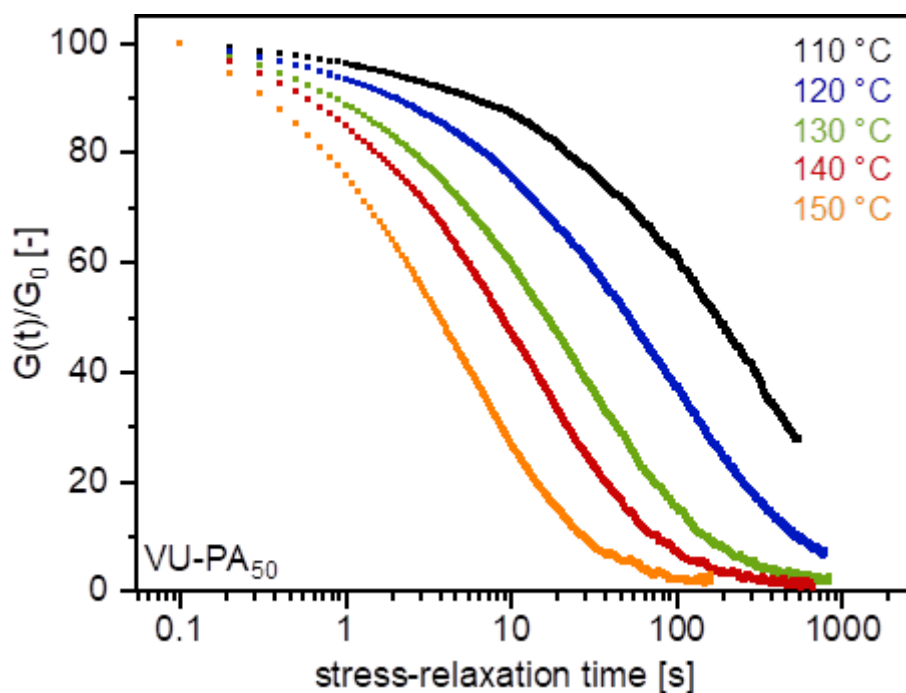
Figure S27-S2. Normalized stress relaxation measurements of the vitrimer VU-PA$_{50}$ in the temperature range of 110–150 °C ($\gamma = 1\%$).
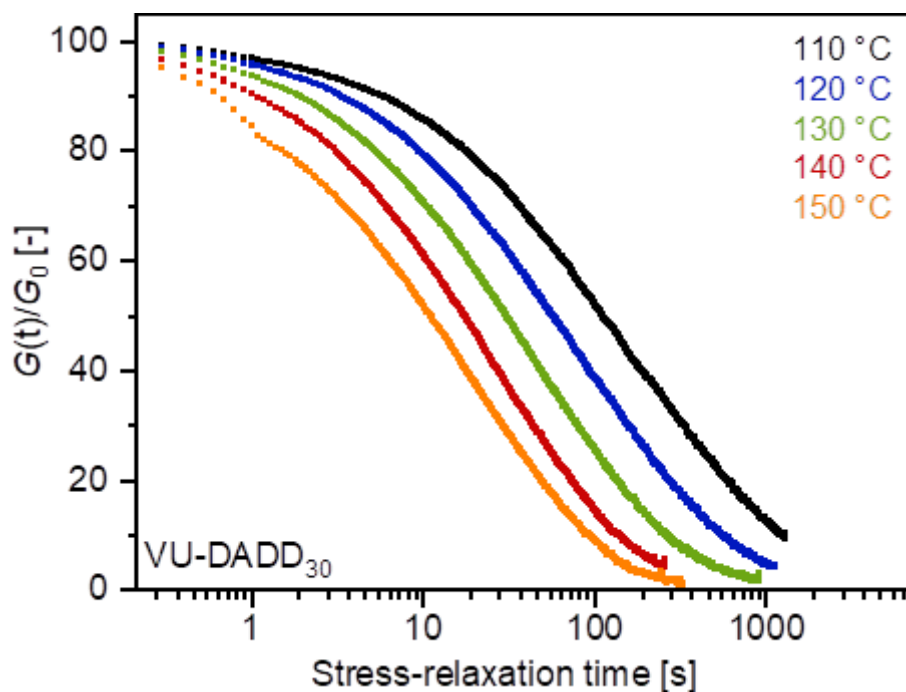
Figure S28-S1. Normalized stress relaxation measurements of the vitrimer VU-DADD$_{30}$ in the temperature range of 110–150 °C ($\gamma = 1\%$).
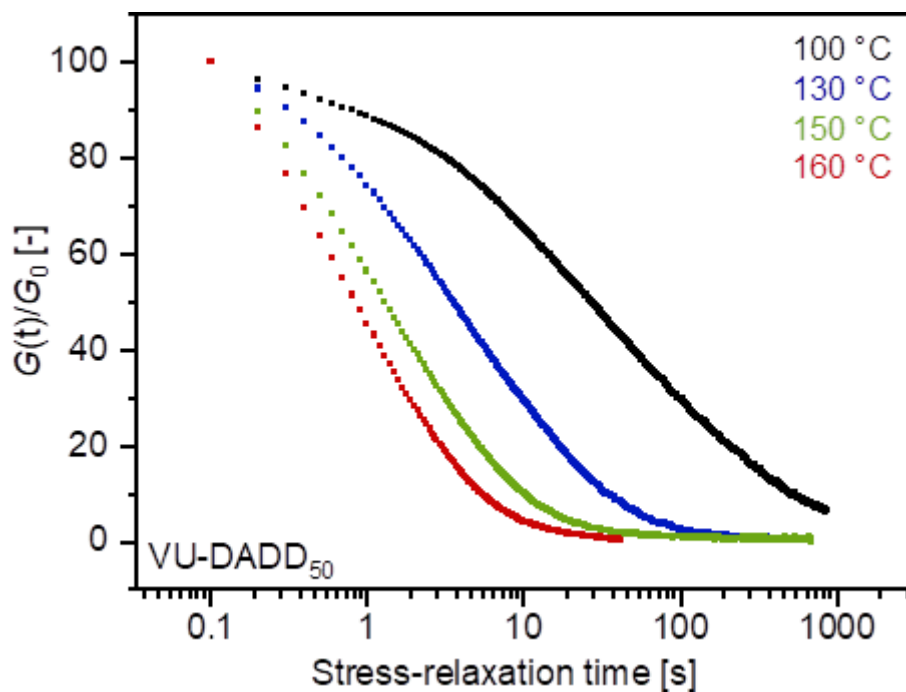
Figure S28-S2. Normalized stress relaxation measurements of the vitrimer VU-DADD$_{50}$ in the temperature range of 100–160 °C ($\gamma = 1\%$).
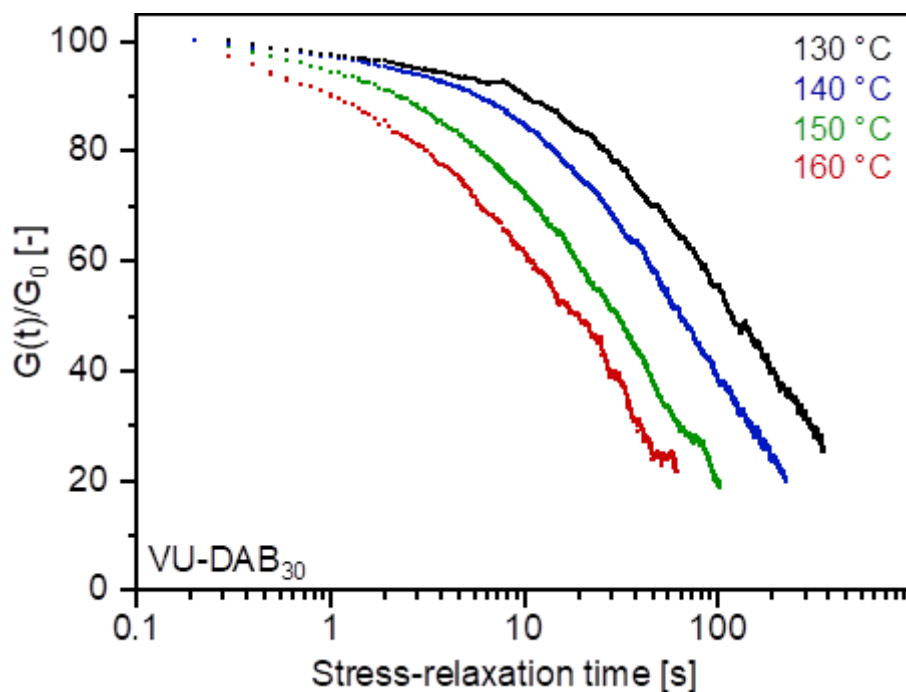
Figure S29-S1. Normalized stress relaxation measurements of the vitrimer VU-DAB$_{30}$ in the temperature range of 110–150 °C ($\gamma = 1\%$).
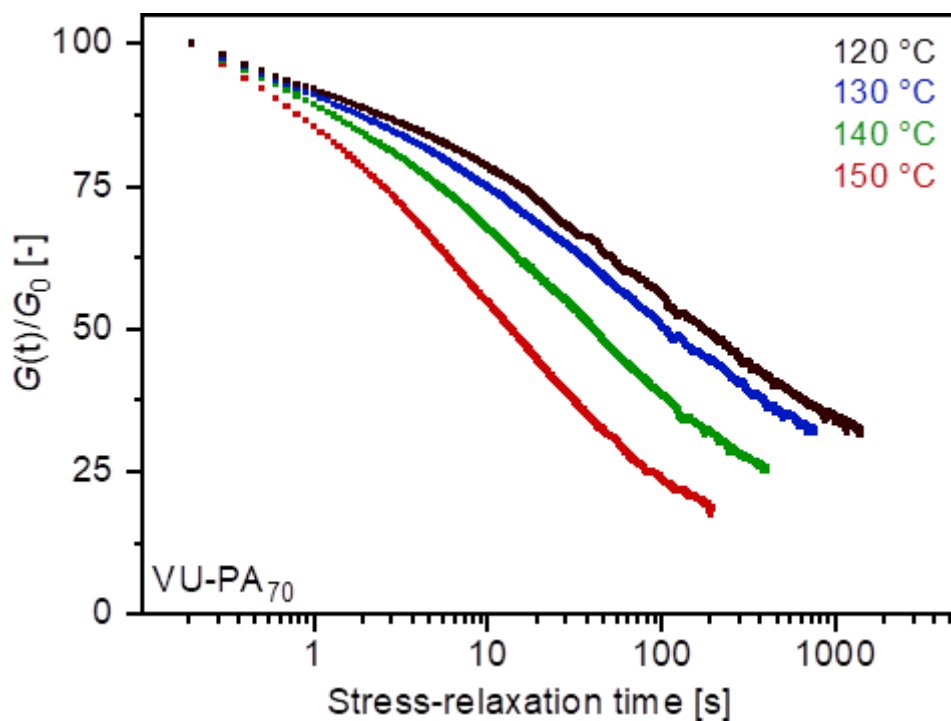
Figure S29-S2. Normalized stress relaxation measurements of the vitrimer VU-PA$_{70}$ in the temperature range of 120–150 °C ($\gamma = 1\%$).
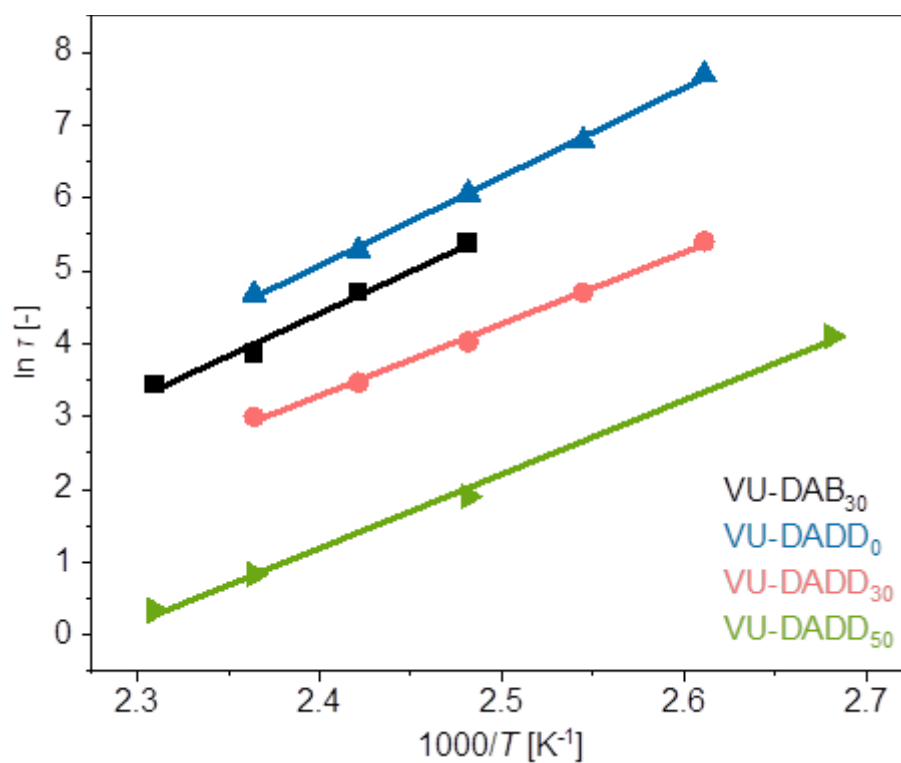
Figure S30-S1. Activation energies of 81.4 ± 3.5 kJ mol^{-1} (VU-DADD$_{30}$), 84.4 ± 2.9 kJ mol^{-1} (VU-DADD$_{50}$) and 96.4 ± 6.8 kJ mol^{-1} (VU-DAB$_{30}$) were calculated from the slope of the linear fits.
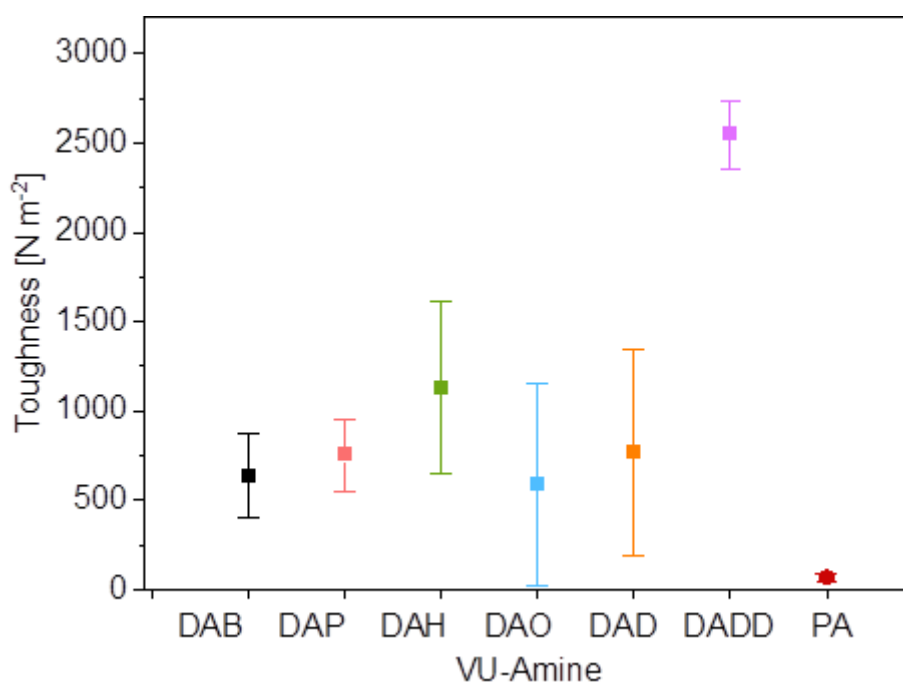
Figure S30-S2. The materials VU-DAB$_0$, VU-DAP$_0$, VU-DAH0, VU-DAO$_0$ and VU-DAD$_0$ show a of 588–1129 N m^{-2}, while VU-DADD$_0$ shows a significant higher value of 2549 N m^{-2}. The elastomeric VU-PA displays a low toughness of 69 N m^{-2}.
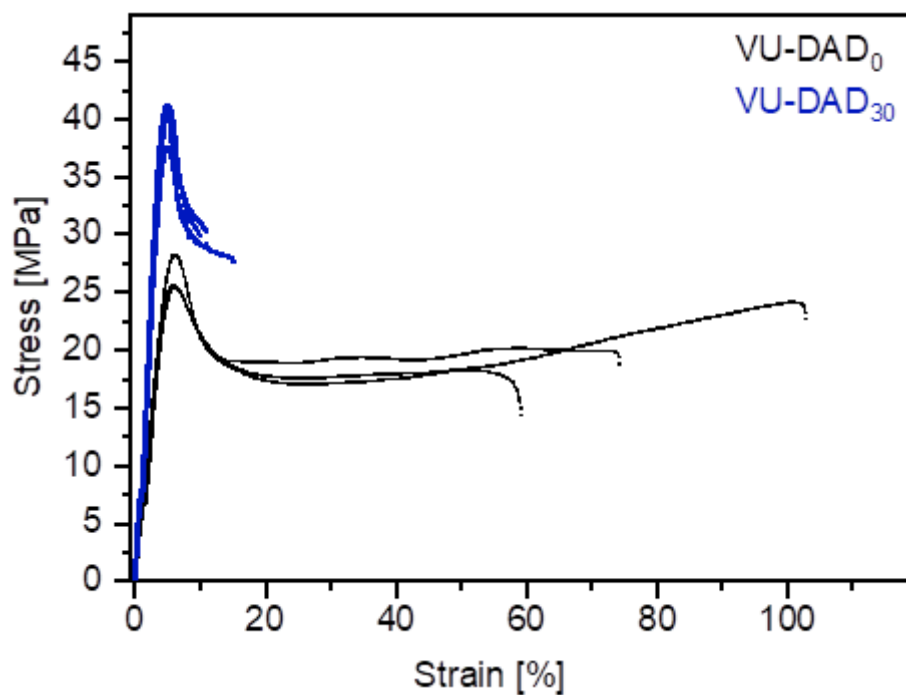
Figure S31-S1. Stress-strain curves of the vitrimers VU-DAD$_0$ and VU-DAD$_{30}$.
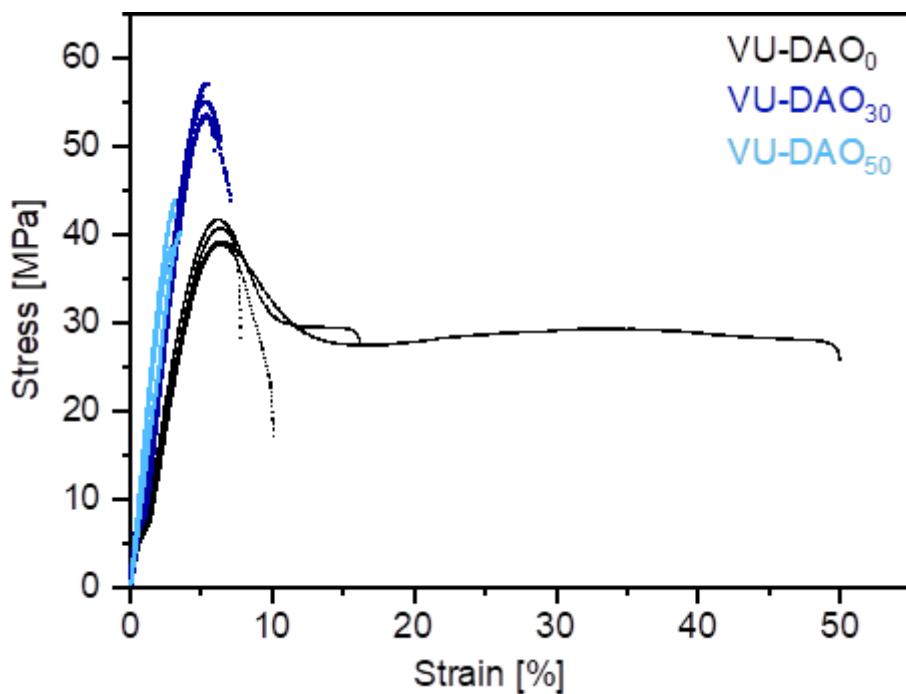
Figure S31-S2. Stress-strain curves of the vitrimers VU-DAO$_0$, VU-DAO$_{30}$ and VU-DAD$_{50}$.
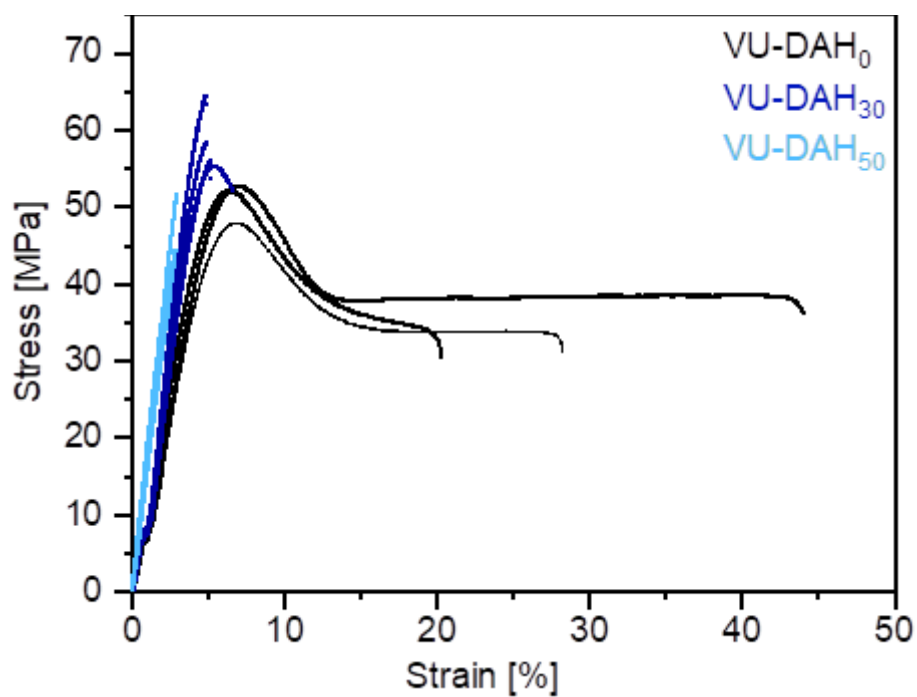
Figure S32-S1. Stress-strain curves of the vitrimers VU-DAH$_0$, VU-DAH$_{30}$ and VU-DAH$_{50}$.
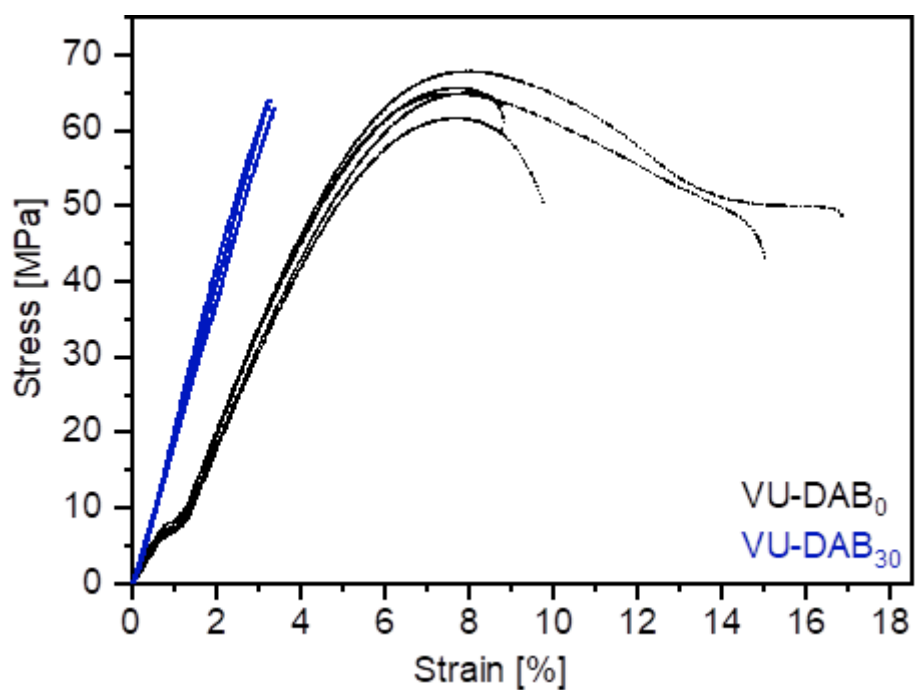
Figure S32-S2. Stress-strain curves of the vitrimers VU-DAB$_0$ and VU-DAB$_{30}$.
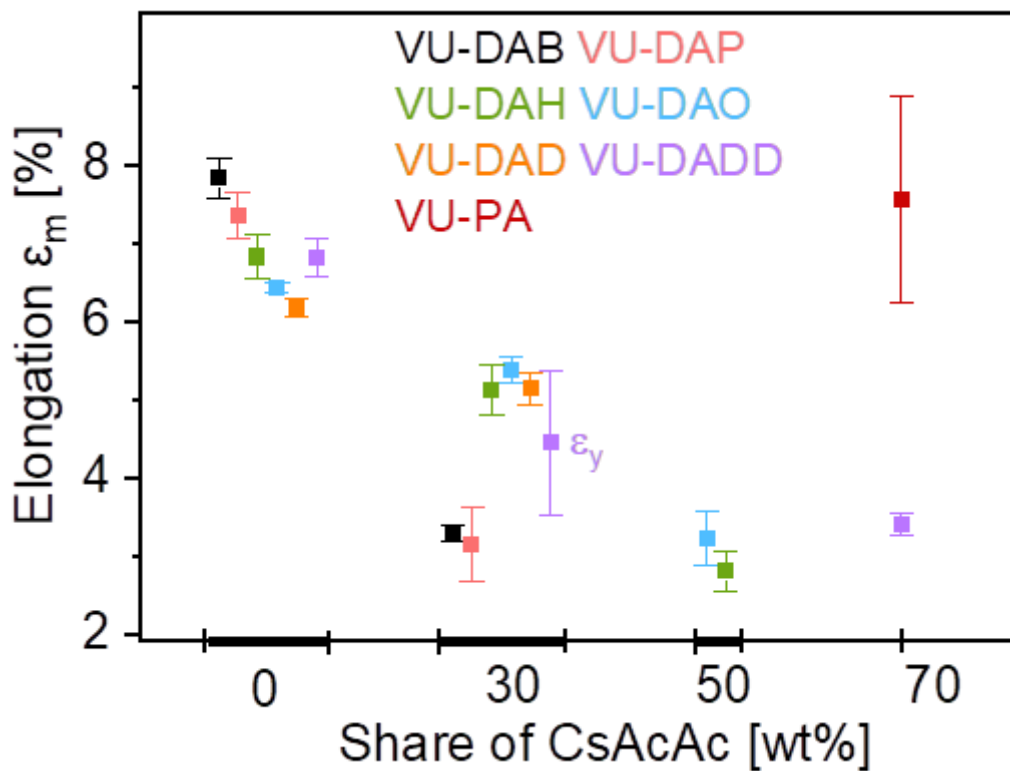
Figure S33-S1. Elongations at maximum stress or break versus the share of CsAcAc.
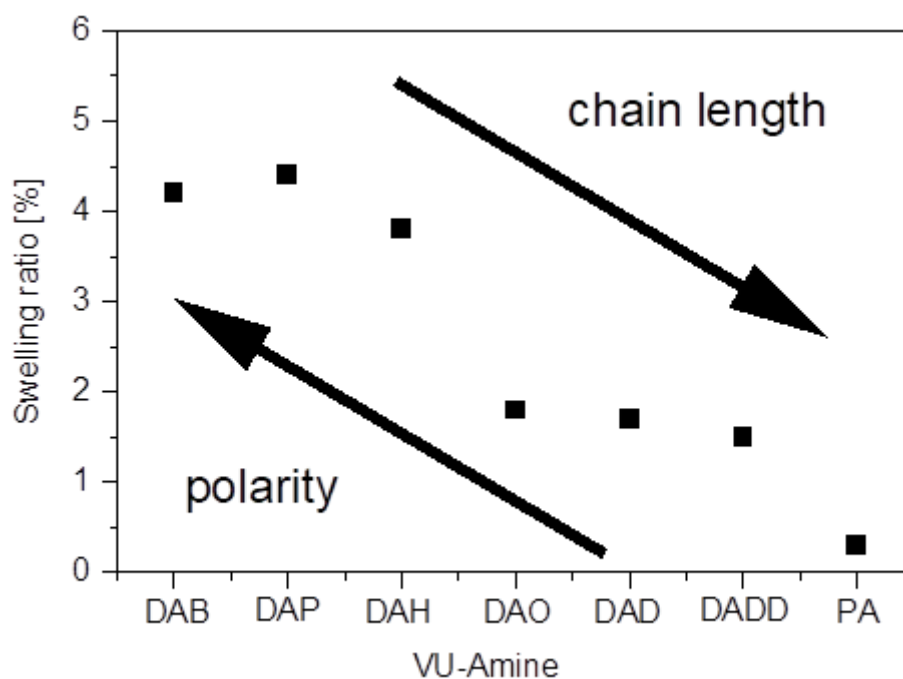
Figure S33-S2. Swelling ratio of the seven matrix vitrimers, showing swelling ratios of 0.3–4.5% in water after 3h at 100 °C, with the polar VU-DAB$_0$, VU-DAP$_0$ and VU-DAH$_0$ showing the highest ratio and the non-polar VU-PA$_0$ the lowest.
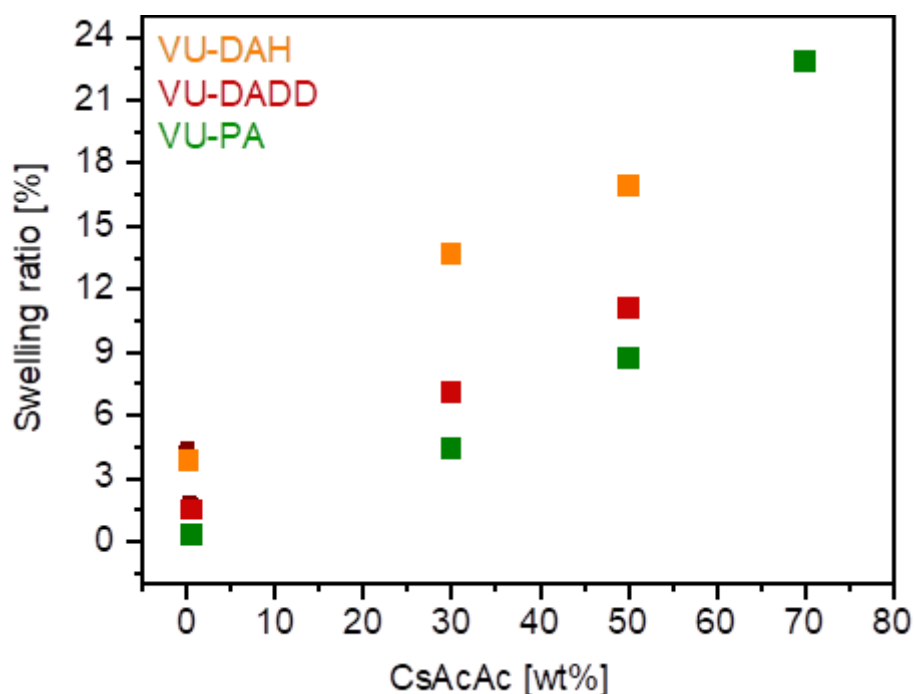
Figure S34-S1. Swelling ratio of exemplary composite vitrimers VU-DAH, VU-DADD and VU-PA with different amounts of starch (0, 30, 50, 70wt%), showing higher swelling ratios with increasing amount of starch, while a massive swelling is still suppressed by the cross-linked matrix.
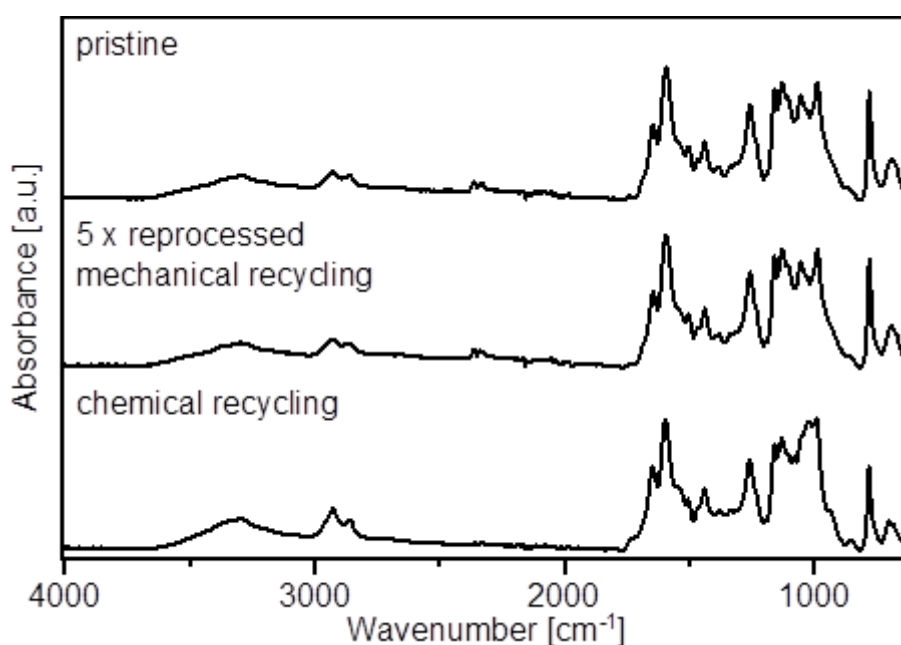
Figure S34-S2. Repetitively measured ATR-FT-IR spectra show rather similar curve shapes of the pristine and after 5 reprocessing cycles, measuring the characteristic conjugated C=C (1592 cm⁻¹) and C=O (1646 cm⁻¹) ester stretching vibrations of the vinylogous urethane bond.
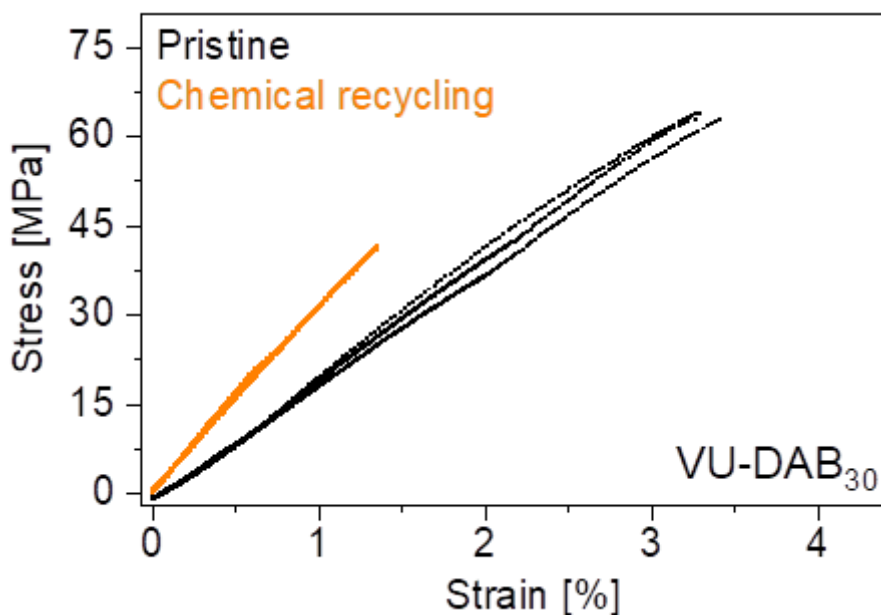
Figure S35-S1. Stress-strain curves of the vitrimer VU-DAB$_{30}$ in comparison of the pristine specimens and specimen after chemical rescycling, showing an increase in brittleness by measuring a higher E-modulus and lower tensile strength.
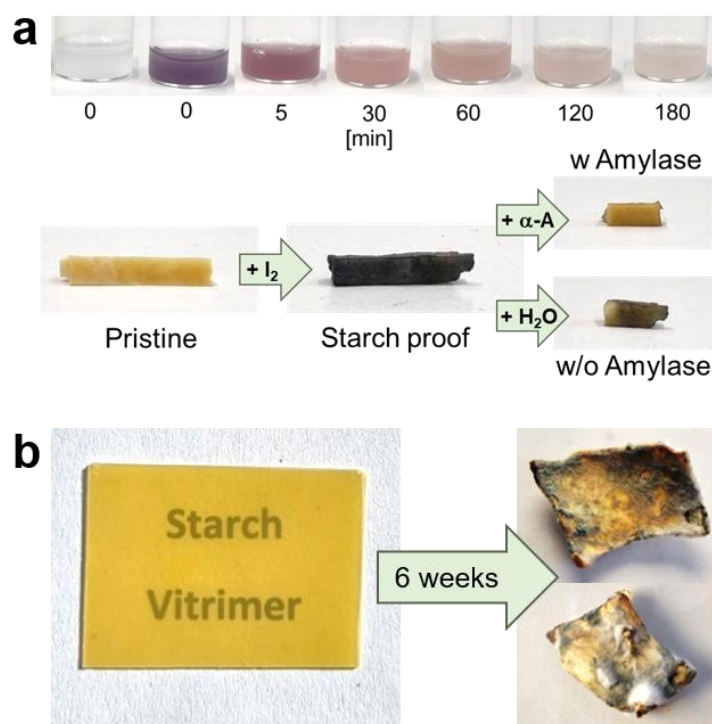
Figure S35-S2. (a) The decrease of purple color (triiodine amylose complex) was monitored as indicator for the enzymatic hydrolysis of starch by amylase. The reaction was monitored for pure corn starch, CsAcAc and the material VU PA70. (b) Pictures of the composite material VU DADD50 before and after 6 weeks under high moisture conditions, showing mold growth and shrinking of the material likewise taking place on native corn starch after a few days.
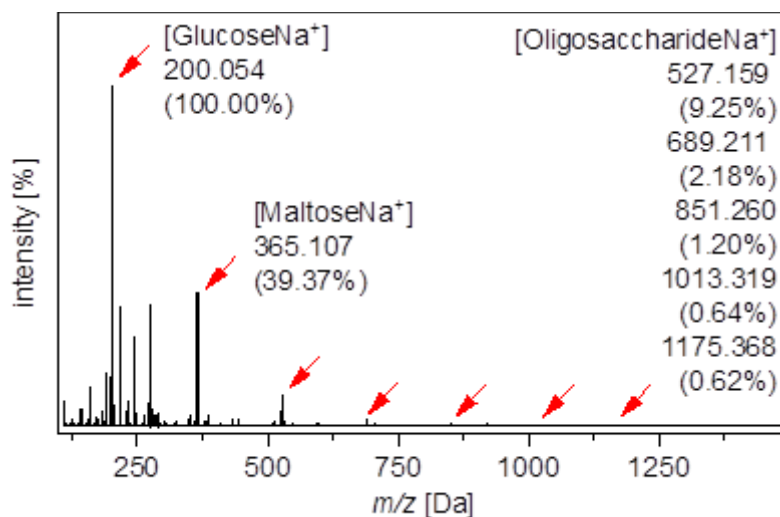
Figure S36-S1. ESI-MS showed the formation of glucose, maltose and oligosaccharides, proving that the enzymatic reaction takes place in the swollen composite materials. m/z = [GlucoseNa+] 200.054 (100.00%), [MaltoseNa+] 365.107 (39.37%) [OligosaccharideNa+] 527.159 (9.25%), 689.211 (2.18%), 851.260(1.20%), 1013.319(0.64%), 1175.368 (0.62%)
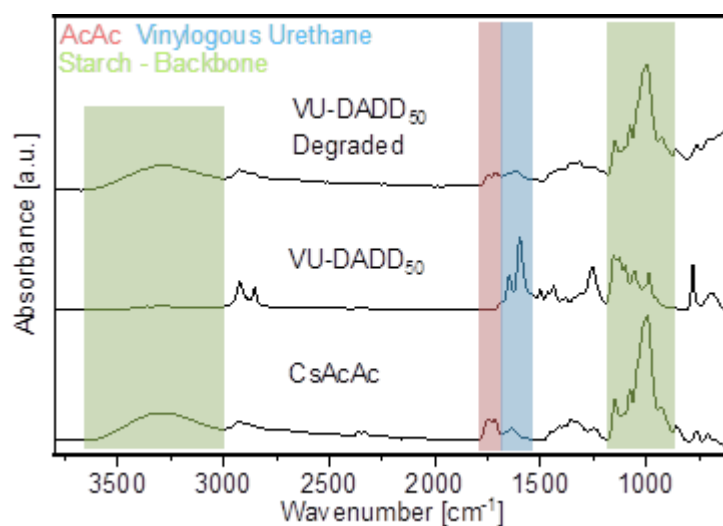
Figure S36-S2. ATR-FT-IR measurements of VU-DADD$_{50}$ before and after 6 weeks under wet conditions show a dramatic decrease of the characteristic vinylogous urethane bands (C=C (1598 cm^{-1}) and C=O ester band (1658 cm^{-1})) and the appearance of the monomers acetoacetate bands (C=O ester (1742 cm^{-1}), C=O ketone (1711 cm^{-1})) as well as the starch-typical AGU bands (CO (995 cm^{-1}, 1078 cm^{-1}, and 1148 cm^{-1}), OH (3000–3600 cm^{-1})).

(1) Witzeman, J. S.; Nottingham, W. D. Transacetoacetylation with tert-butyl acetoacetate: synthetic applications. *The Journal of Organic Chemistry* **1991**, *56* (5), 1713-1718. DOI: 10.1021/jo00005a013.
(2) Regazzi, A.; Dumont, P. J. J.; Harthong, B.; Imbault, D.; Peyroux, R.; Putaux, J.-L. Effectiveness of Thermo-Compression for Manufacturing Native Starch Bulk Materials. *Journal of Materials Science* **2016**, *51* (11), 5146-5159. DOI: 10.1007/s10853-016-9817-7.

9.5   Unpublished Results – Supporting Information
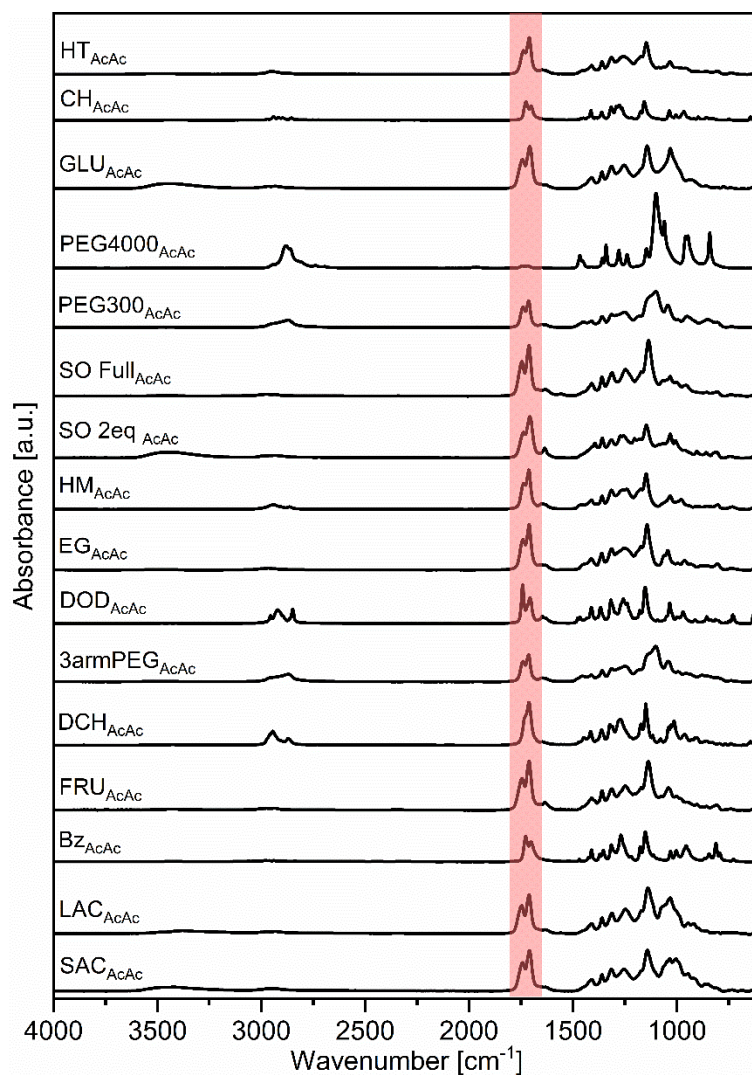
Figure A1: ATR-FT-IR spectra of the acetoacetylated alcohols showing the characteristic acetoacetate C=O stretching vibrations (red). The spectra of the acetoacetylated aromatic alcohols are exclusively shown in publication 2.
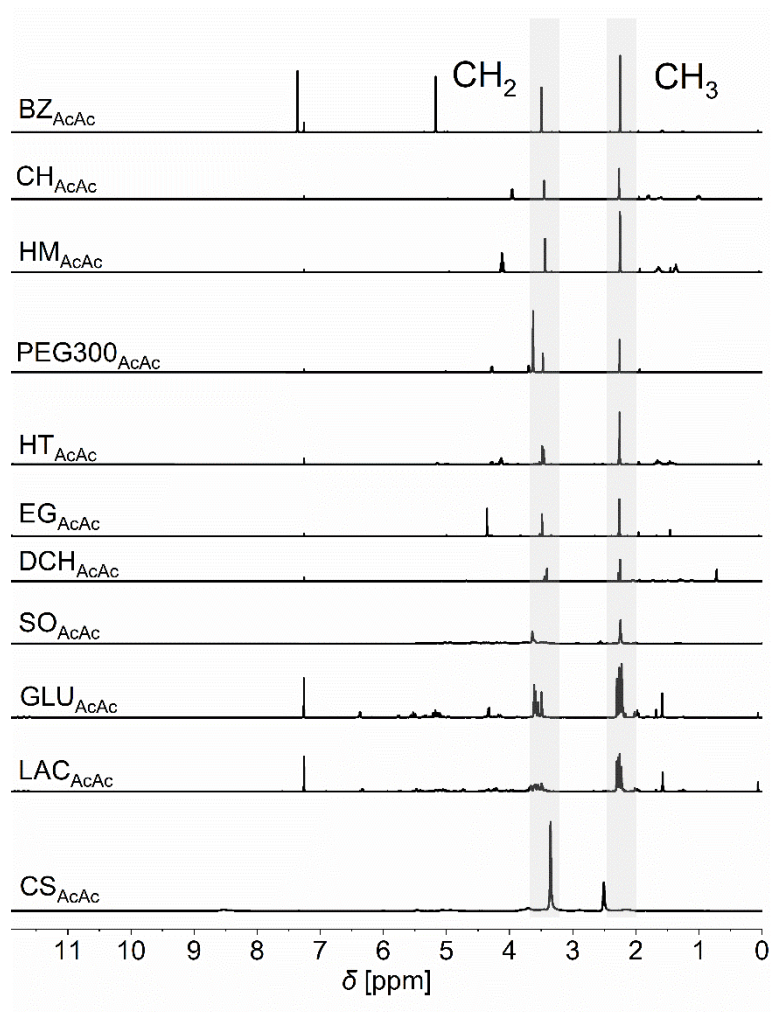
Figure A2: ^{1}H NMR spectra of several acetoacetate monomers showing the characteristic CH$_2$ and CH$_3$ groups of the acetoacetate group. The spectra were recorded in deuterated chloroform (300 MHz, 298 K). CS$_{AcAc}$ was recorded in deuterated DMSO.
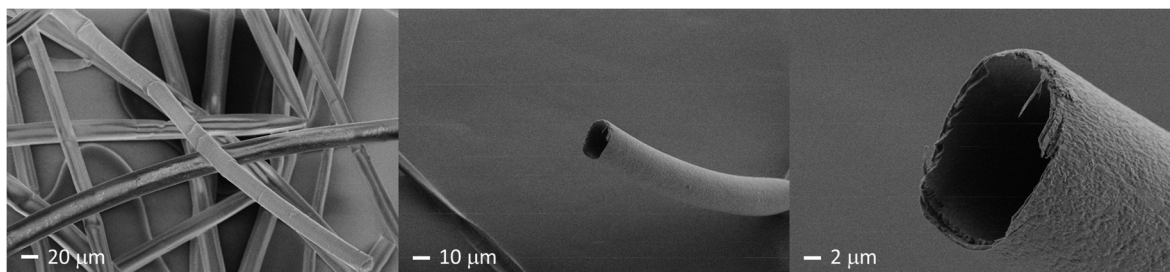
Figure A3: SEM images of hollow and intact acetoacetylated milkweed fibers. The supramolecular structure stays intact even after the modification reaction.

179
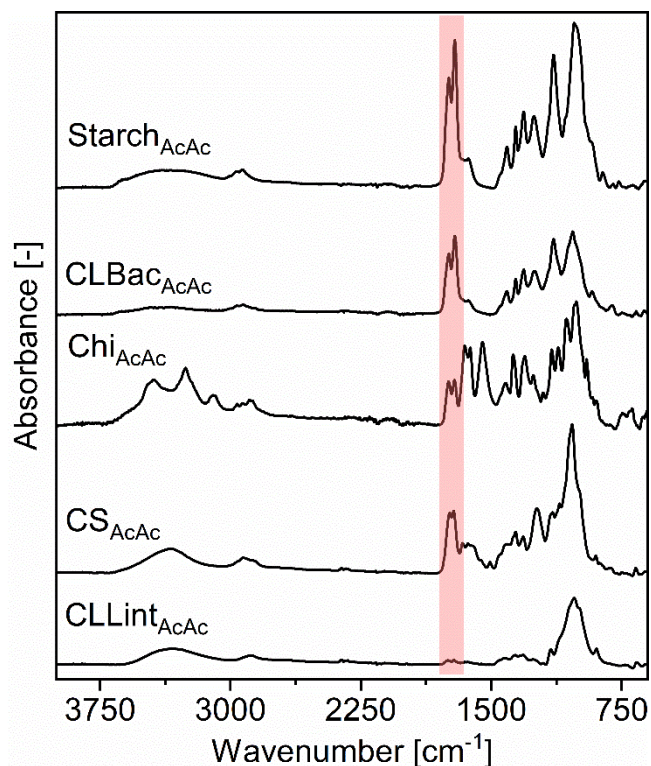
Figure A4: ATR-FT-IR spectra of the acetoacetylated biopolymers, showing the characteristic acetoacetate C=O stretching vibrations (red).
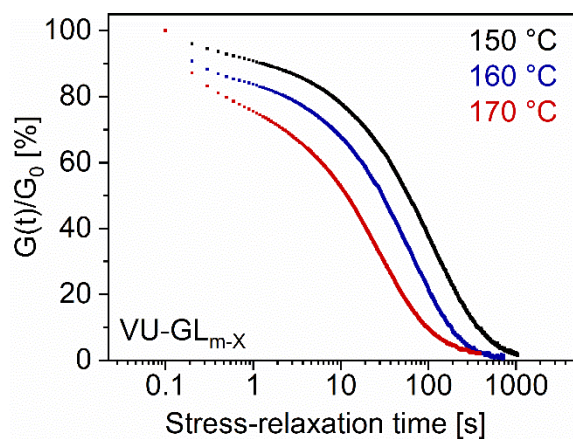
Figure A5: Stress-relaxation curves of VU-GL$_{m-X}$ in the range of 150–170 °C ($\gamma = 1\%$).
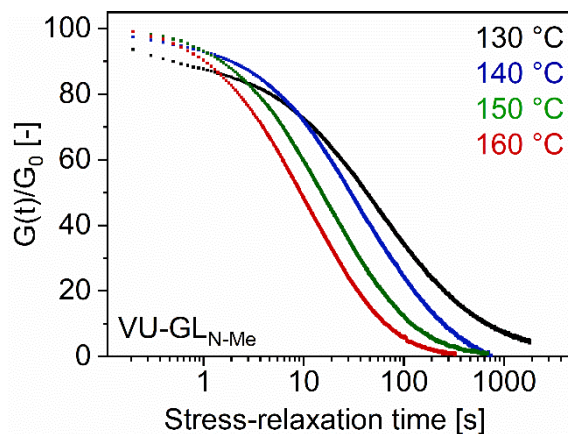
Figure A6: Stress-relaxation curves of VU-GL$_{N-Me}$ in the range of 130–160 °C (γ = 1%).
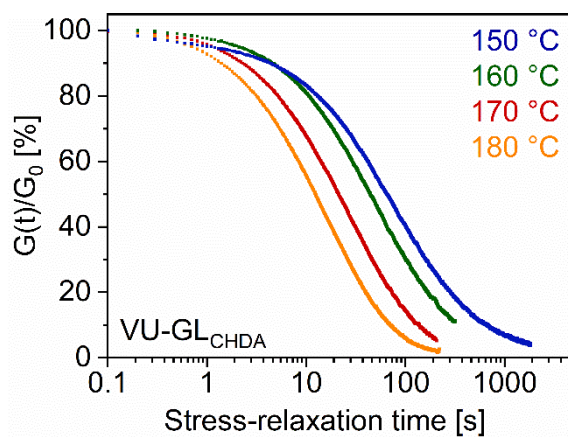
Figure A7: Stress-relaxation curves of VU-GL$_{CHDA}$ in the range of 140–180 °C (γ = 1%).
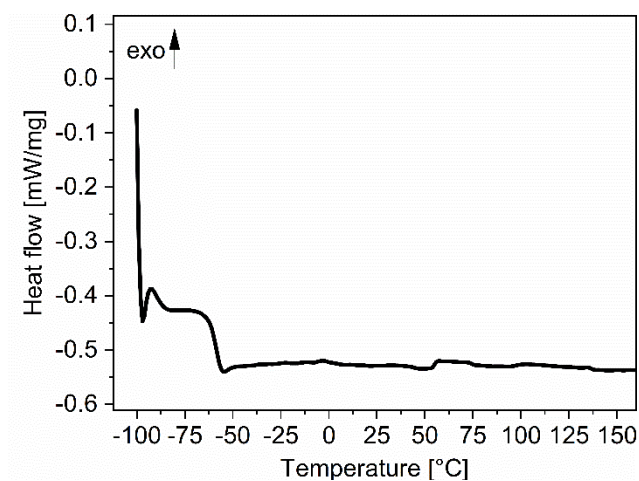
Figure A8: DSC measurement of the vitrimer VU-GL$_{J3000}$ showing a glass transition temperature of -62 °C (on-set) and -58 °C (mid) in the second heating curve.
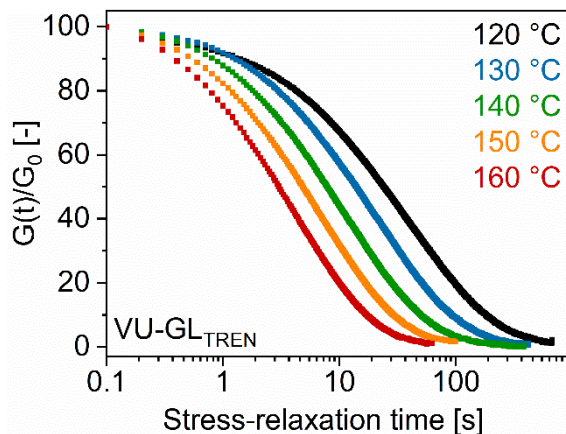
Figure A9: Stress-relaxation curves of VU-GL$_{TREN}$ in the range of 120–160 °C.
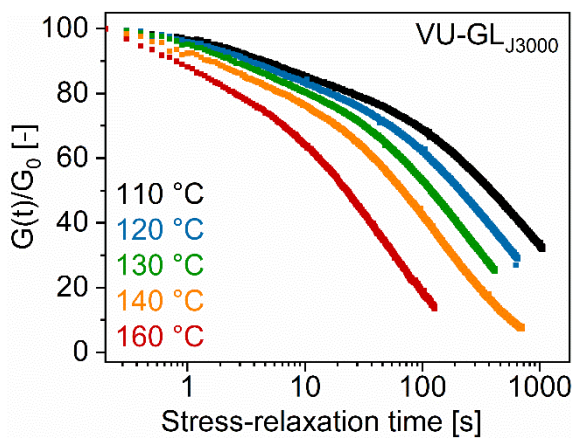
Figure A10: Stress-relaxation curves of VU-GL$_{J3000}$ in the range of 110–160 °C.
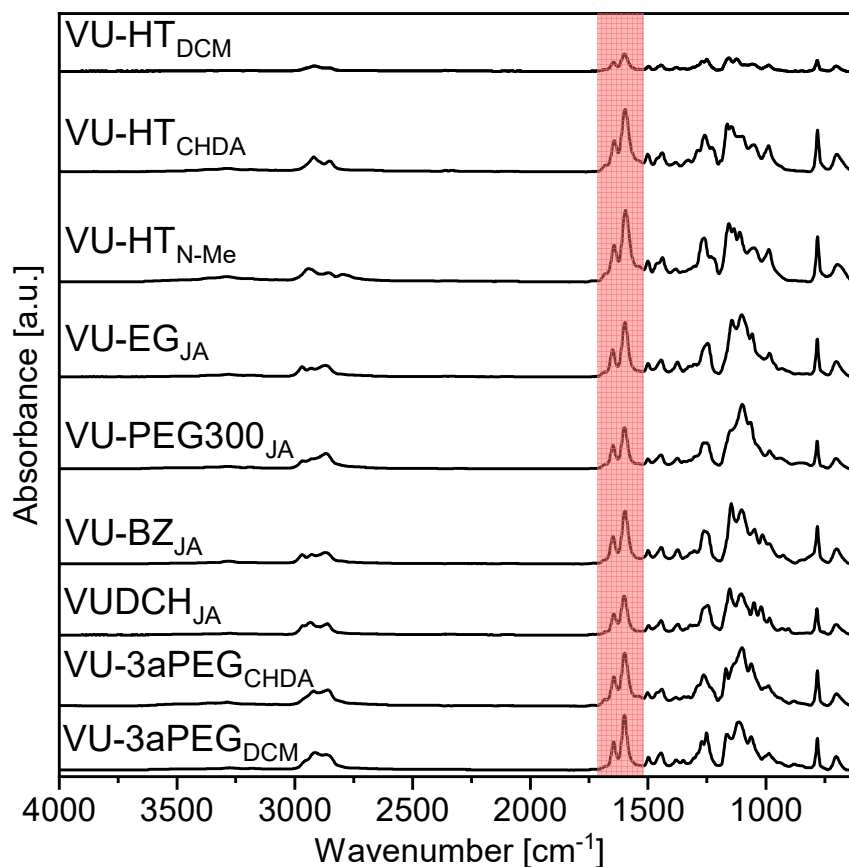
Figure A11: ATR-FT-IR spectra of the prepared vinylogous urethane vitrimers show the formation of the characteristic C=C bands (1595–1597 cm^{-1}) and C=O ester bands (1647–1649 cm^{-1}) of the vinylogous urethane bonds.
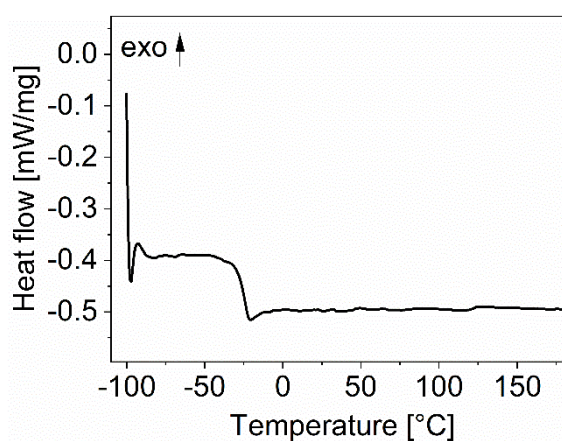
Figure A12: DSC measurements of the vitrimers VU-PEG300$_{J403}$ showing a glass transition temperature of -30 °C (on-set) and -26 °C (mid).
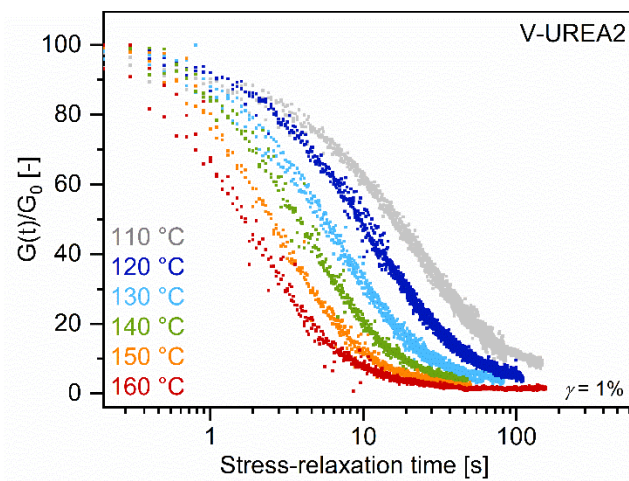
Figure A13: Stress-relaxation curves of V-UREA2.
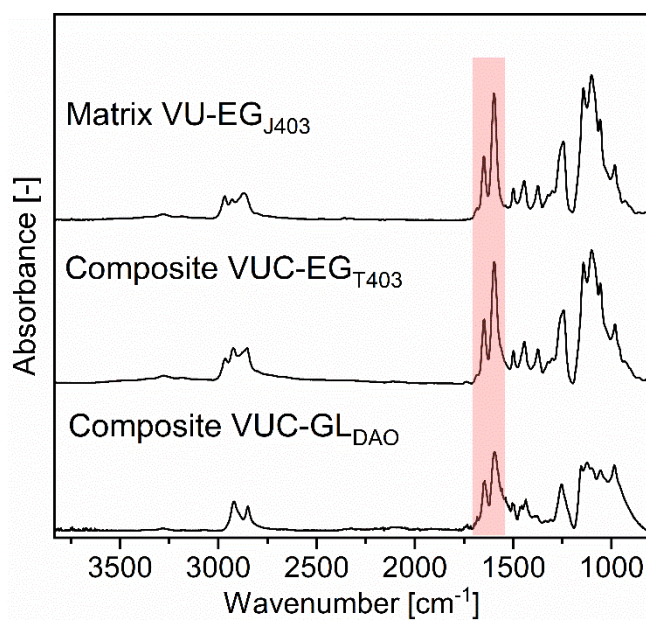
Figure A14: ATR-FT-IR spectra of the matrix vitrimer VU-EG$_{J403}$, VUC-EG$_{J403}$ and VUC-EG$_{DAO}$.

9.6   Safety and Disposal

The chemicals that were used in this work are listed in **Table 9** together with their GHS-Pictograms, Hazard- and Precautionary-Statements.

Table 9: Used substances with their GHS symbols and their Hazard- and Precautionary-Statements.

Substance	Symbol	Hazard-Statements	Precautionary-Statements
(1R,2R)-(+)-1,2-Diphenyl-ethylendiamin		H315, H319, H335	P261, P271, P280, P302 + P352, P305 + P351 + P338
1,1,1-tris(4-hydroxyphenyl)ethane		H320, H411	P501, P273, P264, P391, P337 + P313, P305 + P351 + P338
1,12-Dodecanediol	-	-	-
1,2,6-Hexantriol	-	-	-
1,3-Benzol-dimethanol		H302, H319	P264, P270, P280, P301 + P312, P305 + P351 + P338, P337 + P313
1,4-Bis-(3-aminopropyloxy)-butan		H314, H332	P261, P271, P280, P303 + P361 + P353, P304 + P340 + P310, P305 + P351 + P338
1,4-Cyclohexane-dimethanol		H318	P280, P305 + P351 + P338 + P310
1,4-Dioxane		H225, H319, H335, H351	P210, P261, P281, P305+P351+P338
1,6-Hexanediol	-	-	-
1.10-Diaminobutane		H314	P260, P280, P303 + P361 + P353, P301 + P330 + P331, P304 + P340 + P310
1.12-Diaminobutane		H302, H314, H317	P206, P280, P301+P330+P331, P303+P361+P353, P305+P351+P338, P310, P362+P364, P501

Substance	Symbol	Hazard-Statements	Precautionary-Statements
1.4-Diaminobutane (Putrescin)		H228, H302, H312, H314, H331	P210, P261, P280, P305+P351+P338, P310
1.5-Diaminopentane (cadaverin)		H314	P280, P305+P351+P338, P310
1.6-Hexanediamine		H302, H312, H314, H335	P261, P280, P305+P351+P338, P310
1.8-Diaminooctane		H302, H314, H317	P260, P270, P280, P301 + P312, P303 + P361 + P353, P305 + P351 + P338
11-hydroxyundecyl-phosphonic acid		H315, H319, H335	P261, P264, P271, P280, P302 + P352, P305 + P351 + P338
2,2,6-Trimethyl-1,3-dioxin-4-one		H225-H319	P210-P305+P351+P338
2,2'-(Ethylenedioxy)-diethylamine		H302, H314, H317, H334	P261, P280, P301 + P312, P303 + P361 + P353, P304 + P340 + P310, P305 + P351 + P338
2,7-Naphthalenediol		H315 - H319 - H335	P261 - P264 - P271 - P280 - P302 + P352 - P305 + P351 + P338
3,3-N-methyl propyl diamine		H302, H311, H314	P260, P280, P301+P330+P331, P303+P361+P353, P305+P351+P338, P310, P361+P364, P501
3-Aminobenzylamin		H302, H314, H410	P260, P273, P280, P301 + P330 + P331, P303 + P361 + P353, P305 + P351 + P338
3-aminopropyl)trime thoxysilane		H302,H314, H318, H317	P261, P270, P280, P301 + P312, P303 + P361 + P353, P305 + P351 + P338
3armpeg	-	-	-

Substance	Symbol	Hazard-Statements	Precautionary-Statements
4,4′-(Propane-2,2-diyl)dicyclohexanol (isomeric mixture)		H319	P305 + P351 + P338
4,4′-Diamino-diphenylmethane		H317, H341, H350, H370, H373, H411	P201, P260, P273, P280, P308+P313
4,4′-Methylen-bis-cyclohexylamin		H302-H314-H317-H373-H412	P280-P301+P330+P331-P303+P361+P353-P305+P351+P338-P310
4,4′-Trimethylenedi piperidine		H315, H319, H335	P261, P271, P280, P302 + P352, P305 + P351 + P338
Acetalydehyd trimer		H315, H319, H335	P261, P304+P340, P305+P351+P338, P312, P321, P332+P313, P337+P313, P362, P403+P233, P405
Acetic acid		H226, H314	P280, P305+P351+P338, P310
Acetone		H225, H319, H336	P210, P305+P351+P338, P370+P378, P403+P235
Alpha-Amylase (aspergillus oryzae		H302, H334	P261, P264, P270, P284, P301 + P312, P304 + P340 + P312
Aniline		H301, H311, H317, H318, H331, H341, H351, H372, H400	P201, P202, P260, P261, P264, P270, P271, P272, P273, P280, P281, P301+P310, P302+P352, P304+P340, P305+P351+P338, P308+P313, P310, P311, P312, P314, P321, P322, P330, P333+P313, P361, P363, P391, P403+P233, P405, P501

187

Substance	Symbol	Hazard-Statements	Precautionary-Statements
Benzylacetoacetate		H315, H319, H412	P264, P264+P265, P273, P280, P302+P352, P305+P351+P338, P321, P332+P317, P337+P317, P362+P364, P501
Benzylamine		H302, H312, H314	P260, P264, P270, P280, P301+P312, P301+P330+P331, P302+P352, P303+P361+P353, P304+P340, P305+P351+P338, P310, P312, P321, P322, P330, P363, P405, P501
Bispenol-A diglycidylether		H315, H317, H319, H411	P261, P264, P273, P280, P302 + P352, P305 + P351 + P338
Bisphenol-A		H317, H318, H335, H360, H411	P201, P202, P261, P273, P302+P352, P304+P340, P305+P351+P338, P308+P313, P333+P313, P363, P403+P233
Cellulose	-	-	-
Chitin	-	-	-
Chitosan	-	-	-
Chloroform		H302, H315, H319, H331, H336, H351, H361d, H372	P201, P202, P235, P260, P264, P270, P271, P280, P281, P301+P330+P331, P302+P352, P304+P340, P305+P351+P338, P308+P313, P310, P311, P314, P332+P313, P337+P313, P362, P403+P233, P405, P501

Substance	Symbol	Hazard-Statements	Precautionary-Statements
Deuterated chloroform		H302, H315, H319, H331, H351, H361d, H372	P260, P280, P301+P312+P330, P304+P340+P311, P305+P351+P338, P403+P233
Deuterated benzene		H225, H304, H315, H319, H340, H350, H372	P201, P202, P210, P233, P240, P241, P242, P243, P260, P264, P270, P280, P281, P301+P310, P302+P352, P303+P361+P353, P305+P351+P338, P308+P313, P314, P321, P331, P332+P313, P337+P313, P362, P370+P378, P403+P235, P405, P501
Deuterated dimethylsulfoxide	-	-	-
Deuterated methanol		H225, H301, H311, H331, H370	P210, P233, P240, P241, P242, P243, P260, P261, P264, P270, P271, P280, P301+P310, P302+P352, P303+P361+P353, P304+P340, P307+P311, P311, P312, P321, P322, P330, P361, P363, P370+P378, P403+P233, P403+P235, P405, P501
D-Fructose	-	-	-
D-Glucose	-	-	-
Dichloro-methane		315, 319, 335, 336, 351, 373	261, 281, 305+351+338
D-Laktose	-	-	-
D-Saccharose	-	-	-
D-Sorbitol	-	-	-

Substance	Symbol	Hazard-Statements	Precautionary-Statements
Ethanol		H225, H319	P210, P233, P240, P241, P242, P305+P351+P338
Ethylacetoacetate		H319	P305+P351+P338
Ethylene glycol		H302, H373	P260, P264, P270, P301+P312, P302, P314, P330, P501
Ethylenediamine		H226, H302, H311, H314, H317, H332, H334, H412	P101, P102, P260, P273, P280, P305+P351+P338, P308+P313, P405, P501
Glycerol	-	-	-
H$_2$O	-	-	-
Hexylamine		H226, H301 +H311 H314, H411	P210, P273,P280 P303 + P361 + P353 P304 + P340 + P310 P305 + P351 + P338
Iodine		H302+H312+ H332 H315, H319, H335, H372, H400	P273, P302+P352, P304+P340, P305+P351+P338
Iron-oxide nanoparticles		H319, H335	P261, P264, P271, P280, P304+P340
Isobutylamine		H225, H301, H314	P210, P280, P301+P310, P305+P351+P338, P310
Isophorene diamine		H302, H312, H314, H317, H412	P260, P261, P264, P270, P272, P273, P280, P301+P312, P301+P330+P331, P302+P352, P303+P361+P353, P304+P340, P305+P351+P338, P310, P312, P321, P322, P330, P333+P313, P363, P405, P501

Substance	Symbol	Hazard-Statements	Precautionary-Statements
Jeffamine® D2000		H302 + H312 H318 H411	P264, P270, P273
Jeffamine® D-230		H302 + H312 H318 H411	P264, P270, P273
Jeffamine® D400		H302 + H312 H318 H411	P264, P270, P273
Jeffamine® T-3000		H302 + H312 H318 H411	P264, P270, P273
Jeffamine® T-403		H302 + H312 H318 H411	P264, P270, P273
Magnesiumsulfate	-	-	-
Melamine		H351, H361f, H373	P202, P260, P280, P308 + P313, P405, P501
Menthane diamine		H301 + H311 + H331, H314	P261, P271, P280, P303 + P361 + P353, P304 + P340 + P310, P305 + P351 + P338
Mesitylene		H226, H304, H315, H332, H335, H411	P210, P273, P301 + P310, P303 + P361 + P353, P304 + P340 + P312
Methylacetoacetate		H318	P280 P305+P351+P338 P310

Substance	Symbol	Hazard-Statements	Precautionary-Statements
m-Phenylen-diamine,		H301, H311, H317, H319, H331, H341, H410	P201, P202, P261, P264, P270, P271, P272, P273, P280, P281, P301+P310, P302+P352, P304+P340, P305+P351+P338, P308+P313, P311, P312, P321, P322, P330, P333+P313, P337+P313, P361, P363, P391, P403+P233, P405, P501
m-Xylylendiamine		H302+H332, H314, H412	P273, P280, P301 + P312, P303 + P361 + P353, P304 + P340 + P310, P305 + P351 + P338
N,N Bis(3-aminopropylpiperazin)		H314	P280, P303 + P361 + P353, P304 + P340 + P310, P305 + P351 + P338, P363, P405
N,*N*-Dimethyl-formamide		H226, H312+H332, H319, H360D	P201, P280, P305+P351+P338, P308+P313
Oleic acid	-	-	-
Parafuchsin base		H350	P201-P308+P313
para-Toluene sulfonic acid monohydrate		H315, H319, H335	P302+P352, P305+P351+P338
PEG300	-	-	-
PEG4000	-	-	-
Phenol		H301, H311, H314, H331, H341, H373	P261,P280, P301+P310, P305+P351+P338, P310

Substance	Symbol	Hazard-Statements	Precautionary-Statements
Piperazin		H228, H334, H361, H314, H318, H302, H317	P201, P202, P210, P240, P241, P260, P264, P270, P272, P280, P284, P301+P312, P301+P330+P331, P303+P361+P353, P304+P340, P305+P351+P338, P310, P308+P313, P321, P333+P313
Priamine® 1074		H315, H318, H410	P273, P280, P305+P351+P338, P310, P391, P501
Priamine® 1075		H315, H318, H410	P273, P280, P305+P351+P338, P310, P391, P501
Resorcin		H302, H313, H315, H318, H400	P273, P280, P305+P351+P338
Sodiumacetate	-	-	-
Starch	-	-	-
tert-Butyl-acetoacetate	-	-	-
Tetrahydrofurane		H225, H302, H319, H335, H351	P210, P280, P301+P312+P330, P305+P351+P338, P370+P378, P403+P235
Toluene		H225, H304, H315, H336, H361d, H373	P210, P240, P301+P310, P302+P352, P308+P313, P314, P403+P233
Trifluoroacetic acid		H314, H332, H412	P260, P261, P264, P271, P273, P280, P301+P330+P331, P303+P361+P353, P304+P312, P304+P340, P305+P351+P338, P310, P312, P321, P363, P405, P501

Substance	Symbol	Hazard-Statements	Precautionary-Statements
Tris(2-aminoethyl)amine		H301, H310, H314	P280, P302+P350, P305+P351+P338, P310
Xylene		H225, H226, H304, H312, H315, H319, H332, H335, H412	P210, P233, P240, P241, P242, P243, P261, P264, P271, P273, P280, P301+P310, P302+P352, P303+P361+P353, P304+P312, P304+P340, P305+P351+P338, P312, P321, P322, P331, P332+P313, P337+P313, P362, P363, P370+P378, P403+P233, P403+P235, P405, P501
α-Alumina platelets	-	-	-

Table 10: Used carcinogenic, mutagenic and toxic for reproduction substances according to the CLP regulations of CMR chemicals.

Substance	Hazard-Statements	CMR-Classification CLP	Amount
Deuterated chloroform	H302, H315, H319, H331, H351, H361d, H372	2	2000 x 0.7 mL
Parafuchsin base	H350	1B	100 g
Deuterated benzene	H225, H304, H315, H319, H340, H350, H372	1B	100 x 0.7 mL
4,4′-Diamino-diphenylmethane	H317, H341, H350, H370, H373, H411	2	100 g
N,N-Dimethyl-formamide	H226, H312+H332, H319, H360D	1B	1 L
Bisphenol-A	H317, H318, H335, H360, H411	1B	1 kg
Chloroform	H302, H315, H319, H331, H336, H351, H361d, H372	2	3 L
Melamine	H351, H361f, H373	2	100 g

Substance	Hazard-Statements	CMR-Classification CLP	Amount
Piperazin	H228, H334, H361, H314, H318, H302, H317	2	400 g
Toluene	H225, H304, H315, H336, H361d, H373	2	1 L

10 Acknowledgement

In this chapter, I thank those who supported me in the past years. I especially thank my Doktorvater professor Volker Abetz, who encouraged and supported me in all stages of the thesis. When I moved from Berlin to Hamburg to start my master's in chemistry, I joined your working group for an internship and felt very comfortable from the beginning. It would take some time, but when I finished my master's and wanted to start a Ph.D. I remembered the welcoming working atmosphere and exciting topics in your group. You accepted me as a Ph.D. student on the novel topic of vitrimers, which I have been burning for ever since. I am also very grateful to you for giving me some thematic freedom, so I have now got my dream job in the field of biopolymers. I would also like to thank you generously for the semester abroad, which took place despite the covid-19 pandemic. Thank you for the guidance and many talks on a professional but also on a private level. I would also like to thank Professor Suwabun Chirachanchai, who welcame me generously in Bangkok and allowed me to spend an incredible semester abroad, both thematically and on a socio-ethical level. Birgit, I would like to thank you for always having an open ear and great help whenever it was needed. I will never forget the yearly barbecues.

Thank you, professor Horst Weller for the review of this dissertation.

Dear AK Abetz, you gave me a great time at the university by joining countless events, conversations and laughs. I would especially like to thank the colleagues in room 363. Tilman, Jincong, and I spent years in a pleasant working atmosphere and I appreciate deep talks and laughter but also quiet moments to concentrate and ambitious work. I like to thank Felix, Niklas, Stephan and Sascha for helpful advice, exciting dart games, and remarkable moments in the social rooms and in private life. Iklima, I will miss you and the intensive discussion on the whiteboard, I really hope we can continue someday.

To my students Musawer, Jannik, Fanny and Gloria, thank you for your sacrificing help in internships and master thesis. Gloria, I wish you the best for your Ph.D. and many promising results.

Florian, Siraphat and Gloria, I thank you and the members of the SFB986 for the work on the project, which I always appreciated. Besides many talks, presentations, summer schools and conferences, I always had a memorable time with you.

Sabrina, our trip to Canada was amazing and I am glad to have been able to do this with you. You were a great and encouraging light at the conference in Canada and the trip around. Maria and Patrick, thank you for being part of my Ph.D. and caring for my social well-being in daily life. Martin, thank you for the numerous DSC and TGA measurements you have always sacrificed and measured with passion.

To the cooperation partners at Universität Hamburg and Technische Universität Hamburg. Lea, Michael and Tobias, thank you for the fruitful cooperation, good discussion and many interesting results. I would like to thank Benedikt and Alexander for the great work together, the pleasant working atmosphere and the regular professional exchange. I learned a lot about mechanical properties, and it always felt like working with good friends.

To my friends and family and especially Beate, Juergen, and my girlfriend Daniela. I thank you with all my heart for your support on many levels. You have given me the strength to go on this long journey, and I could not have done it without you.

11 Declaration of Academic Integrity

Hereby I confirm that I wrote the present work independently and that it has not been submitted in any form for another degree at any university or other institute. Information derived from the published and unpublished work of others has been acknowledged in the text and a list of references is given in the bibliography.

Hamburg, 24.10.2023   Philipp Haida

_____

Place, Date, Signature